



HAL
open science

Ecodynamics of trace metals and metalloids in Pyrenean lakes in relation to climate change and anthropogenic pressure

Bastien Duval

► To cite this version:

Bastien Duval. Ecodynamics of trace metals and metalloids in Pyrenean lakes in relation to climate change and anthropogenic pressure. Analytical chemistry. Université de Pau et des Pays de l'Adour; Universidad del País Vasco, 2020. English. NNT : 2020PAUU3046 . tel-03917523

HAL Id: tel-03917523

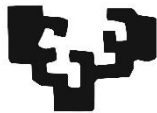
<https://theses.hal.science/tel-03917523>

Submitted on 2 Jan 2023

HAL is a multi-disciplinary open access archive for the deposit and dissemination of scientific research documents, whether they are published or not. The documents may come from teaching and research institutions in France or abroad, or from public or private research centers.

L'archive ouverte pluridisciplinaire **HAL**, est destinée au dépôt et à la diffusion de documents scientifiques de niveau recherche, publiés ou non, émanant des établissements d'enseignement et de recherche français ou étrangers, des laboratoires publics ou privés.

eman ta zabal zazu



Universidad
del País Vasco

Euskal Herriko
Unibertsitatea



Ecodynamics of metals and metalloids in Pyrenean lakes in relation to climate change and anthropogenic pressure

Bastien Duval

October 2020

Supervised by:

Alberto de Diego

David Amouroux

**AUTHORISATION OF THE THESIS SUPERVISOR
FOR ITS PRESENTATION**

Mr/Ms. ALBERTO DE DIEGO with National ID Card num. 22734269R

In his/her capacity as Supervisor of the Doctoral Thesis: **Ecodynamics of metals and metalloids in Pyrenean lakes in relation to climate change and anthropogenic pressure**

completed within the Doctoral Programme: **Scientific Cross-Disciplinary Approaches to Heritage and Landscape**

by the PhD student Mr/Ms. **BASTIEN DUVAL** ,
having reviewed the SIMILARITY REPORT issued by the tool provided for this purpose by the university, hereby authorises the presentation of the aforementioned Doctoral Thesis, given that it fulfils the conditions necessary for its viva.

In LEIOA on 1 of OCTOBER, 2020

THE THESIS SUPERVISOR

Alberto de Diego

Signed: 

**AUTHORISATION OF THE THESIS SUPERVISOR
FOR ITS PRESENTATION**

Mr/Ms. DAVID AMOUROUX with National ID Card
num. 171064350957 _

In his/her capacity as Supervisor of the Doctoral Thesis: **Ecodynamics of metals and metalloids in Pyrenean lakes in relation to climate change and anthropogenic pressure**

completed within the Doctoral Programme: **Scientific Cross-Disciplinary Approaches to Heritage and Landscape**

by the PhD student Mr/Ms. **BASTIEN DUVAL** ,

having reviewed the SIMILARITY REPORT issued by the tool provided for this purpose by the university, hereby authorises the presentation of the aforementioned Doctoral Thesis, given that it fulfils the conditions necessary for its viva.

In LEIOA on 1 of OCTOBER, 2020

THE THESIS SUPERVISOR

David Amouroux

Signed: _____



**AUTHORISATION OF THE DOCTORAL PROGRAMME'S ACADEMIC
COMMISSION**

The Academic Commission of the Doctoral Programme in **Scientific Cross-Disciplinary Approaches to Heritage and Landscape**

during its meeting held on **30 of September, 2020**, agreed to authorise the presentation of the Doctoral Thesis entitled: **Ecodynamics of metals and metalloids in Pyrenean lakes in relation to climate change and anthropogenic pressure**

supervised by Dr. **ALBERTO DE DIEGO** and **DAVID AMOUROUX**

and presented by Mr/Ms. **BASTIEN DUVAL**

and registered with the **Department of Analytical Chemistry**.

In LEIOA on 1 of October, 2020

THE COORDINATOR OF THE DOCTORAL PROGRAMME



Signed: Juan Manuel Madariaga

DEPARTMENT AUTHORISATION

The Board of the Department of **ANALYTICAL CHEMISTRY**

during its meeting held on 25 of September, 2020 agreed to authorise

the processing of the Doctoral Thesis entitled: **Ecodynamics of metals and metalloids in Pyrenean lakes in relation to climate change and anthropogenic pressure**

supervised by Dr. **ALBERTO DE DIEGO** and **DAVID AMOUROUX**

and presented by Mr/Ms. **BASTIEN DUVAL**

to this Department.

In LEIOA, on 25 of September, 2020

APPROVED BY THE DEPARTMENT DIRECTOR AND DEPARTMENT SECRETARY


Signed: Olatz Zuloaga


Signed.: Irantzu Martinez

PHD DEGREE CERTIFICATE
DOCTORAL THESIS VIVA CERTIFICATE

PhD STUDENT MR/MS. **BASTIEN DUVAL**

TITLE OF THE THESIS: **Ecodynamics of metals and metalloids in Pyrenean lakes in relation to climate change and anthropogenic pressure**

After having witnessed the completion of the viva by the author and their response to any objections and/or suggestions made, the Panel appointed by the Postgraduate Commission of the University of the Basque Country to examine the Doctoral Thesis indicated above, meeting on the indicated date, agreed _____ to award the following grade:
unanimously or by majority vote

DISTINCTION / MERIT / PASS / FAIL

Viva language(s) (in the event of there being more than one language, please specify the percentage of the thesis defended in each):

Spanish _____

Basque _____

Others (specify which and the corresponding percentage) _____

In _____ on _____ of _____, _____

CHAIRPERSON,

SECRETARY,

Signed:

Signed:

Dr. _____

Dr: _____

MEMBER 1,

MEMBER 2,

MEMBER 3,

Signed:

Signed:

Signed:

Dr. _____

Dr. _____

Dr. _____

PHD STUDENT

Signed _____

Remerciements

« *Do or do not. There is no try.* »

Et il avait raison le petit bonhomme vert ! La gestation fut longue et compliquée, mais enfin je vais pouvoir ajouter un livre à ~~ma bibliothèque~~ la bibliothèque de ma nouvelle colocataire. Marie, désolé d'avoir passé nos premières journées de vie commune sur mon ordinateur.

Ce manuscrit de thèse est loin d'être uniquement le fruit de mon travail, et des dizaines de personnes y ont contribué, de loin ou de près, que ce soit d'un point de vue purement scientifique ou tout simplement grâce à un soutien morale et physique, merci à tous de m'avoir accompagné pendant ces quatre années.

Je tiens tout d'abord à remercier mes deux directeurs de thèse, Alberto de Diego et David Amouroux, pour la confiance que vous m'avez accordée. Alberto, merci de m'avoir remonté le moral dans les moments les plus durs grâce à un optimisme à toute épreuve. Merci à toi David, tu m'as appris que l'on pouvait travailler dans la rigueur tout en restant dans la bonne humeur ! L'autonomie que vous m'avez donnée, ajoutée à toutes les connaissances que vous m'avez apportées m'ont permis de grandir d'un point de vue professionnel. Ce pour quoi je voudrais surtout vous remercier énormément, c'est tout simplement pour m'avoir donné le « goût de la montagne » Sans vous, et donc sans cette thèse, j'aurais probablement passé mes week-ends d'été de ces quatre dernières années en mode farniente.

J'aimerais également remercier très fortement Emmanuel Tessier qui m'a constamment accompagné, que ce soit au labo ou sur le terrain. Merci pour ta patience (et il en a fallu !), et ton expertise dans tous les domaines (y compris sur l'ouverture des portes !!!). Les discussions sont toujours passionnantes avec toi.

Merci également à Luis Angel Fernández pour toutes les discussions que l'on a pu avoir sur la science et la vie en général. Merci également pour tous tes conseils au laboratoire à l'UPV/EHU, ce fut un vrai plaisir de travailler avec toi.

Je souhaite remercier toutes les personnes du laboratoire IPREM (UPPA) et de l'IBeA (UPV/EHU) que ce soit pour votre aide au laboratoire ou sur le terrain : Kepa, Andrea, Alice, Javier, Nestor, Iciar, Marina, Mireia, Leire, Laura, Marizol. Belen, Thibaut, Gorka, Sylvain, Julien, Josean, Olaia, Silvia, Ainara, Cristina, Jérémy, Asmodée, Thomas etc ...

Remerciements tout particuliers également à Manue, Mathieu et Marine qui m'ont accueilli comme il se doit à l'Iprem, et à Robin, Cloé et Aurore, que je bichonne encore tous les jours comme mes petits bébés (*#levieuxc'estmoi*). Merci pour toutes les sorties, les randonnées, les repas, les week-ends confinement / Age of Empire / bières (coucou Thomas !).

Merci également à tous ceux qui ont participé à la Mercury Conference 2019. Quelle semaine !!!

Merci Gabriella Lobos pour la découverte de ce magnifique pays qu'est le Chili. J'espère pouvoir y revenir très rapidement !

Merci à l'Orchestre Arpège (meilleur orchestre de la Terre entière et même de l'univers intergalactique) pour les soirées détente post-confinement !

Merci à ma famille, l'imputrescible Gégé, la magnifique Julie et la ~~capricieuse~~ sensible Tatab. Je vous aime, mes chéris adorés de tout mon cœur !!!! Vive les chuletón !!!

Et enfin un immense, incroyable et magnifique merci à l'amour de ma vie : Julia. Merci de ta patience, de ton soutien indéfectible et de ton amour, tout simplement. Merci d'avoir toujours été là ces derniers mois, même quand je faisais ma tête de con. L'amour entre nous deux n'est jamais unidirectionnel, sache-le ! Si proto-docteur a su effectuer sa mue avec succès, c'est forcément grâce à toi !

Acknowledgements

« *Do or do not. There is no try.* »

The little green man was right. It took time and hard work, but I can finally add a book to ~~my bookcase~~ my new flatmate's bookcase. Marie, I am sorry I spent these first days in our shared home glued to my computer screen.

This thesis is not the fruit of my work alone. Dozens of people have contributed to its writing, be it from a scientific standpoint or through moral and physical support. Thank you all for your presence during these four years.

I would like to thank my supervisors, Dr. Alberto de Diego and Dr. David Amouroux, for their trust. Alberto, thank you for your unwavering optimism, and for making me smile on the roughest days. David, thank you for teaching me that rigour and pleasure are not incompatible. By pushing me to be independent and teaching me your knowledge, you have helped me grow on a professional level. I could never thank you enough for making me appreciate the mountains as I do now. Without you, and without this thesis, I would have spent the past four summers lazying at home.

I wish to thank Emmanuel Tessier for always being here for me, at the lab and in the field. Thank you for being patient (oh so patient!), and for sharing your expertise in every possible topic (even door-opening!). Every single conversation I have had with you has been fascinating.

Thank you, Luis Angel Fernández, for our numerous talks on science and life in general and thank you for all the advice you gave me at the UPV/EHU lab. Working with you was a great pleasure.

I would also like to thank everyone working at the IPREM (UPPA) and IBeA (UPV/EHU) labs for their help at the lab and on the field: Kepa, Andrea, Alice, Javier, Nestor, Iciar, Marina, Mireia, Leire, Laura, Marizol. Belen, Thibaut, Gorka, Sylvain, Julien, Josean, Olaia, Silvia, Ainara, Cristina, Jérémy, Asmodée, Thomas, etc.

Many thanks to Manue, Mathieu, and Marine, who welcomed me with open arms at the IPREM, and to Robin, Cloé, and Aurore, who will forever be my babies (*#I'llalwaysbeolder*). Thank you for our nights out, our hikes, our dinners together, and our Age of Empire-playing and beer-drinking (Thomas, this one's for you) weekends during lockdown.

Thank you to everyone who participated in the 2019 Mercury Conference. What a week!

Thank you, Gabriella Lobos, for showing me the wonderful country of Chile. I hope to go back there soon!

Thank you, Orchestre Arpège (number one orchestra on Earth and in every galaxy) for amazing post-lockdown chillout session.

I wish to thank my family: my immortal Gégé, my beautiful Julie and my ~~temperamental~~ emotional Tabtab. I love you all, you are my world! Hooray to the chuletón!

And of course, last but not least, thank you to the love of my life: Julia. Thank you for your patience, thank you for your constant support, but most of all, thank you for your love. Thank you for always being by my side, even when I am being a moron. Our love will never be unidirectional, let me tell you! If proto-doctor managed to grow so much, he owes it all to you.

Abstract

The Pyrenean high mountain lakes are iconic elements of the landscape and the history of the territory. Their management and conservation, within the current context of climate change and increasing anthropogenic pressure, requires detailed knowledge of their biogeochemical functioning. This doctoral thesis has been carried out in the framework of the project REPLIM (a network of observatories of aquatic ecosystems sensitive to climate change in the Pyrenees) that aims to investigate the past, present and future of lakes and peatbogs in the Pyrenees in the general context of global change. Five sampling campaigns were carried out in 2017-2019 in more than 20 alpine lakes located in the Central – Western Pyrenees. The collection and analysis of subsurface and deep-water samples allowed us to study the occurrence, geographical distribution, depth profiles and seasonal trends of a large array of chemical and physical parameters to better characterize the aquatic geochemistry of those lakes. Specifically, the cycle of carbon dioxide (CO₂) and the fate of Potentially Harmful Trace Elements (PHTEs) were investigated in detail. The mercury (Hg) was specially studied through the development of a new analytical procedure based on the use of graphene nanoparticles for the measurement of trace concentrations in natural waters. Investigations were conducted on the distribution and the fate of mercury species in the water column, as well as in sediment archives to better constrain mercury biogeochemical processes in space and time.

The new and robust procedure for total alkalinity (TA) and dissolved inorganic carbon (DIC) measurements developed in this work allowed us to determine the other two parameters of the CO₂ system, the pH, and the fugacity of CO₂ (fCO₂). The bedrock characteristics of the watershed appear to be the most important parameters influencing the acid status of the studied lakes: lakes lying on granitic basin rather than on sedimentary rocks are more sensitive to acidification changes. Moreover, fCO₂ values nowadays are above the atmospheric pCO₂ meaning that lakes are sources of CO₂. Nevertheless, anthropogenic emissions of CO₂ are constantly increasing and therefore it is crucial to monitor alpine lakes closely to understand the effects of the excess of atmospheric CO₂.

The measurement of various physico-chemical parameters in alpine lakes allowed us to discriminate and classify the studied lakes according to their water geochemistry, highlighting the importance of the trophic status of the lakes, the geological background (granitic vs sedimentary rocks) and the atmospheric inputs. The occurrence, sources, and behaviour of the PHTEs in the studied lakes were investigated with evidence of a contrast between geological and atmospheric inputs. Intensive monitoring of four lakes revealed some PHTEs (arsenic, copper, nickel, molybdenum, cobalt, and cadmium) to be highly sensitive to environmental changes such as temperature and redox conditions.

Monitoring natural concentrations of total mercury in aquatic systems, especially from remote areas, remains a difficult challenge and there is a need for the development of low cost and easy handling analytical methods. The method for analysis of trace mercury concentrations developed and optimized

in this work was successfully operational and exhibits suitable limit of detection as low as 0.38 ng L⁻¹ using 200 mL of the water sample, and excellent reproducibility (< 5% as RSD).

Hg speciation results in the water column demonstrated the pristine state and the dynamic of the Pyrenean lakes. The homogeneity in the total mercury concentrations in the studied lakes confirmed the absence of local sources and the potential use of these ecosystems as sentinels of regional to global Hg contamination. While inorganic mercury (iHg(II)) did not show seasonal variations, monomethylmercury (MMHg) was significantly higher in autumn 2018 and dissolved gaseous mercury (DGM) varied strongly within and among lakes reaching concentration values never recorded until now for pristine areas in some specific samples. Incubation experiments confirmed that drastic environmental changes occurring daily and seasonally in alpine lakes are providing conditions that can promote Hg methylation (stratified anoxic waters), MMHg demethylation and iHg(II) photoreduction (intense UV light).

The historical Hg record in sediment archives highlighted temporal trends in Hg accumulation rates (HgARs) with a progressive increase since the 16th Century and the industrialization, mirroring the Hg production in Almadén mines (Southern Spain). Hg stable isotopes in these cores also emphasized the anthropogenic pressure characterized by higher odd MIF- $\Delta^{199}\text{Hg}$ values and provided new insights on the dry and wet deposition processes occurring in alpine lakes using even MIF- $\Delta^{200}\text{Hg}$ as a new paleoclimate proxy.

Overall, environmental changes in lake ecosystems, induced by either Climate Change (temperature, and light intensity) or anthropogenic pressure (lake productivity, atmospheric CO₂) are likely to produce unexpected cascading impacts among CO₂, specific PHTEs (arsenic, copper, nickel, molybdenum, cobalt, and cadmium) and Hg biogeochemical cycles in mountainous ecosystems.

Keywords:

Pyrenees; global change; alpine lakes; continental water; trace elements; metals; mercury species; sediments; mercury isotopes; acidification; inorganic carbon cycle

Laburpena

Pirinioetako goi-mendi aintzirak lurralde honetako historiaren eta paisaiaren elementu ikonikoak dira. Klima-aldaketako eta gero eta presio antropogeniko handiagoko gaur egungo testuinguruan, haien kudeaketa eta zaintza egokiak ezaugarri biogeokimikoen ezaguera sakona eskatzen du. Doktorego-Tesi hau *klima aldaketarekiko sentikorrek diren ekosistemen (aintziren, zohikaztegien) behatokiaren* izenburua duen REPLIM proiektuaren esparruan eraman da aurrera. REPLIM proiektuaren helburu nagusia Pirinioetako aintziretako eta zohikaztegiak iragana, oraina eta etorkizuna ikertzea da, aldaketa globalaren testuinguru batean. Bost laginketa-kanpaina burutu genituen 2017 eta 2019 bitartean, erdiko eta mendebaldeko Pirinioetako 20 aintziratatan baino gehiagotan. Azpi-gainazaleko uren laginketak eta analisiak parametro fisiko eta kimiko askoren zenbatekoa, distribuzio geografikoa, sakoneraren araberako soslaia eta urtaroko joera ikertzeko aukera eman ziguten, aintzira horien ur-geokimika hobeto ezaugarritzeko. Karbono dioxidoaren (CO₂-aren) zikloa eta potentzialki kaltegarriak izan daitezkeen aztarna-mailako elementuak (PHTEs delakoak) ikertu genituen espezifikoki. Arreta berezia jaso zuen merkurioak (Hg-k). Elementu honen aztarna-mailako kontzentrazioak ur naturaletan neurtzeko grafenozko nanopartikulak erabiltzen dituen prozedura analitiko berri bat garatu genuen. Halaber, espazioaren eta denboraren araberako merkurioaren prozesu biogeokimikoak hobeto ulertzen saiatzeko, elementu honen espezie kimikoen patua eta distribuzioa aztertu genituen uretan eta baita sedimentuzko zutabeetan ere.

Alkalinitate osoa (ingeleraz TA) eta disolbatutako karbono ez-organikoa (ingeleraz DIC) neurtzeko lan honetan garatutako prozedura sendoak CO₂-aren sistemaren beste bi parametroak, pH-a eta CO₂-aren iheskortasuna (ingeleraz fCO₂), determinatzea ahalbidetu digu. Aztertutako aintziren estatus azidoaren gainean eragin gehien duten parametroak arroaren ezaugarri litologikoak dira: arroka granitikoetan dauden aintzirak azidifikazio-aldaketekiko sentikorrak dira arroka sedimentarioetan kokatuta daudenak baino. Halaber, neurtutako fCO₂-aren balioak atmosferaren pCO₂-aren balioetik goitik daude, gaur egun aintzirak CO₂-aren iturri direla baieztatuz. CO₂-aren igorpen antropogenikoa, edozein kasutan, gora doa etengabe eta, ondorioz, funtsezkoa da aintzira alpinoen monitorizazioarekin jarraitzea, atmosferako gehiegizko CO₂-aren ondorioak ulertu nahi baditugu.

Aintzira alpinotako hainbat parametro fisiko kimikoren neurketak aintzirok uraren geokimikaren arabera taldekatzea ahalbidetu digu, aintziren egoera trofikoaren, hondo geologikoaren (hots, arroka granitiko vs. sedimentario) eta ekarpen atmosferikoen garrantzia azpimarratuz. PHTE delakoen agerpena, iturriak eta portaera ikertu genituen aukeratutako aintziretan, ekarpen atmosferikoaren eta geologikoaren arteko desberdintasuna garbi geratu zelarik. Lau aintziratatan egindako monitorizazio sakonaren ostean ondorioztatu genuen hainbat PHTE (arsenikoa, kobrea, nikela, molibdenoa, kobalto eta kadmioa) tenperatura eta errebox potentzial bezalako ingurumeneko aldagaien aldaketekiko oso sentikorrak direla.

Merkurio osoaren kontzentrazio naturalen monitorizazioa ur sistematan, bereziki urruneko lekuetan dauden sistematan, erronka izaten jarraitzen du eta, hortaz, kostu baxuko eta erabilerrazak diren metodo analitikoaren garapena behar-beharrezkoa izaten da. Lan honetan merkurioaren aztarna-mailako kontzentrazioa neurtzeko garatu eta optimizatu dugun metodoak erabilgarritasuna erakutsi du. Bere detekzio-muga 0.38 ng L^{-1} -koa da 200 mL lagin erabiliz, eta bere erreplikakortasuna %5 baino baxuagoa da desbiderazio estandar erlatibo terminotan.

Ur-zutabeetan lortutako merkuriozko espeziazioaren emaitzek erakutsi zuten Pirinioetako aintziren dinamika eta haien egoera pristinoa. Merkurio ez-hegazkorrari dagokionez, aztertutako aintziretan aurkitutako homogenezotasunak tokiko iturrien absentsia baieztatu zuen eta baita ekosistema hauek merkurioaren bidezko kontaminazio erregionala eta globala aztertzeko duten gaitasuna konfirmatu ere. Merkurio ez-organikoak (ingeleraz iHg(II)-k) urtaroko aldakortasunik erakutsi ez zuen bitartean, monometilmerkurioak (MMHg-k), aldiz, kontzentrazio esanguratsuki altuagoak erakutsi zituen 2018ko udazkenean, eta disolbatutako merkurio hegazkorraren (ingeleraz DGM-aren) kontzentrazioa nabarmenki aldatu zen bai aintzira bakoitzean zein aintzira desberdinen artean, hainbat laginetan orain arte inoiz neurtu ez diren kontzentrazio altuak neurtu genituelarik. Inkubazio-esperimentuek baieztatu zuten egunean zehar eta urtaroen artean gertatzen diren ingurumeneko aldaketa sakonak merkurioaren metilazioa (estratotan banatutako ur anoxikoak), MMHg-aren demetilazioa eta iHg(II)-aren fotorreduzioa (UM-ko argi indartsua) gertatzeko baldintzak faboratzen ari direla.

Sedimentuen zutabetan aurkitutako merkurio historikoaren errejistroak aldaketak erakutsi zituen merkurioaren metaketa-koefizientetan (ingeleraz, HgARs-etan), 16. mendetik eta industrializaziotik aurrera etengabeko igoera ikusi zelarik, nolabait, Espainiako hegoaldean dagoen Almadengo merkuriozko meagintzaren testigu. Zutabeetan neurtutako merkuriozko isotopo egonkorren kontzentrazioek presio antropogenikoaren garrantzia azpimarratu zuten, horren adierazle den masaren araberako frakzionazio bakoiti (ingeleraz, $\text{odd MIF-}\Delta^{199}\text{Hg}$) altuen ondorioz. Gainera, proxy paleoklimatiko bezala erabilita, masatik independentea den frakzionazio bikoitiak (ingeleraz, $\text{even MIF-}\Delta^{200}\text{Hg-ak}$), aintzira alpinotan gertatzen diren deposizio lehorreko eta umeleko prozesuak aztertzeko gako berriak eskaini zizkigun.

Laburbilduz, aintziretako ekosistematan gerta daitezkeen ingurumeneko aldaketek, bai klima-aldaketak (tenperaturak eta argiaren intentsitateak) zein presio antropogenikoak (aintziraren ekoizpenak, atmosferako CO_2 -ak) eraginda, ezusteko bata bestearen atzetiko inpaktuak sor ditzakete goimendietako CO_2 -aren, PHTE delako batzuen (arseniko, kobre, nikel, molibdeno, kobalto eta kadmioaren) eta merkuriozko ziklo biogeokimikoaren artean.

Hitz gakoak:

Pirinioak; aldaketa globala; aintzira alpinoak; barruko urak; aztarna-mailako elementuak; metalak; merkuriozko espezieak; sedimentuak; merkuriozko isotopoak; azidifikazioa; karbono ez-organikoaren zikloa

Résumé

Les lacs de haute montagne Pyrénéens sont des éléments emblématiques et historiques du paysage. Leur gestion et leur conservation, dans le contexte actuel du changement climatique et de l'augmentation de la pression anthropique, nécessite une connaissance approfondie de leur fonctionnement biogéochimique. Cette thèse a été effectuée dans le cadre du projet REPLIM (un réseau d'observatoires des écosystèmes aquatiques sensibles au changement climatique dans les Pyrénées) dont le but est d'étudier le passé, le présent et le futur des lacs et tourbières Pyrénéens dans le contexte du changement global. Cinq campagnes d'échantillonnage ont été réalisées entre 2017 et 2019 dans plus de 20 lacs alpins situés dans les Pyrénées Centrales - Occidentales. La récupération et l'analyse d'échantillons d'eau prélevés à la surface et à différentes profondeurs nous ont permis d'étudier la présence, la répartition géographique, les profils de profondeurs et les variations saisonnières d'une vaste gamme de paramètres chimiques et physiques pour mieux caractériser la géochimie de l'eau de ces lacs. Plus particulièrement, le cycle du dioxyde de carbone (CO_2) et le devenir des Eléments Traces Potentiellement Dangereux (PHTEs) ont été analysés en détail. Le mercure (Hg) a été spécialement étudié au travers du développement d'une nouvelle procédure analytique basée sur l'utilisation de nanoparticules de graphène pour la détermination de concentrations trace dans les eaux naturelles. Des recherches ont également été réalisées sur la distribution et le devenir des espèces mercurielles dans la colonne d'eau, ainsi que dans des archives de sédiments afin de mieux comprendre les processus biogéochimiques du mercure dans le temps et l'espace.

La nouvelle procédure robuste pour l'analyse de l'Alcalinité Totale (TA) et du Carbone Inorganique Dissous (DIC) développée dans ce travail nous a permis de déterminer les deux autres paramètres du système du CO_2 , le pH et la fugacité du CO_2 ($f\text{CO}_2$). Les spécificités du substrat rocheux du bassin versant apparaissent comment étant les paramètres les plus influant en ce qui concerne l'état de l'acidité des lacs étudiés : les lacs reposant sur des roches granitiques, plutôt que sur des roches sédimentaires, sont plus sensibles à l'acidification. De plus, actuellement, les valeurs de $f\text{CO}_2$ sont au-dessus du $p\text{CO}_2$ atmosphérique, ce qui signifie que les lacs sont des sources de CO_2 . Néanmoins, les émissions anthropiques de CO_2 sont en constante augmentation et, par conséquent, il est primordial de surveiller attentivement les lacs alpins afin de comprendre les effets de cet accroissement du CO_2 atmosphérique.

La mesure de plusieurs paramètres physico-chimiques dans les lacs alpins nous a permis de distinguer et classer les lacs étudiés en fonction de leur géochimie de l'eau, mettant en évidence l'importance de l'état trophique des lacs, des caractéristiques géologiques (roches granitiques vs roches sédimentaires) et des apports atmosphériques. La présence, les sources et le comportement des PHTEs dans les lacs étudiés ont été examinés, avec l'évidence d'un contraste entre les apports géologiques et atmosphériques. Le suivi intensif de quatre lacs a démontré que quelques PHTEs (arsenic, cuivre, nickel, molybdène, cobalt et cadmium) sont très sensibles aux changements environnementaux comme la température et les conditions redox.

La mesure des concentrations naturelles de mercure total dans les systèmes aquatiques, particulièrement des zones isolées, reste une tâche complexe et il est nécessaire de développer des méthodes analytiques moins coûteuses et faciles d'utilisation. La méthode pour l'analyse de concentrations traces de mercure développée et optimisée dans ce travail a été appliquée avec succès et a montré une limite de détection basse ($0,38 \text{ ng L}^{-1}$ avec 200 mL d'échantillon d'eau) et une excellente répétabilité ($\text{RSD} < 5\%$).

Les résultats de spéciation du Hg dans la colonne d'eau ont démontré l'état intact et la dynamique des lacs Pyrénéens. Dans les lacs étudiés, l'homogénéité dans les concentrations de mercure total a confirmé l'absence de sources locales et l'utilisation potentielle de ces écosystèmes en tant que sentinelles de la contamination régionale et globale du Hg. Alors que le mercure inorganique (iHg(II)) n'a pas montré de variations saisonnières, le monométhylmercure (MMHg) a été significativement plus élevé en automne 2018 et le mercure gazeux dissous (DGM) a fortement varié parmi les lacs atteignant des valeurs de concentrations jamais enregistrées jusqu'à présent pour des zones isolées dans quelques échantillons en particulier. Les expériences d'incubation ont confirmé le fait que de considérables changements environnementaux se produisant chaque jour et chaque saison dans les lacs alpins permettent des conditions qui favorisent la méthylation du Hg (eaux anoxiques stratifiées), la déméthylation du MMHg et la photo-réduction du iHg(II) (intense lumière UV).

L'enregistrement historique du Hg dans des archives de sédiments lacustres a mis en lumière les tendances temporelles des taux d'accumulation du Hg (HgARs) avec une augmentation progressive depuis le 16^{ème} siècle et l'industrialisation, reflétant la production de Hg dans les mines d'Almadén (Sud de l'Espagne). Les isotopes stables du Hg dans ces carottes ont également mis en évidence la pression anthropique caractérisée par des valeurs plus élevées de $\text{MIF}-\Delta^{199}\text{Hg}$ impair et ont apporté de nouvelles connaissances sur les processus de dépôts secs et humides ayant lieu dans les lacs alpins avec l'utilisation du $\text{MIF}-\Delta^{200}\text{Hg}$ comme nouveau proxy paléoclimatique.

Globalement, les changements environnementaux dans les écosystèmes des lacs, provoqués à la fois par le Changement Climatique (température et intensité lumineuse) et la pression anthropique (productivité du lac, CO_2 atmosphérique) sont susceptibles d'entraîner des répercussions inattendues parmi le CO_2 , certains PHTEs (arsenic, cuivre, nickel, molybdène, cobalt et cadmium) et le cycle biogéochimique du Hg dans les écosystèmes montagnards.

Mots clés:

Pyrénées ; changement global ; lacs alpins ; eau continentale ; éléments traces ; métaux ; espèces mercurielles ; sédiments ; isotopes du mercure ; acidification ; cycle du carbone inorganique

Resumen

Los lagos de alta montaña de los Pirineos son elementos icónicos del paisaje y la historia de dicho territorio. Su gestión y conservación, en el contexto actual de cambio climático y de aumento de la presión antropogénica, requiere un conocimiento detallado de los procesos biogeoquímicos. Esta tesis doctoral se ha llevado a cabo dentro del marco del proyecto REPLIM (Red de Observatorios de Ecosistemas Sensibles al Cambio Climático en el Pirineo) que tiene como objetivo investigar el pasado, presente y futuro de lagos y turberas de los Pirineos dentro de un contexto general de cambio global. Se han realizado cinco campañas de muestreo entre los años 2017 y 2019 en más de 20 lagos alpinos situados en el Pirineo Central-Occidental. La recolección y el análisis de muestras de aguas superficiales y profundas permitieron estudiar la presencia, distribución geográfica, perfiles de profundidad y tendencias estacionales de una gran variedad de parámetros químicos y físicos para caracterizar mejor la geoquímica acuática de esos lagos. Concretamente, se ha investigado en detalle la problemática de elementos traza potencialmente nocivos (PHTEs), la biogeoquímica de las especies de mercurio y el ciclo del carbono inorgánico. Además, se ha propuesto un nuevo procedimiento analítico basado en el uso de nanopartículas de grafeno que permite medir la concentración de mercurio en aguas naturales. Se realizaron investigaciones sobre la distribución y el destino de las especies de mercurio en la columna de agua, así como en los archivos de sedimentos para entender mejor los procesos biogeoquímicos del mercurio en el espacio y el tiempo.

El nuevo y sólido procedimiento para determinar la alcalinidad total (TA) y carbono inorgánico disuelto (DIC) desarrollado en este trabajo nos permitió determinar los otros dos parámetros del sistema del CO₂, el pH y la fugacidad del CO₂ (fCO₂). Las características del lecho rocoso de la cuenca parecen ser el parámetro más influyente sobre la acidez de los lagos estudiados: los lagos que se encuentran en una cuenca granítica en lugar de sobre rocas sedimentarias son más sensibles a procesos de acidificación. Además, los valores de la fCO₂ hoy en día están por encima de la pCO₂ atmosférica, lo que significa que los lagos son fuentes de CO₂. Sin embargo, las emisiones antropogénicas de CO₂ están aumentando constantemente y, por lo tanto, es crucial vigilar de cerca los lagos alpinos para comprender los efectos de un aumento progresivo de CO₂ atmosférico.

La medida de varios parámetros físicoquímicos en lagos alpinos nos ha permitido clasificar los lagos estudiados de acuerdo a la geoquímica de sus aguas, al destacar la importancia del estado trófico de los lagos, el lecho rocoso (rocas graníticas vs. sedimentarias) y las aportaciones atmosféricas. Se ha investigado la presencia, fuentes y comportamiento de los PHTEs en los lagos estudiados, evidenciando una clara diferencia entre las aportaciones geológicas y atmosféricas. La vigilancia intensiva de cuatro de los lagos reveló que algunos PHTEs (arsénico, cobre, níquel, molibdeno, cobalto y cadmio) son muy sensibles a cambios ambientales, tales como la temperatura y las condiciones redox.

La monitorización de la concentración natural de mercurio total en sistemas acuáticos, especialmente en zonas remotas, sigue siendo un reto en la actualidad y es por ello necesario desarrollar métodos analíticos de bajo costo y fácil manejo que permitan esta medida. El método de análisis de concentraciones traza de mercurio, desarrollado y optimizado durante este estudio, funcionó con éxito y presenta un límite de detección adecuado de tan sólo $0,38 \text{ ng L}^{-1}$ utilizando 200 mL de muestra de agua, así como una excelente reproducibilidad ($< 5\%$ como RSD).

Los resultados de la especiación de Hg en la columna de agua demostraron el estado prístino y permitieron el estudio de la dinámica de estas especies en los lagos pirenaicos. La homogeneidad en las concentraciones de mercurio total en los lagos estudiados confirmó la ausencia de fuentes locales y el uso potencial de estos ecosistemas como centinelas de la contaminación de Hg regional a global. Mientras que el mercurio inorgánico (iHg(II)) no mostró variaciones estacionales, el monometilmercurio (MMHg) fue significativamente más alto en el otoño de 2018 y el mercurio gaseoso disuelto (DGM) varió de forma clara dentro y entre los lagos alcanzando, en algunas muestras específicas, concentraciones nunca antes registradas en áreas prístinas. Los experimentos de incubación confirmaron que los cambios ambientales drásticos que se producen en lagos alpinos tanto a lo largo del día como entre diferentes estaciones del año están creando condiciones que pueden promover la metilación del Hg (aguas anóxicas estratificadas) y la demetilación del MMHg, así como la fotorreducción del iHg (luz ultravioleta intensa).

El registro histórico de Hg en los archivos de sedimentos puso de relieve las tendencias estacionales de los ratios de acumulación de Hg (HgAR), con un aumento progresivo a partir del siglo XVI y de la industrialización, reflejando la producción de mercurio en las minas de Hg de Almadén (sur de España). Los isótopos estables de Hg estable en estos archivos de sedimento destacan también la presión antropogénica, caracterizada por valores más altos del $\text{MIF-}\Delta^{199}\text{Hg}$, y proporcionaron nueva información sobre los procesos de deposición seca y húmeda que se producen en los lagos alpinos a través de la utilización del $\text{MIF-}\Delta^{200}\text{Hg}$ como nuevo proxy paleoclimático.

En general, los cambios ambientales en los ecosistemas lacustres, inducidos tanto por el cambio climático (temperatura e intensidad de la luz) como por la presión antropogénica (productividad de los lagos, CO_2 atmosférico) supondrán probablemente impactos inesperados y en cascada en los ciclos biogeoquímicos del CO_2 , algunos PHTEs específicos (arsénico, cobre, níquel, molibdeno, cobalto y cadmio) y el ciclo biogeoquímico del Hg en ecosistemas montañosos.

Palabras clave:

Pirineos, cambio global, lagos alpinos, aguas continentales, elementos traza, metales, especies de mercurio, sedimentos, isótopos de mercurio, acidificación, ciclo del carbono inorgánico

Table of Contents

1. Preface.....	1
1.1. REPLIM Project	2
1.2. PhD Project.....	4
2. General Introduction.....	7
2.1. Climate Change (CC)	8
2.2. Mountain Critical Zone: the case of the Pyrenees	11
2.3. High mountain lakes in the Pyrenees as witness of environmental changes	13
2.4. Potential Harmful Trace Elements (PHTEs)	16
2.5. Mercury (Hg)	18
2.6. Outline of the thesis.....	21
2.7. References.....	21
3. Sampling and analytical strategy	27
3.1. Studied areas.....	28
3.2. Sampling strategy	34
3.3. Analytical methods.....	41
3.3.1. Physicochemical parameters.....	41
3.3.2. Major anions.....	43
3.3.3. Major, trace and ultra-trace elements	45
3.3.4. Organometals (Hg species).....	51
3.3.5. Dissolved Gaseous Mercury (DGM).....	57
3.3.6. Mercury species incubations.....	60
3.3.7. Total selenium (Se)	63
3.3.8. Silicate	64
3.3.9. Total Organic Carbon (TOC).....	65
3.3.10. Carbon Dioxide (CO ₂) system parameters.....	66
3.4. References.....	72
4. Accurate determination of the total alkalinity and the CO₂ system parameters in high altitude lakes from the Western Pyrenees (France – Spain).....	75
4.1. Abstract	76
4.2. Introduction.....	77
4.3. Experimental section.....	80
4.3.1. Studied area and sampling.....	80
4.3.2. Analytical methods.....	82
4.3.3. Calculation procedures.....	82
4.4. Results and discussion.....	84
4.5. Conclusions.....	91
4.6. References.....	92
5. A simple determination of trace mercury concentrations in natural waters using Dispersive Micro-Solid Phase Extraction preconcentration based on functionalized graphene nanosheets	97
5.1. Abstract	98
5.2. Introduction.....	99
5.3. Material and methods.....	101

5.3.1.	Preparation of nanoparticles suspension.....	101
5.3.2.	Procedure for mercury preconcentration (optimum conditions).....	102
5.3.3.	Instrumentation and method for mercury analysis.....	103
5.3.4.	Calibration for mercury quantification.....	103
5.3.5.	Sampling of natural waters.....	104
5.4.	Results and discussion.....	105
5.4.1.	Optimisation of the Hg preconcentration method.....	105
5.4.2.	Optimization of the storage conditions.....	107
5.4.3.	Potential interferences: matrix effects.....	109
5.4.4.	Method blank levels and optimization.....	112
5.4.5.	Analytical performances.....	112
5.5.	References.....	115
6.	Occurrence, distribution, and characteristics concentrations of Potential Harmful Trace Elements (PHTEs) in Pyrenean lakes and their relation to aquatic biogeochemistry	121
6.1.	Abstract.....	122
6.2.	Introduction.....	123
6.3.	Subsurface lake water geochemistry.....	125
6.3.1.	Physico-chemical characteristics and PHTEs concentrations.....	125
6.3.2.	Intra-lake variability: effect of geographical position of the sampling point.....	131
6.3.3.	Intra-lake variability: effect of the sampling time within the same day.....	133
6.3.4.	Filtered vs unfiltered trace element concentrations.....	135
6.4.	Lake classification.....	137
6.4.1.	Trophic status and water quality.....	137
6.4.2.	Classification of the lakes according to the water geochemistry.....	139
6.4.3.	Characteristic concentrations and major sources of Potential Harmful Trace Elements (PHTEs)	147
6.4.4.	Water column dynamics and trace elements distribution in selected alpine lakes....	160
6.5.	References.....	166
7.	Dynamics, distribution, and transformations of mercury species from Pyrenean high-altitude lakes.....	173
7.1.	Abstract.....	174
7.2.	Introduction.....	175
7.3.	Material and methods.....	176
7.4.	Results and discussion.....	177
7.4.1.	Major biogeochemical characteristics.....	177
7.4.2.	Hg measurement outliers for total Hg and DGM.....	178
7.4.3.	Total Hg (Hg _{TOT}) in all lake waters.....	178
7.4.4.	Mercury compounds distribution in the water.....	179
7.4.5.	Mercury species transformations and volatilization in the water column of selected alpine lakes.....	191
7.5.	Implication for Hg cycling in alpine lakes.....	198
7.6.	References.....	199

8. Mercury stable isotopes in Pyrenean lacustrine archives: influence of human pollution and climate variability during the Late Holocene.....	205
8.1. Abstract	206
8.2. Introduction.....	207
8.3. Material and Methods.....	209
8.3.1. Study sites.....	209
8.3.2. Sediment sequence and age-depth models.....	210
8.3.3. Mercury concentrations and fluxes.....	210
8.3.4. Mercury stable isotopes composition	211
8.4. Results and Discussion	213
8.4.1. Variability of mercury accumulation in lacustrine sediments.....	213
8.4.2. Stable isotopes to refine mercury atmospheric sources and historical pollution in Southwestern Europe.....	216
8.4.3. Even-MIF isotope reflects mercury deposition pathways and climatic implications in the Pyrenees.....	221
8.4.4. Hg deposition in Pyrenean lakes and peatland records	225
8.5. Conclusion	227
8.6. References.....	228
General conclusions	235
Annexe 1: Major, trace and ultra-trace elements results obtained by Q-ICP-MS.....	239
Annexe 2: Major, trace and ultra-trace elements results obtained by HR-ICP-MS.....	266
Annexe 3: Organometals results (Hg and Sn)	283
Annexe 4: Results for other parameters (temperature, conductivity, redox potential, TOC, Silicate, DIC, TA, pH, fCO₂, major anions).....	299
Annexe 5: Hg isotope data (Lake Marboré and Lake Estanya)	309

List of Figures

Figure 2-1: Observations and indicators of recent Climate Change induced by human activities. (a) Globally average combined land and ocean surface temperature anomaly; (b) Globally averaged sea level change; (c) Globally averaged greenhouse gas concentrations; (d) Global anthropogenic CO ₂ emissions. <i>From Climate Change 2014 Synthesis Report of the Intergovernmental Panel on Climate Change (IPCC)</i>	10
Figure 2-2: The mountain critical zone processes together with the potential impact of Climate Change (red lightning).	11
Figure 2-3: Reconstruction of the mining-related pollution legacy in high-altitude lacustrine ecosystems (Lake Marboré) [9].	14
Figure 2-4: Typical mixing pattern for a dimictic lake.	15
Figure 2-5: Typical summer thermal stratification. Lake is separated into three separate sections I) Epilimnion II) Metalimnion and III) Hypolimnion.	15
Figure 2-6: Periodic table of the elements. Red framed elements are the PHTEs considered in this work.	16
Figure 2-7: Global Hg budget in the main environmental compartments and pathways that are of importance in the global mercury cycle. <i>Figure from UNEP 2013 [27]</i>	19
Figure 2-8: The mercury geochemical cycle. Hg is methylated in anoxic environments. The toxic methylmercury accumulates in aquatic species (bioaccumulation), and its concentrations increase with each trophic level (biomagnification), causing a threat to humans whose diets rely on fish [35].	20
Figure 3-1: Studied lakes together with geology of their catchments (adapted with permission from Zaharescu <i>et al.</i> [1]); circles show position of the lakes, and colors indicate the elevation of the corresponding lakes. Lake acronyms are detailed in Table 3-1.	32
Figure 3-2: Snow cover duration (from 1st September to 31st August) obtained from Theia Snow collection [3] according to the elevation of the studied lakes depending on the year.	33
Figure 3-3: Transport of the material.	34
Figure 3-4: Water collection using a Go-Flo sampler ((a) subsurface; (b) deep water; (c) sub-sampling.	36
Figure 3-5: Lakes from Cauterets area (Replim1): ARA (a), BAD (b), CAM (c), OPA (d), PEY (e), NER (f), POU (g) and PAR (h)	39
Figure 3-6: Lakes from Ayous area: GEN (Replim5) (a), BER (Replim3) (b) and ROU (Replim5) (c)	39
Figure 3-7: Lake Sabocos (Replim5)	40
Figure 3-8: Lakes from Panticosa area (Replim1): ARN (a), ORD (b), PAN (c), BAC (d), AZU (e), XUA (f), COA (g) and PEC (h)	40
Figure 3-9: EXO2 multiparametric probe.	43
Figure 3-10: (a) Coefficient of determination R ² and (b) the slope b associated to each linear regression between results obtained by Q-ICP-MS and results obtained by HR-ICP-MS.	49
Figure 3-11: Comparison of (a) MMHg concentrations (ng L ⁻¹) obtained in purged and unfiltered samples (last Lake Gentau depth not shown) and (b) iHg(II) concentrations (ng L ⁻¹) obtained in purged and unfiltered samples for June 2019 sampling campaign. Square blue points correspond to samples collected in not well oxygenated depths (anoxic water). Red dashed line is the linear regression using all the samples while blue dashed line included only samples from oxic water.	56
Figure 3-12: In-field purging system.	58
Figure 3-13: FIA manifold used for silicate determination	65
Figure 3-14: Equipment used for the determination of TA and DIC that includes the VINDTA 3C system coupled with a CM5015 coulometer and a 785 DMP Titrino.	67
Figure 4-1: Location of the Pyrenean lakes considered in this study.	80
Figure 4-2: Fitting between the experimental curve (black dots) and the calculated curve (red striped dots) for the titration of the lake AZU sample when TA and E ⁰ are refined.	86

Figure 4-3: Fitting between the experimental curves (black dots) and the calculated curve (red striped dots) for the titration of the lake AZU sample when a) TA, E^0 and the a_0 values in Equation 4-2 are refined, b) TA, E^0 and both the pK_a and the total concentration of the new acid-base species were refined and c) all the above mentioned parameters were simultaneously refined.	87
Figure 5-1: Transmission Electron Microscopy TEM of (a) Graphene, (b) Graphene + APDC and (c) Graphene + APDC + Hg(II).	102
Figure 5-2: Recovery ($n = 4$) of Hg (a) as a function of the volume of nanoparticles suspension and (b) as a function of the time in the ultrasonic bath. Theoretical Hg (ng) as a function of the absorbance given by AMA-254 to (c) Rank 1 and (d) Rank 2 for 20 mL and 200 mL of water sample.	106
Figure 5-3: Ratio between the recovery of Hg for the testing temperature T ($n = 3$) and the recovery of Hg for the reference temperature T_{ref}	109
Figure 5-4: Recovery of Hg (a) as a function of the concentration of natural organic matter (NOM) ($n = 4$) and (b) as a function of the concentration of sodium chloride (NaCl) ($n = 5$). Ratio ($n = 2$) between control samples (high purity water) and real samples from (c) Lake Des Carolins (freshwater) and (d) St Jean de Luz (seawater) as a function of the spiked mercury.	111
Figure 6-1: (a) Major and trace elements (median concentrations above $1 \mu\text{g L}^{-1}$) and (b) ultra-trace elements (median concentrations below $1 \mu\text{g L}^{-1}$) concentrations in unfiltered subsurface water samples of the 20 studied lakes over the four sampling campaigns. Dots are minimum and maximum, white circles are outliers and black crosses are extreme values, bars indicate 10 th and 90 th percentile, boxes indicate 25 th and 75 th , marks within each box are medians and red crosses are mean. Note that Hg corresponds to non-gaseous Hg.	130
Figure 6-2: Relative Standard Deviation (RSD) calculated for each (a) major and trace element and (b) ultra-trace element considered using the results obtained after the analysis of the three samples collected at different parts of each lake. Bars indicate 10 th and 90 th percentile, boxes indicate 25 th and 75 th marks within each box are medians and red crosses are mean. Note that Hg corresponds to non-gaseous Hg.	132
Figure 6-3: Dissolved Fraction (DF) in subsurface water samples calculated for each major, trace and ultra-trace element considered using the results obtained by ICP-MS. Dots are minimum and maximum, white circles are outliers and black crosses are extreme values, bars indicate 10 th and 90 th percentile, boxes indicate 25 th and 75 th , marks within each box are medians and red crosses are mean. For each element, the number n of samples above the LOD for both filtered and unfiltered samples are indicated. Note that Hg corresponds to non-gaseous Hg.	136
Figure 6-4: Trophic State Index (TSI) calculated for all the sampled lakes according to the sampling campaign. TSI below the dashed line (TSI = 40) indicate oligotrophic lakes. Error bars for Lakes ARA, GEN, AZU and SAB are associated to the samples from different times of the day.	138
Figure 6-5: Relation between TOC and NO_3^- with ΔTOC corresponding to the increase of TOC between spring value and autumn values, and ΔNO_3^- corresponding to the decrease of NO_3^- between spring value and autumn values.	139
Figure 6-6: Loading plots on the PC1-PC2 and PC1-PC3 planes obtained after Principal Component Analysis of the dataset.	141
Figure 6-7: Score plots on the PC1-PC2 and PC1-PC3 planes obtained after Principal Component Analysis of the dataset.	142
Figure 6-8: Ca concentrations and TA values according to the classification extracted from the PC1, importance of the weathering supplying alkalinity: Low (Lakes CAM, PEY, OPA, NER, POU, GEN, ROU, BER, ARN, BAC, PEC, COA, PAN and XUA), Medium (Lakes ARA, BAD, AZU and ORD) and High (Lake SAB).	143
Figure 6-9: Na and Cl ⁻ concentrations according to the classification extracted from the PC2, importance of the marine influence and/or eutrophication: Very weak (Lakes ARA, BAD, CAM, PEY, OPA, NER, POU, AZU, ARN, BAC, PEC, COA, XUA and SAB) and Weak (Lakes GEN, ROU, BER, PAN and ORD).	144
Figure 6-10: Negative correlation between elevation and i) Na and ii) Cl ⁻ concentrations (SAB not considered).	145

Figure 6-11: Concentrations of SO_4^{2-} as a function of Mg concentrations. Black dashed line is the new threshold proposed in this work (grey dashed line is the old one from <i>Camarero et al.</i> [10]) and set up at 0.7 mg L^{-1} to distinguish between atmospheric and geological supply of SO_4^{2-} : below this limit, SO_4^{2-} is mainly originated from atmospheric depositions. Significant correlations between SO_4^{2-} from geological supply and Mg have been found ($r = 0.98$ for Lakes AZU and ARN; $r = 0.77$ for Lakes ARA, BAD, BAC, PEC, PAN and ORD).....	146
Figure 6-12: Enrichment factors (EF) for unfiltered subsurface water samples using the upper continental crust (UCC) [54] and the Maladeta (MDT) [55] bedrock as references. Green boxes have been generated using data from low alkaline lakes (Category 1) and blue boxes have been generated using data from medium and high alkaline lakes (Categories 2 and 3). Dots are minimum and maximum, white circles are outliers and block crosses are extreme values, bars indicate 10 th and 90 th percentile, boxes indicate 25 th and 75 th , marks within each box are medians and red crosses are mean. Note that Hg corresponds to non-gaseous Hg.....	157
Figure 6-13: Depth profiles of temperature, percentage of dissolved oxygen saturation, chlorophyll-a (RFU) and the chemical parameters obtained during (a) Replim3 and (b) Replim4 in Lake Azules. .	162
Figure 6-14: Depth profiles of temperature, percentage of dissolved oxygen saturation, chlorophyll-a (RFU) and the chemical parameters obtained during (a) Replim3 and (b) Replim4 in Lake Arratille	163
Figure 6-15: Depth profiles of temperature, percentage of dissolved oxygen saturation, chlorophyll-a (RFU) and the chemical parameters obtained during (a) Replim3 and (b) Replim4 in Lake Sabocos	164
Figure 6-16: Depth profiles of temperature, percentage of dissolved oxygen saturation, chlorophyll-a (RFU) and the chemical parameters obtained during (a) Replim3 and (b) Replim4 in Lake Gentau	165
Figure 7-1: Reactivity model of Hg compounds. Solid arrows correspond to the reaction pathways that can be calculated with the incubation experiments, and dotted arrows the pathways that cannot be quantified. MMHg Loss is calculated as the sum of Oxidative and Reductive Demethylation.	177
Figure 7-2: Boxplot representations of unfiltered and filtered iHg(II), MMHg and percentage of MMHg (calculated as ratio between MMHg and non-gaseous Hg (MMHg + iHg(II))), and DGM and percentage of DGM (calculated as ratio between DGM and total Hg ($\text{Hg}_{\text{TOT}} = \text{MMHg} + \text{iHg(II)} + \text{DGM}$)) in subsurface water samples of the 19 studied lakes. Bars indicate 10 th and 90 th percentile, boxes indicate 25 th and 75 th , marks within each box are medians, and red crosses are mean.	182
Figure 7-3: Daily variation of DGM in Lakes Arratille, Gentau and Sabocos	183
Figure 7-4: Depth profiles of temperature, percentage of dissolved oxygen saturation, chlorophyll-a (RFU) and some other chemical parameters including mercury speciation obtained in (a) June 2018, (b) October 2018 and (c) June 2019 in Lake Gentau. Red dot points correspond to the LoD.	185
Figure 7-5: Depth profiles of temperature, percentage of dissolved oxygen saturation, chlorophyll-a (RFU) and some other chemical parameters including mercury speciation obtained in (a) June 2018, (b) October 2018 and (c) June 2019 in Lake Sabocos. Red dot points correspond to the LoD.....	187
Figure 7-6: Depth profiles of temperature, percentage of dissolved oxygen saturation, chlorophyll-a (RFU) and some other chemical parameters including mercury speciation obtained during (a) June 2018 and (b) October 2018 in Lake Arratille.	189
Figure 7-7: Depth profiles of temperature, percentage of dissolved oxygen saturation, chlorophyll-a (RFU) and some other chemical parameters including mercury speciation obtained during (a) June 2018 and (b) October 2018 in Lake Azul.....	190
Figure 7-8: Linear relationship between MMHg Demethylation and MMHg Loss. The two black squares, out of the trend, correspond to MMHg demethylation / MMHg loss under dark conditions in the middle depth of Lake Sabocos (June 2019).	197
Figure 7-9: Hg transformations ($\text{ng m}^{-3} \text{ day}^{-1}$) and fluxes ($\text{ng m}^{-2} \text{ day}^{-1}$) in Lake Gentau.....	198
Figure 8-1: Study sites: (a) Map of Europe (https://d-maps.com/carte.php?num_car=69122&lang=fr); (b) Average annual precipitation map of Spain (http://atlasnacional.ign.es/wane/Clima); (c) Location of Lake Marboré ($42^{\circ}41'N$; $0^{\circ}2'E$, 2612 m asl) and Lake Estanya ($42^{\circ}02'N$; $0^{\circ}32'E$, 670 m asl) (<i>Pictures by J.P. Corella</i>).	209
Figure 8-2: From top to bottom, variation over time of HgAR, $\delta^{202}\text{Hg}$, $\Delta^{199}\text{Hg}$ and $\Delta^{200}\text{Hg}$ in Lake Marboré and Lake Estanya. Each parameter is on its own y-axis while sharing the same x-axis.	215

Figure 8-3: $\delta^{202}\text{Hg}$ vs $\Delta^{199}\text{Hg}$ plot for both Lakes Marboré and Lake Estanya together with literature data: both MDF and odd-MIF increase along with contamination.	218
Figure 8-4: (a) $\Delta^{199}\text{Hg}$ vs $1/\text{HgAR}$ plot for both Lakes Marboré and Lake Estanya with strong linear relationship for lake Marboré; (b) $\delta^{202}\text{Hg}$ vs $1/\text{HgAR}$ plot for both Lakes Marboré and Lake Estanya.	219
Figure 8-5: $\Delta^{199}\text{Hg}$ vs $1/\text{Hg}$ plot for both Lake Marboré and Lake Estanya, together with other lakes [28,30] and peats [38] to highlight some strong linear relationship (dashed lines).	220
Figure 8-6: $\delta^{202}\text{Hg}$ vs $\Delta^{200}\text{Hg}$ plot for both Lake Marboré and Lake Estanya together with typical wet (cloud waters and precipitations) [37] and dry (GEM) [37,39] deposition Hg isotope signatures in the Central Pyrenees.	223
Figure 8-7: Reconstructed historical Hg wet deposition in Lake Marboré and Lake Estanya.	224
Figure 8-8: $\Delta^{199}\text{Hg}$ comparison between Lake Marboré and Peat Estibere [38].	226

List of Tables

Table 3-1: Some physical characteristics of the sampled lakes. Note that max depth was either measured or estimated from size using allometric relation, and volume of the lake was also estimated from max depth using a geometric approximation (error can be large). Pre-Devonian Granitic rocks (pDe-GR), Devonian sedimentary rocks (De-SR) include limestone, sandstone, and shale. Permo-Triassic sedimentary rocks (PT-SR) include conglomerate, sandstone, lutite and andesite. Cretaceous sedimentary rocks (Cr-SR) are mainly composed by carbonate rocks.	30
Table 3-2: Overall of the sampling strategy.	37
Table 3-3: LOD for major anions analysis.	45
Table 3-4: Operating conditions for the Q-ICP-MS and the HR-ICP-MS.	47
Table 3-5: LOD and analytical uncertainties for major and trace cations analysed by Q-ICP-MS (filtered and unfiltered) and HR-ICP-MS (unfiltered). Subscripts 1, 2, 3 and 4 stand for, respectively, Replim1, Replim2, Replim3 and Replim4.	50
Table 3-6: Operating conditions of the GC-ICP-MS.	54
Table 3-7: Operating conditions for the incubation experiments. Note that PFA Teflon bottles (Nalgene) were used to allow in-situ transmission of both UV A and B during incubation [18].	61
Table 3-8: Summary of the parameters analysed together with their associated analytical protocol. .	70
Table 4-1: Values of the $a_0 - a_5$ parameters used in the calculation of the stoichiometric constants of the carbonate system [15].	83
Table 4-2: Salinity, DIC, NPOC and silicate concentrations measured in sub-surface waters of the lakes.	84
Table 4-3: Values of the refined parameters as well as the residual sum of squares (RSS), along with their uncertainties, calculated with the help of the Microsoft Excel macro SolverAid when 1) TA and E_0 are refined, 2) TA, E_0 and the a_0 values in Equation 4-2 were refined, 3) TA, E_0 and both the pK_a and the total concentration of the new acid-base species [New-Spe] were refined and 4) when all the above mentioned parameters were refined.	88
Table 4-4: Values of all the parameters used to characterise the CO_2 system (TA, DIC, pH and fCO_2) as well as the predicted new acid-base species concentration and pK_{new} values of the studied lakes.	89
Table 5-1: Storage design for isochronous measurements to evaluate stability of the filters.	108
Table 5-2: Methods for analysis of mercury species in natural waters.	114
Table 6-1: Main chemical parameters of the studied lakes measured by the multiparametric probe (temperature, conductivity, redox potential), the TOC analyser (TOC as NPOC), Flow Injection Analysis (Silicate), the VINDTA 3C Instrument (DIC, Total Alkalinity) and the ionic chromatograph (Cl^- , NO_3^- and SO_4^{2-}). pH was calculated according to <i>Kortazar et al.</i> [41]. Chlorophyll-a is not mentioned as it was always below LOD. Dissolved oxygen, as mentioned in 3.3.1 Physicochemical parameters, was calibrated only once before each sampling campaign and the sensor is sensitive to elevation: the whole lakes were oversaturated in subsurface but the values measured differ among lakes because of elevation. All the methodological details can be found 3.Sampling and analytical strategy.	129
Table 6-2: Temperature, pH and concentrations of several elements measured in water samples collected in four selected lakes at different times of the day.	134
Table 6-3: Loadings of the variables on PC1, PC2 and PC3 after Principal Component Analysis of the dataset. Bold values are significant at 95 % confidence interval.	141
Table 6-4: Scores of the observations on PC1, PC2 and PC3 after Principal Component Analysis of the dataset, together with the proposed classification of these lakes: for PC1, Class 1 (Score < 0) / Class 2 (0 < Score < 3) and Class 3 (Score > 3); for PC2, Class 1 (Score < 0) / Class 2 (Score > 0); for PC3, Class 1 (Score < 0.5) / Class 2 (Score > 0.5).	142
Table 6-5: Characteristic concentrations for unfiltered subsurface water samples as minimum, median and maximum concentration as well as the calculated threshold for our study together with data extracted from bibliography (remote and alpine lakes) for the following PHTEs: As, U, Cu, Mo, V, Ni and Cr.	153

Table 6-6: Characteristic concentrations for unfiltered subsurface water samples as minimum, median and maximum concentration as well as the calculated threshold for our study together with data extracted from bibliography (remote and alpine lakes) for the following PHTEs: Pb, Se, Sb, Co, Cd, Tl and Hg	155
Table 6-7: Summary of the results obtained after multiple linear regression of data conducted on each PHTEs using 21 various variables (Catchment influence, Elevation, Maximum depth, Temperature, pH, Ca, Na, Mg, K, Al, Sr, Fe, Mn, Ba, Ti, Cl ⁻ , NO ₃ ⁻ , SO ₄ ²⁻ , TOC, Silicate and Total Alkalinity) according to the geological classification of the studied lakes (Low Alkaline vs Medium and High Alkaline Lakes). Significant variables with its normalized coefficient associated are shown in this table, together with the equation of the model.	158
Table 7-1: Comparison of filtered (F) and unfiltered (UF) inorganic mercury (iHg(II)), monomethylmercury (MMHg) and Dissolved Gaseous Mercury (DGM) concentrations in the subsurface water samples of the 19 studied lakes with literature data for worldwide pristine areas (oceans, boreal lakes, high altitude lakes) and local areas (freshwaters and estuary). %MMHg is calculated as the ratio between MMHg and non-gaseous Hg (MMHg + iHg). %DGM is calculated as ratio between DGM and total Hg (Hg _{TOT} = MMHg + iHg(II) + DGM). *THg, **Reactive Hg and ***Surface and Depth samples.	181
Table 7-2: Methylation (M), Demethylation (D), MMHg Loss (L), Net Methylation (NM) and Reduction (R) potentials (mean ± SD, n=3 for M, D, L and NM, n=2 for R) in unfiltered waters performed under varying light and dark conditions at different depths for Lakes Gentau, Sabocos and Arratille and for sampling campaigns June and October 2018 and June 2019, together with data from the literature. Detection limits are 0.03, 4, 4 and 1 % day ⁻¹ for Methylation, Demethylation, MMHg Loss and Reduction yields, respectively. n.d. is not determined.....	195
Table 8-1: Mean values (± 2SD) of Hg isotopic composition obtained for reference materials NIST-8610 (UM-Almadén), IAEA-405 (estuarine sediment) and NIST-1944 (marine sediment), and for triplicate Hg extraction for lakes Marboré and Estanya.....	212

1.Preface

1.1. REPLIM Project

The Pyrenean high mountain lakes and peat bogs are iconic elements of the landscape and the history of the territory. Their management and conservation, within the current context of climate change and increasing anthropogenic pressure, requires a detailed knowledge of the biotic and abiotic processes in these systems, which should include their natural variability and the synergistic effects of the anthropogenic activities on the climate change. The REPLIM project, “Network of observatories of sensitive ecosystems (lakes, wetlands) to Climate Change in the Pyrenees”, aims to establish a monitoring network in lakes and peat bogs of the Pyrenees to characterize the impact of climate change on these vulnerable mountain ecosystems, both locally and throughout the territory. The REPLIM network will also make it possible to identify the impacts that occurred before the industrial revolution and the Great Acceleration of the second half of the 20th century and quantify the most recent ones. Finally, the REPLIM project will attempt to model the effects that the projected climate change will have on these ecosystems in the near future.

REPLIM aims to contribute to the challenge of assessing the impact of climate change in the territory and the development of mitigation and adaptation policies based on scientific knowledge. To this end, REPLIM focuses on increasing the cooperation between scientists, managers, and citizens from the Pyrenean area, to establish a network of observatories of lakes and peatlands that make possible to characterize the climate change and its effects along the Pyrenees.

The main objectives of the project are to:

- Establish a monitoring network of lakes and peatlands that brings together scientists and managers specialized in climate change research in high mountain systems.
- Define the most appropriate protocols for the characterization of the impacts of Climate Change and human activities in the lakes and peat bogs of the Pyrenees.
- Prepare a report on the current situation of the lakes and peat bogs of the Pyrenees, their recent evolution, and the possible impacts of the climate change on them.
- Encourage and integrate citizen science activities into the network.

With the aims of identifying the most appropriate protocols and indicators to characterize the effects of climate change and on high mountain lakes and peat bogs in the Pyrenees, a multidisciplinary methodology will be applied to the sites of the network. It will include the:

- Installation of temperature sensors at different depths and sediment traps in lakes.
- Installation of piezometers to periodically determine the water table depth in peatlands.
- Determination of periodic output flow in peatland using permanent weirs.
- Seasonal measurements of the chemical composition and some biological properties in waters.
- Measurement of greenhouse gas fluxes in peatlands.

- Development of common procedures to be followed to carry out the samplings and subsequent analytical determination in the selected lakes and peatlands.
- Processing of the monitoring results to know the physicochemical and biological state of the selected lakes and peatlands.
- Development of participation and citizen science programs that will make the public aware of the impacts of climate change, helping to define a management strategy integrated with the social and economic development of the Pyrenean territory.
- Presentation of the results in an interactive geoportal to allow the dissemination of results to managers and citizens and facilitate the understanding of the effect of the climate change on these sensitive ecosystems.

The results of REPLIM will contribute to the development and implementation of the Pyrenean Climate Change Observatory strategy and action plan for the 2016-2019 period.

The main expected results of the project will be the:

- Establishment of a network of climate change observatories located in Pyrenean lakes and peatlands that are sustainable and lasting over time.
- Publication of a methodological manual describing the monitoring protocols in the field applicable to the requirements of the Habitats Directive (HD) and the Water Framework Directive (WFD).
- Development of computer tools for the collection, storage and management of the information generated, to assess the impacts of Climate Change on sensitive high mountain ecosystems.
- Substantial improvement of the knowledge of the status of the selected Pyrenean peat bogs and lakes, as well as their evolution in recent centuries and their status at the beginning of the 20th century, prior to global warming. Moreover, the project will give valuable information to assess the potential effect of future scenarios of climate change in lakes and peat bogs.
- Promotion of citizen participation for the collection of data in the selected ecosystems thereby increasing awareness of the problems related to climate change.

REPLIM is a cross-border network of research institutions (Spanish National Research Council, Aragon, and Catalonia; National Centre for Scientific Research, Occitanie; University of Pau and Pays de l'Adour, Nouvelle-Aquitaine; University of the Basque Country, Basque Country; University of Navarra, Navarra; Centre de Recerca Ecològica i Aplicacions Forestals, Catalonia) whose research area focus specifically on lakes and wetlands, and their relationship with Climate Change.

1.2. PhD Project

Keeping in mind that high altitude lakes are sentinels of global environmental change related to climate variability and anthropogenic pressure, this PhD project aims to evaluate how specific lake ecosystems in the Pyrenees are affected by metal and metalloid contamination and how such contamination can be constrained by climatic, hydrological, and local to long-range anthropogenic inputs.

The work presented here is the result of joined actions carried out by two of the research groups involved in the REPLIM: the IBeA (University of the Basque Country, UPV/EHU) and the IPREM (University of Pau and Pays de l'Adour, UPPA). They are complementary in the field of analytical and environmental chemistry. The knowledge and equipment provided by these two groups allow them to get precise information about trace metals and metalloids.

The Basque group (IBeA, Ikerketa eta Berrikuntza Analitikoa) led by Juan Manuel Madariaga is part of the Department of Analytical Chemistry in the University of the Basque Country (UPV/EHU). It counts with a long experience in the analysis of chemicals, both organic and inorganic, in a broad range of environmental samples, from solid (sediment, soil, particulate, vegetal and animal tissues) to liquid ones (natural and sewage water) using both direct non-destructive techniques (Raman, IR, XRF spectroscopy, LIBS) and more conventional destructive ones (GC-MS, GC-MS/MS, LC-MS/MS, ICP-MS and GC-ICP/MS). The group also addresses a deep knowledge of different statistic and chemometric techniques for multivariate data treatment and interpretation. General facilities for sample collection and treatment are hosted in its laboratories, including sediment and water samplers, passive sampling devices, freeze-driers, planetary ball mills, microwave ovens and focused ultrasound sonicators and facilities for long-term sample storage.

The IPREM (Institute of Analytical Sciences and Physico-Chemistry for Environment and Materials) aims to the development of fundamental knowledge in physico-chemistry, analytical chemistry, and microbiology, in relation to applications concerning the structure of the living, the management of the environment and the functional properties of different classes of materials. This institute organizes its research around three different poles: Analytical, Physical and Theoretical Chemistry (CAPT), Physico-chemistry of surfaces and polymer materials (PCM), and Environmental Chemistry and Microbiology (CME). This last has been pioneering the development of innovative methods of speciation analysis since now more than 2 decades to understand biogeochemical cycles and environmental impacts of trace elements and metals in the environment. Part of its work is based in laboratory experiments to better characterize the molecular forms of trace elements and metals, the mechanisms of their transformations and the relative contribution of biotic and abiotic processes. To improve the knowledge on the origin, anthropogenic contribution of chemical forms of trace metals in the environment and, study the environmental mechanisms of isotopic fractionation, analytical methods are also developed to determine the isotopic composition of trace elements and metals "at the molecular level". The CME team leans on various analytical means including several equipment of mass spectrometry for elemental (Q-ICP-MS, HR-ICP-MS), molecular (ESI Q-TOF, ESI MS/MS), speciation (GC-ICP-MS) and isotopic (MC-ICP-MS) analysis. To improve the knowledge on the contribution of chemical forms in the environment,

this team has an advanced experience in coupling gas-chromatography with MC-ICP-MS to achieve compound specific isotopic analysis (CSIA) of mercury. The group also counts with sampling devices for atmospheric, aquatic and sediment samples, clean labs sample handling and sample preparation techniques (Hotblock, Microwave, High pressure Asher).

The PhD project, conducted over four years, has resulted in five sampling campaigns conducted in 20 lakes, with more than 180 water samples collected. This cross-border collaboration brought new insights about high mountain lakes from the Pyrenees, using a physico-chemical point of view. Both laboratories were fully involved and more than 40 people participated in either the sampling campaigns or the analysis of the collected samples. Innovation and knowledge of both laboratories also lead to the creation of a new and simple methodology for the determination of trace mercury in water samples. Finally, collaboration with other cross-border partners contributes to the knowledge of the mercury biogeochemical cycle in lakes using mercury isotopic analysis in lake sediments. All this work has been presented in international conferences (Spectratom 2018 Conference, ISOBAY 18, European Winter Conference 2019, Goldschmidt Conference 2019 and ICMGP 2019) and part of this work has been already published in peer-reviewed international journals (Microchemical Journal, Science of the Total Environment Journal). The following PhD manuscript gather all the methodologies, results, and discussions about these four years work.

2. General Introduction

2.1. Climate Change (CC)

Climate Change (CC) is an evolution of the climate corresponding to a lasting change (from decades to million years) from statistical parameters of the global Earth's climate or of various regional climates. These changes can be either due to intrinsic processes to the Earth, or more recently to the human activities. Indeed, since the industrial revolution, the climate has increasingly been affected by human activities, mainly as greenhouse gas emission, which are causing global warming and climate change.

Climate Change research has taken additional relevance to the realization that human activities can accelerate Climate Changes. Indeed, warming of the climate is unequivocal, and since the 1950s, many of the observed changes are unprecedented over decades to millennia. The atmosphere and ocean have warmed, the sea level has risen, and the greenhouse gas concentrations have increased (**Figure 2-1**). Other direct and/or indirect changes in the global or regional climate parameters have been observed. Regions of high salinity, where evaporation dominates, have become more saline, while regions of low salinity, where precipitation dominates, have become fresher since the 1950s. Uptake of carbon dioxide (CO₂) by the ocean is also responsible for ocean acidification. Indeed, around 30 % of CO₂ emitted is absorbed by the oceans, lowering its concentration in the atmosphere but making the oceans more acidic: the pH of ocean surface water has decreased by 0.1, corresponding to a 26 % increase in acidity [1]. Worldwide, snow cover decreases under the global warming, highlighted by the melting of the permafrost, of the Arctic sea-ice extent, the glacial retreat.

The primary cause of this global change is the increasing atmospheric concentrations of greenhouse gases, occurring mainly since the pre-industrial era. This has led to atmospheric concentrations of carbon dioxide, methane and nitrous oxide that are unprecedented for at least the last 800,000 years. CO₂ is the primary greenhouse gas. It enters the atmosphere through burning fossil fuels (coal, natural gas, and oil), solid waste, trees, and other biological materials, and because of certain chemical reactions (e.g., manufacture of cement). CO₂ is removed from the atmosphere (or "sequestered") when plants absorb it as part of the biological carbon cycle. Apart from forest, oceans [1], wetlands [2] are also known as sinks of CO₂ and participate actively in the cycle of this important greenhouse gas. The case of lakes is more complex but inland lakes emit CO₂ to the atmosphere [3]. Nevertheless, their low buffer capacity, in particular in high-altitude and remote lakes, threatens this equilibrium between surface lake water and atmosphere. See **4 Accurate determination of the total alkalinity and the CO₂ system parameters in high altitude lakes from the Western Pyrenees (France – Spain)** introduction.

In recent decades, changes in climate have caused impacts on natural and human systems on all continents and across the oceans. Impacts are due to observed climate change, irrespective of its cause, indicating the sensitivity of natural and human systems to changing climate. The World Health Organization (WHO) estimates that the warming and precipitation trends due to anthropogenic Climate Change in the past 30 years has already caused the death of over 150,000 humans every year. Many prevalent human diseases are linked to climate fluctuations, from cardiovascular mortality and respiratory illnesses due to heatwaves, to altered transmission of infectious diseases and malnutrition

from crop failures. A recent study reviewed data to bring to the fore the relationship between Climate Change and health concerns in many regions of the world. The most vulnerable regions to Climate Change are the temperate latitudes, where the increase in temperature will be the most important, the regions around the Pacific and Indian oceans, where the rainfall variability is expected to be larger, and the cities where the urban heat island (an urban area that is significantly warmer than its surrounding rural areas due to human activities) is important [4].

Continued emission of greenhouse gases will cause further warming and long-lasting changes in all components of the climate system, increasing the likelihood of severe, pervasive and irreversible impacts for people and ecosystems. Limiting climate change would require substantial and sustained reductions in greenhouse gas emissions, which, together with adaptation, can limit climate change risks.

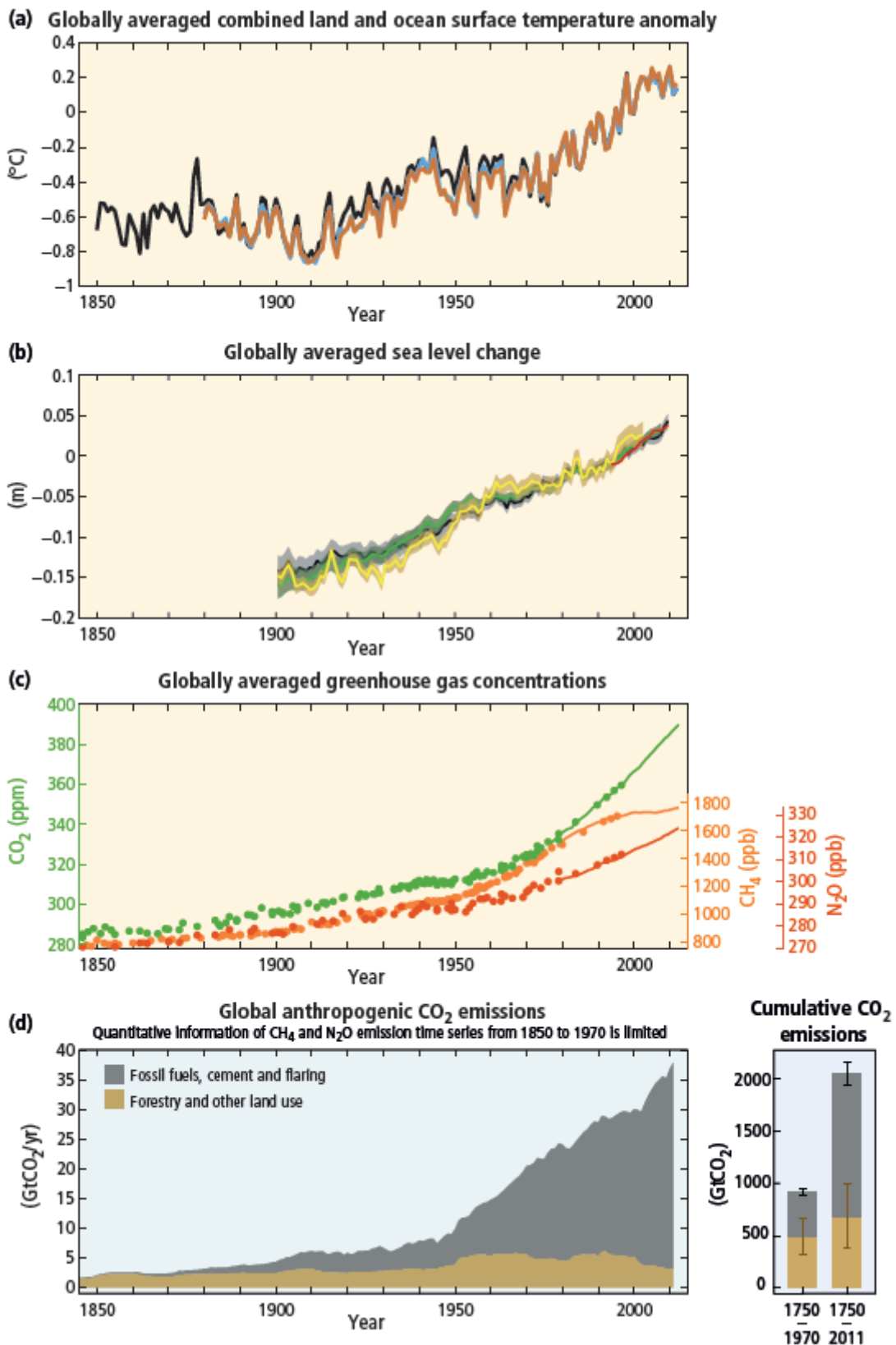


Figure 2-1: Observations and indicators of recent Climate Change induced by human activities. (a) Globally average combined land and ocean surface temperature anomaly; (b) Globally averaged sea level change; (c) Globally averaged greenhouse gas concentrations; (d) Global anthropogenic CO_2 emissions. From *Climate Change 2014 Synthesis Report of the Intergovernmental Panel on Climate Change (IPCC)*.

2.2. Mountain Critical Zone: the case of the Pyrenees

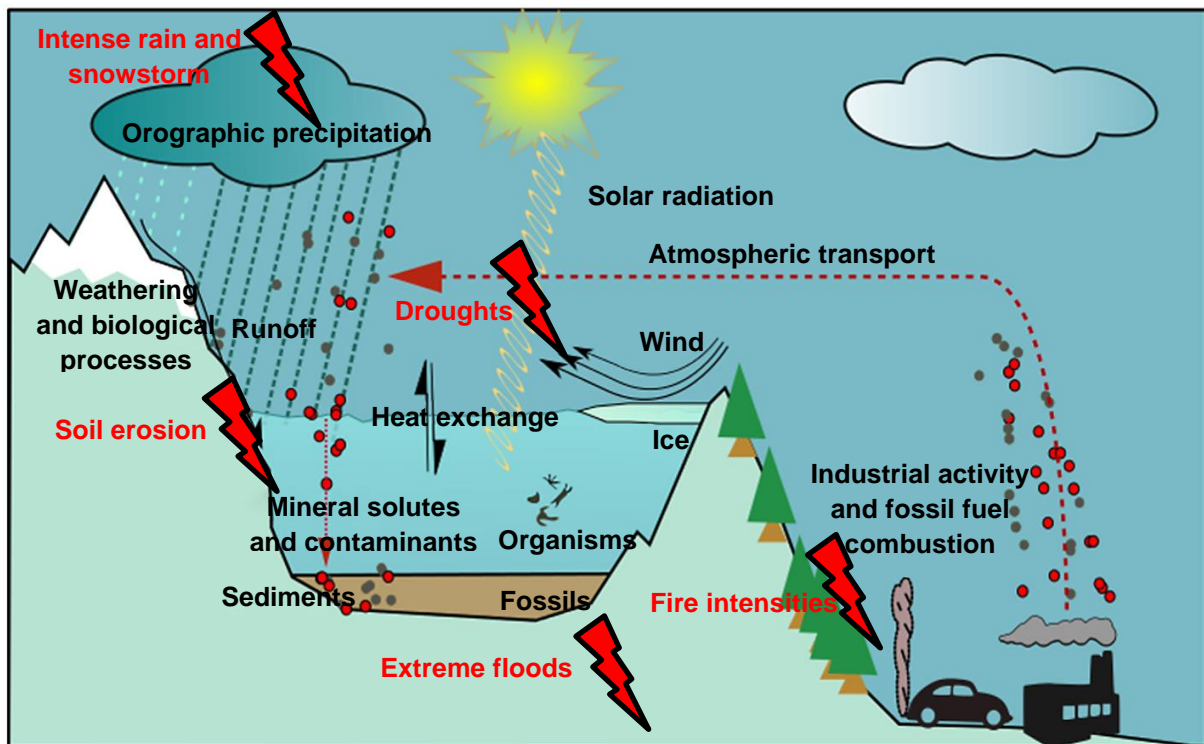


Figure 2-2: The mountain critical zone processes together with the potential impact of Climate Change (red lightning).

High mountain areas are of particular importance in terms of cultural heritage but also in terms of economic issues. Indeed, preservation of the biodiversity of these remote areas is a key point in the development of leisure activities as tourism or mountain sports. Then, the primary importance of these ecosystems has encouraged authorities to take decision by the creation of protected areas. Nevertheless, high mountain areas are unstable and affected by Global Change induced by human activities at both local and global scale.

According to *Brantley et al.* [5]: "All life on Earth is supported by the fragile skin of the planet defined from the outer extent of vegetation down to the lower limits of groundwater". *Le Roux et al.* [6] defined the specificities of the mountain as a particular Critical Zone (**Figure 2-2**). Main specificity concerns the high topographic variability, with large slopes increasing the risk of extreme hydrogeochemical events. Orographic precipitation, produced when moist air is lifted as it moves over a mountain range, leads to higher atmospheric depositions than expected. High complexity of the geology in the mountain, such as the presence of young and easily erodible soils, explains potential microscale natural sources of organic matter and specific chemical elements. Weathering and biological processes are also influenced by the high seasonality occurring in the mountain environment (snow deposition, snowmelt, heavy storm rains, and spring floods) and intense solar radiation. Vegetation, forests, and flora are also strongly dependent on the altitude in the Mountain Critical Zone.

These ecosystems are extremely sensitive to environmental change zones: they are anthropogenically limited (low direct impacts), with a short growing season (due to long winter) and low warmth. The eventual vulnerability of an ecosystem to some perturbation depends on both the degree of exposure, and the sensitivity to it [7]. Thus, Climate Change may strongly affect the Mountain Critical Zone processes with an increase in rain and snowstorm, in droughts, in soil erosion, in extreme floods, and in fire intensities.

The most noticeable consequences of Climate Change on the Mountain Critical Zone are about the increase in the temperature (+1.2 °C average temperatures rise from 1949 to 2010 in the Pyrenees), the decrease in the precipitations (-2.5 % per decade over the last 50 years in the Pyrenees) and the decrease of the snow cover (*OPCC1 project* [8]).

Indirect consequences of the Climate Change in the Pyrenees are also numerous. The winter tourism is the main source of income and the driving force of local development in many areas of the Pyrenees. However, in recent years, this sector of the tourism industry has been identified as being extremely vulnerable to the effects of Climate Change. Indeed, the increase in average of maximum and minimum winter temperatures recording during the last century led to a decrease of the number of days with enough snow accumulation for the practice of the various types of alpine skiing. Moreover, the snow line has been in higher altitude in the recent years. Both processes also delayed the season start date leading to economic implications. To reduce the impact of the lack of snow, ski resorts are forced to use artificial snow, which has impacts not only in terms of economy but also in terms of environmental issues. Another possible impact of Climate Change on tourism may be linked to landscape changes such as degradation of iconic features of the alpine landscape (peatbogs, lakes, and glaciers), the reduction and/or changes in the biodiversity. The most iconic change is the unprecedented retreat of the Pyrenean glaciers which survival is compromised beyond a few decades [9]. The extreme weather events, induced by Climate Change, may also affect not only the biodiversity of the mountain zone, but also the infrastructures directly and indirectly related to tourism in the Pyrenees (refuges, telecommunication networks, mountain roads etc ...). Finally, in the tourism sector, Climate Change could also have positive impact with the increase of average temperature in spring and autumn, lengthening the summer tourism season.

Agriculture and livestock, like tourism, are key factors in terms of economy regarding the Pyrenees. Nevertheless, the increase in the concentration of atmospheric CO₂, the consequent increase in air temperature, as well as changes in seasonal precipitation patterns and the greater frequency and intensity of extreme climate events will affect agriculture (less productivity of crop), pastures (less productivity of pastures) and the livestock (thermal stress and risk of spreading of disease) sector in the Pyrenees.

Energy production might be affected by Climate Change, negatively but also positively. Indeed, on the one hand, the decrease in precipitations together with the increase in drought events affects the accumulation capacity of the reservoirs used to produce hydroelectricity. Wind power production might be also affected as wind speed is decreasing because of Climate Change. On another hand, the

increase of the solar radiation index throughout the Pyrenees Mountain range could favoured the solar power production.

Flora and fauna in the Pyrenees are also unique and take part of the cultural heritage. Yet, Climate Change that induces a change in the distribution and diversity of high mountain species affects them.

2.3. High mountain lakes in the Pyrenees as witness of environmental changes

High mountain lakes (i.e., those located above the local tree line) are iconic elements of the Pyrenean landscape and constitute a good candidate to evaluate the impact of Climate Change all along the mountain range. Indeed, their physical, chemical, and biological properties respond rapidly to climate-related changes, and they are sensitive to even small inputs from diffusive or background atmospheric pollution. However, long-term instrumental records of meteorological parameters (temperature, sea levels etc ...) are scarce. To fill this gap, numerous proxies (ice cores, tree rings, pollen etc ...) have been used to reconstruct past climatic fluctuations. As an example, a short sediment core from the small and karstic Lake Estanya (Pyrenees, Spain) provides a detailed record of the complex environmental, hydrological, and anthropogenic interactions occurring since medieval times (around 800 years) [10].

Most of the existing alpine lakes originated during the last glaciation due to the action of ice upon the bedrocks: alpine lakes are young ecosystems. Alpine lakes are among the ecosystems with larger similarities throughout the planet. In the Pyrenees, there are about 1000 alpine lakes (> 0.5 ha surface area), located mostly between 2000 and 2500m asl. Considering maximum depth, lakes can be divided into two different categories that will further influence their dynamic: shallow lakes (maximum depth bellow 10-15 m) and deep lakes (maximum depth above 15 m). Depositional dynamic of lakes originating from glacial-related processes are strongly influenced by cryosphere processes in the watersheds (snow accumulation and melting, ice-cover, precipitations). These high altitude ecosystems are characterized by high solar insolation and UV radiation, low temperatures and long ice-cover periods, and very pure waters.

Alpine lakes are characterized by catchment-to-lake-surface-area ratio usually low, as the catchment surface is commonly smaller than lowland lakes. Therefore, atmospheric deposition and catchment weathering are important processes influencing greatly the lake water geochemistry [11]. Thus, mountain lake catchments are viewed and used as excellent proxies of background diffuse contamination. Indeed, high altitude lakes accumulate in their sediments organic and inorganic contaminants. As an example, *Corella et al.* [12] reconstructed the timing and magnitude of trace metal pollutants fluxes over the last 3000 years in the Central Pyrenees by analysing some potential harmful trace elements (Pb, Hg, Zn, As and Cu) in sediment cores retrieved from lake Marboré (2612m asl.) **(Figure 2-3).**

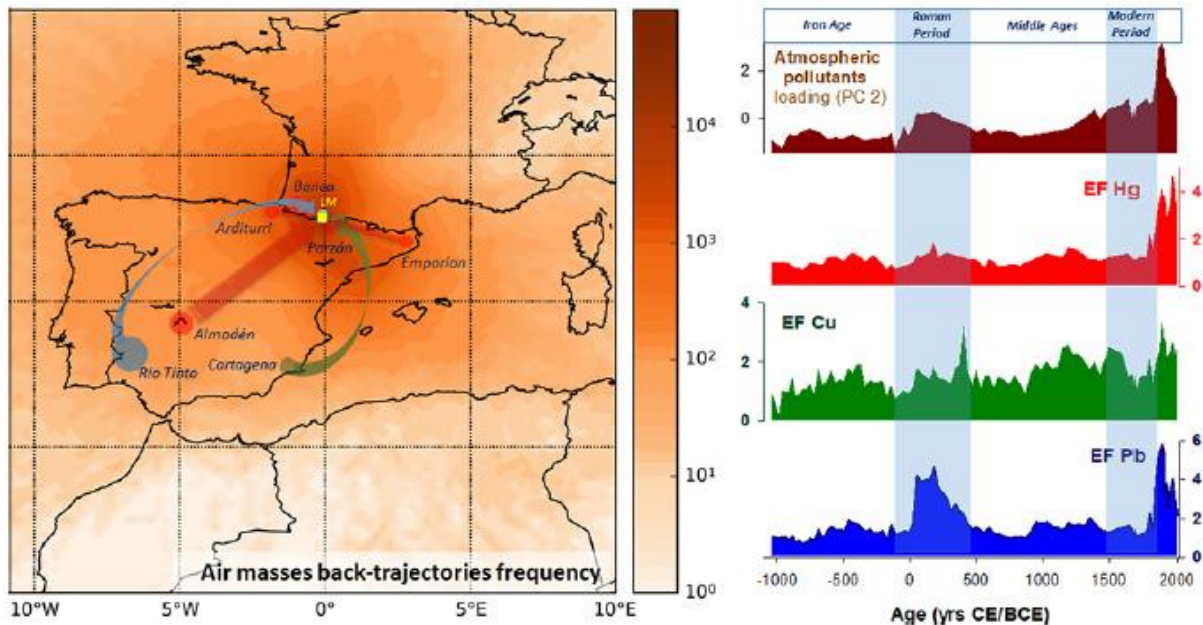


Figure 2-3: Reconstruction of the mining-related pollution legacy in high-altitude lacustrine ecosystems (Lake Marboré) [9].

High mountain lakes in the Pyrenees are pristine areas as indicated by their trophic status. According to the total phosphorus (TP) concentration measured on a survey performed along the Pyrenees in summer year 2000, more than 70 % of the lakes could be classified as ultraoligotrophic ($TP < 4.7 \mu\text{g L}^{-1}$), 22 % as oligotrophic ($4.7 < TP < 9.3 \mu\text{g L}^{-1}$) and 6 % as mesotrophic ($9.3 < TP < 31 \mu\text{g L}^{-1}$) [13]. During the ice-free season, light penetrates until the bottom in more than 75 % of the lakes, so autotrophic biota may develop. UV radiation in these ecosystems can be quite high and may have a direct consequence on the development of microorganisms.

Annual hydrological cycle in lakes is characterized by a large seasonal variability depending on water availability, thermal regime and length of the ice-covered period. Water stratification is an important phenomenon regarding the dynamics of lakes. It occurs when water masses with different properties – salinity (halocline), oxygenation (chemocline), density (pycnocline), temperature (thermocline) – form layers that act as barriers to water mixing which could lead to anoxia or euxinia. These layers are normally arranged according to density, with the less dense water masses sitting above the denser layers. Water stratification also creates barriers to nutrient mixing between layers. This can affect the primary production in an area by limiting photosynthetic processes. When nutrients from the benthos cannot travel up into the photic zone, phytoplankton may be limited by nutrient availability. Lower primary production also leads to lower net productivity waters. The most known and studied stratification is the thermal one and concern changes in the temperature profile with depth within a lake system. Different types of lakes exist according to their physical cycle but most of them are holomictic lakes that means they have a uniform temperature and density from top to bottom at a specific time during the year. Polymictic lakes are holomictic lakes that are too shallow to develop thermal stratification, thus their

waters can mix from top to bottom throughout the ice-free period. Dimictic lakes mix from the surface to bottom twice each year (**Figure 2-4**) during spring and fall overturn, and present a summer stratification with warmer surface layers and an inverse winter stratification with colder surface layers. During summer stratification, three distinct sections compose the lake water column: the epilimnion (warmer and more oxygenated top layer), the metalimnion (thermal layer, thermocline) and the hypolimnion (colder and less oxygenated bottom layer) (**Figure 2-5**). Monomictic are lakes where the mixing occurs only once per year.

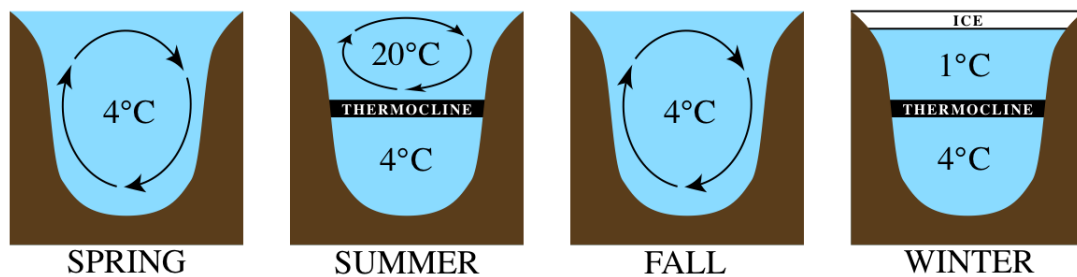


Figure 2-4: Typical mixing pattern for a dimictic lake.

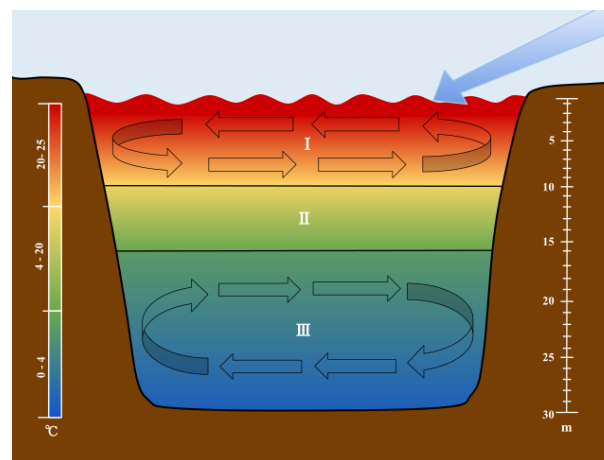


Figure 2-5: Typical summer thermal stratification. Lake is separated into three separate sections I) Epilimnion II) Metalimnion and III) Hypolimnion.

Biological cycles follow the same seasonal patterns with phases of variable productivity in phytoplankton communities. Study of Lake Redó [14], a dimictic oligotrophic mountain lake located in the Pyrenees, emphasize four various main production episodes, in relation to the physical functioning of the lake. Indeed, highest chlorophyll-a concentrations, an indicator of the biological productivity, have been measured during spring overturn, in the hypolimnion during summer stratification, during autumn overturn, and under the ice at the beginning of the ice-covered period.

2.4. Potential Harmful Trace Elements (PHTEs)

Potentially Harmful Trace Elements (PHTEs), or more generally trace elements, are among the most effective environmental contaminants, and their release into the environment is increasing since the last decades. Through many processes and pathways, PHTEs may enter the different environmental compartments [15]. Considering the contributions of soil erosion and eolian dust, *Sen and Peucker-Ehrenbrink* [16] examined the influence of human activities on 77 elements, and it has been found that 62 of them surpass their corresponding natural fluxes. Many of these elements are considered to be PHTEs and the following ones will be studied in this work (**Figure 2-6**): Arsenic (As), Uranium (U), Copper (Cu), Molybdenum (Mo), Vanadium (V), Nickel (Ni), Chromium (Cr), Lead (Pb), Selenium (Se), Antimony (Sb), Cobalt (Co), Cadmium (Cd), Thallium (Tl), Zinc (Zn), Silver (Ag), Titanium (Ti), Tin (Sn) and Mercury (Hg).

1 IA																	18 VIIIA	
1 H Hydrogen 1.008	2 IIA												13 IIIA	14 IVA	15 VA	16 VIA	17 VIIA	2 He Helium 4.002602
3 Li Lithium 6.94	4 Be Beryllium 9.0121831											5 B Boron 10.81	6 C Carbon 12.011	7 N Nitrogen 14.007	8 O Oxygen 15.999	9 F Fluorine 18.99840323	10 Ne Neon 20.1797	
11 Na Sodium 22.98976928	12 Mg Magnesium 24.305											13 Al Aluminium 26.9815385	14 Si Silicon 28.086	15 P Phosphorus 30.973761998	16 S Sulfur 32.06	17 Cl Chlorine 35.45	18 Ar Argon 39.948	
19 K Potassium 39.0983	20 Ca Calcium 40.078	21 Sc Scandium 44.955908	22 Ti Titanium 47.88	23 V Vanadium 50.9415	24 Cr Chromium 51.9961	25 Mn Manganese 54.938044	26 Fe Iron 55.845	27 Co Cobalt 58.933194	28 Ni Nickel 58.6934	29 Cu Copper 63.546	30 Zn Zinc 65.38	31 Ga Gallium 69.723	32 Ge Germanium 72.630	33 As Arsenic 74.9216	34 Se Selenium 78.96	35 Br Bromine 79.904	36 Kr Krypton 83.796	
37 Rb Rubidium 85.4678	38 Sr Strontium 87.62	39 Y Yttrium 88.90584	40 Zr Zirconium 91.224	41 Nb Niobium 92.90638	42 Mo Molybdenum 95.94	43 Tc Technetium (98)	44 Ru Ruthenium 101.07	45 Rh Rhodium 102.90550	46 Pd Palladium 106.42	47 Ag Silver 107.8682	48 Cd Cadmium 112.411	49 In Indium 114.818	50 Sn Tin 118.710	51 Sb Antimony 121.757	52 Te Tellurium 127.60	53 I Iodine 126.90447	54 Xe Xenon 131.29	
55 Cs Caesium 132.90545196	56 Ba Barium 137.327	57 - 71 Lanthanoids	72 Hf Hafnium 178.49	73 Ta Tantalum 180.94788	74 W Tungsten 183.84	75 Re Rhenium 186.207	76 Os Osmium 190.23	77 Ir Iridium 192.222	78 Pt Platinum 195.084	79 Au Gold 196.966569	80 Hg Mercury 200.59	81 Tl Thallium 204.38	82 Pb Lead 207.2	83 Bi Bismuth 208.98040	84 Po Polonium (209)	85 At Astatine (210)	86 Rn Radon (222)	
87 Fr Francium (223)	88 Ra Radium (226)	89 - 103 Actinoids	104 Rf Rutherfordium (261)	105 Db Dubnium (262)	106 Sg Seaborgium (266)	107 Bh Bohrium (264)	108 Hs Hassium (265)	109 Mt Meitnerium (268)	110 Ds Darmstadtium (271)	111 Rg Roentgenium (272)	112 Cn Copernicium (285)	113 Nh Nihonium (286)	114 Fl Flerovium (289)	115 Mc Moscovium (288)	116 Lv Livermorium (293)	117 Ts Tennessine (294)	118 Og Oganesson (294)	
57 La Lanthanum 138.90547	58 Ce Cerium 140.12	59 Pr Praseodymium 140.90766	60 Nd Neodymium 144.242	61 Pm Promethium (145)	62 Sm Samarium 150.36	63 Eu Europium 151.964	64 Gd Gadolinium 157.25	65 Tb Terbium 158.92535	66 Dy Dysprosium 162.500	67 Ho Holmium 164.93033	68 Er Erbium 167.259	69 Tm Thulium 168.93422	70 Yb Ytterbium 173.045	71 Lu Lutetium 174.967				
89 Ac Actinium (227)	90 Th Thorium 232.0377	91 Pa Protactinium 231.03688	92 U Uranium 238.02891	93 Np Neptunium (237)	94 Pu Plutonium (244)	95 Am Americium (243)	96 Cm Curium (247)	97 Bk Berkelium (247)	98 Cf Californium (251)	99 Es Einsteinium (252)	100 Fm Fermium (257)	101 Md Mendelevium (258)	102 No Nobelium (259)	103 Lr Lawrencium (260)				

Figure 2-6: Periodic table of the elements. Red framed elements are the PHTEs considered in this work.

Even if PHTEs constitute less than 0.1 % of the Earth's crust [17], several studies have shown that the contamination by PHTEs is widespread: they can be found in remote areas that are far from contamination sources. Indeed, atmospheric deposition is the main phenomenon controlling Hg, Zn and Pb concentration in the terrestrial compartment of the Svalbard archipelago in the Arctic Ocean [18]. Lichens, used as a good proxy for the assessment of local to long-range atmospheric transport [19], have been collected in James Ross Island, at the north-east of the Antarctica Peninsula, and elemental analysis have been conducted: long-distance transport of some PHTEs such as Co, Hg, Se and As has been demonstrated [20]. The presence of various PHTEs (Pb, Hg, Ag, As, Bi, Cd, Co, Cr, Cs, Cu, Mo, Ni, Sb, Sn, Tl, U, Zn) in ice cores from Polar Regions and high altitude glaciers, evaluated over the past few centuries, suggests that today there are no glaciers on Earth where atmospheric depositions of

anthropogenic origin cannot be detected [21]. The occurrence and distribution of PHTEs is worldwide and thus mountain areas are not an exception [12].

PHTEs are naturally present at low concentrations in rocks and bedrocks, and because of physical and chemical weathering, they are thus also naturally present in soil and surface waters. Various natural processes therefore enable their dispersal throughout the environment [22]. According to *Le Roux et al.* [6], the following sources can be distinguished:

- Terrigenous or lithogenic sources: dispersal from **wind erosion of rocks and soils** (i.e., >20 % of natural derived Cu, Ni, Pb, Sb and Zn in the environment).
- Volcanic sources: dispersal through **volcanic activities** (i.e., ~ 20 % of As, Cd, Cr, Cu, Hg, Ni, Pb and Sb) up to the stratosphere.
- Sea spray: dispersal through suspending **marine water droplets** (i.e., ~ 10 % of total PHTEs emissions).
- Biogenic sources: **biomass fires** driven either by natural or anthropogenic processes.

Anthropogenic sources of PHTEs are mainly due to high-temperature combustion activities resulting in volatilization of trace elements or their release in the form of very fine aerosols (<μm). In the case of erosion or dust emission, without any underlying high-temperature process, emissions tend to be much more localized (i.e., mining activities). According to *Le Roux et al.* [6], the following activities are important sources of PHTEs:

- Energy production by **combustion** (wood, coal, and oil): the dominating anthropogenic source of PHTEs emission (As, Cd, Cu, Hg, Ni, Pb, Sb, Se, V, and Zn).
- **Metallurgical** industry: emission of dust near the extraction and point of exploitation, high-temperature processing of ores emits aerosols rich in trace elements (Cd, Cu, Ni, Pb, V, and Zn).
- Other **industrial processes**: high-temperature processing and manufacturing (As, Cr, Cu, Ni, Pb, and Zn).
- **Transport**: road traffic (Cd, Cu, Fe, Ni, Pb, and Zn), erosion of brake pads (Cu, and Sb), erosion of train rails (Cu).
- **Waste treatment**: incineration of household waste (As, Cr, Cu, Ni, Pb, Sb, Se, V, and Zn).
- **Livestock** and, especially, **agricultural activities**: perturbation of natural soil cycle leading to release of PHTEs.

More information on PHTEs are gathered in introduction of **6 Occurrence, distribution, and characteristics concentrations of Potential Harmful Trace Elements (PHTEs) in Pyrenean lakes and their relation to aquatic** biogeochemistry.

The responsibility of humans regarding the dispersion of aerosols and PHTEs by anthropogenic activities is undeniable, but it is important to consider the intensification of natural processes in the

biogeochemical cycle of PHTEs. On one-part, human activities are modifying the natural atmospheric transport of substances in a direct way: agricultural practices and deforestation may enhance production of dust and Aeolian transport from land; changes in the wildfires regime affect the emission of ashes and gases from burning biomass. On another part, Climate Change also accelerates many of these processes: droughts and losses of snow cover that enhance dust production, melting of organic permafrost that increases CO₂ and methane emissions from soil, changes in the prevailing winds and patterns of circulation of air masses that carry airborne substances.

2.5. Mercury (Hg)

Mercury is a chemical element taking part of the PHTEs. The symbol of mercury, Hg, is coming from the Latin, itself derived from the Greek *hydrargyrum* that means silver water. Hg atomic number is 80 and its average atomic mass is 200.59 g mol⁻¹. Hg has a low melting point ($T_{\text{melting}} = 38.84 \text{ }^{\circ}\text{C}$), therefore it appears under its liquid form at normal conditions of temperature and pressure. Moreover, mercury is highly volatile because of its relatively high vapour pressure (0.180 Pa à 293 K). Mercury has seven various stable isotopes (*abundances in SRM 3133 NIST*): ¹⁹⁶Hg (0.155 %), ¹⁹⁸Hg (10.04 %), ¹⁹⁹Hg (16.94 %), ²⁰⁰Hg (23.14 %), ²⁰¹Hg (13.17 %), ²⁰²Hg (29.73 %) and ²⁰⁴Hg (6.83 %) [23]. Regarding its electronic structure ([Xe] 4f¹⁴ 5d¹⁰ 6s²), mercury is classified as a transition metal IIB presenting an unsaturated “d” layer hence it is easily polarizable. The global annual mean lifetime of Hg(0) against the net photochemical oxidation is estimated to be about 1 year [24], and recent findings on the rapid photochemistry of oxidized mercury have postulated that global atmospheric Hg lifetime could increase by a factor of 2 [25,26]. Therefore, mercury is a ubiquitous element and can appear in all environmental compartments (atmosphere, soils and sediments, and aquatic environment) under different chemical forms: elemental mercury (Hg(0)), divalent inorganic form (iHg(II) or Hg²⁺ or Hg(II)), and organic forms including monomethylmercury (MMHg), dimethylmercury (DMHg) and ethylmercury (C₂H₅Hg). It is possible to define three various steps regulating the biogeochemical cycle of Hg:

- Emission from natural and/or anthropogenic sources or reemission.
- Transport and deposition in aquatic and terrestrial environments.
- Chemical transformations and accumulation in living organisms.

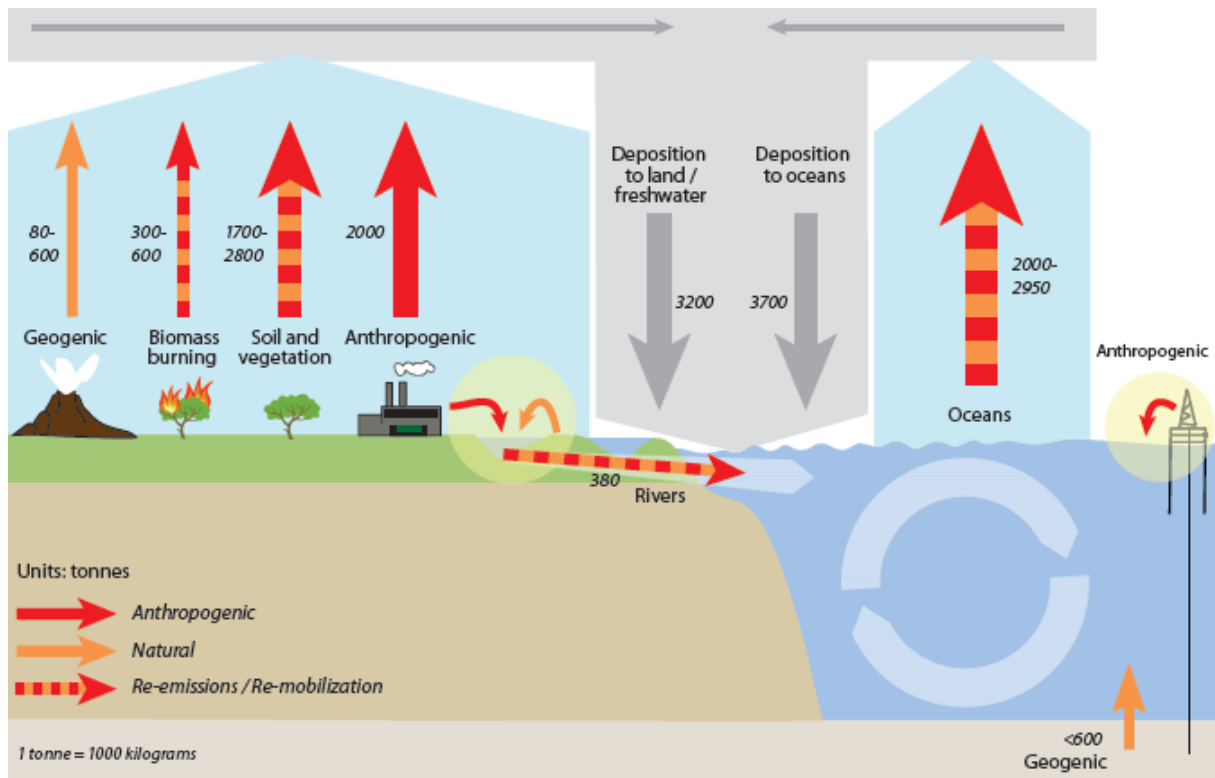


Figure 2-7: Global Hg budget in the main environmental compartments and pathways that are of importance in the global mercury cycle. *Figure from UNEP 2013 [27].*

Sources of Hg (**Figure 2-7**) [27] can be either from natural or anthropogenic origins.

Natural sources of Hg are geogenic and consist in the direct release of Hg present at trace levels in the earth's crust (between 21 and 56 $\mu\text{g kg}^{-1}$ [28], mainly as cinnabar HgS). Thus, natural erosion (water, wind) of these ores in rocks and soils [29], natural fires and volcanic degassing [30], and hydrothermal activities [31] allow Hg to enter the different environmental compartments. These natural sources of Hg account for about 10 % of the 5500-8900 tons of Hg emitted and re-emitted in the atmosphere every year [27].

But nowadays, anthropogenic emissions are about three times higher than the natural ones [27,32,33]. It is important to distinguish between the "unintentional" (or "by-product") discharge of mercury (coal burning, mining, industrial activities that process ores to produce various metals or process other raw materials to produce cement) from the intentional discharge of mercury. In the latest, artisanal and small-scale gold mining is the largest of these: gold is extracted from rocks, soils and sediments by amalgamation with Hg.

Finally, re-emission of mercury account for about 60 % of emitted and re-emitted Hg in the atmosphere [27]. Indeed, Hg derived from atmospheric emissions (natural or anthropogenic) is deposited in terrestrial and aquatic compartments (soils, surface waters, plants), thus can be re-emitted into the air. This re-emission is the result of natural processes that transform organic and inorganic mercury forms into elemental Hg, which is volatile [34].

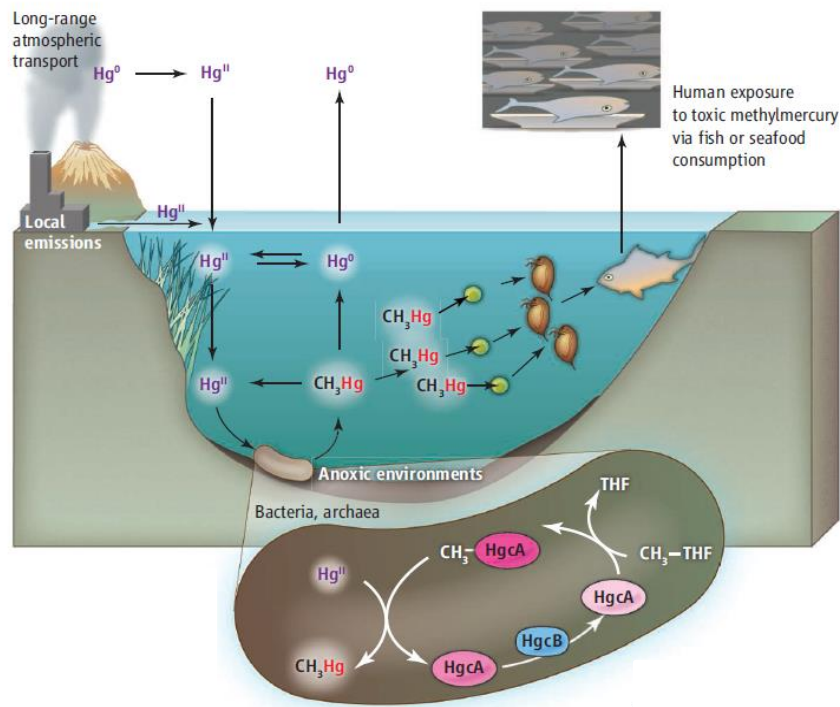


Figure 2-8: The mercury geochemical cycle. Hg is methylated in anoxic environments. The toxic methylmercury accumulates in aquatic species (bioaccumulation), and its concentrations increase with each trophic level (biomagnification), causing a threat to humans whose diets rely on fish [35].

In aquatic environment (**Figure 2-8**), presence of Hg may represent an important source of pollution for the atmosphere (volatilization of Hg (0)), for the sediments (iHg(II)) as well as for the food web (accumulation of MMHg). Therefore, it is important to understand better the biogeochemical cycle of mercury in the aquatic compartment. Hg can reach this compartment by many ways. First, in the atmosphere, more than 95 % of the Hg is under elemental form Hg(0) [36]. Thus, as mentioned previously, Hg(0) lifetime is important in the atmosphere but once it is oxidized, Hg becomes reactive and can be rapidly deposit at the surface of oceans. This atmospheric deposition, either by dry or wet processes is also important in lakes with large surface area-to-volume ratios and small catchment-to-lake surface areas [33].

The various Hg forms are subject to numerous reactions in the aquatic compartment (redox reactions, methylation/demethylation, and photochemical reactions) (**Figure 2-8**). First, volatilization of Hg(0) into the atmosphere is mainly occurring while iHg(II) is transferred from water to sediments and vice-versa through sedimentation and remobilization phenomena. In deepest water, biological activity (bacteria, phytoplankton) is responsible of numerous reactions involving mercury, while at the surface water, abiotic reactions (photoreduction, photodemethylation) are mainly occurring [37,38]. Methylmercury (MeHg) production is a critical process that occurs within aquatic ecosystems. The largest source of MeHg to freshwater lakes and wetlands is in situ microbial production. Indeed, microorganisms such as Sulphate and Iron Reducing Bacteria (SRB and IRB, respectively) can methylate iHg(II) into MeHg. SRB are known as the main responsible of methylation in anoxic aquatic environment but yield of this reaction

vary strongly depending on the involving bacteria [39]. Nevertheless, it is important to note that abiotic methylation can also occur [40], but this phenomenon is photochemically reversible. The activity of methylating microbes is controlled by temperature, redox conditions, pH, and the presence of suitable electron donors. Once produced, MeHg is bioaccumulated and biomagnified within the food web, and can reach dangerous levels in fishes, birds, and mammals [41].

See introductions of **5 A simple determination of trace mercury concentrations in natural waters using Dispersive Micro-Solid Phase Extraction preconcentration based on functionalized graphene nanosheets**, **7 Dynamics, distribution, and transformations of mercury species from Pyrenean high-altitude lakes** and Erreur ! Source du renvoi introuvable. Erreur ! Source du renvoi introuvable. for more information on mercury cycle.

2.6. Outline of the thesis

This work has been carried out in the framework of REPLIM that aims to investigate the past, present and future of lakes and peatbogs in the Pyrenees in a general context of global change.

In chapter **3 Sampling and analytical strategy**, the analytical procedure for an effective and accurate assessment of the water geochemistry in alpine lake waters was described. A special care has been taken during all the analysis process starting by a thorough cleaning of all the material in the laboratory, a careful and homogenous treatment of the samples on field and a proper storage prior the return to the laboratory. To fulfil this objective, the methodology for an **4 Accurate determination of the total alkalinity and the CO₂ system parameters in high altitude lakes from the Western Pyrenees (France – Spain)** and a **5 A simple determination of trace mercury concentrations in natural waters using Dispersive Micro-Solid Phase Extraction preconcentration based on functionalized graphene nanosheets** were developed.

Results for the sampling described allowed us to study **6 Occurrence, distribution, and characteristics concentrations of Potential Harmful Trace Elements (PHTEs) in Pyrenean lakes and their relation to aquatic biogeochemistry** as well as **7 Dynamics, distribution, and transformations of mercury species from Pyrenean high-altitude lakes**.

Finally, thanks to the REPLIM network, Erreur ! Source du renvoi introuvable. Erreur ! Source du renvoi introuvable..

2.7. References

- [1] K. Caldeira, M.E. Wickett, Anthropogenic carbon and ocean pH, *Nature*. 425 (2003) 365–365. <https://doi.org/10.1038/425365a>.

- [2] W.J. Mitsch, B. Bernal, A.M. Nahlik, Ü. Mander, L. Zhang, C.J. Anderson, S.E. Jørgensen, H. Brix, Wetlands, carbon, and climate change, *Landscape Ecology*. 28 (2013) 583–597. <https://doi.org/10.1007/s10980-012-9758-8>.
- [3] N.R. Urban, A. Desai, Are the Great Lakes a significant net source or sink of CO₂?, *SIL Proceedings*, 1922-2010. 30 (2009) 1283–1288. <https://doi.org/10.1080/03680770.2009.11923931>.
- [4] J.A. Patz, D. Campbell-Lendrum, T. Holloway, J.A. Foley, Impact of regional climate change on human health, *Nature*. 438 (2005) 310–317. <https://doi.org/10.1038/nature04188>.
- [5] S.L. Brantley, M.B. Goldhaber, K.V. Ragnarsdottir, Crossing Disciplines and Scales to Understand the Critical Zone, *Elements*. 3 (2007) 307–314. <https://doi.org/10.2113/gselements.3.5.307>.
- [6] G. Le Roux, S.V. Hansson, A. Claustres, Inorganic Chemistry in the Mountain Critical Zone, in: *Developments in Earth Surface Processes*, Elsevier, 2016: pp. 131–154. <https://doi.org/10.1016/B978-0-444-63787-1.00003-2>.
- [7] F. Lloret, Trade-offs in High Mountain Conservation, in: J. Catalan, J.M. Ninot, M.M. Aniz (Eds.), *High Mountain Conservation in a Changing World*, Springer International Publishing, Cham, 2017: pp. 37–59. https://doi.org/10.1007/978-3-319-55982-7_2.
- [8] OPCC-CTP, *Climate change in the Pyrenees: Impacts, vulnerabilities and adaptation.*, 2018. ISBN : 978-84-09-06268-3
- [9] A. Moreno, M. Bartolomé, J.I. López-Moreno, J. Pey, P. Corella, J. García-Orellana, C. Sancho, M. Leunda, G. Gil-Romera, P. González-Sampériz, C. Pérez-Mejías, F. Navarro, J. Otero-García, J. Lapazarán, E. Alonso-González, C. Cid, J. López-Martínez, B. Oliva-Urcia, S.H. Faria, M.J. Sierra, R. Millán, X. Querol, A. Alastuey, J.M. García-Ruiz, The case of a southern European glacier disappearing under recent warming that survived Roman and Medieval warm periods, *Glaciers/Paleoclimate*, 2020. <https://doi.org/10.5194/tc-2020-107>.
- [10] M. Morellón, B. Valero-Garcés, P. González-Sampériz, T. Vegas-Vilarrúbia, E. Rubio, M. Rieradevall, A. Delgado-Huertas, P. Mata, Ó. Romero, D.R. Engstrom, M. López-Vicente, A. Navas, J. Soto, Climate changes and human activities recorded in the sediments of Lake Estanya (NE Spain) during the Medieval Warm Period and Little Ice Age, *J Paleolimnol*. 46 (2011) 423–452. <https://doi.org/10.1007/s10933-009-9346-3>.
- [11] L. Camarero, M. Rogora, R. Mosello, N.J. Anderson, A. Barbieri, I. Botev, M. Kernan, J. Kopáček, A. Korhola, A.F. Lotter, G. Muri, C. Postolache, E. Stuchlík, H. Thies, R.F. Wright, Regionalisation of chemical variability in European mountain lakes: *Regionalisation of mountain lakes chemistry*, *Freshwater Biology*. 54 (2009) 2452–2469. <https://doi.org/10.1111/j.1365-2427.2009.02296.x>.
- [12] J.P. Corella, M.J. Sierra, A. Garralón, R. Millán, J. Rodríguez-Alonso, M.P. Mata, A.V. de Vera, A. Moreno, P. González-Sampériz, B. Duval, D. Amouroux, P. Vivez, C.A. Cuevas, J.A. Adame, B. Wilhelm, A. Saiz-Lopez, B.L. Valero-Garcés, Recent and historical pollution legacy in high altitude Lake Marboré (Central Pyrenees): A record of mining and smelting since pre-Roman times in the Iberian Peninsula, *Science of The Total Environment*. 751 (2021) 141557. <https://doi.org/10.1016/j.scitotenv.2020.141557>.
- [13] J. Catalan, L. Camarero, M. Filip, S. Pla, M. Ventura, T. Buchaca, F. Bartumeus, G. de Mendoza, A. Miró, E.O. Casamayor, J.M. Medina-Sánchez, M. Bacardit, M. Altuna, M. Bartrons, D.D. de Quijano, High mountain lakes: extreme habitats and witnesses of environmental changes, *Limnetica*. 25 (2006) 551–584. <https://doi.org/10.23818/limn.25.38>.
- [14] M. Ventura, L. Camarero, T. Buchaca, F. Bartumeus, D.M. Livingstone, J. Catalan, The main features of seasonal variability in the external forcing and dynamics of a deep mountain lake (Redó, Pyrenees), *Journal of Limnology*. 59 (2000). <https://doi.org/10.4081/jlimnol.2000.s1.97>.
- [15] C. Bini, M. Wahsha, Potentially Harmful Elements and Human Health, in: C. Bini, J. Bech (Eds.), *PHEs, Environment and Human Health*, Springer Netherlands, Dordrecht, 2014: pp. 401–463. https://doi.org/10.1007/978-94-017-8965-3_11.
- [16] I.S. Sen, B. Peucker-Ehrenbrink, Anthropogenic Disturbance of Element Cycles at the Earth's Surface, *Environmental Science & Technology*. 46 (2012) 8601–8609. <https://doi.org/10.1021/es301261x>.

- [17] H.B. Bradl, Chapter 1 Sources and origins of heavy metals, in: *Interface Science and Technology*, Elsevier, 2005: pp. 1–27. [https://doi.org/10.1016/S1573-4285\(05\)80020-1](https://doi.org/10.1016/S1573-4285(05)80020-1).
- [18] S.N. Aslam, C. Huber, A.G. Asimakopoulos, E. Steinnes, Ø. Mikkelsen, Trace elements and polychlorinated biphenyls (PCBs) in terrestrial compartments of Svalbard, Norwegian Arctic, *Science of The Total Environment*. 685 (2019) 1127–1138. <https://doi.org/10.1016/j.scitotenv.2019.06.060>.
- [19] J.P.G. Barre, G. Deletrez, J. Frayret, H. Pinaly, O.F.X. Donard, D. Amouroux, Approach to spatialize local to long-range atmospheric metal input (Cd, Cu, Hg, Pb) in epiphytic lichens over a meso-scale area (Pyrénées-Atlantiques, southwestern France), *Environmental Science and Pollution Research*. 22 (2015) 8536–8548. <https://doi.org/10.1007/s11356-014-3990-5>.
- [20] S.P. Catán, D. Bubach, M. Arribere, M. Ansaldo, M.J. Kitaura, M.C. Scur, J.M. Lirio, Trace elements baseline levels in *Usnea antarctica* from Clearwater Mesa, James Ross Island, Antarctica, *Environmental Monitoring and Assessment*. 192 (2020). <https://doi.org/10.1007/s10661-020-8212-7>.
- [21] P. Gabrielli, P. Vallenga, Contaminant Records in Ice Cores, in: J.M. Blais, M.R. Rosen, J.P. Smol (Eds.), *Environmental Contaminants*, Springer Netherlands, Dordrecht, 2015: pp. 393–430. https://doi.org/10.1007/978-94-017-9541-8_14.
- [22] J.M. Pacyna, E.G. Pacyna, An assessment of global and regional emissions of trace metals to the atmosphere from anthropogenic sources worldwide, *Environmental Reviews*. 9 (2001) 269–298. <https://doi.org/10.1139/er-9-4-269>.
- [23] J.D. Blum, B.A. Bergquist, Reporting of variations in the natural isotopic composition of mercury, *Analytical and Bioanalytical Chemistry*. 388 (2007) 353–359. <https://doi.org/10.1007/s00216-007-1236-9>.
- [24] P.A. Ariya, M. Amyot, A. Dastoor, D. Deeds, A. Feinberg, G. Kos, A. Poulain, A. Ryjkov, K. Semeniuk, M. Subir, K. Toyota, Mercury Physicochemical and Biogeochemical Transformation in the Atmosphere and at Atmospheric Interfaces: A Review and Future Directions, *Chemical Reviews*. 115 (2015) 3760–3802. <https://doi.org/10.1021/cr500667e>.
- [25] A. Saiz-Lopez, S.P. Sitkiewicz, D. Roca-Sanjuán, J.M. Oliva-Enrich, J.Z. Dávalos, R. Notario, M. Jiskra, Y. Xu, F. Wang, C.P. Thackray, E.M. Sunderland, D.J. Jacob, O. Travnikov, C.A. Cuevas, A.U. Acuña, D. Rivero, J.M.C. Plane, D.E. Kinnison, J.E. Sonke, Photoreduction of gaseous oxidized mercury changes global atmospheric mercury speciation, transport and deposition, *Nature Communications*. 9 (2018). <https://doi.org/10.1038/s41467-018-07075-3>.
- [26] A. Saiz-Lopez, A.U. Acuña, T. Trabelsi, J. Carmona-García, J.Z. Dávalos, D. Rivero, C.A. Cuevas, D.E. Kinnison, S.P. Sitkiewicz, D. Roca-Sanjuán, J.S. Francisco, Gas-Phase Photolysis of Hg(I) Radical Species: A New Atmospheric Mercury Reduction Process, *Journal of the American Chemical Society*. 141 (2019) 8698–8702. <https://doi.org/10.1021/jacs.9b02890>.
- [27] UNEP, *Global mercury assessment 2013: sources, emissions, releases and environmental transport*, UNEP Chemicals Branch, Geneva, Switzerland, 2013.
- [28] K. Hans Wedepohl, The composition of the continental crust, *Geochimica et Cosmochimica Acta*. 59 (1995) 1217–1232. [https://doi.org/10.1016/0016-7037\(95\)00038-2](https://doi.org/10.1016/0016-7037(95)00038-2).
- [29] J.O. Nriagu, A global assessment of natural sources of atmospheric trace metals, *Nature*. 338 (1989) 47–49. <https://doi.org/10.1038/338047a0>.
- [30] D.M. Pyle, T.A. Mather, The importance of volcanic emissions for the global atmospheric mercury cycle, *Atmospheric Environment*. 37 (2003) 5115–5124. <https://doi.org/10.1016/j.atmosenv.2003.07.011>.
- [31] J.C. Varekamp, P.R. Buseck, Global mercury flux from volcanic and geothermal sources, *Applied Geochemistry*. 1 (1986) 65–73. [https://doi.org/10.1016/0883-2927\(86\)90038-7](https://doi.org/10.1016/0883-2927(86)90038-7).
- [32] N. Pirrone, S. Cinnirella, X. Feng, R.B. Finkelman, H.R. Friedli, J. Leaner, R. Mason, A.B. Mukherjee, G.B. Stracher, D.G. Streets, K. Telmer, Global mercury emissions to the atmosphere from anthropogenic and natural sources, *Atmospheric Chemistry and Physics*. 10 (2010) 5951–5964. <https://doi.org/10.5194/acp-10-5951-2010>.

- [33] D. Obrist, J.L. Kirk, L. Zhang, E.M. Sunderland, M. Jiskra, N.E. Selin, A review of global environmental mercury processes in response to human and natural perturbations: Changes of emissions, climate, and land use, *Ambio*. 47 (2018) 116–140. <https://doi.org/10.1007/s13280-017-1004-9>.
- [34] M.S. Gustin, S.E. Lindberg, P.J. Weisberg, An update on the natural sources and sinks of atmospheric mercury, *Applied Geochemistry*. 23 (2008) 482–493. <https://doi.org/10.1016/j.apgeochem.2007.12.010>.
- [35] A.J. Poulain, T. Barkay, Cracking the Mercury Methylation Code, *Science*. 339 (2013) 1280–1281. <https://doi.org/10.1126/science.1235591>.
- [36] W.F. Fitzgerald, D.R. Engstrom, R.P. Mason, E.A. Nater, The Case for Atmospheric Mercury Contamination in Remote Areas, *Environmental Science & Technology*. 32 (1998) 1–7. <https://doi.org/10.1021/es970284w>.
- [37] M. Monperrus, E. Tessier, D. Point, K. Vidimova, D. Amouroux, R. Guyoneaud, A. Leynaert, J. Grall, L. Chauvaud, G. Thouzeau, O.F.X. Donard, The biogeochemistry of mercury at the sediment–water interface in the Thau Lagoon. 2. Evaluation of mercury methylation potential in both surface sediment and the water column, *Estuarine, Coastal and Shelf Science*. 72 (2007) 485–496. <https://doi.org/10.1016/j.ecss.2006.11.014>.
- [38] M. Monperrus, E. Tessier, D. Amouroux, A. Leynaert, P. Huonnic, O.F.X. Donard, Mercury methylation, demethylation and reduction rates in coastal and marine surface waters of the Mediterranean Sea, *Marine Chemistry*. 107 (2007) 49–63. <https://doi.org/10.1016/j.marchem.2007.01.018>.
- [39] R. Bridou, M. Monperrus, P.R. Gonzalez, R. Guyoneaud, D. Amouroux, Simultaneous determination of mercury methylation and demethylation capacities of various sulfate-reducing bacteria using species-specific isotopic tracers, *Environmental Toxicology and Chemistry*. 30 (2011) 337–344. <https://doi.org/10.1002/etc.395>.
- [40] V. Celo, D.R.S. Lean, S.L. Scott, Abiotic methylation of mercury in the aquatic environment, *Science of The Total Environment*. 368 (2006) 126–137. <https://doi.org/10.1016/j.scitotenv.2005.09.043>.
- [41] D.C. Evers, Y.-J. Han, C.T. Driscoll, N.C. Kamman, M.W. Goodale, K.F. Lambert, T.M. Holsen, C.Y. Chen, T.A. Clair, T. Butler, Biological Mercury Hotspots in the Northeastern United States and Southeastern Canada, *BioScience*. 57 (2007) 29–43. <https://doi.org/10.1641/B570107>.

3. Sampling and analytical strategy

3.1. Studied areas

Water samples were collected from 20 different high mountain lakes in the Central Pyrenees, most of them at an altitude higher than 2000 m above the sea level (asl): 11 in the French areas of Cauterets and Ayous and 9 in the Spanish areas of Panticosa and Sabocos. Those in Cauterets were Lac d'Arratille (**ARA**), Lac de la Badète (**BAD**), Grand lac de Cambalès (**CAM**), Lac de Peyregnets de Cambalès (**PEY**), Lac de Petite Opale (**OPA**), Lac de Pourtet (**POU**), Lac Nère (**NER**) and Lac du Paradis (**PAR**); while those in Ayous were Lac Gentau (**GEN**), Lac Roumassot (**ROU**) and Lac Bersau (**BER**). The sampled lakes in Panticosa were Ibón de Coanga (**COA**), Ibón de los Arnales (**ARM**), Ibón Azul Alto (**AZU**), Embalse de Bachimaña Bajo (**BAC**), Ibón de los Baños de Panticosa (**PAN**), Ibón de Ordicuso Inferior (**ORD**), Ibón de Xuans (**XUA**) Ibón de Pecico de la Canal (**PEC**) and, finally, Ibón de Sabocos (**SAB**) was also investigated. These small lakes show similar physical properties (lake size: 0.37 – 12.82 Ha; catchment size: 15 – 3229 Ha; maximum depth: 3 – 35 m) but differ from their catchment characteristics and geological background, i.e., mainly granite core (pDe-GR) versus sedimentary rocks (Devonian, De-SR; Permo-Triassic, PT-SR; Cretaceous Cr-SR) [1,2] (**Figure 3-1**). The lakes are located at different altitudes, from around 1600 m asl (PAN and PAR) to around 2600 m asl (XUA). Bioclimatic conditions are also substantially different with a decrease in the temperature (2 – 19 °C) and an increase in the precipitations at higher altitude. It is worth noting that most of the physical parameters listed in **Table 3-1** are season-dependent, meaning that temperature, precipitation, and ice cover duration will have a strong influence, especially on the water level. The snow cover duration (from 1st September to 31st august) is also a good climatic indicator and was determined according to *Gascoin et al.* [3] using data from Theia Snow collection (<https://www.theia-land.fr/product/neige/>). The **Figure 3-2** displays the snow cover duration as a function of the elevation of the studied lakes. The snow cover duration was significantly higher in 2017-2018; therefore, the winter 2017-2018 was colder and/or with much higher wet deposition and snow accumulation than the winters 2016-2017 and 2018-2019.

Firstly, the eight lakes of the Cauterets Area (**Figure 3-5**) are covering a 900 m altitudinal gradient and spanning about 7 km distance. This zone of the Pyrenees, historical passage for French-Spanish exchange, is a mosaic of crystalline, granitic, and sedimentary rocks [1]. All these lakes are within the Parc National des Pyrénées (PNP), so the anthropogenic inputs are limited and restricted to pastoralism, fishing, and hiking. PEY, CAM and OPA are directly connected, and the same observation can be made for ARA and BAD, as well as for NER and POU. On one side, the lakes CAM, PEY, NER and POU have a granitic basin (igneous rocks containing mainly quartz and feldspar) while OPA, besides the same type of basin, can be influenced by Devonian sedimentary rocks (limestone, sandstone, shale) in its surroundings. On the other side, the basin and/or catchment areas of the lakes ARA, BAD and PAR are mainly composed by Devonian sedimentary rocks, but granitic rocks are also present in their surroundings. While all the other lakes exhibit similar characteristics, PAR (1620 m asl) differs for several reasons. It is the only lake below 2000 m asl, located in a small forest catchment close to a park service road. It is also the smaller lake with a surface of 0.43 ha and a maximum depth of 3 m, which encourage the constant resuspension of sediments. Adding the strong vegetation surrounding the lake that

significantly influences its physico-chemical characteristics, this hydrosystem is gradually transforming into a wetland, with enhanced organic matter content. BAD also has a specificity regarding its water level. Indeed, a buried pipe links this lake with electricity facilities down the valley so the water of BAD can be freely dragged. For instance, the water level in October 2017 (Replim2) was a few meters lower than in June 2017 (Replim1).

In the Ayous area (**Figure 3-6**), BER is in the PNP while the other two lakes (ROU and GEN) are located close to it. The three lakes are directly connected and lie on Permo-Triassic volcanic rocks (conglomerate, sandstone, lutite, and andesite) while Carboniferous rocks are mainly present in the environment. Even if they are part of environmental protected areas, the agropastoralism, present for centuries, and, therefore, the presence of gaggles, represent an important source of organic matter and nutrients, especially in GEN (1942 m asl). Moreover, the mineral contributions from the pic d' Ayous, essentially iron, turn the bottom of the lake GEN into an anoxic zone. It is worth noting that recreational fishing is also one of the main activities in all the French lakes and can influence the water quality of the studied lakes. Thus, this lake can be considered as more eutrophic in comparison with the other ones investigated.

The eight lakes of the Panticosa area (**Figure 3-8**) are covering a 1000 m altitudinal gradient and spanning about 10 km. Even if the geological structure on this side of the Pyrenees is like the Cauterets area, mostly granitic [4], climatic conditions in the Panticosa area differ, leading to visible changes in the vegetation. PAN, XUA, COA, ARN and BAC have a basin mainly composed by granite while PEC, AZU and ORD lie on Devonian rocks. Three of these lakes can be directly influenced by local human activity because of the production of electricity coming from hydroelectric dams. Indeed, the flow of water is controlled upstream of BAC (2178 m asl), PAN (1640 m asl) and PEC (2460 m asl). It is also worth noting that PAN and BAC are connected to other lakes upstream so they will directly influence the geochemistry of PAN and BAC by dragging any mobile elements into these lakes. Finally, PAN is directly located in the small town of Baños de Panticosa where tourism activities are well developed (hotels, thermal baths, fishing, hiking) and can eventually influence the water biogeochemistry of the lake.

On its side, the basin of SAB (1900 m asl) (**Figure 3-7**) is dominated by sedimentary rocks (Devonian and Cretaceous) and the lake is located close to a ski resort. All facilities linked to this touristic activity, which is operational the whole year, contribute to the presence of hikers and skiers nearby this lake. Moreover, in analogy to GEN, agropastoralism with bovine and equine cattle and recreational fishing are important activities in this area [5], also leading to the occurrence of an anoxic zone at SAB's bottom.

Table 3-1: Some physical characteristics of the sampled lakes. Note that max depth was either measured or estimated from size using allometric relation, and volume of the lake was also estimated from max depth using a geometric approximation (error can be large). Pre-Devonian Granitic rocks (pDe-GR), Devonian sedimentary rocks (De-SR) include limestone, sandstone, and shale. Permo-Triassic sedimentary rocks (PT-SR) include conglomerate, sandstone, lutite and andesite. Cretaceous sedimentary rocks (Cr-SR) are mainly composed by carbonate rocks.

Lake name	ID Lake	Latitude	Longitude	Elevation (m asl)	Size (Ha)	Catchment (Ha)	Max depth (m) (*calculated)	Volume (m ³) (calculated)	Prevailing bedrock
Cauterets area									
Lac d'Arratille	ARA	42.8009	-0.1748	2256	5.87	296.4	12	264307	De-SR
Lac de la Badète	BAD	42.7938	-0.1820	2341	6.97	79.9	7	243990	De-SR
Grand lac de Cambalès	CAM	42.8297	-0.2251	2344	3.46	179.7	15	208745	pDe-GR
Lac de Peyregnets de Cambalès	PEY	42.8324	-0.2379	2493	1.17	15.2	9	52987	pDe-GR
Lac de Petite Opale	OPA	42.8284	-0.2177	2290	0.64	129.3	6*	25788	pDe-GR
Lac Nère	NER	42.8350	-0.2029	2304	2.91	94.8	12	178522	pDe-GR
Lac de Pourtet	POU	42.8432	-0.2031	2403	5.95	48.7	13	387705	pDe-GR
Lac du Paradis	PAR	42.8487	-0.1603	1620	0.43	25.4	3	16570	De-SR
Ayous Area									
Lac Gentau	GEN	42.8482	-0.4874	1942	8.62	186.2	20	993736	PT-SR
Lac Roumassot	ROU	42.8480	-0.4793	1843	5.15	268.2	16	424200	PT-SR
Lac Bersau	BER	42.8392	-0.4952	2080	12.82	61.4	35	2266475	PT-SR

Table 3-1 (continued)

Panticosa Area									
Ibón de Arnales	ARN	42.7738	-0.2435	2320	2.60	93.5	9	84579	pDe-GR
Ibón de Ordicuso Inferior	ORD	42.7571	-0.2478	2100	0.37	14.9	3	14171	De-SR
Ibón de los Baños de Panticosa	PAN	42.7589	-0.2370	1640	5.50	3229	15	470072	pDe-GR
Ibón Azul Alto	AZU	42.7898	-0.2461	2420	3.89	151.4	8	273527	De-SR
Ibón de Pecico de la Canal	PEC	42.7992	-0.2251	2460	0.91	167.5	9*	38954	De-SR
Ibón de Xuans	XUA	42.7773	-0.2090	2600	2.97	41.3	15	183875	pDe-GR
Ibón de Coanga	COA	42.7774	-0.2199	2304	0.58	27.9	5	23208	pDe-GR
Ibón de Bachimaña Bajo	BAC	42.7813	-0.2266	2178	3.08	1470.1	13*	193335	pDe-GR
Ibón de Sabocos	SAB	42.6926	-0.2574	1900	9.56	231.7	25	1183798	Cr-SR

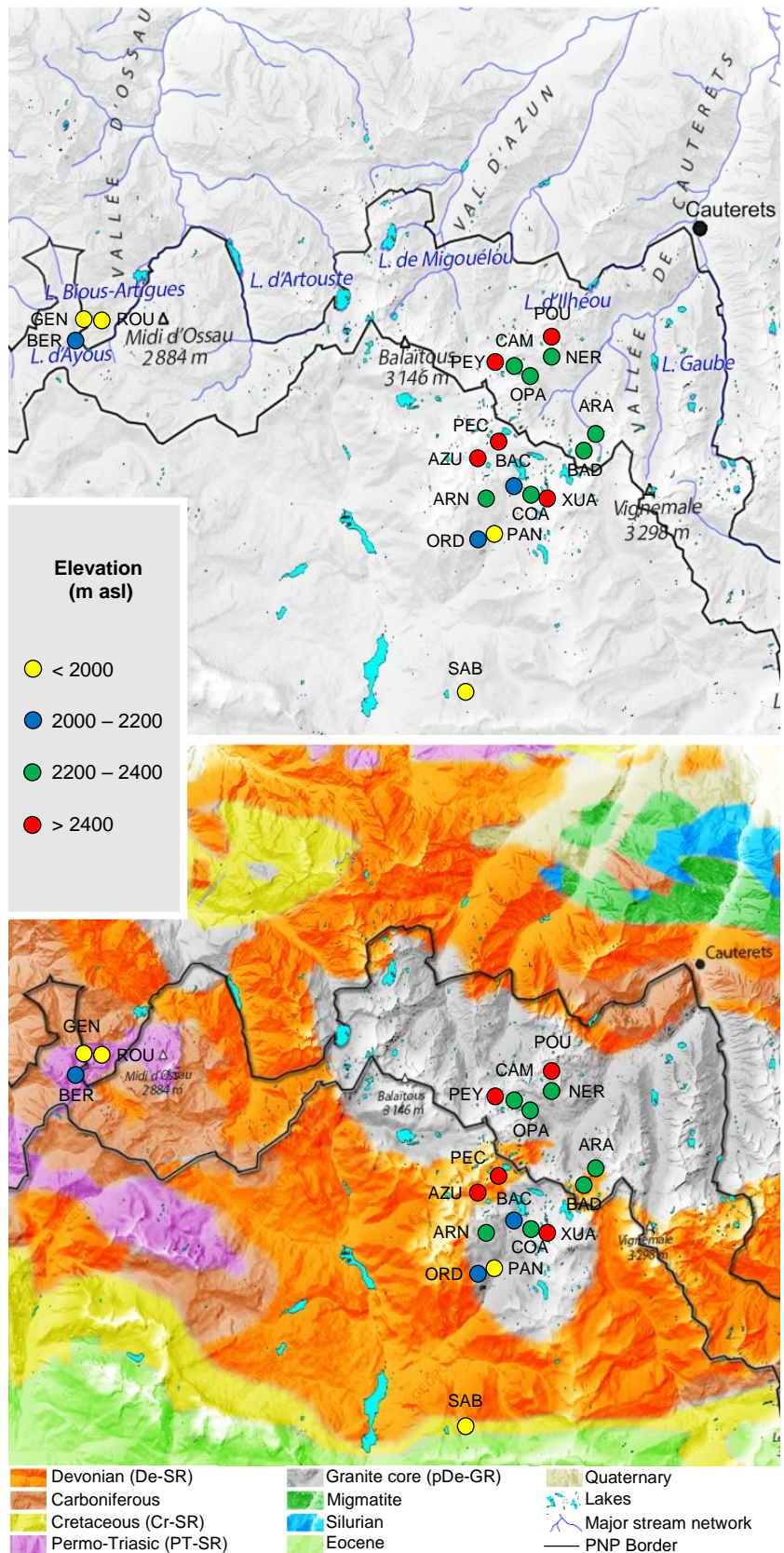


Figure 3-1: Studied lakes together with geology of their catchments (adapted with permission from Zaharescu *et al.* [1]); circles show position of the lakes, and colors indicate the elevation of the corresponding lakes. Lake acronyms are detailed in **Table 3-1**.

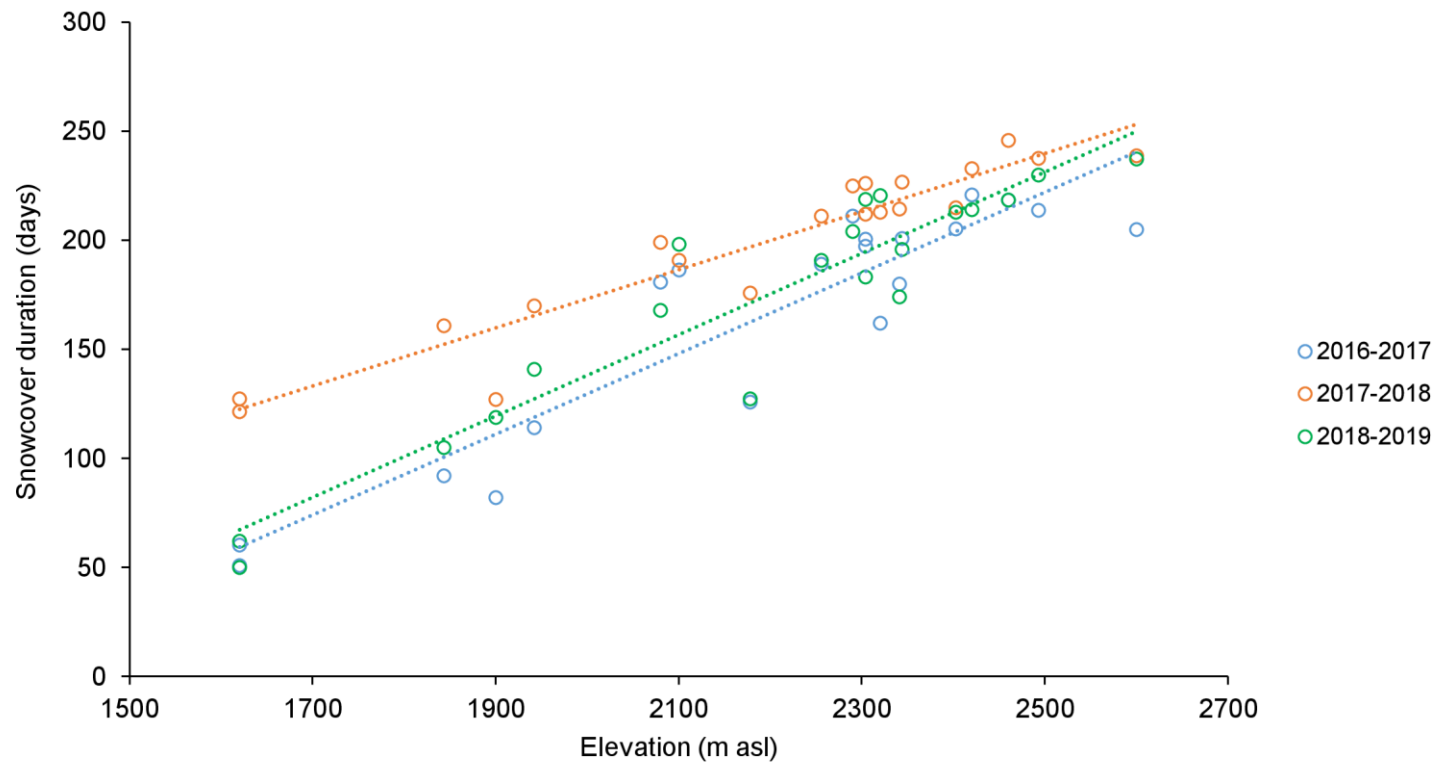


Figure 3-2: Snow cover duration (from 1st September to 31st august) obtained from Theia Snow collection [3] according to the elevation of the studied lakes depending on the year.

3.2. Sampling strategy

Water samples, either unfiltered and/or filtered, were collected during five field campaigns in June 2017 (**Replim1**), October 2017 (**Replim2**), June 2018 (**Replim3**), October 2018 (**Replim4**) and June 2019 (**Replim5**) (**Table 3-2**). For the area of Cauterets, the necessary material for all the lakes was first transported in hiking backpacks, with the help of donkeys only for the first sampling campaign, to the Wallon Refuge (1865 m asl) where the field laboratory was settled (**Figure 3-3**). Then the sampling was performed in 3-4 consecutive days. In the same way, the Refugio de Casa de Piedra (1636 m asl) and the Refugio de los Ibones de Bachimaña (2200 m asl) were used as field laboratories for the 3-4 days of samplings in the area of Panticosa. Finally, the Refugio de Sabocos (1900 m asl) and the Refuge d'Ayous (1980 m asl), respectively located next to the lakes SAB and GEN, were used as field laboratories. Each lake was reached by foot so at least eight people were involved for each sampling for a total of 26 people for all the sampling campaigns.



Figure 3-3: Transport of the material.

Subsurface (~0.5 m depth) water samples were collected during all the sampling campaigns to investigate possible spatial and seasonal variations in the water hydrological and geochemical characteristics (temperature, dissolved oxygen, silicates, TOC, DIC, total alkalinity, anions, major and trace cations). Thus, in details, intra-lake variability has been evaluated in June and October 2017 (Replim1 and 2) performing a triplicate sampling in each lake, at upstream, centre, and downstream locations. During the following sampling campaigns, a single subsurface sampling has been conducted at the deepest point of each lake. Moreover, during June 2018, October 2018 and June 2019 (Replim3, 4 and 5), water column profiles were investigated in GEN (5 depths), ARA (3 depths), SAB (6 depths) and AZU (3 depths), by sampling at different depths along the day. Besides, in-situ water incubation experiments over 7h (usually from 9 a.m. to 4 p.m. UTC+2) using isotopically enriched Hg species ($^{199}\text{iHg(II)}$, $^{201}\text{MMHg}$) were conducted in the June 2018, October 2018 and June 2019 campaigns at lakes GEN, ARA and SAB to investigate Hg species transformation mechanisms in the water column (methylation, demethylation, reduction). All the sampling strategy is summarized in **Table 3-2**.

A key point in the determination of trace elements is the rigour. Every step of the analytical protocol must be done uniformly and very carefully with material as clean as possible to obtain results comparable over time. Thus, thorough cleaning of all the material in the laboratory, a careful and homogenous treatment of the samples on field and a proper storage prior to the laboratory return are the main critical steps involved in the analytical protocol. Therefore, Quality Assurance (QA) and Quality Control (QC) was insured by the application of standardized operating protocols involving replicate tests, blanks controls and certified reference materials.

Briefly, all the material needed up to the lake was transported by hiking. An inflatable rubber boat (*Fish HunterTM FH280, Decathlon, France*) was used to reach the sampling points. To collect the subsurface water samples, a manually operated ultra-clean sampler (*Go-Flo Water Sampler 5L Teflon Coated, General Oceanics, USA*) (**Figure 3-4**) was deployed using powder-free gloves and avoiding the surface microlayer. For depth sampling, the Go-Flo sampler was deployed using a Kevlar cable and operated at the required depth with a plastic-coated messenger. Back ashore, the water sample was distributed with a clean silicone tubing in dedicated flasks according to the parameter to be further analysed.

Note:

Due to time constraints, for June 2019 (Replim5), only results for mercury are available and will be discussed in this manuscript.

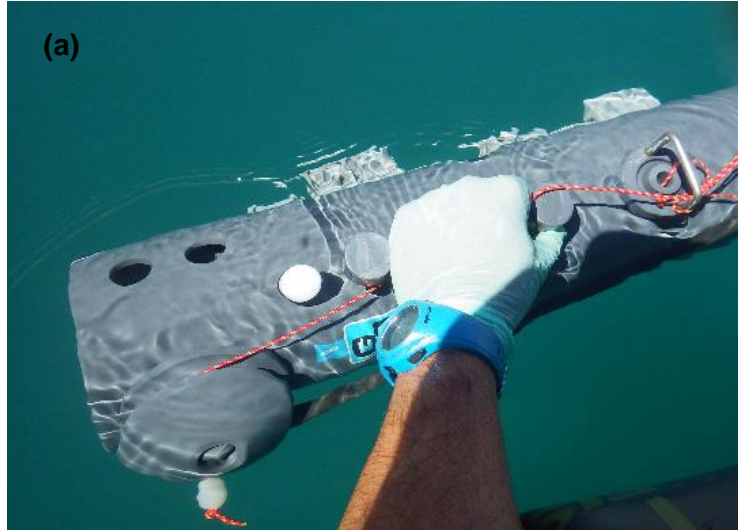


Figure 3-4: Water collection using a Go-Flo sampler ((a) subsurface; (b) deep water; (c) sub-sampling).

Table 3-2: Overall of the sampling strategy.

ID Lake	June 2017 (Replim1)	October 2017 (Replim2)	June 2018 (Replim3)	October 2018 (Replim4)	June 2019 (Replim5)
Cauterets area					
ARA	Subsurface (triplicate)	Subsurface (triplicate)	Profile study	Profile study	-
BAD	Subsurface (triplicate)	Subsurface (triplicate)	Subsurface (singlicate)	Subsurface (singlicate)	-
CAM	Subsurface (triplicate)	Subsurface (triplicate)	Subsurface (singlicate)	Subsurface (singlicate)	-
PEY	Subsurface (triplicate)	Subsurface (triplicate)	Subsurface (singlicate)	Subsurface (singlicate)	-
OPA	Subsurface (triplicate)	Subsurface (triplicate)	Subsurface (singlicate)	Subsurface (singlicate)	-
NER	Subsurface (triplicate)	-	-	-	-
POU	Subsurface (triplicate)	-	-	-	-
PAR	Subsurface (triplicate)	Subsurface (triplicate)	Subsurface (singlicate)	Subsurface (singlicate)	-
Ayous area					
GEN	-	-	Profile study	Profile study	Profile study
ROU	-	-	Subsurface (singlicate)	Subsurface (singlicate)	Subsurface (singlicate)
BER	-	-	Subsurface (singlicate)	Subsurface (singlicate)	Subsurface (singlicate)

Table 3-2 (continued)

Panticosa area					
ARN	Subsurface (triplicate)	Subsurface (triplicate)	Subsurface (singlicate)	Subsurface (singlicate)	Subsurface (singlicate)
ORD	Subsurface (triplicate)	-	Subsurface (singlicate)	Subsurface (singlicate)	Subsurface (singlicate)
PAN	Subsurface (triplicate)	Subsurface (triplicate)	Subsurface (singlicate)	Subsurface (singlicate)	Subsurface (singlicate)
AZU	Subsurface (triplicate)	Subsurface (triplicate)	Profile study	Profile study	Subsurface (singlicate)
PEC	Subsurface (triplicate)	-	Subsurface (singlicate)	Subsurface (singlicate)	Subsurface (singlicate)
XUA	Subsurface (triplicate)	-	-	-	-
COA	Subsurface (triplicate)	Subsurface (triplicate)	Subsurface (singlicate)	Subsurface (singlicate)	Subsurface (singlicate)
BAC	Subsurface (triplicate)	Subsurface (triplicate)	Subsurface (singlicate)	Subsurface (singlicate)	Subsurface (singlicate)
SAB	-	-	Profile study	Profile study	Profile study

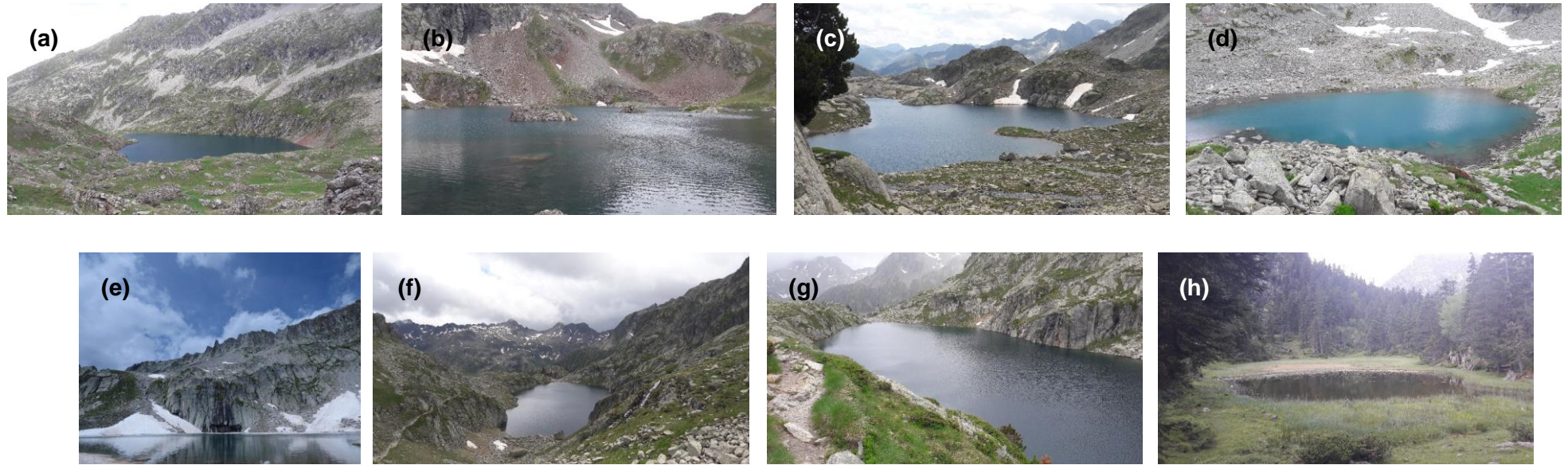


Figure 3-5: Lakes from Causerets area (Replim1): ARA (a), BAD (b), CAM (c), OPA (d), PEY (e), NER (f), POU (g) and PAR (h)



Figure 3-6: Lakes from Ayous area: GEN (Replim5) (a), BER (Replim3) (b) and ROU (Replim5) (c)

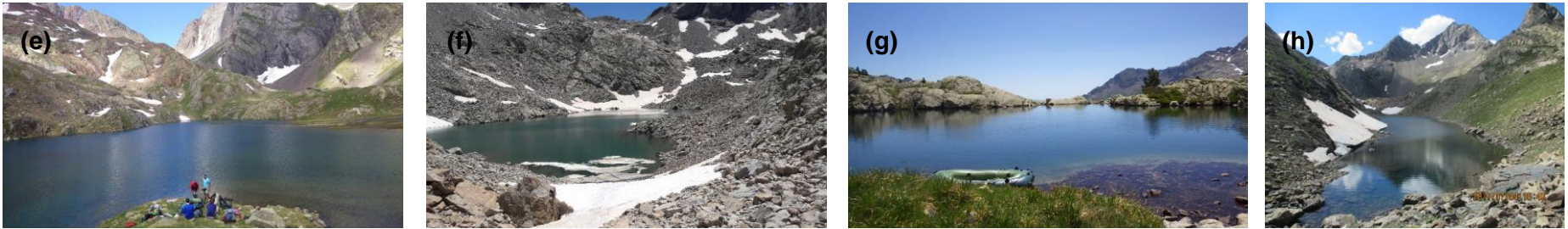


Figure 3-8: Lakes from Panticosa area (Replim1): ARN (a), ORD (b), PAN (c), BAC (d), AZU (e), XUA (f), COA (g) and PEC (h)



Figure 3-7: Lake Sabocos (Replim5)

3.3. Analytical methods

The **Table 3-8** resume all the parameters analysed together with their associated analytical protocol. The results obtained and discussed in this manuscript are gathered in **ANNEXE 1, 2, 3 and 4**.

3.3.1. Physicochemical parameters

Determination of several physicochemical parameters, that directly influence the chemical composition of the lake water, was carried out on site using an EXO2 multiparametric probe (*YSI Inc., USA*) (**Figure 3-9**): depth, temperature, conductivity, salinity, dissolved oxygen (DO), pH, oxidation-reduction potential (ORP) and chlorophyll-a (Chl-a).

The probe determines the depth with a non-vented strain gauge, which measures the pressure exerted by the water column. As the atmospheric pressure changes with altitude, it is important to calibrate the depth sensor before each measurement.

The probe is equipped with a combination temperature/conductivity sensor. The temperature sensor uses a thermistor whose resistance changes with temperature: an algorithm is used to perform the conversion. No calibration or maintenance of the temperature sensor is required, and the accuracy is ± 0.01 °C from -5 to 35 °C. The conductivity sensor uses four internal, pure-nickel electrodes to measure solution conductance. Two of the electrodes are current driven, and two are used to measure the voltage drop. The measured voltage drop is then converted into a conductance value in milliSiemens. Thus, the conductance is multiplied by the cell constant (approximately 5.1 cm^{-1}) to obtain the conductivity value in milliSiemens per cm (mS cm^{-1}). Calibration is performed with a 12.88 mS cm^{-1} (at 25 °C) standard solution (*Crison Instruments S.A., Spain*) which allows adjusting the value of the cell constant, and the accuracy is ± 0.5 % for 0 to 100 mS cm^{-1} and 1 % for 100 to 200 mS cm^{-1} . Salinity is determined automatically from the conductivity and temperature sensor according to algorithms found in Standard Methods for the Examination of Water and Wastewater (23rd edition, 2015) [6]. The use of the Practical Salinity Scale results in unitless values since the measurements are carried out in reference to the conductivity of standard seawater at 15 °C.

The dissolved oxygen (DO) measurement using an optical sensor is based on the influence of DO on an indicator dye. When there is no oxygen present, the lifetime (T) and intensity (I) of the signal, measured via a photodiode, is maximal. As oxygen is in contact with the membrane surface of the sensor, the lifetime becomes shorter and intensity decreases. Thus, the lifetime and the intensity of the luminescence are inversely proportional to the amount of oxygen present, and oxygen can be quantified by the Stern-Volmer equation:

Equation 3-1

$$\frac{I_0}{I} = \frac{T_0}{T} = 1 + K_{SV} \times [O_2]$$

where I_0 and I are the luminescence intensities in absence and presence of oxygen, T_0 and T the luminescence lifetime in absence and presence of oxygen, K_{SV} the Stern-Volmer constant (quantifies the quenching efficiency and therefore the sensitivity of the sensor) and $[O_2]$ the oxygen content.

The sensor gives the DO as oxygen saturation (%) or concentration ($mg\ L^{-1}$), and the accuracy is $\pm 1\%$ from 0 to 200 % oxygen saturation and $\pm 5\%$ from 200 to 500 % oxygen saturation. One calibration was performed at the beginning of each sampling campaign with water. It is then critical to consider that the atmospheric pressure will affect the DO measurement in decreasing this parameter with altitude. Thus, calibration should have been done in each sampling location, which is complicated to set up due to time constraints. The results of DO, discussed in this manuscript, must be taken carefully and reflect semi-quantitative values rather than quantitative values: precise but not fully accurate.

A combination pH/ORP sensor is used for the determination of these two parameters. The probe measures the pH with two electrodes, one for hydrogen ions and one as reference. The sensor is a glass bulb filled with a solution of stable pH and the inside of the glass surface experiences constant binding of H^+ ions. Before each sampling campaign, calibration was performed with three different buffer solutions (pH = 4.01, 7.00 and 10.00; *Hamilton Bonaduz AG, Switzerland*). These measurements can reach accuracies of ± 0.1 pH units within $\pm 10^\circ C$ of calibration temperature and ± 0.2 pH units for the entire temperature range. The ORP is measured by the difference in potential between an electrode, which is relatively chemically inert, and a reference electrode. The ORP sensor consists of a platinum button found on the tip of the probe. The potential associated with this metal is read versus the Ag/AgCl reference electrode of the combination sensor that uses a gelled electrolyte. A one-point calibration was performed with a 425 mV (at $25^\circ C$) buffer solution (*Hamilton Bonaduz AG, Switzerland*). ORP values are presented in millivolts, with an accuracy of ± 20 mV in Redox standard solution and are not compensated for temperature. The pH/ORP sensor is stored in acetate/acetic acid buffer of pH = 4 while not used.

The Total Algae (TAL) sensor unit includes a dual-channel fluorescence sensor that allows the determination of chlorophyll a (Chl-a) (excitation with a blue-emitting LED at 470 ± 15 nm) and phycoerythrin (BGA-PE) (excitation with a blue-shifted beam at 525 ± 15 nm). This manuscript will only focus on Chl-a results. The probe generates data in either RFU (Relative Fluorescence Units) or $\mu g\ L^{-1}$ of pigment. However, RFU is recommended as the default unit rather than $\mu g\ L^{-1}$ of pigment. Indeed, on one hand, RFU (0 to 100 %) is obtained by normalisation of the sensor's output with a secondary standard, rhodamine WT dye (*Acros Organics, Belgium*). It allows the correction of the sensor's drift such as biofouling and declining sensitivity over time and improve the accuracy of the measurements with better linearity. On the other hand, the $\mu g\ L^{-1}$ of pigment unit is just an estimation of pigment concentration based on the correlation between sensor outputs and extracted pigments from laboratory-grown blue-green algae. Thus, this unit is very dependent upon the composition of the algal population, the time of the day, the physiological health of the algae, and other environmental factors. Chl-a results will be discussed as RFU units and as a semi-quantitative variable.



Figure 3-9: EXO2 multiparametric probe.

3.3.2. Major anions

1. Sampling

Only filtrated samples were analysed, and no specific decontamination of the material was required. Indeed, the plastic material used in this case (containers, syringes, and polyamide 0.45 μ m filters) were directly used as received from the supplier, without a previous specific cleaning procedure. On field, after collecting a water sample using Go-Flo sampler (**3.2 Sampling strategy**), the filter and the syringe connected together were rinsed with the water sample. Approximately 50 mL of water were used to rinse the filter and the plastic container. Then, 40 mL of the water sample was filtered using the previously rinsed syringe-filter unit. About 10 mL of headspace was kept in the container to prevent an eventual collapse due to swelling of the sample if frozen during storage. The samples dedicated to major anions analysis were kept in a portable cooler (5-10 °C), protected from light, during transportation to the laboratory where they were stored in the fridge (4 °C).

2. Analysis

The analysis of typically considered major anions (Fluoride F⁻, Chloride Cl⁻, Nitrite NO₂⁻, Bromide Br⁻, Nitrate NO₃⁻, Phosphate PO₄³⁻, and Sulphate SO₄²⁻) was carried out using ionic chromatography by external standard calibration according to the EPA Method 300.1 [7,8]. Briefly, a small volume of sample (20 μ L) was injected into the ion chromatograph. Then, analytes were separated and measured using a system composed of a guard column, an analytical column, a suppressor device, and a conductivity

detector. For the introduction of the sample, the AS40 autosampler (*Dionex Corporation, USA*) was used. Together with an ASRS 300 (4 mm) suppressor, an IonPac AS23 (4 × 250 mm) column and IonPac AG23 (4 × 50 mm) precolumn (*Dionex Corporation, USA*) were used for the separation, whereas quantification was performed with an ICS 2500 ionic chromatograph with an ED50 suppressed conductivity detector (*Dionex Corporation, USA*). Finally, 4.5 mmol L⁻¹ sodium carbonate (Na₂CO₃) / 0.8 mmol L⁻¹ sodium bicarbonate (NaHCO₃) solution was used as mobile phase. 25 mA of suppression current and 1 mL min⁻¹ flow rate were the optimized chromatographic conditions. The program employed for data acquisition was Chromeleon 6.60 (*Dionex Corporation, USA*).

External calibration was carried out using 8 calibration solutions prepared by appropriate dilution in water (Millipore water purification system, *Millipore Co., USA*; 18.2MΩ cm) of 1000 mg L⁻¹ commercial solutions (*Sigma-Aldrich, USA*). Laboratory and in-field blanks were also regularly analysed all along the process to check for contamination issues.

3. Validation of the results

The limit of detection (LOD), associated to a specific technique, is the minimum concentration of an analyte in a sample that can be detected. In the case of the analysis of major anions, the in-field blanks did not display any signal on the chromatogram. Therefore, the calibration curve was used to calculate the LOD as follow:

Equation 3-2

$$\text{Signal} = a + \text{Concentration} \times b$$

where a is the intercept of the regression line and b the slope of the regression line.

Equation 3-3

$$LOD_{\text{concentration}} = \frac{3 \times \sigma_a}{b}$$

where σ_a is the standard deviation associated to the intercept of the regression line, and b the slope of the regression line.

Analysis of the samples has been achieved during four different analytical sessions, corresponding to the first four sampling campaigns (Replim1 – Replim4), and the LODs together with the number of samples analysed in each case are listed in the **Table 3-3**. Chloride (100%), Nitrate (88%) and Sulphate (96%) have been detected in almost all the samples whereas Fluoride (22%), Nitrite (0%), Bromide (3%), and Phosphate (0%) were mainly below the LOD.

Table 3-3: LOD for major anions analysis.

	F ⁻	Cl ⁻	NO ₂ ⁻	Br ⁻	NO ₃ ⁻	PO ₄ ³⁻	SO ₄ ²⁻	n
LOD_{Replim1} (µg L⁻¹)	33	24	19	38	50	81	35	47
n >LOD	0	47	0	0	45	0	47	
LOD_{Replim2} (µg L⁻¹)	11	25	27	43	142	52	102	34
n >LOD	16	34	0	0	27	0	34	
LOD_{Replim3} (µg L⁻¹)	1	22	-	6	12	41	213	40
n >LOD	13	40	-	4	40	0	39	
LOD_{Replim4} (µg L⁻¹)	2	9	-	54	65	90	292	34
n >LOD	5	34	-	0	24	0	29	

3.3.3. Major, trace and ultra-trace elements

1. Sampling

Two different kinds of samples were analysed: filtered and unfiltered.

Considering the very low concentrations expected in the samples and the potential contaminations, working with clean material is required. In that sense, an acid nitric bath at 10% v/v was prepared with a mix of nitric acid at 65 % (*PanReac, Spain*) and Elix quality water (*Merck Millipore, USA*) and plastic containers were soaked for 24 hours. Then, they were rinsed twice with Milli-Q water and dried in a clean atmosphere before being stored in Zip-lock bags. Syringes and syringe-filters were also cleaned using 10 % HNO₃ solution prepared with sub-boiling twice-distilled 69 % nitric acid and Milli-Q quality water (*Millipore Co., USA*; 18.2MΩ cm). First, the syringe is filled with 10 % HNO₃, the filter is connected, and the acid is pushed through the latter. Then, this step was repeated using Milli-Q water instead of 10 % HNO₃. Both materials (filters and syringes) were dried in a clean atmosphere and stored in Zip-lock bags until their use.

Sampling was done following the recommendations of EPA Method 1669 [9].

For the filtered samples, the water sample collected with the Go-Flo sampler (**3.2 Sampling strategy**) was used to fill the syringe, previously connected to the filter. That portion of the sample was passed through the filter and used to rinse one plastic container before being discarded. Then, about 40 mL of the water sample was filtered and used to fill the plastic container. A headspace volume of about 10 mL is kept in the plastic container to prevent an eventual collapse of the container due to swelling of the sample if frozen before analysis.

For the unfiltered samples, after rinsing the plastic container with the water sample, it was directly filled with about 40 mL of the water sample.

To prevent eventual adsorption on the wall, losses and/or transformations during storage, all samples were acidified using about 580 μL of sub-boiling twice-distilled HNO_3 69 %. The plastic container was closed, transported to the laboratory as fresh as possible (4 °C) and protected from light, and finally stored in a freezer (-20 °C) until analysis.

2. Analysis

Quantification has been done with ICP-MS by internal standard calibration according to EPA Method 1640 [10], using two types of equipment: one classical quadrupole Q-ICP-MS with Collision/Reaction Cell (filtered and unfiltered samples) (NexION 300, Perkin Elmer Inc., USA) and one High Resolution HR-ICP-MS (unfiltered samples only) (Element XR, Thermo Scientific, Germany), thus enabling future intercomparison of the results. Operating conditions of both equipments are summarized in **Table 3-4**.

For both methods, no additional sample treatment was needed, and the samples were analysed directly from the plastic container used for sampling. Indeed, given the remote location of the sampling lakes, resulting in ultra-clear water, the matrix of the samples was not considered complex, and possible interferences due to the matrix were negligible: no need for digestion of the samples. Besides, salt concentrations in the water samples were expected to be very low so problems related to the potential presence of salts in the analysis by ICP-MS were negligible and no dilution step was required.

For the analysis by Q-ICP-MS, quality control was insured by analysis of all the calibration standards several times per session, replication of one sample every ten samples to correct for drift in the sensitivity of the equipment, analysis of reference material (SRM 1640a, Trace Elements in Natural Water; *Sigma-Aldrich, USA*), and laboratory and in-field blanks analysis. To reduce potential polyatomic interferences for some elements (Na, Mg, K, Ca, Ti, V, Cr, Mn, Fe, Co, Ni, Cu, Zn, As and Cd), Helium (He) was used to fill the Collision/Reaction cell device (collision mode with kinetic energy discrimination KED).

With the HR-ICP-MS, resolution was adapted to each element likely to be affected by spectral overlaps. However, physical correction of this problem has an inherent disadvantage in that the higher resolving capability will go along with lower sensitivity (decrease in the transmission). Quality control was ensured by analysis of all the calibrations standards several times per session, and laboratory and in-field blanks analysis.

Table 3-4: Operating conditions for the Q-ICP-MS and the HR-ICP-MS.

Q-ICP-MS NexION 300 (Perkin Elmer)		HR-ICP-MS Element XR (Thermo Scientific)	
Forward power	1600 W	Forward power	1200 W
Plasma gas flow (Ar)	18 L min ⁻¹	Plasma gas flow (Ar)	15.90 L min ⁻¹
Auxiliary gas flow (Ar)	1.2 L min ⁻¹	Auxiliary gas flow (Ar)	1 L min ⁻¹
Nebulizer gas flow (Ar)	0.90-1.00 L min ⁻¹	Nebulizer gas flow (Ar)	0.745 L min ⁻¹
Sample flow	0.4 mL min ⁻¹	Sample flow (Azote)	10 L min ⁻¹
Cell gas flow (He)	2.0 mL min ⁻¹		
(depending on elements)	4.0 mL min ⁻¹		
Integration time	1000 ms	Integration time	100 ms
Dwell time	50 ms	Dwell time	10 ms
Sweeps	20	Sweeps	10
Reading	1	Reading	5
Replicates	3	Replicates	5
Internal Standard	⁹ Be, ⁴⁵ Sc, ⁷⁴ Ge, ⁸⁹ Y, ¹¹⁵ In, ²⁰⁹ Bi	Internal Standard	¹⁰³ Rh
Isotopes measured	²³ Na, ²⁴ Mg, ²⁷ Al, ³⁹ K, ⁴⁴ Ca, ⁴⁷ Ti, ⁵¹ V, ⁵² Cr, ⁵⁵ Mn, ⁵⁶ Fe, ⁵⁹ Co, ⁶⁰ Ni, ⁶³ Cu, ⁶⁶ Zn, ⁷⁵ As, ⁸⁸ Sr, ⁹⁸ Mo, ¹⁰⁷ Ag, ¹¹¹ Cd, ¹²⁰ Sn, ¹²¹ Sb, ¹³⁷ Ba, ¹⁸⁴ W, ²⁰⁵ Tl, ²⁰⁸ Pb	Isotopes measured	
		Low Resolution	⁴³ Ca, ⁷⁵ As, ⁸⁸ Sr, ⁹⁵ Mo, ¹⁰⁹ Ag, ¹¹¹ Cd, ¹¹⁸ Sn, ¹²¹ Sb, ¹³⁸ Ba, ¹⁸² W, ²⁰⁵ Tl, ²⁰⁸ Pb, ²³² Th, ²³⁸ U
		Medium Resolution	²³ Na, ²⁶ Mg, ²⁷ Al, ³⁹ K, ⁴⁷ Ti, ⁵¹ V, ⁵² Cr, ⁵⁵ Mn, ⁵⁶ Fe, ⁵⁹ Co, ⁶² Ni, ⁶³ Cu, ⁶⁶ Zn

3. Validation of the results

Analytical uncertainties for both methodologies (**Table 3-5**) have been evaluated using replicate analysis of the same sample. The LOD associated to each element (**Table 3-5**) was calculated according to two different ways.

For the results obtained by the Q-ICP-MS, the calibration curve was used with the same formula as for the determination of instrumental LODs for major anions (**Equation 3-3**). The major elements (Ca, Na, Mg and K) were detected in all the samples (filtered and unfiltered), and other trace (Al, Sr, Fe, Mn, Ba) and ultra-trace (As, Ti, Mo, V, Sb, Zn and W) elements in more than 50% of the samples (filtered and unfiltered). Nevertheless, most of the ultra-trace elements (Cu, Ni, Cr, Pb, Co, Cd, Tl, Ag, and Sn), potentially harmful to human health or the environment, were below the limit of detection (filtered and unfiltered).

Laboratory blanks were used in the case of the HR-ICPMS for the calculation of the LOD, using the following formula:

Equation 3-4

$$LOD_{concentration} = 3 \times \sigma_{blank}$$

where σ_{blank} (ng L⁻¹) is the standard deviation associated to the laboratory blank analysis.

The HR-ICP-MS provided better results because most of the elements analysed, either major, trace or ultra-trace, have shown lower limit of detection. Only two elements have not been detected in most of the samples: Ag and Sn. In pristine natural waters, Ag occurs at low ng L⁻¹ levels (0.1 – 5 ng L⁻¹) [11] not detectable with classical methodologies such as detection by ICP-MS and quantification by external calibration. Regarding Sn, it is an ubiquitous contaminant in laboratory vessels (including quartz and many plastics), which may explain the relative high limit of detection in comparison with other trace elements.

Another trace element showed a high limit of detection, for both techniques: Zn. This was probably due to laboratory contamination that may occur in both the material and Milli-Q water used for the preparation of the calibration curve and the blank solutions. Other lab manipulations also increase the contamination by Zn in water samples. For example, when filtering the samples with PVDF filters, the contamination by Zn was higher, and the results obtained when comparing filtered and non-filtered samples supported this fact. This contamination occurs randomly so even if it has been detected in more than 90 % of the samples (HR-ICP-MS, unfiltered samples), Zn levels will not be discussed furthermore in this manuscript.

To compare the efficiency and suitability of the two methods, a linear regression analysis has been performed with the results obtained by Q-ICP-MS and HR-ICP-MS. The coefficient of determination R² and the slope b, together with its associated standard error $\pm b$, are displayed in the **Figure 3-10**. Except for Al, Co, Cu, Zn and W, most of the elements well detected using Q-ICP-MS display a strong linear relationship with the ones obtained by HR-ICP-MS. Nevertheless, when looking at the slopes associated to each regression, which is under the value of one, it becomes obvious that using the Q-ICP-MS

methodology will lead to an underestimation of the results. This is probably due to the quantification process. Indeed, the standard solutions used for the Q-ICP-MS could be stored for a maximum of one month whereas the ones for HR-ICP-MS were prepared daily. Moreover, we have used the results obtained firstly by Q-ICP-MS to adjust more properly the calibration curves for the HR-ICP-MS, thereby avoiding that some points appear out of the curve (extreme values). Only one element, Sr, displays results always higher with the Q-ICP-MS, this is due to some manipulation problems with the commercial solution used for the HR-ICP-MS methodology.

As a resume, the Q-ICP-MS methodology, used daily for various analysis (sediments, waters, plants etc ...), will be qualified as a semi-quantitative method. With an estimation of the concentrations, its results allow us to compare the variation of each element within the samples, either unfiltered or filtered. For a better accuracy and precision regarding the unfiltered samples, results coming from the HR-ICP-MS methodology will be used within this manuscript (except for Sr).

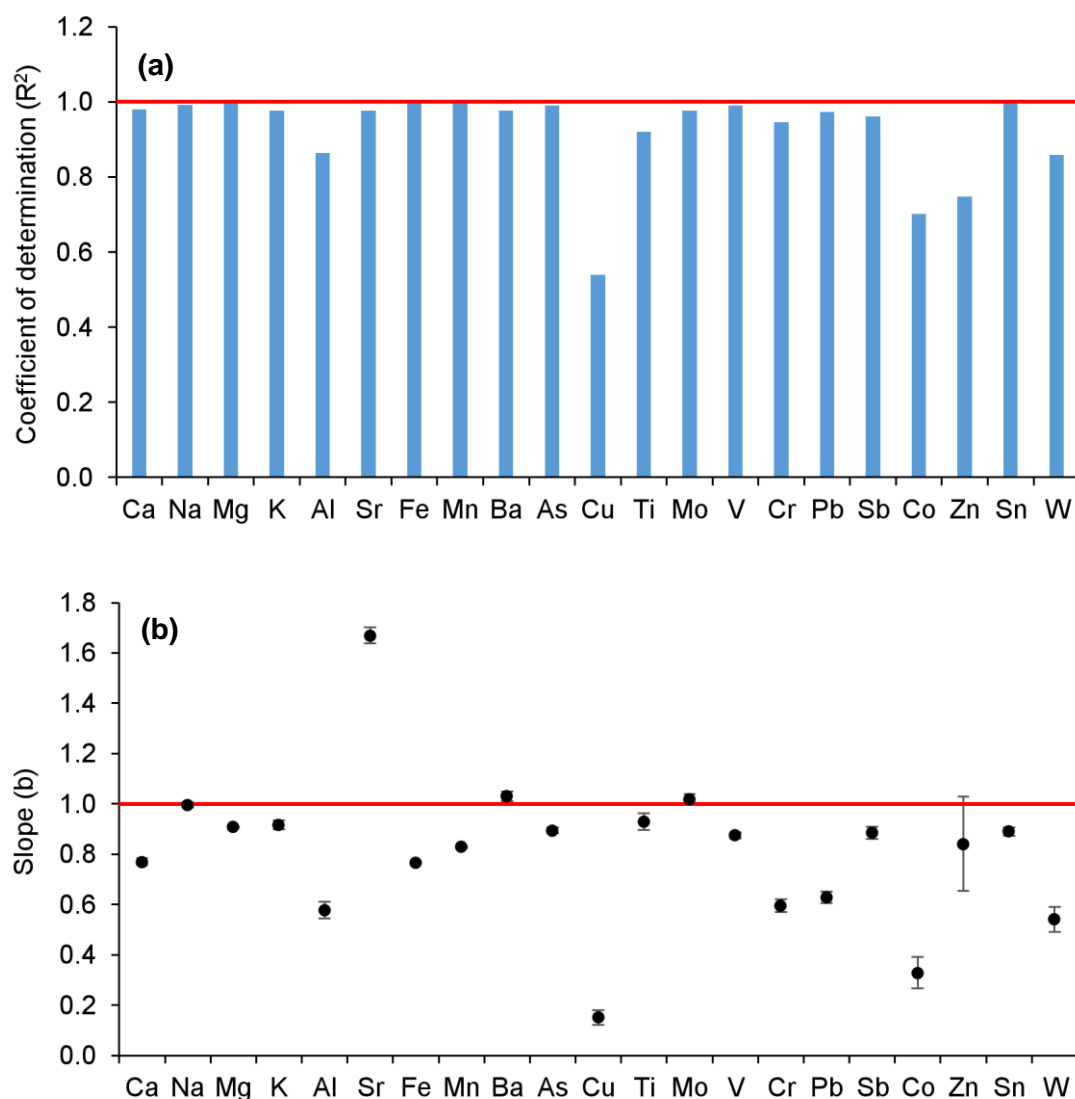


Figure 3-10: (a) Coefficient of determination R^2 and (b) the slope b associated to each linear regression between results obtained by Q-ICP-MS and results obtained by HR-ICP-MS.

Table 3-5: LOD and analytical uncertainties for major and trace cations analysed by Q-ICP-MS (filtered and unfiltered) and HR-ICP-MS (unfiltered). Subscripts 1, 2, 3 and 4 stand for, respectively, Replim1, Replim2, Replim3 and Replim4.

	Ca	Na	Mg	K	Al	Sr	Fe	Mn	Ba		As	U	Cu	Ti	Mo	V	Ni	Cr	Pb	Sb	Co	Cd	Tl	Zn	Ag	Sn	W	<i>n</i>				
Q-ICP-MS	LOD ₁ (µg L ⁻¹)	7	19	3	3	2	0.1	0.7	0.01	0.01	(ng L ⁻¹)	46	-	15	3	6	10	20	7	4	10	4	9	3	493	9	5	4	92			
	n > LOD	92	92	92	92	48	92	76	92	92		91	-	73	92	74	90	0	71	46	70	51	1	6	57	56	4	84				
	(%)	100	100	100	100	52	100	83	100	100		99	-	79	100	80	98	0	77	50	76	55	1	7	62	61	4	91				
	Q-ICP-MS	LOD ₂ (µg L ⁻¹)	6	26	4	12	0.4	0.04	0.6	0.04	0.02	(ng L ⁻¹)	93	-	66	66	9	39	62	40	45	4	26	9	5	2367	18	8	4	65		
		n > LOD	65	65	65	65	65	65	56	65	65		65	-	65	48	65	64	0	12	3	65	1	0	0	35	0	28	65			
		(%)	100	100	100	100	100	100	86	100	100		100	-	100	74	100	98	0	18	5	100	2	0	0	54	0	43	100			
		Q-ICP-MS	LOD ₃ (µg L ⁻¹)	15	18	15	4	2	0.2	8.1	0.4	0.2	(ng L ⁻¹)	131	-	83	13	22	41	82	33	117	6	111	90	19	165	-	20	11	80	
			n > LOD	80	80	79	80	39	79	23	71	74		76	-	3	73	68	49	2	24	1	78	0	0	0	46	-	37	42		
			(%)	100	100	99	100	49	99	29	89	93		95	-	4	91	85	61	3	30	1	98	0	0	0	58	-	46	53		
			Q-ICP-MS	LOD ₄ (µg L ⁻¹)	15	1	2	1	1	0.2	0.7	0.4	0.1	(ng L ⁻¹)	68	-	41	30	8	27	77	37	15	17	51	30	11	836	-	5	17	68
				n > LOD	68	68	68	68	24	67	62	53	63		61	-	13	68	67	54	2	26	15	46	4	1	0	36	-	18	23	
				(%)	100	100	100	100	35	99	91	78	93		91	-	19	100	99	79	3	38	22	68	6	1	0	53	-	26	34	
Q-ICP-MS				n > LOD	305	305	304	305	176	303	217	281	294		293	-	154	281	274	257	4	133	65	259	56	2	6	174	-	87	214	305
				(%)	100	100	100	100	58	99	71	92	96		96	-	50	92	90	84	1	44	21	85	18	1	2	57	36	28	70	
HR-ICP-MS				LOD (µg L ⁻¹)	7	1	0.3	9	0.3	0.002	0.07	0.004	0.002	(ng L ⁻¹)	0.5	0.1	18	2	2	0.1	11	3	2	2	0.1	0.5	0.2	264	6	19	44	143
	n > LOD			143	143	143	143	143	143	143	143	143		143	143	143	143	143	143	143	143	143	143	143	143	142	129	2	35	143		
	(%)			100	100	100	100	100	100	100	100	100		100	100	100	100	100	100	100	100	100	100	100	100	99	90	1	24	100		
Q-ICP-MS Analytical																																
Uncertainties		5		6	5	3	8	3	4	3	2		5	-	6	9	4	8	4	19	5	4	8	17	5	4	22	8	9			
(%)																																
HR-ICP-MS Analytical																																
Uncertainties		2	2	2	2	9	2	2	2	2		2	3	10	3	2	2	9	3	3	2	2	2	2	2	35	8	6	6			
(%)																																

3.3.4. Organometals (Hg species)

The following analytical protocol is set up for the determination of both Hg and Sn species. Nevertheless, only results for Hg species will be presented and discussed in this manuscript. Results for Sn species (Mono-, Di- and Tributyltin, MBT, DBT and TBT) are gathered in **ANNEXE 3**.

It is also important to note that among the Hg species, the analysis carried out by capillary GC-ICP-MS allowed us to quantify the methylated species (MeHg), i.e., the sum of monomethylmercury (MMHg) and dimethylmercury (DMHg). Nevertheless, the later discussion about the purge sample experiment will highlight the fact that the measured MeHg are mainly in the form of MMHg (**5 Purge experiment**).

1. Sampling

Working with ultra-clean material is essential for determination of mercury and tin content, especially in water samples from remote areas. In that sense, time and effort have been dedicated for the cleaning of material used during the analytical process. Teflon containers were filled with nitric acid (HNO_3 , Analytical Grade, *Fisher Scientific, USA*) solution (10% v/v, deionized water), sonicated for 2h, and deionized water was used to rinse them. Then a second cleaning has been processed by filling the Teflon containers with a second solution of HNO_3 (10% v/v, deionized water). They have been sonicated 2h and rinsed with deionized water. Finally, a last cleaning using a solution of hydrochloric acid (HCl, Analytical Grade, *Fisher Scientific, USA*) (10% v/v, deionized water) to fill the Teflon containers has been done. After a last sonication of 2h, Teflon containers have been rinsed three times with deionized water and dried in a clean atmosphere, under a laminar flow hood. Concerning the syringe, silicone, and Teflon tubings, cleaning has been processed in a similar way, using two HNO_3 bath solutions (10% v/v, deionized water) and one HCl bath solution (10% v/v, deionized water). All components were also dried in a clean atmosphere, under a laminar flow hood. Sterivex filter units do not require any cleaning protocol and can be used directly from their original package.

The particles in the water have a key role in the transport and fate of Hg species [12]. Thus, to evaluate their influence on the distribution of Hg species, two kinds of samples were collected and further analysed: filtered (dissolved fraction) and unfiltered (total fraction). It is worth noting that considering the general pristine state of the studied lakes, the particles were scarce and thus it was impossible to collect and analysed them.

For the filtered samples, after collecting a water sample using Go-Flo sampler (**3.2 Sampling strategy**), a Teflon container of 250 mL has to be rinsed three times with an aliquot of the water sample and filled with around 250 mL of the water sample. Then, a Teflon tube is connected to the syringe, and both are rinsed three times using the water sample from the 250 mL Teflon container. This last is also used to fill the syringe at the half before connecting the Sterivex Filter unit (PVDF, 0.22 μm) in place of the Teflon tube. The water sample collected in the syringe is passed through the filter and used to rinse three times a 125 mL Teflon container. Finally, according to this protocol the 125 mL Teflon is filled with 125 mL of the water sample.

For the unfiltered samples, a 125 mL Teflon container is directly rinsed three times with the water sample from the sampler and then filled with 125 mL of the water sample. In-field, all samples, filtered and unfiltered, were acidified at 0.5% v/v adding 625 μ L of acetic acid (CH_3COOH 99%, Trace metal grade, *Fisher Scientific, USA*) [13]. Teflon containers were closed tightly and stored in double PE Zip-lock bags in a portable cooler (5-10 $^{\circ}\text{C}$), protected from light, during transportation to the fridge of the laboratory (5-10 $^{\circ}\text{C}$).

2. Isotopic Dilution Analysis (IDA)

The quantification by Isotopic Dilution Analysis (IDA) [14] is based on the measurement of the isotopic ratio in a sample where the natural isotopic abundance has been altered by the spike of an isotope tracer's solution. Isotopic dilution allows being free from the intensity variations that could be observed on the chromatogram (loss, dilution, transformations etc ...), thus, significantly increasing accuracy and precision of the measurement. Moreover, the enrichment of samples in stable isotopes at the beginning of the analytical protocol also makes possible the evaluation of interconversion reactions (methylation, demethylation).

Two different modes of IDA application exist: species-unspecific (SU) and species-specific (SS).

The SU spiking mode was usually used because of a lack of mercury isotopically enriched spikes (MMHg, iHg(II)) commercially available. This mode only allows correcting the errors derived from the detection step. Indeed, the isotopically enriched spikes are introduced online in the equipment before the ionisation and detection process. The SU spiking mode does not make possible to correct the loss or transformations that occur during the analytical process.

With the SS spiking mode, isotopically enriched spikes are added during the analytical protocol, and IDA is applied specifically to one or more species, depending on whether the single or multiple IDA technique is used.

With classical or simple isotope dilution analysis (S-IDA), only one species enriched in one isotope is added to the sample. Loss or non-quantitative extraction during the analytical protocol are corrected, but not the inter-conversions (MMHg to iHg and vice versa) because each analyte is quantified independently of the others.

In double isotope dilution analysis (D-IDA), two isotope tracer's solutions, with known abundance, are spiked to the sample (e.g., $^{199}\text{iHg(II)}$ and $^{201}\text{MMHg}$) and will react the same way than the studied species (e.g., $^{202}\text{iHg(II)}$ and $^{202}\text{MMHg}$). The natural isotopic composition of the sample is altered, and the quantification is based on the measurement of the mixed isotope ratios. Data obtained by D-IDA can be processed specifically for two species (i.e., double species-specific isotope dilution analysis, D-SS-IDA) or for the whole system (i.e., isotope pattern deconvolution, IPD). D-SS-IDA model consists of the specific measurement of Hg species separately, and only two isotopes are considered for the quantification of each Hg species (e.g., $^{199}\text{iHg(II)}/^{202}\text{iHg(II)}$ for iHg(II) and $^{201}\text{MMHg}/^{202}\text{MMHg}$ for MMHg). Both D-SS-IDA and IPD allow correcting losses and inter-conversions that occur during the whole analytical process. However, IPD takes into account all the different isotopic patterns of both spikes and

endogenous species, so it is more reliable than the D-SS-IDA. It also provides the determination of methylation and demethylation rates from the inter-conversions.

3. Analysis

Back to the laboratory, the quantification is carried out by the double species-specific isotopic dilution method (D-SS-IDA) and analysis by capillary GC-ICP-MS [13,15]. The operating conditions are listed in **Table 3-6**.

For that purpose, a derivatization step followed by a liquid/liquid extraction are needed. The sample in the 125 mL Teflon container is sonicated for 10 min to desorb potential inner-wall adsorbed mercury. About 100 mL of that sample are precisely weighted ($\pm 10^{-5}$ g) in a Boston clear glass vial followed by the addition of 5 mL of acetic acid/acetate buffer (0.1 mol L^{-1} , pH = 4.9). The sample is spiked with weighted amounts of isotope tracer's solution ($^{199}\text{iHg(II)}$ inorganic mercury, $^{201}\text{MMHg}$ methylmercury, and $^{119}\text{BuSn}$ mix of Mono-, Di- and Tributyltin; *ISC-Science, Spain*). Then, the sample is stored at room temperature, protected from light, in a laminar flow hood at least for 12 hours. After this equilibration time, the pH must be adjusted between 4.85 and 5.05 using additions of ultrapure NH_3 and/or HCl solutions (*Optima Grade, Fisher Scientific, USA*). 70 μL of derivatizing agent, sodium tetraethylborate (NaBEt_4 , 5% v/v in Milli-Q water) (*Merseburger Spezialchemikalien, Germany*) and 250 μL of GC organic solvent (Isooctane, *Sigma-Aldrich*) are added to the mixture. After an agitation step of 20 min using an elliptic table (400 rpm), the organic phase containing Hg and Sn species is recovered and transferred in a GC vial equipped with a 200 μL micro insert. Finally, it is stored at $-20 \text{ }^\circ\text{C}$ until analysis.

For quality control purpose, laboratory and in-field blanks were processed regularly. An internal standard solution ($0.5 \text{ } \mu\text{g L}^{-1}$ ^{203}Tl and ^{205}Tl , mass close to Hg) is also introduced together with the sample in the nebulizer for mass bias correction.

Table 3-6: Operating conditions of the GC-ICP-MS.

Gas Chromatograph	
Trace Ultra GC (<i>Thermo Scientific, USA</i>)	
Column	Rxi-5ms Restek, 30m, ID 0.25mm, df 25µm
Injector temperature	250 °C
Injection volume	2 µL (splitless)
Temperature program	Start at 80 °C (30 sec), 60 °C min ⁻¹ until 260 °C (60 sec)
Carrier gas flow (He)	5 mL min ⁻¹
Interface	
Interface temperature	280 °C
Interface length	0.50 m
ICP-MS	
XSeries II (<i>Thermo Scientific, USA</i>)	
Forward power	1200 W
Plasma gas flow (Ar)	14 L min ⁻¹
Auxiliary gas flow (Ar)	0.8 L min ⁻¹
Nebulizer gas flow (Ar)	0.65 L min ⁻¹
Make up gas flow (Ar)	235 mL min ⁻¹
Acquisition mode	Transient Time resolved analysis
Acquisition time	550 sec
Dwell time	20 ms
Detection mode	Pulse
Isotopes measured	¹¹⁷ Sn, ¹¹⁸ Sn, ¹¹⁹ Sn, ¹²⁰ Sn, ¹⁹⁹ Hg, ²⁰⁰ Hg, ²⁰¹ Hg, ²⁰² Hg, ²⁰⁴ Hg, ²⁰³ Tl, ²⁰⁵ Tl

4. Validation of the results

For iHg(II), laboratory blanks were used for the calculation of the LOD using the formula from **Equation 3-3**. iHg(II) was above the LOD in all the samples from Replim1 to Replim5 with LOD of respectively 26, 27, 57, 9 and 34 pg L⁻¹. It is in good agreement with recent publications from *Monperrus et al.* [15] and *Cavalheiro et al.* [13] where the LOD, calculated using the same formula mentioned above, were respectively of 53 and 42 pg L⁻¹.

It is worth noting that to obtain more accurate results, blanks levels (90, 50, 170, 100 and 104 pg L⁻¹ for respectively Replim1, 2, 3, 4 and 5), also quantified with D-SS-IDA method, were subtracted to the iHg(II) concentrations measured in the lake water samples.

In the case of MMHg, the analysis of all the laboratory and in-field blanks did not display any signal at the corresponding retention time: it was below LOD. Thus, the LOD was calculated with the background signal using one chromatogram extracted from one blank analysis. The following formula was used:

Equation 3-5

$$LOD = \frac{3 \times \sigma_{background} \times R}{m}$$

where $\sigma_{background}$ is the standard deviation associated to the mean of the background signal amplitude close to the retention time, R the response factor concentration/signal, and m the average mass of sample weighted at the beginning of the analytical process.

LOD for MMHg were 3 pg L⁻¹ for Replim1, Replim2 and Replim3, and 4 pg L⁻¹ for Replim4 and Replim5. As an analogy with iHg, these LOD are consistent with already published works: 16 pg L⁻¹ [15] and 12 pg L⁻¹ [13].

Except for Replim1 (n=92) and Replim2 (n=59) where 31 and 9 of the samples analysed have shown results <LOD, MMHg was detected in all the samples from Replim3 (n=80), Replim4 (n=68) and Replim5 (n=43). Detection of MMHg in these pristine ecosystems is very tricky as only a few thousands of counts per second (cps) are finally detected on the chromatogram. Thus, a slight decrease in the sensitivity of the equipment and/or losses of mercury compounds during the analytical protocol will imply a decrease in the signal observed on the chromatogram: the more the user practice, the better are the results.

5. Purge experiment

Another concern drove our attention regarding the results for organomercury species. Indeed, the unfiltered non-gaseous mercury, calculated as the sum of iHg(II) and MMHg, ranges from 0.11 to 3.13 ng L⁻¹ in the subsurface water samples with a median value of 0.39 ng L⁻¹, while dissolved gaseous mercury (DGM) ranges from 0.02 to 10.79 ng L⁻¹ with a median value of 0.11 ng L⁻¹. Therefore, some possible Hg transformations might occur during the sampling leading to an underestimation of iHg(II) concentrations (degradation of DGM into iHg(II) during acidification). To answer properly to that question, in the last sampling campaigns June 2019, we collected in 125 mL Teflon container the water sample that has been previously purged to collect DGM species on gold-coated sand trap. These "purged samples" were acidified adding high-purity HCl (1% v/v) (Trace metal grade) and analysed by GC-ICP-MS following the protocol described in **3. Analysis**. The **Figure 3-11** shows a comparison between results obtained in purged and unfiltered samples for both MMHg and iHg(II). On the one hand, with good coefficient of determination R² (0.91) and a slope not significantly different from 1 (0.94±0.07), the results for iHg(II) analysis confirm the fact that gaseous Hg (DGM) is not a significant contributor to Hg(II) measured in unpurged samples. On the other hand, the slope obtained for the MMHg analysis is lower than 1 (R² = 0.98, slope = 0.75±0.02), thus suggesting that in unpurged samples some DMHg was also occurring. Regarding the methylated species quantified by GC-ICP-MS, removing the samples exhibiting suboxic to anoxic conditions (three last depths from Gentau, 8, 12 and 17.5m; last depth from Sabocos, 25m), the slope becomes not significantly different from 1 (R² = 0.91, slope = 0.92±0.09). Overall, in most of the cases, DMHg is negligible in comparison with MMHg, and the methylated species measured are mainly in the form of MMHg.

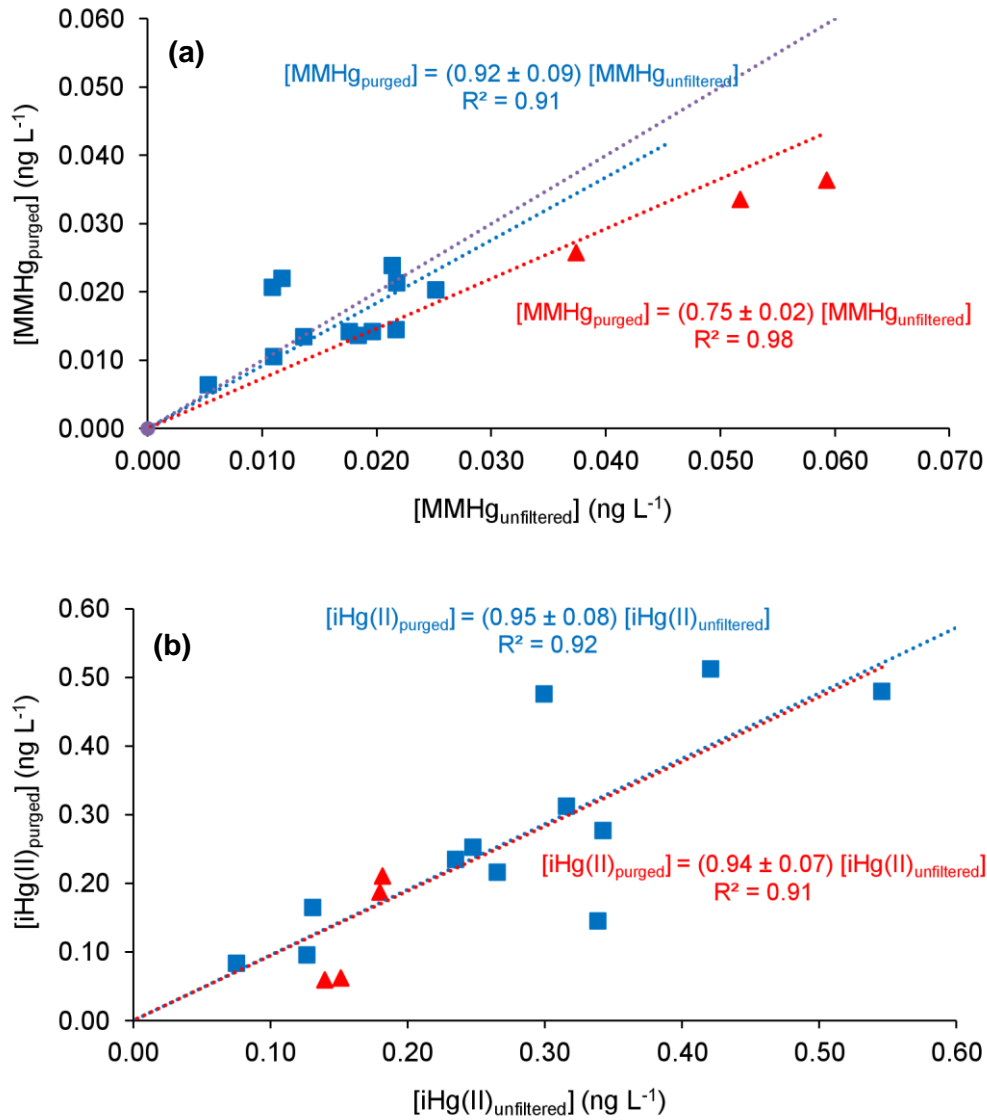


Figure 3-11: Comparison of (a) MMHg concentrations (ng L^{-1}) obtained in purged and unfiltered samples (last Lake Gentau depth not shown) and (b) iHg(II) concentrations (ng L^{-1}) obtained in purged and unfiltered samples for June 2019 sampling campaign. Square blue points correspond to samples collected in not well oxygenated depths (anoxic water). Red dashed line is the linear regression using all the samples while blue dashed line included only samples from oxic water.

3.3.5. Dissolved Gaseous Mercury (DGM)

The following analytical procedure is set up for the determination of DGM, which include both the Hg(0) and the DMHg. Nevertheless, regarding the very small levels of MeHg, i.e., the sum of MMHg and DMHg, in comparison with DGM, we can assume that DGM is mainly elemental mercury Hg(0).

1. Sampling

In analogy with the protocol for **Organometals (Hg species)**, specific cleaning procedure has been applied to the material used for DGM analysis. All plastic and glassware (containers, tubing, fittings, and moisture trap) were soaked successively in two HNO₃ solutions (10% v/v, deionized water) and one HCl solution (10% v/v, deionized water). Drying was processed in a clean atmosphere, under a laminar flow hood. Regarding the gold-coated sand traps, they were heated three times at 600°C during 1 min, under argon flow (100 mL min⁻¹). They were cooled down under a laminar flow hood and closed tightly with caps.

After collecting a water sample using Go-Flo sampler (**3.2 Sampling strategy**), the Teflon 250 mL container was rinsed three times with an aliquot of the water sample. Then, the Teflon container was filled overflow without headspace and following the Winkler method (introducing the silicone tubing down to the bottom to remove all bubbles). Teflon containers were closed tightly and stored in double PE Zip-lock bags in a portable cooler (5-10 °C).

The samples for gaseous Hg species (DGM) were processed close to the sampling site within 1 to 4 hours after sampling by stripping out and trapping the volatile Hg species from the water sample into a gold-coated sand trap [16,17] (**Figure 3-12**). For that purpose, the water sample was gently transferred through a gastight Teflon line into a Teflon purge vessel connected to a gold-coated sand trap and subsequently purged under an argon flow (500 mL min⁻¹, 20 min). The moisture was eliminated by an appropriate trap maintained at - 20 °C and the contamination from the atmosphere was minimised by connecting a second gold trap to the purge line. Gold traps were sealed with polypropylene Teflon-lined caps, stored in double PE zip-lock bags, and kept in the dark at 4 °C until analysis. All this procedure was carried out in an in-field laboratory close to the sampling usually installed in a mountain hut.

All this procedure was carried out in an in-field laboratory mounted in a van close to the sampling sites (**Figure 3-12**) or in the field laboratory inside the mountain hut.

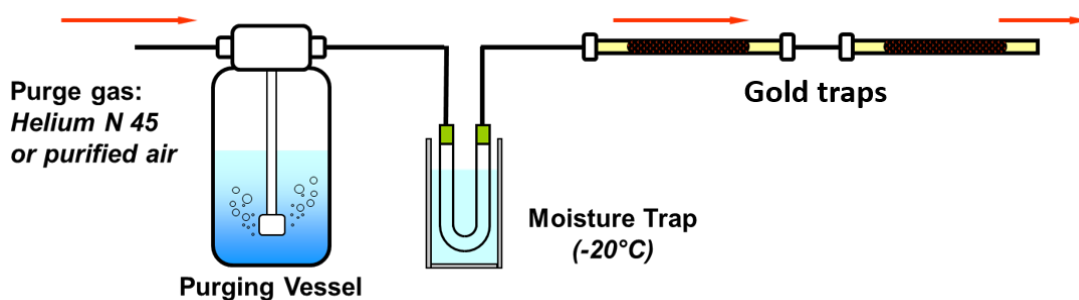


Figure 3-12: In-field purging system.

2. Analysis

The analysis was done by double amalgamation on gold-AFS (DA/Au-AFS) [17]. Briefly, gold-coated sand traps were thermodesorbed (1 min at 600°C followed by 1 min cooling) under argon flow (100 mL min⁻¹) to transfer and amalgamate the mercury onto an analytical preconcentration pure gold trap (gold wool, *Brooks rand Labs, USA*). Then, a 30-sec flash heating at 800 °C was applied to the analytical trap to transfer the mercury to the detector.

Thermodesorption efficiency was controlled by carrying out two consecutive analyses of the gold-coated sand trap. Gaseous mercury quantification was done by external calibration of the DA/Au-AFS device using a controlled Hg(0) source. Finally, the analysis of purge blanks allowed us estimating the efficiency of the sample treatment procedure.

3. Validation of the results

Analysis of the purge blanks allowed us estimating the efficiency of the sample treatment procedure. Considering the five sampling campaigns, the purge efficiency was assessed to reach $(95 \pm 3) \%$ ($n=12$), which allowed us to validate the method employed for the collection of the Hg gaseous species in lake water.

Regarding the limit of detection, it was calculated either with the results from a second analysis of a trap associated to a sample (sample blanks) or the results from the analysis of traps that were only transported during the sampling campaigns (storage blanks). The **Equation 3-3** was used to calculate LOD. LOD were quite constant over the sampling campaigns with values of 0.4, 0.1, 0.5, 0.2 and 0.2 pg L^{-1} for Replim1, Replim2, Replim3, Replim4 and Replim5, respectively, which is consistent with the LOD of 0.4 pg L^{-1} reported by *Bouchet et al.* [17].

4. Hg gaseous fluxes at air-water interface

According to *Sharif et al.* [18], gaseous Hg fluxes at the air-water interface (volatilization flux densities [FD]) ($\text{pmol m}^{-2} \text{h}^{-1}$) were calculated using the following equation:

Equation 3-6

$$\text{Volatilization FD} = k_w \times \left([\text{DGM}] - \frac{[\text{TGM}]}{H} \right)$$

where DGM is the concentration of DGM (i.e., $\text{Hg}(0)_{\text{aq}}$) measured in the subsurface water (pmol m^{-3}), TGM is the concentration of TGM (i.e., $\text{Hg}(0)_{\text{g}}$) measured in the atmosphere. As a reference value for atmospheric concentration of TGM we used the measurement performed at the Pic du Midi (2860 m asl) between February 2012 and January 2013 [19] (1.8 ng m^{-3}). H is the dimensionless Henry's Law constant corrected for water temperature and salinity [20] and k_w is the $\text{Hg}(0)$ gas transfer velocity (m h^{-1}) at the air-water interface. k_w was calculated, according to *Sharif et al.* [18] and using a specific model developed for CO_2 exchanges in sheltered lakes [21], as a function of wind speed.

The wind speed has been measured during daytime in Lake Gentau ($w = (3.2 \pm 1.4) \text{ m s}^{-1}$ in June 2018; $w = (1.4 \pm 0.8) \text{ m s}^{-1}$ in October 2018; $w = (2.6 \pm 2.0) \text{ m s}^{-1}$ in June 2019), Lake Sabocos ($w = (1.5 \pm 1.2) \text{ m s}^{-1}$ in June 2018; $w = (2.8 \pm 2.1) \text{ m s}^{-1}$ in October 2018; $w = (2.0 \pm 2.0) \text{ m s}^{-1}$ in June 2019), Lake Arratille ($w = (1.5 \pm 0.7) \text{ m s}^{-1}$ in June 2018) and Lake Azul ($w = (0.8 \pm 0.8) \text{ m s}^{-1}$ in June 2018). Thus, to estimate the FD in all the sampled lakes, two wind speed ranges will be considered: smooth breeze at 1 m s^{-1} to stronger wind at 3 m s^{-1} , which corresponds well to sheltered lakes conditions as proposed by *Cole and Caraco* [21].

3.3.6. Mercury species incubations

As mentioned in **3.2 Sampling strategy**, intensive monitoring was performed in ARA, GEN, SAB and AZU in order to better understand the dynamic of these lakes. In that sense, mercury species transformation potentials (methylation, demethylation, reduction) were determined through in-situ water incubations performed using isotopically enriched mercury species ($^{199}\text{iHg(II)}$, $^{201}\text{MMHg}$) according to the procedure published elsewhere [22–24].

Unfiltered water samples were collected to perform the incubation experiments. All material used for this methodology underwent the same cleaning procedure described for **3.3.4 Organometals (Hg species)** and **3.3.5 Dissolved Gaseous Mercury (DGM)**. Different conditions of incubation were tested depending on sampling depth (subsurface, middle depth, and bottom) or light exposure (Diurnal vs Dark) (**Table 3-7**).

After collecting a water sample using Go-Flo sampler (**3.2 Sampling strategy**), a first set of samples were prepared. Three 125 mL Teflon container (triplicate) per condition were directly filled with the water sample up to the top. Isotopically enriched spikes were added to each of the replicate to obtain concentrations in $^{199}\text{iHg(II)}$ and $^{201}\text{MMHg}$ of respectively 2 and 0.2 ng L⁻¹. It corresponds to about 10 times the natural concentrations observed in the studied ecosystems: high enough to overlap the natural concentrations and low enough to avoid any biotic stress. Using a simple mooring line at the sampling point, incubation bottles, either protected from the light or not, were placed at the corresponding depth. After 7 hours, the Teflon containers were collected, and the incubation processes were stopped by adding high-purity HCl (1 % v/v). Teflon containers were closed tightly and stored in double PE zip-lock bags in a portable cooler (5-10 °C), protected from light, and further transported and stored in the laboratory (5-10 °C). This first set of samples allows the determination of methylation, demethylation and MMHg loss rates.

A second set of samples was prepared to determine Hg reduction rates. After collection of water using the Go-Flo sampler (**3.2 Sampling strategy**), two 250 mL Teflon containers (duplicate) per condition were filled overflow without headspace and somehow following the protocol for the Winkler method and spiked with 2 and 0.2 ng L⁻¹ isotopically enriched $^{199}\text{iHg(II)}$ and $^{201}\text{MMHg}$, respectively, like in the previous case. They were incubated together with the samples of the first set. The difference in this case is that, at the end of the 7 hours, the elemental Hg (Hg(0)) was immediately recovered in gold-coated sand traps by purging the water samples.

Quantification was carried out by isotope pattern deconvolution (IPD) isotope dilution analysis (IDA) and analysis by capillary GC-ICP-MS for the water samples following the same protocol used for the determination of organomercury species (**3.3.4 Organometals (Hg species)**) [18]. The particularity is that the samples were spiked with other enriched isotope solution ($^{198}\text{iHg(II)}$ and $^{202}\text{MMHg}$).

The gaseous species trapped in the gold-coated sand traps were quantified by IPD and analysed by thermal desorption cryogenic trapping (CT) followed by GC-ICP-MS [18].

Table 3-7: Operating conditions for the incubation experiments. Note that PFA Teflon bottles (Nalgene) were used to allow in-situ transmission of both UV A and B during incubation [18].

Lake name	Sampling Depth	Light exposure	Water temperature (°C)	Incubation time (h)
Lac Gentau, June 2018 <ul style="list-style-type: none"> • Good weather • Analytes: iHg(II), MMHg and DGM 	Subsurface (0.5m)	Diurnal and Dark	6.87	7.4
	Middle depth (8m)	Diurnal and Dark	4.37	8.5
	Bottom (17m)	Dark	4.40	8.7
Lac Gentau, October 2018 <ul style="list-style-type: none"> • Cold, Rainy morning, Sunny spell midday, Cloudy afternoon • Analytes: iHg(II), MMHg and DGM 	Subsurface (0.5m)	Diurnal and Dark	12.80	7.2
	Middle depth (8m)	Diurnal and Dark	12.62	6.0
	Bottom (17m)	Dark	6.05	7.2
Lac Gentau, June 2019 <ul style="list-style-type: none"> • Cold, Windy, Sunny spell morning • Analytes: iHg(II), MMHg and DGM 	Subsurface (0.5m)	Diurnal and Dark	7.57	8.7
	Middle depth (8m)	Diurnal and Dark	5.82	8.5
	Bottom (17m)	Dark	4.30	8.5
Ibón de Sabocos, June 2018 <ul style="list-style-type: none"> • Good weather • Analytes: iHg(II), MMHg 	Subsurface (0.5m)	Diurnal and Dark	17.25	6.3
	Bottom (27m)	Dark	4.80	6.3
Ibón de Sabocos, October 2018 <ul style="list-style-type: none"> • Cold, Cloudy afternoon • Analytes: iHg(II), MMHg 	Subsurface (0.5m)	Diurnal and Dark	10.70	6.3
	Bottom (23m)	Dark	5.70	6.3
Ibón de Sabocos, June 2019 <ul style="list-style-type: none"> • Windy, Cloudy • Analytes: iHg(II), MMHg and DGM 	Subsurface (0.5m)	Diurnal and Dark	11.87	6.8
	Middle depth (9m)	Diurnal and Dark	7.07	6.8
	Bottom (25m)	Dark	4.87	6.8
Lac d'Arratille, June 2018 <ul style="list-style-type: none"> • Good weather • Analytes: iHg(II), MMHg and DGM 	Subsurface (0.5m)	Diurnal and Dark	5.70	6.0
	Middle depth (6m)	Dark	4.87	5.3
Lac d'Arratille, October 2018 <ul style="list-style-type: none"> • Rain, Wind, Bad weather • Analytes: iHg(II), MMHg and DGM 	Subsurface (0.5m)	Diurnal and Dark	8.32	5.3
	Bottom (12m)	Dark	5.64	6.7

The Hg species incubation experiment allowed us to calculate methylation (M) (iHg(II) into MMHg), demethylation (D) (MMHg into iHg(II)), MMHg loss (L) (MMHg into iHg(II) and Hg(0)) and reduction (R) (iHg(II) into Hg(0)) potentials (in % day⁻¹) according to *Rodriguez-Gonzales et al.* [24] with the following formula:

Equation 3-7

$$\text{Methylation (M)} = \frac{{}^{199}\text{MMHg}_t - {}^{199}\text{MMHg}_{t0}}{{}^{199}\text{iHg(II)}_{t0}} \times \frac{1440}{t} \times 100$$

Equation 3-8

$$\text{Demethylation (D)} = \frac{{}^{201}\text{iHg(II)}_t - {}^{201}\text{iHg(II)}_{t0}}{{}^{201}\text{MMHg}_{t0}} \times \frac{1440}{t} \times 100$$

Equation 3-9

$$\text{MMHg Loss (L)} = \frac{{}^{201}\text{MMHg}_{t0} - {}^{201}\text{MMHg}_t}{{}^{201}\text{MMHg}_{t0}} \times \frac{1440}{t} \times 100$$

Equation 3-10

$$\text{Reduction (R)} = \frac{{}^{199}\text{Hg(0)}_t - {}^{199}\text{Hg(0)}_{t0}}{{}^{199}\text{iHg(II)}_{t0}} \times \frac{1440}{t} \times 100$$

where t is the time of incubation (min); ^{xxx}iHg(II)_{t0}, ^{xxx}MMHg_{t0} and ^{xxx}Hg(0)_{t0} are the concentrations measured at the beginning of the incubation experiment, ^{xxx}iHg(II)_t, ^{xxx}MMHg_t and ^{xxx}Hg(0)_t are the concentrations measured at the end of the incubation experiment.

To predict the variations of MMHg concentrations in the lake, the potential net mercury methylation (ng L⁻¹ day⁻¹) was calculated using the methylation and demethylation rates (day⁻¹) according to the following formula:

Equation 3-11

$$\text{Net Methylation} = M \times [\text{iHg(II)}]_{\text{ambient}} - D \times [\text{MMHg}]_{\text{ambient}}$$

where M is the methylation potential (day⁻¹), [iHg(II)]_{ambient} is the ambient iHg(II) concentration (ng L⁻¹), D is the demethylation potential (day⁻¹), [MMHg]_{ambient} is the ambient MMHg concentration (ng L⁻¹).

It is worth noting that we chose to use demethylation rates instead of MMHg loss rates to avoid an underestimation of the net methylation since we have only determined MMHg production from iHg(II). Thus, in that case, we specifically consider the most significant reversible methylation/demethylation pathways between iHg(II) and MMHg forms.

3.3.7. Total selenium (Se)

1. Sampling

New Falcon tubes and Polypropylene containers do not need any cleaning step: they are fully suitable for Se analysis.

Two different kinds of samples were analysed: filtered and unfiltered.

For the filtered samples, after collecting a water sample using Go-Flo sampler (**3.2 Sampling strategy**), a Teflon container of 250 mL was rinsed three times with an aliquot of the water sample and filled with around 250 mL of the water sample. Then, a Teflon tube was connected to the syringe, and both were rinsed three times using the water sample from the 250 mL Teflon container. This last was also used to fill the syringe at the half before connecting the Sterivex Filter unit in place of the Teflon tube. The water sample collected in the syringe was passed through the filter and used to rinse three times a 15 mL Falcon tube. Finally, according to this protocol the 15 mL Falcon tube was filled with 15 mL of the water sample.

For the unfiltered samples, a 15 mL Falcon tube was directly rinsed three times with the water sample from the sampler and then filled with 15 mL of the water sample. In-field, all samples, filtered and unfiltered, were acidified at 1% v/v adding 150 μ L of nitric acid (HNO_3 , *Optima Grade, Fisher Scientific, USA*). Falcon tubes were closed tightly and stored in double PE Zip-lock bags in a portable cooler (5-10 °C), protected from light, during transportation to the fridge of the laboratory (5-10 °C).

2. Analysis

Back to the laboratory, unfiltered samples were digested. The 15 mL sample was weighted, and 300 μ L of HNO_3 and 150 μ L of HCl (final concentration of respectively 3% v/v and 1% v/v) were added prior to digestion using a DigiPrep (*SCP Science, Canada*). The facility method consisted in a temperature gradient for 30 min (0-90 °C), followed by a constant heating at 90°C for 3 hours. Finally, unfiltered digested samples were weighted and filtered using Sterivex filter unit prior to their analysis.

Analysis of both filtered and unfiltered samples was carried out by Q-ICP-MS (Agilent 7900) using H_2 as cell gas to reduce argon-based polyatomic interferences. Quality of the analytical protocol was assured by replicate analysis ($n \geq 2$), and multiple analysis of laboratory and in-field blanks ($n \geq 6$).

Andrea Romero (personal communication) gathers more detailed on the analytical performances and the development of the analytical method [2].

3.3.8. Silicate

1. Sampling

The sample used for silicate determination were the same as for major anions determination. Therefore, all details on the sampling are described in **3.3.2 Major anions**.

2. Analysis

Analysis was carried out by means of Flow Injection Analysis (FIA) [25] using the manifold depicted in **Figure 3-13**. The method employed is based on the classical Molybdenum Blue method but injecting the molybdate reagent (MR) in a sample carrier stream to improve sensibility. Detection was carried out spectrophotometrically at 810 nm. A molybdate reagent was prepared by dissolving 4.5 g of ammonium molybdate tetrahydrate ($(\text{NH}_4)_6\text{Mo}_7\text{O}_{24}\cdot 4\text{H}_2\text{O}$, Merck KGaA, Germany) in 400 mL of Milli-Q water and adding 3.7 mL of concentrated sulphuric acid (H_2SO_4 , Merck KGaA, Germany). Then, Oxalic acid (OA) was prepared by dissolving 25 g of oxalic acid ($\text{C}_2\text{H}_2\text{O}_4$, Merck KGaA, Germany) in 400 mL of Milli-Q water. Finally, Ascorbic acid (AA) was prepared by dissolving 12.5 g of ascorbic acid ($\text{C}_6\text{H}_8\text{O}_6$, Merck KGaA, Germany) in 400 mL of Milli-Q water. All three solutions were adjusted up to 500 mL using Milli-Q water.

The FIA system used for the analysis consisted in a 4-channel MiniPuls 2 peristaltic pump (*Gilson Inc., USA*) and an E60-CE model injection valve (*Valco Instruments Co. Inc., USA*) with an automated single injection port. All the Teflon tubings have an inner diameter of 0.8 mm. As a detector, an Ultrospec III model spectrophotometer (*Pharmacia LKB Biotechnology AB, Sweden*) with a nominal precision of 0.001 absorbance units was used. The analogue signal from the detector was sent to the computer using a PowerChrom 280 analogue to digital convertor (*eDAQ Pty Ltd, Australia*) with a precision of 0.001 mV.

For silicate content determination, external calibration was used with silicon standard solutions (CertiPUR, 1000 mg(Si) L⁻¹, *Sigma-Aldrich, USA*) in a matrix similar to the samples in salinity. Here, Milli-Q water was used as the salinity in the samples was very low or insignificant. According to the expected concentration in the samples, three different calibration ranges were prepared (0.05 to 0.3 mg(Si) L⁻¹; 0.3 to 1.5 mg(Si) L⁻¹; 1.5 to 6 mg(Si) L⁻¹). For each of these calibration ranges, three laboratory blank solutions were also measured. All samples, together with the calibration solutions, were analysed once.

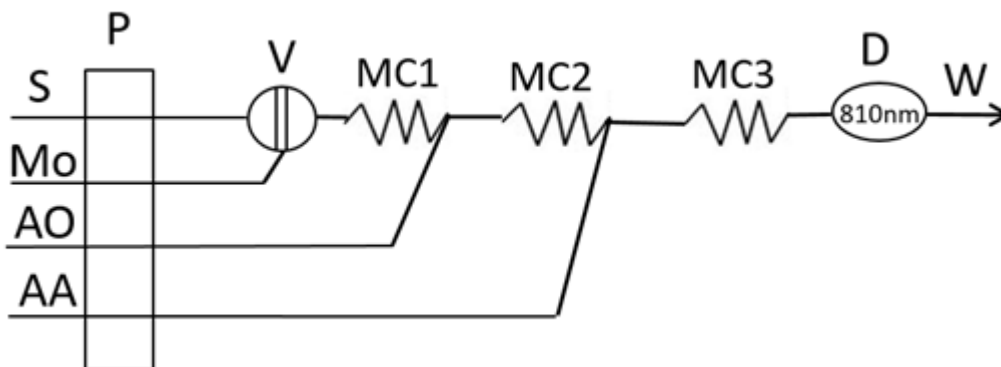


Figure 3-13: FIA manifold used for silicate determination

P: Peristaltic pump / V: Injection valve (500 μL) / D: Detector / MC1, MC2 and MC3: Mixing coils (100, 25 and 45 cm, respectively) / S: Sample (750 $\mu\text{L min}^{-1}$) / Mo: Molybdate reagent (750 $\mu\text{L min}^{-1}$) / AO: Oxalic acid reagent (750 $\mu\text{L min}^{-1}$) / AA: Ascorbic acid reagent (750 $\mu\text{L min}^{-1}$) / W: Waste.

3.3.9. Total Organic Carbon (TOC)

1. Sampling

100 mL narrow neck glass bottles were rinsed successively with tap, deionized and Milli-Q water, and then dried in an oven. The glass caps were first cleaned from sealant vacuum grease with the help of a paper tissue before being cleaned with a detergent and rinsed with water in the same way as the bottles. Once dried, a thin layer of vacuum grease was applied to them again.

With the help of the silicon tubing connected to the Go-Flo sampler, the glass bottle was filled from the bottom, letting the water overflow until an approximate volume similar to that of the bottle was removed. Then, once the bottle was filled, a plastic pipette was used to leave a headspace of 1 % the volume of the bottle to allow the water expansion. For chemical preservation, 50-125 μL of the saturated HgCl_2 solution was added to the bottle using a micropipette and a new tip each time (0.02-0.05 % v/v) to prevent altering the carbon distributions in the sample due to biological activity. The bottle was closed with its glass cap, the cap was wrapped tightly using sealant tape, and the bottle was mixed gently. As fresh as possible and protected from light, the bottles wrapped in air bubble plastic bags were transported to the fridge of the laboratory (5-10 $^{\circ}\text{C}$).

2. Analysis

Total Organic Carbon was determined by catalytic combustion of the sample at 680 °C using a special analyser, Shimadzu TOC-V (*Shimadzu Corporation, Japan*). 20 mL of the samples were placed into the automatic sampler. As the organic carbon concentrations are very low in these samples, the inorganic carbon was first stripped from the sample using 20 µL of a 2 mol L⁻¹ HCl solution (*Bernd Kraft GmbH, Germany*), which transforms it to carbon dioxide (CO₂) in a quantitative way and purged away for 90 sec with the carrier gas, a synthetic air mixture (Zero K50S) 99.999 % free of CO₂ (*Carbueros Metálicos, Spain*). Then, 100 µL of the acidified sample was injected in the combustion column. The organic carbon was converted to CO₂, and it was quantitatively determined with the help of a high sensitivity Non Dispersive InfraRed (NDIR) detector. If volatile organic compounds are present, then the method yields the Non Purgeable Organic Carbon (NPOC) instead.

External calibration, prepared daily with Milli-Q water up to 6 mg(C) L⁻¹, was carried out using a NIST traceable potassium hydrogen phthalate solution (*Panreac Química SLU, Spain*). To ensure precision of the results, replicate analysis were processed for laboratory blanks (n=10), standard solutions (n=5) and samples (n=3).

3. Validation of the results

The LOD was calculated according to **Equation 3-3** using the laboratory blanks results. Analysis of the four sampling campaigns samples were done along three different analytical sessions. The LODs obtained for these three analytical sessions were 0.12, 0.25 and 0.17 mg(C) L⁻¹, and all the results obtained were above the LOD associated to their analytical session.

A reproducibility of 5% (RSD) was obtained after replicate analysis of the same sample.

3.3.10. Carbon Dioxide (CO₂) system parameters

1. Sampling

250 mL narrow neck glass bottles were rinsed successively with tap, deionized and Milli-Q water, and then dried in a clean atmosphere. The glass caps were first cleaned from sealant vacuum grease with the help of a paper tissue before being cleaned with a detergent and rinsed with water in the same way as the bottles. Once dried, a thin layer of vacuum grease was applied to them again.

With the help of the silicon tubing connected to the Go-Flo sampler, the glass bottle was filled from the bottom, letting the water overflow until an approximate volume similar to that of the bottle has been delivered. Then, once the bottle was filled, the use of a plastic pipette allowed to leave a headspace of 1 % the volume of the bottle. For chemical preservation, 50-125 µL of the saturated HgCl₂ (*Merck, Germany*) solution was added to the bottle using a micropipette and a new tip each time (0.02-0.05 % v/v). The bottle was closed with its glass cap, the cap was wrapped tightly using the sealant tape, and the bottle was mixed gently. As fresh as possible and protected from light, the bottles wrapped in air bubble plastic bags were transported to the fridge of the laboratory (5-10 °C).

2. Analysis

Total Alkalinity and Dissolved Inorganic Carbon were measured using a VINDTA 3C instrument (Versatile Instrument for the Determination of Total inorganic carbon and titration Alkalinity) (*Marianda, Germany*) (**Figure 3-14**). The method for their determination in the high-altitude lakes has been adapted from *Kortazar et al.* who determined TA and DIC in estuarine waters [26], and has been already published [27]. It is fully described in the next chapter of this manuscript. Here we describe a short resume of the procedure.

All the acidity constant that are used for the calculation of the TA are at 25 °C so it is important working at a constant temperature of 25 °C. For that purpose, samples were placed in a Julabo CORIO CD-BC26 Heating Circulator (*Julabo GmbH, Germany*) also connected to the VINDTA system to guarantee a temperature of 25 °C.



Figure 3-14: Equipment used for the determination of TA and DIC that includes the VINDTA 3C system coupled with a CM5015 coulometer and a 785 DMP Titrino.

Dissolved Inorganic Carbon was quantified first in the samples by means of a coulometric determination [28] using the VINDTA 3C instrument fitted with a CM5015 Coulometer with the CM5011 emulator (*UIC Inc., USA*). The inorganic carbon was stripped from the sample pumped by the VINDTA 3C (20 mL using the small pipette) system using 10% v/v phosphoric acid (H_3PO_4) solution (*PanReac, Spain*), which transforms it to CO_2 in a quantitative way. The gas carrier, 99.999% nitrogen (N_2) (*Messer Group GmbH, Germany*), was filtrated ahead the equipment with a CO_2 trap (*Supelco, Sigma Aldrich, USA*). After, the CO_2 transported is titrated coulometrically in a special cell with cathode solution, anode solution and KI (*UIC Inc., USA*). Counts were measured every minute until the increment went four times below the blank, measured at the beginning of the analytical session. A moisture trap made up with a few grams of granulated anhydrous magnesium perchlorate (*Alfa Aesar, Thermo Fisher (Kandel) GmbH, Germany*) was also placed before the cell to remove water. It is worth noting that the VINDTA system cleans the tubes and the small pipette with a few millilitres of the sample to be analysed at the beginning of the experiment.

To ensure the accuracy of the DIC measurements, Certified Reference Material for oceanic CO₂ measurements (*A. Dickson, Scripps Institution of Oceanography, USA*) was analysed. A correction factor was calculated by dividing the average experimentally obtained CRM values by the certified one. This factor was applied to the DIC values obtained experimentally for the samples collected for better accuracy of the results.

4. Total Alkalinity (TA)

Total Alkalinity was determined in the samples by means of an open cell potentiometric titration using the VINDTA 3C instrument. The titration was carried out with hydrochloric acid (HCl, Tracepur) (*Merck KGaA, Germany*) until a pH value around 4 was reached, corresponding to the carbonic acid end-point. Since the values of the DIC and TA are very similar in these samples, the previously determined DIC values were used to predict the concentration of HCl needed to titrate each sample. Four different HCl solutions were prepared (0.03, 0.015, 0.036 and 0.1 mol L⁻¹). To ensure the cleanliness of the system, a milli-Q water solution was used to remove the acid residue in the titration cell. Moreover, a few millilitres of samples were passed through the tubes and the pipettes to rinse them before the TA determination.

An extremely accurate determination of the titrant HCl concentration is mandatory. For that, a potentiometric standardisation with tris(hydroxymethyl)aminomethane (Tris) (*Panreac Química SLU, Spain*) was performed and the equivalence volume was calculated using Gran's equations [29].

Once the titration was completed, TA was determined by non-linear least squares procedure with volume fitting using the Levenberg-Marquardt Algorithm (LMA) using the Microsoft Office Excel spreadsheet. The added volume values were theoretically calculated with the following equations:

Equation 3-12

$$V_{\text{calc},i} = \frac{m_0 \cdot (\text{term} - \text{TA})}{(C_{\text{H}}^0 - \text{term}) \cdot \delta_{\text{sample}}}$$

where C_{H}^0 is the concentration of the HCl titrant, δ_{sample} is the density of the sample, m_0 the sample mass and *term* is defined as:

Equation 3-13

$$\begin{aligned} \text{term} = & [\text{H}^+]_{\text{F}} + [\text{HSO}_4^-] + [\text{HF}] + [\text{H}_3\text{PO}_4] + [\text{organic acids}] - [\text{HCO}_3^-] - 2[\text{CO}_3^{2-}] - [\text{B}(\text{OH})_4^-] - [\text{OH}^-] \\ & - [\text{HPO}_4^{2-}] - 2[\text{PO}_4^{3-}] - [\text{SiO}(\text{OH})_3^-] - [\text{NH}_3] - [\text{organic bases}] \end{aligned}$$

The difference between the calculated volume and the experimental volume was minimised using the Solver complement available in the Microsoft Office Excel software by refining the standard potential of the electrode (E^0), TA and the total concentration and acidity constant of the organic alkalinity. In reality, the organic alkalinity would be the sum of all the acid-base species that are not considered in the classical equation for TA determination (i.e., without [organic acids] and [organic bases]).

5. pH and fugacity of CO₂ (fCO₂)

Using DIC and TA values, other parameters that characterise the CO₂ system such as the pH and the fugacity (fCO₂) were calculated with the help of the CO2SYS software [27]. Since this program has been developed for marine measurements, The MATLAB script version used in this work was modified to implement the set of stability constants for the carbonate system published by *Kortazar et al.* [26] and the organic alkalinity contribution (concentration and associated pK_a) determined previously with the TA.

Table 3-8: Summary of the parameters analysed together with their associated analytical protocol.

Parameter	Matrix	Method	Material	Reagents
Physicochemical parameters (depth, temperature, conductivity, salinity, dissolved oxygen, pH, oxidation-reduction potential and chlorophyll-a)	Unfiltered water	Multiparametric probe (in-situ measurements)	-	-
Major anions (Fluoride F ⁻ , Chloride Cl ⁻ , Nitrite NO ₂ ⁻ , Bromide Br ⁻ , Nitrate NO ₃ ⁻ , Phosphate PO ₄ ³⁻ , and Sulphate SO ₄ ²⁻)	Filtered water	Ionic chromatography	Plastic containers (50 mL); syringes; syringe-filters (polyamide, 0.45 µm); Zip-lock bags	<u>Cleaning:</u> none <u>In-situ treatment:</u> none <u>Analysis:</u> Milli-Q water (18.2 MΩ cm); 4.5 mmol L ⁻¹ Na ₂ CO ₃ / 0.8 mmol L ⁻¹ NaHCO ₃ ; Standards commercial solutions of the anions of interest
Major, trace and ultra-trace elements	Filtered and unfiltered water	ICP-MS or HR-ICP-MS	Plastic containers (50 mL); syringes; syringe-filters (PVDF, 0.45 µm); Zip-lock bags	<u>Cleaning:</u> Elix water (10-15 MΩ cm); Milli-Q water (18.2 MΩ cm); HNO ₃ (Analytical grade) <u>In-situ treatment:</u> sub-boiling twice-distilled HNO ₃ (Tracepur grade) for acidification <u>Analysis:</u> Milli-Q water (18.2 MΩ cm); Standards commercial solutions of the cations of interest; Internal standards (usually Sc, Y, In, Bi, Ge or similar); Argon
Organometals (Inorganic mercury iHg(II), Monomethylmercury MMHg and Butyltin BuSn)	Filtered and unfiltered water	GC-ICP-MS using isotope dilution analysis	Teflon containers (125 or 250 mL + one single 250 mL for filtration operation); Luer-lock Teflon or PP syringes (plunger without rubber); Sterivex Filter units (PVDF, 0.22µm); Teflon tubings (10 cm length, ¼ inch OD, for filtration operation); PE Wash bottle; Zip-lock bags	<u>Cleaning:</u> deionized water (13 MΩ cm); HNO ₃ (Analytical grade); HCl (Analytical grade) <u>In-situ treatment:</u> CH ₃ COOH (Trace metal grade) for acidification <u>Analysis:</u> Milli-Q water (18.2 MΩ cm); CH ₃ COOH (Trace metal grade) and Sodium acetate trihydrate (ACS grade) for buffer preparation; NH ₃ and HCl (Optima grade) for pH adjustment; NaBEt ₃ as derivatizing agent; Isooctane (HPLC grade) as organic solvent; Thallium (Claritas PPT® Grade) as internal standard; ²⁰¹ Hg-enriched Monomethylmercury, ¹⁹⁹ Hg-enriched Inorganic mercury and ¹¹⁹ Sn-enriched Butyltin mix standard solutions; Argon and Helium
Dissolved Gaseous Mercury (DGM)	Unfiltered water	Preconcentration on gold trap and detection by Double amalgamation on gold-AFS (DA/Au-AFS)	Teflon containers (250 mL); Nitrogen cylinder or Pump-Rotameter; Gas washing bottle; dewar vessel; gold-coated sand trap; Zip-lock bags	<u>Cleaning:</u> deionized water (13 MΩ cm); HNO ₃ (Analytical grade); HCl (Analytical grade) <u>In-situ treatment:</u> Ice cubes and ethanol or acetone (Analytical or technical grade) for moisture trap preparation <u>Analysis:</u> Pure metallic mercury standard for quantification by Headspace injection/Double amalgamation on gold-AFS (DA/Au-AFS); Argon

Table 3-8 (continued)

Total selenium	Filtered and unfiltered water	ICP-MS	Polypropylene (PP) Falcon tubes (15 mL) and a PP or Teflon 250 mL for filtration operation; Luer-lock Teflon or PP syringes (plunger without rubber); Sterivex Filter units (PVDF, 0.22µm); Teflon tubings (10 cm length, ¼ inch OD, for filtration operation); PE Wash bottle; Zip-lock bags	<p><u>Cleaning:</u> none</p> <p><u>In-situ treatment:</u> HNO₃ (Optima grade) for acidification</p> <p><u>Analysis:</u> HNO₃ and HCl (Trace metal grade) for digestion; Single element calibration standard for ICP-MS for total selenium determination</p>
Silicate	Filtered and unfiltered water	Flow Injection Analysis (FIA)	Plastic containers (50 mL); syringes; syringe-filters (polyamide, 0.45 µm); Zip-lock bags	<p><u>Cleaning:</u> Tap water, Elix water (10-15 MΩ cm) and Milli-Q water (18.2 MΩ cm)</p> <p><u>In-situ treatment:</u> none</p> <p><u>Analysis:</u> Milli-Q water (18.2 MΩ cm); ammonium molybdate tetrahydrate; H₂SO₄; oxalic acid; ascorbic acid; Silicon standard solution for external calibration</p>
Total Organic Carbon (TOC)	Unfiltered water	TOC analyser	100 mL narrow neck glass bottles provided with glass caps; protective air bubble plastic bags; silicon rubber tubing; plastic pipette; sealant tape; micropipette; tips	<p><u>Cleaning:</u> Tap water, Elix water (10-15 MΩ cm) and Milli-Q water (18.2 MΩ cm)</p> <p><u>In-situ treatment:</u> Saturated HgCl₂ solution for sample preservation</p> <p><u>Analysis:</u> Milli-Q quality water (18.2 MΩ cm); HCl (p.a. tracepur); HK-Phtalate (NIST traceable standard); carrier gas Zero K50S 99.999 % free of CO₂</p>
Dissolved Inorganic Carbon (DIC) and Total Alkalinity (TA)	Unfiltered water	VINDTA	250 mL narrow neck glass bottles provided with glass caps; protective air bubble plastic bags; silicon rubber tubing; plastic pipette; sealant tape; micropipette; tips	<p><u>Cleaning:</u> Tap water, Elix water (10-15 MΩ cm) and Milli-Q water (18.2 MΩ cm)</p> <p><u>In-situ treatment:</u> Saturated HgCl₂ solution for sample preservation</p> <p><u>Analysis:</u></p> <ul style="list-style-type: none"> - DIC: H₃PO₄ (p.a. tracepur); Anode and Cathode solutions; KI (p.a.) - TA: HCl (Tracepur); NaCl rinsing solution; tris(hydroxymethyl)aminomethane (Tris)

3.4. References

- [1] D.G. Zaharescu, P.S. Hooda, C.I. Burghilea, A. Palanca-Soler, A Multiscale Framework for Deconstructing the Ecosystem Physical Template of High-Altitude Lakes, *Ecosystems*. 19 (2016) 1064–1079. <https://doi.org/10.1007/s10021-016-9987-9>.
- [2] M. Bueno, B. Duval, E. Tessier, A. Romero-Rama, L. Kortazar, L.A. Fernandez, A. De Diego, D. Amouroux, Selenium distribution and speciation in waters of pristine alpine lakes from central-western Pyrenees (France-Spain), *Environ. Sci.: Processes Impacts*. (2022) 10.1039/D1EM00430A. <https://doi.org/10.1039/D1EM00430A>.
- [3] S. Gascoin, M. Grizonnet, M. Bouchet, G. Salgues, O. Hagolle, Theia Snow collection: high-resolution operational snow cover maps from Sentinel-2 and Landsat-8 data, *Earth System Science Data*. 11 (2019) 493–514. <https://doi.org/10.5194/essd-11-493-2019>.
- [4] E. Serrano-Cañadas, Glacial evolution of the upper Gallego Valley (Panticosa mountains and Ribera de Biescas, Aragonese Pyrenees, Spain), *Pirineos : Revista de Ecología de Montaña*. 138 (1991) 23. <https://doi.org/10.3989/pirineos.1991.v138.191>.
- [5] Z. Santolaria, T. Arruebo, J.S. Urieta, F.J. Lanaja, A. Pardo, J. Matesanz, C. Rodriguez-Casals, Hydrochemistry dynamics in remote mountain lakes and its relation to catchment and atmospheric features: the case study of Sabocos Tarn, Pyrenees, *Environmental Science and Pollution Research*. 22 (2015) 231–247. <https://doi.org/10.1007/s11356-014-3310-0>.
- [6] L.L. Bridgewater, R.B. Baird, A.D. Eaton, E.W. Rice, American Public Health Association, American Water Works Association, Water Environment Federation, eds., *Standard methods for the examination of water and wastewater*, 23rd edition, American Public Health Association, Washington, DC, 2017.
- [7] J.D. Pfaff, D.P. Hautman, Determination of inorganic anions in drinking water by ion chromatography, 40. ISBN : 13 : 978-1289186807.
- [8] N. Prieto-Taboada, O. Gómez-Laserna, I. Martínez-Arkarazo, M.A. Olazabal, J.M. Madariaga, Optimization of two methods based on ultrasound energy as alternative to European standards for soluble salts extraction from building materials, *Ultrasonics Sonochemistry*. 19 (2012) 1260–1265. <https://doi.org/10.1016/j.ultsonch.2012.03.002>.
- [9] Method 1669: Sampling Ambient Water for Trace Metals at EPA Water Quality Criteria Levels, 39.
- [10] Method 1640: Determination of Trace Elements in Water by Preconcentration and Inductively Coupled Plasma-Mass Spectrometry, 65.
- [11] C.M. Wood, Silver, in: *Fish Physiology*, Elsevier, 2011: pp. 1–65. [https://doi.org/10.1016/S1546-5098\(11\)31023-0](https://doi.org/10.1016/S1546-5098(11)31023-0).
- [12] A.G. Bravo, D.N. Kothawala, K. Attermeyer, E. Tessier, P. Bodmer, J.L.J. Ledesma, J. Audet, J.P. Casas-Ruiz, N. Catalán, S. Cauvy-Fraunié, M. Colls, A. Deininger, V.V. Evtimova, J.A. Fonvielle, T. Fuß, P. Gilbert, S. Herrero Ortega, L. Liu, C. Mendoza-Lera, J. Monteiro, J.-R. Mor, M. Nagler, G.H. Niedrist, A.C. Nydahl, A. Pastor, J. Pegg, C. Gutmann Roberts, F. Pilotto, A.P. Portela, C.R. González-Quijano, F. Romero, M. Rulík, D. Amouroux, The interplay between total mercury, methylmercury and dissolved organic matter in fluvial systems: A latitudinal study across Europe, *Water Research*. 144 (2018) 172–182. <https://doi.org/10.1016/j.watres.2018.06.064>.
- [13] J. Cavalheiro, C. Sola, J. Baldanza, E. Tessier, F. Lestremau, F. Botta, H. Preud'homme, M. Monperrus, D. Amouroux, Assessment of background concentrations of organometallic compounds (methylmercury, ethyllead and butyl- and phenyltin) in French aquatic environments, *Water Research*. 94 (2016) 32–41. <https://doi.org/10.1016/j.watres.2016.02.010>.
- [14] S. Clémens, M. Monperrus, O.F.X. Donard, D. Amouroux, T. Guérin, Mercury speciation in seafood using isotope dilution analysis: A review, *Talanta*. 89 (2012) 12–20. <https://doi.org/10.1016/j.talanta.2011.12.064>.
- [15] M. Monperrus, E. Tessier, S. Veschambre, D. Amouroux, O. Donard, Simultaneous speciation of mercury and butyltin compounds in natural waters and snow by propylation and species-specific

- isotope dilution mass spectrometry analysis, *Analytical and Bioanalytical Chemistry*. 381 (2005) 854–862. <https://doi.org/10.1007/s00216-004-2973-7>.
- [16] D. Amouroux, E. Tessier, C. Pécheyran, O.F.X. Donard, Sampling and probing volatile metal(loid) species in natural waters by in-situ purge and cryogenic trapping followed by gas chromatography and inductively coupled plasma mass spectrometry (P-CT–GC–ICP/MS), *Analytica Chimica Acta*. 377 (1998) 241–254. [https://doi.org/10.1016/S0003-2670\(98\)00425-5](https://doi.org/10.1016/S0003-2670(98)00425-5).
- [17] S. Bouchet, E. Tessier, M. Monperrus, R. Bridou, J. Clavier, G. Thouzeau, D. Amouroux, Measurements of gaseous mercury exchanges at the sediment–water, water–atmosphere and sediment–atmosphere interfaces of a tidal environment (Arcachon Bay, France), *Journal of Environmental Monitoring*. 13 (2011) 1351. <https://doi.org/10.1039/c0em00358a>.
- [18] A. Sharif, M. Monperrus, E. Tessier, S. Bouchet, H. Pinaly, P. Rodriguez-Gonzalez, P. Maron, D. Amouroux, Fate of mercury species in the coastal plume of the Adour River estuary (Bay of Biscay, SW France), *Science of The Total Environment*. 496 (2014) 701–713. <https://doi.org/10.1016/j.scitotenv.2014.06.116>.
- [19] X. Fu, N. Maruszczak, X. Wang, F. Gheusi, J.E. Sonke, Isotopic Composition of Gaseous Elemental Mercury in the Free Troposphere of the Pic du Midi Observatory, France, *Environmental Science & Technology*. 50 (2016) 5641–5650. <https://doi.org/10.1021/acs.est.6b00033>.
- [20] M.E. Andersson, K. Gårdfeldt, I. Wängberg, D. Strömberg, Determination of Henry's law constant for elemental mercury, *Chemosphere*. 73 (2008) 587–592. <https://doi.org/10.1016/j.chemosphere.2008.05.067>.
- [21] J.J. Cole, N.F. Caraco, Atmospheric exchange of carbon dioxide in a low-wind oligotrophic lake measured by the addition of SF₆, *Limnology and Oceanography*. 43 (1998) 647–656. <https://doi.org/10.4319/lo.1998.43.4.0647>.
- [22] M. Monperrus, E. Tessier, D. Amouroux, A. Leynaert, P. Huonnic, O.F.X. Donard, Mercury methylation, demethylation and reduction rates in coastal and marine surface waters of the Mediterranean Sea, *Marine Chemistry*. 107 (2007) 49–63. <https://doi.org/10.1016/j.marchem.2007.01.018>.
- [23] S. Bouchet, D. Amouroux, P. Rodriguez-Gonzalez, E. Tessier, M. Monperrus, G. Thouzeau, J. Clavier, E. Amice, J. Deborde, S. Bujan, J. Grall, P. Anschutz, MMHg production and export from intertidal sediments to the water column of a tidal lagoon (Arcachon Bay, France), *Biogeochemistry*. 114 (2013) 341–358. <https://doi.org/10.1007/s10533-012-9815-z>.
- [24] P. Rodriguez-Gonzalez, S. Bouchet, M. Monperrus, E. Tessier, D. Amouroux, In situ experiments for element species-specific environmental reactivity of tin and mercury compounds using isotopic tracers and multiple linear regression, *Environmental Science and Pollution Research*. 20 (2013) 1269–1280. <https://doi.org/10.1007/s11356-012-1019-5>.
- [25] J. Ma, R.H. Byrne, Flow injection analysis of nanomolar silicate using long pathlength absorbance spectroscopy, *Talanta*. 88 (2012) 484–489. <https://doi.org/10.1016/j.talanta.2011.11.019>.
- [26] L. Kortazar, D. Milea, O. Gómez-Laserna, L.A. Fernández, Accurate determination of total alkalinity in estuarine waters for acidification studies, *TrAC Trends in Analytical Chemistry*. 114 (2019) 69–80. <https://doi.org/10.1016/j.trac.2019.01.010>.
- [27] L. Kortazar, B. Duval, O. Liñero, O. Olamendi, A. Angulo, D. Amouroux, A. de Diego, L.A. Fernandez, Accurate determination of the total alkalinity and the CO₂ system parameters in high-altitude lakes from the Western Pyrenees (France – Spain), *Microchemical Journal*. 152 (2020) 104345. <https://doi.org/10.1016/j.microc.2019.104345>.
- [28] A.G. Dickson, C.L. Sabine, J.R. Christian, C.P. Barger, North Pacific Marine Science Organization, eds., *Guide to best practices for ocean CO₂ measurements*, North Pacific Marine Science Organization, Sidney, BC, 2007. ISBN : 978-1-897176-07-8.
- [29] G. Gran, Determination of the equivalence point in potentiometric titrations. Part II, *The Analyst*. 77 (1952) 661. <https://doi.org/10.1039/an9527700661>.

**4. Accurate determination of the total alkalinity
and the CO₂ system parameters in high
altitude lakes from the Western Pyrenees
(France – Spain)**

4.1. Abstract

Studies on the CO₂ system in alpine lakes are performed by scientists of different areas and, therefore, it is crucial to establish common procedures to investigate the chemical properties of these ecosystems to reach comparable results and perform meaningful long-term studies. In this work, a robust procedure was developed to determine the total alkalinity in high altitude mountain lakes which allows the determination of the CO₂ system parameters with improved precision and accuracy. In the potentiometric titration of the samples with HCl, used for the Total Alkalinity determination, the fitting between experimental and calculated titration points was greatly improved by incorporating the contribution of new acid-base species, which had not been accounted for in previous works. This methodology can be used not only for alpine lakes but also for other natural water systems where the contribution of an extended set of acid-base species is normally not considered. A modified script has been also developed for the Matlab version of the CO₂SYST program, which allows an adequate calculation of the rest of the CO₂ system parameters. The calculated pK_a values of the new acid-base species are consistent in nearly all the lakes, ranging from 6.5 to 7, suggesting the similar nature of the acid-base species in all the lakes and that in the Ayous area a different number and/or type of species could be present. Furthermore, the values of all the chemical parameters studied were explained considering the geochemistry of the bedrock.

Keywords:

Total Alkalinity; Data analysis; CO₂ system; High altitude mountain lakes; Pyrenees

L. Kortazar, B. Duval, O. Liñero, O. Olamendi, A. Angulo, D. Amouroux, A. de Diego, L.A. Fernandez, Accurate determination of the total alkalinity and the CO₂ system parameters in high-altitude lakes from the Western Pyrenees (France – Spain), *Microchemical Journal*. 152 (2020) 104345. <https://doi.org/10.1016/j.microc.2019.104345>.

4.2. Introduction

Alpine lakes are iconic landscapes in mountain regions, where they frequently play an important role as economic and touristic resources. From an environmental point of view, as these ecosystems are usually far from local sources of pollution, they are particularly sensitive to the atmospheric deposition of pollutants and climate change due to climatic factors, shallow soil cover, the modest dimension of the watershed and rapid flushing rates. Alpine lakes are often located in crystalline bedrocks, which implies low ionic strength waters with a poor buffer capacity. It has been reported that physical, chemical, and biological lake properties respond rapidly to climate-related changes [1–5]. Studies performed in lakes can provide some of the early indications of the effects of climate change on the ecosystem's structure and function as well as the consequences for ecosystem services [5]. Particularly, the study of the Pyrenean lakes is of special interest due to their geographical situation, which makes the chemistry of precipitation to be influenced by the air masses with different origins: Mediterranean, Atlantic, Saharan and Continental [1].

Since the industrial revolution times, CO₂ is being produced and emitted to the atmosphere in important quantities. The CO₂ concentration in the atmosphere has increased from pre-industrial levels of around 280 parts per million (ppm) up to 415 ppm in May 2019 [6,7] (updated regularly at: <https://www.esrl.noaa.gov/gmd/ccgg/trends/>), which means about a 50% increment. The CO₂ concentration is predicted to keep rising and may reach levels of around 936 ppm by the year 2100 according to the Representative Concentration Pathway (RCP) 8.5 of the IPCC which is the “high emission scenario” [6], and could have negative effects in different ecosystems.

For instance, a large part of the excess of the emitted CO₂ is absorbed by various natural sinks, the most well-known being oceans, which absorb the excess of CO₂, lowering its concentration in the atmosphere but making the oceans more acidic [6,8,9]. This phenomenon is known as ocean acidification. The pH of the ocean has lowered about 0.1 units from pre-industrial levels [10] and by the end of the century, the average surface ocean pH could be 0.2 - 0.4 units lower than it is today [6,11]. Although this phenomenon is referred to oceanic waters, every natural water system is being affected by this excess of atmospheric CO₂ in different ways and its study in different natural water bodies is of great interest. Since the effects of the increase of the atmospheric CO₂ concentration will be appreciated with difficulty in short periods, it is crucial to use a proper methodology to study the CO₂ system to obtain results with the highest possible accuracy and precision. This has been the highest priority for oceanographers in the last decades.

When the “quality” of analytical measurements is being tested, it is very important to consider the scientific application that they are required for, and the maximum uncertainty that is considered appropriate for that application. A quite recent report describing plans for a Global Ocean Acidification Observing Network (GOA-ON) articulates two such applications: a “weather” goal and a “climate” goal [12]. The former is defined as a set of measurements of a quality that is sufficient to identify relative spatial patterns and short-term variations, supporting mechanistic responses to the impact on local, immediate ocean acidification dynamics. This implies an uncertainty of ~10 μmol kg⁻¹ in measurements

of total alkalinity (TA) and dissolved inorganic carbon (DIC) (~0.5 %). The “climate” goal is defined as a set of measurements of a quality that is enough to assess long-term trends with a defined level of confidence, supporting detection of the long-term anthropogenically driven changes in hydrographic conditions. This objective is much more demanding and implies an uncertainty of ~2 μmol kg⁻¹ in measurements of TA and DIC (~0.1 %). These “weather” and “climate” goals were used by Bockmon and Dickson [13] at their interlaboratory comparison studies.

To characterise the CO₂ chemistry, four measurable parameters can be used: TA, (DIC), pH and partial pressure of CO₂ (pCO₂) or fugacity (fCO₂) [14]. Given the thermodynamic relation between all of them, it is only necessary to experimentally measure two of them to calculate the other two if the temperature, ionic strength, pressure and the concentrations of other acid-base species are known [9,14–16]. The equations used to obtain a complete description of the carbon dioxide system are the mass-conservation equations and the equilibrium constants, which are gathered in the book “Guide to Best Practices for Ocean CO₂ Measurements” [17]. These four parameters are described in the following.

TA is a mass-conservation expression for the hydrogen ion. The most used definition for alkalinity nowadays is that formulated by Andrew Dickson [18]. According to him: “The total alkalinity of a natural water is thus defined as the number of moles of hydrogen ion equivalent to the excess of proton acceptors (bases formed from weak acids with a dissociation constant $K \leq 10^{-4.5}$, at 25 °C and zero ionic strength) over proton donors (acids with $K > 10^{-4.5}$) in one kilogram of sample.”

The total alkalinity is expressed according to **Equation 4-1**:

Equation 4-1

$$\begin{aligned} \text{TA} = & [\text{HCO}_3^-] + 3[\text{CO}_3^{2-}] + [\text{B}(\text{OH})_4^-] + [\text{OH}^-] + [\text{HPO}_4^{2-}] + 2[\text{PO}_4^{3-}] + [\text{SiO}(\text{OH})_3^-] \\ & + [\text{HS}^-] + 2[\text{S}^{2-}] + [\text{NH}_3] - [\text{H}^+] - [\text{HSO}_4^-] - [\text{HF}] \\ & - [\text{H}_3\text{PO}_4] + [\text{organic bases}] - [\text{organic acids}] \end{aligned}$$

The contribution from organic species such as the bases of humic and fulvic acids is usually assumed to be negligible in systems like seawater. However, several studies have shown that the TA contribution from dissolved organic carbon (DOC) can be significant, especially in river, estuary and coastal waters, where the concentration of DOC is usually higher [19–22]. Conversely, since neither the detailed nature of DOC nor the dissociation constants for these organic species are well known, the effect of organic acids and bases on the alkalinity is very difficult to estimate [23]. However, ignoring the contribution of these systems would produce important errors when determining TA and, subsequently, the rest of the parameters for studying the CO₂ system.

DIC is the sum of the three species of the carbonate system in water: dissolved CO₂, HCO₃⁻ and CO₃²⁻. The pH of the water will determine the relative proportion of each of them. pH is the minus logarithm of the hydrogen ion concentration and, finally, pCO₂ is the partial pressure of CO₂ in air in equilibrium with a water sample, which is a measure of the degree of saturation of the sample with CO₂ gas. In thermodynamics, the fCO₂ of a real gas replaces the mechanical partial pressure used for ideal gases.

This chemical system has been widely studied in seawater and lately it is being studied in estuary waters as well [15], where accurate measurements of the carbonate system have become a high priority in the

last decades. Regarding high-altitude mountain systems, it has been found that CO₂ release from inland waters contribute significantly to the global carbon budget [24–28], although they have not been widely studied yet. This means that inland lakes are not CO₂ sinks, but instead, they emit this gas to the atmosphere. However, an anthropogenic increase of the atmospheric CO₂ concentration will affect the equilibrium between the atmosphere and the surface of the lakes. The concentration of CO₂ in water would increase, whereas the pH would still decrease. Considering the usually low buffer capacity of high-altitude mountain lakes, small changes in the proton concentration will be more noticeable than in other natural waters with a higher buffer capacity, such as seawater. An important decrease on the pH would be harmful for all the organisms that inhabit these ecosystems.

Even if the lakes are very important for the global CO₂ budget, the methodology employed up to now is far from being acceptable for this kind of studies, considering the weather and climate goals mentioned before. For instance, *Finlay et al.* [27] studied the seasonality of pCO₂ in some lakes with data collected over 36 years. They estimated the pCO₂ and the CO₂ flux from conductivity, temperature and pH measurements. Moreover, they estimated the DIC from a previously derived relationship between DIC and conductivity. Whereas these methodologies may be valid to obtain approximate values, they cannot be considered acceptable for accurate studies of the CO₂ system. *Wen et al.* [29] studied the CO₂ emissions from lakes and reservoirs of China based on the pCO₂ values. These values were estimated from pH, TA, salinity and temperature, where pH was measured using a multiparametric probe with an uncertainty of 0.01 units in pH and TA was measured following an old-fashioned standard procedure [30] with a measurement error of 100 μmol L⁻¹. Moreover, the dissociation constants they used for the CO₂ system are intended to be used in seawater and are not suitable for freshwater [31,32]. According to up to date standards, these methodologies would be deemed unacceptable to study the CO₂ system in other natural water systems such as seawater, and, therefore, they should not be considered adequate for inland waters either.

Taking into account everything mentioned before, we have considered necessary to establish a proper calculation strategy for the determination of TA with high accuracy and precision to study the effects of the increased emissions of CO₂ in the carbonate system of high-altitude mountain lakes. The developed methodology was tested in alpine lakes from the Pyrenees, although it could be used in other natural water systems. Furthermore, a preliminary analysis of the results was performed by linking them with the bedrock of the area.

4.3. Experimental section

4.3.1. Studied area and sampling

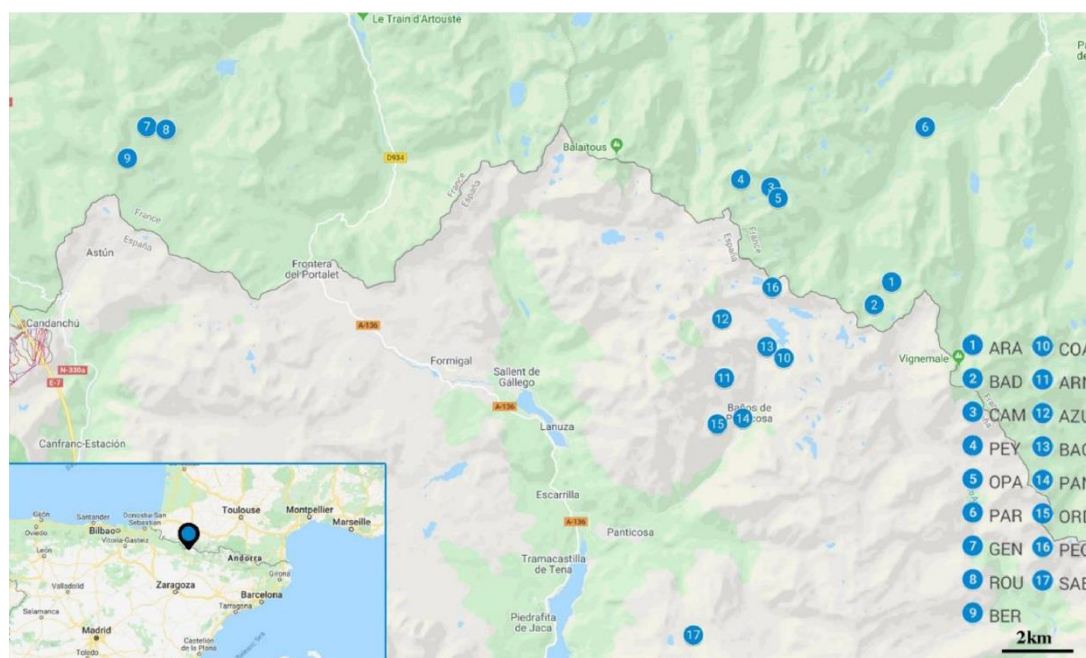


Figure 4-1: Location of the Pyrenean lakes considered in this study.

Water samples were collected from 17 different high mountain lakes in the Pyrenees, most of them at an altitude higher than 2000 m: 9 in the French areas of Cauterets and Ayous and 8 in the Spanish areas of Panticosa and Sabocos (**Figure 4-1**). Those in Cauterets were Lac d'Arratille (ARA), Lac de la Badete (BAD), Grand lac de Cambales (CAM), Lac de Peyregnets de Cambales (PEY), Lac de Petite Opale (OPA) and Lac du Paradis (PAR); while those in Ayous were Lac Gentau (GEN), Lac Roumassot (ROU) and Lac Bersau (BER). The sampled lakes in Panticosa were Ibon de Coanga (COA), Ibon de los Arnales (ARN), Ibon Azul Alto (AZU), Embalse de Bachimana Bajo (BAC), Ibon de los Banos de Panticosa (PAN), Ibon de Ordicuso Inferior (ORD) and Ibon de Pecico de la Canal (PEC) and, finally, Ibon de Sabocos (SAB) was also sampled.

The lakes are located at different altitudes, from around 1600m above the sea level (asl) (PAN and PAR) to around 2500m asl (PEY).

Firstly, the six lakes of the Cauterets Area are covering a 900m altitudinal gradient and span about 7 km distance. This zone of the Pyrenees is a mosaic of crystalline, granitic and sedimentary rocks [33]. All these lakes are within the Parc National des Pyrenees (PNP), so the anthropogenic inputs are limited and restricted to pastoralism, fishing and hiking. PAR (1620m asl) is the only lake below 2000m asl. and close to a Park service road. It is also the smaller lake (0.4 Ha) showing a high content of organic matter so a probable future transformation into a wetland cannot be discarded. In the Ayous area, ROU, GEN

and BER are located close to the PNP. However, the agropastoralism, and, therefore, the presence of gaggles, represents an important source of organic matter and nutrients, especially in GEN (1942m asl). Moreover, the mineral contributions from the pic d'Ayous, essentially iron, turn the bottom of lake GEN into an anoxic zone so this lake can be considered as eutrophic. It is worth noting that recreational fishing is also one of the main activities in all the French lakes.

The six lakes of the Panticosa area cover a 1000m altitudinal gradient and span about 10 km. Even if the geological structure on this side of the Pyrenees is similar, mostly granitic [34], climatic conditions in the Panticosa area differ from the Cauterets area, leading to visible changes in the vegetation. Three of these lakes can be influenced by local human activity because of the production of electricity coming from hydroelectric dams. Indeed, the flow of water is controlled upstream of BAC (2178m asl), PAN (1640m asl) and PEC (2460m asl). On its side, basin of SAB (1900m asl) is dominated by sedimentary rocks (Devonian and Cretaceous) and the lake is located close to a ski resort. All facilities of this touristic activity, which are operational the whole year, contribute to the presence of hikers and skiers nearby this lake. Moreover, by analogy to Gentau, agropastoralism with bovine and equine cattle and fishing are important activities in this area [35], showing also an anoxic zone at its bottom.

The sampling campaign addressed in this work took place in October 2018. The areas of Cauterets and Panticosa were sampled in 3 - 4 consecutive days. The samplings in Ayous and Sabocos were performed in a full working day each, where several samples were taken along the day in the same spot to study daily variations. All the lakes were reached by foot and the necessary material was transported in hiking backpacks. Sub-surface water samples (~0.5 m) were collected at the deepest point of each lake, which was reached with an inflatable boat. Physico-chemical parameters were also measured at each lake using an EXO2 multiparametric probe (YSI Inc., OH, USA). The measured parameters were conductivity (and its derived parameters, like salinity), temperature, pH, oxidation–reduction potential (ORP), Optical Dissolved Oxygen (ODO), Fluorescent Dissolved Organic Matter (fDOM) and depth. The water samples were taken using a 5 L capacity GO-FLO Teflon Trace Metal Bottle (General Oceanics, FL, USA). At the lake shore, the sample was divided in different sub-samples for specific parameters analysis. Sub-samples for the analysis of alkalinity and dissolved inorganic carbon were collected in 250 mL borosilicate brown glass bottles fitted with glass stoppers. Then, a headspace of 1 % of the bottle volume was left to allow for water expansion and a 100 μL spike of a saturated HgCl_2 solution (60 g L^{-1}) was added to stop biological activity from altering the carbon distribution in the samples, as recommended by the standard operating procedures (SOPs) [17]. Besides, sub-samples for the analysis of organic carbon were collected in 100 mL borosilicate glass bottles fitted with glass stoppers in which HgCl_2 spikes were also added. Finally, samples used for silicate and major anions (phosphate, fluoride and sulphate) analysis were collected in 50 mL polypropylene bottles. All these samples were kept at 4 °C until measurement.

4.3.2. Analytical methods

Silicate was measured by means of flow injection analysis (FIA) using the molybdenum blue method proposed by *Ma et al.* [36] and using the equipment described by *Kortazar et al.* [37], while phosphate was measured using ion chromatography (IC) [38] along with fluoride and sulphate. Total organic carbon (TOC) was measured as nonpurgeable organic carbon (NPOC) using a TOC-VCSH system with an automatic sampler (Shimadzu Corporation, Kyoto, Japan).

TA and DIC were measured using a VINDTA 3C system (Marianda, Kiel, Germany) [15]. TA was determined using a potentiometric titration while DIC determination was performed coulometrically [17] with a CM5015 Coulometer with the CM5011 emulator supplied by UIC Inc. (UIC Inc., Rockdale, IL, USA).

Since the TA values of these samples differ widely, it was deemed necessary to perform first the determination of the DIC in all the samples. Afterwards, considering that the TA values are usually very similar to DIC, samples were separated into 4 - 5 different groups and HCl titrant solutions of adequate concentration were prepared for each group. This working procedure assured a proper quality of the potentiometric titrations. The used HCl concentrations were 0.003, 0.015, 0.036 and 0.1 mol L⁻¹. HCl was standardised by potentiometric titration using Tris (tris(hydroxymethyl)aminomethane), and the equivalence volume was calculated using Gran II equations [39]. The HCl 0.1 mol L⁻¹ solution was titrated both with a Certified Reference Material (CRM) provided by Andrew Dickson's laboratory (A. Dickson, Scripps Institution of Oceanography, San Diego) and with Tris in order to verify the usefulness of Tris and Gran II equations for this purpose.

4.3.3. Calculation procedures

Silicate was measured using flow injection analysis (FIA) using the molybdenum blue method proposed by *Ma et al.* [36] and using the equipment. In the case of DIC, correction factors were calculated, using the CRMs, by dividing the average experimentally obtained CRM values of the day with the certified ones. These correction factors were then applied to the experimental results to obtain traceable DIC values. For the determination of TA this procedure was not applicable due to the CRM's high TA concentration and matrix difference. Instead, a nonlinear least squares procedure with volume fitting using the Levenberg-Marquardt Algorithm (LMA) was used to calculate the TA using the Microsoft Office Excel program. The calculation procedure was previously published by *Kortazar et al.* [15] for estuarine waters but had to be modified for alpine lakes due to the matrix difference. All the equations to determine the stoichiometric constants used were in the total proton and in the mol kg_{solution}⁻¹ scales. The equations for the calculation of the dissociation constants of sulphuric acid and the self-ionisation of water were taken from the book "CO₂ in Seawater: Equilibrium, Kinetics, Isotopes" [16]. The pK₁ and pK₂ values for the carbonate system were published by *Kortazar et al.* [15]. These constants are based in those proposed by *Millero* [40]:

Equation 4-2

$$pK = pK_1^0 + a_0 \cdot S^{0.5} + a_1 \cdot S + a_2 \cdot S^{1.5} + \frac{(a_3 \cdot S^{0.5} + a_4 \cdot S)}{T} + a_5 \cdot S^{0.5} \cdot \ln T$$

where $i = 1$ or 2 , correspond to the first or the second dissociation equilibria of the carbonate system, respectively, and pK_0 refers to the thermodynamic constant that was calculated according to the equations proposed by *Millero*:

Equation 4-3

$$pK_1^0 = -126.34048 + \frac{6320.813}{T} + 19.568224 \ln T$$

Equation 4-4

$$pK_2^0 = -90.18333 + \frac{5143.692}{T} + 14.613358 \ln T$$

The values of the parameters a_0 to a_5 can be found in *Kortazar et al.* [15] and are gathered in **Table 4-1**.

Table 4-1: Values of the $a_0 - a_5$ parameters used in the calculation of the stoichiometric constants of the carbonate system [15].

	For pK_1	For pK_2
a_0	15 (kept fixed)	21 (kept fixed)
a_1	0.0450 ± 0.0047	0.1453 ± 0.0072
a_2	-0.000852 ± 0.000042	-0.00517 ± 0.000064
a_3	-594.5 ± 6.5	-768.5 ± 9.9
a_4	-8.4 ± 1.4	-19.4 ± 2.1

As mentioned before, TA was determined by means of non-linear least-squares regression with volume fitting. This means that the added volume values were theoretically calculated, v_{calc} , and their differences with the experimental ones, v_{exp} , were minimised by refining certain parameters. In the present work, several models with different refined parameters were essayed in order to choose the most suitable ones.

For each titration point v_{calc} was calculated with the following equation:

Equation 4-5

$$v_{calc,i} = \frac{m_0 \cdot (\text{term} - TA)}{(C_H^0 - \text{term}) \cdot \delta_{sample}}$$

where C_H^0 is the concentration of the HCl titrant, δ_{sample} is the density of the sample and term is defined as:

Equation 4-6

$$\begin{aligned} \text{term} = & [\text{H}^+]_{\text{F}} + [\text{HSO}_4^-] + [\text{HF}] + [\text{H}_3\text{PO}_4] + [\text{organic acids}] \\ & - [\text{HCO}_3^-] - 2[\text{CO}_3^{2-}] - [\text{B}(\text{OH})_4^-] - [\text{OH}^-] - [\text{HPO}_4^{2-}] \\ & - 2[\text{PO}_4^{3-}] - [\text{SiO}(\text{OH})_3^-] - [\text{NH}_3] - [\text{organic bases}] \end{aligned}$$

Once TA and DIC were calculated, the rest of the parameters that characterise the CO₂ system, such as, pH or fCO₂ were calculated with the help of the CO2SYS software [41,42]. In this work, the MATLAB script version modified by *Orr. et al.* [43] was used and further modified as will be explained below. The script was executed in the GNU Octave software environment (John W. Eaton.,FSF, Inc).

4.4. Results and discussion

Among the measured anions that could contribute to the TA, fluoride (< 0.002 mg L⁻¹) and phosphate (< 0.090 mg L⁻¹) were under the limit of detection (LOD) and, therefore, their contribution was considered negligible. **Table 4-2** collects the concentrations of DIC, NPOC and silicate along with the salinity found in the investigated lakes.

Table 4-2: Salinity, DIC, NPOC and silicate concentrations measured in sub-surface waters of the lakes.

ID Lake	Salinity	DIC ($\mu\text{mol kg}^{-1}$)	NPOC ($\mu\text{mol kg}^{-1}$)	SiO(OH) ₃ ⁻ ($\mu\text{mol kg}^{-1}$)
ARA	0.028	776.94	149.87	50.17
BAD	0.029	778.48	105.32	43.35
CAM	0.006	162.29	90.44	19.74
PEY	0.003	79.41	136.97	8.52
OPA	0.011	306.91	93.26	25.10
PAR	0.022	641.62	191.84	67.77
GEN	0.014	367.98	108.90	14.75
ROU	0.014	358.60	155.49	12.17
BER	0.008	237.32	132.21	9.24
AZU	0.029	803.34	78.66	28.63
ARN	0.011	308.67	–	26.02
BAC	0.013	357.95	87.87	15.64
PEC	0.016	443.61	89.90	23.31
COA	0.004	124.64	156.51	12.28
PAN	0.013	371.60	169.20	31.40
ORD	0.020	572.54	386.39	30.12
SAB	0.058	1691.23	252.41	11.65

As can be appreciated, DIC values are much lower than those values usually found in other natural waters such as seawater, where DIC is around $2400 \mu\text{mol kg}^{-1}$. Besides that, values differ substantially among lakes, which corresponds, mainly, to differences in the bedrock composition. The higher values are found in SAB whose basin lies on Devonian sedimentary rocks (limestone, sandstone, shale), and Cretaceous sedimentary rocks (limestone, sandstone) compose its south catchment area. During Cretaceous, more chalk (CaCO_3 deposited by the shells of marine invertebrates) was formed than in any other period in the Phanerozoic, including Devonian and Permo-Triassic (conglomerate, sandstone, lutite, andesite, shale). These carbonate rocks, composed mainly by limestone, are very sensitive to weathering, explaining the high DIC in this lake. The basins and/or catchment of the lakes ARA, BAD, PAR, AZU, PEC and ORD are mainly composed by Devonian sedimentary rocks, but granitic rocks are also present in their surroundings. While the second ones are igneous rocks containing mainly quartz and feldspar and hard to dissolve, the first ones contain limestone.

This could explain their reasonably high DIC ($600 - 800 \mu\text{mol kg}^{-1}$) although it is not as high as in SAB. Among these lakes, PEC shows the lowest DIC values probably due to a higher granitic basin percentage. These lakes also present the highest concentrations of silicate, which might be related to the sandstone (quartz and feldspar) highly soluble of the Devonian rocks. The lakes from the Ayous area have a Permo-Triassic volcanic bedrock which also agrees with the lower DIC ($300 \mu\text{mol kg}^{-1}$). DIC values around $400 \mu\text{mol kg}^{-1}$ are observed for lakes PAN and BAC, which are connected to other lakes upstream, either rich in carbonate or not. The DIC values, around $300 \mu\text{mol kg}^{-1}$, measured in lakes ARN and OPA are related to the Devonian rocks located in the surroundings dragging CaCO_3 in their granitic basin. Finally, CAM, PEY, and COA have a granitic basin which agrees with their very low DIC values.

The relative standard deviation (RSD) of the NPOC values is 5 %, and for silicate is 2 %, where both uncertainties were calculated as the square root of the sum of the variances due to repetition and the intrinsic one. In the case of DIC, the uncertainty was calculated in the same way and the RSD values were below 1 %. These are rather high RSD values for this kind of studies, but considering the low DIC values obtained, it is normal to have higher RSD values.

Taking into account the relative high concentrations of NPOC and the low DIC values, the contribution of organic alkalinity can be considered significant. Regarding the determination of TA, the 0.1 mol L^{-1} HCl solution was used to evaluate the usability of Tris for its standardisation. Using the CRM, the HCl concentration obtained was $0.10462 \pm 0.00003 \text{ mol L}^{-1}$ (0.03 % RSD), while using Tris the HCl concentration obtained was $0.1044 \pm 0.0009 \text{ mol L}^{-1}$ (0.9 % RSD). The repeatability obtained using the CRM was considerably better than using Tris. The reason might be that the calculation of the equivalence volume using Gran II equations is very dependent of the amount of titration points used. It could probably be improved by performing more and smaller volume additions of the titrant. However, the relative difference between both values is of 0.2 % and both are statistically comparable at a 99 % of confidence level. Therefore, Tris was used for the standardisation of HCl when its concentration was $< 0.1 \text{ mol L}^{-1}$.

For the determination of TA, first, the curve fitting was performed by refining both E_0 and TA, as it is usually done. As an example, **Figure 4-2** shows both the experimental and calculated curves for the case of AZU, where the black dots correspond to the experimental titration points while the red striped dots correspond to the fitted curve using the refined parameters. This model will be called (1) for now on.

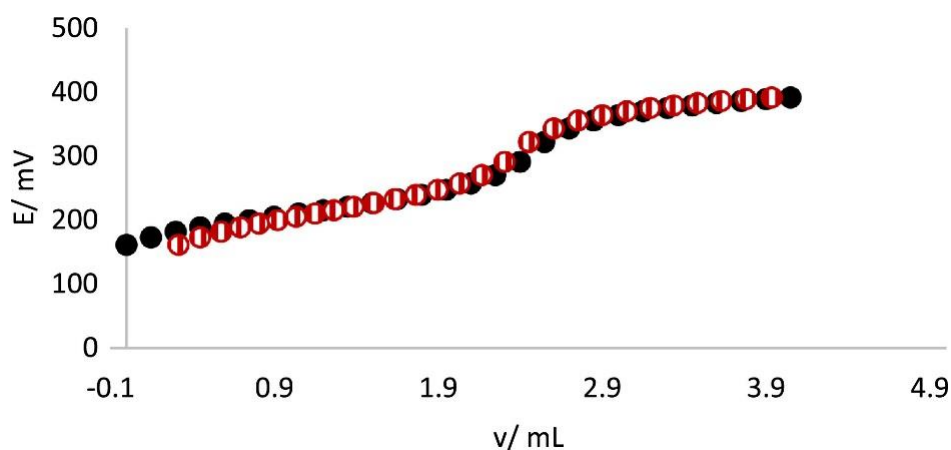


Figure 4-2: Fitting between the experimental curve (black dots) and the calculated curve (red striped dots) for the titration of the lake AZU sample when TA and E^0 are refined.

As can be seen, the fitting between both curves is not perfect. This suggests that all the acid-base species present in the water were not considered. Therefore, different refinement approaches were tested and contrasted, as can be seen in **Figure 4-3**, again for the case of AZU used as an example.

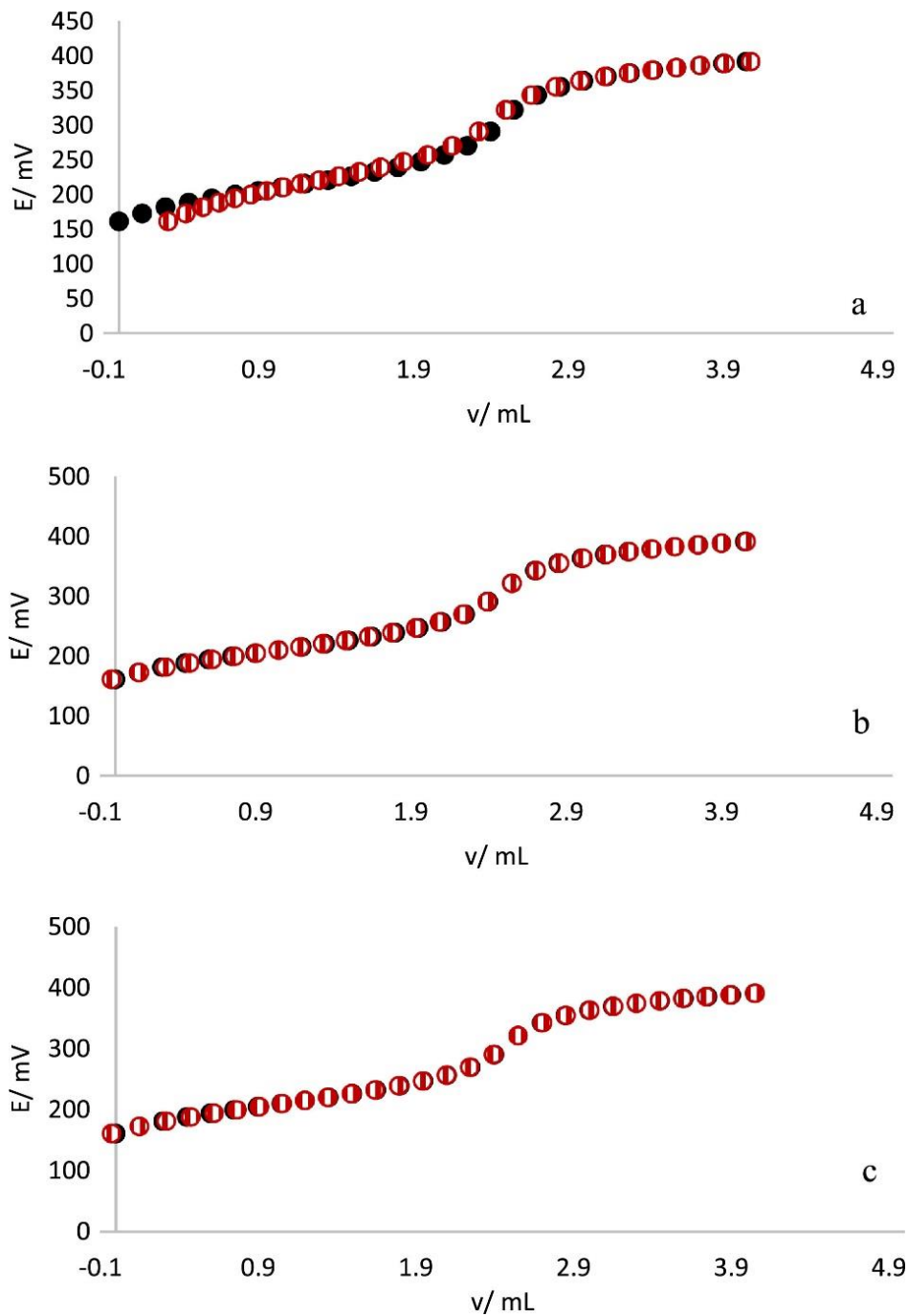


Figure 4-3: Fitting between the experimental curves (black dots) and the calculated curve (red striped dots) for the titration of the lake AZU sample when a) TA, E^0 and the a_0 values in **Equation 4-2** are refined, b) TA, E^0 and both the pK_a and the total concentration of the new acid-base species were refined and c) all the above mentioned parameters were simultaneously refined.

In **Figure 4-3.a**, besides the TA and E_0 , the a_0 values in **Equation 4-2** for the calculation of both pK_a values of the carbonate system were also refined. These last two values were refined according to the work published by *Kortazar et al.* [15] for the determination of TA in estuarine waters. This model will be called (2).

As mentioned before, the contribution of organic alkalinity might be significant and therefore it seemed necessary to consider its contribution. Since the nature and concentration of the possible acid-base organic species was unknown, a single species was considered for each lake and both its pK_a and total concentration were refined as shown in **Figure 4-3.b**, which will be called model (3). This “new species alkalinity” would be the sum of all the acid-base species that was not considered in **Equation 4-1**, and probably, not only the organic alkalinity. Finally, in **Figure 4-3.c**, the previously mentioned 6 parameters were refined and will be called model (4).

Table 4-3 shows the values of the refined parameters as well as the residual sum of squares (RSS) along with their uncertainties, calculated with the help of the Microsoft Excel macro SolverAid (<http://www.bowdoin.edu/~rdelevie/excellaneous/>). The RSS is a measure of the discrepancy between the empirical data and an estimation model.

Table 4-3: Values of the refined parameters as well as the residual sum of squares (RSS), along with their uncertainties, calculated with the help of the Microsoft Excel macro SolverAid when 1) TA and E_0 are refined, 2) TA, E_0 and the a_0 values in **Equation 4-2** were refined, 3) TA, E_0 and both the pK_a and the total concentration of the new acid-base species [New-Spe] were refined and 4) when all the above mentioned parameters were refined.

Model	RSS	TA ($\mu\text{mol kg}^{-1}$)	E_0 (mV)	a_0 (pK_1)	a_0 (pK_2)	pK_{new}	[New-Spe] ($\mu\text{mol kg}^{-1}$)
1)	0.5	818 ± 18	586 ± 2	–	–	–	–
2)	0.2	833 ± 24	585 ± 2	14.5 ± 0.2	(21 ± 91)	–	–
3)	0.005	852 ± 2	585.8 ± 0.2	–	–	6.58 ± 0.04	196 ± 7
4)	0.003	850 ± 2	585.8 ± 0.2	15 ± 1	(21 ± 41)	6 ± 2	(189 ± 22)

First, it has to be mentioned that the a_0 parameter for the pK_2 of the carbonate system is negligible in this example due to the sample's pH. This is the reason for having such high uncertainties. Both **Figure 4-2** and **Figure 4-3** and **Table 4-3** show that in models 1) and 2) the experimental and calculated curves do not match fully. The high RSS values obtained indicate that these two models are not appropriate for the determination of TA. The RSS of model 4) is the lowest one. However, the high correlation between the pK_{new} and the concentration of the new acid-base species results in very large uncertainties. This model has too many parameters to be refined for the relatively low amount of data used in the calculation. Therefore, model 3) seems to be the most adequate for the calculation of TA in these lakes. The correlation between the pK_{new} and the concentration of the new acid-base species is also quite high in this case, resulting in a RSD value for [New-Spe] close to 5 %.

As mentioned before, the Matlab script version of CO2SYS was used to calculate pH and fCO₂ from TA and DIC. This script had to be modified to take into account two new important aspects: 1) the set of stability constants for the carbonate system published by *Kortazar et al.* [15], which have been used in this work and 2) the contribution of the new acid-base species to the TA. To fulfil this last requirement, the script was modified to allow the addition of the new acid-base species total concentration and its pK_{new} values as input parameters. Provisions were also made to ensure convergence of the calculations since the low TA and DIC values of some samples sometimes prevented it. To ease the calculations, an Excel template was developed to manually add the input parameters into the script, which was also used to collect all the output parameters. The script and the Excel template are available upon request.

Table 4-4 shows the values of all the parameters used to characterise the CO₂ system (TA, DIC, pH and fCO₂) as well as the predicted new acid-base species concentration and pK_{new} values obtained for the studied lakes.

Table 4-4: Values of all the parameters used to characterise the CO₂ system (TA, DIC, pH and fCO₂) as well as the predicted new acid-base species concentration and pK_{new} values of the studied lakes.

	[New-Spe] ($\mu\text{mol kg}^{-1}$)	pK_{new}	DIC ($\mu\text{mol kg}^{-1}$)	TA ($\mu\text{mol kg}^{-1}$)	pH	fCO₂
ARA	256	7.07	777	815	7.23	1998
BAD	171	6.76	778	825	7.37	1450
CAM	143	6.40	162	154	6.36	1618
PEY	110	6.00	79	85	5.94	1034
OPA	194	6.76	307	291	6.74	1788
PAR	187	6.74	642	618	6.99	2639
GEN	549	7.24	368	378	6.74	2462
ROU	384	7.28	359	374	6.87	1943
BER*	13	7.31	237	222	7.41	446
AZU	196	6.58	803	852	7.27	1803
ARN	158	6.53	309	309	6.79	1737
BAC	258	6.85	358	350	6.75	2194
PEC	765	7.46	444	438	6.79	2489
COA	264	6.46	125	106	6.02	1523
PAN	359	7.00	372	334	6.64	2718
ORD	199	6.75	573	540	6.90	2740
SAB	243	6.57	1691	1839	7.71	1584
ARA	256	7.07	777	815	7.23	1998

*The discrepancies between BER and the rest of the lakes in the Ayous area might indicate an experimental error when measuring this sample and, therefore, it will not be considered for the discussion

As can be seen, pK_{new} ranges between 6.5 and 7.0 in all the lakes except for those of Ayous. This might indicate that whatever it is being considered as acid-base species shows a similar nature for all these lakes. Furthermore, these pK_a values are in agreement with those found by *Yang et al.* [44] for organic acids found coastal waters. It might be hypothesised that in the lakes of the Ayous area a different number and/or type of acid-base species would be present compared to the rest of the lakes, but this aspect clearly deserves further investigation. Furthermore, considering that the concentration of the refined species is sometimes higher than the NPOC, it can be concluded that not only organic matter is being considered but also something else.

Concerning the CO_2 system parameters, the obtained pH values range between 6.0 and 7.7. As expected, SAB showed the highest pH value, which is logical considering the carbonate-based basin. PEY, the highest lake located on granitic bedrocks, shows always the lowest pH values, which corresponds with the lowest TA and DIC values. Moreover, according to *Skjelkvale et al.* [3] low pH values can be caused by organic cations (humic acids) and, as can be seen, PEY shows one of the highest new species concentration and NPOC concentrations. Finally, the fugacity shows, as published before, that these lakes contribute to increase the CO_2 (g) concentration in the atmosphere. The atmospheric pCO_2 is around 415 ppm nowadays and if the fugacity is above that value it means that the equilibrium is displaced to the gas phase, and thus, CO_2 is released to the atmosphere. As can be seen in **Table 4-4** the fugacities of these lakes are well above this atmospheric value and therefore it is crucial to monitor them closely to understand the effects of the excess of atmospheric CO_2 .

Regarding the precisions/uncertainties of the measured/derived variables, some observations can be made. Even if **Table 4-4** does not show the uncertainties of the results, general RSD values were calculated for each parameter to discuss them briefly. Most uncertainties were calculated as the square root of the sum of variances due to repetition and the intrinsic one, calculated differently in every case. In the case of the pH and the fugacity, only the standard deviation due to the repetition was considered and, thus, even if the repeatability is supposed to be the main contribution to the total uncertainty, the RSD values could be slightly higher.

The intrinsic uncertainty of TA was the one obtained from the fitting of titration data with the help of the SolverAid Excel macro. In general, RSD values were below 2 %, with very few exceptions. As happened for the DIC values, this RSD is quite high, but it can be explained by the low TA values. The RSD for the concentration of the new acid-base species was generally below 5 %, whereas for the pK_{new} was below 1 %. In the case of pH and fugacity, values were below 1 % and below 3 %, respectively. Considering these RSD values, the methodology can be considered precise, much more than those found in bibliography [27,29]. As previously stated, the low TA and DIC values of some samples imply higher RSD values, but the repeatability is as good as in other works which make use of this equipment [15]. The uncertainties of pH and fugacity derived from the refined parameters need further investigation, although there is a recent published work that study the uncertainty propagation for the marine CO_2 system [43].

4.5. Conclusions

A robust procedure was developed to determine the total alkalinity in high altitude mountain lakes, which allows the determination of the CO₂ system parameters with improved precision and accuracy that can also be useful for any other inland freshwater body with similar characteristics. This approach, derived from that developed for the accurate determination of acidification parameters in estuarine waters, allows the determination of TA in a highly improved way, compared to the currently available methodologies which have reported uncertainties of 100 μmol L⁻¹. Moreover, the methodologies used for the determination of TA in lakes are far from being acceptable for studies of the CO₂ system. The fitting between the experimental and calculated titration curves is very good and the obtained values are in good agreement with the expected ones. The obtained uncertainties are reasonably low, which indicates the high precision of this methodology. Moreover, the modified script for the Matlab version of CO2SYS allows the calculation of the rest of the parameters of the CO₂ system in a precise way. The incorporation of a new acid-base species to explain the deviation between the experimental and calculated curves is a great advantage that could be also used in any other natural water systems where not all acid-base species present in the samples, particularly those of organic nature, are explicitly known or can be adequately quantified. Moreover, most of the obtained results were explained taking into account the characteristics of the bedrock of the lakes' basin. However, further investigation is necessary in some cases, such as to explain the higher pH in the Ayous area. This methodology will help researchers from different areas to share common practices allowing the comparison and use of results from others, which would encourage multidisciplinary and long-term studies in these important ecosystems.

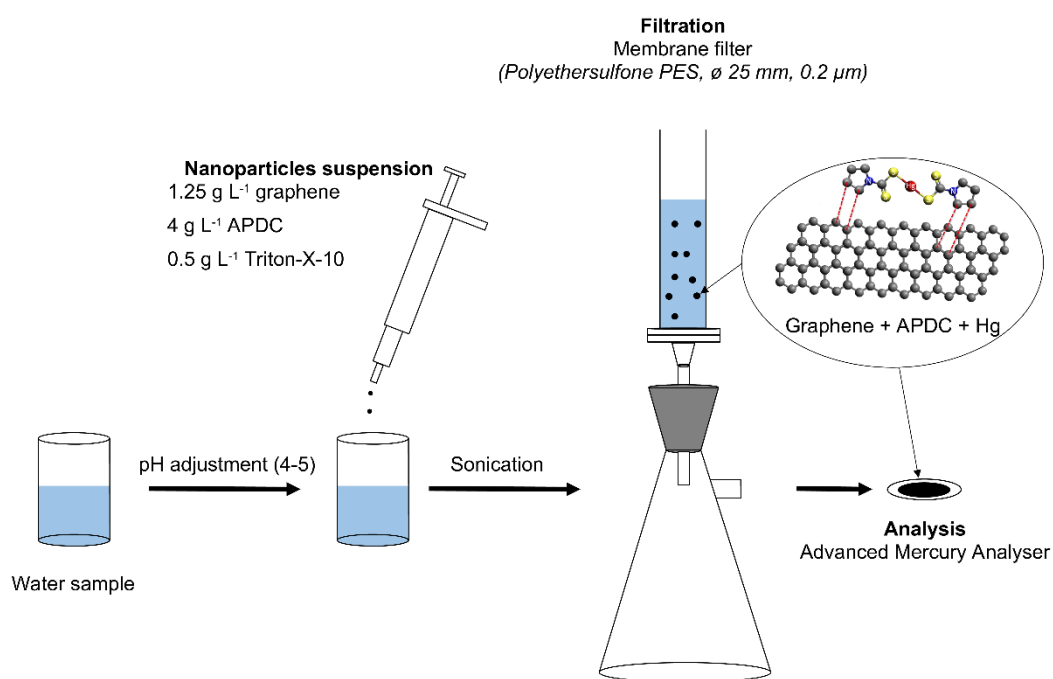
4.6. References

- [1] L. Camarero, J. Catalan, A simple model of regional acidification for high mountain lakes : Application to the Pyrenean Lakes (North-East Spain), *Water Research*. 32 (1998) 1126–1136. [https://doi.org/10.1016/S0043-1354\(97\)00291-1](https://doi.org/10.1016/S0043-1354(97)00291-1).
- [2] R. Mosello, A. Lami, A. Marchetto, M. Rogora, B. Wathne, L. Lien, J. Catalan, L. Camarero, M. Ventura, R. Psenner, K. Koinig, H. Thies, S. Sommaruga-Wögrath, U. Nickus, D. Tait, B. Thaler, A. Barbieri, R. Harriman, Trends in the Water Chemistry of High Altitude Lakes in Europe, *Water, Air and Soil Pollution: Focus*. 2 (2002) 75–89. <https://doi.org/10.1023/A:1020138221582>.
- [3] B.L. Skjelkvaale, R.F. Wright, Mountain lakes; sensitivity to acid deposition and global climate change, *Ambio*. 27 (1998) 280–286.
- [4] R. Mosello, B.M. Wathne, L. Lien, H.J.B. Birks, Al:Pe projects: Water chemistry and critical loads, *Water, Air, & Soil Pollution*. 85 (1995) 493–498. <https://doi.org/10.1007/BF00476877>.
- [5] R. Adrian, C.M. O'Reilly, H. Zagarese, S.B. Baines, D.O. Hessen, W. Keller, D.M. Livingstone, R. Sommaruga, D. Straile, E. Van Donk, G.A. Weyhenmeyer, M. Winder, Lakes as sentinels of climate change, *Limnology and Oceanography*. 54 (2009) 2283–2297. https://doi.org/10.4319/lo.2009.54.6_part_2.2283.
- [6] T. Stocker, ed., *Climate change 2013: the physical science basis: Working Group I contribution to the Fifth assessment report of the Intergovernmental Panel on Climate Change*, Cambridge University Press, New York, 2014. ISBN : 978-1-107-66182-0
- [7] C. Le Quéré, R.J. Andres, T. Boden, T. Conway, R.A. Houghton, J.I. House, G. Marland, G.P. Peters, G.R. van der Werf, A. Ahlström, R.M. Andrew, L. Bopp, J.G. Canadell, P. Ciais, S.C. Doney, C. Enright, P. Friedlingstein, C. Huntingford, A.K. Jain, C. Jourdain, E. Kato, R.F. Keeling, K. Klein Goldewijk, S. Levis, P. Levy, M. Lomas, B. Poulter, M.R. Raupach, J. Schwinger, S. Sitch, B.D. Stocker, N. Viovy, S. Zaehle, N. Zeng, The global carbon budget 1959–2011, *Earth System Science Data*. 5 (2013) 165–185. <https://doi.org/10.5194/essd-5-165-2013>.
- [8] C. Le Quéré, R.M. Andrew, J.G. Canadell, S. Sitch, J.I. Korsbakken, G.P. Peters, A.C. Manning, T.A. Boden, P.P. Tans, R.A. Houghton, R.F. Keeling, S. Alin, O.D. Andrews, P. Anthoni, L. Barbero, L. Bopp, F. Chevallier, L.P. Chini, P. Ciais, K. Currie, C. Delire, S.C. Doney, P. Friedlingstein, T. Gkritzalis, I. Harris, J. Hauck, V. Haverd, M. Hoppema, K. Klein Goldewijk, A.K. Jain, E. Kato, A. Körtzinger, P. Landschützer, N. Lefèvre, A. Lenton, S. Lienert, D. Lombardozzi, J.R. Melton, N. Metzl, F. Millero, P.M.S. Monteiro, D.R. Munro, J.E.M.S. Nabel, S. Nakaoka, K. O'Brien, A. Olsen, A.M. Omar, T. Ono, D. Pierrot, B. Poulter, C. Rödenbeck, J. Salisbury, U. Schuster, J. Schwinger, R. Séférian, I. Skjelvan, B.D. Stocker, A.J. Sutton, T. Takahashi, H. Tian, B. Tilbrook, I.T. van der Laan-Luijkx, G.R. van der Werf, N. Viovy, A.P. Walker, A.J. Wiltshire, S. Zaehle, *Global Carbon Budget 2016*, *Earth System Science Data*. 8 (2016) 605–649. <https://doi.org/10.5194/essd-8-605-2016>.
- [9] J.-P. Gattuso, L. Hansson, eds., *Ocean acidification*, Oxford University Press, Oxford ; New York, 2011. ISBN : 978-0-19-959109-1
- [10] K. Caldeira, M.E. Wickett, Anthropogenic carbon and ocean pH, *Nature*. 425 (2003) 365–365. <https://doi.org/10.1038/425365a>.
- [11] M. Gledhill, E.P. Achterberg, K. Li, K.N. Mohamed, M.J.A. Rijkenberg, Influence of ocean acidification on the complexation of iron and copper by organic ligands in estuarine waters, *Marine Chemistry*. 177 (2015) 421–433. <https://doi.org/10.1016/j.marchem.2015.03.016>.
- [12] J. Newton, R. Feely, E. Jewett, P. Williamson, J. Mathis, *Global Ocean Acidification Observing Network: Requirements and Governance Plan*, 61.
- [13] E.E. Bockmon, A.G. Dickson, An inter-laboratory comparison assessing the quality of seawater carbon dioxide measurements, *Marine Chemistry*. 171 (2015) 36–43. <https://doi.org/10.1016/j.marchem.2015.02.002>.
- [14] A.G. Dickson, *The carbon dioxide system in seawater: Equilibrium chemistry and measurements. Guide to Best Practices for Ocean Acidification Research and Data Reporting*. (2010) 17-40.

- [15] L. Kortazar, D. Milea, O. Gómez-Laserna, L.A. Fernández, Accurate determination of total alkalinity in estuarine waters for acidification studies, *TrAC Trends in Analytical Chemistry*. 114 (2019) 69–80. <https://doi.org/10.1016/j.trac.2019.01.010>.
- [16] R.E. Zeebe, D.A. Wolf-Gladrow, *CO₂ in seawater: equilibrium, kinetics, isotopes*, Elsevier, Amsterdam ; New York, 2001. ISBN : 978-0-444-50946-8
- [17] A.G. Dickson, C.L. Sabine, J.R. Christian, C.P. Barger, North Pacific Marine Science Organization, eds., *Guide to best practices for ocean CO₂ measurements*, North Pacific Marine Science Organization, Sidney, BC, 2007.
- [18] A.G. Dickson, An exact definition of total alkalinity and a procedure for the estimation of alkalinity and total inorganic carbon from titration data, *Deep Sea Research Part A. Oceanographic Research Papers*. 28 (1981) 609–623. [https://doi.org/10.1016/0198-0149\(81\)90121-7](https://doi.org/10.1016/0198-0149(81)90121-7).
- [19] Y.H. Ko, K. Lee, K.H. Eom, I.-S. Han, Organic alkalinity produced by phytoplankton and its effect on the computation of ocean carbon parameters: *Organic Alkalinity, Limnology and Oceanography*. 61 (2016) 1462–1471. <https://doi.org/10.1002/lno.10309>.
- [20] W.-J. Cai, Y. Wang, R.E. Hodson, Acid-Base Properties of Dissolved Organic Matter in the Estuarine Waters of Georgia, USA, *Geochimica et Cosmochimica Acta*. 62 (1998) 473–483. [https://doi.org/10.1016/S0016-7037\(97\)00363-3](https://doi.org/10.1016/S0016-7037(97)00363-3).
- [21] H.-C. Kim, K. Lee, Significant contribution of dissolved organic matter to seawater alkalinity, *Geophysical Research Letters*. 36 (2009). <https://doi.org/10.1029/2009GL040271>.
- [22] C.W. Hunt, J.E. Salisbury, D. Vandemark, Contribution of non-carbonate anions to total alkalinity and overestimation of pCO₂ in New England and New Brunswick rivers, *Biogeosciences*. 8 (2011) 3069–3076. <https://doi.org/10.5194/bg-8-3069-2011>.
- [23] F.J. Millero, D. Pierrot, K. Lee, R. Wanninkhof, R. Feely, C.L. Sabine, R.M. Key, T. Takahashi, Dissociation constants for carbonic acid determined from field measurements, *Deep Sea Research Part I: Oceanographic Research Papers*. 49 (2002) 1705–1723. [https://doi.org/10.1016/S0967-0637\(02\)00093-6](https://doi.org/10.1016/S0967-0637(02)00093-6).
- [24] J.J. Cole, Y.T. Prairie, N.F. Caraco, W.H. McDowell, L.J. Tranvik, R.G. Striegl, C.M. Duarte, P. Kortelainen, J.A. Downing, J.J. Middelburg, J. Melack, Plumbing the Global Carbon Cycle: Integrating Inland Waters into the Terrestrial Carbon Budget, *Ecosystems*. 10 (2007) 172–185. <https://doi.org/10.1007/s10021-006-9013-8>.
- [25] B.A. Denfeld, P. Kortelainen, M. Rantakari, S. Sobek, G.A. Weyhenmeyer, Regional Variability and Drivers of Below Ice CO₂ in Boreal and Subarctic Lakes, *Ecosystems*. 19 (2016) 461–476. <https://doi.org/10.1007/s10021-015-9944-z>.
- [26] V. Ducharme-Riel, D. Vachon, P.A. del Giorgio, Y.T. Prairie, The Relative Contribution of Winter Under-Ice and Summer Hypolimnetic CO₂ Accumulation to the Annual CO₂ Emissions from Northern Lakes, *Ecosystems*. 18 (2015) 547–559. <https://doi.org/10.1007/s10021-015-9846-0>.
- [27] K. Finlay, R.J. Vogt, G.L. Simpson, P.R. Leavitt, Seasonality of pCO₂ in a hard-water lake of the northern Great Plains: The legacy effects of climate and limnological conditions over 36 years, *Limnology and Oceanography*. 64 (2019). <https://doi.org/10.1002/lno.11113>.
- [28] Y.T. Prairie, Carbocentric limnology: looking back, looking forward, *Canadian Journal of Fisheries and Aquatic Sciences*. 65 (2008) 543–548. <https://doi.org/10.1139/f08-011>.
- [29] Z. Wen, K. Song, Y. Shang, C. Fang, L. Li, L. Lv, X. Lv, L. Chen, Carbon dioxide emissions from lakes and reservoirs of China: A regional estimate based on the calculated pCO₂, *Atmospheric Environment*. 170 (2017) 71–81. <https://doi.org/10.1016/j.atmosenv.2017.09.032>.
- [30] L.L. Bridgewater, R.B. Baird, A.D. Eaton, E.W. Rice, American Public Health Association, American Water Works Association, Water Environment Federation, eds., *Standard methods for the examination of water and wastewater*, 23rd edition, American Public Health Association, Washington, DC, 2017. ISBN : 978-0-87553-287-5
- [31] F.J. Millero, Thermodynamics of the carbon dioxide system in the oceans, *Geochimica et Cosmochimica Acta*. 59 (1995) 661–677. [https://doi.org/10.1016/0016-7037\(94\)00354-0](https://doi.org/10.1016/0016-7037(94)00354-0).

- [32] R.N. Roy, L.N. Roy, K.M. Vogel, C. Porter-Moore, T. Pearson, C.E. Good, F.J. Millero, D.M. Campbell, The dissociation constants of carbonic acid in seawater at salinities 5 to 45 and temperatures 0 to 45°C, *Marine Chemistry*. 44 (1993) 249–267. [https://doi.org/10.1016/0304-4203\(93\)90207-5](https://doi.org/10.1016/0304-4203(93)90207-5).
- [33] D.G. Zaharescu, P.S. Hooda, C.I. Burghilea, A. Palanca-Soler, A Multiscale Framework for Deconstructing the Ecosystem Physical Template of High-Altitude Lakes, *Ecosystems*. 19 (2016) 1064–1079. <https://doi.org/10.1007/s10021-016-9987-9>.
- [34] E. Serrano-Cañadas, Glacial evolution of the upper Gallego Valley (Panticosa mountains and Ribera de Biescas, Aragonese Pyrenees, Spain), *Pirineos : Revista de Ecología de Montaña*. 138 (1991) 23. <https://doi.org/10.3989/pirineos.1991.v138.191>
- [35] Z. Santolaria, T. Arruebo, J.S. Urieta, F.J. Lanaja, A. Pardo, J. Matesanz, C. Rodriguez-Casals, Hydrochemistry dynamics in remote mountain lakes and its relation to catchment and atmospheric features: the case study of Sabocos Tarn, Pyrenees, *Environmental Science and Pollution Research*. 22 (2015) 231–247. <https://doi.org/10.1007/s11356-014-3310-0>.
- [36] J. Ma, R.H. Byrne, Flow injection analysis of nanomolar silicate using long pathlength absorbance spectroscopy, *Talanta*. 88 (2012) 484–489. <https://doi.org/10.1016/j.talanta.2011.11.019>.
- [37] L. Kortazar, S. Alberdi, E. Tynan, L.A. Fernández, An adapted flow injection analysis method of phosphate for estuarine samples avoiding matrix effects, *Microchemical Journal*. 124 (2016) 416–421. <https://doi.org/10.1016/j.microc.2015.09.027>.
- [38] O. Gómez-Laserna, P. Cardiano, M. Diez-García, N. Prieto-Taboada, L. Kortazar, M.Á. Olazabal, J.M. Madariaga, Multi-analytical methodology to diagnose the environmental impact suffered by building materials in coastal areas, *Environmental Science and Pollution Research*. 25 (2018) 4371–4386. <https://doi.org/10.1007/s11356-017-0798-0>.
- [39] G. Gran, Determination of the equivalence point in potentiometric titrations. Part II, *The Analyst*. 77 (1952) 661. <https://doi.org/10.1039/an9527700661>.
- [40] F.J. Millero, Carbonate constants for estuarine waters, *Marine and Freshwater Research*. 61 (2010) 139. <https://doi.org/10.1071/MF09254>.
- [41] E. Lewis, D. Wallace, L.J. Allison, Program developed for CO₂ system calculations, 1998. <https://doi.org/10.2172/639712>.
- [42] D.E. Pierrot, D.W.R. Wallace, E. Lewis, MS Excel Program Developed for CO₂ System Calculations, (2011). https://doi.org/10.3334/CDIAC/otg.CO2SYS_XLS_CDIAC105a.
- [43] J.C. Orr, J.-M. Epitalon, A.G. Dickson, J.-P. Gattuso, Routine uncertainty propagation for the marine carbon dioxide system, *Marine Chemistry*. 207 (2018) 84–107. <https://doi.org/10.1016/j.marchem.2018.10.006>.
- [44] B. Yang, R.H. Byrne, M. Lindemuth, Contributions of organic alkalinity to total alkalinity in coastal waters: A spectrophotometric approach, *Marine Chemistry*. 176 (2015) 199–207. <https://doi.org/10.1016/j.marchem.2015.09.008>.

5. A simple determination of trace mercury concentrations in natural waters using Dispersive Micro-Solid Phase Extraction preconcentration based on functionalized graphene nanosheets



5.1. Abstract

In this work, we developed an innovative analytical method for the trace and ultra-trace determination of total mercury (Hg) concentration in natural water samples (fresh and seawaters). In this method, Dispersive Micro-Solid Phase Extraction (DMSPE) is applied using graphene nanosheets to quantitatively preconcentrate dissolved Hg from natural water samples, before its direct analysis by commercially available pyrolysis gold amalgamation and atomic absorption spectroscopy (AAS). In this new methodology, only two easy steps are necessary, saving time and effort. First, the operator has to add 500 μL of nanoparticles suspension containing graphene, Ammonium Pyrrolidine DithioCarbamate (APDC) and Triton-X-100 in the water sample. This solution is filtered under vacuum and the Hg complex on the functionalized graphene can be simply collected on a membrane filter (Polyethersulfone PES, 0.2 μm). The filter obtained can then be analysed back at the laboratory by direct pyrolysis of the PES filter using a commercial mercury analyser. Different parameters have been tested to optimize this preconcentration procedure, such as the sample volume, the amount of nanoparticles suspension and the extraction time. The stability conditions of the Hg preconcentrated on PES filters during storage and before analysis has also been investigated. The influence of the occurrence of marine salts (sodium chloride), natural organic matter or competing metals (calcium) in the sample has also been evaluated to prevent possible matrix effects. This method is fully operational after application to real water sample matrices and exhibits suitable limit of detection, as low as 0.38 ng L⁻¹ using 200 mL of the water sample, and excellent reproducibility (< 5 % as RSD).

Keywords:

Mercury; Preconcentration; Ultra-trace analysis; Graphene nanosheets; Dispersive Micro-Solid Phase Extraction (DMSPE); Water sample

B. Duval, A. Gredilla, S. Fdez-Ortiz de Vallejuelo, E. Tessier, D. Amouroux, A. de Diego, A simple determination of trace mercury concentrations in natural waters using dispersive Micro-Solid phase extraction preconcentration based on functionalized graphene nanosheets, *Microchemical Journal*. 154 (2020) 104549. <https://doi.org/10.1016/j.microc.2019.104549>.

5.2. Introduction

Among other pollutants, mercury (Hg) is of major concern in aquatic environments. While mercury is present at low concentration in natural waters [1], its specific biogeochemical cycling allows bioaccumulation and biomagnification in the food chain leading to serious consequences for animals and higher predators, including humans [2,3]. Consequences of mercury contamination are not only noticeable in terms of people's health [4,5] but also in the economic sphere [6–9].

Thereby, mercury concentrations in topsoil, atmosphere and oceanic surface waters have increased respectively by a factor of 1.2, 4-6 and 3 since the pre-industrial period [8,10]. Besides, the numerous ecological studies about mercury show that primary anthropogenic mercury emissions are still increasing [9,10]. Therefore, the scenarios for the future are quite pessimistic, predicting a change in mercury emission of -4 % to 96 % [11].

Monitoring natural concentrations of total mercury in aquatic systems remains a difficult challenge since Hg is mainly occurring at ultra-trace levels: 0.3 to 8 ng L⁻¹ in waters free from local sources of mercury, either anthropogenic or natural, and 10 to 40 ng L⁻¹ for waters influenced by mercury mining and/or industrial pollution [12]. Indeed, a wide range of study has highlighted such levels of mercury in natural waters either seawater [1,8] or freshwater [13].

The development of low cost and easy handling analytical methods is then a necessity and it is required to fulfil some of the objectives of the Minamata Convention on Mercury, a global treaty to protect human health and the environment from the adverse effects of mercury. In that sense, Solid Phase Extraction (SPE) procedures to preconcentrate Hg before its analysis have shown a great interest in the scientific community due to its efficiency and simplicity. Most of the studies focus on the preparation of micro-column filled with specific adsorbents for Hg preconcentration. Polymers such as zwitterion-functionalized polymer microspheres (ZPMs) [14] or ion-imprinted polymer (IIP) especially designed for Hg adsorption [15] can be successfully used for rapid enrichment of mercury species. More simple in its preparation yet more expensive, the use of aminated Amberlite XAD-4 resin [16] or silica reversed-phase (RP-C₁₈) [17] respectively followed by FI-CVG-AAS and GC/MS analysis allows determination of Hg species, but its applicability to real samples remains difficult due to high limits of detection.

The investigation of new materials for Hg selective preconcentration made a great step forward in recent years. Indeed, due to their specific properties, nanomaterials have attracted increasing interest in the development of preconcentration methods for contaminants [18], and, more recently, Hg analysis. Then, the micro-column used to preconcentrate Hg can be packed with nanocomposites, previously functionalized for specific adsorption of Hg: magnetite (Fe₃O₄) nanoparticles [19], graphene oxide (GO) [20], multiwalled carbon nanotubes (MWCNTs) [17,21], carbon nanotube sponges (CNT sponges) [22]. Hence, all these methodologies include synthesis of the adsorbent, preparation of the column, elution of the Hg species directly followed by analysis, preventing direct application on the field. Moreover, multiplication of the preparation steps, from collection to analysis, may be problematic considering the potential contaminations or losses of Hg [23].

The use of field techniques reduces travelling and storage times of the samples, and facilitate the acquisition of results in developing countries and/or remote areas. In that sense, *K. Leopold et al.* [24–26] have conducted various studies in the last decade to develop a passive sampler for reagent-free on-site Hg preconcentration: nanogold-coated dipsticks. Thermal desorption of trapped Hg followed by AFS detection allows determination of Hg contents lower than the ppt level (ng L^{-1}), and applicability to real samples, either seawater or freshwater, have been demonstrated. Nevertheless, implementation of this methodology in developing countries remains difficult because of the heavy preparation of the dipsticks (cleaning, coating, and functionalization) and their high cost (reagents and chemicals): sampling campaigns would need numerous of this passive sampler. Also, dipsticks have to be regenerated by thermal annealing at $600\text{ }^{\circ}\text{C}$ for 20 min before each use, which greatly lengthens the preparation time of a sampling campaign. Finally, reproducible production of the nanogold-coated dipsticks remains difficult. As an alternative to expensive gold materials, *Tavares et al.* [27] have produced magnetite nanoparticles using iron oxide nanoparticles coated with silica shells functionalized with dithiocarbamate groups in order to take advantage of the strong affinities between Hg and thiol group (R-SH) [28,29] to preconcentrate Hg prior to its analysis by thermal decomposition AAS with gold amalgamation. Again, synthesis of the nanoparticles includes numerous steps and reagents, and requires important scientific knowledge. Besides, extraction of Hg using these nanoparticles with recovery close to 100% necessitates at least 24 hours. Finally, the limit of detection of 1.8 ng L^{-1} , reached with this procedure prevents its application in pristine areas.

Several studies conducted by *Sitko et al.* have already been made using modified graphene nanomaterials for Dispersive Micro-solid Phase Extraction (DMSPE) such as carbon nanotubes [30], multiwalled carbon nanotubes (MWCNTs) [31], graphene oxide (GO) [32] or graphene nanosheets [33] in order to preconcentrate various elements (Mn, Fe, Co, Ni, Cu, Zn, Se, Pb, Cd). Nevertheless, none of these works deals with Hg, probably because of the high limit of detection of the apparatus (wavelength-dispersive X-ray fluorescence WDXRF, total-reflection X-ray fluorescence spectrometry TXRF, or energy-dispersive X-ray fluorescence spectrometry EDXRF) and the difficulties of working with such element (contaminations or losses).

In this work, we have used the specific properties of graphene nanosheets, a cheap material, to develop an innovative analytical method. Firstly, graphene is flexible so it can be easily attached to a support, which makes it a worthwhile candidate in the use of Micro-solid Phase Extraction (MSPE). It is as well hydrophobic and non-polar with a strong affinity for carbon-based ring compound due to the hexagonal arrays of carbon atoms in its structure. Graphene shows also a huge specific surface ($2630\text{ m}^2\text{ g}^{-1}$) [34], which encourages its use as a sorbent in MSPE. It should be noted that this amazing material could be synthesized easily and affordably in most of the laboratories all around the world, including those of developing countries. Among graphene-based material, graphene nanosheets display great adsorption capacities. Indeed, both surfaces of a planar sheet of graphene are accessible to adsorption of analytes [35]. Also, nanostructured material as graphene nanosheets allows the adsorption of the organic compound via non-covalent interactions [36].

In the proposed method, based on *Kocot et Sitko* [33], dissolved Hg in water samples is first preconcentrated using a nanoparticles suspension consisting of graphene nanosheets as an adsorbent, Ammonium Pyrrolidine DithioCarbamate (APDC) as a chelating agent and Triton-X-100 as a surfactant. To obtain high recovery of the Hg on the nanoparticles, the procedure is optimized for various analytical parameters such as the amount of nanoparticles, sonication time and sample volume. The Hg-rich nanoparticles are then collected in a Polyethersulfone (PES) filter, whose stability at different storage conditions is also checked. The potential existence of matrix effects due to the presence of chloride salts (estuarine or seawater), organic matter (continental water) and metals (calcium) able to compete with mercury for the binding sites of the sorbent is investigated, and the applicability of the whole method is finally verified by the analysis of real samples (seawater and lake water).

Together with the in-field preconcentration of a large volume of water on a small and light membrane filter and the direct analysis of this filter back to the lab greatly enhance the simplicity of all the analytical process for a precise and accurate determination of mercury content in water samples: from the sampling to the result!

5.3. Material and methods

5.3.1. Preparation of nanoparticles suspension

The principle of our method is based on the adsorption of mercury on graphene nanosheets. Nevertheless, metal ions in the form of hydrophilic complexes, including dissolved mercury, cannot be adsorbed directly on the graphene surface with a great efficiency [33]. Therefore, it is necessary to functionalize the graphene nanosheets using a chelating agent that will be adsorbed on the graphene nanosheets via non-covalent interactions (π - π stacking) [35]. Ammonium Pyrrolidine DithioCarbamate (APDC) was chosen as a chelating agent due to some specificity in its structure. Indeed, strong affinities between APDC and mercury, mainly due to the presence of thiol groups (R-SH) in the structure of APDC, lead to the chelation of mercury by APDC (covalent bonds) [33]. -SH groups have already shown one of the strongest binding affinity either for inorganic mercury (sulphur-containing organic matter or polymers with Hg(II)) or organic mercury (sulphur-containing organo-metallic compounds or thiolate-like species with MeHg) [29]. We also need to add some Triton-X-100 in the nanoparticles suspension to increase the viscosity of the solution, hence improving the buoyancy of graphene nanosheets and, in this way, to obtain a real suspension of nanoparticles.

Then, following the recommendations of *Kocot and Sitko* [33], that applied DMSPE for the preconcentration of Co, Ni, Cu and Pb, the graphene/APDC/Triton-X-100 nanoparticles suspension was prepared as follows: 25 mg of graphene nanosheets ($\sim 5 \mu\text{m}$ diameter, 1-5 nm thickness, *Green Stone Swiss Co.*), 80 mg of APDC (*Purum p.a. $\geq 98.0\%$, Sigma-Aldrich*) and 10 mg of Triton-X-100 (*Laboratory-grade, Sigma-Aldrich*) in 20 mL of high purity water (18.2 M Ω cm), sonicated for 60 min, to obtain concentrations of 1.25 g L⁻¹; 4 g L⁻¹ and 0.5 g L⁻¹ for graphene, APDC and Triton-X-100, respectively. To avoid the aggregation of the graphene and to ensure its homogeneity within the nanoparticles suspension, the solution was sonicated 5 min before each use.

5.3.2. Procedure for mercury preconcentration (optimum conditions)

The chelation between APDC and mercury can effectively occur only with a pH between 4 and 5, so initially, the pH of the water sample containing mercury was adjusted by the addition of ultrapure HCl and/or NH₃ solutions (*Optima grade, Fisher Scientific*). In the second step, 0.5 mL of nanoparticles suspension was added to either 20 mL or 200 mL of the aqueous solution to be analysed. Then, the solution containing the complex formed by Hg, APDC and graphene was sonicated for 5 min and collected on a membrane filter (*Polyethersulfone PES, ϕ 25 mm, 0.2 μ m, Pall Corporation*) by filtration (*250 mL Erlenmeyer glass flask*) under vacuum. **Figure 5-1** shows Transmission Electron Microscopy (TEM) images of water samples containing (a) graphene alone, (b) graphene and APDC, and (c) Hg, APDC and graphene. This figure really highlights an increase of the size in the observed particles from graphene alone (67 nm) to the complex Hg/APDC/Graphene (700 nm to 1.89 μ m). Consequently, the size of this complex is larger than the membrane filter pores and is quantitatively retained by the filtering PES membrane. We noticed that the size of the complex Hg/APDC/Graphene remains lower than the certified commercial size of graphene nanosheets (*\sim 5 μ m diameter, 1-5 nm thickness*). In our study, we assume that both the time in the ultrasonic bath (about 60 min) and the use of Triton-X-100 during the preparation of the nanoparticles suspension would promote the dislocation of aggregates, hence reducing the size in comparison with the raw graphene nanosheets [37].

Finally, the membrane filter obtained is dried for 5 min in a laminar flow hood (*Class 100*) and kept into polycarbonate filters holder (*Petri slides*) at low temperature (-7°C) before its analysis.

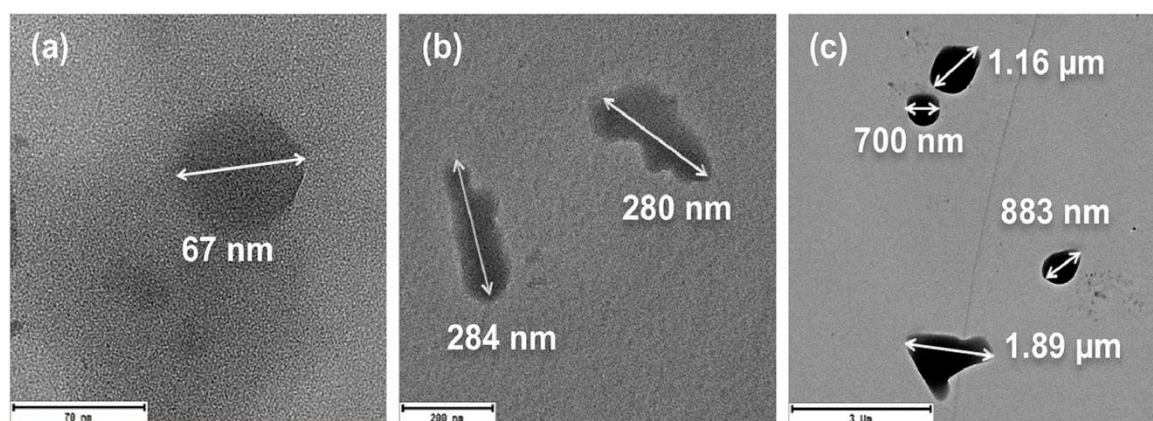


Figure 5-1: Transmission Electron Microscopy TEM of (a) Graphene, (b) Graphene + APDC and (c) Graphene + APDC + Hg(II).

5.3.3. Instrumentation and method for mercury analysis

Direct pyrolysis gold amalgamation and atomic absorption spectroscopy (AAS), using an Advanced Mercury Analyser (*Altec AMA-254, SymaLab*), allows the quantification of Hg in solid samples. The whole membrane filter is dropped on a nickel boat especially designed for this instrument ($1000 \mu\text{L}$, *SymaLab*). To increase analytical performances, nickel boats used for the analysis of the PES filters were previously cleaned by burning at $750 \text{ }^\circ\text{C}$ daily, using the AMA-254. This step has been repeated until a relative standard deviation under 10 % between two successive burnings is obtained. After the introduction of the sample into the analyser using the nickel boat, an increase in temperature up to $750 \text{ }^\circ\text{C}$ under oxygen atmosphere allows first the drying of the matrix, and then the decomposition of the sample and its dry mineralization. Decomposition products and mercury are driven by the oxygen stream through a catalytic tube continuously heated at $550 \text{ }^\circ\text{C}$. This catalytic tube allows decomposition and reduction of methylmercury to gaseous elemental mercury $\text{Hg}(0)$ and the removal of halogens. Then, total mercury vapour is trapped in a quartz tube filled with gold-coated sand that allows the preconcentration of mercury, and so improve the sensitivity of the instrument. A few seconds later, the gold amalgamator is heated at about $950 \text{ }^\circ\text{C}$. The quantification of this released mercury is carried out using two absorption cells (1 cm and 10 cm lengths, wavelength = 253.65 nm), both of them thermostatically controlled at $125 \text{ }^\circ\text{C}$, that allows sequential quantification of mercury at two different ranks (Rank 1 < 25 ng Hg , and Rank 2 > 25 ng Hg).

All instrumental parameters have been optimized for analysis of PES filters as follow: drying step of 150 sec, decomposition step of 150 sec and waiting step of 45 sec. Accuracy and reproducibility of the AMA-254 were assessed by using the Certified Reference Material BCR-320R (channel sediment $0.85 \pm 0.09 \text{ mg kg}^{-1}$ of total Hg), analysed regularly all along the measurement process according to the EPA method 7473 (SW-846).

5.3.4. Calibration for mercury quantification

To quantify the accumulated mass of mercury on the PES filter, the AMA-254 was calibrated using an external matrix-matched calibration curve in the absolute mass of mercury ($2.3 - 207 \text{ ng Hg}$). Indeed, matrix effects can occur during the analysis of the PES filters and there is no existing certified reference material with a similar matrix. The Hg(II) standard solution (*Strem Chemicals, USA*) was prepared in 1% HCl with a concentration of $400 \mu\text{g Hg L}^{-1}$ and various amounts were directly dropped into a nickel boat containing a PES filter resulting in absolute Hg masses of 2, 4, 10, 21, 31, 42, 53, 85, 144 and 207 ng. Here, we used Hg(II) considering the low fraction of MeHg in natural waters (< 10 % of total mercury) and assuming there would not be any difference in the adsorption process using either Hg(II) and/or MeHg (**5.3.1 Preparation of nanoparticles suspension**). The absorbance (A) resulting from the analysis of unused filters was used for blank correction. The calibration functions obtained provide a reliable way to determine Hg content in the PES filters for both absorption cells, Rank1 ($R^2 = 0.99947$) and Rank2 ($R^2 = 0.99996$), with slopes of respectively (36.4 ± 0.3) and (560 ± 1) ng Hg AbsorbanceUnit⁻¹.

The calibration curves according to the present procedure under the optimized conditions were also set up in the absolute mass of mercury (1.9 – 210 ng). Various samples containing 200 mL of high purity water were spiked with known amounts of Hg(II) standard solution ($[Hg] = 400 \mu\text{g L}^{-1}$) resulting in absolute Hg masses of 2, 4, 8, 13, 19, 22, 43, 85, 148 and 211 ng. These samples were subjected to the preconcentration process previously described (**5.3.2 Procedure for mercury preconcentration (optimum conditions)**). The obtained calibration functions provide a reliable way to determine Hg content in the PES filters for both absorption cells, Rank1 ($R^2 = 0.99974$) and Rank2 ($R^2 = 0.99971$), with slopes of respectively (38.6 ± 0.1) and (576 ± 3) ng Hg Absorbance Unit⁻¹.

Coefficients of determination R^2 of the four different calibration curves are all above 0.99947, suggesting validated good linear relationship. Nevertheless, taking into account the standard deviations, the slopes given by these models are significantly different at a 95 % confidence level. This could be explained by the relative difficulty to weigh correctly the mass of Hg(II) standard solution added directly in the nickel boat in the case of matrix-matched calibration. Indeed, in practice, when the operator drops the solution into the nickel boat, the balance is not stable either due to adsorption on the nickel boat surface and/or evaporation. Therefore, in this work, we decided to use the calibration curves obtained according to the procedure developed in this study under optimized conditions for data treatment.

5.3.5. Sampling of natural waters

To check the suitability of the proposed method to the analysis of natural waters, real samples were collected in April 2017 at two locations of the Pyrénées-Atlantiques (Nouvelle-Aquitaine, France). Freshwater was collected from Lac Des Carolins ($43^{\circ}20'15''$ N, $0^{\circ}24'23''$ W), at a depth of 40 cm using acid cleaned polyethylene bottles (2 L) that were rinsed three times with the sampling water. Important wildlife in the surroundings of the lake has a great influence on its biogeochemical characteristics, especially concerning the relatively high content of organic matter measured in the sample ($[DOC] = 5.6 \text{ mg L}^{-1}$). Coastal seawater was collected in the same way out of the Bay of St Jean de Luz ($43^{\circ}23'37''$ N, $1^{\circ}39'44''$ W, Bay of Biscay, North-East Atlantic Ocean). Time collection of the samples corresponds to high tide, and the seawater is characterized by a lower amount of organic matter ($[DOC] = 0.90 \text{ mg L}^{-1}$) and a high salinity (35.6 PSU). All water samples were filtered through a PES membrane ($0.2 \mu\text{m}$), acidified with ultra-pure hydrochloric acid (1 % v/v) and stored at 4 °C for no longer than two days before further manipulation and analysis.

5.4. Results and discussion

5.4.1. Optimisation of the Hg preconcentration method

1. Amount of nanoparticles

The amount of nanoparticles used in the preconcentration step will have a great influence on the efficiency of the proposed procedure. Enough nanoparticles must be available to chelate all the mercury present in the sample. Furthermore, an extra amount of nanoparticles will i) ensure that the possible presence of other competing metals will not negatively affect the effectiveness of Hg sequestration and ii) allow the use of a larger volume of sample to eventually improve the detection limit of the method. In this work, the influence of the amount of nanoparticles has been studied. High purity water samples of 25 mL (n=4) were spiked with 100 ng of mercury (Hg(II) standard solution), and various amounts of nanoparticles have been added (expressed as volume of nanoparticles suspension added, from 100 μ L to 2000 μ L). Then, all the samples were subjected to the preconcentration procedure with a sonication time of 5 min. Blanks (n=4) were also produced for the various amounts of nanoparticles, following the same procedure with unspiked high purity water. The results are shown in **Figure 5-2.a**, which provides the mercury recovery, obtained as a function of the amount of nanoparticles. No significant change was noticed in the recovery but the best condition selected was for a volume of nanoparticles suspension of 500 μ L, to ensure that all the mercury in the sample would be trapped even in the presence of a high amount of other competing metals. Indeed, a large amount of nanoparticles suspension leads to an increase in the blanks signal. The graphene shows similar properties to activated carbon so it can adsorb the gaseous species of mercury present in the air during the preparation of the nanoparticles suspension [38–40]. This could lead to the contamination in the blanks, making necessary to work under a clean atmosphere and to minimize the amount of nanoparticles suspension.

2. Sonication time

In previous works about preconcentration of metals using graphene nanoparticles as a sorbent, it is shown that the contact time between the nanoparticles suspension and the water sample does not appear as a critical variable as sorption occurs immediately [30,41]. Nevertheless, this parameter has been investigated here (**Figure 5-2.b**) within the time range of 1-15 min in the ultrasonic bath. So, high purity water samples of 25 mL (n=4) were spiked with 100 ng of mercury, and preconcentrated using 500 μ L of nanoparticles suspension with various sonication times (1-15 min). Blanks (n=4) were also performed for each condition, following the same procedure with unspiked high purity water. Results depicted in **Figure 5-2.b** show that sorption of mercury is significantly less effective when the time in the ultrasonic bath is lower than 1 min. Besides, for 2 min of sonication, the procedure shows a lower reproducibility (two replicates with about 87% of recovery and two replicates with about 100% recovery) confirming that the sorption of mercury does not occur immediately. Finally, longer sonication times result in poorer reproducibility. This might be due to the influence of the ultrasonic bath that could degrade the non-covalent interactions (π - π stacking) between graphene nanosheets and APDC. Therefore, sonication time of 5 min allows an effective and reproducible activation of the binding sites.

For in-field direct application, we can imagine that the use of the ultrasonic bath can be easily replaced by a simple shaking, with longer time.

3. Sample volume

The volume of the water sample used during the method of preconcentration is one of the critical steps in the analytical performance. Indeed, the choice of a larger volume of samples leads to an increase in the preconcentration factor and, hence, to a decrease in the detection limits, provided that the nanoparticles present (same amount, lower concentration) can sequester quantitatively all the mercury that can be much more diluted in the medium. Calibration curves were obtained as described in **5.3.4 Calibration for mercury quantification** using two different volumes of ultrapure water, i.e. 20 and 200 mL **Figure 5-2.c and d** show the absorbance obtained after the analysis of the filters produced according to the procedure described in **5.3.2 Procedure for mercury preconcentration (optimum conditions)** as a function of the theoretical amount of mercury added to the sample. Blanks (n=3 for 20 mL and n=2 for 200 mL of the sample) have been carried out for the two volumes, following the same procedure with unspiked high purity water. From 1.6 ng to 210 ng of mercury added to the test solution, no significant change can be observed in the efficiency of the preconcentration when working with 20 or 200 mL. A larger volume could have been tested, nevertheless, increasing the volume above 200 mL will be more time consuming for the operator in charge of the procedure because the filtration step will be much longer, especially with samples containing a high content of organic matter and/or suspended material. For future use of this method to quantify mercury in an aquatic environment, it is then important to adapt the sample volume to the specification of the water sample, especially when the concentration of Hg is very low.

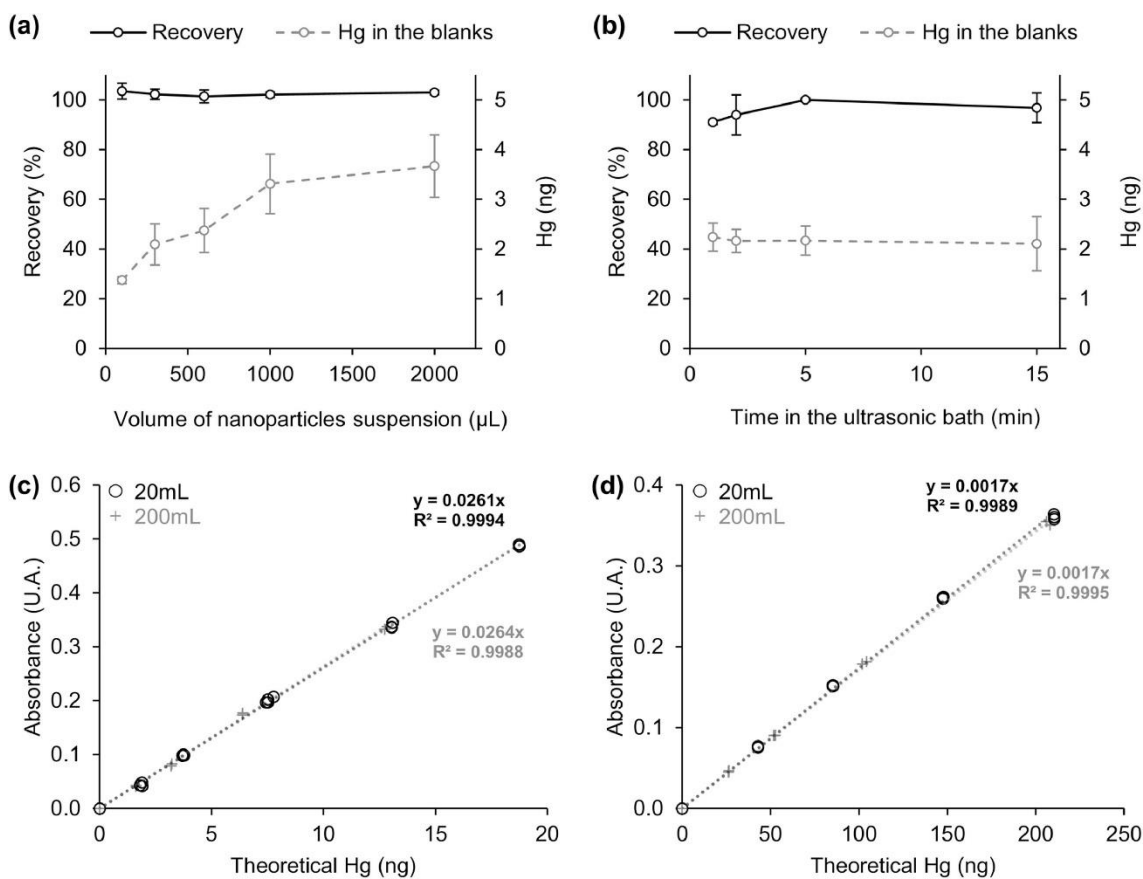


Figure 5-2: Recovery (n = 4) of Hg (a) as a function of the volume of nanoparticles suspension and (b) as a function of the time in the ultrasonic bath. Theoretical Hg (ng) as a function of the absorbance given by AMA-254 to (c) Rank 1 and (d) Rank 2 for 20 mL and 200 mL of water sample.

5.4.2. Optimization of the storage conditions

The possible application of this preconcentration method directly in the field, in remote areas, implies the transportation of the filters from the sampling site back to the laboratory for their analysis. Thus, storage conditions of the filters is an important factor to take into account to minimize sample contamination as well as potential losses of mercury by evaporation. On the one hand, elemental mercury (Hg(0)) is present at trace levels in the ambient air. Typically, Total Gaseous Mercury (TGM) concentrations averages about 1.5 ng m³ in background ambient air throughout the world [42]. In our laboratory, TGM concentrations have been reported by *Lusilao-Makiese et al.* [40] (6.3 ± 1.6 ng m³), and are higher than the background ambient air levels due to the activities that take place in the laboratory (analysis and development of methodologies for metals and metalloids). This concentration, though, remains quite low for a laboratory building located in an urban area. Then, as Hg(0) is subject to adsorption on all solid surfaces, it could eventually be adsorbed on the Hg-enriched filters produced in the preconcentration step and lead to an overestimation of the Hg content. On the other hand, the complex formed by Hg, APDC and graphene may be sensitive to degradation by light, temperature, oxygen, humidity etc... Then the exposure of the filters to various environmental conditions could lead to desorption of the mercury from the filters.

To avoid such problems, the stability of Hg-enriched filters has been evaluated using various storage conditions according to an isochronous design [43–45]. It is based on a storage design of the samples at various temperatures for different time intervals allowing all measurements to be done at the same time i.e. at the end of the study. In classical stability studies, measurements of the samples are achieved throughout the study i.e. at a different time so any drift of the measurement system over time can lead to incorrect conclusions. Thus, isochronous measurements only require repeatability conditions whereas classical stability studies require also long-term reproducibility.

The storage design set up in this study is shown in **Table 5-1**. Hg-enriched filters were obtained according to the present procedure under optimized conditions (500 µL of nanoparticles suspension, 5 min sonication time), using 25 mL of high purity water samples spiked with 100 ng of mercury (n=3). Then, the filters were kept into polycarbonate filter holders (Petri slides) and Zip-lock bags at the corresponding temperature for the required time. It has been assumed that mercury is stable on the filters at low temperature (-7 °C). Thus, this reference temperature (i.e. -7 °C in a freezer) is the temperature at which the samples were always transported or kept before the analysis and the testing temperatures (i.e. 4 °C in a cool room and 21 °C in a flow hood at ambient temperature) were the conditions at which test samples were stored for a selected period of time, before returning to the reference temperature. The total amount of Hg in all the filters was measured together at the end of the experiment.

To distinguish the various storage conditions of the filters and their efficiency, a Kruskal-Wallis test (nonparametric test), followed by a Conover and Iman test has been performed. **Figure 5-3** summarizes the data collected in the isochronous measurement experiment along with the results of the Kruskal-Wallis test. On the one hand, after eight weeks of storage, the ratio between the recovery of the testing

temperature T1 (21 °C) and the recovery of the reference temperature decreases significantly down to $84.7 \pm 1.9 \%$. On the other hand, after eight weeks, the decrease of this ratio with the testing temperature T2 (4 °C) is less important ($93.2 \pm 1.4 \%$) but still significant. The only storage condition that does not show a significant difference with the results from the reference temperature is as follows: one week of storage at 4 °C. This allows the in-field application of the mercury preconcentration method as it is usually possible to keep the filters at low temperature (4 °C) in a portable fridge before coming back to the lab where the filters can be stored at low temperature ($< -7 \text{ °C}$). If filters must be stored for a longer time, it is recommended to do it at freezing temperature, and even in that case, possible loss of mercury should be expected.

Table 5-1: Storage design for isochronous measurements to evaluate stability of the filters.

Storage t (weeks) \ Temperature (°C)	0	1	2	3	4	5	6	7	8	9	10	11	12	
	T ₁ (21°C)													
T ₂ (4°C)														
T _{ref} (-7°C)														
Analysis														✘

 Storage at temperature T
 Storage at very low temperature (T_{ref})

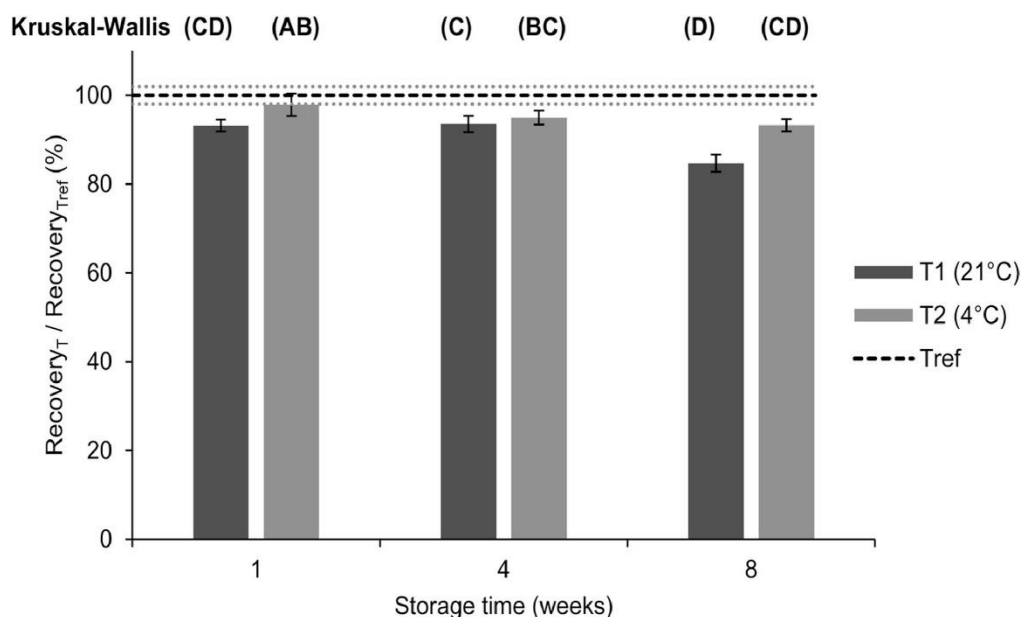


Figure 5-3: Ratio between the recovery of Hg for the testing temperature T ($n = 3$) and the recovery of Hg for the reference temperature T_{ref} .

5.4.3. Potential interferences: matrix effects

The potential occurrence of matrix effects due to the presence of interfering compounds in the sample was also investigated. For the sake of simplicity, the possible effect of salinity, organic matter and competing metals were modelled with NaCl, natural organic matter (NOM) and Ca^{2+} , respectively. Then, applicability to real samples with high organic matter content, and high salinity was demonstrated.

1. Organic matter

According to various studies about the adsorption of dissolved mercury and the influence of organic matter on this process, the efficiency of our new methodology could be eventually reduced by the presence of organic matter [46–48]. The reference material Suwanee River natural organic matter (SRNOM), purchased from International Humic Substances Society (IHSS, USA) was used to model organic matter. A solution with $NOM = 500 \text{ mg L}^{-1}$ was prepared by dissolving 12.5 mg of NOM in 25 mL of high purity water. Firstly, high purity water samples of 25 mL ($n=4$) were spiked with 100 ng of mercury, and various amounts of natural organic matter solution were added ($[NOM] = 0 - 18.4 \text{ mg L}^{-1}$). Blanks ($n=4$) were also produced in the same extent and under the same conditions with unspiked high purity water. The whole samples were preconcentrated using 500 μL of nanoparticles suspension and 5 min sonication time. Recoveries in **Figure 5-4.a**, calculated using the theoretical amount of Hg in the water sample and the amount of Hg obtained from the analysis of the Hg-enriched filter, show us

that for NOM < 5 mg L⁻¹ there is no significant influence of the organic matter on the preconcentration of mercury on the nanoparticles (98±2 % < R < 105±1 %). Nevertheless, for NOM > 5 mg L⁻¹, the recovery decreases steadily down to 84±3 % for NOM = 18.4 mg L⁻¹.

The potential influence of organic matter was also tested with real samples from Lac des Carolins ([DOC] = 5.6 mg L⁻¹). 200 mL of water sample from this lake (n=2) spiked with a known amount of mercury (1.6 – 208 ng of mercury), and control solutions (n=2) with the same amount of mercury in 200 mL of high purity water were simultaneously prepared. Then, samples were stored at room temperature, protected from light, in a laminar flow hood at least for 12 hours (equilibrium step). The samples were then treated according to the procedure described in **5.3.2 Procedure for mercury preconcentration (optimum conditions)**. The percentage of controls, calculated as the ratio between mercury found in the real sample and mercury found in the controls for the same amount of spiked mercury (**Figure 5-4.c**) demonstrates that our new methodology for mercury preconcentration can be applied successfully to samples with a relatively high content of organic matter.

Bravo et al. [49] have studied the influence of organic matter on mercury species concentrations within 29 streams across Europe. In this study, total organic carbon (TOC) values range from 0.6 to 22.2 mg L⁻¹ and 76 % of the streams show TOC < 5 mg L⁻¹, suggesting that our method is applicable to many freshwater systems.

2. Salinity

By analogy with organic matter, it has been shown that the presence of chloride salts might reduce the efficiency of the adsorption because of the formation of the resistant complex HgCl₄⁻ leading to an inhibition of the mercury adsorption on other sorbents [50,51]. The presence of chloride salts and their influence on the efficiency of the preconcentration procedure have been studied to determine applicability to seawater samples. Firstly, sodium chloride (*NaCl*, Merck KGaA, Denmark) has been added to high purity water samples of 25 mL (NaCl, 0 – 36 g L⁻¹), also spiked with 100 ng of mercury. Replicates (n=4) of these synthesized solutions allowed us to produce Hg-enriched filters that have been analysed by AMA-254. Recoveries in **Figure 5-4.b**, calculated using the theoretical amount of Hg in the water sample and the amount of Hg obtained from the analysis of the Hg-enriched filter, show us that for NaCl < 22 g L⁻¹ there is no significant influence of sodium chloride on the preconcentration of mercury on nanoparticles (100±1 % < R < 107±1 %). Nevertheless, the recovery decreases slightly until 93±2 % for NaCl = 36 g L⁻¹. For most natural waters, including groundwater, continental and estuarine waters, the presence of moderate amounts of salt should not lead to significant errors derived from the occurrence of matrix effects. Even in the case of high salinity seawaters, the effect should not be very pronounced (about 7 % suppression of the analytical signal).

To validate this hypothesis, we decided to apply the method of preconcentration to real samples with high salinity. 200 mL of water sample (n=2) from St Jean de Luz were spiked with a known amount of mercury (1.9 – 208 ng of mercury). Control solutions (n=2) with the same amount of mercury in 200 mL of high purity water samples were simultaneously prepared. After an equilibration step of 12 hours, Hg-enriched filters were produced according to the preconcentration procedure. The percentage of control,

depicted in **Figure 5-4.d**, demonstrates that our new methodology for mercury preconcentration can be applied successfully to samples with high salinity. Elsewhere, even if seawater contains high amounts of potential sources of exhaustion of the binding sites (sulphate, chloride, sodium, potassium etc...), the successful application of our new methodology to real seawater samples underlines the absence of competition of these ions with Hg for binding to the APDC.

3. Competing metals

With the variety of metal ions that could bind competitively with the chelating agent (APDC), calcium (Ca^{2+}) is usually the major species present in water samples, and so it has been selected to investigate the competition with mercury for the chelation step. High purity water samples of 25 mL containing various amount of calcium ($\text{Ca}^{2+} = 0 - 18.5 \text{ mg L}^{-1}$) were spiked with 100 ng of mercury. The ratio between results obtained for the reference filter (without calcium) and other conditions ($R = 102 - 109 \%$) confirms that mercury is predominately bond to the APDC in all the conditions tested. Considering the strong binding affinity between $-\text{SH}$ groups from APDC and Hg, a high competition or influence from the presence of other ions than Ca^{2+} is not expectable

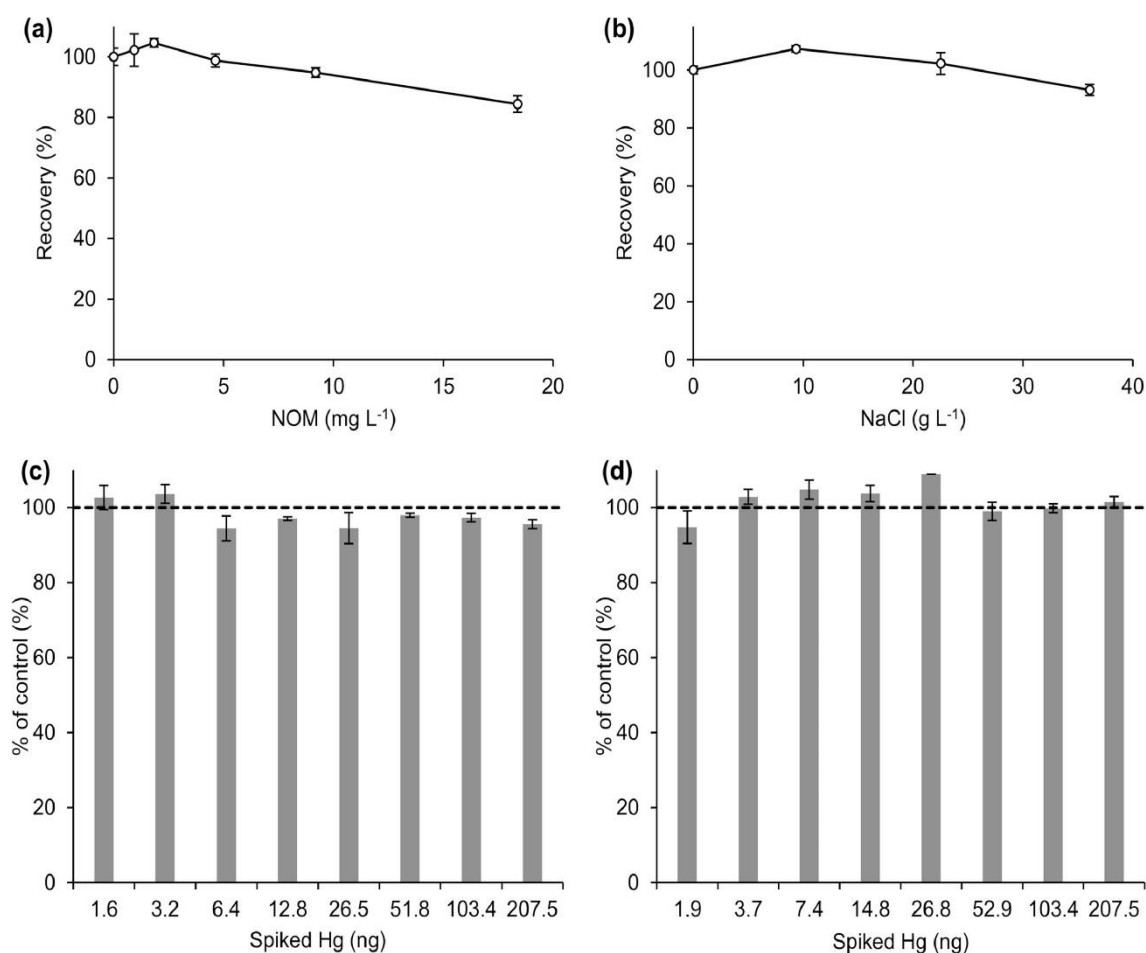


Figure 5-4: Recovery of Hg (a) as a function of the concentration of natural organic matter (NOM) ($n = 4$) and (b) as a function of the concentration of sodium chloride (NaCl) ($n = 5$). Ratio ($n = 2$) between control samples (high purity water) and real samples from (c) Lake Des Carolins (freshwater) and (d) St Jean de Luz (seawater) as a function of the spiked mercury.

5.4.4. Method blank levels and optimization

Working under clean conditions is also a crucial consideration for successful analysis at very low concentration levels, in particular with mercury. In that sense, as mentioned in previous sections, for each change in a parameter during the preconcentration procedure (sample volume, nanoparticles suspension, sonication time, and amount of Ca^{2+} , NaCl and organic matter in the sample) replicates of high purity water were submitted to the same protocol. Low levels and good reproducibility for these blank samples lead to a very good limit of detection.

Firstly, to check any contamination before their use, unused PES membrane filters have been analysed using the AMA-254. The absorbance obtained was 0.0025 ± 0.0006 ($n=15$) and this value is not significantly different (t-test, $p < 0.05$) from the value given by the analysis of empty nickel boats, 0.0018 ± 0.0002 ($n=9$), suggesting that no cleaning step is necessary for the PES filters.

Secondly, most of the experiments have been conducted in a trace metals laboratory whereas the last experiments, about real samples, took place in a clean laboratory, dedicated to ultra-trace mercury analysis. In the first cases, plastic flasks of 25 mL, cleaned in a 10% HNO_3 bath, were used as a container and the blanks levels reached 1.9 ± 0.2 ng Hg per filter. In the clean laboratory, special attention was paid to the procedure for cleaning all vessels used for sampling (polyethylene vials) and sample preparation (glass vials, glass filtration system, and filter holders) with successive acid baths (10% HNO_3 , 10% HNO_3 and 10% HCl), reducing the blank levels down to 0.60 ± 0.03 ng Hg per filter.

Finally, it has been shown that graphene on its own can adsorb volatile Hg species, so it is probably responsible for the Hg content in the blank filters. This hypothesis was confirmed by the analysis of graphene directly by AMA-254: 0.82 ± 0.01 mg Hg kg^{-1} . One possibility to reduce such contamination, and therefore to reduce the blank levels, should be to buy new graphene nanosheets that will be managed only in a glove box under argon flux. Another solution could be to find a purification process not affecting graphene nanosheets structure and properties.

5.4.5. Analytical performances

The analytical performances of the method developed in this work are summarized in **Table 5-2** together with other methods for determination of mercury species at trace and ultra-trace levels. Traditional and/or newly developed methods highlight various problems preventing their application in-field and/or in developing countries: heavy sample preparation, high cost due to reagents and/or apparatus, and high limits of detection. Indeed, very sensitive analytical methods commonly used for the determination of Hg species, CV-AFS (LOD < 0.06 ng L^{-1}) [52,53] and GC-ICP-MS (LOD < 0.04 ng L^{-1}) [13], require a strong knowledge in analytical chemistry, and maintenance. Moreover, the use of these techniques implies a significant economic cost, due to either the equipment or the reagents. The use of a commercial mercury analyser for the analysis of the filters produced according to our new procedure greatly simplifies all the analytical process. Most of the newly developed methodologies focus on preconcentration of the Hg species followed by an elution step [15,17,20,54,55], making their application in the field laborious, if not impossible, which is not the case in our new method with the direct analysis

of the filter. Finally, the most interesting published analytical methods for in-field Hg preconcentration need also strong knowledge in analytical chemistry for the preparation of the nanogold-coated passive sampler [26] and the magnetite nanoparticles [27] while the functionalization of the graphene nanosheets in our study appears much simpler. Moreover, in this work, just a few minutes are necessary to recover the whole Hg species on the functionalized graphene nanosheets whereas *Tavares et al.* [27] need 24 hours. Overall, the novelty and the superiority of our work lie mainly on its simplicity all along its process: sampling (easily transportable filter), preconcentration (quickly and effortlessly producible adsorbent) and analysis (direct analysis of the solid without any elution step needed using a cheap equipment).

This new method for quantification of mercury by DMSPE using graphene nanosheets and direct analysis by pyrolysis gold amalgamation and atomic absorption spectroscopy (AAS) resolves many of these limitations and can be still improved. It provides a LOD as low as 0.38 ng L^{-1} for 200 mL of samples, with a large linear range ($0.38 - 1038 \text{ ng L}^{-1}$). As concentration levels of total mercury in water samples (sea, estuarine, fresh) range in the ng L^{-1} , in most of the cases, our method is applicable, only with 600 mL of water sample for triplicate analysis. In the case of water samples presenting smaller mercury content, usually coming from pristine areas, such as ocean and many remote water bodies, the matrix is not complex, making the filtration step easier to manage. Therefore, for these particular cases, increasing the volume up to 1 L should allow a reduction of the LOD to match the Hg concentration in the sample.

Table 5-2: Methods for analysis of mercury species in natural waters.

<i>Method</i>	<i>Volume (L)</i>	<i>Water type</i>	<i>Hg species</i>	<i>Quantification</i>	<i>RSD (%)</i>	<i>LOD (ng.L⁻¹)</i>	<i>Note</i>	<i>Reference</i>
Procedure presented in this work	0.2 (5min extraction)	Fresh and seawater	THg	External calibration	4.2 (Blanks) 3.0 (Standard) 3.2 (Fresh water) 4.5 (Seawater)	0.4	APDC/Graphene Nanosheets - DMSPE, filtration, and double gold amalgamation before AAS detection	This work
GC-ICP-MS	0.1	Fresh and seawater	Hg ²⁺ MeHg ⁺	Isotopic Dilution (equilibration time 12h)	2.5 3.4	0.04 0.01	Alkyl derivatization to produce volatile species, extraction in GC organic solvent	[13]
CV-AFS (EPA 245.7)	0.25	Fresh water	THg	External calibration	n.d.	0.04	KBr oxidation, SnCl ₂ reduction, purge of Hg(0), and AFS detection	[53]
CV-AFS (EPA 1631)	0.1	Fresh water	THg	External calibration	~5	0.06	BrCl oxidation, SnCl ₂ reduction, purge of Hg(0), and double gold amalgamation before AFS detection	[52]
IIP-CV-AAS	0.1	Fresh and seawater	Hg ²⁺	External calibration	2.4	0.5	Preparation of the IIP for Hg ²⁺ specific adsorption IIP - SPE column, elution by EDTA, and AAS detection	[15]
MWCNTs-GC-MS	0.025	Fresh and seawater	Hg ²⁺ MeHg ⁺ EtHg ⁺	Internal standard quantification	6.2 6.8 7.2	4 3 3	Complexation of Hg species by NaDDC, MWCNTs - SPE column, elution by ethyl acetate with online alkyl derivatization	[17]
IL-GO-ETAAS	0.005	Fresh water	THg	External calibration	3.9	14	Preparation of the IL-GO hybrid nanomaterial for Hg adsorption IL-GO – SPE column, elution by 20% HNO ₃ and ETAAS detection	[20]
NG-COOH-FI-CV-AAS	0.010	Fresh water	Hg ²⁺ MeHg ⁺ EtHg ⁺	External calibration	<3	9.8	NG-COOH as solid-phase sorbent for US-D-IL-μ-SPE Elution by HNO ₃ and analysis by FI-CV-AAS	[54]
GO-ICP-MS	0.010	Fresh water	Hg ²⁺ MeHg ⁺ EtHg	External calibration	4.5 3.1 3.7	0.005 0.006 0.009	GO as the SPE adsorbent Elution by benzoic acid	[55]
AuNP-AFS	n.d. (10min direct extraction)	Fresh and seawater	THg	External calibration	4.9	0.2	Nanogold-coated dipsticks (AuNP) - SPE Thermal desorption, double gold amalgamation before AFS detection	[26]
NPs-AAS	1	Fresh and seawater	THg	External calibration	<10	1.8	Fe ₃ O ₄ @SiO ₂ SiDTC – DMSPE (24h extraction step), double gold amalgamation before AAS detection	[27]

5.5. References

- [1] B. Gworek, O. Bemowska-Kalabun, M. Kijeńska, J. Wrzosek-Jakubowska, Mercury in Marine and Oceanic Waters—a Review, *Water, Air, & Soil Pollution*. 227 (2016). <https://doi.org/10.1007/s11270-016-3060-3>.
- [2] Z.F. Anual, W. Maher, F. Krikowa, L. Hakim, N.I. Ahmad, S. Foster, Mercury and risk assessment from consumption of crustaceans, cephalopods and fish from West Peninsular Malaysia, *Microchemical Journal*. 140 (2018) 214–221. <https://doi.org/10.1016/j.microc.2018.04.024>.
- [3] M. Arcagni, R. Juncos, A. Rizzo, M. Pavlin, V. Fajon, M.A. Arribére, M. Horvat, S. Ribeiro Guevara, Species- and habitat-specific bioaccumulation of total mercury and methylmercury in the food web of a deep oligotrophic lake, *Science of The Total Environment*. 612 (2018) 1311–1319. <https://doi.org/10.1016/j.scitotenv.2017.08.260>.
- [4] J. Aaseth, B. Hilt, G. Bjørklund, Mercury exposure and health impacts in dental personnel, *Environmental Research*. 164 (2018) 65–69. <https://doi.org/10.1016/j.envres.2018.02.019>.
- [5] F. Khan, S. Momtaz, M. Abdollahi, The relationship between mercury exposure and epigenetic alterations regarding human health, risk assessment and diagnostic strategies, *Journal of Trace Elements in Medicine and Biology*. 52 (2019) 37–47. <https://doi.org/10.1016/j.jtemb.2018.11.006>.
- [6] K. Sundseth, J.M. Pacyna, E.G. Pacyna, J. Munthe, M. Belhaj, S. Astrom, Economic benefits from decreased mercury emissions: Projections for 2020, *Journal of Cleaner Production*. 18 (2010) 386–394. <https://doi.org/10.1016/j.jclepro.2009.10.017>.
- [7] W. Zhang, G. Zhen, L. Chen, H. Wang, Y. Li, X. Ye, Y. Tong, Y. Zhu, X. Wang, Economic evaluation of health benefits of mercury emission controls for China and the neighboring countries in East Asia, *Energy Policy*. 106 (2017) 579–587. <https://doi.org/10.1016/j.enpol.2017.04.010>.
- [8] C.H. Lamborg, C.R. Hammerschmidt, K.L. Bowman, G.J. Swarr, K.M. Munson, D.C. Ohnemus, P.J. Lam, L.-E. Heimbürger, M.J.A. Rijkenberg, M.A. Saito, A global ocean inventory of anthropogenic mercury based on water column measurements, *Nature*. 512 (2014) 65–68. <https://doi.org/10.1038/nature13563>.
- [9] UNEP, Global mercury assessment 2013: sources, emissions, releases and environmental transport, UNEP Chemicals Branch, Geneva, Switzerland, 2013.
- [10] C.T. Driscoll, R.P. Mason, H.M. Chan, D.J. Jacob, N. Pirrone, Mercury as a Global Pollutant: Sources, Pathways, and Effects, *Environmental Science & Technology*. 47 (2013) 4967–4983. <https://doi.org/10.1021/es305071v>.
- [11] D.G. Streets, Q. Zhang, Y. Wu, Projections of Global Mercury Emissions in 2050, *Environmental Science & Technology*. 43 (2009) 2983–2988. <https://doi.org/10.1021/es802474j>.
- [12] J. Wiener, D. Krabbenhoft, G. Heinz, A. Scheuhammer, Ecotoxicology Of Mercury, in: D. Hoffman, B. Rattner, G. Allen Burton Jr, J. Cairns Jr (Eds.), *Handbook of Ecotoxicology*, Second Edition, CRC Press, 2002. <https://doi.org/10.1201/9781420032505.ch16>.
- [13] J. Cavalheiro, C. Sola, J. Baldanza, E. Tessier, F. Lestremau, F. Botta, H. Preud'homme, M. Monperrus, D. Amouroux, Assessment of background concentrations of organometallic compounds (methylmercury, ethyllead and butyl- and phenyltin) in French aquatic environments, *Water Research*. 94 (2016) 32–41. <https://doi.org/10.1016/j.watres.2016.02.010>.
- [14] X. Jia, J. Zhao, H. Ren, J. Wang, Z. Hong, X. Zhang, Zwitterion-functionalized polymer microspheres-based solid phase extraction method on-line combined with HPLC–ICP-MS for mercury speciation, *Talanta*. 196 (2019) 592–599. <https://doi.org/10.1016/j.talanta.2019.01.013>.
- [15] M. Soleimani, M.G. Afshar, Highly selective solid phase extraction of mercury ion based on novel ion imprinted polymer and its application to water and fish samples, *J Anal Chem*. 70 (2015) 5–12. <https://doi.org/10.1134/S1061934815010189>.
- [16] O. Çaylak, Ş.G. Elçi, A. Höl, A. Akdoğan, Ü. Divrikli, L. Elçi, Use of an aminated Amberlite XAD-4 column coupled to flow injection cold vapour generation atomic absorption spectrometry for

- mercury speciation in water and fish tissue samples, *Food Chemistry*. 274 (2019) 487–493. <https://doi.org/10.1016/j.foodchem.2018.08.107>.
- [17] J. Muñoz, M. Gallego, M. Valcárcel, Speciation of Organometallic Compounds in Environmental Samples by Gas Chromatography after Flow Preconcentration on Fullerenes and Nanotubes, *Anal. Chem.* 77 (2005) 5389–5395. <https://doi.org/10.1021/ac050600m>.
- [18] A. Kaur, U. Gupta, A review on applications of nanoparticles for the preconcentration of environmental pollutants, *Journal of Materials Chemistry*. 19 (2009) 8279. <https://doi.org/10.1039/b901933b>.
- [19] A. Tadjarodi, A. Abbaszadeh, A magnetic nanocomposite prepared from chelator-modified magnetite (Fe₃O₄) and HKUST-1 (MOF-199) for separation and preconcentration of mercury(II), *Microchim Acta*. 183 (2016) 1391–1399. <https://doi.org/10.1007/s00604-016-1770-2>.
- [20] A.C. Sotolongo, E.M. Martinis, R.G. Wuilloud, An easily prepared graphene oxide–ionic liquid hybrid nanomaterial for micro-solid phase extraction and preconcentration of Hg in water samples, *Anal. Methods*. 10 (2018) 338–346. <https://doi.org/10.1039/C7AY02201H>.
- [21] T.A. Labutin, V.N. Lednev, A.A. Ilyin, A.M. Popov, Femtosecond laser-induced breakdown spectroscopy, *J. Anal. At. Spectrom.* 31 (2016) 90–118. <https://doi.org/10.1039/C5JA00301F>.
- [22] L. Wang, J.-B. Zhou, X. Wang, Z.-H. Wang, R.-S. Zhao, Simultaneous determination of copper, cobalt, and mercury ions in water samples by solid-phase extraction using carbon nanotube sponges as adsorbent after chelating with sodium diethyldithiocarbamate prior to high performance liquid chromatography, *Anal Bioanal Chem.* 408 (2016) 4445–4453. <https://doi.org/10.1007/s00216-016-9542-8>.
- [23] T. Stoichev, D. Amouroux, R.C.R. Martin-Doimeadios, M. Monperrus, O.F.X. Donard, D.L. Tsalev, Speciation Analysis of Mercury in Aquatic Environment, *Applied Spectroscopy Reviews*. 41 (2006) 591–619. <https://doi.org/10.1080/05704920600929415>.
- [24] A. Zierhut, K. Leopold, L. Harwardt, M. Schuster, Analysis of total dissolved mercury in waters after on-line preconcentration on an active gold column, *Talanta*. 81 (2010) 1529–1535. <https://doi.org/10.1016/j.talanta.2010.02.064>.
- [25] J. Huber, L.-E. Heimbürger, J.E. Sonke, S. Ziller, M. Lindén, K. Leopold, Nanogold-Decorated Silica Monoliths as Highly Efficient Solid-Phase Adsorbent for Ultratrace Mercury Analysis in Natural Waters, *Analytical Chemistry*. 87 (2015) 11122–11129. <https://doi.org/10.1021/acs.analchem.5b03303>.
- [26] M. Schlathauer, J. Friedland, M. Lindén, K. Leopold, Sustainable and reagent-free mercury trace determination in natural waters using nanogold dipsticks, *Microchemical Journal*. 147 (2019) 253–262. <https://doi.org/10.1016/j.microc.2019.03.032>.
- [27] D.S. Tavares, C. Vale, C.B. Lopes, T. Trindade, E. Pereira, Reliable quantification of mercury in natural waters using surface modified magnetite nanoparticles, *Chemosphere*. 220 (2019) 565–573. <https://doi.org/10.1016/j.chemosphere.2018.12.149>.
- [28] J. Li, Y. Liu, Y. Ai, A. Alsaedi, T. Hayat, X. Wang, Combined experimental and theoretical investigation on selective removal of mercury ions by metal organic frameworks modified with thiol groups, *Chemical Engineering Journal*. 354 (2018) 790–801. <https://doi.org/10.1016/j.cej.2018.08.041>.
- [29] Y. Huang, Y. Gong, J. Tang, S. Xia, Effective removal of inorganic mercury and methylmercury from aqueous solution using novel thiol-functionalized graphene oxide/Fe-Mn composite, *Journal of Hazardous Materials*. 366 (2019) 130–139. <https://doi.org/10.1016/j.jhazmat.2018.11.074>.
- [30] B. Zawisza, R. Skorek, G. Stankiewicz, R. Sitko, Carbon nanotubes as a solid sorbent for the preconcentration of Cr, Mn, Fe, Co, Ni, Cu, Zn and Pb prior to wavelength-dispersive X-ray fluorescence spectrometry, *Talanta*. 99 (2012) 918–923. <https://doi.org/10.1016/j.talanta.2012.07.059>.
- [31] K. Kocot, B. Zawisza, E. Marguá, I. Queralt, M. Hidalgo, R. Sitko, Dispersive micro solid-phase extraction using multiwalled carbon nanotubes combined with portable total-reflection X-ray fluorescence spectrometry for the determination of trace amounts of Pb and Cd in water samples, *Journal of Analytical Atomic Spectrometry*. 28 (2013) 736. <https://doi.org/10.1039/c3ja50047k>.

- [32] B. Zawisza, R. Sitko, E. Malicka, E. Talik, Graphene oxide as a solid sorbent for the preconcentration of cobalt, nickel, copper, zinc and lead prior to determination by energy-dispersive X-ray fluorescence spectrometry, *Analytical Methods*. 5 (2013) 6425. <https://doi.org/10.1039/c3ay41451e>.
- [33] K. Kocot, R. Sitko, Trace and ultratrace determination of heavy metal ions by energy-dispersive X-ray fluorescence spectrometry using graphene as solid sorbent in dispersive micro solid-phase extraction, *Spectrochimica Acta Part B: Atomic Spectroscopy*. 94–95 (2014) 7–13. <https://doi.org/10.1016/j.sab.2014.02.003>.
- [34] M.D. Stoller, S. Park, Y. Zhu, J. An, R.S. Ruoff, Graphene-Based Ultracapacitors, *Nano Letters*. 8 (2008) 3498–3502. <https://doi.org/10.1021/nl802558y>.
- [35] R. Sitko, B. Zawisza, E. Malicka, Graphene as a new sorbent in analytical chemistry, *TrAC Trends in Analytical Chemistry*. 51 (2013) 33–43. <https://doi.org/10.1016/j.trac.2013.05.011>.
- [36] M. Valcárcel, S. Cárdenas, B.M. Simonet, Y. Moliner-Martínez, R. Lucena, Carbon nanostructures as sorbent materials in analytical processes, *TrAC Trends in Analytical Chemistry*. 27 (2008) 34–43. <https://doi.org/10.1016/j.trac.2007.10.012>.
- [37] J. Gigault, B. Grassl, G. Lespes, A new analytical approach based on asymmetrical flow field-flow fractionation coupled to ultraviolet spectrometry and light scattering detection for SWCNT aqueous dispersion studies, *The Analyst*. 137 (2012) 917–923. <https://doi.org/10.1039/C2AN15449H>.
- [38] D. Amouroux, E. Tessier, C. Pécheyran, O.F.X. Donard, Sampling and probing volatile metal(loid) species in natural waters by in-situ purge and cryogenic trapping followed by gas chromatography and inductively coupled plasma mass spectrometry (P-CT-GC-ICP/MS), *Analytica Chimica Acta*. 377 (1998) 241–254. [https://doi.org/10.1016/S0003-2670\(98\)00425-5](https://doi.org/10.1016/S0003-2670(98)00425-5).
- [39] X.Q. Wang, P. Wang, P. Ning, Y.X. Ma, F. Wang, X.L. Guo, Y. Lan, Adsorption of gaseous elemental mercury with activated carbon impregnated with ferric chloride, *RSC Advances*. 5 (2015) 24899–24907. <https://doi.org/10.1039/C5RA01011J>.
- [40] J. Lusilao-Makiese, E. Tessier, D. Amouroux, E. Cukrowska, Analytical Performances of Nanostructured Gold Supported on Metal Oxide Sorbents for the Determination of Gaseous Mercury, *International Journal of Analytical Chemistry*. 2014 (2014) 1–8. <https://doi.org/10.1155/2014/490291>.
- [41] E.R. Pereira, B.M. Soares, J.V. Maciel, S.S. Caldas, C.F.F. Andrade, E.G. Primel, F.A. Duarte, Development of a dispersive liquid–liquid microextraction method for iron extraction and preconcentration in water samples with different salinities, *Analytical Methods*. 5 (2013) 2273. <https://doi.org/10.1039/c3ay26294d>.
- [42] Europäische Kommission, Ambient Air Pollution by Mercury (Hg) Position Paper: 17 October 2001, 2011. <https://nbn-resolving.org/urn:nbn:de:101:1-2012111733715> (accessed September 30, 2020).
- [43] A. Lamberty, H. Schimmel, J. Pauwels, The study of the stability of reference materials by isochronous measurements, *Fresenius' Journal of Analytical Chemistry*. 360 (1998) 359–361. <https://doi.org/10.1007/s002160050711>.
- [44] T.P.J. Linsinger, A.M.H. van der Veen, B.M. Gawlik, J. Pauwels, A. Lamberty, Planning and combining of isochronous stability studies of CRMs, *Accreditation and Quality Assurance*. 9 (2004) 464–472. <https://doi.org/10.1007/s00769-004-0818-x>.
- [45] B.M. Gawlik, R. Loos, G. Bidoglio, G. Fauler, X. Guo, E. Lankmayr, T. Linsinger, Testing sample stability in short-term isochronous stability studies for EU-wide monitoring surveys of polar organic contaminants in water, *TrAC Trends in Analytical Chemistry*. 36 (2012) 36–46. <https://doi.org/10.1016/j.trac.2012.04.001>.
- [46] Y. Yang, L. Liang, D. Wang, Effect of dissolved organic matter on adsorption and desorption of mercury by soils, *Journal of Environmental Sciences*. 20 (2008) 1097–1102. [https://doi.org/10.1016/S1001-0742\(08\)62155-5](https://doi.org/10.1016/S1001-0742(08)62155-5).
- [47] F. Wu, H. Liu, M. Zhang, W. Ma, X. Huang, S. Liu, J. Dai, Adsorption Characteristics and the Effect of Dissolved Organic Matter on Mercury(II) Adsorption of Various Soils in China, *Soil and Sediment*

- [48] X. Wang, X. Pan, G.M. Gadd, Soil dissolved organic matter affects mercury immobilization by biogenic selenium nanoparticles, *Science of The Total Environment*. 658 (2019) 8–15. <https://doi.org/10.1016/j.scitotenv.2018.12.091>.
- [49] A.G. Bravo, D.N. Kothawala, K. Attermeyer, E. Tessier, P. Bodmer, J.L.J. Ledesma, J. Audet, J.P. Casas-Ruiz, N. Catalán, S. Cauvy-Fraunié, M. Colls, A. Deininger, V.V. Evtimova, J.A. Fonvielle, T. Fuß, P. Gilbert, S. Herrero Ortega, L. Liu, C. Mendoza-Lera, J. Monteiro, J.-R. Mor, M. Nagler, G.H. Niedrist, A.C. Nydahl, A. Pastor, J. Pegg, C. Gutmann Roberts, F. Pilotto, A.P. Portela, C.R. González-Quijano, F. Romero, M. Rulík, D. Amouroux, The interplay between total mercury, methylmercury and dissolved organic matter in fluvial systems: A latitudinal study across Europe, *Water Research*. 144 (2018) 172–182. <https://doi.org/10.1016/j.watres.2018.06.064>.
- [50] C. Green-Ruiz, Effect of salinity and temperature on the adsorption of Hg(II) from aqueous solutions by a Ca-montmorillonite, *Environmental Technology*. 30 (2009) 63–68. <https://doi.org/10.1080/09593330802503859>.
- [51] X. Huang, J. Yang, J. Wang, J. Bi, C. Xie, H. Hao, Design and synthesis of core–shell Fe₃O₄@PTMT composite magnetic microspheres for adsorption of heavy metals from high salinity wastewater, *Chemosphere*. 206 (2018) 513–521. <https://doi.org/10.1016/j.chemosphere.2018.04.184>.
- [52] G.L. Lescord, K.A. Kidd, J.L. Kirk, N.J. O’Driscoll, X. Wang, Derek.C.G. Muir, Factors affecting biotic mercury concentrations and biomagnification through lake food webs in the Canadian high Arctic, *Science of The Total Environment*. 509–510 (2015) 195–205. <https://doi.org/10.1016/j.scitotenv.2014.04.133>.
- [53] K. Eklöf, J. Fölster, L. Sonesten, K. Bishop, Spatial and temporal variation of THg concentrations in run-off water from 19 boreal catchments, 2000–2010, *Environmental Pollution*. 164 (2012) 102–109. <https://doi.org/10.1016/j.envpol.2012.01.024>.
- [54] H. Shirkhanloo, A. Khaligh, H.Z. Mousavi, A. Rashidi, Ultrasound assisted-dispersive-ionic liquid-micro-solid phase extraction based on carboxyl-functionalized nanoporous graphene for speciation and determination of trace inorganic and organic mercury species in water and caprine blood samples, *Microchemical Journal*. 130 (2017) 245–254. <https://doi.org/10.1016/j.microc.2016.09.012>.
- [55] S. Yang, D. Zhang, H. Cheng, Y. Wang, J. Liu, Graphene oxide as an efficient adsorbent of solid-phase extraction for online preconcentration of inorganic and organic mercurials in freshwater followed by HPLC-ICP-MS determination, *Analytica Chimica Acta*. 1074 (2019) 54–61. <https://doi.org/10.1016/j.aca.2019.04.066>.

**6. Occurrence, distribution, and characteristics
concentrations of Potential Harmful Trace
Elements (PHTEs) in Pyrenean lakes and
their relation to aquatic biogeochemistry**

6.1. Abstract

High altitude ecosystems are of primary importance for the preservation of the biodiversity and water resources. They are also essential to help sustain the economic development of touristic regions. These ecosystems are very unstable due to human activity and are already affected by climate change on both local and global scale. Various studies have demonstrated chemical contamination of anthropogenic origin in Pyrenean lakes and ecosystems. This contamination is due to both local pollution (mining, industry, road traffic) and atmospheric transport from regional or global pollution sources. The use of alpine lakes as proxies of global environmental changes implies a deep understanding of their hydrological functioning and physicochemical dynamics, taking especially into consideration the combined effects of seasonal variations, altitudinal gradient, and the own properties of the lake. One of the possibilities to study alpine lakes dynamics is to focus on the presence and the fate of trace elements. Indeed, the dynamic of metals and metalloids is directly related to hydrology and geochemical processes, themselves sensitive to changes in environmental conditions such as temperature, atmospheric deposition, or biological productivity. Even if several research projects have highlighted the presence and the impact of contaminants such as toxic metals, metalloids and organometals in Pyrenean ecosystems, the chemical cycle of these elements has been barely investigated in detail. In this study, a seasonal sampling has been conducted to investigate the distribution and the fate of Potential Harmful Trace Elements (PHTEs) (As, Sb, Cd, Cr, Cu, Ni, Pb, Zn, etc...) within the water column of several alpine lakes, and how such contamination can be constrained by climatic, hydrological and local to long range anthropogenic inputs. Water samples were collected in June 2017, October 2017, June 2018, and October 2018 in 20 different lakes of the Central Pyrenees on both French and Spanish slopes to understand the spatial and seasonal variations of PHTEs contamination within the lake ecosystems. During the first two sampling campaigns, spatial variability has been evaluated in each lake by collecting subsurface water samples at input, output, and center of the lake. In 2018, a more in-depth study was performed in lakes Gentau, Arratille, Azules and Sabocos, by sampling at different depths along the day. A classification of the lakes according to their water geochemistry was done, highlighting the importance of the trophic status of the lakes, the geological background, and the atmospheric inputs. The occurrence, sources, and behaviour of the PHTEs in the studied lakes were investigated. Finally, the intensive monitoring of the four lakes mentioned above allow to identify some PHTEs sensitive to environmental changes induced either by Climate Change or anthropogenic pressure.

Keywords:

Potential Harmful Trace Elements; Water; Lakes; Pyrenees

6.2. Introduction

High altitude ecosystems are of primary importance for the preservation of the biodiversity. They are also essential to help sustain the economic development of touristic regions. These ecosystems are very unstable due to human activity and are already affected by climate change [1–4] with increasing temperature, decreasing precipitations, glacier recession, and decreasing of the snow cover as main observable phenomena. All these environmental perturbations of high altitude ecosystems may have strong impact on the functioning of sensitive aquatic systems, such as high altitude lake ecosystems. *Sánchez-España et al.* [4], in a recent study conducted in the Lake Enol (1070m asl, North West Spain), also suggested that climate factors (warmer and drier spring and autumn) are reducing oxygen levels in deep waters through a long and increasingly steep thermal stratification.

The use of alpine lakes as proxies of global environmental changes [4–8] implies a deep understanding of their natural processes and physicochemical dynamics [9]. For this purpose, *Camarero et al.* [10] have focused on the main chemical parameters of mountain lake waters and their relation to environmental drivers such as weathering, sea salt inputs, atmospheric deposition of nitrogen (N) and sulphur (S), and biological activity of soils in the catchment that consumes nitrate (NO_3^-) and produces dissolved organic carbon (DOC). Various studies have also demonstrated chemical contamination of anthropogenic origin in Pyrenean lakes [11–17]: Potential Harmful Trace Elements (PHTEs), PolyBrominated Diphenyl Ether (PBDE), PolyChlorinated Biphenyl (PCB), pesticides, Polycyclic Aromatic Hydrocarbon (PAH). This contamination is due to both local pollution (mining, industry, road traffic) and atmospheric transport from regional or global pollution sources.

Therefore, it is important to investigate the presence and fate of contaminants in alpine lakes, especially those known as Potential Harmful Trace Elements (PHTEs), which constitute a threat for aquatic ecosystems because of their persistency in the environment and their potential toxicity on biological functions [18–21]. PHTEs dynamics are directly related to hydrological and geochemical processes, themselves sensitive to changes in environmental conditions. Combined, the concentration of PHTEs constitutes less than 0.1 % of the Earth's crust [22], and several studies have shown that the contamination by PHTEs is widespread and that PHTEs can be found in remote areas that are far from contamination sources. For example, lead isotopes analysis in Greenland ice cores highlighted large-scale atmospheric pollution by this toxic metal over thousands of years [23]. An evaluation of various contaminants of anthropogenic origin, including lead and mercury, over the past few centuries has been possible using ice cores from polar regions and high altitude glaciers [24]. *Cooke et al.* [25] review the use of lake sediment, peat, ice, marine sediment and tree rings as environmental archives of the global biogeochemical mercury cycle. Released by different sources, both natural and anthropic, PHTEs can be dispersed in the environment through various physical processes and accumulated in plants and, ultimately, in human body, causing serious health problems such as intoxication, neurological disturbance and cancer [26]. Some elements are essential to human health (Fe, Cu, Zn) whereas some others are toxic (As, Hg, Pb), responsible for serious human diseases with frequent lethal

consequences. They can reach high altitude lakes through direct atmospheric deposition and/or release from sediments and soils from the catchment [27].

Worldwide, the occurrence of PHTEs in surface waters of alpine lakes has been scarcely studied. In the Alps, human activities in the lowlands (industries and intensive agriculture) resulted in the transport and deposition of pollutants in alpine areas [28]. The ICP Waters Programme supported investigations to assess the effects of cross-border air pollution on aquatic ecosystems, especially on PHTEs such as As, Cu, V, Ni, Cr, Cd, Se and Zn [29]. *Hofer et al.* [30] also reported Pb, Cd, Ni, Cu and Zn concentrations in surface waters from 17 alpine lakes in the Alps. In the Himalaya, PHTEs biogeochemical cycle in the aquatic compartment has been studied in only two alpine lakes, regarding seasonal variations with the influence of the monsoon [31], and in relation to elevation particularly with higher enrichment of Cd and Pb in high altitude lakes [32].

The presence and potential impact of such contaminants have been successfully highlighted studying sediment cores from Pyrenean lakes [12,27,33,34]. Nevertheless, their biogeochemical cycle, especially in the aquatic compartment, has been barely investigated in this mountain range [35,36]. Indeed, *Zaharescu et al.* [36] investigated the sources of some trace elements (As, Cd, Co, Cu, Mn, Ni, Pb and Zn) in the Lake Respomuso (2200 m asl., Central Pyrenees) by analysis of surface waters and sediments from the lake and its catchment. In this lake, the main source of these trace elements appears to be the bedrock, rich in metal-bearing minerals. The other study dealing with trace elements in Pyrenean lake waters has been conducted by *Bacardit and Camarero* [35] on three different alpine lakes from the Central Pyrenees (Lakes Légunabens, Plan and Vidal d'Amunt). In this work, only three trace elements, Pb, Zn and As, have been quantified in atmospheric depositions, sediments and surface waters from the lakes and their catchment. Terrestrial inputs from the catchment to the lakes dominate for the three trace elements, with distinct sources for Pb (anthropogenic origin) and As (weathering of As-rich rocks).

Overall, even if alpine lakes are sensitive to changes in atmospheric pollution and climate, offering strong research opportunities, there is a lack of knowledge about the aquatic biogeochemical cycle of PHTEs in such remote areas. This is probably due to the difficult accessibility to these remote environments with all required material and to the extremely low concentrations of the PHTEs, usually below the $\mu\text{g L}^{-1}$, avoiding their quantification without ultra-trace sampling protocols, clean lab methodologies and high sensitivity instruments (**3 Sampling and analytical strategy**).

This work presents an integrated investigation conducted in twenty high altitude pristine lakes from the Central Pyrenees. These small lakes show similar physical properties (i.e., size, depth) but differ mainly from their catchment characteristics and geological background (i.e., granitic vs sedimentary rocks). They also span a wide range of altitude, from 1620 to 2600 m asl. To study the water hydrological and geochemical characteristics (temperature, dissolved oxygen, conductivity, redox potential, chlorophyll-a, silicates, TOC, DIC, Total Alkalinity, pH, anions, major, trace and ultra-trace elements), subsurface (~0.5 m depth) water samples from all the lakes were collected in June 2017 (Replim1), October 2017 (Replim2), June 2018 (Replim3) and October 2018 (Replim4), and a more in-depth study was performed in three of these lakes by sampling at different depths along the same day in June 2018 (Replim3) and

October 2018 (Replim4). All the procedures used to collect and analyse the samples have been fully described in **3 Sampling and analytical strategy**.

The more specific objectives of this study were to i) evaluate the effectiveness of the sampling strategy in terms of intra-lake variability and truly dissolved vs total concentration of PHTEs, ii) establish a categorisation of the lakes according to their water chemical composition and iii) contribute to the knowledge on PHTEs biogeochemical cycle by an evaluation of the main sources and processes controlling their fate in alpine lake waters. This study is also the first one to report 15 PHTEs detected and quantified in all the water samples collected in alpine lakes.

6.3. Subsurface lake water geochemistry

6.3.1. Physico-chemical characteristics and PHTEs concentrations

Statistical descriptors of the main physico-chemical parameters of the 74 subsurface water samples collected during the four sampling campaigns are summarized in **Table 6-1**, and those of the concentrations of major, trace and ultra-trace cations are shown in **Figure 6-1**.

The 24 major/minor and trace/ultra-trace elements detected in all the samples can be separated in two categories according to their concentration. On the one hand, major/minor and trace elements, with concentrations mainly above the ppb level ($\mu\text{g L}^{-1}$), occurred in the following order of abundance: Ca > Na > Mg > K > Al > Sr > Fe > Mn > Ba. On the other hand, ultra-trace elements, mainly PHTEs, occurred in the following order of abundance: As > U > Cu > Ti > Mo > V > Ni > Cr > Pb > Se > Sb > Co > Cd > Tl > non-gaseous Hg.

Temperatures of the lake water varied strongly among and within the studied lakes, ranging from 2 to 19 °C. Altitude is a key factor explaining these variations with an opposite correlation with temperature ($r = -0.48$). The highest temperature was found in June 2017 at ORD (2100 m asl), a low altitude, shallow and well exposed to sunlight lake, while the lowest one was recorded in June 2018 (Replim3) in CAM (2344 m asl) while ice was still covering a part of the lake. Over the four sampling campaigns, the temperature has been always measured in 6 lakes (ARA, CAM, AZU, ARN, COA and PAN) and the lowest values were recorded in June 2018 (Replim3). As previously highlighted, this can be explained by the fact that a few days before June 2018 sampling many of the studied lakes were still partially frozen (high snow accumulation during winter 2017-2018, **Figure 3-2**).

Regarding the dissolved oxygen (DO), most of the subsurface lake waters were oversaturated. The fluorescence signal of the chlorophyll-a in the samples, as Relative Fluorescence Units (RFU), was always below the limit of detection. Indeed, there was no significant difference between the signal measured by the probe out of the water and the signal measured at 0.5m depth. These two parameters will be discussed later using the depth profiles obtained in some specific lakes.

Conductivity (5 to 130 $\mu\text{S cm}^{-1}$), pH (4.87 to 7.91), Total Alkalinity (TA) (14 to 1839 $\mu\text{mol kg}^{-1}$) and Dissolved Inorganic Carbon (DIC) (33 to 1727 $\mu\text{mol kg}^{-1}$) are all together significantly correlated ($r = 0.74$, 0.74 and 0.75 respectively between pH and conductivity, pH and TA, and pH and DIC; $p\text{-value} < 0.05$) with the lowest values for the granitic lake PEY and the highest values for the limestone and dolomite enriched lake SAB. This variability is a direct consequence of weathering of Calcium (Ca) mainly as calcite (180 to 22229 $\mu\text{g L}^{-1}$) and, to a lesser extent, dolomite with an important Magnesium (Mg) content (51 to 6129 $\mu\text{g L}^{-1}$): a strong correlation ($r = 0.78$; $p\text{-value} < 0.05$) can be observed between pH and the sum of Ca and Mg concentrations.

Strontium (Sr) (0.3 to 73.8 $\mu\text{g L}^{-1}$) was strongly associated with Ca ($r = 0.93$; $p\text{-value} < 0.05$). The presence of Barium (Ba) (0.1 to 5.4 $\mu\text{g L}^{-1}$) in surface waters was strongly controlled by the abundance of Ba in the bedrock. Along with the four sampling campaigns, the highest Ba concentrations were found in AZU ($4.7 \pm 0.4 \mu\text{g L}^{-1}$) and SAB ($4.3 \pm 0.1 \mu\text{g L}^{-1}$). Therefore, both Sr and Ba are also indicative of calcareous rocks, in association with Ca, Mg and Sr.

The presence of Aluminium (Al) (6 to 96 $\mu\text{g L}^{-1}$) might be related to atmospheric transport of dust. Its distribution in the lake waters is strongly dependent on pH: Al is characterised by a low solubility that increases sharply with decreasing pH, therefore directly influencing its toxicity. This is well supported by the negative correlation between Al and Ca ($r = -0.40$; $p\text{-value} < 0.05$): lower Ca induces high sensitivity to acidification hence increases of Al concentrations. Al is also well correlated ($r = 0.91$; $p\text{-value} < 0.05$) with Ti (22 to 1882 ng L^{-1}).

The most significant sources of Chloride (Cl⁻) in freshwaters are rainfall and marine aerosols [37]. Cl⁻ in the high altitude lakes of this study (69 to 684 $\mu\text{g L}^{-1}$) is significantly correlated with Sodium (Na) (35 to 1084 $\mu\text{g L}^{-1}$) ($r = 0.83$; $p\text{-value} < 0.05$) and to Potassium (K) (20 to 202 $\mu\text{g L}^{-1}$) ($r = 0.61$; $p\text{-value} < 0.05$). The sulphate (SO₄²⁻) concentrations ranged between $< 0.21 \text{ mg L}^{-1}$ and 7.56 mg L^{-1} . The highest SO₄²⁻ concentrations, of geological origin, are found in ARA ($3.0 \pm 0.4 \text{ mg L}^{-1}$), BAD ($3.9 \pm 1.1 \text{ mg L}^{-1}$) and AZU ($6.1 \pm 1.2 \text{ mg L}^{-1}$).

Total Organic Carbon (TOC) (0.6 to 4.6 mg L^{-1}) and Nitrate (NO₃⁻) (< 0.065 to 1.13 mg L^{-1}) were low and varied strongly among lakes and sampling campaigns. Together with Silicate (0.1 to 7.0 mg L^{-1}), TOC and NO₃⁻ can be indicators of possible biological activity, especially the production of phytoplankton (including diatoms for silicates), in the studied lakes [10]. The highest concentrations of Silicate over the four sampling campaigns were found in Lakes ARA (4.7 ± 0.2), BAD (4.6 ± 0.7) and PAR (6.5 ± 0.3), in relation to the sandstone (quartz and feldspar) highly soluble of the Devonian rocks.

Fe and Mn concentrations ranged respectively from 3 to 68 $\mu\text{g L}^{-1}$ and from 0.2 to 10.9 $\mu\text{g L}^{-1}$. The fate of Fe and Mn dissolved in lake waters is complex as they are relatively immobile under most environmental conditions due to limited solubility. These two elements, mainly from lithogenic origin, can be rapidly adsorbed onto particles depending on the physico-chemical characteristics of the water, in particular pH, redox potential and dissolved oxygen. Strong variations of dissolved oxygen occur in stratified lakes, with hypoxic to anoxic zone at the bottom part of these lakes. Therefore, the study of depth profile in such lakes, that will be discussed later, will provide new insights on the biogeochemical

cycle of these two particular elements. It is also important to underline that various PHTEs can be either trapped or released together with Fe and Mn [38].

PHTEs (As, U, Cu, Mo, V, Ni, Cr, Pb, Se, Sb, Co, Cd, Tl and non-gaseous Hg) were found at very low concentrations in the lake waters, below the maximum allowable concentrations (MAC) set by the Council Directive 98/83/EC for human consumption. Arsenic (As) concentrations varied strongly (31 to 8910 ng L⁻¹) with the highest values over the four sampling campaigns in lakes AZU (5000 ± 920 ng L⁻¹) and PEC (8400 ± 600 ng L⁻¹) close to the MAC (10 µg L⁻¹). Such enrichment in As has already been attributed to local geological sources. Indeed, the sediments of Pyrenean lakes present a remarkably higher As content compared to other alpine lakes [12]. Arsenic can be released from hydrothermal and magmatic ore deposits in granites or metamorphic rocks, which are naturally rich in As as sulphide minerals in the Pyrenees [35].

Other PHTEs have shown much higher concentrations in some lakes, also probably linked to the characteristics of the bedrock of the affected lakes and their associated catchment. Indeed, Uranium (U) (5 to 2402 ng L⁻¹) is a non-essential element and is chemotoxic, radiotoxic and carcinogen. The highest concentrations were found in PAR (2310 ± 80 ng L⁻¹). Vanadium (V) (23 to 397 ng L⁻¹) also presented its higher concentrations in PAR (392 ± 4 ng L⁻¹) probably due to the presence of carnotite minerals present in sandstone (K₂(UO₂)₂(VO₄)₂·3H₂O) also supported by the important content of K in this lake (190 ± 10 µg L⁻¹). Nevertheless, PAR is the only lake with concentrations of V at least 3 times higher than the rest of the studied lakes. The status of this lake can also be responsible for this anomaly in V concentration. Indeed, it is a very shallow lake, partly occupied by a peatland, with the highest organic matter content (TOC = 2.6 ± 0.4 mg L⁻¹), and reactivity at the water-sediment interface is important. V buried in the anoxic sediments of Lake PAR might be remobilized, and released into the water column [39].

U veins can also appear in granitic rocks. That is the case of Lake OPA where important U (1400 ± 300 ng L⁻¹) and K (130 ± 10 µg L⁻¹) were measured, while V (100 ± 8 ng L⁻¹) was not significantly different from the results obtained in all the other lakes except PAR (Kruskal-Wallis test, p-value = 0.292). Toxicity of V highly depends on its speciation and oxidation state. Airborne anthropogenic V might be an important source, especially for high altitude lakes without V geological inputs.

Molybdenum (Mo) (6 to 618 ng L⁻¹) and Selenium (Se) (12 to 89 ng L⁻¹) are both essential elements, and both deficiencies and excesses can cause health problems. Mo species are strongly adsorbed by clay particles, oxyhydroxides (Fe, Al and Mn) and can coprecipitate with organic matter and/or other cations. Nevertheless, all these reactions depend on the pH and redox potential; therefore, the occurrence and mobility of Mo in lake water are difficult to predict. Highest concentrations of Mo were also found in PAR (570 ± 40 ng L⁻¹), probably also because of the remobilization of Mo at the water-sediment interface. Se is widely present as a micronutrient, replacing sulphur in many sulphide minerals such as pyrite, chalcopyrite, pyrrhotite and sphalerite. Therefore, we have found a significant correlation between Se and SO₄²⁻ in our results (r = 0.83; p-value < 0.05) and the highest concentrations of Se were

found in the lakes with the highest concentration of SO_4^{2-} , ARA ($60 \pm 2 \text{ ng L}^{-1}$), BAD ($70 \pm 10 \text{ ng L}^{-1}$) and AZU ($60 \pm 10 \text{ ng L}^{-1}$) (*Andrea Romero, personal communication*) [40].

Although possible local soils and bedrocks sources should not be discarded, Lead (Pb) (13 to 503 ng L^{-1}) was found associated to Al ($r = 0.81$) and Ti ($r = 0.87$) suggesting an important input of Pb from dust depositions. Precipitation might be an important source of Nickel (Ni) (23 to 797 ng L^{-1}) and Copper (Cu) (94 to 434 ng L^{-1}) in the lakes under study, as suggested for other lakes [3].

Atmospheric transport and both dry and wet deposition are the main sources of Mercury (Hg) in high altitude lakes. In our study, the concentration of non-gaseous Hg in subsurface waters ranged from 0.1 to 2.9 ng L^{-1} . Even if Hg occurs at very low concentrations in marine systems and remote lakes, it is very important because of its biomagnification capacity, also depending on its speciation.

This study is one of the first providing results in surface water samples from various alpine lakes for some important potential toxic elements: Chromium (Cr) (23 to 279 ng L^{-1}), Antimony (Sb) (5 to 85 ng L^{-1}), Cobalt (Co) (5 to 80 ng L^{-1}), Cadmium (Cd) (1 to 12 ng L^{-1}) and Thallium (Tl) (0.2 to 2.5 ng L^{-1}). In our study, the highest Cr concentrations were found in ARA ($150 \pm 60 \text{ ng L}^{-1}$), BAD ($180 \pm 50 \text{ ng L}^{-1}$) and PAR ($160 \pm 10 \text{ ng L}^{-1}$). Sb has no known function in living organisms, and, because of its low natural abundance, it is a useful indicator of anthropogenic contamination. The highest concentrations were found in GEN ($70 \pm 10 \text{ ng L}^{-1}$), ROU ($70 \pm 5 \text{ ng L}^{-1}$) and AZU ($69 \pm 7 \text{ ng L}^{-1}$). The concentration of Cd did not present strong variations within the sampled lakes ($3 \pm 2 \text{ ng L}^{-1}$). The studied lakes differ mainly from their geological substrate, and the small variations in Cd observed suggests that the weathering of rocks and the catchment should not significantly influence Cd distribution. The constant concentrations of Cd measured in the studied lakes are rather due to a common source, maybe atmospheric, rather than local and specific processes occurring in the lakes. Cobalt, as well as Mo and Se, is an essential micronutrient, but excess doses or deficiencies are toxic. Small variations were also detected in Co concentrations along with the whole data set ($15 \pm 10 \text{ ng L}^{-1}$), with some punctual high concentrations. Finally, the toxicity of Tl is similar to that of Cd, Hg and Pb, but the fate of this element in lake water has been poorly studied as it occurs at extremely low concentrations. Together with non-gaseous Hg, this element, mainly below the ppt level (ng L^{-1}), was the less abundant and detected for the first time in the high altitude lakes of our study, with small variations among lakes ($0.7 \pm 0.4 \text{ ng L}^{-1}$).

Overall, it is worth noting that the samples collected in PAR presented significantly higher values for many of the measured parameters (TOC, trace and ultra-trace elements, Silicate). This lake is completely different from the other ones, mainly because of i) its very small size (close to a pond) and the very low depth that enhances resuspension of sediments and organic material, ii) the remobilization of trace elements from organic sediment diagenesis and peat leachates, iii) its gradual transformation into a wetland/peatland, and iv) its low altitude together with the dense forest vegetation surrounding the lake.

The studied lakes span a wide range of chemical characteristics in particular related to their sensitivity to acidification, a consequence of the widely different lithological characteristics of the lake catchments (i.e., easily erodible sedimentary rocks vs granite).

Table 6-1: Main chemical parameters of the studied lakes measured by the multiparametric probe (temperature, conductivity, redox potential), the TOC analyser (TOC as NPOC), Flow Injection Analysis (Silicate), the VINDTA 3C Instrument (DIC, Total Alkalinity) and the ionic chromatograph (Cl⁻, NO₃⁻ and SO₄²⁻). pH was calculated according to Kortazar *et al.* [41]. Chlorophyll-a is not mentioned as it was always below LOD. Dissolved oxygen, as mentioned in **3.3.1 Physicochemical parameters**, was calibrated only once before each sampling campaign and the sensor is sensitive to elevation: the whole lakes were oversaturated in subsurface but the values measured differ among lakes because of elevation. All the methodological details can be found **3.Sampling and analytical strategy**.

Sampling	Lakes		Elevation (m asl)	Temperature (°C)	pH	Conductivity (µS cm ⁻¹)	Redox Potential (mV)	TOC (mg L ⁻¹)	Silicate (mg L ⁻¹)	DIC (µmol kg ⁻¹)	Total Alkalinity (µmol kg ⁻¹)	Cl ⁻ (mg L ⁻¹)	NO ₃ ⁻ (mg L ⁻¹)	SO ₄ ²⁻ (mg L ⁻¹)
June 2017	16	Min	1620	4.63	6.01	7.2	97	0.63	1.20	92	80	0.15	0.12	0.28
		Max	2600	18.3	7.47	61	270	2.90	6.20	800	830	0.49	0.90	6.50
		Median		8.84	6.93	23	160	1.10	2.20	310	310	0.19	0.65	1.60
		Mean		9.29	6.89	28	160	1.40	2.70	390	400	0.21	0.57	1.70
		SD		3.30	0.44	19	51	0.70	1.50	260	270	0.10	0.24	1.60
October 2017	11	Min	1620	7.22	6.00	7.0	46	1.30	0.54	87	84	0.15	< 0.14	0.35
		Max	2493	11.1	7.91	72	150	3.10	7.00	880	910	0.48	0.75	7.60
		Median		9.85	7.07	36	110	1.90	2.40	410	400	0.19	0.37	2.30
		Mean		9.80	7.07	39	110	2.10	2.60	480	490	0.22	0.39	2.40
		SD		1.10	0.53	23	32	0.69	1.90	290	310	0.10	0.24	2.10
June 2018	16	Min	1620	2.43	4.87	5.4	36	0.62	0.10	33	14	0.10	0.10	< 0.21
		Max	2493	18.7	7.65	130	320	2.40	6.40	1700	1800	0.50	1.13	5.40
		Median		6.87	6.88	28	170	0.86	2.40	350	360	0.20	0.47	1.70
		Mean		8.49	6.77	39	160	1.10	2.70	570	570	0.22	0.49	1.80
		SD		4.80	0.64	35	79	0.51	1.50	480	510	0.10	0.28	1.50
October 2018	16	Min	1620	5.33	5.94	4.5	36	0.94	0.81	79	85	0.14	< 0.10	< 0.29
		Max	2493	13.4	7.71	100	260	4.60	6.40	1700	1800	0.68	0.82	6.80
		Median		9.32	6.79	25	170	1.60	1.50	370	380	0.22	0.17	1.70
		Mean		9.30	6.92	38	170	1.80	2.20	590	610	0.27	0.31	1.70
		SD		2.56	0.49	29	63	0.87	1.40	500	550	0.15	0.30	1.60

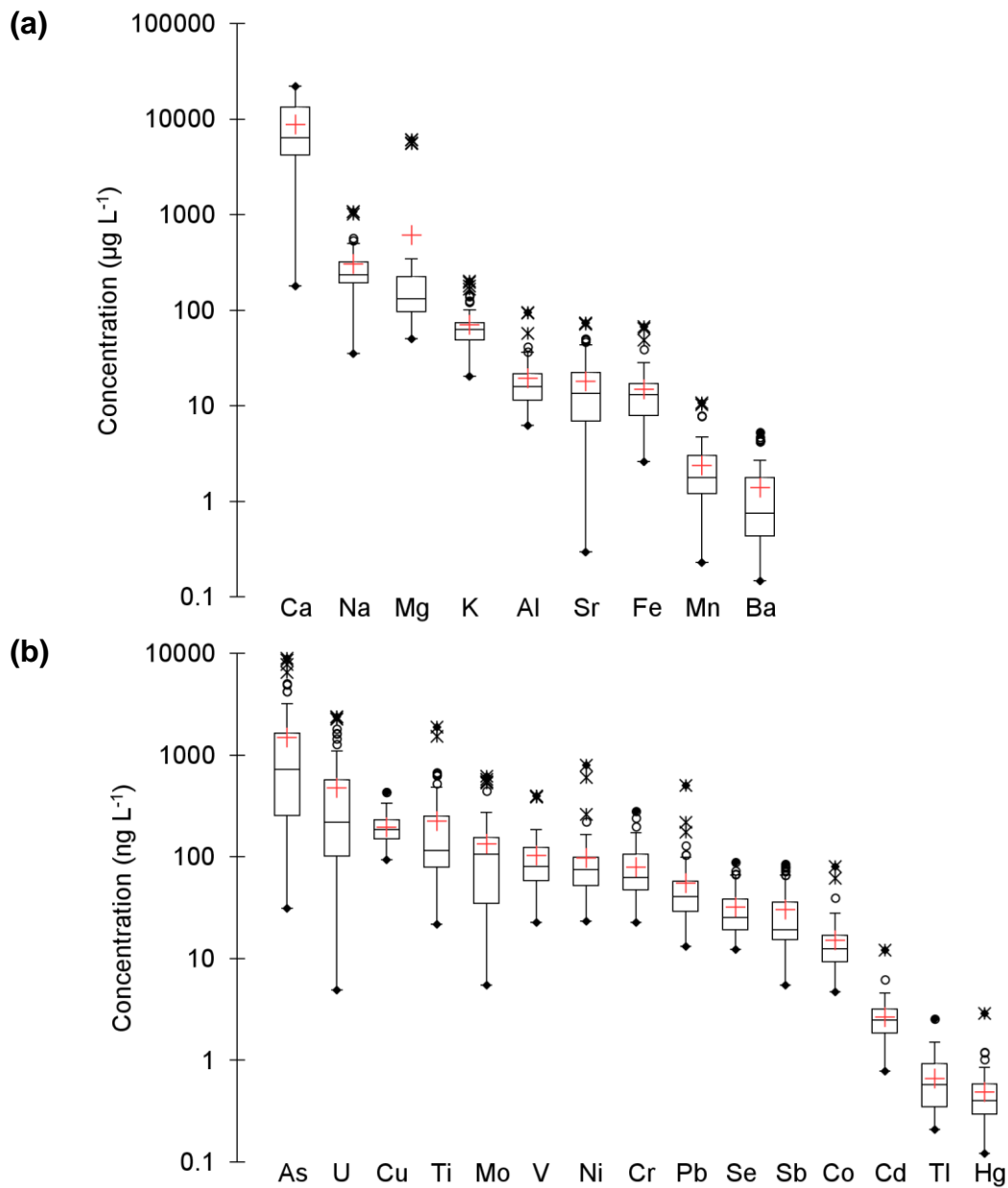


Figure 6-1: (a) Major and trace elements (median concentrations above 1 µg L⁻¹) and (b) ultra-trace elements (median concentrations below 1 µg L⁻¹) concentrations in unfiltered subsurface water samples of the 20 studied lakes over the four sampling campaigns. Dots are minimum and maximum, white circles are outliers and black crosses are extreme values, bars indicate 10th and 90th percentile, boxes indicate 25th and 75th, marks within each box are medians and red crosses are mean. Note that Hg corresponds to non-gaseous Hg.

6.3.2. Intra-lake variability: effect of geographical position of the sampling point

In most of the publications related to the geochemistry of lake waters, the spatial variation in the sampling process has not been evaluated, that means the potential variations observed in the chemical parameters linked to the sampling location in each lake and sampling campaign. Indeed, water samples were collected either at the outflow or at the central part of each lake (usually the deepest part of the lake), assuming that the inter-lake variability in the chemistry variables is larger than the intra-lake variability [29,30,42,43], regardless of the lake size. In another way, *Pertsemli and Voutsas* [44] collected three water samples at different locations and mixed them to ensure that the sample is well representative of the site. In *Markert et al.* [45], considering the large size of the studied lakes (> 1640 ha), the sampling points were chosen carefully according to the local status, i.e. low direct anthropogenic influence: in this publication, results are rather representative of a specific area of the lake rather than representative of its global status.

In this work, a triplicate sampling in each studied lake was carried out during the first two sampling campaigns (June 2017 and October 2017) to assess the intra-lake variability in water geochemistry. The uncertainty associated to the analytical measurement has been evaluated **in 3.Sampling and analytical strategy**, and only Al (9 %), Cu (10 %), and Ni (9 %) have shown values above 3 %, mainly due to random contamination and/or possible interferences (i.e. double Carbon interferes with Aluminium). **Figure 6-2** depicts the Relative Standard Deviation (RSD) calculated for each major and trace element considered using the results obtained after the analysis of the three samples collected at different parts of each lake. The red dashed lines associated with each element correspond to the uncertainty associated to the analytical measurement.

Overall, the median value for each element is below 15 % (except Ni (21 %)), which is very low assuming that the uncertainty related to the sampling process is more important than the analytical one. Moreover, in this figure, elements range from the most abundant (Ca) to the less one (non-gaseous Hg), and no clear trend is observed regarding this classification. Usually, higher uncertainty is expected at lower concentrations due to the drop in the precision of the instrument, a lower recovery or potential sample contamination. Therefore, in our study, the uncertainty is not related to the analysis processes.

In addition, only a few elements have shown median RSD above 10 %: Al (12 %), Cu (15 %), Ti (10 %), Ni (21 %), Pb (15 %), Cd (12 %) and non-gaseous Hg (14 %). Apart from local sources (rich ores), Hg, Pb and Cd contributions from atmospheric compartment is also important in high altitude lakes [12]. Al and Ti, terrigenous elements (weathering of rocks) are also atmospherically transported to the lake with the dust [3]. Climatic conditions (precipitation, wind, and temperature) may strongly vary between a short distance and timescale in high altitude environments and might be partly responsible for the variation of non-gaseous Hg, Pb, Cd, Al and Ti concentrations among the selected sampling points. Indeed, it has been shown that periods of high deposition of crustal elements occurs during both spring/early summer and late summer/autumn, which correspond to the biannual sampling periods of our study [3]. On the one hand, during spring and early summer, extreme events, more important, are responsible for strong

atmospheric depositions. On the other hand, air masses from the South (North Africa and the Iberian Peninsula) are more important during late summer and autumn [11].

Apart from these phenomena, Ni and Cu have shown in our study one of the most important analytical uncertainties due to random contaminations and consequently we can assume that the sampling process has probably increased the global uncertainty related to these two elements for the same reason.

At the light of these results, we decided to sample just a single point of the lake (the deepest one) in the two last campaigns (June 2018 and October 2018) of the study.

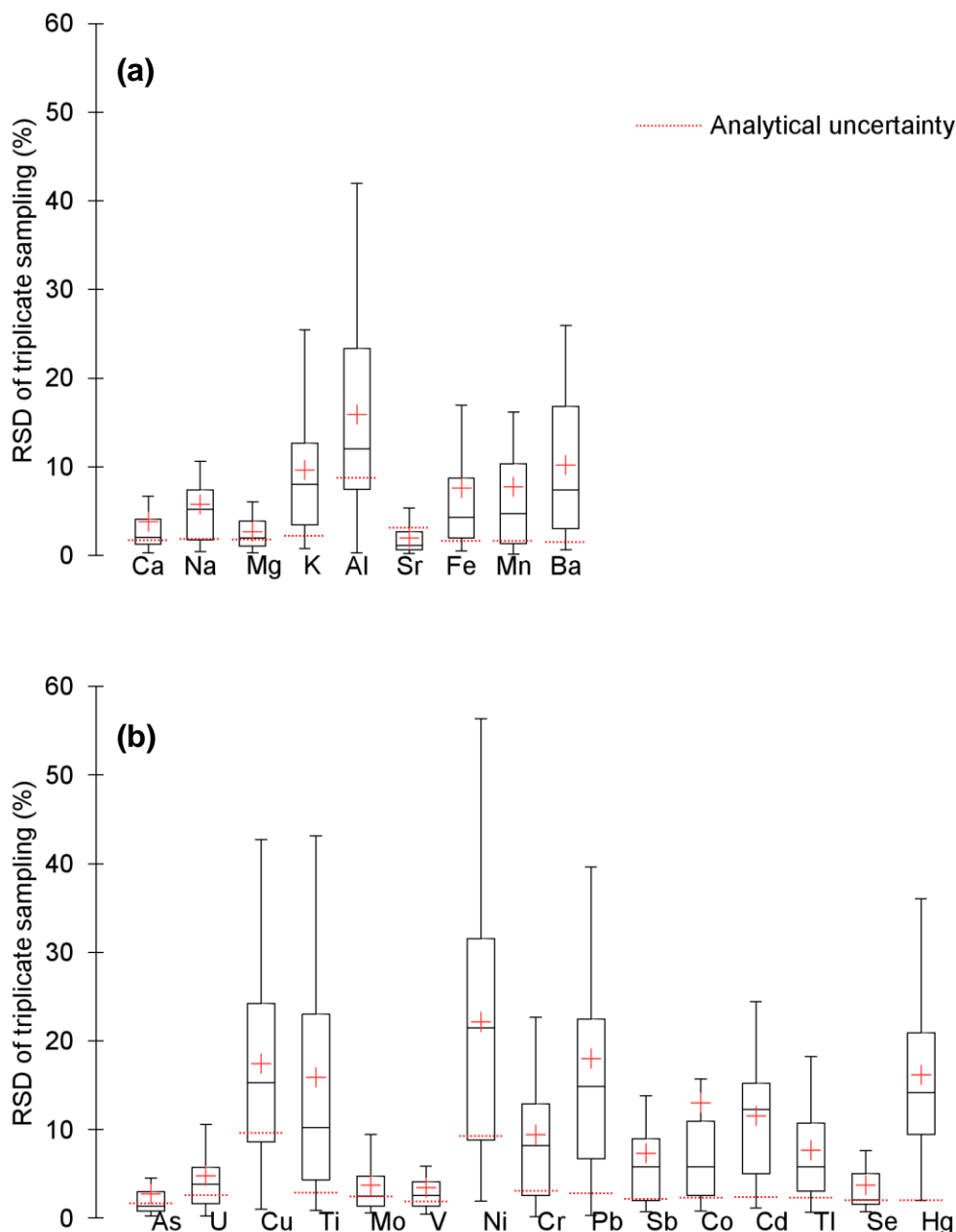


Figure 6-2: Relative Standard Deviation (RSD) calculated for each (a) major and trace element and (b) ultra-trace element considered using the results obtained after the analysis of the three samples collected at different parts of each lake. Bars indicate 10th and 90th percentile, boxes indicate 25th and 75th marks within each box are medians and red crosses are mean. Note that Hg corresponds to non-gaseous Hg.

6.3.3. Intra-lake variability: effect of the sampling time within the same day

In June 2018 and October 2018, water samples were collected at four selected lakes (GEN, ARA, AZU and SAB) at different times of the day at the same point of the lake to investigate the reactivity of some of the trace and ultra-trace elements in high altitude lakes.

Over the 24 elements investigated, only nine of them have shown a clear diurnal variation: Al, Fe, Mn, Cu, Ti, Ni, Pb, Cd and non-gaseous Hg (**Table 6-2**). As mentioned previously, variation for some of these elements may be due to an increase or decrease in the magnitude of the deposition processes including snow melting much higher during the day, but reactivity might also be partially responsible. Indeed, these trace elements are reactive and can precipitate rapidly as (oxy)hydroxide species, poorly soluble in the water. The precipitation reaction, as well as dissolution, depends on some variables such as pH, temperature and organic matter [46]. Considering the oligotrophic status of the studied lakes and the small content of organic matter ($\text{TOC} < 4.6 \text{ mg L}^{-1}$), organic matter itself and/or biological productivity should not be the most important driving force responsible of the precipitation reactions.

For Al, Fe, Mn, Ti and Pb, pH seems to have a great influence with an opposite relation: increasing concentrations of the trace elements as pH decreases, even by less than one pH unit. Indeed, significant correlations have been found between pH and Fe ($r = -0.69$; $p\text{-value} < 0.05$), Mn ($r = -0.68$; $p\text{-value} < 0.05$), Ti ($r = -0.60$; $p\text{-value} < 0.05$) and Pb ($r = -0.53$; $p\text{-value} < 0.05$). In the case of Al ($r = -0.44$; $p\text{-value} = 0.06$), the larger analytical uncertainty associated to Al (9 %) might prevent a significant correlation. These oxyanions have the particularity to express high variations in their pH-dependent diagrams [47] in the range of 4 to 8 pH values, which corresponds to the values registered during the four sampling campaigns in our study.

Cd presents significant correlations with both pH ($r = -0.47$; $p\text{-value} < 0.05$) and temperature ($r = -0.78$; $p\text{-value} < 0.05$).

Hg displays a biogeochemical cycle much more complex in aquatic ecosystems, especially regarding its speciation with inter-species conversions (reduction, demethylation, methylation etc ...) and important reemissions of gaseous Hg (i.e., $\text{Hg}(0)$) from the surface water directly to the atmospheric compartment [48]. Mercury species dynamic and cycling will be further presented and discussed in detail in **7 Dynamics, distribution, and transformations of mercury species from Pyrenean high-altitude lakes** and Erreur ! Source du renvoi introuvable. Erreur ! Source du renvoi introuvable..

Ni and Cu results do not express any clear trend regarding pH and temperature. As for Hg, this might be related to the complexity of their biogeochemical cycle.

Overall, even if some elements are showing significant daily variations in their water concentrations, for further discussions we can assume that seasonal and spatial inter-lake variability will be more important than daily variations.

Table 6-2: Temperature, pH and concentrations of several elements measured in water samples collected in four selected lakes at different times of the day.

Lake	Time	T° (°C)	pH	Al (µg L ⁻¹)	Fe (µg L ⁻¹)	Mn (µg L ⁻¹)	Cu (ng L ⁻¹)	Ti (ng L ⁻¹)	Ni (ng L ⁻¹)	Pb (ng L ⁻¹)	Cd (ng L ⁻¹)	Non-gaseous Hg (ng L ⁻¹)
ARA (June 2018)	08:30	5.86	7.09	9.50	13.7	3.23	161	99	120	42	3.0	0.12
	11:05	5.70	6.99	9.82	15.4	3.30	145	90	103	20	2.3	0.21
	13:25	5.72	6.94	9.00	14.8	3.06	141	87	102	39	2.5	0.18
	16:00	6.64	6.88	13.1	13.0	2.96	204	89	109	48	2.5	0.21
GEN (June 2018)	06:30	6.89	6.70	17.8	11.8	3.28	202	382	164	58	1.9	0.85
	10:50	6.87	6.72	20.8	11.4	3.05	256	356	260	93	3.7	0.39
	15:50	6.87	6.90	15.9	11.8	3.27	196	317	150	40	1.7	0.69
	21:10	7.21	6.64	17.6	22.9	10.9	434	329	797	174	2.6	0.40
AZU (June 2018)	09:35	4.87	7.17	13.9	11.0	2.97	158	131	98	44	3.0	0.31
	12:00	5.03	7.58	11.6	10.3	2.61	132	101	91	35	2.8	0.39
SAB (June 2018)	09:45	16.6	7.65	10.0	7.84	2.40	231	31	114	21	1.2	0.72
	12:35	17.2	7.53	12.2	9.84	2.70	285	39	85	42	0.9	0.66
	15:35	18.7	7.47	10.9	8.09	1.67	263	92	86	18	0.9	0.75
GEN (October 2018)	07:50	12.6	6.74	7.15	15.3	7.77	192	43	36	38	1.4	0.26
	12:50	12.8	6.75	6.62	17.6	10.4	137	45	25	35	1.1	0.34
	17:45	12.8	6.71	13.9	24.9	7.88	242	485	50	34	1.4	0.19
SAB (October 2018)	09:30	10.4	7.71	11.0	10.7	1.80	197	125	61	17	0.9	0.61
	14:05	10.7	7.64	6.30	10.4	1.24	171	22	64	13	0.8	0.61
	16:10	10.8	7.67	8.65	10.9	1.26	208	36	64	36	0.8	0.56

6.3.4. Filtered vs unfiltered trace element concentrations

As mentioned in **3.Sampling and analytical strategy**, the HR-ICPMS was only used to analyse unfiltered samples. Consequently, the results obtained after the analysis of the samples by Q-ICP-MS (and GC-ICP-MS for non-gaseous mercury) were used to evaluate the tendency of metals to get adsorbed onto suspended particles by comparison of the concentrations found in filtered (< 0.22 µm for Se and non-gaseous Hg; < 0.45 µm for others) and unfiltered samples. For most of the ultra-trace elements, the results obtained after the Q-ICP-MS analysis are close or below the LOD. **Figure 6-3**, consequently, does not display results for Ni, Cd, Pb, Tl and Co. In addition, the amount of data is smaller for many trace elements.

Dissolved Fraction (DF) is defined as the ratio between the concentrations of the element considered in the sample after ($[X]_{Filtered}$) and before ($[X]_{Unfiltered}$) filtration:

Equation 6-1

$$DF = \frac{[X]_{Filtered}}{[X]_{Unfiltered}}$$

The **Figure 6-3** displays the DF in subsurface water samples calculated for each major, trace and ultra-trace element considered using the results obtained by ICP-MS (only unfiltered samples were analysed by HR-ICP-MS).

The solubility of an element in wet deposition (precipitation and snow) may be related to the origin and the mechanism of aerosol formation, both of which affect the size and the chemical properties of the particles. Thus, resuspension of terrigenous substrates produces coarse particles with a high content of insoluble species, whereas soluble species are often gaseous species in origin that have been adsorbed onto particles [49].

Most of the elements exhibit Dissolved Fraction close to one, so mainly present in dissolved form, with median Dissolved Fraction of 0.99, 1.03, 0.98, 1.02, 0.98, 0.95, 0.95, 0.90, 1.01, 0.92, 0.90, 0.80 and 0.97 respectively for Ca, Na, Mg, K, Sr, Ba, As, Cu, Mo, V, Cr, Se and Sb. Only Al (median DF = 0.56), Fe (median DF = 0.41), Mn (median DF = 0.58), Ti (median DF = 0.59) and Hg (median DF = 0.72) show DF well below one. Consequently, it can be concluded that an important fraction of these elements can be found associated with particles (organic matter and/or suspended inorganic solids). Variability of the DF is particularly high for these elements supporting the hypothesis of important reactivity: regular precipitation and dissolution reactions that can occur either during atmospheric transport or in the water column itself. The analysis of the snowpack of the Maladeta valley (Central Pyrenees) made by *Bacardit et Camarero (2010)* [49] highlighted the association of Al, Ti and Fe to particles by comparison of the dissolved and particulate fractions. In waters from Lakes Légunabens, Plan and Vidal d'Amunt, Pb was bound mostly to particles while As and Zn were detected mostly as dissolved forms [35].

The case of Cu differs well as we observed important variability regarding the sampling point and the daytime of sampling but according to the results of the ICP-MS analysis of 22 samples, the DF for Cu is

close to one (median DF = 0.90). It confirms the hypothesis that the variations observed previously for Cu (intra-lake variability) can be due to either contamination or differences in the deposition process rather than to an important reactivity regarding this element.

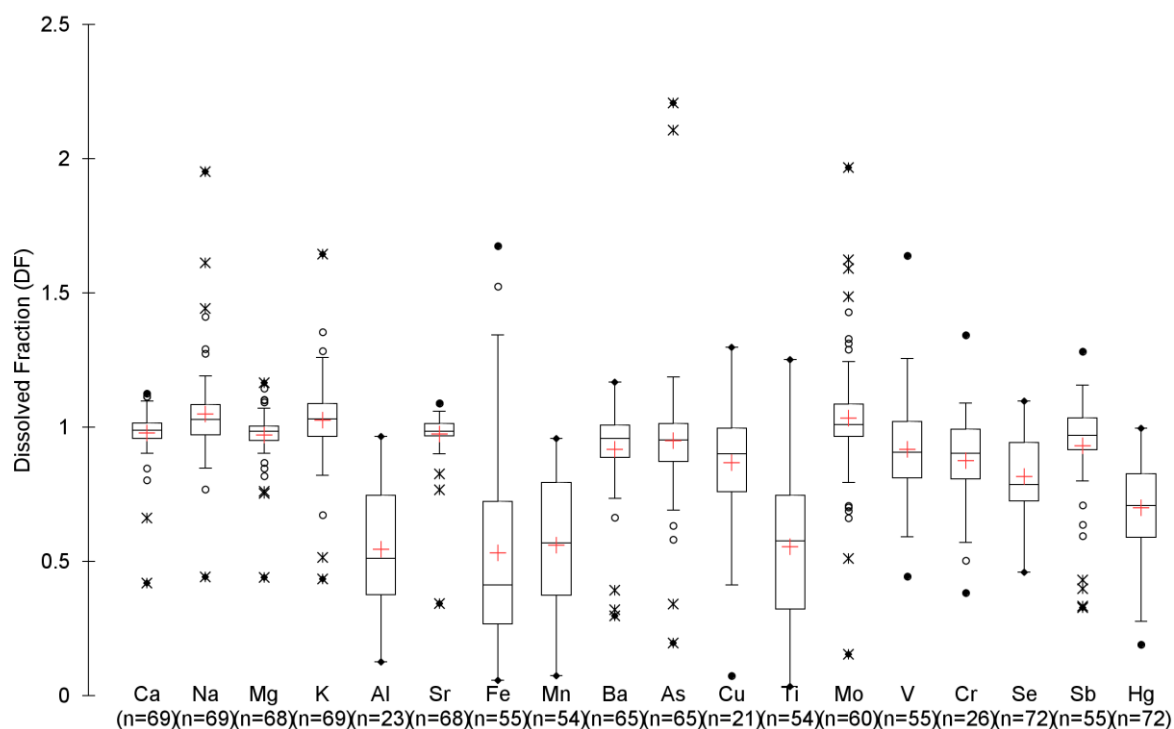


Figure 6-3: Dissolved Fraction (DF) in subsurface water samples calculated for each major, trace and ultra-trace element considered using the results obtained by ICP-MS. Dots are minimum and maximum, white circles are outliers and black crosses are extreme values, bars indicate 10th and 90th percentile, boxes indicate 25th and 75th, marks within each box are medians and red crosses are mean. For each element, the number n of samples above the LOD for both filtered and unfiltered samples are indicated. Note that Hg corresponds to non-gaseous Hg.

6.4. Lake classification

6.4.1. Trophic status and water quality

The Trophic State Index (TSI) was first proposed in 1977 by *Carlson* [50] and is defined as the total weight of biomass in a given water body at the time of measurement. This index, from 0 to 100, can be calculated using several parameters such as total phosphorus (TP), total nitrogen (TN), chlorophyll and Secchi disk transparency (SD). Each major division (10, 20, 30 etc.) represents a doubling in algal biomass. In our study, TP, TN and SD were not evaluated and chlorophyll-a was only measured at subsurface in all the lakes, with values below the limit of detection. Thus, it was not possible to calculate the chlorophyll-a concentration over all the water body. The only parameters that could probably estimate the trophic status of 20 studied lakes are Nitrate (NO_3^-), TOC and to a lesser extent Silicate. Indeed, the presence of phytoplankton communities is highly dependent on the quality and ratio of macro- and micronutrients (nitrogen N and phosphorous P) [11]. Diatoms are a major group of microalgae found in all aquatic systems, and represent a major component at the base of the marine food web, responsible for up to 50 % of total lake and oceanic primary production and 25 % of all oxygen produced on the planet [51]. Thus, these microorganisms intake NO_3^- (and to a lesser extent Silicate for diatoms) to develop themselves, subsequently increasing the TOC values in the lakes, especially during the spring-summer time.

Therefore, in order to evaluate the trophic status and classify the 19 studied lakes (PAR excluded), the TSI was calculated using TOC values according to *Dunalska* [52] and using the following formula:

Equation 6-2

$$TSI (TOC) = 20.59 + 15.71 \ln TOC$$

The TSI estimated for the lakes under study over the four sampling campaigns vary from 13 to 45 with a median value of 24 (**Figure 6-4**). A TSI below 30 to 40 is typical from oligotrophic lakes, where waterbodies have the lowest level of biological productivity, while TSI from 40 to 50 is characteristic of a mesotrophic lake with a moderate level of biological productivity. Lake ORD presents the highest TSI in the three sampling campaigns this lake was sampled, and it is the only one showing TSI above 40 (TSI = 45 in October 2018). This lake is shallow and relatively densely vegetated in comparison with the rest of the lakes. Apart from this lake, all the samples analysed showed a TSI value typical from oligotrophic lakes. In the Central Pyrenees, the trophic status of high altitude lakes range between ultraoligotrophic to mesotrophic [10,11,37]. Pasture is the most important source of eutrophication but is restricted to small and very shallow lakes. Therefore, our data about TOC and TSI are in accordance with previous studies that use TP to define the trophic status of high altitude lakes in the Pyrenees.

There are strong variations of TSI between sampling campaigns, and a significant increase (Kruskal-Wallis test, p-value < 0.05) occurs during the algal summer bloom. Indeed, an increase in TSI of 7 ± 3 between June 2017 and October 2017 for the ten lakes sampled in these two sampling campaigns (ARA, BAD, CAM, PEY, OPA, AZU, ARN, BAC, COA and PAN), and of 8 ± 3 between June 2018 and

October 2018 (ARA, BAD, CAM, PEY, OPA, GEN, ROU, BER, BAC, PEC, COA, PAN, ORD and SAB) were observed. This increase in the TSI is probably due to the more important primary productivity during summer: decreasing NO_3^- associated to increasing TOC (significant negative correlation between NO_3^- and TOC; $r = 0.59$; $p\text{-value} < 0.05$; **Figure 6-5**).

NO_3^- appears to be a limiting nutrient in the primary production as it was below the limit of detection in autumn samples for lakes PEY (both October 2017 and 2018), GEN, BER and ROU (October 2018). The highest decrease in NO_3^- during summer was found in Lakes ARA, BAD and COA. Lakes GEN, BER and ROU are impacted by agropastoralism, probably leading gradually to their eutrophication. COA, like ORD, is a shallow lake. ARA and BAD are also impacted by agropastoralism but to a lesser extent than the three lakes from the Ayous location (GEN, ROU and BER).

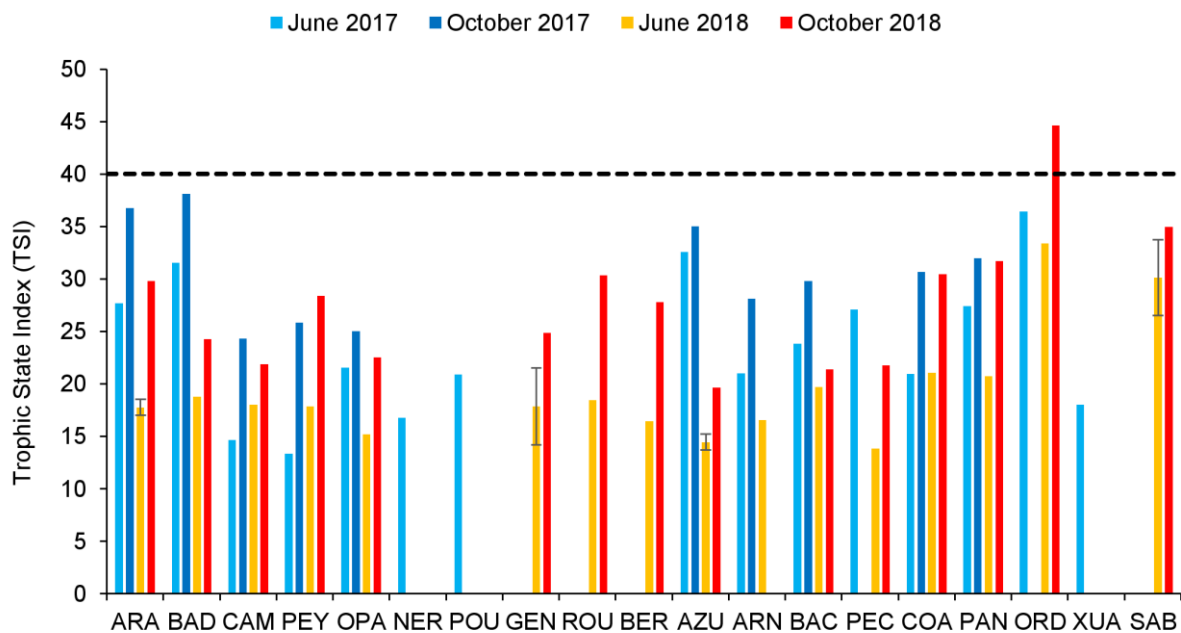


Figure 6-4: Trophic State Index (TSI) calculated for all the sampled lakes according to the sampling campaign. TSI below the dashed line (TSI = 40) indicate oligotrophic lakes. Error bars for Lakes ARA, GEN, AZU and SAB are associated to the samples from different times of the day.

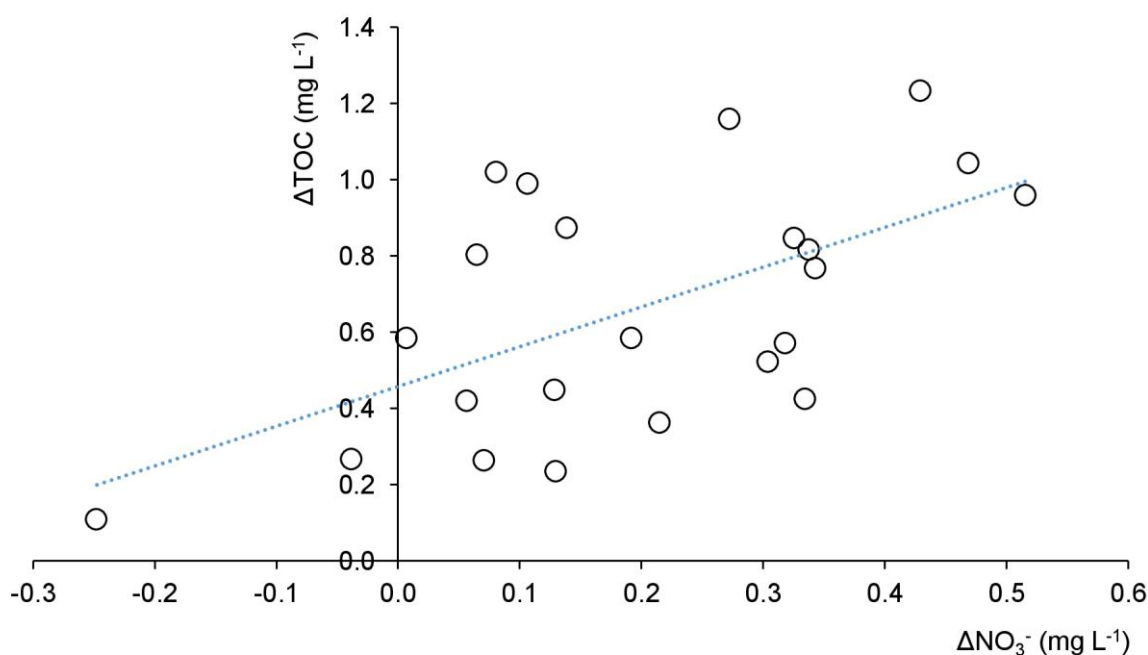


Figure 6-5: Relation between TOC and NO_3^- with ΔTOC corresponding to the increase of TOC between spring value and autumn values, and ΔNO_3^- corresponding to the decrease of NO_3^- between spring value and autumn values.

6.4.2. Classification of the lakes according to the water geochemistry

Water chemistry varies widely within and among the studied lakes. Principal Component Analysis (PCA) was carried out to investigate the main sources of variation in data. PCA is an ordination method that allows analysis and a visualisation of a dataset described by various quantitative variables. This statistical method uses an orthogonal transformation to convert a set of observations of possibly correlated variables into a set of values of linearly uncorrelated variables called principal components. The variables in the first principal component (PC1) explain most of the total variance of the system under study, and their loadings help identifying what contributes most to the differences among the individual sites. Similarly, the projection of the sites on the first principal components (scores) helps identifying groups of samples with similar characteristics. As a resume, PCA reduces the dimensions of a multivariate data to two or three principal components, that allows us visualizing the main sources of variance in the data matrix by means of the scores and loadings plots.

PCA of the data matrix made up of the main physicochemical parameters analysed in unfiltered subsurface water samples (Altitude, Ca, Na, Mg, K, Al, Sr, Fe, Mn, Ba, Cl⁻, NO_3^- , SO_4^{2-} , TOC, DIC, Silicate and TA) as variables and the water samples collected at the different studied lakes during the

four sampling campaigns as objects was carried by means of XLSTAT out in order to i) identify the major sources of variability, and ii) to look for groups of lakes with similar characteristics. Lake PAR was not considered because it differs too much from all the other studied lakes and would behave as a statistical outlier.

The data set were previously centred and scaled to rend normalized variables (mean value = 0; standard deviation = 1).

The main results of the PCA analysis are displayed in **Table 6-3**, **Figure 6-6**, **Table 6-4** and **Figure 6-7**. Three principal components were extracted explaining approximately 66 % of the total variance. PC1 explained 36 % of variance and was positively correlated with Ca (loading = 0.97), Mg (0.80), Sr (0.96), DIC (0.98) and TA (0.97). This PC indicates mainly the weathering of rocks supplying alkalinity. PC2 explained 18 % of variance and was positively correlated with Na (0.84), Cl⁻ (0.83) and Mn (0.62), and negatively with Elevation (-0.83): it could be both linked to atmospheric deposition or eutrophication. Finally, PC3 explained 13 % of the variance and is positively correlated with Silicate (0.76) and NO₃⁻ (0.59). It might indicate a mixture of lithogenic inputs (weathering of siliceous rocks) and primary productivity (consumption of Si and NO₃⁻).

Using the scores of the observations on each of the three PCs (**Table 6-4** and **Figure 6-7**), a classification of the lakes according to the chemical characteristics of their unfiltered subsurface waters can be proposed. Depending on these scores together with data previously published by *Camarero et al.* [10], different classes have been created for each PC. The cut off for each class has also been chosen to minimize the overlapping of the data for the main variables of a PC.

Table 6-3: Loadings of the variables on PC1, PC2 and PC3 after Principal Component Analysis of the dataset. Bold values are significant at 95 % confidence interval.

Principal Component (% of total variance)	PC1 36	PC2 18	PC3 13
Elevation	-0.32	-0.83	-0.02
Ca	0.97	-0.08	0.11
Na	-0.21	0.84	0.37
Mg	0.80	0.07	-0.49
K	0.20	0.17	0.20
Al	-0.47	-0.19	-0.51
Sr	0.96	-0.03	-0.08
Fe	-0.28	0.13	-0.38
Mn	-0.04	0.62	0.01
Ba	0.66	0.12	-0.29
Cl ⁻	-0.01	0.83	0.28
NO ₃ ⁻	0.13	-0.53	0.59
SO ₄ ²⁻	0.64	-0.35	0.45
TOC	0.49	0.28	-0.09
DIC	0.98	0.00	-0.14
Silicate	0.26	-0.12	0.76
TA	0.97	0.00	-0.15

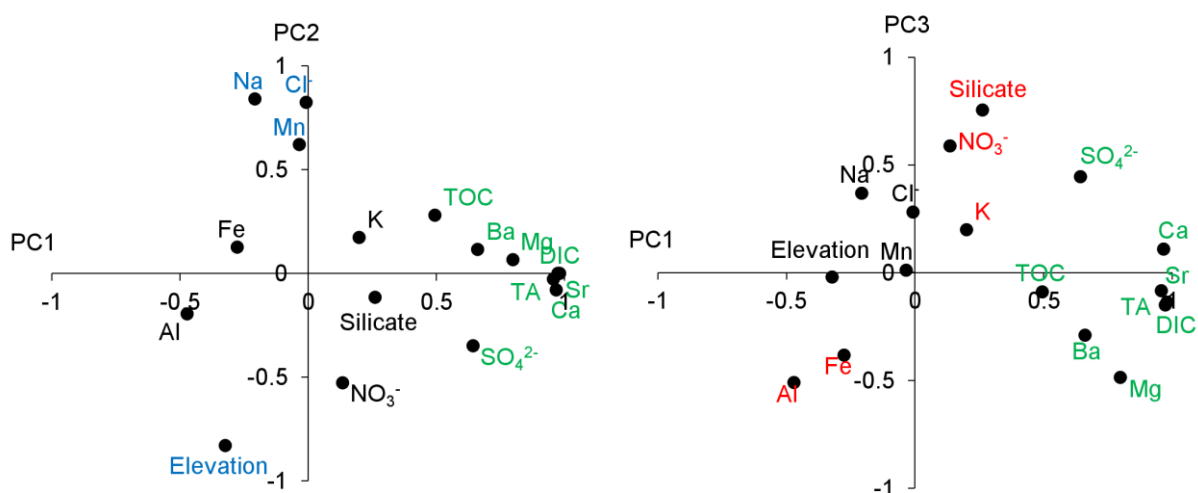


Figure 6-6: Loading plots on the PC1-PC2 and PC1-PC3 planes obtained after Principal Component Analysis of the dataset.

Table 6-4: Scores of the observations on PC1, PC2 and PC3 after Principal Component Analysis of the dataset, together with the proposed classification of these lakes: for PC1, Class 1 (Score < 0) / Class 2 (0 < Score < 3) and Class 3 (Score > 3); for PC2, Class 1 (Score < 0) / Class 2 (Score > 0); for PC3, Class 1 (Score < 0.5) / Class 2 (Score > 0.5).

Lake	PC1 Score	PC1 Class	PC2 Score	PC2 Class	PC3 Score	PC3 Class
ARA	0.8 ± 0.5	Class 2	-0.8 ± 0.4	Class 1	1.4 ± 0.6	Class 2
BAD	1.8 ± 0.6	Class 2	-1.5 ± 1.0	Class 1	1.7 ± 0.7	Class 2
CAM	-2.1 ± 0.2	Class 1	-0.6 ± 0.7	Class 1	-0.2 ± 0.2	Class 1
PEY	-3.4 ± 0.7	Class 1	-1.4 ± 0.6	Class 1	-3.1 ± 1.9	Class 1
OPA	-1.4 ± 0.3	Class 1	-0.6 ± 0.3	Class 1	0.0 ± 0.4	Class 1
NER	-2.2	Class 1	-1.0	Class 1	-0.5	Class 1
POU	-2.1	Class 1	-0.6	Class 1	-0.1	Class 1
GEN	-1.0 ± 0.1	Class 1	3.0 ± 0.9	Class 2	0.0 ± 0.5	Class 1
ROU	-0.9 ± 0.1	Class 1	2.7 ± 0.1	Class 2	0.0 ± 0.5	Class 1
BER	-1.6 ± 0.6	Class 1	0.9 ± 0.7	Class 2	-1.0 ± 0.3	Class 1
AZU	2.4 ± 1.0	Class 2	-1.8 ± 0.1	Class 1	0.9 ± 0.3	Class 2
ARN	-1.3 ± 0.5	Class 1	-1.1 ± 0.3	Class 1	0.9 ± 0.3	Class 2
BAC	-0.9 ± 0.1	Class 1	-0.3 ± 0.3	Class 1	0.4 ± 0.3	Class 1
PEC	-0.6 ± 0.6	Class 1	-2.1 ± 0.5	Class 1	0.7 ± 0.3	Class 2
COA	-2.1 ± 0.1	Class 1	-0.5 ± 0.4	Class 1	-1.0 ± 0.6	Class 1
PAN	-0.2 ± 0.3	Class 1	2.9 ± 1.9	Class 2	1.8 ± 0.5	Class 2
ORD	0.7 ± 0.1	Class 2	1.4 ± 0.9	Class 2	0.2 ± 0.4	Class 1
XUA	-2.2	Class 1	-1.7	Class 1	-0.3	Class 1
SAB	6.1 ± 0.3	Class 3	0.4 ± 0.4	Class 1	-2.4 ± 0.3	Class 1

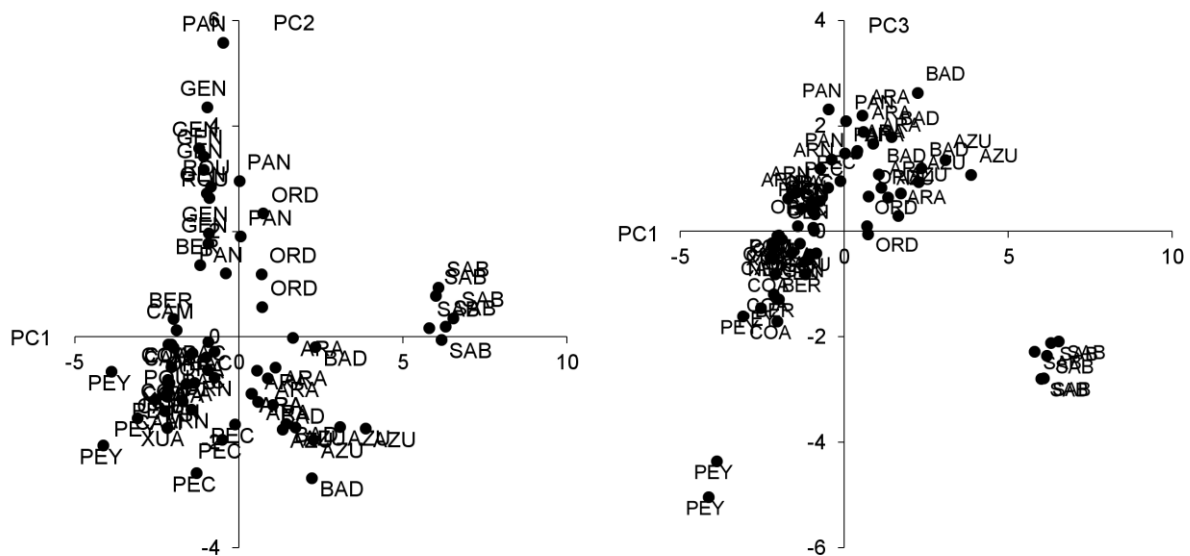


Figure 6-7: Score plots on the PC1-PC2 and PC1-PC3 planes obtained after Principal Component Analysis of the dataset.

The PC1, explaining most of the variance, relates to the influence of the weathering of rocks supplying alkalinity, mainly dependent on the composition of the geological basin of the lakes. Indeed, dissolution of calcium carbonate CaCO_3 , and to a lesser extent magnesium carbonate MgCO_3 , contributes significantly to the alkalinity of lake water as indicated by the strong and significant correlation between Ca and TA ($r = 0.93$; $p\text{-value} < 0.05$). From this PC, three different classes have been extracted (**Table 6-4**): low weathering (Class 1) ($n=14$), medium weathering (Class 2) ($n=4$) and high weathering (Class 3) ($n=1$). The highest values of Ca (median = $21358 \mu\text{g L}^{-1}$) and TA (median = $1810 \mu\text{mol kg}^{-1}$) were found in SAB whose basin lies on Devonian (limestone, sandstone, shale) and Cretaceous (limestone, sandstone) sedimentary rocks, rich in limestone (mainly CaCO_3) and dolomite (mainly $\text{CaMg}(\text{CO}_3)_2$). It is worth noting that during Cretaceous, more chalk (CaCO_3 deposited by the shells of marine invertebrates) was formed than in any other period in the Phanerozoic, including Devonian and Permian-Triassic (conglomerate, sandstone, lutite, andesite, shale). These carbonate rocks are very soluble and sensitive to weathering, explaining the high values for Ca and TA. The contribution of Mg (concentrations up to 100 times higher in SAB), through dolomite dissolution, to the TA is also much more important than in any other lake [53]. The second class, medium weathering, includes the four lakes whose basin lies exclusively on Devonian sedimentary rocks (ARA, BAD, AZU and ORD; $13559 \mu\text{g L}^{-1}$ and $733 \mu\text{mol kg}^{-1}$ median values of Ca and TA). Finally, the last fourteen lakes make up the third class ($5427 \mu\text{g L}^{-1}$ and $302 \mu\text{mol kg}^{-1}$ median values of Ca and TA), low weathering, with the lowest values of Ca and TA observed for the lakes lying on non-erodible granites. Overall, this PC1 expresses well a weathering rate gradient related to soil and bedrock mineralogy from non-erodible granite to high soluble sedimentary rocks (**Figure 6-8**).

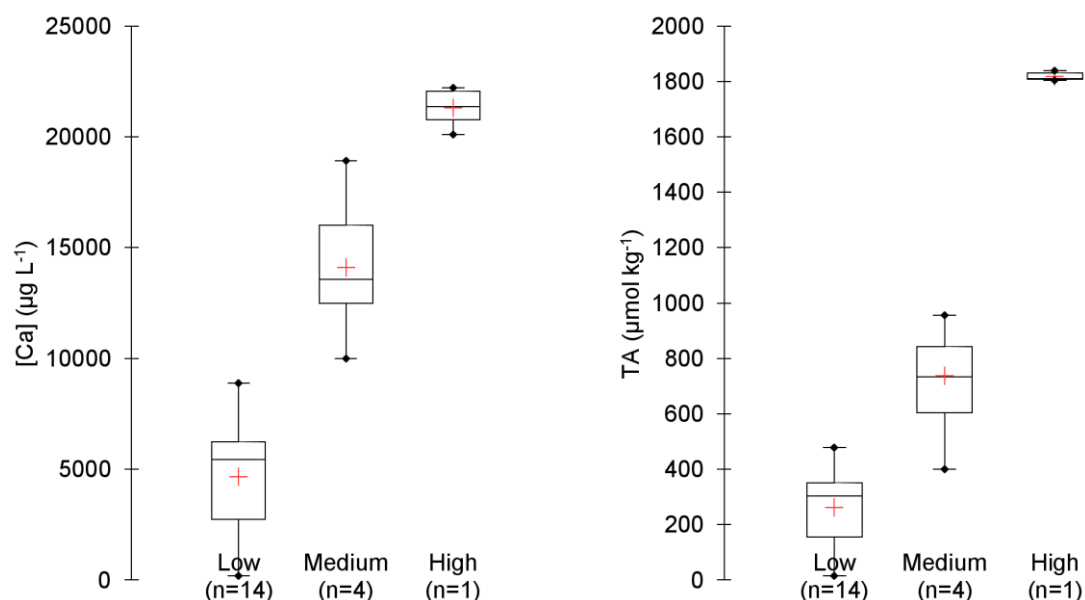


Figure 6-8: Ca concentrations and TA values according to the classification extracted from the PC1, importance of the weathering supplying alkalinity: Low (Lakes CAM, PEY, OPA, NER, POU, GEN, ROU, BER, ARN, BAC, PEC, COA, PAN and XUA), Medium (Lakes ARA, BAD, AZU and ORD) and High (Lake SAB).

The important weight of both Na and Cl⁻ on PC2 suggests an influence of atmospheric depositions through sea-salt inputs (marine aerosols). Nevertheless, Cl⁻ can also be originated from cattle urine, therefore a witness of pastoralism activities [37]. Additionally, positive loading of Mn on this PC2 suggests that hypoxia/anoxia is important in these lakes, also a symptom of eutrophication by cattle. The negative loading of NO₃⁻ on this PC2 is also supporting the eutrophication factor: lower NO₃⁻ implies higher eutrophication as explained in **6.4.1 Trophic status and water quality**. Pasturage is the most important eutrophication agent for the lakes in the Pyrenees, and specially occurs in the Ayous area where GEN, BER and ROU are located. Concentrations of Na, Cl⁻ and Mn, the three chemical variables with the highest loadings on PC2, allow classifying the lakes in two classes: very weak (Class 1) (n=14) and weak (Class 2) (n=5) marine influence and/or eutrophication (**Table 6-4** and **Figure 6-9**).

Na and Cl⁻ have also an opposite relation with elevation as shown on **Figure 6-10**: decreasing concentrations as elevation increases ($r = 0.67$ for Na and $r = 0.66$ for Cl⁻ without SAB; p-values < 0.05). Due to orographic effect, heavy rain usually deposits at the mountain foothills, not at the summits: lakes located at higher altitude may be less influenced by sea-salt depositions. In addition to this process influencing directly the wet and dry depositions, at very high altitude, vegetation is scarce and influence of the leaching from the catchment on the lake water might be less important than at lower altitude so dry depositions of sea-salt are expected to be lower. One lake, SAB, does not follow the same trend as it is in the very weak marine influence class. This is probably due to the location of this lake, the southernmost lake.

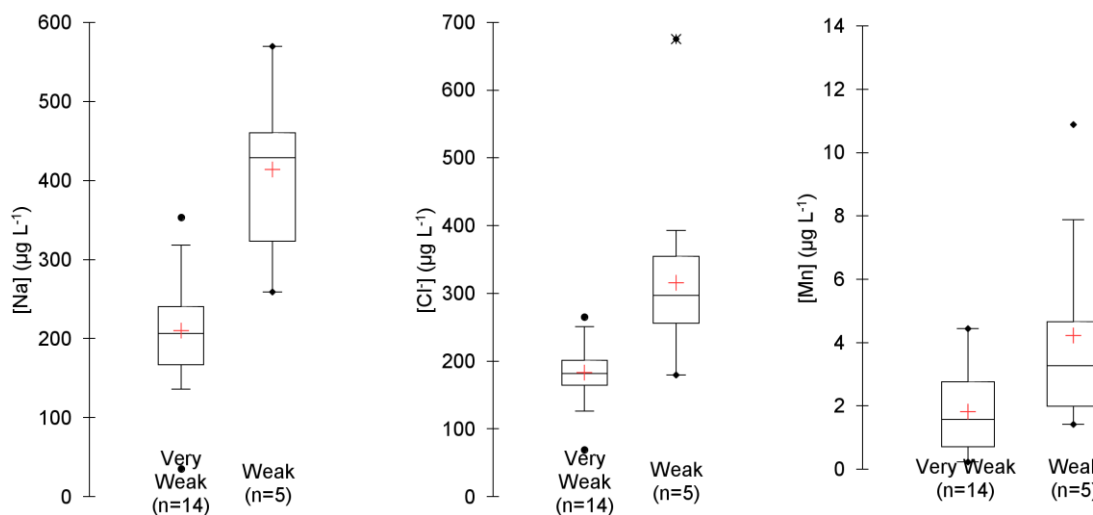


Figure 6-9: Na and Cl⁻ concentrations according to the classification extracted from the PC2, importance of the marine influence and/or eutrophication: Very weak (Lakes ARA, BAD, CAM, PEY, OPA, NER, POU, AZU, ARN, BAC, PEC, COA, XUA and SAB) and Weak (Lakes GEN, ROU, BER, PAN and ORD).

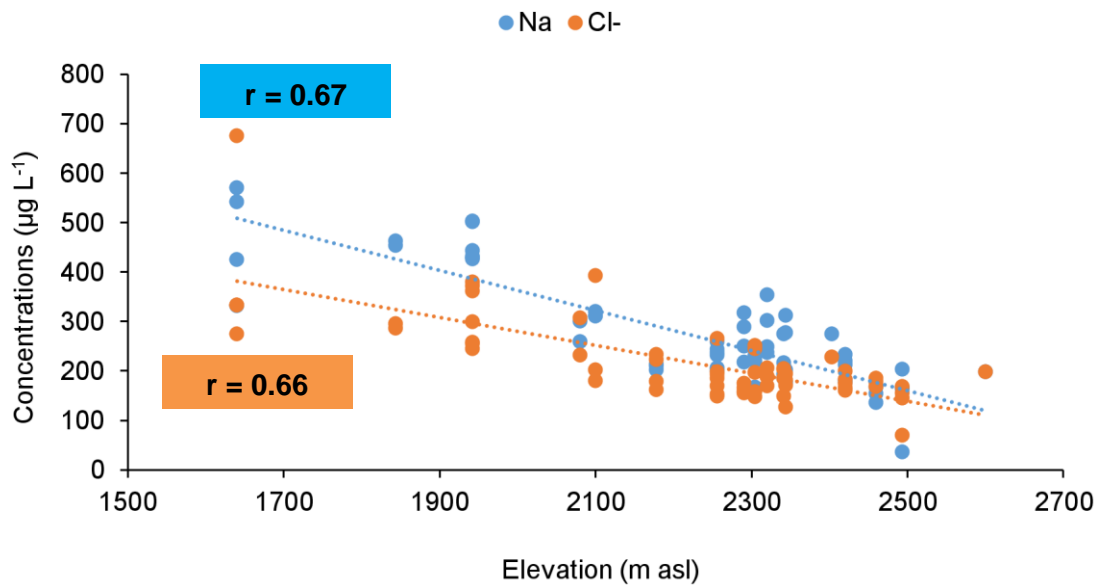


Figure 6-10: Negative correlation between elevation and i) Na and ii) Cl⁻ concentrations (SAB not considered).

Finally, the PC3 is mainly characterized by positive loadings of Silicate and NO₃⁻ and might be related to a mixture of lithogenic inputs and primary productivity. Silicate may reach lake waters through weathering of siliceous rocks, but also from atmospheric mineral depositions. Moreover, Silicate (Si) is an essential macronutrient, especially in the development of diatoms microorganisms that consume both Silicate and NO₃⁻. Silicate is also important for the carbon cycle (calculation of alkalinity) [41]. Only two classes are defined with this PC: low (Class 1) (n=13) and high (Class2) (n=6).

Among the main parameters, SO₄²⁻ is of particular interest. Indeed, sulphate occurs as the principal anion in lake waters. It provides sulphur S to the lake water, an essential plant nutrient just as nitrate or phosphate. The PC1 and PC3, related to the weathering processes, explains most of the variability of SO₄²⁻ (respectively 0.64 and 0.45): weathering of soil mineral, through mineral-bearing S and Mg²⁺, might be the main sources of S in high altitude lakes. Nevertheless, even if the contribution is less important, especially with reducing emissions of S, it is important to make the difference between the geological and atmospheric supply of sulphur. *Camarero et al.* [10] proposed a threshold of SO₄²⁻ concentrations: below 50 µeq L⁻¹ (2.40 mg L⁻¹) in lake water, atmospheric deposition of S is the main controlling factor, whereas above this threshold geological supply of S is dominant. Nevertheless, this study uses data obtained in a sampling campaign carried out in 2000, and S emissions have declined by about 80 % in Spain and in France between 2000 and 2016 (<http://www.emep.int/Emerge>). Therefore, considering this recent and significant decrease in the S emissions, we proposed here lowering this threshold to 15 µeq L⁻¹ (0.72 mg L⁻¹). **Figure 6-11** displays the concentrations of SO₄²⁻ against the concentrations of Mg²⁺ and allows classifying lakes as a function of S deposition processes.

With this new limit, half of the lakes display SO_4^{2-} values below the established limit, in relation to their geological background. On the one hand, CAM, PEY, OPA, NER, POU, COA and XUA are mainly lying on non-soluble granites, explaining well the atmospheric inputs. On the other hand, GEN, ROU and BER, lying on Cretaceous sedimentary rocks, expressed higher Mg^{2+} concentrations but low SO_4^{2-} . It might be rather due to production of sulphide under more anoxic conditions and its precipitation in those two lakes.

The other lakes, lying on well soluble sedimentary rocks, have shown a strong relation between SO_4^{2-} and Mg^{2+} (**Figure 6-11**) highlighting their geological supply of S ($r = 0.98$ for AZU and ARN; $r = 0.77$ for ARA, BAD, BAC, PEC, PAN and ORD; p -value < 0.05 ; Mg^{2+} 100 fold higher in SAB because of dolomites and high SO_4^{2-} content).

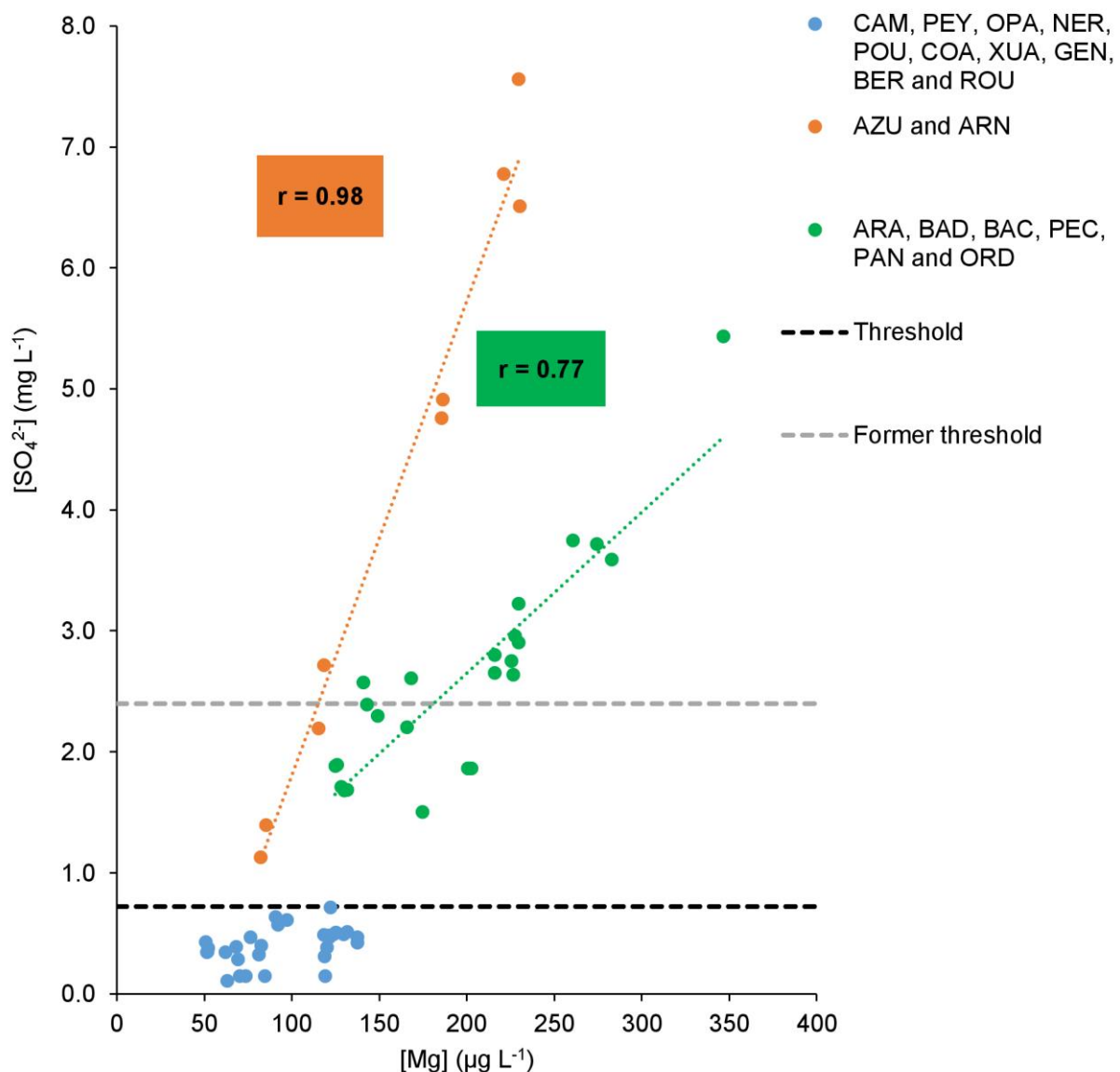


Figure 6-11: Concentrations of SO_4^{2-} as a function of Mg concentrations. Black dashed line is the new threshold proposed in this work (grey dashed line is the old one from *Camarero et al.* [10]) and set up at 0.7 mg L⁻¹ to distinguish between atmospheric and geological supply of SO_4^{2-} : below this limit, SO_4^{2-} is mainly originated from atmospheric depositions. Significant correlations between SO_4^{2-} from geological supply and Mg have been found ($r = 0.98$ for Lakes AZU and ARN; $r = 0.77$ for Lakes ARA, BAD, BAC, PEC, PAN and ORD).

6.4.3. Characteristic concentrations and major sources of Potential Harmful Trace Elements (PHTEs)

Discussion about the main parameters in the paragraphs above brings insights about the typology of the studied high-altitude lakes. The main outcome from this statistical analysis was the predominant importance of the geological background on the water chemistry of these lakes with the evidence for a gradient from non-soluble granite, where atmospheric inputs are more relevant than weathering inputs, to easily erodible sedimentary rocks. Therefore, to a better understanding and interpretation of PHTEs distribution among these lakes, it is necessary to split the lakes in three main categories depending on the influence of weathering of rocks supplying alkalinity (cf PC1):

- Category 1 with low weathering and more acidic lakes: 14 lakes (ARN, BAC, BER, CAM, COA, GEN, NER, OPA, PAN, PEC, PEY, POU, ROU and XUA).
- Category 2 with medium weathering: 4 lakes (ARA, BAD, ORD and AZU).
- Category 3 with high weathering and more alkaline lake: 1 lake (SAB).

Note that PAR has been removed from this discussion because, as mentioned previously, it is an outlier in many ways.

In order to investigate the occurrence and origin of PHTEs in the studied lakes, three complementary different tools were used: i) estimation of the characteristic concentrations (minimum, maximum, median and threshold) of each lake category, ii) calculation of enrichment factors (EF), and iii) Multiple Linear Regression (MLR) of data. The results obtained will be discussed all together in this section

Table 6-5 and **Table 6-6** present a summary of the results (minimum, maximum, median and threshold) obtained for PHTEs in unfiltered subsurface water samples. Three different groups of lakes have been defined according to the classification proposed in **6.4.2 Classification of the lakes according to the water geochemistry**. Bibliographic data extracted from remote and/or alpine lakes is also presented in **Table 6-5** and **Table 6-6** for comparison purposes.

The threshold values have been calculated according to the guidelines from the Idaho Geological Survey [54] for non-normal distributed data, which do not meet the steady state condition and for which possible seasonal effects were not corrected:

Equation 6-3

$$\text{Threshold} = \text{Median} + 1.65 \times (\text{interquartile range})$$

Figure 6-12 displays the Crustal Enrichment Factors (EF_{UCC}) calculated for each PHTEs of interest in the unfiltered subsurface water samples. EF_{UCC} is defined as the concentration ratio of a given element to that of one element which originates mainly from rock and soil dust (usually Al or Ti), normalized to the same reference concentration ratio characteristic of the upper continental crust (UCC) given by *Wedepohl (1995)* [55].

Equation 6-4

$$EF_{UCC} = \frac{\frac{[X]_{sample}}{[Al\ or\ Ti]_{sample}}}{\frac{[X]_{UCC}}{[Al\ or\ Ti]_{UCC}}}$$

where X is the element of interest. Crustal enrichment factors (EF_{UCC}) have been already used in previous studies to estimate the relative contribution of elements from natural versus anthropogenic sources, either in sediments [12] or atmospheric depositions [49] in the Pyrenees.

Enrichment factors below 10 times the mean crustal composition are unlikely to indicate contributions other than crustal sources while values between 10 and 100 suggest moderate enrichment and values above 100 a high enrichment. Enrichment factors interpretation has to be done carefully, especially because of the variable composition of the Earth's crust. Therefore, we also calculated the EF_{MDT} in a similar way than the EF_{UCC} , but using the Maladeta bedrock (Central Pyrenees) [56] as a reference.

The non-parametric test Kruskal-Wallis was used to check if there were significant differences between EF according to the geological category.

Multiple Linear Regression (MLR) of data was carried out (XLSTAT software) in an attempt to explain the variations in PHTEs concentrations within lakes (dependent variables) using a combination of explanatory factors (independent variables).

The independent variables considered in the calculation were either physical parameters (elevation, catchment size to lake size ratio, maximum depth of the lake, temperature) or chemical parameters (pH, Ca, Na, Mg, K, Al, Sr, Fe, Mn, Ba, Cl⁻, SO₄²⁻, NO₃⁻, DOC, Si, TA). The significance of each parameter was evaluated using the stepwise procedure. With this procedure, the selection process starts by adding the variable with the largest contribution to the model (the criterion used is Student's t statistic). If a second variable is such that the probability associated with its t statistic (the ratio between the corresponding standard deviation of the parameter and the parameter itself) is less than the "probability for entry", it is added to the model. The same for a third variable. After the third variable is added, the impact of removing each variable present in the model after it has been added is evaluated (still using the t statistic). If the probability is greater than the "Probability of removal", the variable is removed. The procedure continues until no more variables can be added or removed.

In order to increase the power of this multivariate regression technique, Cat2 and Cat3 have been grouped together as the five lakes with more important weathering.

A summary of the results is shown in **Table 6-7**.

In the next paragraphs, an element-by-element discussion of the results shown in **Table 6-5** and **Table 6-6** (characteristic concentrations), **Figure 6-12** (EFs) and **Table 6-7**. (MLR) follows to i) compare the occurrence of PHTEs in the studied lakes with that in other similar environments, ii) characterize the different groups of lakes concerning the PHTEs in their unfiltered sub-surface waters, iii) investigate the magnitude of anthropogenic sources of PHTEs to the lakes, and iv) identify the physico-chemical variables more directly implicated in the variability of the data.

Arsenic has shown a wide range of concentrations with significant differences within and among each category of lakes: from 31 to 8910 ng L⁻¹ in more acidic lakes (Cat1), from 445 to 6462 ng L⁻¹ in medium alkaline lakes (Cat2) and from 124 to 172 ng L⁻¹ in the alkaline lake SAB (Cat3). The thresholds set up for Cat1 and Cat2, respectively 2949 and 4525 ng L⁻¹, are higher than most of the median As concentrations measured in water of many lakes worldwide, either from remote locations or not [29,42,43,45,57–59]. This may present a risk to arsenic sensitive biota to the concerned lakes and these strong variations in the As content may be related to local geological sources. Such strong variations in As concentrations have been already documented in the catchment of Lake Respomuso (Central Pyrenees, 2130 m asl) [36] and in the three lakes studied by *Bacardit and Camarero* [35] in a close area. Arsenic presents an important enrichment (>100) in more than 90% of the samples, and it was significantly higher in medium and high alkaline lakes (Kruskall-Wallis test, p-value < 0.05). The EF were lower when using the MDT reference rather than the UCC, supporting the hypothesis of local sources of As. The best MLR models obtained for medium and high alkaline lakes (Categories 2&3) highlight the significant influence of Sulphate on the As distribution. This is well supported by the strong positive correlation ($r = 0.69$) between As and Sulphate in these lakes. Dissolution of sulphide and sulpharsenide minerals, notably arsenopyrite FeAsS, in the easily erodible bedrock lakes might be responsible of the presence of As in those lakes. Moreover, desorption of As from soils and/or at the sediment-water interface might be enhanced by the presence of sulphate as mentioned in a recent study [60].

U concentrations were found to be higher in the less alkaline lakes (Category1) with a threshold set up at 1395 ng L⁻¹ while it was at 425 and 191 ng L⁻¹ respectively in medium (Category2) and high alkaline lakes (Category3). None publications related to high altitude lakes document the concentrations of U in such environment but lower concentrations, a few ng L⁻¹, were found in remote lakes such as in Antarctica [57] or in Lake Kawagama (Canada) [58]. When looking at the EF, no differences (Kruskall-Wallis test, p-value = 0.75) were found between lake categories, and most of the samples were highly enriched (>100), suggesting a common source of U in all the lakes. This assumption is well supported by the results of the MLR. Indeed, in the non-easily erodible lakes of Category1, the main significant variable explaining the distribution of U is the concentration of potassium. Transport of U-bearing minerals (i.e. carnotite) by Iberian and north African dust might be responsible of most of the U in low alkaline lakes where lower pH can promote the dissolution of these minerals [61]. Another possibility would be local sources from bearing rocks but mining of U ores was very small in the Pyrenees.

Cu, which is known to be atmospherically transported and deposited through precipitations [3] over long distances, is present in the high altitude lakes independently of the geological background. Indeed, the distribution is not significantly different among categories with thresholds at 292 ng L⁻¹ in low alkaline lakes (Category1), 325 ng L⁻¹ in medium alkaline lakes (Category2), and 310 ng L⁻¹ in high alkaline lakes (Category3). Nevertheless, when looking at the EF, Cu was mainly moderately enriched (10 < EF < 100). There were also significantly higher EF in medium and high alkaline lakes (Kruskall-Wallis, p < 0.05) suggesting small local inputs from weathering of Cu-bearing minerals in those lakes. The MLR technique does not provide us with relevant information due to the small coefficient of multiple determination associated to the model (0.32 for Category1 and 0.41 for Categories2&3).

Mo concentrations were in the same range than in the remote lakes from Antarctica [57]: from 6 to 544 ng L⁻¹ (threshold = 192 ng L⁻¹) in less alkaline lakes (Category1), from 104 to 247 ng L⁻¹ (threshold = 249 ng L⁻¹) in medium alkaline lakes (Category2) and from 38 to 55 ng L⁻¹ in the high alkaline lake SAB (threshold = 46 ng L⁻¹). As mentioned previously, Mo mobility is hardly predictable because it depends on many parameters. EF indicated moderately enrichment (between 10 and 100) for most of the samples with significantly higher EF (Kruskall-Wallis, p-value < 0.05) observed for the medium to high alkaline lakes suggesting that weathering processes are influencing the concentrations of Mo. The results from the MLR suggest a strong influence of sulphate on the distribution of Mo, especially for low alkaline lakes with a positive correlation between Mo and sulphate (r = 0.60) where sulphate is mainly atmospherically originated.

V concentrations were extremely low in comparison with data from other remote lakes. Indeed, concentrations range from 30 to 174 ng L⁻¹ in low alkaline lakes (Category1), from 42 to 186 ng L⁻¹ in medium alkaline lakes (Category2) and from 23 to 35 ng L⁻¹ in the high alkaline lake SAB (Category 3), while the minimum value documented for V in the Alps was 300 ng L⁻¹ [29]. Usually of anthropogenic origin (combustion of coal/oil and road traffic), V is a good indicator for the remoteness of a studied area. This element shows also extremely low EF values, independently from the geological substrate of the lake (Kruskall-Wallis, p-values = 0.20). Nevertheless, the best MLR models obtained for V highlight strong differences according to the geological background. Indeed, while Na, probably from geological origin, is triggering the distribution of V in erodible lakes (Categories 2&3), V is associated to SO₄²⁻ in non-erodible lakes (Category1) where sulphate is mainly atmospherically deposited. Therefore, these types of lakes could eventually be used to follow the atmospheric deposition of V.

Ni is showing a comparable behaviour to that of Cu with no clear dependence of concentrations on the geological substrate, therefore suggesting atmospheric depositions as the main source of Ni. Indeed, the thresholds calculated for the low alkaline lakes (148 ng L⁻¹), for the medium alkaline lakes (120 ng L⁻¹), and for the lake SAB (110 ng L⁻¹) were comparable. Concentrations are also globally lower than all the bibliographic data for remote lakes. According to the EF, Ni was non enriched to moderately enriched in the studied lakes with higher EF in medium to high alkaline lakes (Kruskall-Wallis, p-value < 0.05). The MLR technique was not able to explain the distribution of Ni

neither for low alkaline (Category1) or medium to high alkaline lakes (Categories2&3), with coefficient of multiple determination of, respectively, 0.20 and 0.36.

Cr is present at very low concentrations in the studied lakes ranging from 23 to 129 ng L⁻¹ in low alkaline lakes, from 59 to 279 ng L⁻¹ in medium alkaline lakes and from 29 to 47 ng L⁻¹ in Lake SAB. For the low alkaline lakes, the range is comparable with the measurement made in the Alps [29] while the more erodible lakes are showing higher concentrations. EF are showing non enrichment for the whole samples when using the Maladeta reference while Cr is moderately enriched in medium alkaline lakes using the UCC reference, then suggesting some local and geological sources.

Pb concentrations were in the range of the studies already made in the Pyrenees by *Zaharescu et al (2009)* [36] and *Bacardit and Camarero (2010)* [35] and highest concentrations were found in the low alkaline lakes suggesting an influence of pH on the distribution of Pb. When taking Maladeta as a reference, Pb was always lower than 10 suggesting non enrichment. Using the UCC reference, EF were significantly higher suggesting possible local geological sources of Pb. Nevertheless, for low alkaline lakes, this potential source of Pb does not influence its distribution as well demonstrated by the best MLR models. Indeed, Ti is the main significant parameter influencing the concentrations of Pb in those low alkaline lakes suggesting a common source, probably Iberian and North Africa dust. This is also well supported by the positive correlation between Ti and Pb for low alkaline lakes ($r = 0.79$).

Se concentrations were extremely low in comparison with other studies in remote lakes, with thresholds of 40 ng L⁻¹ for low alkaline lakes (Category1), 81 ng L⁻¹ for medium alkaline lakes (Category2) and 23 ng L⁻¹ for Lake SAB. Se was constant and did not significantly change over sampling campaign, suggesting local geological sources. These sources might be significant as the EF calculated were the second highest (after As), and dependant on the geological substrate (Kruskall-Wallis, p-value < 0.05). The MLR analysis on the low alkaline lakes highlight well the importance of Sulphate, with positive correlation observed ($r = 0.72$) between sulphate and Se concentration. Se in lake waters behave the same as Sulphate as it replaces sulphur in sulphide minerals such as pyrite, chalcopyrite, pyrrhotite and sphalerite.

Sb is present at very low concentrations in the studied lakes, ranging from 5 to 85 ng L⁻¹ in low alkaline lakes (Category1), from 10 to 80 ng L⁻¹ in medium alkaline lakes (Category2) and from 33 to 36 ng L⁻¹ in Lake SAB. It displays moderate to intense EF values both in low or medium to high alkaline lakes. Sb in low alkaline lakes was the highest in lakes GEN and PEC where Ca was also the highest, explaining the results obtained for the MLR statistical method. In addition, Sb in medium to high alkaline lakes was the highest in Lake AZU.

The concentration of Co in the lakes investigated in this work was lower than the values reported by *Zaharescu et al (2009)* [36] for the catchment of Lake Resposuso. Calculated thresholds were 20, 28 and 14 ng L⁻¹ from low alkaline to high alkaline lakes. Co EF were among the lowest calculated ones, indicating no anthropogenic enrichment of Co. Only for low alkaline lakes, Fe is the main

variable explaining the distribution of Co, and both parameters are significantly correlated in these lakes ($r = 0.86$; $p\text{-value} < 0.05$). Therefore, once in the lake, Co probably behaves closely together with other oxide-hydroxide elements.

Cd is present at very low concentrations but the moderate values of EF obtained may suggest an anthropogenic origin. Nevertheless, the MLR model was not able to further explain the distribution and origin of Cd.

TI concentration was much lower than in some remote lakes from Antarctica [56], the only pristine lakes in which the TI concentration has been measured so far. This element shows a clear dependence with geology: highest concentrations in low alkaline lakes (0.2 to 2.5 ng L^{-1}) and lowest ones in medium (0.2 to 0.8 ng L^{-1}) and high alkaline lakes (0.3 to 0.3 ng L^{-1}). EF were very low, suggesting no anthropogenic inputs. The MLR models calculated for TI suggest a common source or behaviour for Al and TI in low alkaline lakes, and for Na and TI in high alkaline lakes.

Non-gaseous Hg, supposed to reach the lake water mainly through wet and dry deposition, exhibits very low concentrations, similar to what can be found in open seawater and independently of the geological substrate. This supports the hypothesis of atmospheric deposition as the main processes responsible of the presence of Hg in the high altitude lakes. EF is also from moderate to intense suggesting long-range transport of both natural and anthropogenic Hg to the lakes. Finally, in the MLR model, TOC is the main parameter influencing the non-gaseous Hg distribution supported the role of organic matter to control Hg level in the aqueous phase as already observed in previous studies [62,63]. The role of Hg and its cycle in lake environments is discussed in the next chapters of this manuscript: **7 Dynamics, distribution, and transformations of mercury species from Pyrenean high-altitude lakes** and Erreur ! Source du renvoi introuvable. Erreur ! Source du renvoi introuvable..

Table 6-5: Characteristic concentrations for unfiltered subsurface water samples as minimum, median and maximum concentration as well as the calculated threshold for our study together with data extracted from bibliography (remote and alpine lakes) for the following PHTEs: As, U, Cu, Mo, V, Ni and Cr.

Reference	Location	Lakes	Elevation (m asl)	Data	As	U	Cu	Mo	V	Ni	Cr
					ng L ⁻¹						
This Work	Central Pyrenees (France/Spain)	14 (Cat1)	1620-2600	Min-Max	31-8910	5-1796	94-434	6-544	30-174	23-797	23-129
				Median	396	328	176	52	82	64	59
				Threshold	2949	1395	292	192	165	148	102
		4 (Cat2)	2100-2420	Min-Max	445-6462	69-434	110-334	104-247	42-186	37-124	59-279
				Median	1112	195	188	143	96	96	121
				Threshold	4525	425	325	249	188	120	194
		1 (Cat3)	1900	Min-Max	124-172	98-146	171-285	38-55	23-35	61-114	29-47
				Median	142	111	219	40	26	74	41
				Threshold	191	123	310	46	32	110	58
<i>Skjelkvåle et al.</i> (2001) [43]	Finland	464		Min-Max	<30-4060		70-13000		10-8340	20-47600	7-2830
				Median	290		420		290	370	290
	Norway	985		Min-Max	<50-12700		30-37700		3-5920	10-7050	1-6140
				Median	<50		330		100	240	70
	Sweden	1036		Min-Max	<30-126000		20-8200		7-3680	10-11100	3-27700
				Median	280		360		150	350	130
	Denmark	19		Min-Max	<30-4000		<100-3200		<1000-3300	<500-5300	<500-500
				Median	1200		600		1000	1000	<500
	Russian Kola	460		Min-Max			100-20000			100-450000	
				Median			730			330	
<i>Chen et al.</i> (2000) [42]	USA	20		Min-Max	0-587						
				Median	587						
<i>Markert et al.</i> (1997) [45]	Argentina	4	Lake Mascardi (Tronador)			1400				<800	<1500
			Lake Mascardi (Catedral)	<300		2600				8700	<2000
			Lake Gutierrez	<1200		<1200				<800	<2000
			Lake Nahuel Huapi	<400		<1100				<500	<1200

Table 6-5 (continued)

<i>Green et al. (2004)</i> [64]	Antarctica	1		Lake Vanda		254			200		
<i>Kakareka et al. (2019)</i> [57]	Antarctica	4		Min-Max	52-989	<1-12	<22-2173	10-1602	155-3907	46-687	44-12063
				Median	422	5	644	264	670	376	1666
<i>Shotyk and Krachler (2009)</i> [58]	Canada	1	356	Lake Kawagama	137	4	470	8	62	289	75
<i>Yang et al. (2002)</i> [65]	Scotland	1	785	Lake Lochnagar			750			200	
<i>Rosseland et al. (2013)</i> [59]	Himalaya (Nepal)	1	782	Lake Phewa	800		500			400	900
<i>Sharma et al. (2015)</i> [32]	Himalaya (Nepal)	2	782	Lake Phewa			1760		260	760	210
				Lake Gosainkunda			300		130	280	710
<i>Deka et al. (2016)</i> [31]	Himalaya (India)	1	3962	P.T. Tso (pre-monsoon)			4200				3100
				P.T. Tso (post-monsoon)			<LOD				<LOD
<i>Hofer et al. (2001)</i> [30]	Alps (Italy/Austria)	17	1092-2387	Min-Max			50-19400			90-2100	
				Median			690			730	
<i>Tornimbeni and Rogora (2012)</i> [29]	Alps (Italy)	32	1895-2672	Min-Max	500-2200		200-2400		300-5400	100-1200	50-100
				Median	1100		400		800	350	100
<i>ICP Water Annual Report (2016)</i> [66]	Alps (Switzerland)	21	1692-2580	Min-Max			100-400			100-6100	
				Median			200			100	
<i>Zaharescu et al. (2009)</i> [36]	Central Pyrenees (Spain)	5	2130	Min-Max	60-9650		980-46800			540-38610	140-1030
				Median	2630		3130			2165	280
<i>Bacardit and Camarero (2010)</i> [35]	Central Pyrenees (France/Spain)	3	1655	Légunabens	2110						
				Plan	310						
				Vidal d'Amunt	140						

Table 6-6: Characteristic concentrations for unfiltered subsurface water samples as minimum, median and maximum concentration as well as the calculated threshold for our study together with data extracted from bibliography (remote and alpine lakes) for the following PHTEs: Pb, Se, Sb, Co, Cd, Tl and Hg

Reference	Location	Lakes	Elevation (m asl)	Data	Pb	Se	Sb	Co	Cd	Tl	Hg	
This Work	Central Pyrenees (France/Spain)	14 (Cat1)	1620-2600	Min-Max	15-503	12-46	5-85	5-61	1-12	0.2-2.5	0.1-2.9	
				Median	42	21	21	10	2	0.6	0.4	
				Threshold	99	40	62	20	5	1.4	0.7	
		4 (Cat2)	2100-2420	Min-Max	17-105	25-89	10-80	8-80	1-4	0.2-0.8	0.1-1.2	
				Median	42	59	18	17	3	0.4	0.3	
				Threshold	81	81	61	28	4	0.8	0.7	
		1 (Cat3)	1900	Min-Max	13-42	18-24	33-36	12-13	1-1	0.3-0.3	0.6-0.8	
				Median	20	20	34	13	1	0.3	0.6	
				Threshold	44	23	36	14	1	0.3	0.8	
<i>Skjelkvåle et al. (2001) [43]</i>	Finland	464		Min-Max	14-2780			1-20300	1-230			
				Median	170			58	11			
	Norway	985		Min-Max	4-15000			1-3200	0-1070			
				Median	140			45	12			
	Sweden	1036		Min-Max	3-12900			1-5500	1-540			
				Median	160			55	10			
	Denmark	19		Min-Max	50-8120			<50-790	<5-266			
				Median	380			70	50			
	Russian Kola	460		Min-Max								
				Median								
	<i>Chen et al. (2000) [42]</i>	USA	20		Min-Max	0-1040				1-114		
					Median	20				73		
<i>Markert et al. (1997) [45]</i>	Argentina	4		Lake Mascardi (Tronador)	<700			<200	<200			
				Lake Mascardi (Catedral)	<2200			<200	<200			
				Lake Gutierrez				<200	<200			
				Lake Nahuel Huapi	<600			<200	<200			

Table 6-6 (continued)

<i>Green et al. (2004)</i> [64]	Antarctica	1		Lake Vanda					12	
<i>Kakareka et al. (2019)</i> [57]	Antarctica	4		Min-Max	<5-1865	32-4295	1-5406	0-286	1-551	<1-31
				Median	178	1240	553	22	40	3
<i>Shotyk and Krachler (2009)</i> [58]	Canada	1	356	Lake Kawagama	57		30	12	8	
<i>Yang et al. (2002)</i> [65]	Scotland	1	785	Lake Lochnagar	820					150
<i>Rosseland et al. (2013)</i> [59]	Himalaya (Nepal)	1	782	Lake Phewa	1000					
<i>Sharma et al. (2015)</i> [32]	Himalaya (Nepal)	2	782	Lake Phewa	650			110	20	
			4300	Lake Gosainkunda	160			1440	3	
<i>Deka et al. (2016)</i> [31]	Himalaya (India)	1	3962	P.T. Tso (pre-monsoon)	7000					6000
				P.T. Tso (post-monsoon)	2000					1000
<i>Hofer et al. (2001)</i> [30]	Alps (Italy/Austria)	17	1092-2387	Min-Max	20-5300					3-100
				Median	220					30
<i>Tornimbeni and Rogora (2012)</i> [29]	Alps (Italy)	32	1895-2672	Min-Max		1000-5700				50-80
				Median		2600				80
<i>ICP Water Annual Report (2016)</i> [66]	Alps (Switzerland)	21	1692-2580	Min-Max	100-100					
				Median	100					
<i>Zaharescu et al. (2009)</i> [36]	Central Pyrenees (Spain)	5	2130	Min-Max	50-3390			20-260	30-990	
				Median	250			70	60	
<i>Bacardit and Camarero (2010)</i> [35]	Central Pyrenees (France/Spain)	3	1655	Légunabens	260					
			2188	Plan	50					
			2684	Vidal d'Amunt	40					

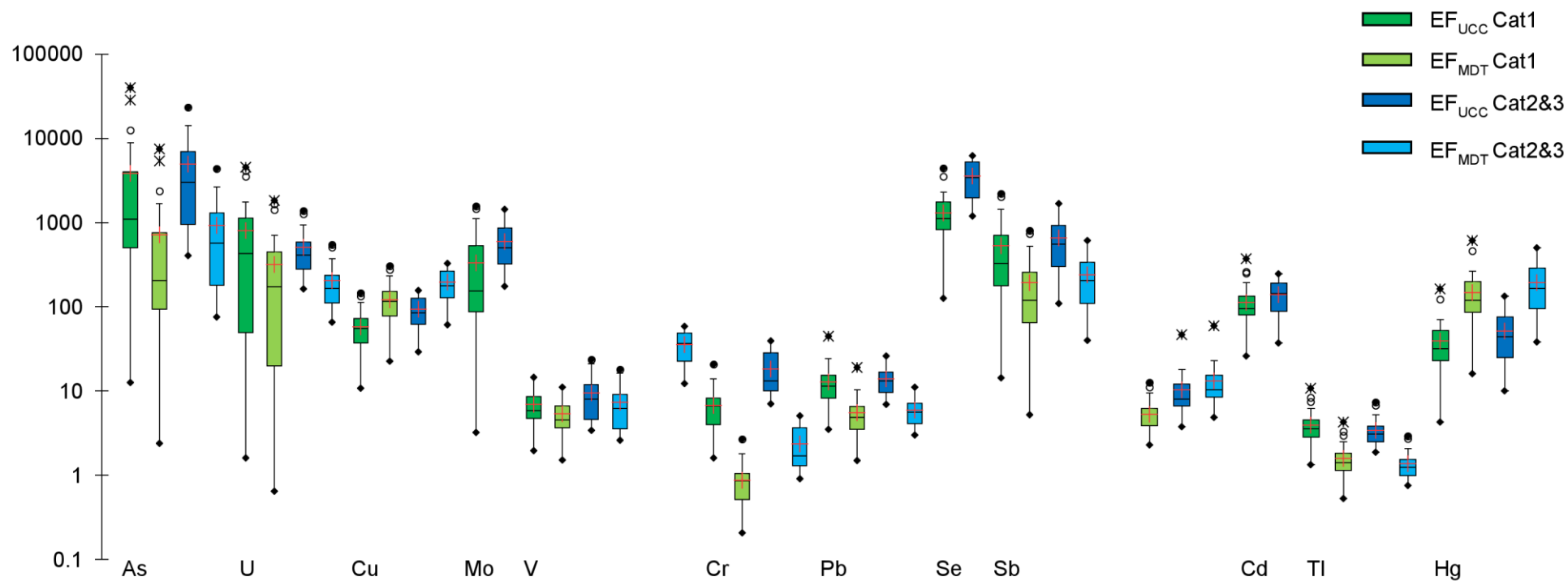


Figure 6-12: Enrichment factors (EF) for unfiltered subsurface water samples using the upper continental crust (UCC) [54] and the Maladeta (MDT) [55] bedrock as references. Green boxes have been generated using data from low alkaline lakes (Category 1) and blue boxes have been generated using data from medium and high alkaline lakes (Categories 2 and 3). Dots are minimum and maximum, white circles are outliers and block crosses are extreme values, bars indicate 10th and 90th percentile, boxes indicate 25th and 75th, marks within each box are medians and red crosses are mean. Note that Hg corresponds to non-gaseous Hg.

Table 6-7: Summary of the results obtained after multiple linear regression of data conducted on each PHTEs using 21 various variables (Catchment influence, Elevation, Maximum depth, Temperature, pH, Ca, Na, Mg, K, Al, Sr, Fe, Mn, Ba, Ti, Cl⁻, NO₃⁻, SO₄²⁻, TOC, Silicate and Total Alkalinity) according to the geological classification of the studied lakes (Low Alkaline vs Medium and High Alkaline Lakes). Significant variables with its normalized coefficient associated are shown in this table, together with the equation of the model.

Low Alkaline Lake (Category1): Lakes ARN, BAC, BER, CAM, COA, GEN, NER, OPA, PAN, PEC, PEY, POU, ROU and XUA				
Element	Samples	Coefficient of multiple determination (adjusted r ²)	Significant variables and associated normalized coefficient (bold is the most influencing variable)	Equation of the model
As	40	0.86	Sr (0.77) Na (-0.66) Ba (-0.34) Cl ⁻ (0.25) SO ₄ ²⁻ (0.29)	As = 1002 + 348.Sr – 12.Na – 1163.Ba + 5557.Cl ⁻ + 790.SO ₄ ²⁻
U	40	0.74	K (0.94) Ba (-0.54) Mg (-0.38) NO ₃ ⁻ (-0.37) pH (0.30)	U = -1422 + 16.K – 423.Ba – 6.0.Mg – 680.NO ₃ ⁻ + 341.pH
Cu	40	0.32	Cl⁻ (0.59) pH (-0.46)	Cu = 562 + 416.Cl ⁻ - 72.pH
Mo	40	0.79	SO₄²⁻ (1.22) Na (0.69) Sr (-0.58) Cl ⁻ (-0.30) Catchment (-0.24)	Mo = 154. SO ₄ ²⁻ + 0.56.Na -12.Sr – 309.Cl ⁻ - 0.13.Catchment
V	40	0.72	SO₄²⁻ (0.93) Al (0.57) Ca (-0.58) Na (0.31) K (0.28)	V = 23 + 41.SO ₄ ²⁻ + 1.1.Al – 0.009.Ca + 0.09.Na + 0.32.K
Ni	40	0.20	Ba (0.47)	Ni = 3.5 + 105.Ba
Cr	40	0.80	SO₄²⁻ (0.73) Fe (0.60) Ba (0.46) Max.Depth (-0.32) Temperature (-0.25)	Cr = 40 + 22.SO ₄ ²⁻ + 1.06.Fe + 17.Ba – 1.4.MaxDepth – 2.3.Temperature
Pb	40	0.78	Ti (0.89)	Pb = 11 + 194.Ti
Se	40	0.94	SO₄²⁻ (0.53) Mg (0.47) TOC (0.40) Na (-0.32) Fe (-0.18) Elevation (0.18) Temperature (-0.13)	Se = -4 + 5.SO ₄ ²⁻ + 0.1.Mg + 8.0.TOC – 0.02.Na – 0.1.Fe + 0.005.Elevation – 0.3.Temperature
Sb	40	0.91	NO₃⁻ (-0.45) Ca (0.89) Catchment (-0.40) Cl ⁻ (0.31) TOC (-0.24) pH (-0.22)	Sb = 83 – 35.NO ₃ ⁻ + 0.009.Ca – 0.05.Catchment + 67.Cl ⁻ - 14.TOC – 11.pH
Co	40	0.91	Fe (0.92) Mn (-0.16) pH (-0.13)	Co = 23 + 0.68.Fe – 0.61.Mn – 2.8.pH
Cd	40	0.34	Sr (-0.53) TOC (0.45)	Cd = 1.9 – 0.19.Sr + 2.1.TOC
TI	40	0.77	Al (0.69) TOC (0.45) Sr (-0.43) Silicate (0.24)	TI = -0.09 + 0.014.Al + 0.47.TOC – 0.035.Sr + 0.14.Silicate
Hg	40	0.23	TOC (0.49) pH (-0.36)	Hg = 2.2 + 0.56.TOC – 0.35.pH

Table 6-7 (continued)

Medium and High Alkaline Lakes (Categories 2&3): Lakes ARA, BAD, ORD, AZU and SAB				
Element	Samples	Coefficient of multiple determination (adjusted r ²)	Significant variables and associated normalized coefficient (bold is the most influencing variable)	Equation of the model
As	24	0.98	SO₄²⁻ (0.65) Mg (-0.68) Silicate (-0.66) Catchment (0.18) Ti (-0.09)	As = 2077 + 726.SO ₄ ²⁻ - 0.51.Mg – 881.Silicate + 25.Catchment – 1521.Ti
U	24	0.94	Ba (-0.69) Na (0.52) pH (0.33) Temperature (0.20) Cl ⁻ (-0.19)	U = -775 – 35.Ba + 1.02.Na + 118.pH + 4.6.Temperature – 401.Cl ⁻
Cu	24	0.41	Temperature (0.66)	Cu = 120 + 8.2.Temperature
Mo	24	0.91	Mg (-2.54) TA (1.60) Al (-0.41) NO ₃ ⁻ (-0.16)	Mo = 109 – 0.063.Mg + 0.20.TA - 5.0.Al – 32.NO ₃ ⁻
V	24	0.95	Na (0.66) Ba (-0.46) Catchment (-0.25) Cl ⁻ (-0.20)	V = 30 + 0.62.Na – 11.Ba – 0.9.Catchment – 199.Cl ⁻
Ni	24	0.36	Mn (0.41) K (-0.41)	Ni = 100 + 9.2.Mn – 0.5.K
Cr	24	0.98	Al (0.23) Ba (-0.70) Silicate (0.30) NO ₃ ⁻ (0.21) Ca (0.16) Catchment (-0.14) SO ₄ ²⁻ (0.13)	Cr = 24 + 2.4.Al – 18.Ba + 11.Silicate + 37.NO ₃ ⁻ + 0.002.Ca – 0.5.Catchment + 4.0.SO ₄ ²⁻
Pb	24	0.74	Al (0.70) Mn (0.49) K (0.32)	Pb = -51 + 3.0.Al + 11.Mn + 0.39.K
Se	24	0.96	Silicate (0.79) SO ₄ ²⁻ (0.61) Fe (-0.12)	Se = -14 + 12.Silicate + 7.7.SO ₄ ²⁻ - 0.30.Fe
Sb	24	1.00	Ba (1.12) Mg (-0.53) SO ₄ ²⁻ (0.14) NO ₃ ⁻ (-0.10) Catchment (0.06)	Sb = 6 + 12.Ba – 0.005.Mg + 1.8.SO ₄ ²⁻ - 7.0.NO ₃ ⁻ + 0.09.Catchment
Co	24	0.13	Na (0.41)	Co = -5 + 0.11.Na
Cd	24	0.94	Ba (0.62) Mg (-1.59) MaxDepth (0.76) Na (0.50)	Cd = -0.3 + 0.26.Ba – 0,001.Mg + 0.09.MaxDepth
Tl	24	0.85	Na (0.77) Catchment (-0.36) TOC (0.32)	Tl = -0.076 + 0.003.Na – 0.004.Catchment + 0,055.TOC
Hg	24	0.77	TOC (0.54) Silicate (-0.51) pH (-0.39) Temperature (0.26)	Hg = 2.9 + 0.14.TOC – 0.09.Silicate – 0.35.pH + 0.01 Temperature

6.4.4. Water column dynamics and trace elements distribution in selected alpine lakes

The studied lakes have been successfully classified according to their water geochemistry using the unfiltered subsurface water samples, highlighting the importance of geological background. This section focuses on the dynamics of some particular lakes, and how different processes affect the chemistry involved in their water column.

The concerned lakes are AZU, ARA, SAB and GEN and they have been chosen according to their importance in the REPLIM Network. They are also relatively easily accessible. They mainly all lied on sedimentary rocks: Devonian rocks for AZU and ARA, Cretaceous rocks for SAB and Permo-Triassic rocks for GEN. These lakes are located at various altitudes (1900 m asl. for SAB, 1942 m asl. for GEN, 2256 m asl. for ARA and 2420 m asl. for AZU) and span a wide range of maximum depth (8 m for AZU, 12 m for ARA, 20 m for GEN and 25 m for SAB). Lake GEN is well impacted by agropastoralism and has shown one of the lowest values of nitrate, either in spring or in autumn, suggesting an important primary productivity in this lake. Lake ARA, which displays one of the most important variation in nitrate content during summer, is also impacted by agropastoralism but to a lesser extent. Lake SAB stood out from the other lakes mainly because of its high alkalinity, and lake AZU is the most pristine.

Analytical results for the water column of those four lakes are displayed in **Figure 6-13** (AZU), **Figure 6-14** (ARA), **Figure 6-15** (SAB) and **Figure 6-16** (GEN).

The physical parameters provided by the multiparametric probe (temperature, dissolved oxygen and chlorophyll) are giving insights on the lakes and allow us to discriminate them more efficiently.

The shallower and more elevated lake AZU expresses constant temperature and dissolved oxygen from surface to bottom of the lake, either in spring or in autumn, respectively of 4.8 ± 0.1 °C and 76 ± 1 % in spring and 5.1 ± 0.2 °C and 71 ± 2 % in autumn. The chlorophyll measured by the probe all along the water column was also not significantly different from zero. This lake is a very pristine and well-mixed lake all over the year.

The less shallow lake ARA behaves differently depending on the time of the year. In spring, temperature was relatively higher at the surface but did not vary significantly along the water column while in autumn a thermocline was observed around 10m with constant temperature above this limit (8.4 ± 0.1 °C) and lower temperature at the bottom part of the lake (from 8.0 to 5.6 °C). In both spring and autumn, a chemocline at around 10m is observed and dissolved oxygen started to decrease at this depth in Lake ARA. Chlorophyll in spring was not significantly different from zero while a very small increase was observed in the signal at the last centimetres of the water column in autumn, probably due to algae material that are growing or accumulating at the lake bottom.

In the deepest and lowest elevated Lake Sabocos, both temperatures and dissolved oxygen vary strongly depending on the depth with lower values at the bottom of the lake, which becomes anoxic. The maximum signal of Chlorophyll (2.3) was detected at 18.62 m depth in spring corresponding to the algae accumulation and oxygen consumption, while in autumn the production was over and the

maximum chlorophyll was identified at the bottom part of the lake, below 23 m depth (33.1 ± 9.9). Primary production in this lake is relatively important during summer time [53], thus our observations suggest that a large part of the algae material accumulates at the lake where it decomposes in the post-productive period (fall).

Lake Gentau differs clearly from the other three lakes. This lake was chemically stratified in spring and autumn suggesting a quasi-permanent stratification (holomixis normally occurs in late fall) probably due to intense agropastoralism and touristic activities that promote the primary production through the release of nutrients into the lake. In this lake three different zone can be set up according to the physical parameters. Epilimnion (0 to 6.5 m depth in spring; 0 to 9 m depth in autumn) is the top layer of the lake, well mixed and where oxygen was at its maximum. Metalimnion (or chemocline) (6.5 to 13.5 m depth in spring; 9 to 16 m depth in autumn) is the middle zone of the lake where primary production is the most important (maximum chlorophyll) and the oxygen is also decreasing. Finally, Hypolimnion (below 13.5 m depth in spring; below 16 m depth in autumn) is characterised by the quasi absence of oxygen. Overall, this lake, where primary production is probably the most important, is well stratified in various layers leading to strong variations of the geochemical parameters along the water column depth.

These differences of dynamics are also well highlighted by the results of the chemical parameters. Indeed, while chemical parameters, either TOC, Silicate, anions or cations, did not significantly vary in the well-mixed Lake AZU, chemistry in Lake GEN varies strongly, especially due to the presence of the anoxic zone. Around the chemocline, in autumn, SO_4^{2-} decreases with the depth, likely due to anaerobic conditions and microbial activity in the hypolimnion layer, as sulphur-reducing bacteria cause the transformation of sulphates to hydrogen sulphide. In autumn, higher concentration of NO_3^- at the bottom part of the lake is probably due to nitrification.

However, the most important phenomena is again linked to the reactivity of Fe and Mn, for which the concentrations increase sharply in the hypolimnion: both elements are released into bottom water by reductive dissolution of Mn and Fe oxides at the water-sediment interface. The Fe and Mn particles are able to remove other dissolved trace elements, which is clearly the case here with increasing concentrations of As, Cu (only spring), Mo, Co and Cd. The same tendency is observed in Lake SAB with increasing concentrations of Fe, Mn, As, Mo, Ni (only spring) and Co when dissolved oxygen is decreasing, and to a lesser extent in Lake ARA with increasing concentrations of Fe, Mn and Co. Fe, Mn and Co have been commonly used as tracers to describe redox conditions along the sediment cores [13].

Environmental changes in lake ecosystems, induced by either Climate Change (temperature gradient) or anthropogenic pressure (lake productivity), are likely to produce unexpected cascading impacts between PHTEs biogeochemical cycles and such mountainous ecosystems. In a near future, increasing redox changes and amplitude due to anthropogenic inputs of nutrients and organic matter will induce a potential increase of primary productivity and microbial activity. In addition, higher temperature maximum and amplitude will possibly increase thermocline duration/extent and biological turnover. Overall, these processes will likely modify the availability of some specific PHTEs such as As, Cu, Ni, Mo, Co and Cd.

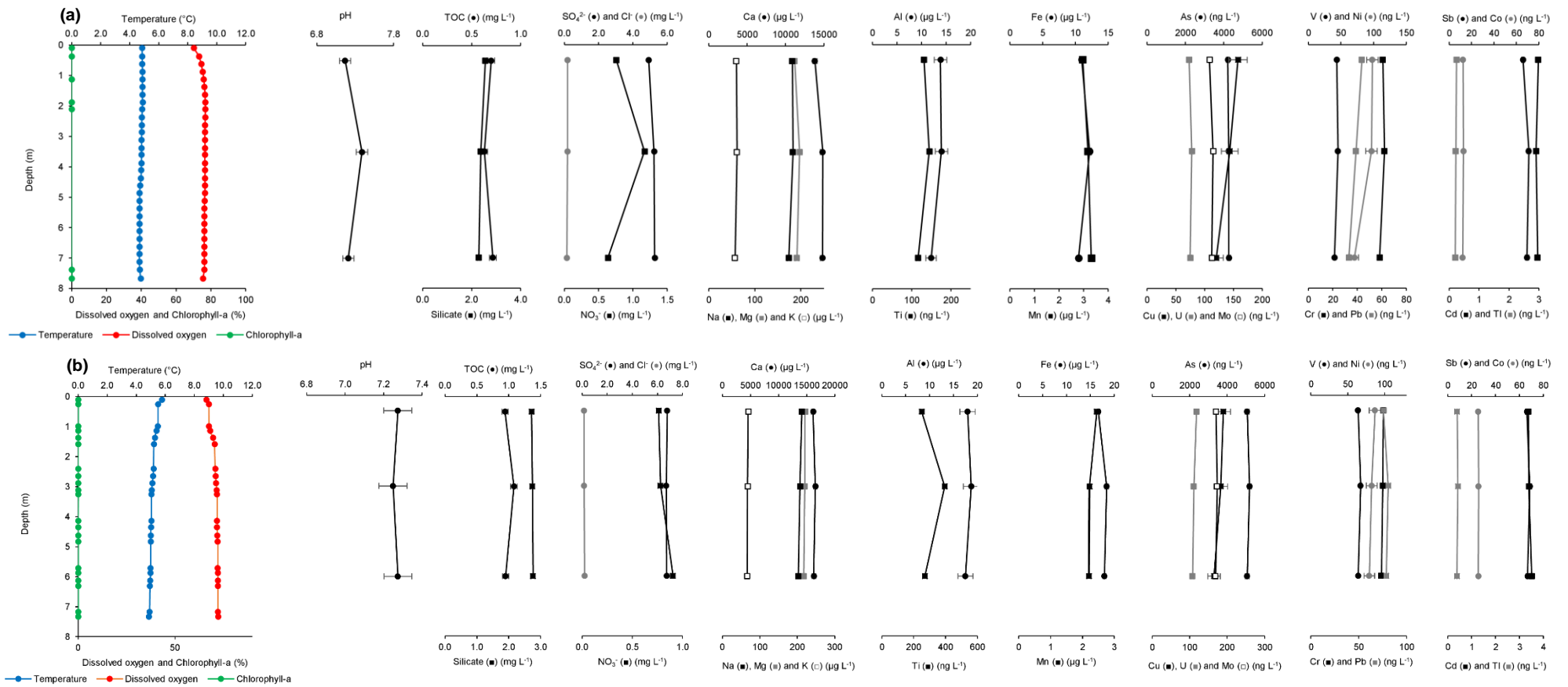


Figure 6-13: Depth profiles of temperature, percentage of dissolved oxygen saturation, chlorophyll-a (RFU) and the chemical parameters obtained during (a) Replim3 and (b) Replim4 in Lake Azules.

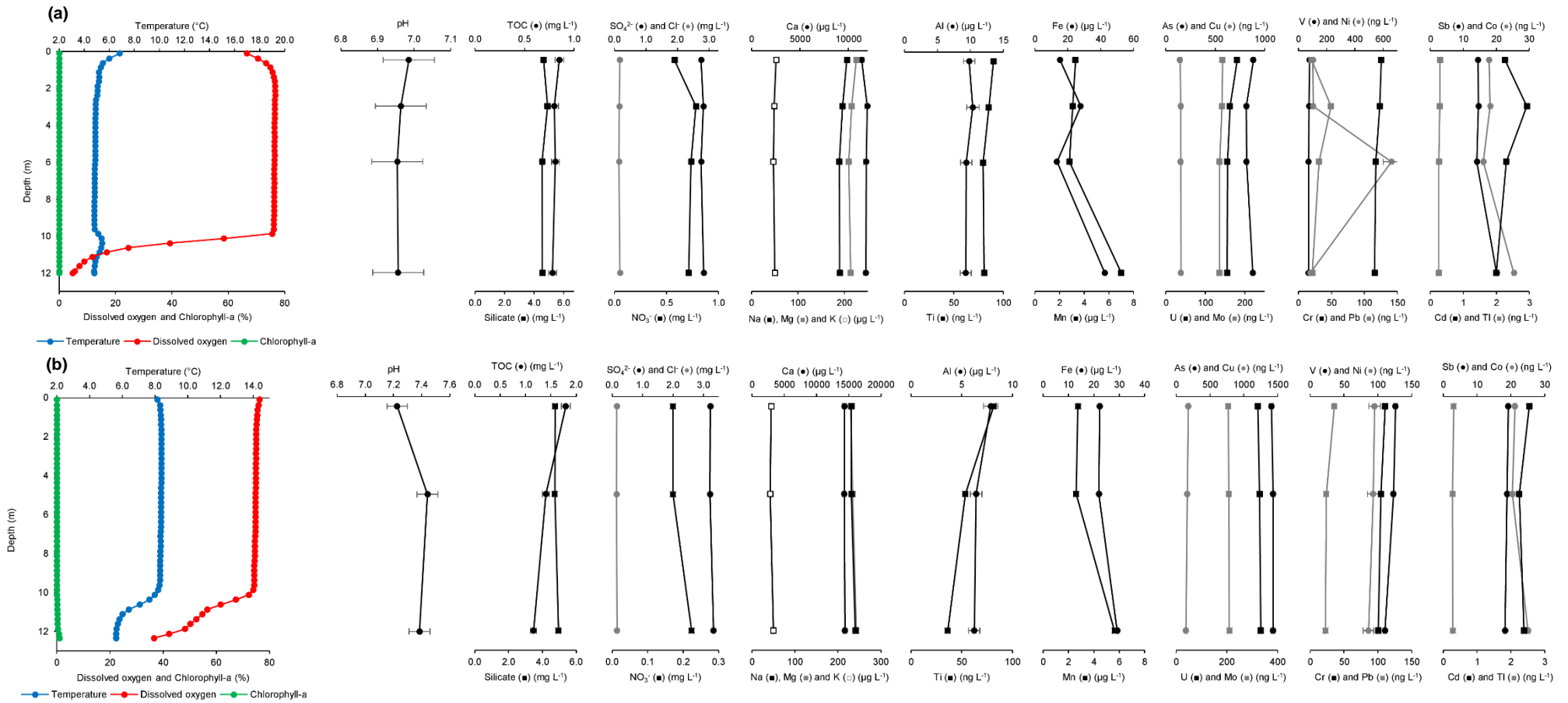


Figure 6-14: Depth profiles of temperature, percentage of dissolved oxygen saturation, chlorophyll-a (RFU) and the chemical parameters obtained during (a) Replim3 and (b) Replim4 in Lake Arratille

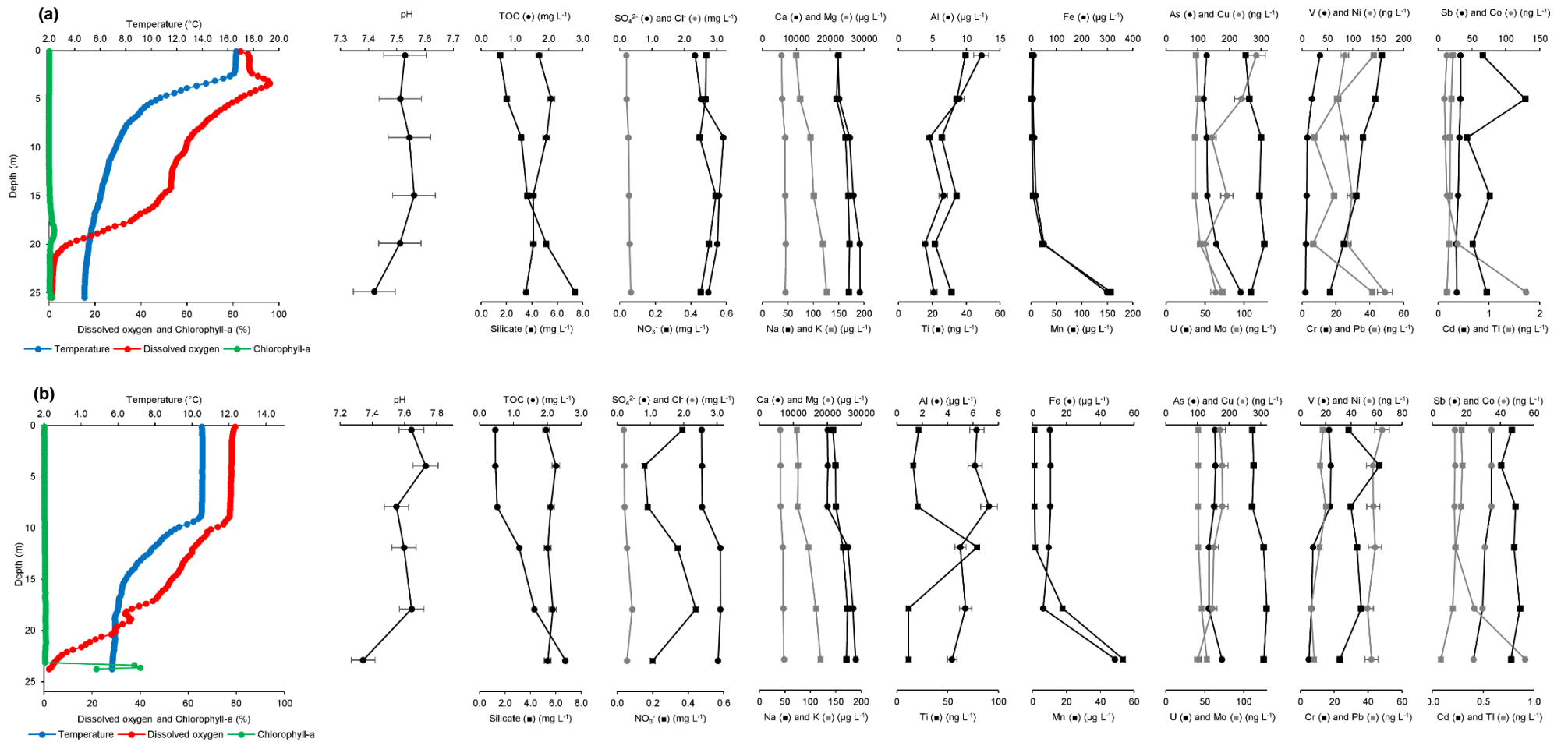


Figure 6-15: Depth profiles of temperature, percentage of dissolved oxygen saturation, chlorophyll-a (RFU) and the chemical parameters obtained during (a) Replim3 and (b) Replim4 in Lake Sabocos

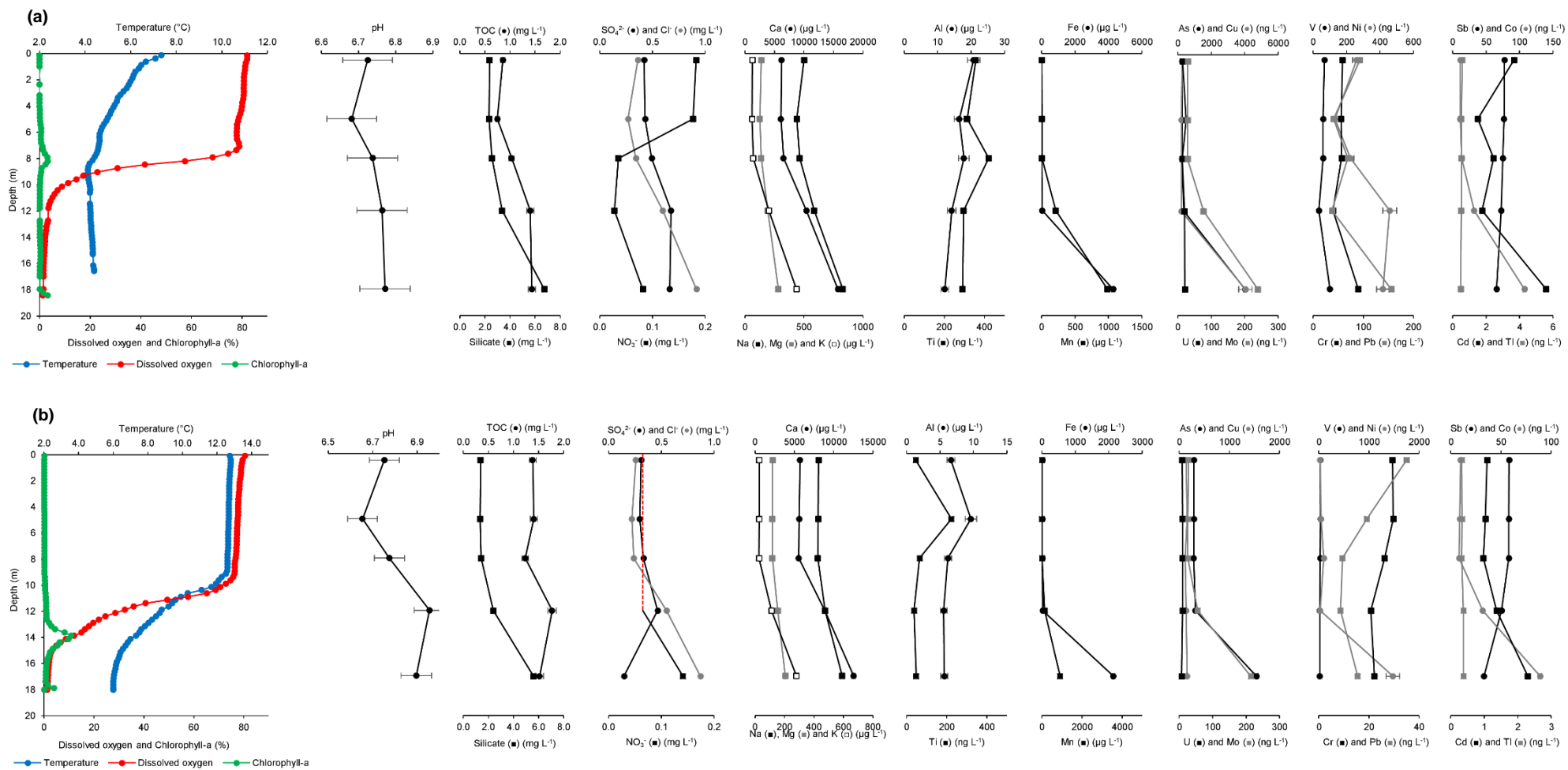


Figure 6-16: Depth profiles of temperature, percentage of dissolved oxygen saturation, chlorophyll-a (RFU) and the chemical parameters obtained during (a) Replim3 and (b) Replim4 in Lake Gentau

6.5. References

- [1] J.S. Baron, T.M. Schmidt, M.D. Hartman, Climate-induced changes in high elevation stream nitrate dynamics, *Global Change Biology*. 15 (2009) 1777–1789. <https://doi.org/10.1111/j.1365-2486.2009.01847.x>.
- [2] A. Martínez Cortizas, Mercury in a Spanish Peat Bog: Archive of Climate Change and Atmospheric Metal Deposition, *Science*. 284 (1999) 939–942. <https://doi.org/10.1126/science.284.5416.939>.
- [3] L. Camarero, M. Bacardit, A. de Diego, G. Arana, Decadal trends in atmospheric deposition in a high elevation station: Effects of climate and pollution on the long-range flux of metals and trace elements over SW Europe, *Atmospheric Environment*. 167 (2017) 542–552. <https://doi.org/10.1016/j.atmosenv.2017.08.049>.
- [4] J. Sánchez-España, M.P. Mata, J. Vegas, M. Morellón, J.A. Rodríguez, Á. Salazar, I. Yusta, A. Chaos, C. Pérez-Martínez, A. Navas, Anthropogenic and climatic factors enhancing hypolimnetic anoxia in a temperate mountain lake, *Journal of Hydrology*. 555 (2017) 832–850. <https://doi.org/10.1016/j.jhydrol.2017.10.049>.
- [5] J. Catalan, L. Camarero, M. Felip, S. Pla, M. Ventura, T. Buchaca, F. Bartumeus, G. de Mendoza, A. Miró, E.O. Casamayor, J.M. Medina-Sánchez, M. Bacardit, M. Altuna, M. Bartrons, D.D. de Quijano, High mountain lakes: extreme habitats and witnesses of environmental changes, *Limnetica*. 25 (2006) 551–584. <https://doi.org/10.23818/limn.25.38>.
- [6] P. González-Sampériz, J. Aranbarri, A. Pérez-Sanz, G. Gil-Romera, A. Moreno, M. Leunda, M. Sevilla-Callejo, J.P. Corella, M. Morellón, B. Oliva, B. Valero-Garcés, Environmental and climate change in the southern Central Pyrenees since the Last Glacial Maximum: A view from the lake records, *CATENA*. 149 (2017) 668–688. <https://doi.org/10.1016/j.catena.2016.07.041>.
- [7] M. Morellón, B. Valero-Garcés, P. González-Sampériz, T. Vegas-Vilarrúbia, E. Rubio, M. Rieradevall, A. Delgado-Huertas, P. Mata, Ó. Romero, D.R. Engstrom, M. López-Vicente, A. Navas, J. Soto, Climate changes and human activities recorded in the sediments of Lake Estanya (NE Spain) during the Medieval Warm Period and Little Ice Age, *Journal of Paleolimnology*. 46 (2011) 423–452. <https://doi.org/10.1007/s10933-009-9346-3>.
- [8] M. Rogora, R. Mosello, S. Arisci, The Effect of Climate Warming on the Hydrochemistry of Alpine Lakes, *Water, Air, and Soil Pollution*. 148 (2003) 347–361. <https://doi.org/10.1023/A:1025489215491>.
- [9] D.G. Zaharescu, P.S. Hooda, C.I. Burghilea, A. Palanca-Soler, A Multiscale Framework for Deconstructing the Ecosystem Physical Template of High-Altitude Lakes, *Ecosystems*. 19 (2016) 1064–1079. <https://doi.org/10.1007/s10021-016-9987-9>.
- [10] L. Camarero, M. Rogora, R. Mosello, N.J. Anderson, A. Barbieri, I. Botev, M. Kernan, J. Kopáček, A. Korhola, A.F. Lotter, G. Muri, C. Postolache, E. Stuchlík, H. Thies, R.F. Wright, Regionalisation of chemical variability in European mountain lakes: *Regionalisation of mountain lakes chemistry*, *Freshwater Biology*. 54 (2009) 2452–2469. <https://doi.org/10.1111/j.1365-2427.2009.02296.x>.
- [11] L. Camarero, J. Catalan, Atmospheric phosphorus deposition may cause lakes to revert from phosphorus limitation back to nitrogen limitation, *Nature Communications*. 3 (2012) 1118. <https://doi.org/10.1038/ncomms2125>.
- [12] L. Camarero, Spreading of trace metals and metalloids pollution in lake sediments over the Pyrénées, *Journal de Physique IV (Proceedings)*. 107 (2003) 249–253. <https://doi.org/10.1051/jp4:20030289>.
- [13] I. Lavilla, A.V. Filgueiras, F. Valverde, J. Millos, A. Palanca, C. Bendicho, Depth Profile Of Trace Elements In a Sediment Core Of a High-Altitude Lake Deposit At The Pyrenees, Spain, *Water, Air, and Soil Pollution*. 172 (2006) 273–293. <https://doi.org/10.1007/s11270-006-9079-0>.
- [14] L. Camarero, J. Catalan, A simple model of regional acidification for high mountain lakes: Application to the Pyrenean Lakes (North-East Spain), *Water Research*. 32 (1998) 1126–1136. [https://doi.org/10.1016/S0043-1354\(97\)00291-1](https://doi.org/10.1016/S0043-1354(97)00291-1).

- [15] J.M. Blais, S. Charpentier, F. Pick, L.E. Kimpe, A.St. Amand, C. Regnault-Roger, Mercury, polybrominated diphenyl ether, organochlorine pesticide, and polychlorinated biphenyl concentrations in fish from lakes along an elevation transect in the French Pyrénées, *Ecotoxicology and Environmental Safety*. 63 (2006) 91–99. <https://doi.org/10.1016/j.ecoenv.2005.08.008>.
- [16] E. Escartín, C. Porte, Biomonitoring of PAH Pollution in High-Altitude Mountain Lakes through the Analysis of Fish Bile, *Environmental Science & Technology*. 33 (1999) 406–409. <https://doi.org/10.1021/es980798a>.
- [17] R.M. Vilanova, P. Fernandez, J.O. Grimalt, Polychlorinated biphenyl partitioning in the waters of a remote mountain lake, *Science of the Total Environment*. 279 (2001) 51–62.
- [18] C.G. Fraga, Relevance, essentiality and toxicity of trace elements in human health, *Molecular Aspects of Medicine*. 26 (2005) 235–244. <https://doi.org/10.1016/j.mam.2005.07.013>.
- [19] A. Mehri, R.F. Marjan, Review article Trace Elements in Human Nutrition: A Review, (2013) 15.
- [20] M. Mikulewicz, K. Chojnacka, B. Kawala, T. Gredes, Trace Elements in Living Systems: From Beneficial to Toxic Effects, *BioMed Research International*. 2017 (2017) 1–2. <https://doi.org/10.1155/2017/8297814>.
- [21] V. Antoniadis, S.M. Shaheen, E. Levizou, M. Shahid, N.K. Niazi, M. Vithanage, Y.S. Ok, N. Bolan, J. Rinklebe, A critical prospective analysis of the potential toxicity of trace element regulation limits in soils worldwide: Are they protective concerning health risk assessment? - A review, *Environment International*. 127 (2019) 819–847. <https://doi.org/10.1016/j.envint.2019.03.039>.
- [22] H.B. Bradl, Chapter 1 Sources and origins of heavy metals, in: *Interface Science and Technology*, Elsevier, 2005: pp. 1–27. [https://doi.org/10.1016/S1573-4285\(05\)80020-1](https://doi.org/10.1016/S1573-4285(05)80020-1).
- [23] K.J.R. Rosman, W. Chisholm, S. Hong, J.-P. Candelone, C.F. Boutron, Lead from Carthaginian and Roman Spanish Mines Isotopically Identified in Greenland Ice Dated from 600 B.C. to 300 A.D. †, *Environmental Science & Technology*. 31 (1997) 3413–3416. <https://doi.org/10.1021/es970038k>.
- [24] P. Gabrielli, P. Vallenga, Contaminant Records in Ice Cores, in: J.M. Blais, M.R. Rosen, J.P. Smol (Eds.), *Environmental Contaminants*, Springer Netherlands, Dordrecht, 2015: pp. 393–430. https://doi.org/10.1007/978-94-017-9541-8_14.
- [25] C.A. Cooke, A. Martínez-Cortizas, R. Bindler, M. Sexauer Gustin, Environmental archives of atmospheric Hg deposition – A review, *Science of The Total Environment*. 709 (2020) 134800. <https://doi.org/10.1016/j.scitotenv.2019.134800>.
- [26] C. Bini, M. Wahsha, Potentially Harmful Elements and Human Health, in: C. Bini, J. Bech (Eds.), *PHEs, Environment and Human Health*, Springer Netherlands, Dordrecht, 2014: pp. 401–463. https://doi.org/10.1007/978-94-017-8965-3_11.
- [27] M. Bacardit, M. Krachler, L. Camarero, Whole-catchment inventories of trace metals in soils and sediments in mountain lake catchments in the Central Pyrenees: Apportioning the anthropogenic and natural contributions, *Geochimica et Cosmochimica Acta*. 82 (2012) 52–67. <https://doi.org/10.1016/j.gca.2010.10.030>.
- [28] M. Rogora, R. Mosello, S. Arisci, M.C. Brizzio, A. Barbieri, R. Balestrini, P. Waldner, M. Schmitt, M. Stähli, A. Thimonier, M. Kalina, H. Puxbaum, U. Nickus, E. Ulrich, A. Probst, An Overview of Atmospheric Deposition Chemistry over the Alps: Present Status and Long-term Trends, *Hydrobiologia*. 562 (2006) 17–40. <https://doi.org/10.1007/s10750-005-1803-z>.
- [29] O. Tornimbeni, M. Rogora, An Evaluation of Trace Metals in High-Altitude Lakes of the Central Alps: Present Levels, Origins and Possible Speciation in Relation to pH Values, *Water, Air, & Soil Pollution*. 223 (2012) 1895–1909. <https://doi.org/10.1007/s11270-011-0993-4>.
- [30] R. Hofer, R. Lackner, J. Kargl, B. Thaler, D. Tait, L. Bonetti, R. Vistocco, G. Flaim, Organochlorine and Metal Accumulation in Fish (*Phoxinus phoxinus*) Along a North-South Transect in the Alps, *Water, Air, and Soil Pollution*. 125 (2001) 189–200. <https://doi.org/10.1023/A:1005272308236>.
- [31] J.P. Deka, S. Singh, P.K. Jha, U.K. Singh, M. Kumar, Imprints of long-range-transported pollution on high-altitude Eastern Himalayan lake water chemistry, *Environmental Earth Sciences*. 75 (2016). <https://doi.org/10.1007/s12665-015-4813-9>.

- [32] C.M. Sharma, S. Kang, M. Sillanpää, Q. Li, Q. Zhang, J. Huang, L. Tripathee, S. Sharma, R. Paudyal, Mercury and Selected Trace Elements from a Remote (Gosainkunda) and an Urban (Phewa) Lake Waters of Nepal, *Water, Air, & Soil Pollution*. 226 (2015). <https://doi.org/10.1007/s11270-014-2276-3>.
- [33] J.P. Corella, A. Saiz-Lopez, M.J. Sierra, M.P. Mata, R. Millán, M. Morellón, C.A. Cuevas, A. Moreno, B.L. Valero-Garcés, Trace metal enrichment during the Industrial Period recorded across an altitudinal transect in the Southern Central Pyrenees, *Science of The Total Environment*. 645 (2018) 761–772. <https://doi.org/10.1016/j.scitotenv.2018.07.160>.
- [34] J.P. Corella, B.L. Valero-Garcés, F. Wang, A. Martínez-Cortizas, C.A. Cuevas, A. Saiz-Lopez, 700 years reconstruction of mercury and lead atmospheric deposition in the Pyrenees (NE Spain), *Atmospheric Environment*. 155 (2017) 97–107. <https://doi.org/10.1016/j.atmosenv.2017.02.018>.
- [35] M. Bacardit, L. Camarero, Modelling Pb, Zn and As transfer from terrestrial to aquatic ecosystems during the ice-free season in three Pyrenean catchments, *Science of The Total Environment*. 408 (2010) 5854–5861. <https://doi.org/10.1016/j.scitotenv.2010.07.088>.
- [36] D.G. Zaharescu, P.S. Hooda, A.P. Soler, J. Fernandez, C.I. Burghilea, Trace metals and their source in the catchment of the high altitude Lake Respomuso, Central Pyrenees, *Science of The Total Environment*. 407 (2009) 3546–3553. <https://doi.org/10.1016/j.scitotenv.2009.02.026>.
- [37] J. Catalan, E. Ballesteros, E. Gacia, A. Palau, L. Camarero, Chemical composition of disturbed and undisturbed high-mountain lakes in the Pyrenees: A reference for acidified sites, *Water Research*. 27 (1993) 133–141. [https://doi.org/10.1016/0043-1354\(93\)90203-T](https://doi.org/10.1016/0043-1354(93)90203-T).
- [38] R. Salminen, Forum of the European Geological Surveys Directors, eds., Background information, methodology and maps, Geological Survey of Finland, Espoo, 2005.
- [39] A. Chappaz, Chromium, tungsten and vanadium diagenesis in lake sediments, (n.d.) 2.
- [40] M. Bueno, B. Duval, E. Tessier, A. Romero-Rama, L. Kortazar, L.A. Fernandez, A. De Diego, D. Amouroux, Selenium distribution and speciation in waters of pristine alpine lakes from central-western Pyrenees (France-Spain), *Environ. Sci.: Processes Impacts*. (2022) 10.1039/D1EM00430A. <https://doi.org/10.1039/D1EM00430A>.
- [41] L. Kortazar, B. Duval, O. Liñero, O. Olamendi, A. Angulo, D. Amouroux, A. de Diego, L.A. Fernandez, Accurate determination of the total alkalinity and the CO₂ system parameters in high-altitude lakes from the Western Pyrenees (France – Spain), *Microchemical Journal*. 152 (2020) 104345. <https://doi.org/10.1016/j.microc.2019.104345>.
- [42] C.Y. Chen, R.S. Stemberger, B. Klaue, J.D. Blum, P.C. Pickhardt, C.L. Folt, Accumulation of heavy metals in food web components across a gradient of lakes, *Limnology and Oceanography*. 45 (2000) 1525–1536. <https://doi.org/10.4319/lo.2000.45.7.1525>.
- [43] B.L. Skjelkvåle, T. Andersen, E. Fjeld, J. Mannio, A. Wilander, K. Johansson, J.P. Jensen, T. Moiseenko, Heavy Metal Surveys in Nordic Lakes; Concentrations, Geographic Patterns and Relation to Critical Limits, *AMBIO: A Journal of the Human Environment*. 30 (2001) 2–10. <https://doi.org/10.1579/0044-7447-30.1.2>.
- [44] E. Pertsemli, D. Voutsas, Distribution of heavy metals in Lakes Doirani and Kerkini, Northern Greece, *Journal of Hazardous Materials*. 148 (2007) 529–537. <https://doi.org/10.1016/j.jhazmat.2007.03.019>.
- [45] B. Markert, F. Pedrozo, W. Geller, K. Friese, S. Korhammer, G. Baffico, M. Díaz, S. Wölfl, A contribution to the study of the heavy-metal and nutritional element status of some lakes in the southern Andes of Patagonia (Argentina), *Science of The Total Environment*. 206 (1997) 1–15. [https://doi.org/10.1016/S0048-9697\(97\)00218-0](https://doi.org/10.1016/S0048-9697(97)00218-0).
- [46] O.S. Pokrovsky, L.S. Shirokova, Diurnal variations of dissolved and colloidal organic carbon and trace metals in a boreal lake during summer bloom, *Water Research*. 47 (2013) 922–932. <https://doi.org/10.1016/j.watres.2012.11.017>.
- [47] V. Hatje, T.E. Payne, D.M. Hill, G. McOrist, G.F. Birch, R. Szymczak, Kinetics of trace element uptake and release by particles in estuarine waters: effects of pH, salinity, and particle loading, *Environment International*. 29 (2003) 619–629. [https://doi.org/10.1016/S0160-4120\(03\)00049-7](https://doi.org/10.1016/S0160-4120(03)00049-7).

- [48] D. Obrist, J.L. Kirk, L. Zhang, E.M. Sunderland, M. Jiskra, N.E. Selin, A review of global environmental mercury processes in response to human and natural perturbations: Changes of emissions, climate, and land use, *Ambio*. 47 (2018) 116–140. <https://doi.org/10.1007/s13280-017-1004-9>.
- [49] M. Bacardit, L. Camarero, Atmospherically deposited major and trace elements in the winter snowpack along a gradient of altitude in the Central Pyrenees: The seasonal record of long-range fluxes over SW Europe, *Atmospheric Environment*. 44 (2010) 582–595. <https://doi.org/10.1016/j.atmosenv.2009.06.022>.
- [50] R.E. Carlson, A trophic state index for lakes1: Trophic state index, *Limnology and Oceanography*. 22 (1977) 361–369. <https://doi.org/10.4319/lo.1977.22.2.0361>.
- [51] M.T. Kiran, M.V. Bhaskar, A. Tiwari, Phycoremediation of Eutrophic Lakes Using Diatom Algae, in: M.N. Rashed (Ed.), *Lake Sciences and Climate Change*, InTech, 2016. <https://doi.org/10.5772/64111>.
- [52] J. Dunalska, Total organic carbon as a new index for monitoring trophic states in lakes, *Oceanological and Hydrobiological Studies*. 40 (2011). <https://doi.org/10.2478/s13545-011-0022-7>.
- [53] Z. Santolaria, T. Arruebo, J.S. Urieta, F.J. Lanaja, A. Pardo, J. Matesanz, C. Rodriguez-Casals, Hydrochemistry dynamics in remote mountain lakes and its relation to catchment and atmospheric features: the case study of Sabocos Tarn, Pyrenees, *Environmental Science and Pollution Research*. 22 (2015) 231–247. <https://doi.org/10.1007/s11356-014-3310-0>.
- [54] X. Dai, J. Welhan, Statistical Guidance for Determining Background Ground Water Quality and Degradation, in: 2014.
- [55] K. Hans Wedepohl, The composition of the continental crust, *Geochimica et Cosmochimica Acta*. 59 (1995) 1217–1232. [https://doi.org/10.1016/0016-7037\(95\)00038-2](https://doi.org/10.1016/0016-7037(95)00038-2).
- [56] E. Arranz Yagüe, *Petrología del macizo granítico de La Maladeta (Huesca-Lérida)*, 1997.
- [57] S. Kakareka, T. Kukharchyk, P. Kurman, Major and trace elements content in freshwater lakes of Vecherny Oasis, Enderby Land, East Antarctica, *Environmental Pollution*. 255 (2019) 113126. <https://doi.org/10.1016/j.envpol.2019.113126>.
- [58] W. Shotyk, M. Krachler, Determination of trace element concentrations in natural freshwaters: How low is “low”, and how low do we need to go?, *Journal of Environmental Monitoring*. 11 (2009) 1747. <https://doi.org/10.1039/b917090c>.
- [59] B.O. Rosseland, H.-C. Teien, S. Basnet, R. Borgstrøm, C.M. Sharma, Trace elements and organochlorine pollutants in selected fish species from Lake Phewa, Nepal, *Toxicological & Environmental Chemistry*. 99 (2017) 390–401. <https://doi.org/10.1080/02772248.2016.1189915>.
- [60] S. Li, C. Yang, C. Peng, H. Li, B. Liu, C. Chen, B. Chen, J. Bai, C. Lin, Effects of elevated sulfate concentration on the mobility of arsenic in the sediment–water interface, *Ecotoxicology and Environmental Safety*. 154 (2018) 311–320. <https://doi.org/10.1016/j.ecoenv.2018.02.046>.
- [61] T. Moreno, X. Querol, S. Castillo, A. Alastuey, E. Cuevas, L. Herrmann, M. Mounkaila, J. Elvira, W. Gibbons, Geochemical variations in aeolian mineral particles from the Sahara–Sahel Dust Corridor, *Chemosphere*. 65 (2006) 261–270. <https://doi.org/10.1016/j.chemosphere.2006.02.052>.
- [62] A.G. Bravo, D.N. Kothawala, K. Attermeyer, E. Tessier, P. Bodmer, J.L.J. Ledesma, J. Audet, J.P. Casas-Ruiz, N. Catalán, S. Cauvy-Fraunié, M. Colls, A. Deininger, V.V. Evtimova, J.A. Fonvielle, T. Fuß, P. Gilbert, S. Herrero Ortega, L. Liu, C. Mendoza-Lera, J. Monteiro, J.-R. Mor, M. Nagler, G.H. Niedrist, A.C. Nydahl, A. Pastor, J. Pegg, C. Gutmann Roberts, F. Pilotto, A.P. Portela, C.R. González-Quijano, F. Romero, M. Rulík, D. Amouroux, The interplay between total mercury, methylmercury and dissolved organic matter in fluvial systems: A latitudinal study across Europe, *Water Research*. 144 (2018) 172–182. <https://doi.org/10.1016/j.watres.2018.06.064>.
- [63] C.T. Driscoll, R.P. Mason, H.M. Chan, D.J. Jacob, N. Pirrone, Mercury as a Global Pollutant: Sources, Pathways, and Effects, *Environmental Science & Technology*. 47 (2013) 4967–4983. <https://doi.org/10.1021/es305071v>.
- [64] W.J. Green, B.R. Stage, B.J. Bratina, S. Wagers, A. Preston, K. O'bryan, J. Shacat, S. Newell, Nickel, Copper, Zinc and Cadmium Cycling with Manganese in Lake Vanda (Wright Valley,

Antarctica), *Aquatic Geochemistry*. 10 (2004) 303–323. <https://doi.org/10.1007/s10498-004-2263-1>.

[65] H. Yang, N.L. Rose, R.W. Battarbee, Distribution of some trace metals in Lochnagar, a Scottish mountain lake ecosystem and its catchment, *Science of The Total Environment*. 285 (2002) 197–208. [https://doi.org/10.1016/S0048-9697\(01\)00931-7](https://doi.org/10.1016/S0048-9697(01)00931-7).

[66] ICP Water annual report, (2016).

7. Dynamics, distribution, and transformations of mercury species from Pyrenean high- altitude lakes

7.1. Abstract

While mercury (Hg) is a major concern in all aquatic environments because of its methylation and biomagnification pathways, very few studies consider Hg cycling in remote alpine lakes which are sensitive ecosystems towards global environmental changes. Nineteen high-altitude pristine lakes from Western / Central Pyrenees were investigated on both northern (France) and southern (Spain) slopes (1620 to 2600 m asl.). Subsurface water samples were collected in June 2017/2018/2019 and October 2017/2018 for Hg speciation analysis of inorganic mercury (iHg(II)), monomethylmercury (MMHg), and dissolved gaseous mercury (DGM) to investigate spatial and seasonal variations. In June 2018/2019 and October 2018, more comprehensive studies were performed in lakes Gentau, Arratille and Sabocos, by taking water column depth profiles. Besides, in-situ incubation experiments using isotopically enriched Hg species ($^{199}\text{iHg(II)}$, $^{201}\text{MMHg}$) were conducted to investigate Hg transformation mechanisms in the water column (methylation, demethylation, reduction). While iHg(II) (0.08 to 1.10 ng L⁻¹ in filtered samples; 0.11 to 1.19 ng L⁻¹ in unfiltered samples) did not show significant seasonal variations in the subsurface water samples, MMHg (<0.03 to 0.035 ng L⁻¹ in filtered samples; <0.03 to 0.062 ng L⁻¹ in unfiltered samples) was significantly higher in October 2018, mainly because of in-situ methylation. DGM (0.02 to 0.68 ng L⁻¹) varies strongly among and within lakes and can exhibit higher levels in comparison with other pristine areas. Depth profiles and incubation experiments highlighted the importance of in-situ biotic methylation triggered by anoxic conditions in bottom waters. In-situ incubations confirm that significant methylation, demethylation and photoreduction extents are taking place in alpine lakes water columns. Overall, drastic environmental changes occurring daily and seasonally in alpine lakes are providing conditions that can both promote Hg methylation (stratified anoxic waters) and MMHg photodemethylation (intense UV light). In addition, light induced photoreduction is a major pathway controlling significant gaseous Hg evasion in the studied lakes. Consequently, both global warming and potential eutrophication may have important implications on those pathways and the fate of Hg in these remote lakes.

Keywords:

Mercury; Biogeochemistry; Alpine lakes; Methylation; Demethylation ; Photoreduction

7.2. Introduction

Natural sources of mercury (Hg) (volcanic activities and degassing, evasion from aquatic and terrestrial surfaces) and increasing anthropogenic sources (e.g. fossil fuel combustion and gold mining), combined to a high volatility, contribute to the global pool of Hg in the atmosphere and lead to long-range dispersion and deposition away from point sources [1–3]. Hg has also created a scenario of global health concerns due to its conversion into an organometallic compound of elevated neurotoxicity and persistence, namely monomethylmercury (MMHg).

Hg is a biogeochemically driven contaminant because its most harmful organometallic species (MMHg) is naturally produced in aquatic systems thanks to a complex interplay between microbial and chemical processes. MMHg is a persistent contaminant because it biomagnifies from one trophic level to another, leading its concentration to increase naturally along food chains. The European Water Framework Directive (WFD-2000/60/EG) classifies Hg as one of the 30th most “precarious dangerous pollutants”. Human exposure to MMHg is actually well defined, and mainly associated with fish consumption [4]. Yet, most risk assessment studies lack fundamental information as to what exactly controls Hg levels in fish. Without detailed knowledge of the Hg biogeochemical cycle and, in particular, the fundamental processes at the origin of MMHg production [5–7], it is difficult to estimate precisely Hg’s health impacts and socio-economical costs [8].

The net production of MMHg in aquatic ecosystems is closely dependent on the environmental conditions, such as presence of methylating microorganisms, temperature, pH, organic matter, redox conditions, ionic strength or solar radiation, which influence both the Hg bioavailability and the competition between methylation and demethylation pathways [9]. Managing bioaccumulation of MMHg in aquatic food chains requires differentiation between the biotic and abiotic pathways that lead to its production and degradation. Microorganisms such as sulphate-reducing or iron-reducing bacteria, among other groups, are known to be widely involved both in the methylation of inorganic Hg (iHg(II)) and demethylation of MMHg [10,11] in aquatic ecosystems.

Among the aquatic compartments, lowland lakes have been widely studied regarding Hg pollution, speciation and species transformations [12–15]. Some publications highlighted a link between organic matter and Hg in lake ecosystems [13,16], with evidence of the catchment influence on the Hg levels. (Photo)demethylation was also observed in lakes [17] at an important rate, more important than the external inputs of MMHg (rain, snow, runoff), suggesting MMHg sources from bottom sediments. Nevertheless, the biogeochemical processes that control the speciation and fate of Hg, and especially MMHg levels, remain poorly established [12]. Alpine lakes are better witnesses of Hg past and present contamination in comparison with lowland lakes. They are usually characterized by a low catchment-to-lake-surface-area ratio, as the catchment surface is commonly smaller than lowland lakes. Therefore, atmospheric deposition and catchment weathering are important processes influencing greatly the lake water geochemistry [18]. Thus, mountain lake catchments are viewed and used as excellent proxies of background diffuse contamination [3,19]. While alpine lakes, through sediment cores analysis, have been successfully used to reconstruct temporal trends in atmospheric Hg deposition [2,3,20], Hg behaviour

in the aquatic compartment of those pristine areas has been barely investigated. For instance, *Guédron et al.* [21,22] and *Alanoca et al.* [23] have reported Hg cycling features in high-altitude Bolivian lakes. Even if those ecosystems are directly influenced by human activities, both urban and mining, Hg species cycling is highly dynamic and MMHg production was driven by eutrophication in these lakes, while intense UV light promoted significant demethylation and reduction pathways. Regarding pristine high-altitude lakes, Hg species distribution has been only investigated in one study on four lakes from the French Alps [24]. Thus, while Hg transformations in the aquatic compartment have been well described in lower altitude or more accessible aquatic systems [15,23,25–32], there is a lack of studies in more pristine areas, such as alpine lakes that are especially sensitive to global changes and long range transport of pollutants [19,33].

In that sense, *Chételat et al.* [12] suggested that profound environmental changes may be impacting the cycling and bioaccumulation of Hg. The responsibility of humans regarding the dispersion of aerosol and Hg by anthropogenic activities is undeniable [34,35], but it is important to take into account the intensification of natural processes occurring though Global Change in the biogeochemical cycle of Hg species. On the one hand, human activities are modifying the natural atmospheric transport of substances in a direct way: agricultural practices and deforestation may enhance production of dust and aeolian transport from land; changes in the wildfire's regime affect the emission of ashes and gases from burning biomass. On the other hand, Climate Change also accelerates many of these processes: droughts and losses of snow cover that enhance dust production, melting of organic permafrost that increases CO₂ and methane emissions from soil, changes in the prevailing winds and patterns of circulation of air masses that carry airborne substances.

In this work, we report for the first time a complete inventory of Hg levels and speciation (iHg(II), MMHg, DGM) in the water column of high-altitude pristine lakes from the Western Pyrenees. The objectives of this study were i) to assess the Hg species levels and variability in the aquatic compartment of these ecosystems, ii) to evaluate the importance of redox and methylation pathways affecting the fate of Hg in mountain lakes, iii) to highlight potential climatic and biogeochemical processes controlling these pathways.

7.3. Material and methods

All the sampling sites and their characteristics have been described in **3 Sampling and analytical strategy** and the analytical methods for the determination of mercury species are gathered in **3.3.4 Organometals (Hg species)** and **3.3.5 Dissolved Gaseous Mercury (DGM)**.

The methodology described in **3.3.4 Organometals (Hg species)** allows to quantify the iHg(II) and the methylated species (MeHg, i.e., the sum of MMHg and DMHg). Nevertheless, the purge sample experiment highlights the fact that the measured MeHg are mainly in the form of MMHg.

The methodology described in **3.3.5 Dissolved Gaseous Mercury (DGM)** allows the measurement of dissolved gaseous mercury species, i.e. the sum elemental mercury Hg(0) and volatile dimethylmercury

DMHg. Nevertheless, regarding the very small levels of methylated species (MeHg) in comparison with DGM, we can assume that DGM is mainly elemental mercury Hg(0).

Calculation of methylation (M), demethylation (D), MMHg loss (L) and Hg reduction (R) potentials as well as calculation of net methylation are described in **3.3.6 Mercury species incubations** and the **Figure 7-1** summarize the reactivity of Hg compounds together with the reaction pathways evaluated using incubation experiments.

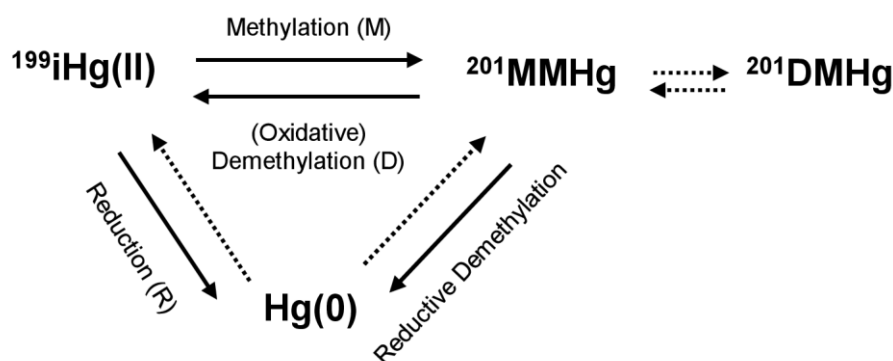


Figure 7-1: Reactivity model of Hg compounds. Solid arrows correspond to the reaction pathways that can be calculated with the incubation experiments, and dotted arrows the pathways that cannot be quantified. MMHg Loss is calculated as the sum of Oxidative and Reductive Demethylation.

As a reminder, non-gaseous mercury is calculated as the sum of the measured iHg(II) and MMHg, while total mercury is calculated as the sum of the measured iHg(II), MMHg and DGM.

7.4. Results and discussion

7.4.1. Major biogeochemical characteristics

Major biogeochemical characteristics of the studied lakes have been discussed previously (**6 Occurrence, distribution, and characteristics concentrations of Potential Harmful Trace Elements (PHTEs) in Pyrenean lakes and their relation to aquatic biogeochemistry**). The oligotrophic status of the studied lakes, the importance of the geological background and the importance of atmospheric processes have been identified to be essential to define the chemical characteristics of the studied lakes.

In this study, Lake Paradis was also not considered because it differs too much from all other studied lakes and would behave as a statistical outlier.

7.4.2. Hg measurement outliers for total Hg and DGM

Regarding total Hg (Hg_{TOT}), defined here as the sum of concentrations of $iHg(II)$, MMHg and DGM in unfiltered samples (DGM only measured in unfiltered samples), seven specific samples stood out as outliers (Grubbs's tests, p -value < 0.05 then p -value = 0.063 > 0.05).

In Lake Coanga in October 2018 at 8:50 a.m., very high levels of $iHg(II)$ were measured in both filtered ($iHg(II)_F = 2.68 \text{ ng L}^{-1}$) and unfiltered ($iHg(II)_{UF} = 2.88 \text{ ng L}^{-1}$) samples. In this sample, filtered and unfiltered MMHg and DGM does not differ strongly from the other samples suggesting that this high $iHg(II)$, either filtered or unfiltered, might be due punctual $iHg(II)$ inputs or simply to contamination during the sample collection: this sample will be discarded from the discussion on $iHg(II)$, and consequently from Hg_{TOT} . In Lake Panticosa in October 2017 at 00:30 p.m., the relatively high levels of both $iHg(II)$ ($iHg(II)_F = 0.64 \text{ ng L}^{-1}$; $iHg(II)_{UF} = 0.68 \text{ ng L}^{-1}$) and DGM ($DGM = 1.21 \text{ ng L}^{-1}$) suggested that this specific sample was enriched in Hg, probably coming either from the catchment (the biggest one, 3229 Ha) or from punctual high Hg inputs. Finally, the last five outliers concern two specific and particular lakes : Lake Gentau (June 2018, 10:50 a.m.) and Lake Sabocos (June 2018, 09:45 a.m., 00:35 p.m. and 3:35 p.m.; June 2019, 00:30 p.m.). This is mainly because Lakes Gentau and Sabocos exhibited important DGM with extremely high values around midday ($DGM = 10.79 \text{ ng L}^{-1}$ in June 2018 for Lake Gentau; $DGM = 4.65 \text{ ng L}^{-1}$ in June 2018 and $DGM = 1.34 \text{ ng L}^{-1}$ in June 2019 for Lake Sabocos) when the light incidence was the highest (**Figure 7-3**). The explanation is not clear, but this important DGM might be due to i) accumulation of DGM under the ice cover during the winter or ii) important $iHg(II)$ provided by the snow melt then converted into $Hg(0)$ by reduction pathways. In both cases, it implies that the sampling has been done right after the winter period, where the lakes are frozen and the catchment is covered by snow, which is the case in June 2018. Indeed, a few days before the sampling, more than 90 % of the studied lakes were completely frozen. However, it remains difficult to explain such exceptionally high levels of DGM measured only in these two lakes. Further studies, with intensive monitoring and sampling during several days at the snowmelt period are needed to fully understand the mechanisms occurring in those Pyrenean Lakes. To avoid bias interpretation, these five samples will be discarded for the discussion on DGM levels and volatilization in high-altitude lakes.

7.4.3. Total Hg (Hg_{TOT}) in all lake waters

In the following discussions, to establish a proper global assessment of the total Hg (Hg_{TOT}) in the subsurface water of the high-altitude lakes, the seven outliers are discarded from the whole database based on the fact that the concentrations observed were too high compared to the normal distribution of our data and that no valid explanation could be given for such higher values.

Hg_{TOT} is quite homogeneous along the five sampling campaigns, ranging from 0.17 to 1.37 ng L^{-1} with a median value of 0.48 ng L^{-1} and an average of $(0.54 \pm 0.26) \text{ ng L}^{-1}$ ($n=66$). The homogeneity in the Hg_{TOT} concentrations in the Pyrenean lakes suggests that local inputs through geogenic paths (erosion, lixiviation) are not significant and does not play a key role in the biogeochemistry of Hg as it was found for other trace elements [36–38]. This also confirms the fact that Hg inputs in alpine environments like the Pyrenees are mainly due to wet and dry atmospheric deposition. Only two previous studies showed

that unfiltered Hg_{TOT} varies from 2 to 14 ng L^{-1} in the precipitation from the Pyrenees (880 m asl) in 2014 [39] and from 2 to 170 ng L^{-1} in the surface snow from the Alps (2448 m asl) in 2008 – 2009 [40]. In our study, Hg species in meltwater and ice were also measured in Lake Cambalès in June 2018. The Hg_{TOT} concentrations were much higher in ice ($\text{Hg}_{\text{TOT}} = 19.41 \text{ ng L}^{-1}$) than in meltwater ($\text{Hg}_{\text{TOT}} = 1.05 \text{ ng L}^{-1}$) and subsurface water ($\text{Hg}_{\text{TOT}} = 0.45 \text{ ng L}^{-1}$). These reported concentrations in atmospheric depositions are much higher than the levels observed in the subsurface water from the high-altitude lakes from this study, suggesting a simple dilution effect or more complex exchanges in lake waters as discussed thereafter.

7.4.4. Mercury compounds distribution in the water

1. Variability in subsurface waters of all lakes

Inorganic mercury (iHg(II)) (Figure 7-2)

Filtered and unfiltered iHg(II) levels ($\text{iHg(II)}_{\text{F}}$ and $\text{iHg(II)}_{\text{UF}}$) in subsurface water from the 19 sampled lakes over the five sampling campaigns were slightly lower than other worldwide lakes [15,21,23,24,27–30] and freshwaters from the same area [31,32] (Table 7-1). $\text{iHg(II)}_{\text{F}}$ ranges from 0.08 to 1.10 ng L^{-1} with a median value of 0.23 ng L^{-1} and $\text{iHg(II)}_{\text{UF}}$ ranges from 0.11 to 1.19 ng L^{-1} with a median value of 0.38 ng L^{-1} , similar to concentration levels found in marine waters [41,42] and typical from a pristine environment.

The filtered fraction of Hg ($\text{iHg(II)}_{\text{F}}$) represents about $68 \pm 16 \%$ (range from 19 to 100 %) of the unfiltered fraction ($\text{iHg(II)}_{\text{UF}}$), suggesting that most of the mercury in the Pyrenean lakes is found in the dissolved fraction. However, subsurface water samples from Azul in Spring 2017 (39 %), Peyregnets (47 %) and Gentau (19 % to 44 %) in Spring 2018 and Cambalès (41%), Peyregnets (49 %) and Gentau (41 %) in Autumn 2018 are exhibiting higher particulate Hg fraction.

In Figure 7-2, the homogeneity observed in the iHg(II) concentrations, either filtered or unfiltered, along the five different seasons demonstrates a rather steady state in the Hg mass balance between the investigated periods. iHg(II) in high altitude Lake Uru Uru (3686 m asl), affected by urban and mining contamination [23], was significantly higher during the dry season over the wet season because of the enhanced evaporation occurring at the end of the dry season. In pristine Pyrenean lakes, the concentration of iHg(II) in Autumn (2017 and 2018) is not significantly higher than in early Spring (2017, 2018 and 2019) (Kruskal-Wallis test, p-value = 0.79 and 0.54 respectively for $\text{iHg(II)}_{\text{UF}}$ and $\text{iHg(II)}_{\text{F}}$).

Monomethylmercury (MMHg) (Figure 7-2)

Filtered and unfiltered MMHg levels (MMHg_{F} and MMHg_{UF}) in subsurface water from the 19 sampled lakes over the five sampling campaigns vary respectively from <0.003 to 0.035 ng L^{-1} and from <0.003 to 0.062 ng L^{-1} (Table 7-1). The median values, 0.008 for MMHg_{F} and 0.011 for MMHg_{UF} , are typical from pristine aquatic environments, in the range of what has been found in Lake Superior ($\text{MMHg}_{\text{F}} = 0.005 \pm 0.001 \text{ ng L}^{-1}$ in April 2000; $\text{MMHg}_{\text{F}} = 0.008 \pm 0.002 \text{ ng L}^{-1}$ in August 2000) [15] and in some high-altitude lakes in the Alps (0.002 – 0.005 ng L^{-1}) [24]. MMHg represents (4±3) % of the filtered non-gaseous Hg and (4±2) % of the unfiltered non-gaseous Hg.

Studying the surface snow from the French Alps (2448 m asl) *Maruszczak et al.* [40] concluded that biotic production of MMHg in the snowpack is unlikely, considering the constant ratio MMHg/THg measured throughout the season in their study. Considering that the main contributor to Hg in the high-altitude lakes is the atmospheric deposition, the higher proportion of MMHg observed in the surface water from the high-altitude lakes in the Alps (4 ± 3 % for MMHg_F and 3 ± 2 % for MMHg_{UF}) in comparison with the surface snow (MMHg vary from non-determined to 1.21 % of the total Hg) might be due to in-situ aquatic methylation.

Regarding the MMHg levels in the surface waters of the investigated Pyrenean lakes, the Autumn 2018 sampling campaign stands out from the other ones (**Figure 7-2**). Indeed, the median values for MMHg_{UF} in Spring 2017, Autumn 2017, Spring 2018, and Spring 2019 were respectively 0.010, 0.006, 0.011 and 0.013 ng L⁻¹ while the median value in Autumn 2018 was 0.025 ng L⁻¹. If we compare Spring 2018 and Autumn 2018, MMHg_{UF} increased significantly in the lakes Arratille (+248 %), Gentau (+360 %), Roumassot (+235 %), Bachimaña (+211 %), Coanga (+231 %), Panticosa (+583 %) and Sabocos (+216 %) and moderately in most of the other studied lakes. Spring - summer algal bloom are controlling the whole biological turnover in those high-altitude and oligotrophic lakes [43], and such intense bloom events can be for example responsible of an increase in the methylation processes in the sediments [28,44]. Arratille, Gentau, Roumassot, Coanga and Sabocos showed the lowest nitrate (NO₃⁻) concentrations (from below LOD to 0.171 mg L⁻¹) in Autumn 2018, which can be an indicator of its removal by higher biological productivity [18,19,43,45]. In-situ methylation rates in lakes have already been linked to the trophic status, with increasing eutrophication leading to increasing organic matter loading and subsequent Hg methylation [21].

Dissolved Gaseous Mercury (DGM) (Figure 7-2)

Dissolved Gaseous Mercury (DGM) varied strongly, from 0.02 to 0.68 ng L⁻¹ (outliers excluded), and, overall, was higher than the measured DGM in other pristine areas (**Table 7-1**). Indeed, DGM in Bolivian lakes vary from 0.001 to 0.017 ng L⁻¹ in Lake Titicaca [21] and from 0.003 to 0.125 ng L⁻¹ in Lake Uru Uru [23]. In the Lake Superior, in Canada, DGM measured in august 2000 was 0.020 ± 0.003 ng L⁻¹ [15]. Even in the Adour Estuary, downstream to the Pyrenees, DGM content was lower than in the Pyrenean Lakes with values ranging from 0.024 to 0.056 ng L⁻¹ [31]. Finally, the DGM measured in the present study, with a median value of 0.11 ng L⁻¹, was in the range of the open ocean waters [42]. DGM accounted for 25 ± 11 % of the Hg_{TOT} and sometimes represent unexpectedly up to 55% of the total Hg.

The homogeneous iHg(II) concentrations contrasts with the high DGM levels measured in the Pyreneans lakes of our study. Photoreduction is probably important in high-altitude lakes from the Pyrenees. This photoreduction might be triggered by important solar radiation, and the general oligotrophic state of the Pyrenean lakes, in comparison with Bolivian [21,23] or Canadian lakes [27], might play a key role in this process. Indeed, organic matter is believed to have an impact on Hg photoreduction, and it is worth noting that DOC concentrations exhibit low to moderate values in the Pyrenean lakes (from 0.62 to 4.63 mg L⁻¹). In that sense, higher Hg photo-reduction to elemental Hg(0) takes place in open water in which low to moderate DOC content has been observed [42].

Table 7-1: Comparison of filtered (F) and unfiltered (UF) inorganic mercury (iHg(II)), monomethylmercury (MMHg) and Dissolved Gaseous Mercury (DGM) concentrations in the subsurface water samples of the 19 studied lakes with literature data for worldwide pristine areas (oceans, boreal lakes, high altitude lakes) and local areas (freshwaters and estuary). %MMHg is calculated as the ratio between MMHg and non-gaseous Hg (MMHg + iHg). %DGM is calculated as ratio between DGM and total Hg ($Hg_{TOT} = MMHg + iHg(II) + DGM$). *THg, **Reactive Hg and ***Surface and Depth samples.

Reference	Location	Elevation (m asl)	Sampling period	iHg(II) _F ng L ⁻¹	iHg(II) _{UF} ng L ⁻¹	MMHg _F (% MMHg _F) ng L ⁻¹	MMHg _{UF} (% MMHg _{UF}) ng L ⁻¹	DGM (% DGM) ng L ⁻¹
This Work	Central Pyrenees (France/Spain)	1640 - 2600	2017-2019	0.08 - 1.10 median = 0.23	0.11 - 1.19 median = 0.38	<0.003 - 0.035 (4 ± 3%) median = 0.008	<0.003 - 0.062 (4 ± 2%) median = 0.011	0.02 - 10.79 (29 ± 18%) median = 0.12
<i>Fitzgerald et al.</i> (and references therein) [42]	Equatorial Pacific Ocean North Pacific Ocean North Atlantic Ocean South Atlantic Ocean			0.03 - 0.39* 0.48 ± 0.32*	0.08 - 1.38** 0.58 ± 0.34*	0.209 ± 0.217 <0.010 - 0.030	<0.010 - 0.116	0.003 - 0.138 0.096 ± 0.062 0.241 ± 0.160
<i>Cavalheiro et al.</i> [32]	Freshwaters (France)		2012	<0.14 - 2.10		<0.04 - 0.14		
<i>Sharif et al.</i> [31]	Adour Estuary (France)		2007 & 2010	0.28 - 0.59	0.40 - 2.66	0.014 - 0.054	0.018 - 0.124	0.024 - 0.056
<i>Emmerton et al.</i> [27]	Boreal Lakes (Canada, n=50)		2012 - 2016		0.36 - 5.33*		<0.01 - 0.344	
<i>Bravo et al.</i> [28]	Boreal Lakes (Sweden, n=10)***	3 - 229	2012 & 2013		0.9 - 7.3		0.2 - 2.9	
<i>Rolfhus et al.</i> [15]	Lake Superior (Canada/USA)	183	April 2000 August 2000		0.57 ± 0.07* 0.47 ± 0.03*		0.005 ± 0.001 0.008 ± 0.002	0.020 ± 0.003
<i>Meuleman et al.</i> [29]	Lake Baïkal (Russia)***	456	1992 & 1993	0.14 - 0.77*		0.002 - 0.038		
<i>Malczyk and Branfireun</i> [30]	Lake Zapotlán (Mexico)	1497	2007 & 2008	0.5 - 2.4*	0.9 - 10.7*	0.006 - 0.119		
<i>Maruszczak et al.</i> [40]	Lake (Alps, n=4)	1648 - 2448	2008		<0.1 - 3.12*		0.002 - 0.005	
<i>Alanoca et al.</i> [23]	Uru Uru Lake (Bolivia)	3686	2010 & 2011	0.7 - 6.3	0.2 - 2.5	0.2 - 3.8	0.2 - 4.5	0.003 - 0.125
<i>Guédron et al.</i> [23]	Lake Titicaca	3809	2013 & 2015	0.10 - 0.82*	0.08 - 1.81*	0.003 - 0.243	0.013 - 0.306	0.001 - 0.017

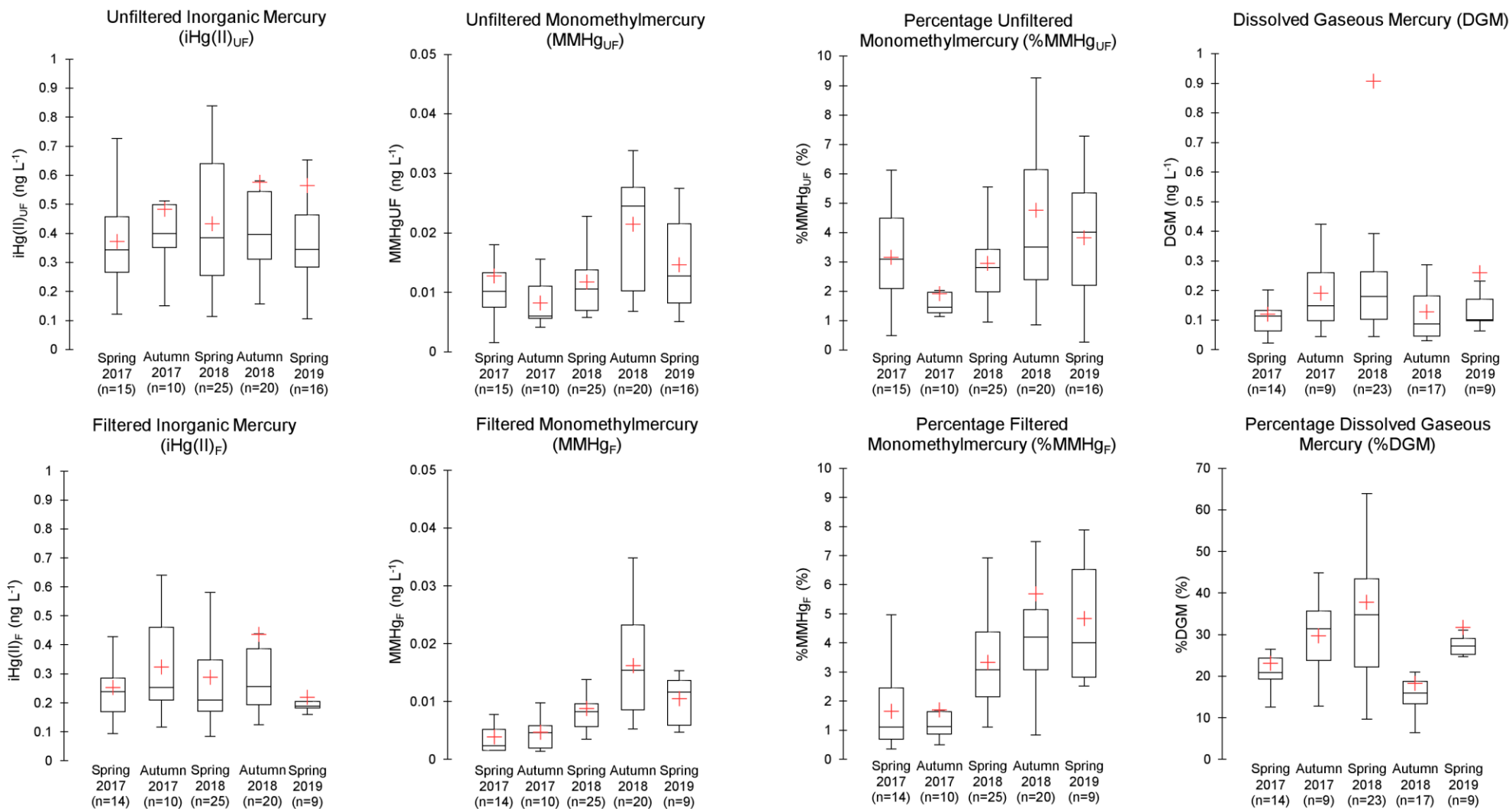


Figure 7-2: Boxplot representations of unfiltered and filtered $iHg(II)$, $MMHg$ and percentage of $MMHg$ (calculated as ratio between $MMHg$ and non-gaseous Hg ($MMHg + iHg(II)$), and DGM and percentage of DGM (calculated as ratio between DGM and total Hg ($Hg_{TOT} = MMHg + iHg(II) + DGM$)) in subsurface water samples of the 19 studied lakes. Bars indicate 10th and 90th percentile, boxes indicate 25th and 75th, marks within each box are medians, and red crosses are mean.

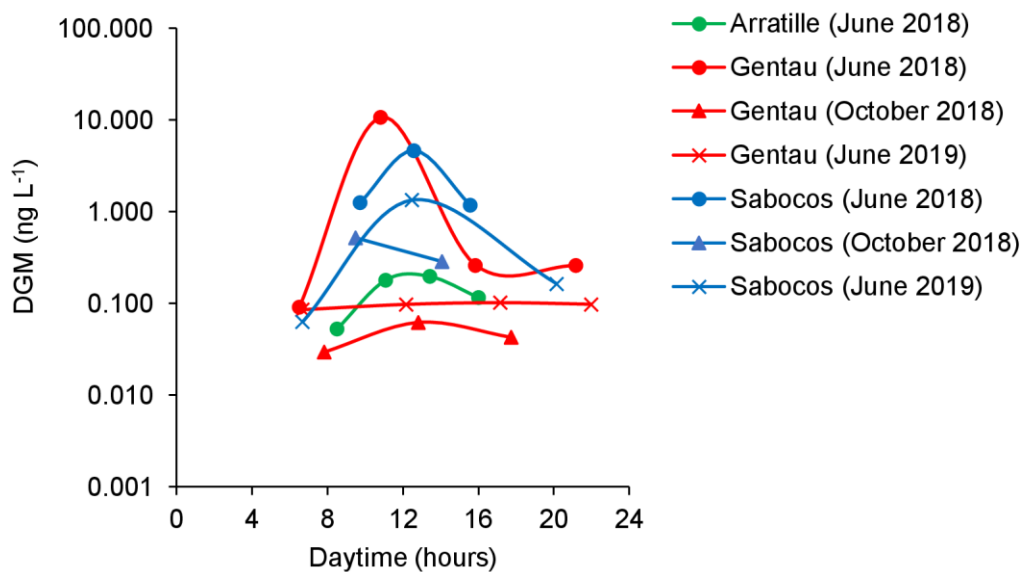


Figure 7-3: Daily variation of DGM in Lakes Arratille, Gentau and Sabocos

2. Mercury compounds distribution in the water column of selected alpine lakes

The **Figure 7-4** (Lake Gentau), **Figure 7-5** (Lake Sabocos), **Figure 7-6** (Lake Arratille) and **Figure 7-7** (Lake Azul) display some physico-chemical parameters like temperature, dissolved oxygen saturation (not corrected from altitude), chlorophyll-a, TOC, Silicate, SO_4^{2-} , Cl^- and NO_3^- that could be useful to understand the mercury species (iHg(II), MMHg and DGM) distribution in the water column of four different lakes intensively monitored during June 2018, October 2018 and June 2019. The results are also summarised in **ANNEXE 3**.

Features and specificities of these four lakes have been already discussed in **6 Occurrence, distribution, and characteristics concentrations of Potential Harmful Trace Elements (PHTEs) in Pyrenean lakes and their relation to aquatic biogeochemistry**. Globally, even if their catchment is mainly composed of easily erodible sedimentary rocks (Devonian, Cretaceous and Permo-Triassic rocks) Gentau, Sabocos, Arratille and Azules span a wide range of physical characteristics with maximum depth from 8 to 25m, altitude from 1900 m to 2420 m.

Lake Gentau (Figure 7-4)

The water column of Lake Gentau was stratified in the three sampling campaigns (June 2018, October 2018, and June 2019). Indeed, this lake is divided in three various sections: epilimnion, metalimnion, and hypolimnion, all along the year except during the short overturn spring and autumn periods [46]. In addition to the oxygen chemocline (located around 7m depth in June 2018, 10m depth in October 2018 and 8m in June 2019), Gentau also presented a thermocline in the June 2018 sampling campaign in the metalimnion part of the lake (at 10m depth).

The highest iHg(II) concentrations, either unfiltered or filtered, were detected at the deepest sampling point of the lake in June (0.75 and 0.66 ng L⁻¹ in unfiltered and filtered samples, respectively) and October 2018 (0.39 and 0.36 ng L⁻¹ in unfiltered and filtered samples, respectively). In June 2019, the surface water samples were characterized by the highest iHg(II) concentrations (0.27 and 0.18 ng L⁻¹ in unfiltered and filtered samples, respectively). *Bravo et al.* [28] have shown that the highest total mercury concentrations in river stream systems were associated with important terrestrial DOM (Dissolved Organic Matter) and low nutrient content. In our study, TOC was low and relatively constant all along the water column during the three sampling campaigns (1.1 ± 0.3 mg L⁻¹ in June 2018, 1.5 ± 0.2 mg L⁻¹ in October 2018, and 1.2 ± 0.1 mg L⁻¹ in June 2019). In addition, nitrate, indicator of the biological productivity, decreased with depth in June 2018 (0.18 to 0.08 mg L⁻¹) while it increased with depth in October 2018 (<0.06 to 0.14 mg L⁻¹), exhibiting the seasonal changes in primary productivity and water column remineralisation of nitrogen. Also, the important increase observed for iHg(II) in the deepest point of the lake in June and October 2018 is probably due to some inputs of iHg(II) at the water-sediment interface.

MMHg concentrations were significantly higher at the deepest point of the lake in comparison with the other four sampled points. Indeed, while unfiltered and filtered MMHg in the water column in June 2018 varied from 0.008 to 0.057 ng L⁻¹ and 0.006 to 0.023 ng L⁻¹ respectively, MMHg unfiltered and filtered levels were respectively 0.426 and 0.318 ng L⁻¹ at 18 m depth. In October 2018, the same trend was observed for MMHg: unfiltered and filtered MMHg varied from 0.027 to 0.055 ng L⁻¹ and 0.011 to 0.026 ng L⁻¹, respectively, while the deepest sampled point (17m depth) exhibited MMHg levels as high as 0.388 and 0.341 ng L⁻¹ for the unfiltered and filtered samples. In June 2019, unfiltered and filtered MMHg concentrations varied from 0.007 to 0.059 ng L⁻¹ and <0.004 to 0.019 ng L⁻¹ respectively, while 0.236 and 0.157 ng L⁻¹ were the unfiltered and filtered MMHg concentrations measured at the deepest sampled point (17.5m depth). Moreover, MMHg represents a higher fraction of the non-gaseous Hg species (MMHg and iHg(II)) at the deepest sampled point, from 36 to 56% for unfiltered MMHg and from 32 to 60% for filtered MMHg. Anoxic conditions observed in the deepest point of Lake Gentau can host anaerobic microbial activities responsible of in-situ Hg biotic methylation in both water and surface sediments [47].

Finally, vertical distribution of DGM in Gentau was quite simple with a constant and progressive decrease from surface waters (10.79 ng L⁻¹ in June 2018; 0.06 ng L⁻¹ in October 2018; 0.10 ng L⁻¹ in June 2019) to the deepest sampled point (0.14 ng L⁻¹ in June 2018 at 18m depth; 0.03 ng L⁻¹ in October 2018 at 17m depth; 0.01 ng L⁻¹ in June 2019 at 17.5m depth). DGM concentrations were also lower in

October 2018 than in June 2018 and 2019 all along the water column. This supports the previous assumption regarding the importance of photo-reduction processes in those high-altitude lakes, induced by significant solar radiation in surface waters.

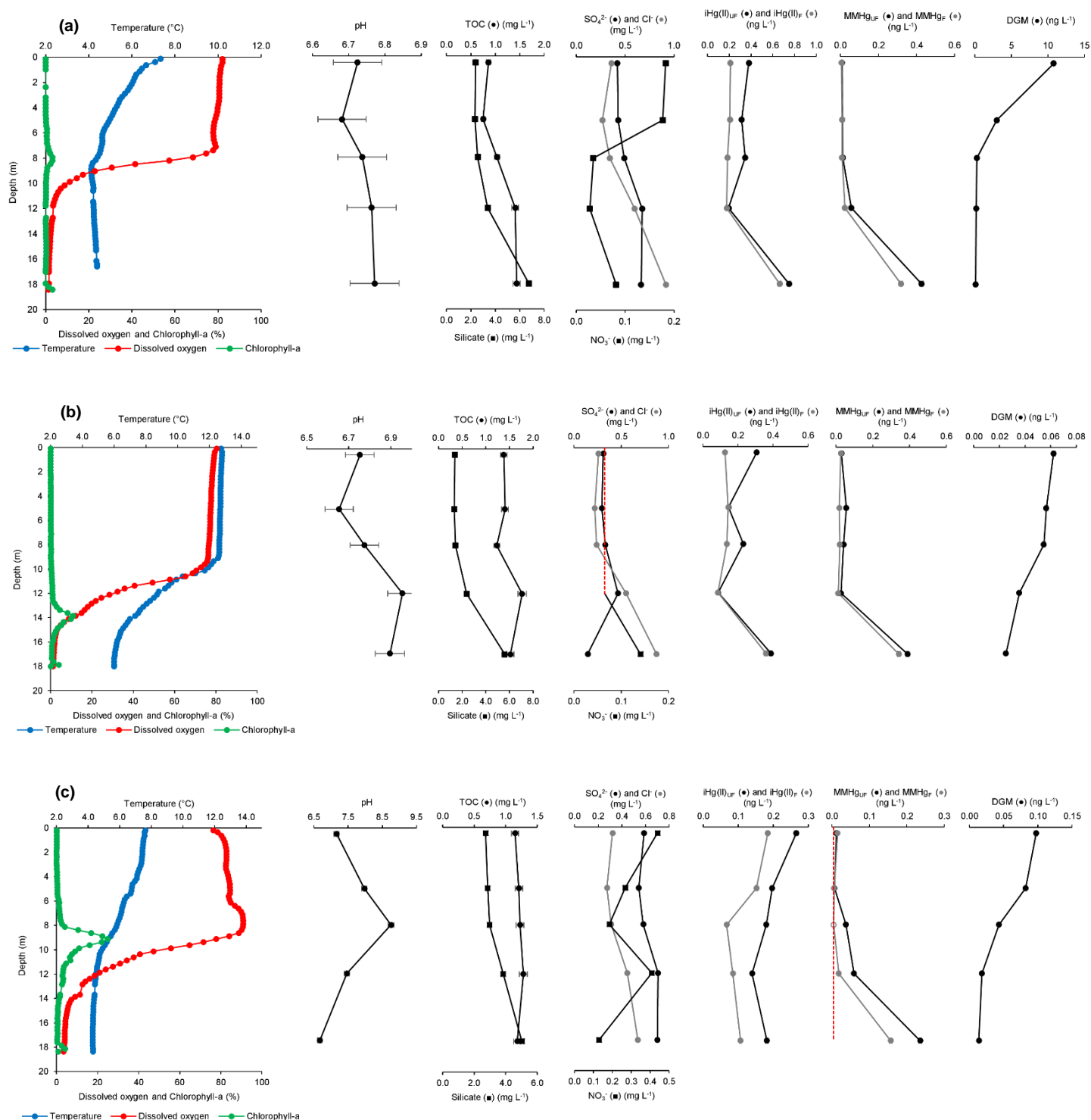


Figure 7-4: Depth profiles of temperature, percentage of dissolved oxygen saturation, chlorophyll-a (RFU) and some other chemical parameters including mercury speciation obtained in (a) June 2018, (b) October 2018 and (c) June 2019 in Lake Gentau. Red dot points correspond to the LoD.

Lake Sabocos (Figure 7-5)

Lake Sabocos is less stratified than Lake Gentau, but oxygen and temperature varied strongly along the water column with depletion of both physico-chemical parameters with depth, leading to almost anoxic conditions in the bottom part of this lake. Indeed, dissolved oxygen varied from 96 to 1% in June 2018, from 79 to 2% in October 2018 and from 84 to 5% in June 2019, and the chemocline, where dissolved oxygen starts decreasing, was located at 4, 10 and 5m in June 2018, October 2018, and June 2019, respectively. The thermocline was located at the same depths than chemocline and temperature varied from 17 to 5°C in June 2018, 11 to 6°C in October 2018 and 12 to 5°C in June 2019. This lake has also one special characteristic : it is the only one considered as alkaline lake with pH values ranging from 7.47 to 7.71 in the surface water (June and October 2018).

iHg(II), either unfiltered or filtered, strongly varied all along the water column in the three sampling campaigns (respectively from 0.39 to 1.29 ng L⁻¹ and from 0.29 to 0.53 ng L⁻¹ in June 2018; from 0.53 to 0.90 ng L⁻¹ and from 0.17 to 0.68 ng L⁻¹ in October 2018; from 0.08 to 0.34 ng L⁻¹ and from 0.02 to 0.21 ng L⁻¹ in June 2019). There is no evidence for a specific trend in the iHg(II) distribution in the Lake Sabocos but the strong variations suggest that important Hg species transformations may occur.

MMHg depth profiles in Lake Sabocos indicate possible in-situ methylation. Production of MMHg in the lake may occur under reducing conditions in both June 2018 and 2019 with the highest MMHg unfiltered and filtered levels measured in the deepest part of the lake where the oxygen level was the lowest (respectively 0.060 and 0.025 ng L⁻¹ and 10 and 7% of the non-gaseous Hg in June 2018; 0.052 and 0.021 ng L⁻¹ and 25 and 42% of the non-gaseous Hg in June 2019). Increase of MMHg levels was not observed in October 2018. In this sampling campaign, no maximum of chlorophyll was detected in the water column, probably indicating a lower biological production.

Regarding the DGM concentrations, the high levels measured in surface waters in both June 2018 and 2019 (4.65 and 1.34 ng L⁻¹ respectively), in comparison with deepest samples (0.56 and 0.06 ng L⁻¹ respectively), is consistent with very high photo-reduction enhanced during spring conditions.

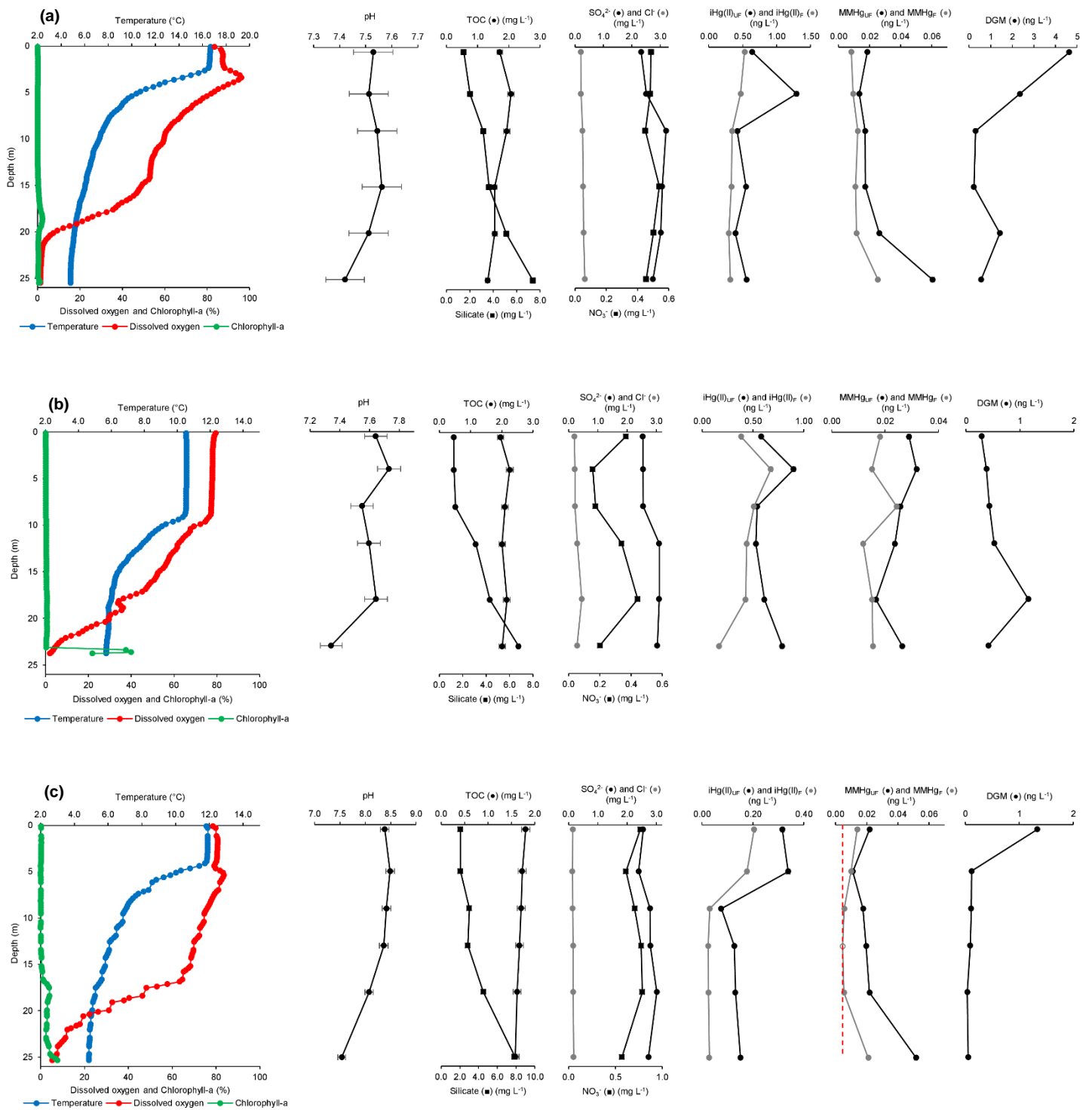


Figure 7-5: Depth profiles of temperature, percentage of dissolved oxygen saturation, chlorophyll-a (RFU) and some other chemical parameters including mercury speciation obtained in (a) June 2018, (b) October 2018 and (c) June 2019 in Lake Sabocos. Red dot points correspond to the LoD.

Lake Arratille (Figure 7-6) and Azul (Figure 7-7)

In the shallow alpine Lake Arratille (2256 m asl.), physico-chemical parameters measured in-situ with the multiparameter probe (temperature, oxygen and chlorophyll) did not vary strongly within the water column. Indeed, the average temperature was 5.0 ± 0.4 °C in June 2018 and 8.0 ± 0.9 °C in October 2018, and the average dissolved oxygen was 65 ± 23 % in June 2018 and 71 ± 10 % in October 2018. Nevertheless, it is worth noting that a short decrease in both temperature and oxygen is observed in the last 2 meters of the lake in both June and October 2018. Concerning the mercury species distribution, no significant difference was observed for unfiltered and filtered iHg(II) (0.26 ± 0.10 and 0.18 ± 0.05 ng L⁻¹, respectively), unfiltered and filtered MMHg (0.010 ± 0.04 and 0.008 ± 0.03 ng L⁻¹, respectively) and DGM (0.13 ± 0.06 ng L⁻¹) along the water column, suggesting a well-mixed lake with clear water.

In the shallower and more elevated Lake Azul (2420 m asl.), dissolved oxygen (76 ± 1 % in June 2018 and 72 ± 2 % in October 2018) and temperature (4.8 ± 0.1 °C in June 2018 and 5.1 ± 0.2 °C in October 2018) did not vary at all along the water column. Regarding Hg species, on the one hand, no specific trend was observed in June 2018 for unfiltered and filtered iHg(II) (0.36 ± 0.05 and 0.30 ± 0.02 ng L⁻¹, respectively) unfiltered and filtered MMHg (0.006 ± 0.001 and 0.004 ± 0.001 ng L⁻¹, respectively) and DGM (0.12 ± 0.04 ng L⁻¹). On the other hand, a significant increase was observed with depth in October 2018 for unfiltered and filtered iHg(II) (from 0.39 to 2.81 ng L⁻¹ and from 0.27 to 2.46 ng L⁻¹, respectively) unfiltered and filtered MMHg (from 0.009 to 0.021 ng L⁻¹ and from 0.009 to 0.021 ng L⁻¹, respectively) and DGM (from 0.09 to 1.33 ng L⁻¹). It might be linked to a sediment punctual remobilisation of Hg.

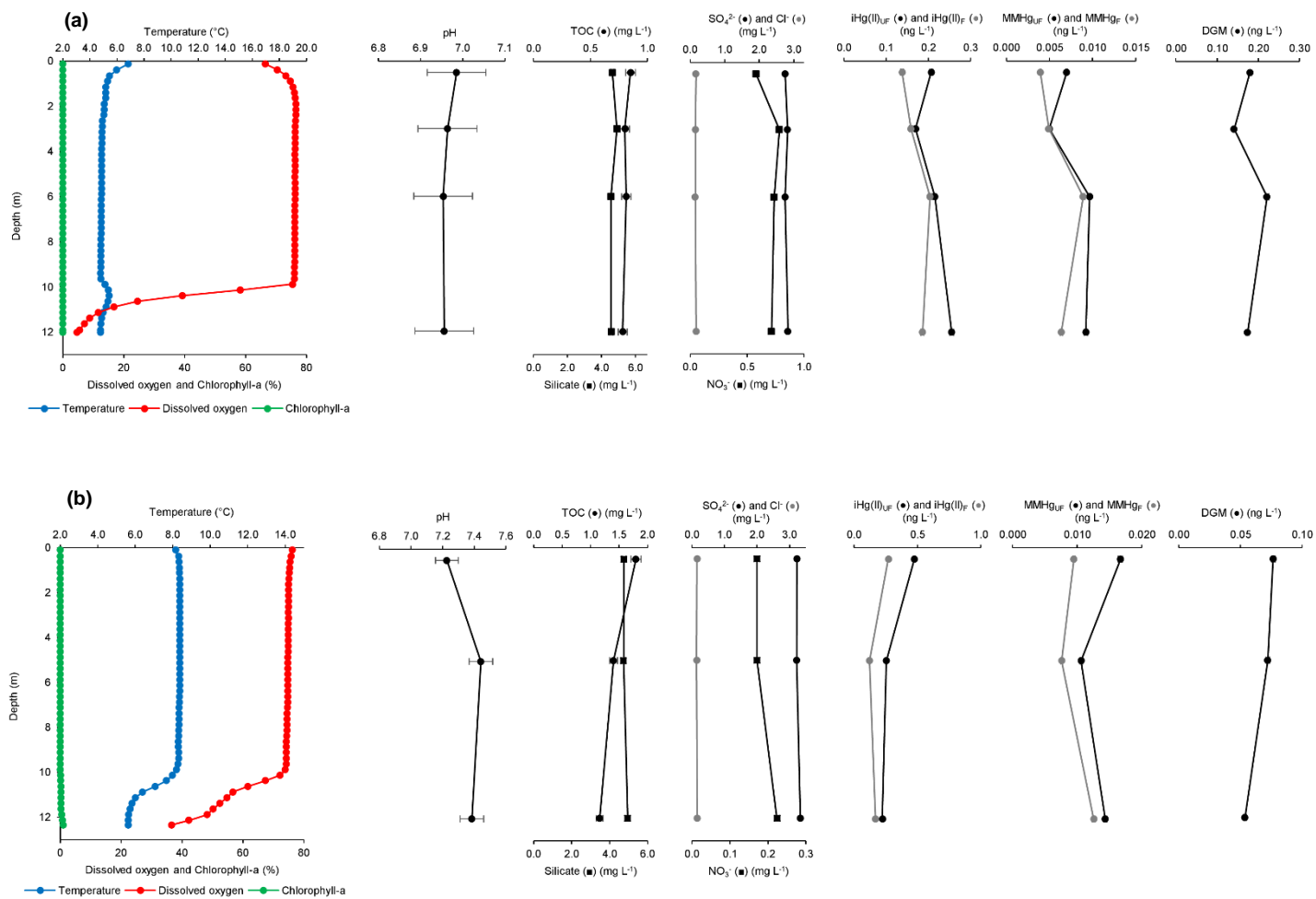


Figure 7-6: Depth profiles of temperature, percentage of dissolved oxygen saturation, chlorophyll-a (RFU) and some other chemical parameters including mercury speciation obtained during (a) June 2018 and (b) October 2018 in Lake Arratille.

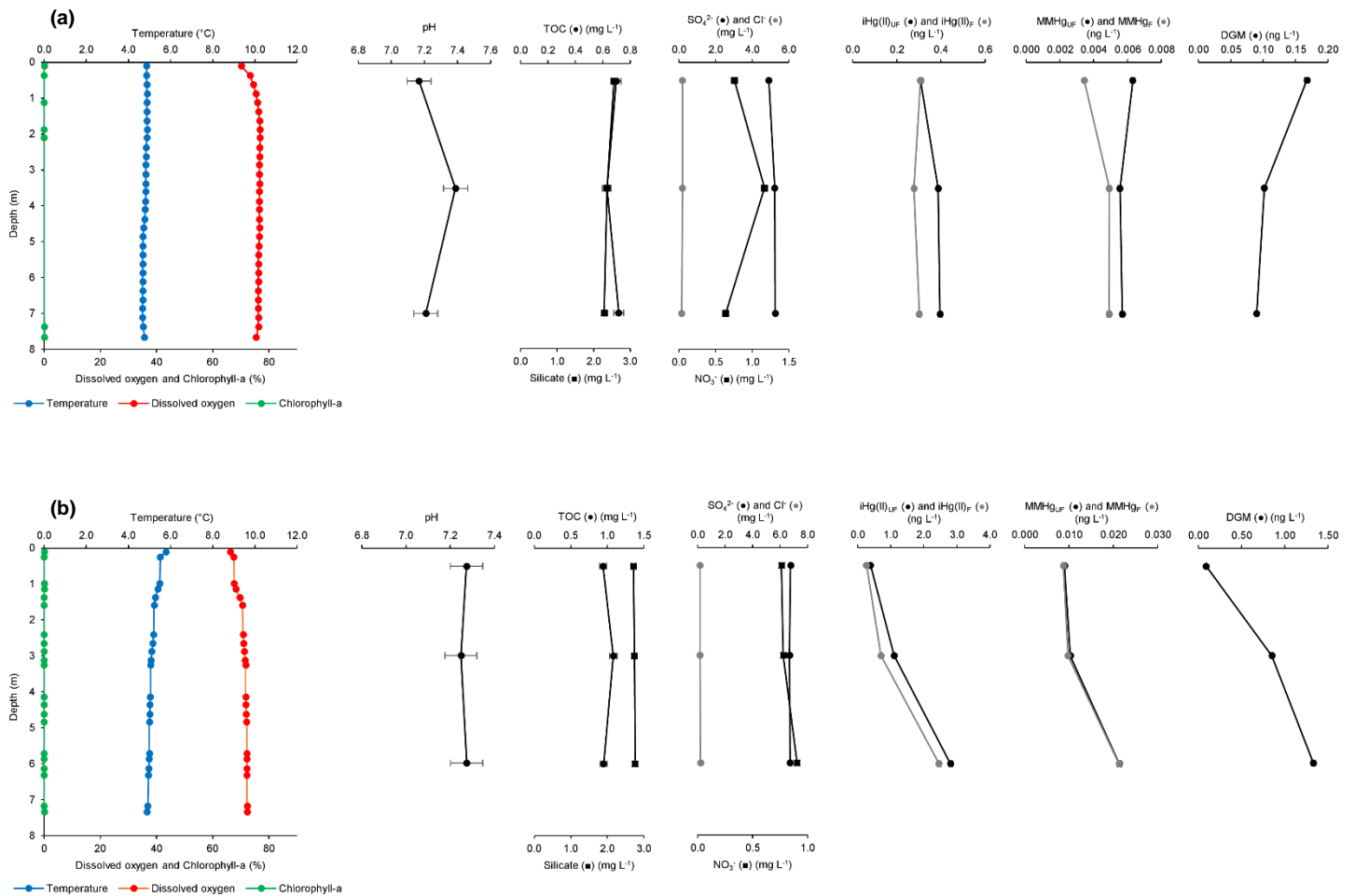


Figure 7-7: Depth profiles of temperature, percentage of dissolved oxygen saturation, chlorophyll-a (RFU) and some other chemical parameters including mercury speciation obtained during (a) June 2018 and (b) October 2018 in Lake Azul.

7.4.5. Mercury species transformations and volatilization in the water column of selected alpine lakes

Hg species incubation experiments were conducted in Lakes Gentau, Sabocos and Arratille as described in **3.3.6 Mercury species incubations**, to quantify the importance of the Hg species transformations occurring in these high-altitude lakes. The obtained results are summarized in **Table 7-2**, together with transformation rates obtained in previous studies.

1. Methylation and demethylation pathways

Inorganic mercury methylation

Methylation potentials under dark and diurnal conditions obtained in unfiltered water samples ranged between <0.03 and 6.97 \% day^{-1} in Lake Gentau, between <0.03 and 0.95 \% day^{-1} in Lake Sabocos, and between <0.03 and 0.44 \% day^{-1} in Lake Arratille (**Table 7-2**). These methylation potentials are in accordance with data obtained for water samples in Canadian lakes[25], high-altitude Bolivian lakes [23] and for marine and coastal waters [31,48] using similar experimental methods. The highest methylation potentials have been measured under dark conditions in the bottom anoxic zone for Lake Gentau which exhibits $4.34 \pm 0.40 \text{ \% day}^{-1}$ in June 2018, $6.97 \pm 0.44 \text{ \% day}^{-1}$ in October 2018 and $1.63 \pm 0.11 \text{ \% day}^{-1}$ in June 2019). For Lake Sabocos, methylation is $0.81 \pm 0.33 \text{ \% day}^{-1}$ in June 2018, $0.95 \pm 0.38 \text{ \% day}^{-1}$ in October 2018 and $0.63 \pm 0.28 \text{ \% day}^{-1}$ in June 2019. No significant difference was observed for methylation potentials for incubation performed under dark or diurnal conditions, confirming that light induced methylation is not significant in those high-altitude pristine lakes. These results also support depth profile measurements and demonstrate that reducing conditions especially in stratified anoxic waters promote Hg methylation due to methylating anaerobic bacteria.

Lower but measurable methylation extent were determined in the oxic subsurface waters of Lake Gentau with $0.42 \pm 0.12 \text{ \% day}^{-1}$ under diurnal conditions and $0.40 \pm 0.17 \text{ \% day}^{-1}$ under dark conditions in June 2018, and $0.21 \pm 0.17 \text{ \% day}^{-1}$ under diurnal conditions in June 2019. In Lake Sabocos, surface water methylation was $0.09 \pm 0.05 \text{ \% day}^{-1}$ under diurnal conditions and $0.26 \pm 0.02 \text{ \% day}^{-1}$ under dark conditions in June 2018, and $0.34 \pm 0.25 \text{ \% day}^{-1}$ under diurnal conditions and $0.17 \pm 0.07 \text{ \% day}^{-1}$ under dark conditions in October 2018. Lake Arratille exhibit methylation potential of $0.44 \pm 0.04 \text{ \% day}^{-1}$ under diurnal conditions in June 2018. The formation of MMHg in the oxic freshwater column is not fully understood. A recent work conducted in Lake Geneva highlights that particles sinking through oxygenated water column can produced MMHg [26]. In our work, even if the methylation rates measured remain low, it is measurable and suggests that reducing conditions occurring in particles microenvironment within the oxic layer could also play a role.

MMHg demethylation

Significant demethylation potentials were measured in the subsurface waters of Lake Gentau ($23.8 \pm 4.4 \text{ \% day}^{-1}$ in June 2018; $23.9 \pm 2.9 \text{ \% day}^{-1}$ in October 2018 and $35.6 \pm 2.2 \text{ \% day}^{-1}$ in June 2019) and

Lake Sabocos ($35.2 \pm 9.7 \text{ \% day}^{-1}$ in June 2018; $9.0 \pm 0.5 \text{ \% day}^{-1}$ in October 2018 and $12.4 \pm 4.2 \text{ \% day}^{-1}$ in June 2019) only at daylight conditions. These important demethylation potentials have been observed in previous studies and were associated to both abiotic and biotic processes [31,47]. In our study, demethylation under dark conditions was detected only in Lake Sabocos within the oxicle in June 2019 ($6.8 \pm 4.7 \text{ \% day}^{-1}$), while in other lakes and season dark demethylation was always below 4 \% day^{-1} . Therefore, our results suggest that in high-altitude pristine lakes, direct light-induced photochemical demethylation in UV exposed surface waters is a significant pathway that contribute to control the extent of MMHg in the water column [22].

Lake Sabocos exhibited an interesting result regarding the middle depth (9m), only studied in June 2019. While in Lake Gentau significant demethylation was measured at the middle depth of the lake (8m) in June 2018 ($13.6 \pm 1.2 \text{ \% day}^{-1}$) and June 2019 ($13.6 \pm 0.4 \text{ \% day}^{-1}$) only under diurnal conditions and in lower extent than for the subsurface, Lake Sabocos exhibited significant demethylation at both diurnal and dark conditions in June 2019 ($8.2 \pm 3.9 \text{ \% day}^{-1}$ and $6.8 \pm 4.7 \text{ \% day}^{-1}$ respectively). Thus, in both stratified lakes, demethylation occurred within the oxicle and cannot be related to UV photochemical reactions (i.e., no UV light). These results suggest that specific microbial activity are involved due to heterotrophic (Gentau, Sabocos) and/or phototrophic (Sabocos) bacteria specifically developing at the oxicle (middle depth).

Demethylation vs total MMHg loss

As mentioned previously, demethylation, especially in subsurface waters, is important in Lake Gentau and Lake Sabocos. As a reminder, demethylation potentials calculated here correspond to the transformation of MMHg into iHg(II). In **Table 7-2**, additionally to the demethylation potentials, total loss of MMHg potential from the experimental water solution has also been determined. Total loss of MMHg correspond to the decrease of MMHg during the incubation and could be connected to both the transformation of MMHg into iHg(II), and the transformation of MMHg into Hg(0) or other precipitated insoluble forms. The linear regression between both MMHg degradation processes (excluding middle depth dark conditions of Lake Sabocos, June 2019) exhibits a very good coefficient of determination ($R^2 = 0.97$; linear trend MMHg Loss = $(1.7 \pm 0.1) \times$ Demethylation) (**Figure 7-8**). The covariation of both calculated potentials (demethylation and loss of MMHg) suggests that similar pathways occur during the different incubation experiments. These results demonstrate that a significant fraction (always below 50%) of the degraded MMHg, not recovered as soluble iHg(II), is converted to Hg(0) (reductive (photo)demethylation) or to insoluble Hg forms as final products.

Net methylation assessment

In anoxic waters, the net methylation assessment (**Table 7-2**) allows to exhibit a potential significant production of MMHg in the bottom part of Lake Gentau with $3.25 \pm 0.30 \text{ ng L}^{-1} \text{ day}^{-1}$ in June 2018, $2.71 \pm 0.17 \text{ ng L}^{-1} \text{ day}^{-1}$ in October 2018, and $0.29 \pm 0.02 \text{ ng L}^{-1} \text{ day}^{-1}$ in June 2019. While lower ones are determined in Lake Sabocos with $0.45 \pm 0.19 \text{ ng L}^{-1} \text{ day}^{-1}$ in June 2018, $0.75 \pm 0.30 \text{ ng L}^{-1} \text{ day}^{-1}$ in October 2018, and $0.09 \pm 0.04 \text{ ng L}^{-1} \text{ day}^{-1}$ in June 2019. On the one hand, at the subsurface, low potential production of MMHg was observed in Lake Arratille with net methylation of $0.07 \pm 0.01 \text{ ng L}^{-1}$

day⁻¹ (diurnal condition) and $0.07 \pm 0.04 \text{ ng L}^{-1} \text{ day}^{-1}$ (dark condition) in June 2018. On the other hand, under diurnal conditions, the subsurface waters of Lake Gentau and Lake Sabocos behave as a sink of MMHg, as net methylation remains negative and varies from -0.01 ± 0.09 to $-0.64 \pm 0.08 \text{ ng L}^{-1} \text{ day}^{-1}$.

2. Reduction and volatilization from alpine lakes

Reduction and volatilization Flux Density in selected alpine lakes (Arratille, Gentau and Sabocos)

High iHg(II) reduction potentials (**Table 7-2**) were measured under diurnal conditions in subsurface waters of Lake Gentau ($81.2 \pm 0.8 \text{ \% day}^{-1}$ in June 2018; $20.8 \pm 0.1 \text{ \% day}^{-1}$ in October 2018 and $16.9 \pm 0.1 \text{ \% day}^{-1}$ in June 2019) and Lake Sabocos (13.2 \% day^{-1} in June 2019), and were less significant in subsurface waters of Lake Arratille ($17.3 \pm 2.9 \text{ \% day}^{-1}$ in June 2018; $2.8 \pm 0.2 \text{ \% day}^{-1}$ in October 2018), but still remained among the highest in comparison to previous studies [23,31,48]. These important reduction potentials are consistent with the high DGM concentrations measured, especially in Lakes Gentau and Sabocos. Regarding the dark conditions, reduction potentials at subsurface waters were detected at lower extents only in June 2018 ($9.1 \pm 2.6 \text{ \% day}^{-1}$) and October 2018 ($1.7 \pm 0.1 \text{ \% day}^{-1}$) for Lake Gentau, June 2019 ($3.5 \pm 0.1 \text{ \% day}^{-1}$) for Lake Sabocos. Therefore, intense UV light occurring in surface waters of high-altitude lakes promotes Hg reduction.

Using the reduction potentials and the non-gaseous Hg measured at the subsurface waters, we can estimate the amount of Hg reduced per day within the first meter depth under diurnal conditions and compare it with the Volatilization Flux Density (FD) calculated as described in **4 Hg gaseous fluxes at air-water interface**. All the fluxes calculated are gathered in **ANNEXE 3**.

In Lake Gentau, the amount of Hg reduced per day was $473 \pm 5 \text{ ng m}^{-2} \text{ day}^{-1}$ in June 2018, $54 \pm 1 \text{ ng m}^{-2} \text{ day}^{-1}$ in October 2018 and $47 \pm 1 \text{ ng m}^{-2} \text{ day}^{-1}$ in June 2019. Median values of Volatilization FD in Lake Gentau were in the same order of magnitude with $48 \text{ ng m}^{-2} \text{ day}^{-1}$ for 1 m s^{-1} wind speed (from 12 to $143 \text{ ng m}^{-2} \text{ day}^{-1}$) and $72 \text{ ng m}^{-2} \text{ day}^{-1}$ for 3 m s^{-1} wind speed (from 18 to $216 \text{ ng m}^{-2} \text{ day}^{-1}$) (n=10). For Lake Sabocos, the quantity of Hg reduced per day was in the same range than Lake Gentau with $46 \pm 1 \text{ ng m}^{-2} \text{ day}^{-1}$ in June 2019, and in the same order of magnitude than the Volatilization FD median values, $121 \text{ ng m}^{-2} \text{ day}^{-1}$ for 1 m s^{-1} wind speed (from 31 to $288 \text{ ng m}^{-2} \text{ day}^{-1}$) and $184 \text{ ng m}^{-2} \text{ day}^{-1}$ for 3 m s^{-1} wind speed (from 46 to $436 \text{ ng m}^{-2} \text{ day}^{-1}$) (n=4). In these two lakes, even if the Volatilization FD median values are not significantly different than the extent of Hg reduced per day, the overall range remains important. The amount of Hg reduced in Lake Arratille was lower than the other two lakes with $31 \pm 5 \text{ ng m}^{-2} \text{ day}^{-1}$ in June 2018 and $14 \pm 1 \text{ ng m}^{-2} \text{ day}^{-1}$ in October 2018, which is also in the same order of magnitude than the Volatilization FD calculated (from 20 to $178 \text{ ng m}^{-2} \text{ day}^{-1}$ for 1 m s^{-1} wind speed and from 30 to $270 \text{ ng m}^{-2} \text{ day}^{-1}$ for 3 m s^{-1} wind speed (n=7)). Overall, the gaseous Hg evasion estimated from the first meter of the water column (subsurface) represents a similar extent than the reduction potential obtained from our incubation experiments. Such results strongly support that UV light induced in-situ reduction is a major pathway controlling significant volatilization of Hg from these alpine lakes.

Volatilization Flux Density (FD) in all the studied lakes and comparison with other fluxes

Median values of Volatilization FD in all the lakes (except Arratille, Sabocos and Gentau discussed below) were $60 \text{ ng m}^{-2} \text{ day}^{-1}$ for 1 m s^{-1} wind speed (from 7 to $375 \text{ ng m}^{-2} \text{ day}^{-1}$) and $92 \text{ ng m}^{-2} \text{ day}^{-1}$ for 3 m s^{-1} wind speed (from 11 to $568 \text{ ng m}^{-2} \text{ day}^{-1}$). Volatilization FD did not vary strongly depending on the sampling campaign with median values from 45 to $111 \text{ ng m}^{-2} \text{ day}^{-1}$ (1 m s^{-1}) and from 68 to $168 \text{ ng m}^{-2} \text{ day}^{-1}$ (3 m s^{-1}).

It is interesting to compare these estimated Volatilization FD with wet Hg deposition fluxes (direct input and snow-ice melt), and mercury accumulation rates in sediments. This later is commonly used as a probe for past Hg contamination in alpine lakes and atmospheric burden.

Wet deposition at the peatland of Pinet (Central Pyrenees, 880m asl) were recently measured at $8.0 \pm 4.6 \text{ ng L}^{-1}$ [39]. Considering that annual precipitation is 1161 mm at Pinet peat (average for the period 2010-2013) [39] and 2000 mm at lake Marboré (Central Pyrenees, 2612 m asl) [3], the studied lakes in this work (from 1620 m asl to 2600 m asl) are subjected to 25 to $44 \text{ ng m}^{-2} \text{ day}^{-1}$ of wet depositions. This is well in accordance with model results of Hg deposition in the Pyrenees Region from European Monitoring and Evaluation Programme (EMEP), ranging from 33 to $49 \text{ ng m}^{-2} \text{ day}^{-1}$ (Website. <http://www.emep.int/>). The median Volatilization FD calculated in this work are 60 to $92 \text{ ng m}^{-2} \text{ day}^{-1}$ (1 and 3 m s^{-1} wind speed, respectively) which is slightly above the maximum wet deposition. Nevertheless, considering the surface of the studied lakes the median Volatilization Flux Density can be estimated to be 2 to 3 mg day^{-1} while considering the surface of the catchment the wet deposition in the high-altitude lakes can be estimated to be 45 to 79 mg day^{-1} . Thus, Hg evasion is not a major loss at the catchment scale for Hg mass balance, but it will drastically affect its water column biogeochemistry.

Lake Marboré has been deeply studied [3,49,50], and the next chapter is also dedicated to the Hg in sediment cores from this lake (*Erreur ! Source du renvoi introuvable. Erreur ! Source du renvoi introuvable.*). In this study, the most recent sample (2004 AD) exhibits a Hg accumulation rate of $40 \mu\text{g m}^{-2} \text{ year}^{-1}$, which corresponds to an average daily Hg fluxes of $110 \text{ ng m}^{-2} \text{ day}^{-1}$. This flux is in the same range as the median Volatilization Flux Density calculated with the gas exchange model.

Overall, the evasion fluxes calculated for the alpine lakes are very significant, and due to the high DGM levels measured in these lakes. It is worth noting that these estimations are made using an empirical water-air gas exchange model providing a rough estimate, and that the calculated Volatilization Flux Density corresponds to the free-ice period (negligible during ice cover). However, it is clear that the Hg deposited in bottom lake sediments will be drastically affected by DGM evasion and direct input from snow melt and runoff.

Table 7-2: Methylation (M), Demethylation (D), MMHg Loss (L), Net Methylation (NM) and Reduction (R) potentials (mean \pm SD, n=3 for M, D, L and NM, n=2 for R) in unfiltered waters performed under varying light and dark conditions at different depths for Lakes Gentau, Sabocos and Arratille and for sampling campaigns June and October 2018 and June 2019, together with data from the literature. Detection limits are 0.03, 4, 4 and 1 % day⁻¹ for Methylation, Demethylation, MMHg Loss and Reduction yields, respectively. n.d. is not determined.

Location	Sampling Period	Sampling Type	Incubation Time (h)	iHg(II) Methylation (%day ⁻¹)		MMHg Demethylation (%day ⁻¹)		MMHg Loss (%day ⁻¹)		Hg Reduction (%day ⁻¹)		Net Methylation (ng L ⁻¹ day ⁻¹)	
				Diurnal	Dark	Diurnal	Dark	Diurnal	Dark	Diurnal	Dark	Diurnal	Dark
Lake Gentau (Central Pyrenees)	June 2018	Subsurface (0.5m)	7.4	0.4 \pm 0.1	0.4 \pm 0.2	23.8 \pm 4.4	<LOD	44.5 \pm 4.4	7.8 \pm 1.9	81.2 \pm 0.8	9.1 \pm 2.6	-0.01 \pm 0.09	0.23 \pm 0.10
		Middle Depth (8m)	8.5	<LOD	<LOD	13.6 \pm 1.2	<LOD	23.3 \pm 0.3	8.7 \pm 3.6	19.5 \pm 0.3	5.2 \pm 0.6	-0.17 \pm 0.01	-0.01 \pm 0.09
		Bottom (17m)	8.7	n.d.	4.3 \pm 0.4	n.d.	<LOD	n.d.	7.0 \pm 3.3	n.d.	<LOD	n.d.	3.25 \pm 0.30
	October 2018	Subsurface (0.5m)	7.2	<LOD	<LOD	23.9 \pm 2.9	<LOD	41.7 \pm 7.8	23.2 \pm 2.8	20.8 \pm 0.1	1.7 \pm 0.1	-0.64 \pm 0.08	<LOD
		Middle Depth (8m)	6.0	0.4 \pm 0.2	0.5 \pm 0.2	<LOD	<LOD	9.1 \pm 7.4	<LOD	<LOD	<LOD	0.08 \pm 0.05	0.11 \pm 0.06
		Bottom (17m)	7.2	n.d.	7.0 \pm 0.4	n.d.	<LOD	n.d.	28.9 \pm 8.6	n.d.	<LOD	n.d.	2.71 \pm 0.17
	June 2019	Subsurface (0.5m)	8.7	0.2 \pm 0.2	<LOD	35.6 \pm 2.2	<LOD	61.5 \pm 7.0	<LOD	16.9 \pm 0.1	<LOD	-0.43 \pm 0.07	<LOD
		Middle Depth (8m)	8.5	<LOD	<LOD	13.6 \pm 0.4	<LOD	31.5 \pm 8.3	<LOD	3.7 \pm 1.4	<LOD	-0.51 \pm 0.01	<LOD
		Bottom (17m)	8.5	n.d.	1.6 \pm 0.1	n.d.	<LOD	n.d.	<LOD	n.d.	<LOD	n.d.	0.29 \pm 0.02
Lake Sabocos (Central Pyrenees)	June 2018	Subsurface (0.5m)	6.3	0.1 \pm 0.0	0.3 \pm 0.0	35.2 \pm 9.7	<LOD	52.8 \pm 15.4	<LOD	n.d.	n.d.	-0.52 \pm 0.18	0.18 \pm 0.01
		Bottom (27m)	6.3	n.d.	0.8 \pm 0.3	n.d.	<LOD	n.d.	<LOD	n.d.	n.d.	n.d.	0.45 \pm 0.19
	October 2018	Subsurface (0.5m)	6.3	0.3 \pm 0.2	0.2 \pm 0.1	9.0 \pm 0.5	<LOD	12.2 \pm 3.7	4.3 \pm 1.7	n.d.	n.d.	-0.06 \pm 0.13	0.10 \pm 0.04
		Bottom (23m)	6.3	n.d.	1.0 \pm 0.4	n.d.	<LOD	n.d.	<LOD	n.d.	n.d.	n.d.	0.75 \pm 0.30
	June 2019	Subsurface (0.5m)	6.8	<LOD	<LOD	12.4 \pm 4.2	<LOD	14.8 \pm 7.5	<LOD	13.2	3.5 \pm 0.1	-0.19 \pm 0.06	<LOD
		Middle Depth (9m)	6.8	0.2 \pm 0.2	0.1 \pm 0.0	8.2 \pm 3.9	6.8 \pm 4.7	22.5 \pm 4.6	24.7 \pm 2.3	3.7 \pm 0.4	2.4 \pm 0.2	-0.14 \pm 0.07	-0.11 \pm 0.08
		Bottom (25m)	6.8	n.d.	0.6 \pm 0.3	n.d.	<LOD	n.d.	<LOD	n.d.	<LOD	n.d.	0.09 \pm 0.04

Table 7-2 (continued)

Lake Arratille (Central Pyrenees)	June 2018	Subsurface (0.5m)	6.0	0.4 ± 0.0	n.d.	<LOD	n.d.	22.6 ± 15.7	n.d.	17.3 ± 2.9	13.6 ± 0.8	0.07 ± 0.01	0.07 ± 0.04
		Middle Depth (6m)	5.3	0.4 ± 0.2	<LOD	<LOD	<LOD	16.4 ± 1.4	7.8 ± 0.6	n.d.	18.7 ± 5.4	n.d.	<LOD
	October 2018	Subsurface (0.5m)	5.3	n.d.	n.d.	n.d.	n.d.	n.d.	n.d.	2.8 ± 0.2	<LOD	n.d.	n.d.
		Bottom (12m)	6.7	n.d.	n.d.	n.d.	n.d.	n.d.	n.d.	n.d.	<LOD	n.d.	n.d.
Lake (Canada) [25]	2002	Oxycline	24	0.6 - 14.8				<12					
Mediterranean Sea [48]	2003 & 2004	Surface Water	24	<0.02 - 6.3	<0.02 - 3.8	3.3 - 24.5	<1.5 - 10.9	1.1 - 16.9				1.0 - 12.3	
Lake Moreno (Argentina) [51]	April 2007	Upper limit of metalimnion (30m depth)	72	27.3 - 50.8	15.4 - 23.5								
Arcachon Bay (France) [47]	2006 & 2007	Water column	24	<0.02 - 0.8	<0.02 - 1.1	1.8 - 11.9	1.3 - 9.0						
Adour river estuary (France) [31]	2007 & 2010	Surface Water	24	<0.01 - 0.4	<0.01 - 0.1	6.6 - 55.3	<2.0 - 22.1	4.3 - 43.5				0.3 - 14.7	-0.02 - 0.00
Lake Uru Uru (Bolivia) [23]	2010 & 2011	Surface Water	24	<0.02 - 4.9	<0.02 - 7.7	<0.02 - 21.0	<0.02 - 20.5	0.1 - 1.0				-0.11 - 0.20	-0.06 - 0.45

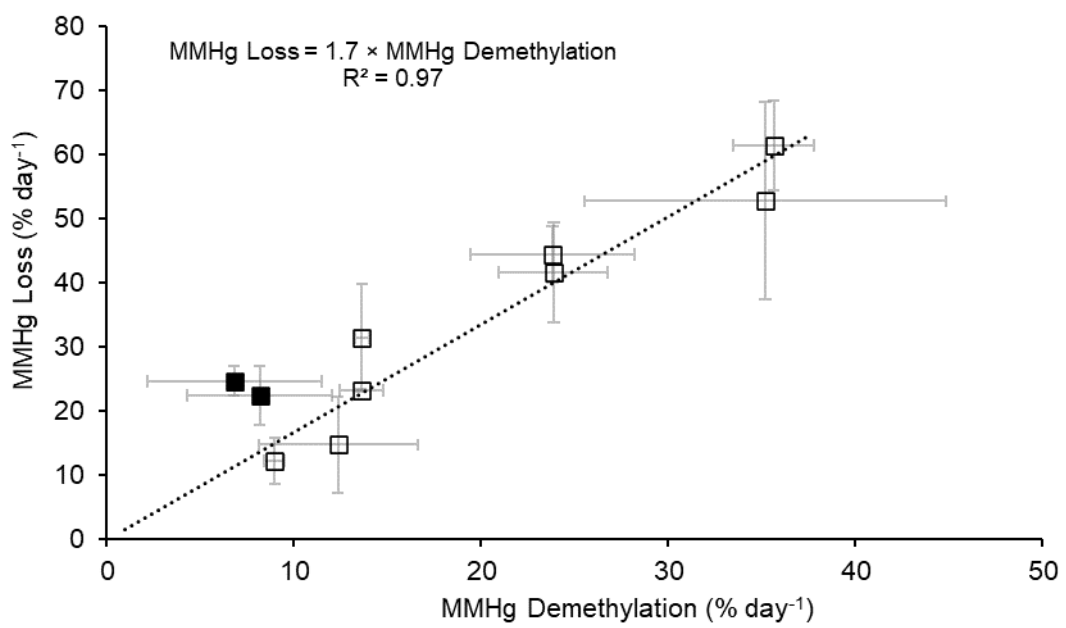


Figure 7-8: Linear relationship between MMHg Demethylation and MMHg Loss. The two black squares, out of the trend, correspond to MMHg demethylation / MMHg loss under dark conditions in the middle depth of Lake Sabocos (June 2019).

7.5. Implication for Hg cycling in alpine lakes

Overall, this work focusing on the water column provides a first global picture of the Hg cycling in the high-altitude lake's ecosystems including various transformations rates measured and estimated volatilization fluxes for the first time. As an example, results obtained from Lake Gentau (**Figure 7-9**) allow us to estimate the fate of Hg in such stratified alpine lakes and to predict the influence of changes in the hydrological cycle, the water column stratification, and the biological productivity due to anthropogenic pressure and/or climate conditions. Indeed, important methylation (290 to 3250 $\text{ng m}^{-3} \text{ day}^{-1}$) occurs in the deepest and anoxic zone of this lake with possible harmful impacts on the biota, while important (photo)demethylation (10 to 640 $\text{ng m}^{-3} \text{ day}^{-1}$) and (photo)reduction (47 to 473 $\text{ng m}^{-3} \text{ day}^{-1}$) leading to Hg evasion (50 to 75 $\text{ng m}^{-2} \text{ day}^{-1}$) take place in the surface of the lake. Direct changes in the alpine ecosystem (e.g. tourism, agropastoralism) or in climatic forcing, such as temperature or light incidence, will have drastic consequences on the Hg cycle at high-altitude lakes. Future in-depth studies must be conducted on these sentinel ecosystems to better constrain fluxes and transformations and obtain a more accurate mass balance of Hg species

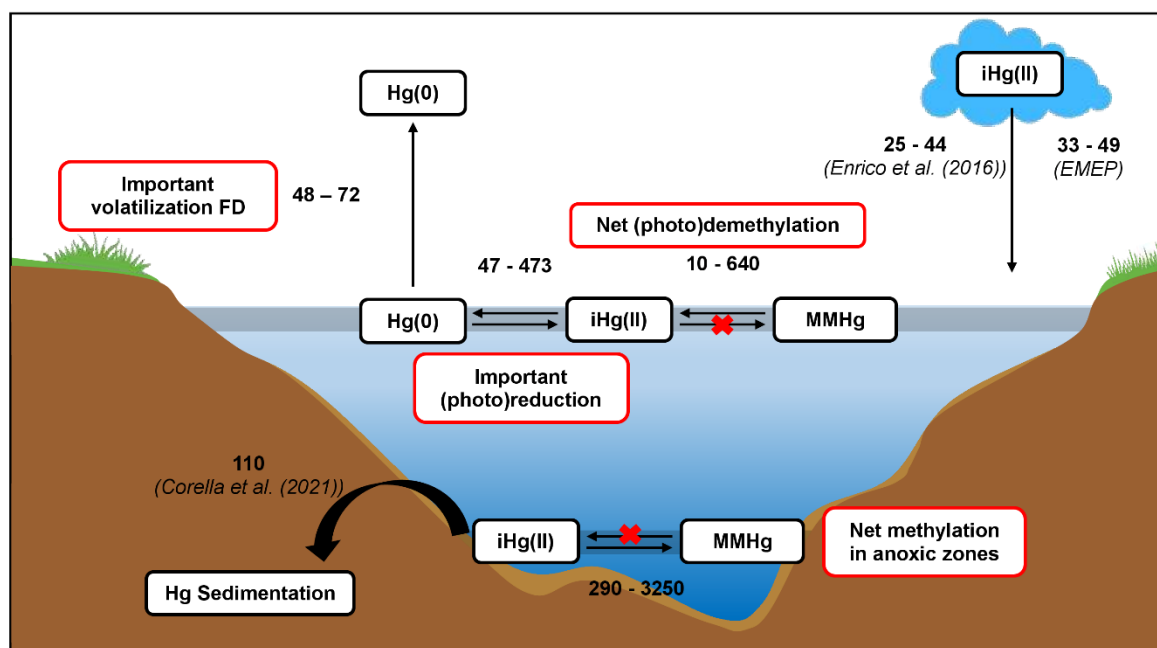


Figure 7-9: Hg transformations ($\text{ng m}^{-3} \text{ day}^{-1}$) and fluxes ($\text{ng m}^{-2} \text{ day}^{-1}$) in Lake Gentau.

7.6. References

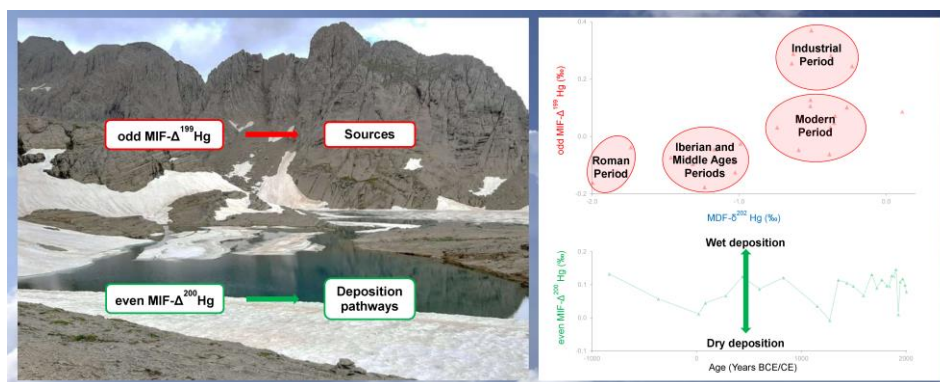
- [1] C.T. Driscoll, R.P. Mason, H.M. Chan, D.J. Jacob, N. Pirrone, Mercury as a Global Pollutant: Sources, Pathways, and Effects, *Environmental Science & Technology*. 47 (2013) 4967–4983. <https://doi.org/10.1021/es305071v>.
- [2] C.A. Cooke, H. Hintelmann, J.J. Ague, R. Burger, H. Biester, J.P. Sachs, D.R. Engstrom, Use and Legacy of Mercury in the Andes, *Environmental Science & Technology*. 47 (2013) 4181–4188. <https://doi.org/10.1021/es3048027>.
- [3] J.P. Corella, M.J. Sierra, A. Garralón, R. Millán, J. Rodríguez-Alonso, M.P. Mata, A.V. de Vera, A. Moreno, P. González-Sampériz, B. Duval, D. Amouroux, P. Vivez, C.A. Cuevas, J.A. Adame, B. Wilhelm, A. Saiz-Lopez, B.L. Valero-Garcés, Recent and historical pollution legacy in high altitude Lake Marboré (Central Pyrenees): A record of mining and smelting since pre-Roman times in the Iberian Peninsula, *Science of The Total Environment*. 751 (2021) 141557. <https://doi.org/10.1016/j.scitotenv.2020.141557>.
- [4] E.M. Sunderland, Mercury Exposure from Domestic and Imported Estuarine and Marine Fish in the U.S. Seafood Market, *Environmental Health Perspectives*. 115 (2007) 235–242. <https://doi.org/10.1289/ehp.9377>.
- [5] H. Hintelmann, K. Keppel-Jones, R.D. Evans, Constants of mercury methylation and demethylation rates in sediments and comparison of tracer and ambient mercury availability, *Environmental Toxicology and Chemistry*. 19 (2000) 2204–2211. <https://doi.org/10.1002/etc.5620190909>.
- [6] N.E. Selin, Global Biogeochemical Cycling of Mercury: A Review, *Annual Review of Environment and Resources*. 34 (2009) 43–63. <https://doi.org/10.1146/annurev.enviro.051308.084314>.
- [7] A.J. Poulain, T. Barkay, Cracking the Mercury Methylation Code, *Science*. 339 (2013) 1280–1281. <https://doi.org/10.1126/science.1235591>.
- [8] K. Sundseth, J.M. Pacyna, E.G. Pacyna, J. Munthe, M. Belhaj, S. Astrom, Economic benefits from decreased mercury emissions: Projections for 2020, *Journal of Cleaner Production*. 18 (2010) 386–394. <https://doi.org/10.1016/j.jclepro.2009.10.017>.
- [9] S.M. Ullrich, T.W. Tanton, S.A. Abdrashitova, Mercury in the Aquatic Environment: A Review of Factors Affecting Methylation, *Critical Reviews in Environmental Science and Technology*. 31 (2001) 241–293. <https://doi.org/10.1080/20016491089226>.
- [10] G.C. Compeau, R. Bartha, Sulfate-Reducing Bacteria: Principal Methylators of Mercury in Anoxic Estuarine Sediment, *Appl Environ Microbiol*. 2 (1985) 498–502.
- [11] R. Bridou, M. Monperrus, P.R. Gonzalez, R. Guyoneaud, D. Amouroux, Simultaneous determination of mercury methylation and demethylation capacities of various sulfate-reducing bacteria using species-specific isotopic tracers, *Environmental Toxicology and Chemistry*. 30 (2011) 337–344. <https://doi.org/10.1002/etc.395>.
- [12] J. Chételat, Mercury in freshwater ecosystems of the Canadian Arctic: Recent advances on its cycling and fate, *Science of the Total Environment*. (2015) 26.
- [13] H.F.V. Braaten, H.A. de Wit, E. Fjeld, S. Rognerud, E. Lydersen, T. Larssen, Environmental factors influencing mercury speciation in Subarctic and Boreal lakes, *Science of The Total Environment*. 476–477 (2014) 336–345. <https://doi.org/10.1016/j.scitotenv.2014.01.030>.
- [14] S.J. Klapstein, N.J. O'Driscoll, Methylmercury Biogeochemistry in Freshwater Ecosystems: A Review Focusing on DOM and Photodemethylation, *Bull Environ Contam Toxicol*. 100 (2018) 14–25. <https://doi.org/10.1007/s00128-017-2236-x>.
- [15] K.R. Rolfhus, H.E. Sakamoto, L.B. Cleckner, R.W. Stoor, C.L. Babiarez, R.C. Back, H. Manolopoulos, J.P. Hurley, Distribution and Fluxes of Total and Methylmercury in Lake Superior, *Environmental Science & Technology*. 37 (2003) 865–872. <https://doi.org/10.1021/es026065e>.
- [16] A.G. Bravo, D.N. Kothawala, K. Attermeyer, E. Tessier, P. Bodmer, J.L.J. Ledesma, J. Audet, J.P. Casas-Ruiz, N. Catalán, S. Cauvy-Fraunié, M. Colls, A. Deininger, V.V. Evtimova, J.A. Fonvielle, T. Fuß, P. Gilbert, S. Herrero Ortega, L. Liu, C. Mendoza-Lera, J. Monteiro, J.-R. Mor, M. Nagler,

- G.H. Niedrist, A.C. Nydahl, A. Pastor, J. Pegg, C. Gutmann Roberts, F. Pilotto, A.P. Portela, C.R. González-Quijano, F. Romero, M. Rulík, D. Amouroux, The interplay between total mercury, methylmercury and dissolved organic matter in fluvial systems: A latitudinal study across Europe, *Water Research*. 144 (2018) 172–182. <https://doi.org/10.1016/j.watres.2018.06.064>.
- [17] P. Sella, C.A. Kelly, J.W.M. Rudd, A.R. MacHutchon, Photodegradation of methylmercury in lakes, *Nature*. 380 (1996) 694–697. <https://doi.org/10.1038/380694a0>.
- [18] L. Camarero, M. Rogora, R. Mosello, N.J. Anderson, A. Barbieri, I. Botev, M. Kernan, J. Kopáček, A. Korhola, A.F. Lotter, G. Muri, C. Postolache, E. Stuchlík, H. Thies, R.F. Wright, Regionalisation of chemical variability in European mountain lakes: *Regionalisation of mountain lakes chemistry*, *Freshwater Biology*. 54 (2009) 2452–2469. <https://doi.org/10.1111/j.1365-2427.2009.02296.x>.
- [19] J. Catalan, L. Camarero, M. Felip, S. Pla, M. Ventura, T. Buchaca, F. Bartumeus, G. de Mendoza, A. Miró, E.O. Casamayor, J.M. Medina-Sánchez, M. Bacardit, M. Altuna, M. Bartrons, D.D. de Quijano, High mountain lakes: extreme habitats and witnesses of environmental changes, *Limnetica*. 25 (2006) 551–584. <https://doi.org/10.23818/limn.25.38>.
- [20] J.P. Corella, A. Saiz-Lopez, M.J. Sierra, M.P. Mata, R. Millán, M. Morellón, C.A. Cuevas, A. Moreno, B.L. Valero-Garcés, Trace metal enrichment during the Industrial Period recorded across an altitudinal transect in the Southern Central Pyrenees, *Science of The Total Environment*. 645 (2018) 761–772. <https://doi.org/10.1016/j.scitotenv.2018.07.160>.
- [21] S. Guédron, D. Point, D. Acha, S. Bouchet, P.A. Baya, E. Tessier, M. Monperrus, C.I. Molina, A. Groleau, L. Chauvaud, J. Thebault, E. Amice, L. Alanoca, C. Duwig, G. Uzu, X. Lazzaro, A. Bertrand, S. Bertrand, C. Barbraud, K. Delord, F.M. Gibon, C. Ibanez, M. Flores, P. Fernandez Saavedra, M.E. Ezpinoza, C. Heredia, F. Rocha, C. Zepita, D. Amouroux, Mercury contamination level and speciation inventory in Lakes Titicaca & Uru-Uru (Bolivia): Current status and future trends, *Environmental Pollution*. 231 (2017) 262–270. <https://doi.org/10.1016/j.envpol.2017.08.009>.
- [22] S. Guédron, D. Achá, S. Bouchet, D. Point, E. Tessier, C. Heredia, S. Rocha-Lupa, P. Fernandez-Saavedra, M. Flores, S. Bureau, I. Quino-Lima, D. Amouroux, Accumulation of Methylmercury in the High-Altitude Lake Uru Uru (3686 m a.s.l, Bolivia) Controlled by Sediment Efflux and Photodegradation, *Applied Sciences*. 10 (2020) 7936. <https://doi.org/10.3390/app10217936>.
- [23] L. Alanoca, D. Amouroux, M. Monperrus, E. Tessier, M. Goni, R. Guyoneaud, D. Acha, C. Gassie, S. Audry, M.E. Garcia, J. Quintanilla, D. Point, Diurnal variability and biogeochemical reactivity of mercury species in an extreme high-altitude lake ecosystem of the Bolivian Altiplano, *Environmental Science and Pollution Research*. 23 (2016) 6919–6933. <https://doi.org/10.1007/s11356-015-5917-1>.
- [24] N. Maruszczak, C. Larose, A. Dommergue, S. Paquet, J.-S. Beaulne, R. Maury-Brachet, M. Lucotte, R. Nedjai, C.P. Ferrari, Mercury and methylmercury concentrations in high altitude lakes and fish (Arctic charr) from the French Alps related to watershed characteristics, *Science of The Total Environment*. 409 (2011) 1909–1915. <https://doi.org/10.1016/j.scitotenv.2011.02.015>.
- [25] C.S. Eckley, H. Hintelmann, Determination of mercury methylation potentials in the water column of lakes across Canada, *Science of The Total Environment*. 368 (2006) 111–125. <https://doi.org/10.1016/j.scitotenv.2005.09.042>.
- [26] E. Gascón Díez, J.-L. Loizeau, C. Cosio, S. Bouchet, T. Adatte, D. Amouroux, A.G. Bravo, Role of Settling Particles on Mercury Methylation in the Oxic Water Column of Freshwater Systems, *Environmental Science & Technology*. 50 (2016) 11672–11679. <https://doi.org/10.1021/acs.est.6b03260>.
- [27] C.A. Emmerton, C.A. Cooke, G.R. Wentworth, J.A. Graydon, A. Ryjkov, A. Dastoor, Total Mercury and Methylmercury in Lake Water of Canada's Oil Sands Region, *Environmental Science & Technology*. 52 (2018) 10946–10955. <https://doi.org/10.1021/acs.est.8b01680>.
- [28] A.G. Bravo, S. Bouchet, J. Tolu, E. Björn, A. Mateos-Rivera, S. Bertilsson, Molecular composition of organic matter controls methylmercury formation in boreal lakes, *Nature Communications*. 8 (2017). <https://doi.org/10.1038/ncomms14255>.
- [29] C. Meuleman, M. Leermakers, W. Baeyens, Mercury speciation in Lake Baikal, *Water, Air, & Soil Pollution*. 80 (1995) 539–551. <https://doi.org/10.1007/BF01189704>.

- [30] E.A. Malczyk, B.A. Branfireun, Mercury in sediment, water, and fish in a managed tropical wetland-lake ecosystem, *Science of The Total Environment*. 524–525 (2015) 260–268. <https://doi.org/10.1016/j.scitotenv.2015.04.015>.
- [31] A. Sharif, M. Monperrus, E. Tessier, S. Bouchet, H. Pinaly, P. Rodriguez-Gonzalez, P. Maron, D. Amouroux, Fate of mercury species in the coastal plume of the Adour River estuary (Bay of Biscay, SW France), *Science of The Total Environment*. 496 (2014) 701–713. <https://doi.org/10.1016/j.scitotenv.2014.06.116>.
- [32] J. Cavalheiro, C. Sola, J. Baldanza, E. Tessier, F. Lestremau, F. Botta, H. Preud'homme, M. Monperrus, D. Amouroux, Assessment of background concentrations of organometallic compounds (methylmercury, ethyllead and butyl- and phenyltin) in French aquatic environments, *Water Research*. 94 (2016) 32–41. <https://doi.org/10.1016/j.watres.2016.02.010>.
- [33] R. Adrian, C.M. O'Reilly, H. Zagarese, S.B. Baines, D.O. Hessen, W. Keller, D.M. Livingstone, R. Sommaruga, D. Straile, E. Van Donk, G.A. Weyhenmeyer, M. Winder, Lakes as sentinels of climate change, *Limnology and Oceanography*. 54 (2009) 2283–2297. https://doi.org/10.4319/lo.2009.54.6_part_2.2283.
- [34] UNEP, Global mercury assessment 2013: sources, emissions, releases and environmental transport, UNEP Chemicals Branch, Geneva, Switzerland, 2013.
- [35] D. Obrist, J.L. Kirk, L. Zhang, E.M. Sunderland, M. Jiskra, N.E. Selin, A review of global environmental mercury processes in response to human and natural perturbations: Changes of emissions, climate, and land use, *Ambio*. 47 (2018) 116–140. <https://doi.org/10.1007/s13280-017-1004-9>.
- [36] M. Bacardit, L. Camarero, Atmospherically deposited major and trace elements in the winter snowpack along a gradient of altitude in the Central Pyrenees: The seasonal record of long-range fluxes over SW Europe, *Atmospheric Environment*. 44 (2010) 582–595. <https://doi.org/10.1016/j.atmosenv.2009.06.022>.
- [37] L. Camarero, M. Bacardit, A. de Diego, G. Arana, Decadal trends in atmospheric deposition in a high elevation station: Effects of climate and pollution on the long-range flux of metals and trace elements over SW Europe, *Atmospheric Environment*. 167 (2017) 542–552. <https://doi.org/10.1016/j.atmosenv.2017.08.049>.
- [38] M. Bueno, B. Duval, E. Tessier, A. Romero-Rama, L. Kortazar, L.A. Fernandez, A. De Diego, D. Amouroux, Selenium distribution and speciation in waters of pristine alpine lakes from central-western Pyrenees (France-Spain), *Environ. Sci.: Processes Impacts*. (2022) 10.1039/D1EM00430A. <https://doi.org/10.1039/D1EM00430A>.
- [39] M. Enrico, G.L. Roux, N. Maruszczak, L.-E. Heimbürger, A. Claustres, X. Fu, R. Sun, J.E. Sonke, Atmospheric Mercury Transfer to Peat Bogs Dominated by Gaseous Elemental Mercury Dry Deposition, *Environmental Science & Technology*. 50 (2016) 2405–2412. <https://doi.org/10.1021/acs.est.5b06058>.
- [40] N. Maruszczak, C. Larose, A. Dommergue, E. Yumvihoze, D. Lean, R. Nedjai, C. Ferrari, Total mercury and methylmercury in high altitude surface snow from the French Alps, *Science of The Total Environment*. 409 (2011) 3949–3954. <https://doi.org/10.1016/j.scitotenv.2011.06.040>.
- [41] C.H. Lamborg, C.R. Hammerschmidt, K.L. Bowman, G.J. Swarr, K.M. Munson, D.C. Ohnemus, P.J. Lam, L.-E. Heimbürger, M.J.A. Rijkenberg, M.A. Saito, A global ocean inventory of anthropogenic mercury based on water column measurements, *Nature*. 512 (2014) 65–68. <https://doi.org/10.1038/nature13563>.
- [42] W.F. Fitzgerald, C.H. Lamborg, C.R. Hammerschmidt, Marine Biogeochemical Cycling of Mercury, *Chemical Reviews*. 107 (2007) 641–662. <https://doi.org/10.1021/cr050353m>.
- [43] Z. Santolaria, T. Arruebo, J.S. Urieta, F.J. Lanaja, A. Pardo, J. Matesanz, C. Rodriguez-Casals, Hydrochemistry dynamics in remote mountain lakes and its relation to catchment and atmospheric features: the case study of Sabocos Tarn, Pyrenees, *Environmental Science and Pollution Research*. 22 (2015) 231–247. <https://doi.org/10.1007/s11356-014-3310-0>.
- [44] P. Lei, L.M. Nunes, Y.-R. Liu, H. Zhong, K. Pan, Mechanisms of algal biomass input enhanced microbial Hg methylation in lake sediments, *Environment International*. 126 (2019) 279–288. <https://doi.org/10.1016/j.envint.2019.02.043>.

- [45] L. Camarero, J. Catalan, Atmospheric phosphorus deposition may cause lakes to revert from phosphorus limitation back to nitrogen limitation, *Nature Communications*. 3 (2012) 1118. <https://doi.org/10.1038/ncomms2125>.
- [46] PNP, ETUDE PISCICOLE DES LACS D'AYOUS, (2013).
- [47] S. Bouchet, D. Amouroux, P. Rodriguez-Gonzalez, E. Tessier, M. Monperrus, G. Thouzeau, J. Clavier, E. Amice, J. Deborde, S. Bujan, J. Grall, P. Anschutz, MMHg production and export from intertidal sediments to the water column of a tidal lagoon (Arcachon Bay, France), *Biogeochemistry*. 114 (2013) 341–358. <https://doi.org/10.1007/s10533-012-9815-z>.
- [48] M. Monperrus, E. Tessier, D. Amouroux, A. Leynaert, P. Huonnic, O.F.X. Donard, Mercury methylation, demethylation and reduction rates in coastal and marine surface waters of the Mediterranean Sea, *Marine Chemistry*. 107 (2007) 49–63. <https://doi.org/10.1016/j.marchem.2007.01.018>.
- [49] J.P. Corella, A. Saiz-Lopez, M.J. Sierra, M.P. Mata, R. Millán, M. Morellón, C.A. Cuevas, A. Moreno, B.L. Valero-Garcés, Trace metal enrichment during the Industrial Period recorded across an altitudinal transect in the Southern Central Pyrenees, *Science of The Total Environment*. 645 (2018) 761–772. <https://doi.org/10.1016/j.scitotenv.2018.07.160>.
- [50] J.P. Corella, B.L. Valero-Garcés, F. Wang, A. Martínez-Cortizas, C.A. Cuevas, A. Saiz-Lopez, 700 years reconstruction of mercury and lead atmospheric deposition in the Pyrenees (NE Spain), *Atmospheric Environment*. 155 (2017) 97–107. <https://doi.org/10.1016/j.atmosenv.2017.02.018>.
- [51] S. Ribeiro Guevara, C.P. Queimaliños, M. del C. Diéguez, M. Arribére, Methylmercury production in the water column of an ultraoligotrophic lake of Northern Patagonia, Argentina, *Chemosphere*. 72 (2008) 578–585. <https://doi.org/10.1016/j.chemosphere.2008.03.011>.

8. Mercury stable isotopes in Pyrenean lacustrine archives: influence of human pollution and climate variability during the Late Holocene



8.1. Abstract

Mercury (Hg) isotopic composition in lake sediments reflects both Hg sources and pathways, including atmospheric trends and watershed-lake interactions. In this work, two sedimentary archives from high alpine (Lake Marboré, 2612 m asl) and mid-mountain (Lake Estanya, 670 m asl) in the Southern Central Pyrenean lakes have been investigated. Temporal trends in Hg accumulation rates (HgARs) show a consistent evolution with a progressive increase since the 16th century likely mirroring the mercury production in Almadén Hg mines (Southern Spain). Shifts in Hg isotope values confirm this trend, with an Industrial Period characterized by higher odd MIF- $\Delta^{199}\text{Hg}$ values compared to pre-16th century. The distinct watershed characteristics of the two investigated lakes and the climatic variations (warm vs cold periods) during the last millennia are also reflected in Hg isotopes even MIF ($\Delta^{200}\text{Hg}$) variability. The studied sedimentary sequences exhibit a significant positive shift for $\Delta^{199}\text{Hg}$ in lake sediment, highlighting the relative contribution of dry and wet depositions in both types of ecosystems but also the potential photoreduction and re-emission of deposited Hg in alpine lakes. The agreement between the high-altitude Lake Marboré Hg record and other Pyrenean Hg peatbog archives confirms the regional increasing trends in Hg levels in Southwestern Europe.

Keywords:

Mercury; Isotopes; Lake Sediments; Oligotrophic; Pyrenees

8.2. Introduction

Mercury (Hg) is a global pollutant present in all surface compartments of the Earth that affects human and ecosystem health [1–3]. Primary anthropogenic Hg emissions greatly exceed natural sources by a factor of 4-6 [4,5], increasing Hg in reservoirs during the last millennia. The global annual mean lifetime of Hg(0) against the net photochemical oxidation is in the range of several months to over a year [6], and recent findings on atmospheric Hg reduction processes have postulated that global atmospheric Hg lifetime could increase by a factor 2 [7,8]. Natural primary emission of Hg from geogenic sources consists in the release of Hg from the continental crust through natural weathering, hydrothermal activities, natural fires and volcanic degassing. Anthropogenic emissions include the use of fossil fuels (mainly coal burning), artisanal and small-scale gold mining, iron and non-ferrous metals production, cement production, oil refining and wastes from consumer products [9].

Mercury concentration records derived from natural archives such as lake sediments [10], peat [11] and ice cores [12,13] have already highlighted the influence of anthropogenic activities on the atmospheric Hg deposition with a clear increase since Roman times. Climate has also a significant role in controlling Hg concentration in sediments before the human imprint in the Hg cycle [14]. *Martínez-Cortizas et al.* [15] proposed the use of the thermal lability of the accumulated Hg in a peat bog as a tool for quantitative paleotemperature reconstruction: to our knowledge, this is the only relevant study relating such conclusion, and none exists for lakes.

The various environmental archives display different enrichment factor depending on their nature or location [5,16]. Indeed, local to regional processes related to emission, transport, redox chemistry, deposition and re-emission play a key role in the complex biogeochemical cycle of Hg [4,17]. On one hand, ombrotrophic mires record the atmospheric Hg pollution [15,18]. Nevertheless, they may suffer from aerial exposure and diagenetic processes altering mercury levels [19–21]. Mercury losses have also been reported recently in boreal peatland [22], mainly as a result of gaseous elemental Hg evasion and through THg stream discharge: both phenomena may have impact on the estimation of historical Hg accumulation rates from peat profiles. On the other hand, lacustrine sedimentary sequences do not suffer from apparent losses of total Hg concentration in the sediment [23]. However, they often show a mixed-signal between run-off and atmospheric Hg inputs [24]. Furthermore, metal remobilization and redox changes in the water column may affect Hg concentrations [19]. Among lacustrine archives, high-altitude lakes have well demonstrated their use as a proxy of past global atmospheric Hg pollution since i) they have small watersheds, and they are scarcely affected by local anthropogenic activities so they can be considered conservative ecosystems over time; ii) they are emplaced in regional convergence regions of atmospheric pollutants and iii) their oligotrophic status reduces *in-situ* transformations [17].

Mercury isotopic composition offers new insights to Hg cycling processes in the environment. Mercury has seven stable isotopes that undergo mass dependent fractionation (MDF, $\delta^{202}\text{Hg}$) during both kinetic and equilibrium reactions as a result of many physical, chemical or biological processes such as evaporation, microbial reduction and methylation / demethylation, photochemical reactions, trophic and metabolic processes [25]. Mass independent fractionation (MIF) also occurs for Hg isotopes, especially

during light-induced reactions. While important odd-MIF ($\Delta^{199}\text{Hg}$, $\Delta^{201}\text{Hg}$) is primarily related to photochemical reactions such as photoreduction of both Hg(II) and MeHg [26], the mechanism responsible of positive even-MIF ($\Delta^{200}\text{Hg}$, $\Delta^{204}\text{Hg}$) in rainfall and snow is not understood yet [27,28]. Several studies have recorded historical variations of Hg isotopic fingerprints in lake sediments [28–35], ice core [36] and peat cores [37,38]. *Enrico et al.* [37,38] used the distinct, conservative even-MIF signatures of rainfall and atmospheric gaseous Hg(0) to discriminate the main deposition pathways in two remote peatlands and reconstructed past atmospheric Hg levels. Dry deposition, characterized by slightly negative $\Delta^{200}\text{Hg}$ [37,39], involves foliar uptake of Hg(0) [40], whereas wet deposition, with positive $\Delta^{200}\text{Hg}$ [27,37], involves the scavenging of gas-phase and aerosol-phase Hg(II) by cloud droplets. For MDF and odd-MIF, a widely observed significant change in the Hg isotopic signatures occurs in sedimentary archives for periods corresponding to the beginning of anthropogenic activities and exhibits increasing $\delta^{202}\text{Hg}$ and $\Delta^{199}\text{Hg}$ values either due to local or regional industrial development [28,30,34–36,38].

In the Pyrenees, several recent studies have described changes in Hg deposition alpine lakes [17,41,42] and peatlands [37,38] during the last millennia. Nevertheless, sources and Hg biogeochemical cycling in lacustrine environments are still poorly understood due to the lack of Hg isotopic analyses, especially in remote areas with limited direct human influence.

In this study, we have selected two of the best dated lacustrine sedimentary sequences from Southern Central Pyrenees along an altitudinal gradient to test climate, anthropogenic and site-specific forcing in Hg deposition during the last 4 kilo annum (ka). We also have compared the Hg lacustrine records with nearby Hg peatbogs to understand the different Hg depositional processes affecting both type of alpine ecological systems. Mercury concentration and isotopic analyses in these lacustrine records are used to determine the main Hg deposition pathways, Hg pollution sources and evaluate the use of Hg isotopes as a paleohydrological and paleoclimate proxy and indicator of variable human impact.

8.3. Material and Methods

8.3.1. Study sites

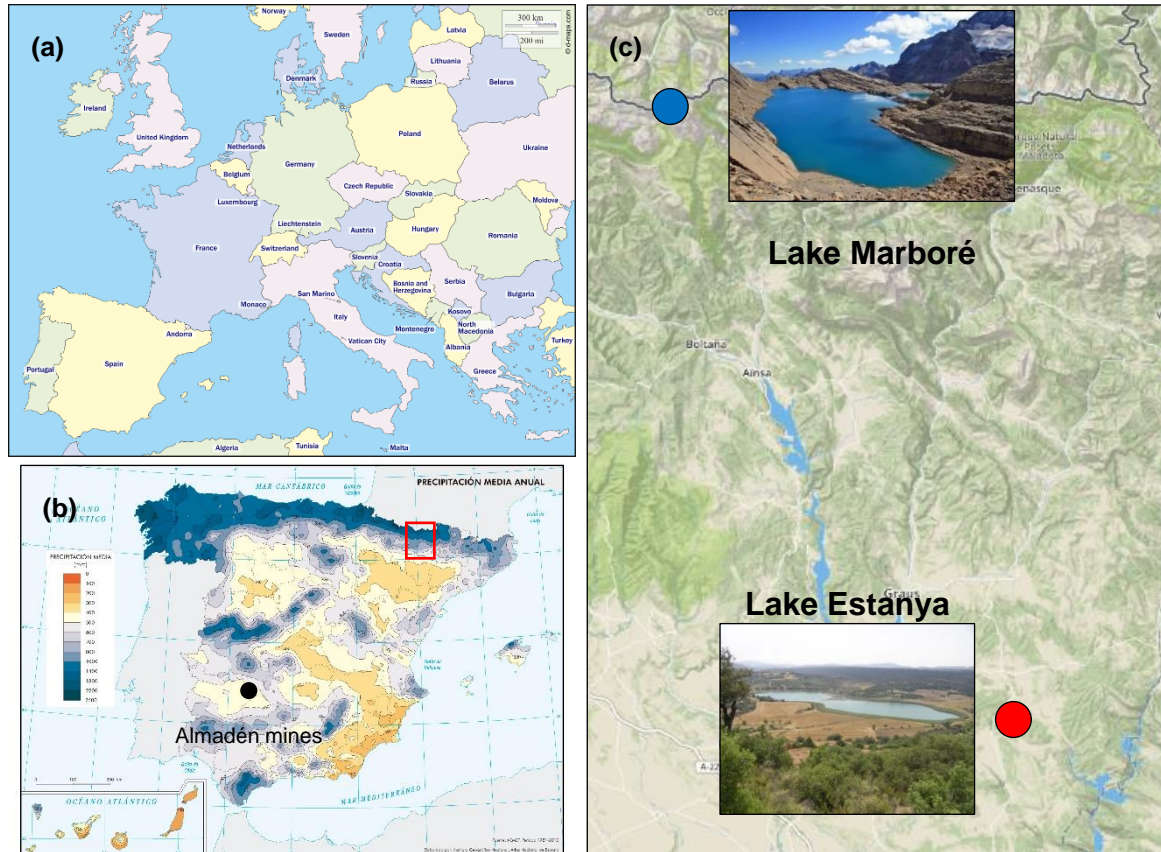


Figure 8-1: Study sites: (a) Map of Europe (https://d-maps.com/carte.php?num_car=69122&lang=fr); (b) Average annual precipitation map of Spain (<http://atlasnacional.ign.es/wane/Clima>); (c) Location of Lake Marboré (42°41'N; 0°2'E, 2612 m asl) and Lake Estanya (42°02'N; 0°32'E, 670 m asl) (Pictures by J.P. Corella).

The two studied lacustrine ecosystems (**Figure 8-1**), Lake Marboré (42°41'N; 0°2'E, 2612 m asl) and Lake Estanya (42°02'N; 0°32'E, 670 m asl), are located in the Southern Central Pyrenees. They show similarities with small surface lake areas of 14.3 and 18.8 ha, small-sized watersheds of 137 and 106 ha and maximum depths of 30 and 24 m in lakes Marboré and Estanya, respectively [43,44]. The watersheds of both lakes are emplaced over carbonate bedrocks [17]. Bioclimatic conditions in both lakes greatly differ with lower temperatures and higher precipitation in Lake Marboré (mean annual temperatures and precipitation of 5°C and 2000 mm) compared to Lake Estanya (mean annual temperatures and precipitation of 14°C and 470 mm) [44].

Lake Marboré is a high-alpine lake located above the tree line. Therefore, the vegetation cover around the lake is very scarce with only a few remains of alpine rocky grass species [45]. The lake's hydrology is controlled by precipitation/evaporation balance, meltwater input along a small NW inlet, outputs

through a surface outlet located in the southern area, and some groundwater fluxes [44,46]. It is a cold dimictic and ultra-oligotrophic lake with alkaline waters. Ice and snow cover Lake Marboré surface 9-10 months per year [47].

Lake Estanya is a karstic lake emplaced in Triassic carbonate, marls and claystones [48,49]. It is a monomictic lake with brackish and oligotrophic waters [49]. Vegetation in the watershed consists of scrublands and oak forest in the high-elevated areas while the lowlands are mostly covered by barley cultivation [49].

8.3.2. Sediment sequence and age-depth models

Both lake sequences have been intensively studied from sedimentological, geochemical and palynological points of view [50] and have robust ^{14}C and ^{210}Pb and ^{137}Cs – based age models. Sediment cores were retrieved from the deepest area of the studied lakes using a UWITEC (MAR11-1U sediment core, 27 m depth, 2011) [51] and Kulleberg (LEG04-1K sediment core, 24 m depth, 2004) [49] floating platforms for Lake Marboré and Lake Estanya respectively. UWITEC gravity cores were additionally collected to preserve the uppermost sediments and the water-sediment interphase in both lakes (MAR11-1G-1U, LEG1A-1M sediment cores) [43,51].

The age-depth models in the two lakes are based on ^{137}Cs , ^{210}Pb and Accelerator Mass Spectrometry (AMS) ^{14}C radiometric dating techniques. The Holocene chronology for the Lake Marboré and Estanya sediment sequences was developed using 10 and 11 AMS ^{14}C dates respectively. ^{210}Pb and ^{137}Cs radiometric dating was applied for the recent sediment in both lakes. Mean annual sedimentation rate (SR) in Lake Marboré was constant during the Late Holocene (SR $\approx 0.6 \text{ mm yr}^{-1}$) while SR in Lake Estanya ranged from 0.2 to 2.1 mm yr^{-1} [43,45,49,51].

The selected section for Marboré Lake spans the last 3 ka (27 samples selected for this study) and it is composed of laminated to banded fine silts composed of silicate minerals and very low organic and carbonate content [51]. The Estanya section spans the last 4 ka (14 samples selected for this study) and includes carbonate-rich silts of mainly detrital origin deposited under relatively high lake level conditions and increased runoff and organic-rich facies with gypsum formed under shallower conditions [43,49]. The reconstructed depositional evolution reflects the impact of climate variability in both lakes and a strong impact of human activities (deforestation, agriculture) in Estanya at least since the 10th century.

8.3.3. Mercury concentrations and fluxes

Mercury analyses were carried out in discrete samples retrieved downcore in the studied cores (27 samples selected for Marboré and 14 samples selected for Estanya). Total Hg concentration measurements were carried out by Cold Vapor Atomic Absorption Spectrophotometry (CV-AAS) using an Advanced Mercury Analyzer (AMA 254, LECO Company). Certified reference materials (CRM) were used to determine the accuracy and precision of the Hg measurements. Certified reference material (CRM) was used to determine the accuracy and precision of the Hg measurements (NCS DC87103, soil, $[\text{Hg}] = 0.017 \pm 0.003 \text{ mg kg}^{-1}$). The repeatability was $S_r \leq 15\%$ and the relative uncertainty associated

with the method ($k = 2$) was $\pm 20\%$. All analyses were run at least in triplicate. Total metal concentrations are expressed in $\mu\text{g g}^{-1}$ of dry weight sediment.

Mass accumulation rates for Hg depositional fluxes estimation (HgAR) were calculated as the product of their concentration in the sediment, the dry bulk density of the sediment, and sedimentation rates according to *Givelet et al.* [50].

8.3.4. Mercury stable isotopes composition

The analytical protocol for the determination of Hg isotopes in sediments is derived from various studies previously conducted [30,52]. Before Hg isotopic analysis, sediment samples (0.5 - 1 g) were first pre-digested overnight at room temperature in a Teflon tube using 3 mL of nitric acid (65 %, INSTRA quality). After addition of 1 mL of hydrochloric acid (37 %, INSTRA quality), the extraction of Hg was carried out using a Hotblock at 85 °C (6 h plus 3 h after the addition of about 1.3 mL of hydrogen peroxide (30 %, ULTREX quality)). Then, an aliquot of about 1.5 mL was recovered in an Eppendorf Safe-Lock tube and centrifuged at 14 500 rpm for 90 seconds. The supernatant was collected and diluted for isotopic measurements (10 % HNO_3 , 2 % HCl, either 0.5 or 1 $\mu\text{g kg}^{-1}$ of Hg depending on the analytical session). Hg isotopic composition was determined using a cold-vapour generator (CVG) with SnCl_2 reduction coupled with MC-ICPMS (Nu Instruments). NIST SRM-997 thallium standard solution was used for mass-bias correction. Sample standard bracketing with NIST SRM-3133 was conducted to report Hg isotopic values as delta notation to allow inter-laboratory comparisons [53] :

Equation 8-1

$$\delta^{xxx}\text{Hg} (\text{‰}) = \left[\left(\frac{\left(\frac{^{xxx}\text{Hg}}{^{198}\text{Hg}} \right)_{\text{sample}}}{\left(\frac{^{xxx}\text{Hg}}{^{198}\text{Hg}} \right)_{\text{NIST 3133}}} \right) - 1 \right] \times 1000$$

where xxx is the mass of each Hg isotope between 199 and 204, ^{198}Hg is used as a reference because it is one of the lighters Hg isotopes (^{196}Hg has a too-small abundance).

Mass Independent Fractionation (MIF) anomalies are expressed with the Δ notation, quantifying the difference between the measured isotope ratio $\delta^{xxx}\text{Hg}$ and the theoretical value $\delta^{xxx}\text{Hg}$, calculated based on the Mass Dependent Fractionation (MDF) fractionation laws. As for the δ notation, we report Hg MIF anomalies as proposed by Blum and Bergquist ¹ to ensure data comparison:

Equation 8-2

$$\Delta^{199}\text{Hg} = \delta^{199}\text{Hg}_{\text{exp}} - \delta^{202}\text{Hg}_{\text{theo}} \times 0.2520$$

$$\Delta^{200}\text{Hg} = \delta^{200}\text{Hg}_{\text{exp}} - \delta^{202}\text{Hg}_{\text{theo}} \times 0.5024$$

$$\Delta^{201}\text{Hg} = \delta^{201}\text{Hg}_{\text{exp}} - \delta^{202}\text{Hg}_{\text{theo}} \times 0.7520$$

$$\Delta^{204}\text{Hg} = \delta^{204}\text{Hg}_{\text{exp}} - \delta^{202}\text{Hg}_{\text{theo}} \times 1.4930$$

To validate each analytical session, reference material NIST-8610 (formerly UM-Almadén) was analyzed regularly along with samples (n=32) (**Table 8-1**). The uncertainty on Hg isotope ratios is evaluated using multiple analyses of a procedural CRM (IAEA-405, estuarine sediment) prepared using a procedure similar to samples. Results obtained are shown in **Table 8-1** and are in good agreement with previously published values. In this manuscript, all reported analytical uncertainties for Hg isotopic values are presented as 2SD of IAEA-405.

Sample standard bracketing with NIST SRM-3133 also allowed us to calculate a Hg recovery related to the extraction of Hg from the sediment samples [30,54]. Recoveries averaged $103 \pm 10 \%$ (n=15) and $98 \pm 10 \%$ (n=14), respectively for Lake Marboré and Lake Estanya.

Table 8-1: Mean values (\pm 2SD) of Hg isotopic composition obtained for reference materials NIST-8610 (UM-Almadén), IAEA-405 (estuarine sediment) and NIST-1944 (marine sediment), and for triplicate Hg extraction for lakes Marboré and Estanya.

Sample	Reference	n	$\delta^{204}\text{Hg}$ ‰	$\delta^{202}\text{Hg}$ ‰	$\delta^{201}\text{Hg}$ ‰	$\delta^{200}\text{Hg}$ ‰	$\delta^{199}\text{Hg}$ ‰	$\Delta^{204}\text{Hg}$ ‰	$\Delta^{201}\text{Hg}$ ‰	$\Delta^{200}\text{Hg}$ ‰	$\Delta^{199}\text{Hg}$ ‰
NIST RM 8610	This study	32	-0.78 \pm 0.18	-0.52 \pm 0.12	-0.42 \pm 0.12	-0.26 \pm 0.10	-0.12 \pm 0.14	0.00 \pm 0.14	-0.03 \pm 0.07	0.00 \pm 0.06	-0.01 \pm 0.12
	Reference values		-0.82 \pm 0.07	-0.56 \pm 0.03	-0.46 \pm 0.02	-0.27 \pm 0.01	-0.17 \pm 0.01	-	-0.04 \pm 0.01	0.00 \pm 0.01	-0.03 \pm 0.02
IAEA 405	This study	7	-0.57 \pm 0.15	-0.39 \pm 0.09	-0.30 \pm 0.13	-0.20 \pm 0.08	-0.11 \pm 0.06	0.02 \pm 0.08	0.00 \pm 0.08	0.00 \pm 0.05	-0.01 \pm 0.06
	Jiménez-Moreno et al. [52]	14	-0.62 \pm 0.21	-0.41 \pm 0.16	-0.31 \pm 0.19	-0.19 \pm 0.12	-0.12 \pm 0.11	-	-0.01 \pm 0.09	0.01 \pm 0.06	-0.02 \pm 0.08
	Guédron et al. [30]	14	-0.50 \pm 0.17	-0.30 \pm 0.11	-0.29 \pm 0.07	-0.22 \pm 0.11	-0.17 \pm 0.15	-	-0.06 \pm 0.06	-0.07 \pm 0.13	-0.10 \pm 0.15
NIST 1944	IPREM (2011-2015)	15	-0.68 \pm 0.17	-0.44 \pm 0.14	-0.32 \pm 0.18	-0.23 \pm 0.13	-0.11 \pm 0.12	-	0.01 \pm 0.12	-0.01 \pm 0.10	-0.00 \pm 0.11
	Sherman and Blum [55]	9	-	-0.44 \pm 0.12	-0.34 \pm 0.08	-0.22 \pm 0.05	-0.10 \pm 0.04	-	-0.01 \pm 0.05	0.00 \pm 0.03	0.01 \pm 0.04
	Sonke et al. [56]	3	-	-0.48 \pm 0.29	-0.38 \pm 0.18	-0.21 \pm 0.23	-0.10 \pm 0.02	-	-0.01 \pm 0.04	0.04 \pm 0.09	0.02 \pm 0.05
	Ma et al. [57]	5	-	-0.45 \pm 0.06	-	-	-	-	-	-	-0.03 \pm 0.02
	Biswas et al. [58]	10	-	-0.42 \pm 0.07	-	-	-	-	-0.02 \pm 0.01	-	-0.02 \pm 0.01
Maboré	This study	3	-1.07 \pm 0.11	-0.59 \pm 0.15	-0.48 \pm 0.10	-0.21 \pm 0.10	-0.20 \pm 0.10	-0.18 \pm 0.18	-0.03 \pm 0.05	0.09 \pm 0.07	-0.05 \pm 0.09
Estanya	This study	3	-2.91 \pm 0.15	-1.98 \pm 0.17	-1.57 \pm 0.16	-1.00 \pm 0.08	-0.57 \pm 0.05	0.04 \pm 0.14	-0.08 \pm 0.03	-0.01 \pm 0.01	-0.07 \pm 0.08

8.4. Results and Discussion

8.4.1. Variability of mercury accumulation in lacustrine sediments

In both lakes sequences, three distinct periods of Hg deposition can be distinguished (**Figure 8-2**).

2000 BCE – 1500 CE. In Lake Marboré, background values of Hg fluxes average $14.4 \pm 1.7 \mu\text{g m}^{-2} \text{y}^{-1}$ (n=12) whereas Lake Estanya recorded lower Hg fluxes of about $4.8 \pm 1.0 \mu\text{g m}^{-2} \text{y}^{-1}$ (n=5). It is worth noting that these are not natural background values since Hg production has been occurring intermittently since the Roman Period [59]. Lake Estanya record is consistent with other pre-anthropogenic Hg fluxes recorded in North America lakes [10,28,34] and peatland from Central Pyrenees [38]. Lake Marboré higher HgAR has also been reported in nearby Lake Montcortés with around $30 \mu\text{g m}^{-2} \text{y}^{-1}$ [41] and in Lake August with around $13.2 \mu\text{g m}^{-2} \text{y}^{-1}$ [10] for the pre-anthropogenic period. High HgAR in some Pyrenean lakes (Marboré, Montcortés) could be related to specific characteristics of the catchments and geographical factors favouring Hg deposition. The Marboré watershed consists of bare rock and very scarce vegetation while forest and agricultural fields surround Lake Estanya (**Figure 8-1**). Moreover, Lake Marboré is ice-covered about 9-10 months per year [47], and snow is known to be a large reservoir that accumulates Hg until melting [60]. Inputs from accumulated snow from the catchment and the lake surface could lead to an important HgAR during the sudden annual snowmelt in summer [61]. This may also promote efficient Hg transport to the lake bottom with very little Hg recycling and re-emission from water column processes. Enrichment factors of both Lake Maboré and Lake Estanya [17] are comparable with other records cited above, supporting the fact that this difference in HgAR could be related with lake and catchment specific features rather than sources or deposition fluxes.

1500 – 1850 CE. This Modern Period (MP) is characterized by a progressive increase in HgAR for both Lake Marboré (i.e. 1500-1890 CE) and Lake Estanya (i.e. 1500-1780 CE), with HgAR respectively of $24.6 \pm 10.4 \mu\text{g m}^{-2} \text{y}^{-1}$ (n=8) and $22.6 \pm 2.3 \mu\text{g m}^{-2} \text{y}^{-1}$ (n=2). This trend corresponds to the increase in Hg production worldwide and especially in nearby Almadén mines. It is worth noting that the increase in HgAR observed in Pyrenean lakes predates the industrial rise reported in North America lakes (at around 1850s CE) [28,34], in good agreement with the delayed increase in Hg production in North America [62]. This difference between environmental archives from both continents suggests that Hg deposited in remote lakes can be largely influenced by regional sources rather than global ones [16].

1850 CE – Present day. The last period corresponds to the Industrial Period (IP) and is well observed in Lake Marboré (1890-2000 CE) with HgAR of $49.2 \pm 11.7 \mu\text{g m}^{-2} \text{y}^{-1}$ (n=6) and in Lake Estanya (1780-1980 CE) with HgAR of $46.0 \pm 7.3 \mu\text{g m}^{-2} \text{y}^{-1}$ (n=5). It is noticeable that although the background levels are different in both lakes, the modern and industrial HgAR values are quite similar. These remarkable increases mirror the Hg production in Almadén [17,41] and are followed by decreases in recent years in both lakes (since 1970 and 1940 CE for Marboré and Estanya, respectively). This earlier late-industrial decline in HgAR is also observed in recent lake sediment [28,30,34] and peat cores [38] and

corresponds with the local to regional decline in Hg emissions due to the deindustrialization of metal industries and declining mining production in Europe, as well as improved technologies limiting Hg emissions from coal power plants, chlor-alkali plants and waste incinerators [9], as a response to policy requirement. The studied natural archives show this decrease at slightly different times. Indeed, we observed parallel main trends in both lakes Marboré and Estanya, but low amplitude changes in Marboré reflect regional-scale changes as influenced by direct atmospheric inputs, while Estanya is subsequently influenced by watershed-scale human activities such as farming, deforestation, etc. Then, in order to obtain regional rather than local information, it is important to choose remote areas such as Lake Marboré.

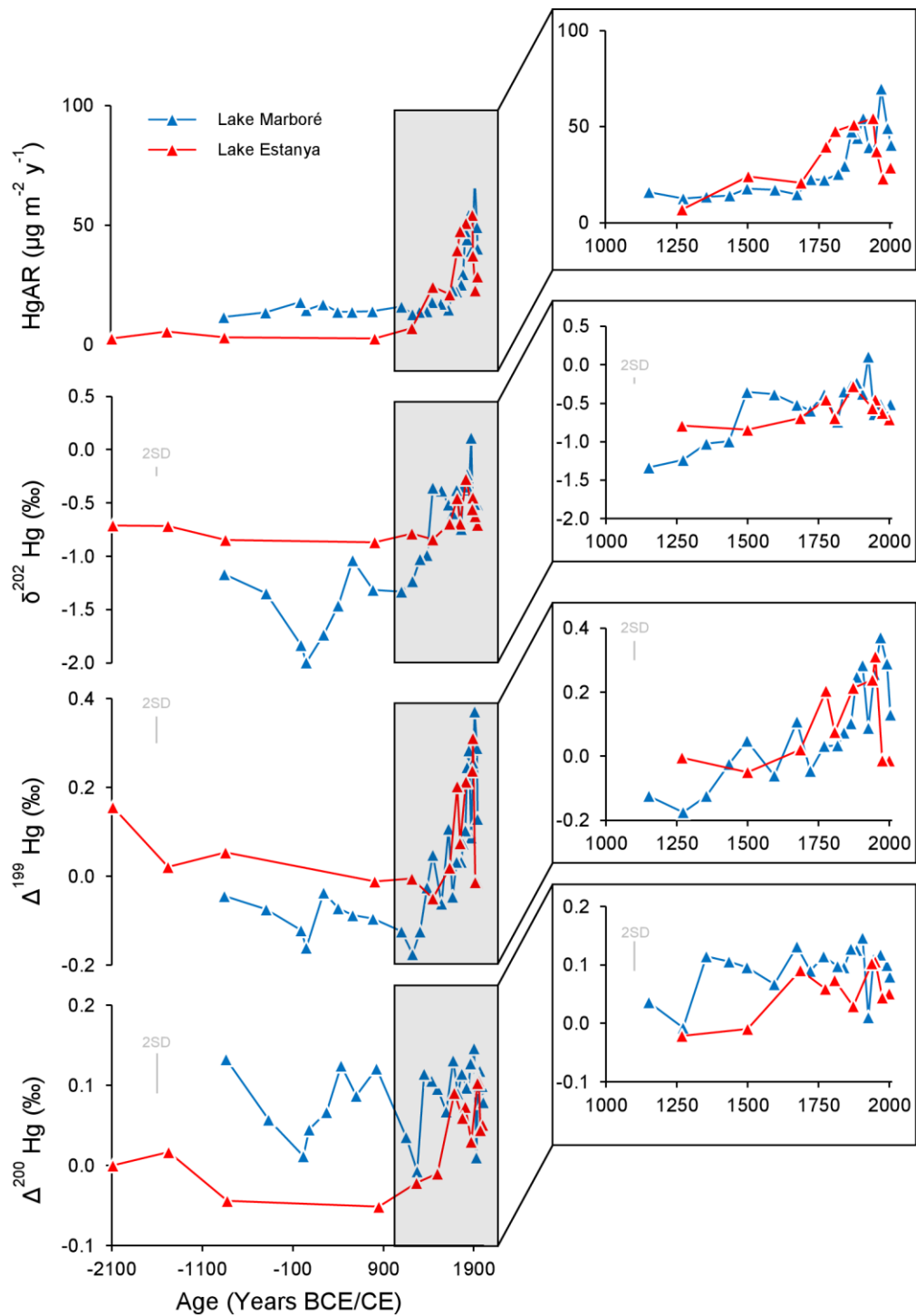


Figure 8-2: From top to bottom, variation over time of HgAR, $\delta^{202}\text{Hg}$, $\Delta^{199}\text{Hg}$ and $\Delta^{200}\text{Hg}$ in Lake Marboré and Lake Estanya. Each parameter is on its own y-axis while sharing the same x-axis.

8.4.2. Stable isotopes to refine mercury atmospheric sources and historical pollution in Southwestern Europe

Mercury stable isotopes provide new insights on the biogeochemical cycle of Hg in the geosphere. Our isotopic results show clear relations between MDF, odd-MIF and even-MIF and the HgAR recorded in the studied sediment cores.

Sediments $\delta^{202}\text{Hg}$ range from -1.99 (90 CE) to 0.11‰ (1930 CE) at Lake Marboré while we observe narrower variations from -0.87 (850 CE) to -0.28‰ (1870 CE) at Lake Estanya. The same pattern is observed for odd-MIF results with $\Delta^{199}\text{Hg}$ values at Lake Marboré and Lake Estanya ranging from -0.18 (1270 CE) to 0.37‰ (1970 CE) and -0.05 (1500 CE) to 0.31‰ (1950 CE) respectively. The profiles reveal increases in both $\delta^{202}\text{Hg}$ and $\Delta^{199}\text{Hg}$ in the upper part of the core sediments corresponding to the last centuries. In contrast, the even-MIF anomalies $\Delta^{200}\text{Hg}$ vary little among the samples with values ranging from -0.01 (1270 CE) to 0.15 ‰ (1910 CE) for Lake Marboré and from -0.05 (850 CE) to 0.11 ‰ (1950 CE) for Lake Estanya sediments. An increase in $\Delta^{200}\text{Hg}$ initiated during the 16th century is evident at Estanya, while the signal inferred by the Marboré sequence remains higher than in Lake Estanya.

The smaller $\delta^{202}\text{Hg}$ and $\Delta^{199}\text{Hg}$ variations at Lake Estanya (except $\Delta^{200}\text{Hg}$) for most of the record up to the last centuries is a unique feature and suggest a strong control of local factors on the Hg cycle until recent times. Two possible in-lake factors might cause MDF and reduce the range of the sediment signatures: i) a strong influence of the catchment via vegetation uptake and ii) limnological processes (biological activity). While HgAR has shown an important increase at the beginning of the 16th century, results from both $\delta^{202}\text{Hg}$ and $\Delta^{199}\text{Hg}$ do not display a significant difference between background (respectively -0.79 ± 0.07 ‰ and 0.04 ± 0.07 ‰) and pre-industrial (respectively -0.77 ± 0.11 ‰ and -0.01 ± 0.05 ‰) values (t-test, $p > 0.05$). Most of the archives, either lakes or peatlands, have shown a positive shift in the $\delta^{202}\text{Hg}$ and $\Delta^{199}\text{Hg}$ values along with the beginning of anthropogenic activities [28,30,34,38,63] (**Figure 8-3**), suggesting that this constant $\delta^{202}\text{Hg}$ and $\Delta^{199}\text{Hg}$ at Lake Estanya is rather due to the control exerted by the lake-watershed system on the fate of external Hg input. The relatively constant $\delta^{202}\text{Hg}$ and $\Delta^{199}\text{Hg}$ close to background values at the beginning of the 16th century when HgAR increased due to global Hg deposition increase could be explained by the change in the vegetation of the catchment that occurred during the 16th century caused by deforestation and land-use for agricultural activities [49]. The period between 1650 and 1750 CE has recorded the highest runoff and soil erosion rates in the Lake Estanya catchment during the last millennium and coincides with the maximum expansion of cultivars at the expenses of natural vegetation in the area according to pollen data [50] and a relative maximum in lake water levels [49]. These environmental conditions occurred in the context of the relatively colder and more humid period recorded during the Little Ice Age (LIA) (14th to 19th centuries CE) in the Pyrenees [64,65]. This climatic period was preceded by a warmer and arid one, the Medieval Climate Anomaly (MCA) (10th to 13th centuries CA) [64–66]. Lakes located in the lowlands (i.e. Estanya) were probably more affected by hydrological changes, whereas sedimentation in high

mountain lakes (i.e. Marboré) was likely more affected by decreasing temperatures and associated effects (ice cover phenology, glacier readvances, etc). Therefore, these abrupt climatic oscillations (MCA-LIA transition) might have influenced in different ways Hg record of lake sediments Marboré and Estanya. In contrast with the 16th century phase, the Industrial Period (1780-1980 CE) was characterized by higher HgAR ($46.0 \pm 7.3 \mu\text{g m}^{-2} \text{y}^{-1}$) as well as higher $\delta^{202}\text{Hg}$ and $\Delta^{199}\text{Hg}$ (respectively $-0.49 \pm 0.15 \text{‰}$ and $0.21 \pm 0.09 \text{‰}$). The $+0.3 \text{‰}$ shift in the $\delta^{202}\text{Hg}$ agrees well with the change in bulk atmospheric Hg emissions observed between 1850 and 2010, from mining to the energy sector [67]. The observed decrease in runoff and soil erosion in the Lake Estanya catchment after 1850 CE as a result of lower human pressure in the region and natural vegetation recovery [49] might have also influenced this change. A similar increase for both $\delta^{202}\text{Hg}$ and $\Delta^{199}\text{Hg}$ has been observed in remote North American lakes over a geographically widespread area since industrialization ($0.22 \pm 0.07 \text{‰}$ and $0.2 \pm 0.03 \text{‰}$, respectively) [63]. The samples dated 1980 and 2000 display $\delta^{202}\text{Hg}$ of -0.62 and -0.70‰ and $\Delta^{199}\text{Hg}$ of -0.01‰ in both samples, similar to pre-industrial and background values. This change has already been observed for EF and HgAR [17] and might be linked to a decrease of Hg emissions in Europe.

The Hg isotopic signal from Lake Marboré displays five distinct periods, following the HgAR and EF variations already documented in a previous publication [42] (**Figure 8-3**): i) Iberian Period (-840 to 20 CE) ii) Roman Period (20 to 440 CE), iii) Middle Ages Period (440 to 1500 CE), iv) Modern Period (1500 to 1890 CE), and v) Industrial Period (1890 to 2000 CE). The Iberian and Middle Ages Periods, reflecting a period of limited anthropogenic influence on Hg cycling, establish a consistent baseline ($\delta^{202}\text{Hg} = -1.21 \pm 0.17 \text{‰}$ and $\Delta^{199}\text{Hg} = -0.09 \pm 0.05 \text{‰}$). This baseline is interrupted by Hg releases during the Roman Period ($\delta^{202}\text{Hg} = -1.85 \pm 0.13 \text{‰}$ and $\Delta^{199}\text{Hg} = -0.11 \pm 0.06 \text{‰}$), expressed as a $\delta^{202}\text{Hg}$ shift by 0.6‰ . Cinnabar (HgS) extraction from Almadén mines for pigment production (vermilion) is well documented and evidenced by archaeological studies, in particular the numerous coins, medals, vessels and other historical objects found in the Almadenejos and Valdeazogues areas [59,68,69]. The production processes included grinding of mined cinnabar followed by drying in furnaces. Romans collected Hg after evaporation and called it hydrargyrum (hence Hg). Arabs brought to Iberia new processes for obtaining Hg, by ore melting and sublimation. The introduction of this new technology might be responsible for some of the changes observed around the 7th – 9th centuries (**Figure 8-2**). Depending on the minerals associated to cinnabar, quartzite, breccia, goethite or pyrite, and depending on the location of the vein (Almadén, El Entredicho, Nuevo Entredicho, Las Cuevas or Nueva Concepción), $\delta^{202}\text{Hg}$ in cinnabar varies greatly from -1.73 to 0.15‰ [70]. Hence, the decrease in $\delta^{202}\text{Hg}$ we infer at Marboré might relate to the characteristic of the veins exploited by Romans in addition to the processing technique. More Hg isotopic analyses depending on the extraction process and the variety of cinnabar are needed to better understand this negative shift during the Roman Period. As mentioned above for others archives, the Modern and Industrial Periods are characterized by less negative $\delta^{202}\text{Hg}$ values of respectively $-0.45 \pm 0.16 \text{‰}$ and $-0.38 \pm 0.29 \text{‰}$ (t-test, $p < 0.05$). However, for Lake Marboré, the main Hg isotopic feature regarding Hg contamination concerns the odd-MIF signal. Indeed, from Iberian and Middle Ages Periods ($\Delta^{199}\text{Hg} = -0.09 \pm 0.05 \text{‰}$), through Modern Period ($\Delta^{199}\text{Hg} = 0.04 \pm 0.06 \text{‰}$), to Industrial Period ($\Delta^{199}\text{Hg} = 0.26 \pm 0.09 \text{‰}$) and recent sample from 2004 ($\Delta^{199}\text{Hg} = 0.13 \text{‰}$) $\Delta^{199}\text{Hg}$ follows a trend parallel to HgAR (**Figure 8-4**), itself related to the Hg Almadén production. A

strong linear relationship between both $1/\text{HgAR}$ and $\Delta^{199}\text{Hg}$ ($r^2 = 0.72$; $p < 0.05$) is well defined by the whole Lake Marboré record, providing evidence for the mixing of two distinct sources affecting atmospheric Hg and allowing the discrimination of natural background (non-Anthropogenic) and industrial emissions. It is worth noting that from the 16th century onwards and the increase in HgAR related to the Hg Almadén production, a $\Delta^{199}\text{Hg}$ vs $1/\text{HgAR}$ relationship is also found for Estanya sediments and confounded with the Marboré trend ($r^2 = 0.57$; $p\text{-value} = 0.018$).

The linear relationship between $1/\text{Hg}$ and $\Delta^{199}\text{Hg}$ has already been observed for the whole core of Lake Luitel ($r^2 = 0.79$; $p < 0.05$) [30] and Lost Lake ($r^2 = 0.85$; $p < 0.05$) [28], as well as for Estibere Peat ($r^2 = 0.56$; $p < 0.05$) and Pinet Peat ($r^2 = 0.50$; $p < 0.05$) [38] excluding recent samples (>1997 CE) (**Figure 8-5**). The slopes related to these regressions depends strongly on different parameters such as main sources, deposition pathways (wet vs dry), and internal lake processes (photoreduction within the lake). Globally lakes from remote areas strongly influenced by direct precipitated Hg such as Lake Marboré or Lost Lake will be more sensitive to atmospheric Hg inputs (higher Hg and $\Delta^{199}\text{Hg}$ variations) than lakes more influenced by gaseous dry deposition to the catchment such as Lake Estanya.

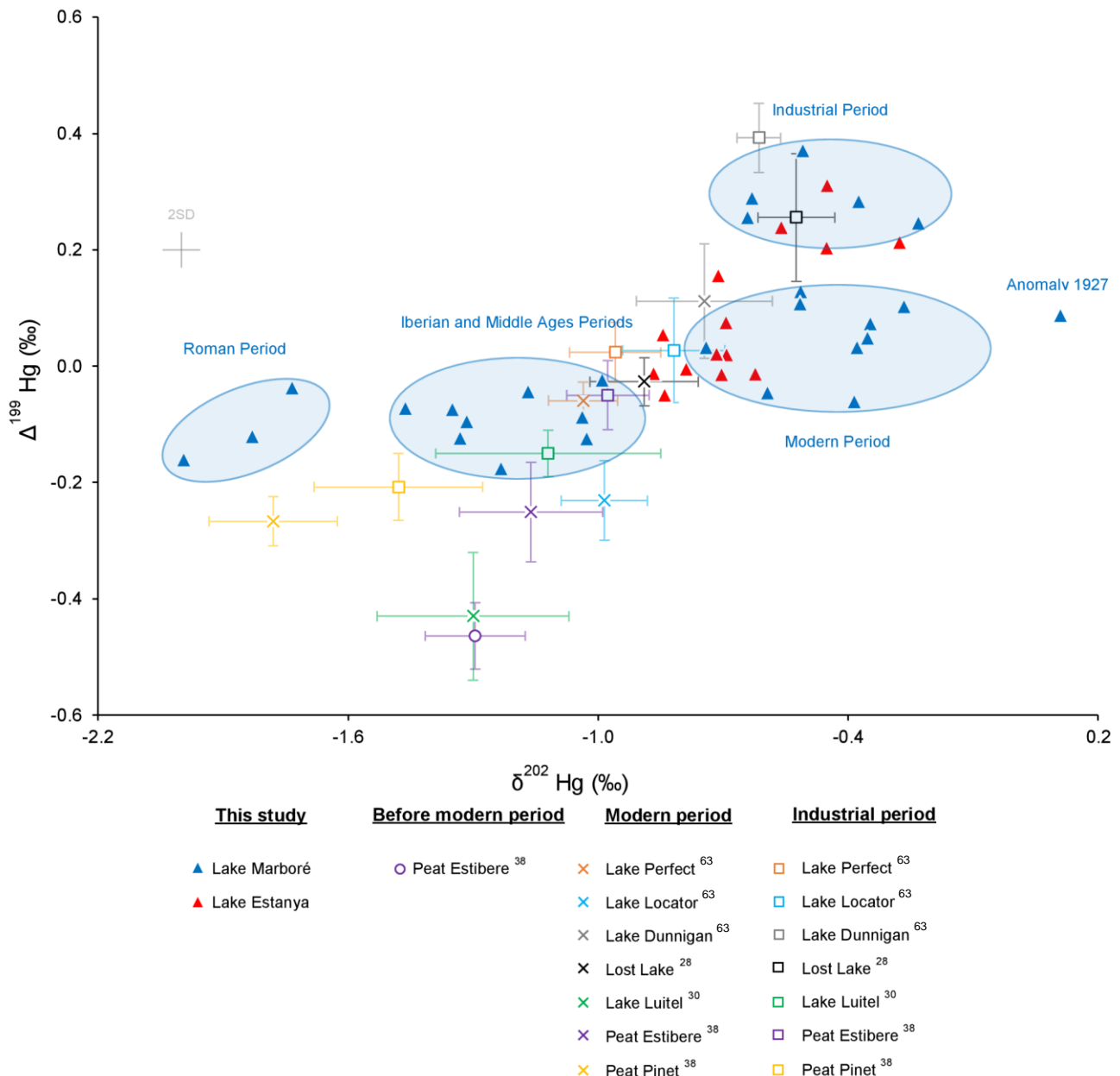


Figure 8-3: $\delta^{202}\text{Hg}$ vs $\Delta^{199}\text{Hg}$ plot for both Lakes Marboré and Lake Estanya together with literature data: both MDF and odd-MIF increase along with contamination.

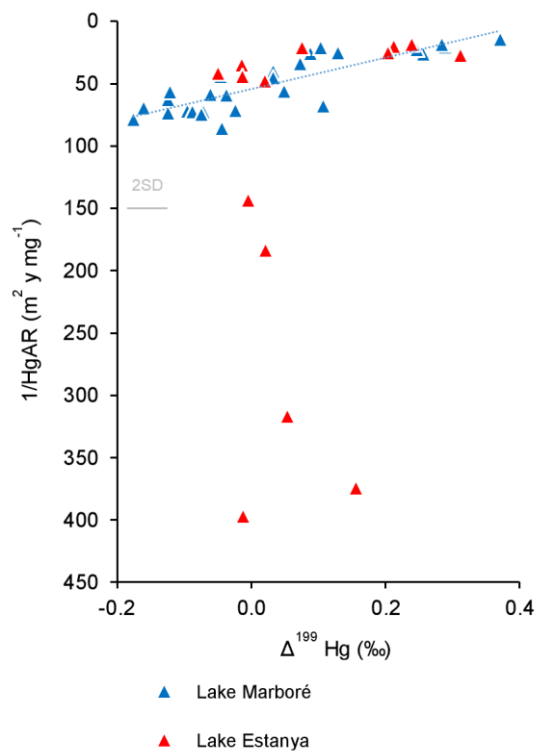


Figure 8-4: (a) $\Delta^{199}\text{Hg}$ vs $1/\text{HgAR}$ plot for both Lakes Marboré and Lake Estanya with strong linear relationship for lake Marboré; (b) $\delta^{202}\text{Hg}$ vs $1/\text{HgAR}$ plot for both Lakes Marboré and Lake Estanya.

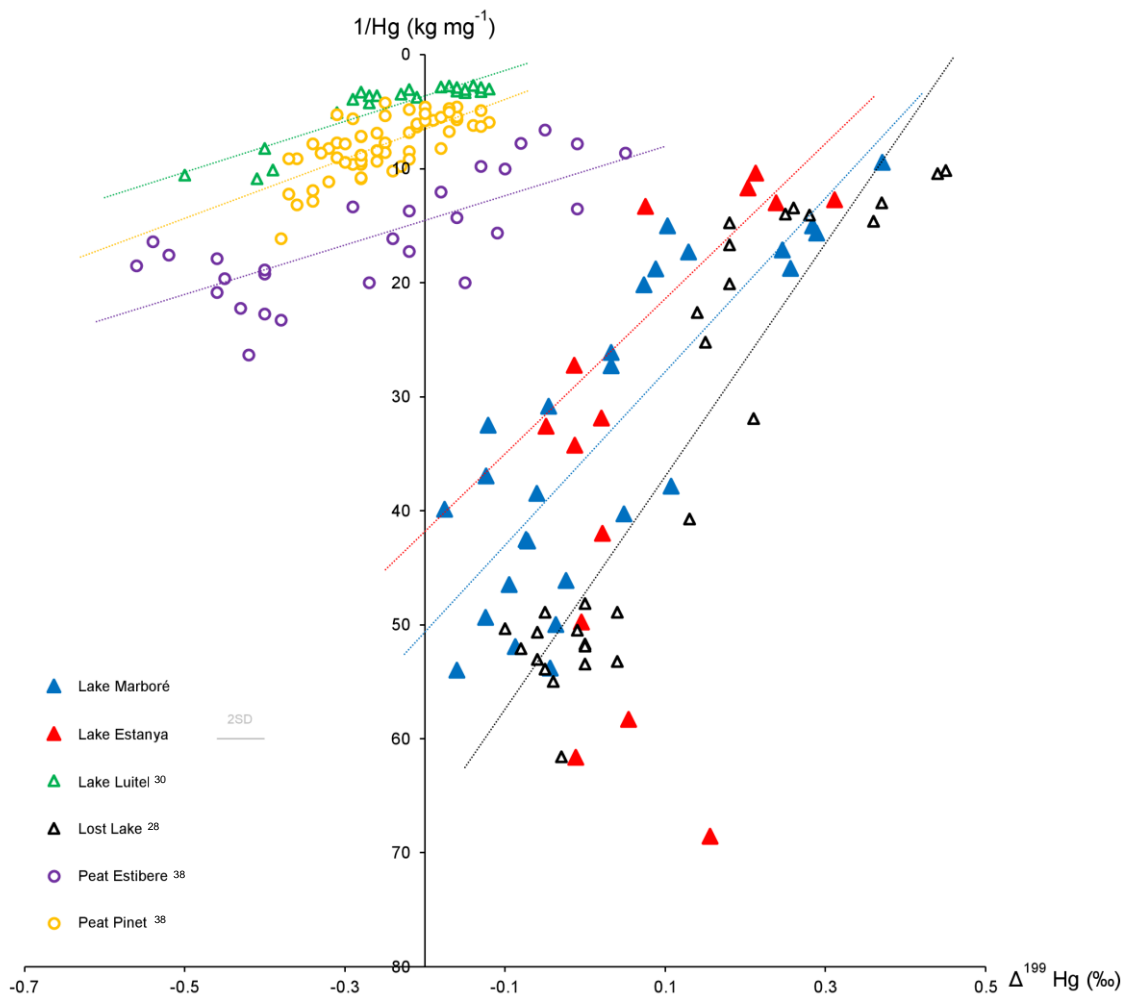


Figure 8-5: $\Delta^{199}\text{Hg}$ vs $1/\text{Hg}$ plot for both Lake Marboré and Lake Estanya, together with other lakes [28,30] and peats [38] to highlight some strong linear relationship (dashed lines).

8.4.3. Even-MIF isotope reflects mercury deposition pathways and climatic implications in the Pyrenees

Mixing models have been recently used to estimate either Hg pollution sources through MDF [34,52,54] and odd-MIF isotopes [30], or deposition pathways through even-MIF isotope [24,28,35,37,38]. According to previous studies on Hg deposition in lakes, main inputs come from the atmospheric compartment either by direct deposition or indirectly as a consequence of run-off phenomena occurring in the catchment [4,19,24,30,71–78].

Wet deposition involves the scavenging of gas-phase and aerosol-phase Hg(II) before their deposition with rainfall and/or snowfall in the lake, whereas gaseous elemental mercury (GEM) dry deposition (Hg(0)) involves surface uptake of Hg(0) directly to the lake by dust transport or through leaching after vegetation uptake. Wet deposition in the northern hemisphere is characterized by significant positive even-MIF $\Delta^{200}\text{Hg}$ [24,28,37,38,79] whereas GEM dry deposition (Hg(0)) shows slight negative $\Delta^{200}\text{Hg}$ values [24,28,37,39].

Downcore sediment from Lake Marboré (**Figure 8-2**) displays positive $\Delta^{200}\text{Hg}$ values of $0.09 \pm 0.04 \text{ ‰}$ (1σ , $n = 27$) suggesting a significant contribution of wet deposition over GEM dry deposition consistent with the absence of vegetation in its catchment and the important precipitation rate (2000 mm per year¹⁷). In this lake, covered by the snow 9-10 months per year, dry deposition likely occurs mainly through GEM adsorption on snow [80]. Indeed, even if gaseous oxidized mercury (GOM) is more prone to dry deposition, its very low abundance in the atmospheric boundary layer makes it less significant than GEM dry deposition.

In contrast, even-MIF $\Delta^{200}\text{Hg}$ is lower ($0.03 \pm 0.05 \text{ ‰}$ [1σ , $n = 14$]) in Lake Estanya and exhibits important variability, with a decrease in the fraction of Hg coming from GEM dry deposition since the 16th century (higher $\Delta^{200}\text{Hg}$, t-test, $p < 0.05$). The relatively constant values in Estanya record before the 16th century suggest that Hg transport to this site seems to have been dominated by GEM dry deposition through foliar uptake followed by run-off from soil catchment. At the onset of the 16th century, both dry and wet depositions raise because of increasing atmospheric Hg levels. Nevertheless, the difference in the lifetime of Hg in the soil and the atmosphere might explain the observed shift in the $\Delta^{200}\text{Hg}$ signal towards relatively more wet deposition. Another possible explanation for this positive shift is the large changes in the lake catchment occurring since the 16th century due to human activities, with the development of large scale agricultural activities and the reduction of the forest cover [50]. These changes in vegetation cover might induce a decrease in the fraction of Hg coming from GEM dry deposition. Finally, changes in local precipitation could also play a role as the 16th – 17th centuries included several wetter phases within the Little Ice Age [49,51].

As determined from a previous work in Central Pyrenees, modern $\Delta^{200}\text{Hg}_{\text{Wet}}$ end-member derived from precipitation ($0.21 \pm 0.04 \text{ ‰}$ (1σ) [37]) and $\Delta^{200}\text{Hg}_{\text{Dry}}$ end-member derived from atmospheric GEM (-

0.05 ± 0.04 ‰, 1σ [37]) allow us to perform an estimate of the mass balance between wet and dry (GEM) deposition in lakes Marboré and Estanya (**Figure 8-6**) using the following formula:

Equation 8-3

$$\Delta^{200}\text{Hg} = F_{\text{Wet}} \times \Delta^{200}\text{Hg}_{\text{Wet}} + F_{\text{Dry}} \times \Delta^{200}\text{Hg}_{\text{Dry}}$$
$$F_{\text{Wet}} + F_{\text{Dry}} = 1$$

The assumption to use this formula along the whole sediment core relies on the hypothesis that the $\Delta^{200}\text{Hg}$ signature in wet and dry deposition did not change over time [38]. Fractions of Hg from wet depositions vary from 16 to 76 % in Lake Marboré with a median value of 57 % whereas fractions of Hg from wet deposition in Lake Estanya ranges from 0 to 60 % with a median value of 33 %. This is consistent with the difference in precipitations observed between both lakes, being higher in Lake Marboré.

As mentioned previously, $\Delta^{200}\text{Hg}$ in Lake Estanya can be affected not only by climate variability but also by the changes of vegetation surrounding the lake, caused by human activities. Lake Marboré watershed, however, has not experienced large changes in vegetation during the last millennia [45], and even-MIF $\Delta^{200}\text{Hg}$ values could be successfully used as a climate proxy. Even if the exact mechanisms involved are not fully understood, the seasonal variation of $\Delta^{200}\text{Hg}$, with significant positive $\Delta^{200}\text{Hg}$, in precipitation samples observed by *Chen et al.* [27] a few years ago bring to light the possible use of $\Delta^{200}\text{Hg}$ as a tool to monitor related climate effects. It is worth noting that the use of Hg as a tool for quantitative paleotemperature reconstruction have been reported in *Martínez-Cortizas et al.* [15]. This assumption is supported by the comparison of the reconstructed wet/dry deposition in this lake using $\Delta^{200}\text{Hg}$ with past climate phases identified in the Pyrenees (**Figure 8-7**). Samples corresponding to warmer periods (MCA and Roman Warm Period) show distinctively lower $\Delta^{200}\text{Hg}$ values than other samples from the sediment core. The two samples dated in the 12th – 13th centuries (1150 and 1270 CE) show lower $\Delta^{200}\text{Hg}$ of respectively 0.04 and -0.01‰ (t-test, p<0.05) and they correspond to the most arid and warm phase of the last millennium, occurring during the MCA [64]. The Roman Warm Period (-250-450 AD), temperatures were also relatively higher in NE Spain [50,81] and, the Marboré samples included in that period – dated -370, 20, 90 and 280 CE – have even-MIF $\Delta^{200}\text{Hg}$ values significantly lower (0.01 to 0.07‰, t-test, p<0.05). Only one more sample, dated 1930 CE displays a similar anomaly with lower $\Delta^{200}\text{Hg}$ (0.01‰), and also higher MDF and lower odd-MIF in comparison with closest dated samples. No clear explanation can be related to this outlier except a local anthropogenic influence, possibly related to the expansion of the Tuquerouye Refuge in 1927 (42°41'N; 0°2'E). Recent values also show a decreasing trend, although wet deposition are estimated to remain higher than 50%. Interestingly, the colder and more humid periods as Dark Ages Cold Period (450 - 900 AD) and the Little Ice Age (1300 - 1850 AD) display higher even-MIF $\Delta^{200}\text{Hg}$ values (respectively 0.09 to 0.12‰ and 0.07 to 0.13‰). Overall, although a better understanding of the relationship between $\Delta^{200}\text{Hg}$ and climatic variations is needed, the occurrence of a consistent even-MIF $\Delta^{200}\text{Hg}$ signal among many climatic periods in remote alpine areas is promising for further paleoclimatic applications.

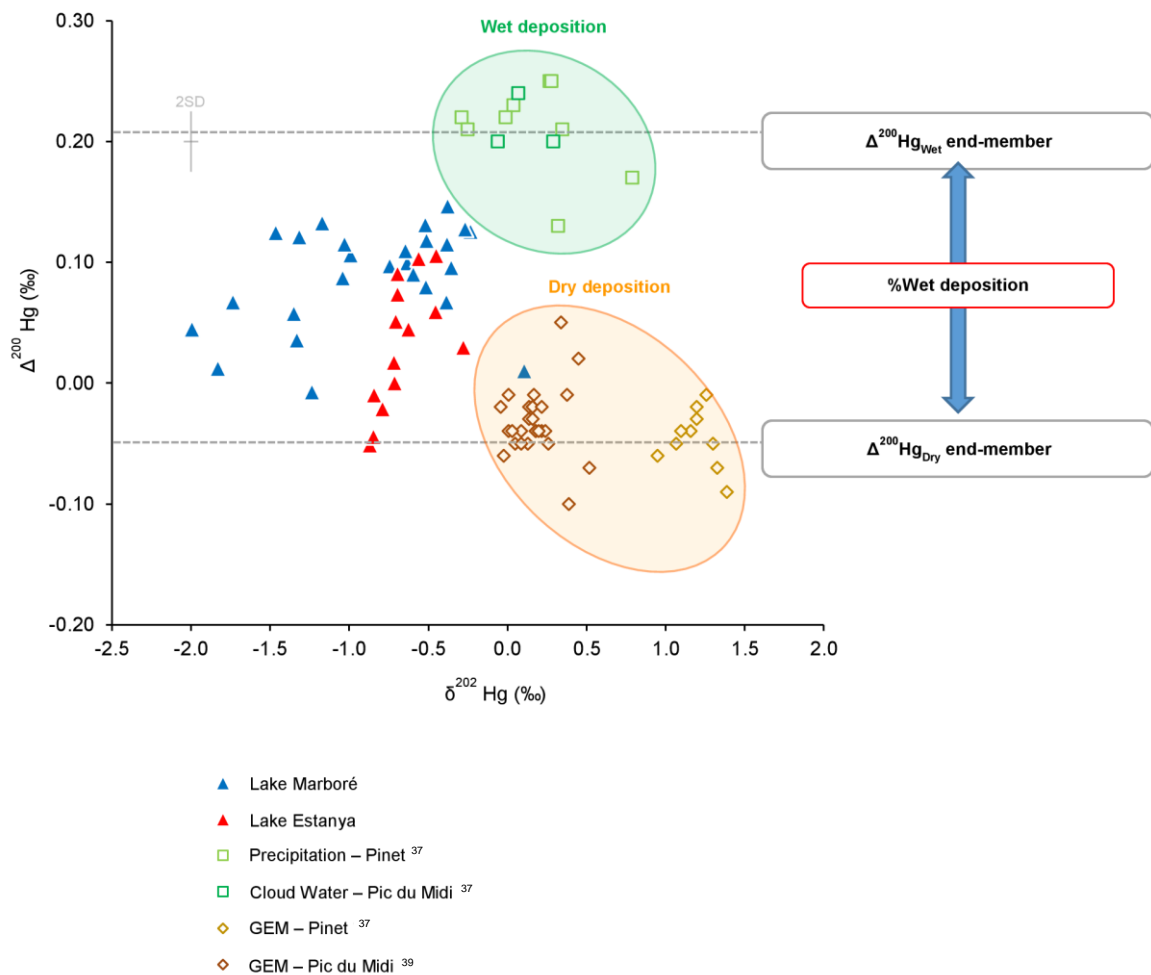


Figure 8-6: $\delta^{202}\text{Hg}$ vs $\Delta^{200}\text{Hg}$ plot for both Lake Marboré and Lake Estanya together with typical wet (cloud waters and precipitations) [37] and dry (GEM) [37,39] deposition Hg isotope signatures in the Central Pyrenees.

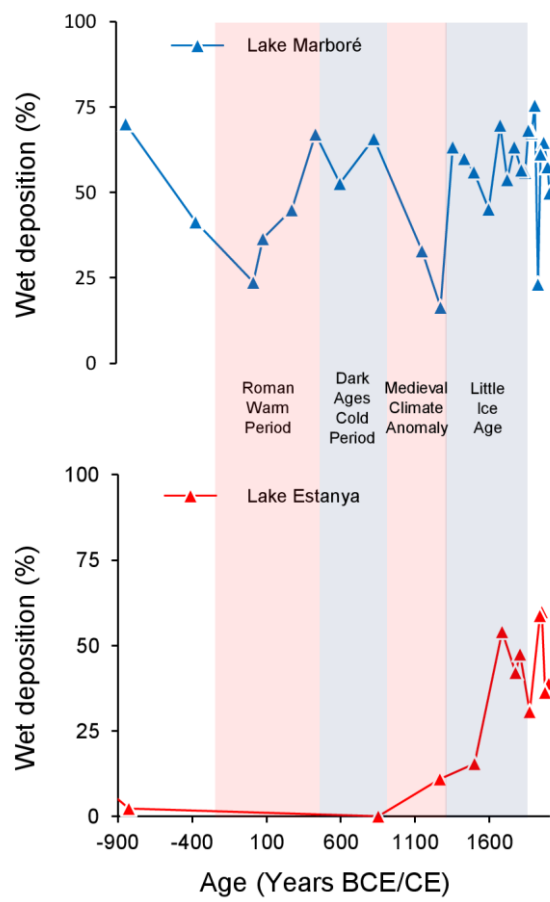


Figure 8-7: Reconstructed historical Hg wet deposition in Lake Marboré and Lake Estanya.

8.4.4. Hg deposition in Pyrenean lakes and peatland records

The Lake Marboré sediment core allows a comparison with another well-studied archive nearby system in the Pyrenees: the Estibere peatland, located at 2120m asl, in the Central Pyrenees at about 18km north-east from Lake Marboré. The peatland receives less annual rainfall than Marboré (1400 mm vs 2000 mm). In addition, isotope signatures of living sphagnum moss and accumulated peat emphasize the strong influence of dry deposition in peat environment [37]. This contrast in the Hg deposition pathways for both ecosystems, lake and peatland, is supported by the significant differences in the even-MIF $\Delta^{200}\text{Hg}$ values (t-test, $p < 0.05$): 0.06 ± 0.03 ‰ for Peat Estibere (905 – 2005 AD) and 0.09 ± 0.04 ‰ for Lake Marboré (829 – 2004 AD).

More interestingly, and except for recent samples (2004 CE for Lake Marboré and 2005 CE for Peat Estibere), the $\Delta^{199}\text{Hg}$ displays a constant shift of 0.33 ± 0.08 ‰ (linear interpolation to reconstruct the $\Delta^{199}\text{Hg}$ values year per year for both dataset) between both archives (**Figure 8-8**). Considering the proximity of both ecosystems and their common atmospheric Hg sources, this shift can be either related to i) deposition pathways or ii) internal processes. Modern wet deposition displays higher $\Delta^{199}\text{Hg}$ than dry deposition: 0.71 ± 0.14 ‰ in precipitation compared to -0.18 ± 0.07 ‰ in atmospheric GEM [37]. Then, the difference in annual precipitation between the lake and the peat could be responsible for this shift in $\Delta^{199}\text{Hg}$. Nevertheless, if we compare the $\Delta^{199}\text{Hg}$ between Peat Estibere and Peat Pinet (precipitation of 1161 mm per year) for the Pre-Industrial Period there is no significant difference (t-test, $p > 0.05$) and there is a shift of about 0.15 ‰ for the Industrial Period. Therefore, while the temporal trends likely reflect variations in atmospheric Hg isotope signatures, the constant shift all along the cores of Lake Marboré and Peat Estibere is likely due to differences in Hg deposition and re-emission pathways. One possible process to account for these differences is in-situ fractionation occurring in Lake Marboré during photoreduction of Hg(II) either when the snow covers the lake or within the water column after melting periods [82]. In addition, Hg photoreduction from foliage might affect Hg isotope composition in peatland [83].

While the HgAR in both archives decreases in the recent samples, the $\Delta^{199}\text{Hg}$ does not follow this tendency in the peat. It has been noticed that during peat diagenesis, non-quantitative retention and loss of Hg occur [22]. *Enrico et al.* [37] have studied the potential influence of photoreduction during peat diagenesis but no effect on sphagnum Hg concentration or Hg isotope composition have been observed. Further in-situ experiments should be conducted to better understand Hg cycle and transformations during peat diagenesis.

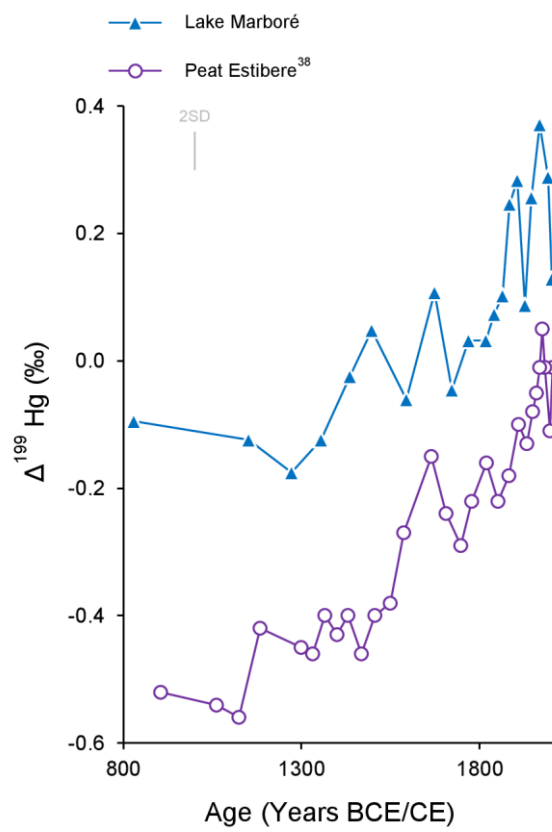


Figure 8-8: $\Delta^{199}\text{Hg}$ comparison between Lake Marboré and Peat Estibere [38].

8.5. Conclusion

We present the first Late Holocene reconstruction of Hg isotope variability in lake sediments in the Iberian Peninsula using two sedimentary archives (Lake Estanya and Maboré) across an altitudinal gradient in the Southern Central Pyrenees. Increasing Hg concentrations and fluxes, recorded in both lakes, agrees well with previous Hg reconstruction in the Pyrenees confirming the regional increasing trends in Hg levels in Southwestern Europe mirroring Hg emissions from global inventories. Hg isotopic composition allowed us to depict the Hg long-term biogeochemical cycling, sources, and transport pathways in the Pyrenees during the last 4000 years. The isotopic signal from Lake Marboré allowed us to better track the regional Hg emissions since low-elevation Lake Estanya Hg signal is more affected by local anthropogenic factors (deforestation and land use activities). Nevertheless, both lakes have shown similar long-term trends in MDF and odd-MIF suggesting common sources.

Lake Marboré isotopic signal suggests that Hg depositional fluxes in high alpine areas mostly occurs via wet deposition. The unique features of this lake, with a small, non-vegetated watershed, ultra-oligotrophic waters and reduced human activities influencing on the Hg cycle, allowed the detection of small variations in the even-MIF synchronously to well-known Late Holocene climatic phases. This agreement between Hg isotopic oscillations and climate variability suggests that Hg isotopic records from remote lakes with similar characteristics could be use as paleoclimatic proxies although further research should be carried out on this topic to confirm this hypothesis. This study also assesses, for the first time, the different isotopic signal recorded in lake and peatbogs in high alpine environments showing a constant offset in the odd-MIF in both record types that stimulates the ongoing debates on lakes/peats as environmental Hg archives.

8.6. References

- [1] M. Arcagni, R. Juncos, A. Rizzo, M. Pavlin, V. Fajon, M.A. Arribére, M. Horvat, S. Ribeiro Guevara, Species- and habitat-specific bioaccumulation of total mercury and methylmercury in the food web of a deep oligotrophic lake, *Science of The Total Environment*. 612 (2018) 1311–1319. <https://doi.org/10.1016/j.scitotenv.2017.08.260>.
- [2] Z.F. Anual, W. Maher, F. Krikowa, L. Hakim, N.I. Ahmad, S. Foster, Mercury and risk assessment from consumption of crustaceans, cephalopods and fish from West Peninsular Malaysia, *Microchemical Journal*. 140 (2018) 214–221. <https://doi.org/10.1016/j.microc.2018.04.024>.
- [3] Q. Xu, L. Zhao, Y. Wang, Q. Xie, D. Yin, X. Feng, D. Wang, Bioaccumulation characteristics of mercury in fish in the Three Gorges Reservoir, China, *Environmental Pollution*. 243 (2018) 115–126. <https://doi.org/10.1016/j.envpol.2018.08.048>.
- [4] C.T. Driscoll, R.P. Mason, H.M. Chan, D.J. Jacob, N. Pirrone, Mercury as a Global Pollutant: Sources, Pathways, and Effects, *Environmental Science & Technology*. 47 (2013) 4967–4983. <https://doi.org/10.1021/es305071v>.
- [5] H.M. Amos, J.E. Sonke, D. Obrist, N. Robins, N. Hagan, H.M. Horowitz, R.P. Mason, M. Witt, I.M. Hedgecock, E.S. Corbitt, E.M. Sunderland, Observational and Modeling Constraints on Global Anthropogenic Enrichment of Mercury, *Environmental Science & Technology*. 49 (2015) 4036–4047. <https://doi.org/10.1021/es5058665>.
- [6] P.A. Ariya, M. Amyot, A. Dastoor, D. Deeds, A. Feinberg, G. Kos, A. Poulain, A. Ryjkov, K. Semeniuk, M. Subir, K. Toyota, Mercury Physicochemical and Biogeochemical Transformation in the Atmosphere and at Atmospheric Interfaces: A Review and Future Directions, *Chemical Reviews*. 115 (2015) 3760–3802. <https://doi.org/10.1021/cr500667e>.
- [7] A. Saiz-Lopez, S.P. Sitkiewicz, D. Roca-Sanjuán, J.M. Oliva-Enrich, J.Z. Dávalos, R. Notario, M. Jiskra, Y. Xu, F. Wang, C.P. Thackray, E.M. Sunderland, D.J. Jacob, O. Travnikov, C.A. Cuevas, A.U. Acuña, D. Rivero, J.M.C. Plane, D.E. Kinnison, J.E. Sonke, Photoreduction of gaseous oxidized mercury changes global atmospheric mercury speciation, transport and deposition, *Nature Communications*. 9 (2018). <https://doi.org/10.1038/s41467-018-07075-3>.
- [8] A. Saiz-Lopez, A.U. Acuña, T. Trabelsi, J. Carmona-García, J.Z. Dávalos, D. Rivero, C.A. Cuevas, D.E. Kinnison, S.P. Sitkiewicz, D. Roca-Sanjuán, J.S. Francisco, Gas-Phase Photolysis of Hg(I) Radical Species: A New Atmospheric Mercury Reduction Process, *Journal of the American Chemical Society*. 141 (2019) 8698–8702. <https://doi.org/10.1021/jacs.9b02890>.
- [9] UNEP, Global mercury assessment 2013: sources, emissions, releases and environmental transport, UNEP Chemicals Branch, Geneva, Switzerland, 2013.
- [10] D.R. Engstrom, W.F. Fitzgerald, C.A. Cooke, C.H. Lamborg, P.E. Drevnick, E.B. Swain, S.J. Balogh, P.H. Balcom, Atmospheric Hg Emissions from Preindustrial Gold and Silver Extraction in the Americas: A Reevaluation from Lake-Sediment Archives, *Environmental Science & Technology*. 48 (2014) 6533–6543. <https://doi.org/10.1021/es405558e>.
- [11] C. Li, J.E. Sonke, G. Le Roux, N. Piotrowska, N. Van der Putten, S.J. Roberts, T. Daley, E. Rice, R. Gehrels, M. Enrico, D. Mauquoy, T.P. Roland, F. De Vleeschouwer, Unequal Anthropogenic Enrichment of Mercury in Earth's Northern and Southern Hemispheres, *ACS Earth and Space Chemistry*. (2020). <https://doi.org/10.1021/acsearthspacechem.0c00220>.
- [12] S.A. Beal, E.C. Osterberg, C.M. Zdanowicz, D.A. Fisher, Ice Core Perspective on Mercury Pollution during the Past 600 Years, *Environmental Science & Technology*. 49 (2015) 7641–7647. <https://doi.org/10.1021/acs.est.5b01033>.
- [13] P.F. Schuster, D.P. Krabbenhoft, D.L. Naftz, L.D. Cecil, M.L. Olson, J.F. Dewild, D.D. Susong, J.R. Green, M.L. Abbott, Atmospheric Mercury Deposition during the Last 270 Years: A Glacial Ice Core Record of Natural and Anthropogenic Sources, *Environmental Science & Technology*. 36 (2002) 2303–2310. <https://doi.org/10.1021/es0157503>.
- [14] M. Pérez-Rodríguez, O. Margalef, J. Corella, A. Saiz-Lopez, S. Pla-Rabes, S. Giral, A. Martínez Cortizas, The Role of Climate: 71 ka of Atmospheric Mercury Deposition in the Southern

- Hemisphere Recorded by Rano Aroi Mire, Easter Island (Chile), *Geosciences*. 8 (2018) 374. <https://doi.org/10.3390/geosciences8100374>.
- [15] A. Martínez Cortizas, Mercury in a Spanish Peat Bog: Archive of Climate Change and Atmospheric Metal Deposition, *Science*. 284 (1999) 939–942. <https://doi.org/10.1126/science.284.5416.939>.
- [16] C.A. Cooke, A. Martínez-Cortizas, R. Bindler, M. Sexauer Gustin, Environmental archives of atmospheric Hg deposition – A review, *Science of The Total Environment*. 709 (2020) 134800. <https://doi.org/10.1016/j.scitotenv.2019.134800>.
- [17] J.P. Corella, A. Saiz-Lopez, M.J. Sierra, M.P. Mata, R. Millán, M. Morellón, C.A. Cuevas, A. Moreno, B.L. Valero-Garcés, Trace metal enrichment during the Industrial Period recorded across an altitudinal transect in the Southern Central Pyrenees, *Science of The Total Environment*. 645 (2018) 761–772. <https://doi.org/10.1016/j.scitotenv.2018.07.160>.
- [18] A. Martínez Cortizas, E. Peiteado Varela, R. Bindler, H. Biester, A. Cheburkin, Reconstructing historical Pb and Hg pollution in NW Spain using multiple cores from the Chao de Lamoso bog (Xistral Mountains), *Geochimica et Cosmochimica Acta*. 82 (2012) 68–78. <https://doi.org/10.1016/j.gca.2010.12.025>.
- [19] H. Biester, R. Bindler, A. Martinez-Cortizas, D.R. Engstrom, Modeling the Past Atmospheric Deposition of Mercury Using Natural Archives, *Environmental Science & Technology*. 41 (2007) 4851–4860. <https://doi.org/10.1021/es0704232>.
- [20] H. Biester, A. Martinez-Cortizas, S. Birkenstock, R. Kilian, Effect of Peat Decomposition and Mass Loss on Historic Mercury Records in Peat Bogs from Patagonia, *Environmental Science & Technology*. 37 (2003) 32–39. <https://doi.org/10.1021/es025657u>.
- [21] S. Bandara, D.G. Froese, V.L. St. Louis, C.A. Cooke, F. Calmels, Postdepositional Mercury Mobility in a Permafrost Peatland from Central Yukon, Canada, *ACS Earth Space Chem*. 3 (2019) 770–778. <https://doi.org/10.1021/acsearthspacechem.9b00010>.
- [22] S. Osterwalder, K. Bishop, C. Alewell, J. Fritsche, H. Laudon, S. Åkerblom, M.B. Nilsson, Mercury evasion from a boreal peatland shortens the timeline for recovery from legacy pollution, *Scientific Reports*. 7 (2017). <https://doi.org/10.1038/s41598-017-16141-7>.
- [23] J. Rydberg, V. Gälman, I. Renberg, R. Bindler, L. Lambertsson, A. Martínez-Cortizas, Assessing the Stability of Mercury and Methylmercury in a Varved Lake Sediment Deposit, *Environmental Science & Technology*. 42 (2008) 4391–4396. <https://doi.org/10.1021/es7031955>.
- [24] J. Chen, H. Hintelmann, W. Zheng, X. Feng, H. Cai, Z. Wang, S. Yuan, Z. Wang, Isotopic evidence for distinct sources of mercury in lake waters and sediments, *Chemical Geology*. 426 (2016) 33–44. <https://doi.org/10.1016/j.chemgeo.2016.01.030>.
- [25] J.D. Blum, L.S. Sherman, M.W. Johnson, Mercury Isotopes in Earth and Environmental Sciences, *Annual Review of Earth and Planetary Sciences*. 42 (2014) 249–269. <https://doi.org/10.1146/annurev-earth-050212-124107>.
- [26] B.A. Bergquist, J.D. Blum, Mass-Dependent and -Independent Fractionation of Hg Isotopes by Photoreduction in Aquatic Systems, *Science*. 318 (2007) 417–420. <https://doi.org/10.1126/science.1148050>.
- [27] J. Chen, H. Hintelmann, X. Feng, B. Dimock, Unusual fractionation of both odd and even mercury isotopes in precipitation from Peterborough, ON, Canada, *Geochimica et Cosmochimica Acta*. 90 (2012) 33–46. <https://doi.org/10.1016/j.gca.2012.05.005>.
- [28] A.Y. Kurz, J.D. Blum, S.J. Washburn, M. Baskaran, Changes in the mercury isotopic composition of sediments from a remote alpine lake in Wyoming, USA, *Science of The Total Environment*. 669 (2019) 973–982. <https://doi.org/10.1016/j.scitotenv.2019.03.165>.
- [29] C.A. Cooke, H. Hintelmann, J.J. Ague, R. Burger, H. Biester, J.P. Sachs, D.R. Engstrom, Use and Legacy of Mercury in the Andes, *Environmental Science & Technology*. 47 (2013) 4181–4188. <https://doi.org/10.1021/es3048027>.
- [30] S. Guédron, D. Amouroux, P. Sabatier, C. Desplanque, A.-L. Develle, J. Barre, C. Feng, F. Guiter, F. Arnaud, J.L. Reyss, L. Charlet, A hundred year record of industrial and urban development in French Alps combining Hg accumulation rates and isotope composition in sediment archives from

- [31] T.A. Jackson, Stratigraphic variations in the $\delta^{201}\text{Hg}/\delta^{199}\text{Hg}$ ratio of mercury in sediment cores as historical records of methylmercury production in lakes, *Journal of Paleolimnology*. 61 (2019) 387–401. <https://doi.org/10.1007/s10933-019-00066-4>.
- [32] T.A. Jackson, Historical variations in the stable isotope composition of mercury in a sediment core from a riverine lake: Effects of dams, pulp and paper mill wastes, and mercury from a chlor-alkali plant, *Applied Geochemistry*. 71 (2016) 86–98. <https://doi.org/10.1016/j.apgeochem.2016.06.001>.
- [33] T.A. Jackson, D.C.G. Muir, W.F. Vincent, Historical Variations in the Stable Isotope Composition of Mercury in Arctic Lake Sediments, *Environmental Science & Technology*. 38 (2004) 2813–2821. <https://doi.org/10.1021/es0306009>.
- [34] R. Yin, R.F. Lepak, D.P. Krabbenhoft, J.P. Hurley, Sedimentary records of mercury stable isotopes in Lake Michigan, *Elementa: Science of the Anthropocene*. 4 (2016) 000086. <https://doi.org/10.12952/journal.elementa.000086>.
- [35] R. Yin, X. Feng, J.P. Hurley, D.P. Krabbenhoft, R.F. Lepak, S. Kang, H. Yang, X. Li, Historical Records of Mercury Stable Isotopes in Sediments of Tibetan Lakes, *Scientific Reports*. 6 (2016). <https://doi.org/10.1038/srep23332>.
- [36] C.M. Zdanowicz, E.M. Krümmel, A.J. Poulain, E. Yumvihoze, J. Chen, M. Štok, M. Scheer, H. Hintelmann, Historical variations of mercury stable isotope ratios in Arctic glacier firn and ice cores: Mercury Stable Isotopes in Glacier Ice, *Global Biogeochemical Cycles*. 30 (2016) 1324–1347. <https://doi.org/10.1002/2016GB005411>.
- [37] M. Enrico, G.L. Roux, N. Maruszczak, L.-E. Heimbürger, A. Clautres, X. Fu, R. Sun, J.E. Sonke, Atmospheric Mercury Transfer to Peat Bogs Dominated by Gaseous Elemental Mercury Dry Deposition, *Environmental Science & Technology*. 50 (2016) 2405–2412. <https://doi.org/10.1021/acs.est.5b06058>.
- [38] M. Enrico, G. Le Roux, L.-E. Heimbürger, P. Van Beek, M. Souhaut, J. Chmeleff, J.E. Sonke, Holocene Atmospheric Mercury Levels Reconstructed from Peat Bog Mercury Stable Isotopes, *Environmental Science & Technology*. 51 (2017) 5899–5906. <https://doi.org/10.1021/acs.est.6b05804>.
- [39] X. Fu, N. Maruszczak, X. Wang, F. Gheusi, J.E. Sonke, Isotopic Composition of Gaseous Elemental Mercury in the Free Troposphere of the Pic du Midi Observatory, France, *Environmental Science & Technology*. 50 (2016) 5641–5650. <https://doi.org/10.1021/acs.est.6b00033>.
- [40] D. Obrist, Y. Agnan, M. Jiskra, C.L. Olson, D.P. Colegrove, J. Hueber, C.W. Moore, J.E. Sonke, D. Helmig, Tundra uptake of atmospheric elemental mercury drives Arctic mercury pollution, *Nature*. 547 (2017) 201–204. <https://doi.org/10.1038/nature22997>.
- [41] J.P. Corella, B.L. Valero-Garcés, F. Wang, A. Martínez-Cortizas, C.A. Cuevas, A. Saiz-Lopez, 700 years reconstruction of mercury and lead atmospheric deposition in the Pyrenees (NE Spain), *Atmospheric Environment*. 155 (2017) 97–107. <https://doi.org/10.1016/j.atmosenv.2017.02.018>.
- [42] J.P. Corella, M.J. Sierra, A. Garralón, R. Millán, J. Rodríguez-Alonso, M.P. Mata, A.V. de Vera, A. Moreno, P. González-Sampériz, B. Duval, D. Amouroux, P. Vivez, C.A. Cuevas, J.A. Adame, B. Wilhelm, A. Saiz-Lopez, B.L. Valero-Garcés, Recent and historical pollution legacy in high altitude Lake Marboré (Central Pyrenees): A record of mining and smelting since pre-Roman times in the Iberian Peninsula, *Science of The Total Environment*. 751 (2021) 141557. <https://doi.org/10.1016/j.scitotenv.2020.141557>.
- [43] M. Morellón, B. Valero-Garcés, T. Vegas-Vilarrúbia, P. González-Sampériz, Ó. Romero, A. Delgado-Huertas, P. Mata, A. Moreno, M. Rico, J.P. Corella, Lateglacial and Holocene palaeohydrology in the western Mediterranean region: The Lake Estanya record (NE Spain), *Quaternary Science Reviews*. 28 (2009) 2582–2599. <https://doi.org/10.1016/j.quascirev.2009.05.014>.
- [44] B. Valero-Garcés, B. Oliva-Urcia, A. Moreno, M. Herrero, M. del Pi. Mata, Á. Salazar, M. Rieradevall, J.M. García-Ruiz, J. Cía, P. Gonzalez Samperiz, A. Sanz, A. Salabarnada, A. Pardo, C. Sancho, F. Barreiro-Lostres, M. Bartolomé, E. Garcia-Prieto, G. Gil-Romera, L. Merino, P.

Tarrats, Dinámica glacial, clima y vegetación en el Parque Nacional de Ordesa y Monte Perdido durante el Holoceno, (2013) 7–37.

- [45] M. Leunda, P. González-Sampérez, G. Gil-Romera, J. Aranbarri, A. Moreno, B. Oliva-Urcia, M. Sevilla-Callejo, B. Valero-Garcés, The Late-Glacial and Holocene Marboré Lake sequence (2612 m a.s.l., Central Pyrenees, Spain): Testing high altitude sites sensitivity to millennial scale vegetation and climate variability, *Global and Planetary Change*. 157 (2017) 214–231. <https://doi.org/10.1016/j.gloplacha.2017.08.008>.
- [46] P.M. Nicolás-Martínez, Morfología del circo de Tucarroya (Macizo de Monte Perdido, Pirineo Aragonés), *Cuadernos de Investigación Geográfica*. 7 (1981) 51. <https://doi.org/10.18172/cig.884>.
- [47] J. Sánchez-España, M.P. Mata, J. Vegas, M. Morellón, J.A. Rodríguez, Á. Salazar, I. Yusta, Limnochemistry of the remote, high mountain Lake Marboré (Ordesa and Monte Perdido National Park, Central Pyrenees): Stratification dynamics and trace metal anomalies, *Limnetica*. (2018) 85–103. <https://doi.org/10.23818/limn.37.08>.
- [48] C. Sancho, El polje de Saganta (Sierras Exteriores Pirenaicas, Provincia de Huesca), *Cuaternario y Geomorfología*. 2 (1988) 207–213.
- [49] M. Morellón, B. Valero-Garcés, P. González-Sampérez, T. Vegas-Vilarrúbia, E. Rubio, M. Rieradevall, A. Delgado-Huertas, P. Mata, Ó. Romero, D.R. Engstrom, M. López-Vicente, A. Navas, J. Soto, Climate changes and human activities recorded in the sediments of Lake Estanya (NE Spain) during the Medieval Warm Period and Little Ice Age, *Journal of Paleolimnology*. 46 (2011) 423–452. <https://doi.org/10.1007/s10933-009-9346-3>.
- [50] P. González-Sampérez, J. Aranbarri, A. Pérez-Sanz, G. Gil-Romera, A. Moreno, M. Leunda, M. Sevilla-Callejo, J.P. Corella, M. Morellón, B. Oliva, B. Valero-Garcés, Environmental and climate change in the southern Central Pyrenees since the Last Glacial Maximum: A view from the lake records, *CATENA*. 149 (2017) 668–688. <https://doi.org/10.1016/j.catena.2016.07.041>.
- [51] B. Oliva-Urcia, A. Moreno, M. Leunda, B. Valero-Garcés, P. González-Sampérez, G. Gil-Romera, M.P. Mata, Last deglaciation and Holocene environmental change at high altitude in the Pyrenees: the geochemical and paleomagnetic record from Marboré Lake (N Spain), *Journal of Paleolimnology*. 59 (2018) 349–371.
- [52] M. Jiménez-Moreno, J.P.G. Barre, V. Perrot, S. Bérail, R.C. Rodríguez Martín-Doimeadios, D. Amouroux, Sources and fate of mercury pollution in Almadén mining district (Spain): Evidences from mercury isotopic compositions in sediments and lichens, *Chemosphere*. 147 (2016) 430–438. <https://doi.org/10.1016/j.chemosphere.2015.12.094>.
- [53] J.D. Blum, B.A. Bergquist, Reporting of variations in the natural isotopic composition of mercury, *Analytical and Bioanalytical Chemistry*. 388 (2007) 353–359. <https://doi.org/10.1007/s00216-007-1236-9>.
- [54] J.P.G. Barre, G. Deletraz, C. Sola-Larrañaga, J.M. Santamaria, S. Bérail, O.F.X. Donard, D. Amouroux, Multi-element isotopic signature (C, N, Pb, Hg) in epiphytic lichens to discriminate atmospheric contamination as a function of land-use characteristics (Pyrénées-Atlantiques, SW France), *Environmental Pollution*. 243 (2018) 961–971. <https://doi.org/10.1016/j.envpol.2018.09.003>.
- [55] L.S. Sherman, J.D. Blum, Mercury stable isotopes in sediments and largemouth bass from Florida lakes, USA, *Science of The Total Environment*. 448 (2013) 163–175. <https://doi.org/10.1016/j.scitotenv.2012.09.038>.
- [56] J.E. Sonke, J. Schäfer, J. Chmeleff, S. Audry, G. Blanc, B. Dupré, Sedimentary mercury stable isotope records of atmospheric and riverine pollution from two major European heavy metal refineries, *Chemical Geology*. 279 (2010) 90–100. <https://doi.org/10.1016/j.chemgeo.2010.09.017>.
- [57] J. Ma, H. Hintelmann, J.L. Kirk, D.C.G. Muir, Mercury concentrations and mercury isotope composition in lake sediment cores from the vicinity of a metal smelting facility in Flin Flon, Manitoba, *Chemical Geology*. 336 (2013) 96–102. <https://doi.org/10.1016/j.chemgeo.2012.10.037>.

- [58] A. Biswas, J.D. Blum, B.A. Bergquist, G.J. Keeler, Z. Xie, Natural Mercury Isotope Variation in Coal Deposits and Organic Soils, *Environmental Science & Technology*. 42 (2008) 8303–8309. <https://doi.org/10.1021/es801444b>.
- [59] P.L.H. Higueras, L.M. Plaza, S.L. Álvarez, J.M.E. Víctor, The Almadén mercury mining district, *CUADERNOS DEL MUSEO GEOMINERO*. 13 (2011) 75–88.
- [60] J. Chételat, M. Amyot, P. Arp, J.M. Blais, D. Depew, C.A. Emmerton, M. Evans, M. Gamberg, N. Gantner, C. Girard, J. Graydon, J. Kirk, D. Lean, I. Lehnherr, D. Muir, M. Nasr, A. J. Poulain, M. Power, P. Roach, G. Stern, H. Swanson, S. van der Velden, Mercury in freshwater ecosystems of the Canadian Arctic: Recent advances on its cycling and fate, *Science of The Total Environment*. 509–510 (2015) 41–66. <https://doi.org/10.1016/j.scitotenv.2014.05.151>.
- [61] N. Maruszczak, C. Larose, A. Dommergue, E. Yumvihoze, D. Lean, R. Nedjai, C. Ferrari, Total mercury and methylmercury in high altitude surface snow from the French Alps, *Science of The Total Environment*. 409 (2011) 3949–3954. <https://doi.org/10.1016/j.scitotenv.2011.06.040>.
- [62] L.D. Hylander, M. Meili, 500 years of mercury production: global annual inventory by region until 2000 and associated emissions, *Science of The Total Environment*. 304 (2003) 13–27. [https://doi.org/10.1016/S0048-9697\(02\)00553-3](https://doi.org/10.1016/S0048-9697(02)00553-3).
- [63] R.F. Lepak, S.E. Janssen, D.R. Engstrom, D.P. Krabbenhoft, M.T. Tate, R. Yin, W.F. Fitzgerald, S.A. Nagorski, J.P. Hurley, Resolving Atmospheric Mercury Loading and Source Trends from Isotopic Records of Remote North American Lake Sediments, *Environmental Science & Technology*. 54 (2020) 9325–9333. <https://doi.org/10.1021/acs.est.0c00579>.
- [64] M. Morellón, A. Pérez-Sanz, J.P. Corella, U. Büntgen, J. Catalán, P. González-Sampériz, J.J. González-Trueba, J.A. López-Sáez, A. Moreno, S. Pla-Rabes, M.Á. Saz-Sánchez, P. Scussolini, E. Serrano, F. Steinhilber, V. Stefanova, T. Vegas-Vilarrúbia, B. Valero-Garcés, A multi-proxy perspective on millennium-long climate variability in the Southern Pyrenees, *Climate of the Past*. 8 (2012) 683–700. <https://doi.org/10.5194/cp-8-683-2012>.
- [65] J.P. Corella, A. Brauer, C. Mangili, V. Rull, T. Vegas-Vilarrúbia, M. Morellón, B.L. Valero-Garcés, The 1.5-ka varved record of Lake Montcortès (southern Pyrenees, NE Spain), *Quat. Res.* 78 (2012) 323–332. <https://doi.org/10.1016/j.yqres.2012.06.002>.
- [66] A. Moreno, A. Pérez, J. Frigola, V. Nieto-Moreno, M. Rodrigo-Gámiz, B. Martrat, P. González-Sampériz, M. Morellón, C. Martín-Puertas, J.P. Corella, Á. Belmonte, C. Sancho, I. Cacho, G. Herrera, M. Canals, J.O. Grimalt, F. Jiménez-Espejo, F. Martínez-Ruiz, T. Vegas-Vilarrúbia, B.L. Valero-Garcés, The Medieval Climate Anomaly in the Iberian Peninsula reconstructed from marine and lake records, *Quaternary Science Reviews*. 43 (2012) 16–32. <https://doi.org/10.1016/j.quascirev.2012.04.007>.
- [67] R. Sun, D.G. Streets, H.M. Horowitz, H.M. Amos, G. Liu, V. Perrot, J.-P. Toutain, H. Hintelmann, E.M. Sunderland, J.E. Sonke, Historical (1850–2010) mercury stable isotope inventory from anthropogenic sources to the atmosphere, *Elementa: Science of the Anthropocene*. 4 (2016) 000091. <https://doi.org/10.12952/journal.elementa.000091>.
- [68] J.M. Esbrí, P. Higueras, Mercury Contents in Waters from the Valdeazogues Watershed (Almadén, Spain), (2005) 7.
- [69] M. Garcia Gomez, J. Diego Caballero Klink, P. Boffetta, S. Espanol, G. Sallsten, J. Gomez Quintana, Exposure to mercury in the mine of Almaden, *Occupational and Environmental Medicine*. 64 (2006) 389–395. <https://doi.org/10.1136/oem.2006.030940>.
- [70] J.E. Gray, M.J. Pribil, P.L. Higueras, Mercury isotope fractionation during ore retorting in the Almadén mining district, Spain, *Chemical Geology*. 357 (2013) 150–157. <https://doi.org/10.1016/j.chemgeo.2013.08.036>.
- [71] M.D. Cohen, R.R. Draxler, R.S. Artz, P. Blanchard, M.S. Gustin, Y.-J. Han, T.M. Holsen, D.A. Jaffe, P. Kelley, H. Lei, C.P. Loughner, W.T. Luke, S.N. Lyman, D. Niemi, J.M. Pacyna, M. Pilote, L. Poissant, D. Ratte, X. Ren, F. Steenhuisen, A. Steffen, R. Tordon, S.J. Wilson, Modeling the global atmospheric transport and deposition of mercury to the Great Lakes, *Elementa: Science of the Anthropocene*. 4 (2016) 000118. <https://doi.org/10.12952/journal.elementa.000118>.
- [72] S. Guédron, D. Point, D. Acha, S. Bouchet, P.A. Baya, E. Tessier, M. Monperrus, C.I. Molina, A. Groleau, L. Chauvaud, J. Thebault, E. Amice, L. Alanoca, C. Duwig, G. Uzu, X. Lazzaro, A.

- Bertrand, S. Bertrand, C. Barbraud, K. Delord, F.M. Gibon, C. Ibanez, M. Flores, P. Fernandez Saavedra, M.E. Ezpinoza, C. Heredia, F. Rocha, C. Zepita, D. Amouroux, Mercury contamination level and speciation inventory in Lakes Titicaca & Uru-Uru (Bolivia): Current status and future trends, *Environmental Pollution*. 231 (2017) 262–270. <https://doi.org/10.1016/j.envpol.2017.08.009>.
- [73] C.R. Hammerschmidt, W.F. Fitzgerald, Methylmercury in Freshwater Fish Linked to Atmospheric Mercury Deposition, *Environmental Science & Technology*. 40 (2006) 7764–7770. <https://doi.org/10.1021/es061480i>.
- [74] R.P. Mason, K.A. Sullivan, Mercury in Lake Michigan, *Environmental Science & Technology*. 31 (1997) 942–947. <https://doi.org/10.1021/es960656l>.
- [75] C. Meuleman, M. Leermakers, W. Baeyens, Mercury speciation in Lake Baikal, *Water, Air, & Soil Pollution*. 80 (1995) 539–551. <https://doi.org/10.1007/BF01189704>.
- [76] A. Økelsrud, E. Lydersen, E. Fjeld, Biomagnification of mercury and selenium in two lakes in southern Norway, *Science of The Total Environment*. 566–567 (2016) 596–607. <https://doi.org/10.1016/j.scitotenv.2016.05.109>.
- [77] K.R. Rolfhus, H.E. Sakamoto, L.B. Cleckner, R.W. Stoor, C.L. Babiarz, R.C. Back, H. Manolopoulos, J.P. Hurley, Distribution and Fluxes of Total and Methylmercury in Lake Superior, *Environmental Science & Technology*. 37 (2003) 865–872. <https://doi.org/10.1021/es026065e>.
- [78] J.G. Wiener, B.C. Knights, M.B. Sandheinrich, J.D. Jeremiason, M.E. Brigham, D.R. Engstrom, L.G. Woodruff, W.F. Cannon, S.J. Balogh, Mercury in Soils, Lakes, and Fish in Voyageurs National Park (Minnesota): Importance of Atmospheric Deposition and Ecosystem Factors, *Environmental Science & Technology*. 40 (2006) 6261–6268. <https://doi.org/10.1021/es060822h>.
- [79] J.D. Demers, J.D. Blum, D.R. Zak, Mercury isotopes in a forested ecosystem: Implications for air-surface exchange dynamics and the global mercury cycle: MERCURY ISOTOPES IN A FORESTED ECOSYSTEM, *Global Biogeochemical Cycles*. 27 (2013) 222–238. <https://doi.org/10.1002/gbc.20021>.
- [80] T.A. Douglas, J.D. Blum, Mercury Isotopes Reveal Atmospheric Gaseous Mercury Deposition Directly to the Arctic Coastal Snowpack, *Environ. Sci. Technol. Lett.* 6 (2019) 235–242. <https://doi.org/10.1021/acs.estlett.9b00131>.
- [81] J.P. Corella, V. Stefanova, A. El Anjoumi, E. Rico, S. Giralt, A. Moreno, A. Plata-Montero, B.L. Valero-Garcés, A 2500-year multi-proxy reconstruction of climate change and human activities in northern Spain: The Lake Arreo record, *Palaeogeography, Palaeoclimatology, Palaeoecology*. 386 (2013) 555–568. <https://doi.org/10.1016/j.palaeo.2013.06.022>.
- [82] A. Spolaor, E. Barbaro, D. Cappelletti, C. Turetta, M. Mazzola, F. Giardi, M.P. Björkman, F. Lucchetta, F. Dallo, K.A. Pfaffhuber, H. Angot, A. Dommergue, M. Maturilli, A. Saiz-Lopez, C. Barbante, W.R.L. Cairns, Diurnal cycle of iodine, bromine, and mercury concentrations in Svalbard surface snow, *Atmospheric Chemistry and Physics*. 19 (2019) 13325–13339. <https://doi.org/10.5194/acp-19-13325-2019>.
- [83] W. Yuan, J. Sommar, C.-J. Lin, X. Wang, K. Li, Y. Liu, H. Zhang, Z. Lu, C. Wu, X. Feng, Stable Isotope Evidence Shows Re-emission of Elemental Mercury Vapor Occurring after Reductive Loss from Foliage, *Environmental Science & Technology*. 53 (2019) 651–660. <https://doi.org/10.1021/acs.est.8b04865>.

General conclusions

The aim of this thesis was to evaluate how aquatic geochemistry and trace elements cycling in alpine lakes can be affected by Global Change, including Climate Change.

Firstly, there is a contradiction between the importance of remote areas, such as alpine lakes, and the few number of studies conducted worldwide on the aquatic compartment of these ecosystems. Therefore, the **first objective** was to establish a guideline for sampling and analytical strategy in order to study a large scope of physico-chemical parameters in water samples from remote alpine lakes. This was an important step, especially regarding the need of long-term continuous, high quality and homogeneous measurements in alpine lakes if the effect of Global Change in these environments are to be investigated. Thus, the various methodology described in the **Chapter 3** can be further used by the scientific community to produce comparable data over time. Additionally, even if the lakes are very important for the global CO₂ budget, the methodology employed up to now to determine the total alkalinity (TA) and the dissolved inorganic carbon (DIC), two major parameters of the CO₂ system were far from being acceptable (estimation using measurement of other parameters such as conductivity, large uncertainties). Then, the **Chapter 4** of this manuscript was dedicated to the development of a new and robust procedure for TA and DIC measurements, thus also allowing the determination of the other two parameters of the CO₂ system, the pH and the fugacity of CO₂ (fCO₂). We encourage greatly the further studies to be based on this accurate protocol. Finally, high altitude lakes are remote areas, which can pose logistical problems in the organization of scientific study: difficulties to reach those environments carrying all the material needed. Thus, the need for newly low cost and easy handling methodologies led us to develop a new method for analysis of trace mercury concentrations in aquatic systems (**Chapter 5**). The analytical performances of this method, based on the micro-solid phase extraction preconcentration using functionalized graphene nanosheets, with a detection limit as low as 0.38 ng L⁻¹ using 200 mL of the water sample and an excellent reproducibility (< 5% as RSD), were promising and can still be improved. Future work must be conducted in order to i) improve the detection limit (purifying the graphene, handling the graphene in a super clean atmosphere, using gloves box for example), ii) test for Hg specific species determination (MMHg, iHg) and iii) test the suitability of this methodology on Hg isotopic analysis (nowadays heavy methodologies are used involving numerous analytical steps).

The primary cause of Global Change is the emission of greenhouse gases, such as carbon dioxide CO₂. Thus, the **second objective** of this thesis was to study the CO₂ parameters (TA, DIC, pH, fCO₂) in alpine lakes from the Pyrenees, using the analytical protocol described previously (**Chapter 4**). It appears that, depending on the bedrock characteristics of their watershed, the studied lakes are very sensitive (granitic basin) or less sensitive (sedimentary rocks) to acidification. Therefore, in order to follow the future Global Changes, regular accurate determination of the CO₂ parameters in the water of acid-sensitive lakes must be conducted. Furthermore, values of fCO₂ in the studied lakes, always above the atmospheric pCO₂ confirm that nowadays, lakes are sources of CO₂. Nevertheless, anthropogenic emissions of CO₂ are constantly increasing and therefore it is crucial to monitor alpine lakes closely to understand the effects of the excess of atmospheric CO₂.

Climate Change has direct consequences on the physical processes occurring in the mountain critical zone, where belong the alpine lakes, which can result in an increase of intense rain and snowstorm, soil erosion, extreme floods, fire intensities and droughts. All these phenomena influences the sources and pathways of Potential Harmful Trace Elements (PHTEs): remobilization, atmospheric deposition, geological supply. The **third objective** was then to classify all the studied lakes according to their surface water geochemistry and to assess, for the first time, the occurrence and sources of a wide range of PHTEs in a large amount of Pyrenean lakes (**Chapter 6**). Additionally, intensive monitoring conducted on the water column of four lakes revealed some PHTEs (arsenic, copper, nickel, molybdenum, cobalt and cadmium) to be highly sensitive to environmental changes such as temperature and redox conditions

Among the PHTEs, mercury (Hg) has historically shown interesting specificities that can make a good candidate to follow Climate and Global changes. It is a global pollutant, atmospherically deposited (wet and dry depositions) and potentially subjected to transformations in the lake ecosystems under the effect of environmental changes. Thus, the **fourth objective** of the thesis was to evaluate sensitivity of Hg to anthropogenic pressure and Climate Change by studying the Hg cycle in both the water column and the sediment archives from high altitude lakes. Hg speciation results in the water column (**Chapter 7**) demonstrated the pristine state and the dynamic of the Pyrenean lakes. The homogeneity in the non-gaseous total mercury (THg) concentrations in the studied lakes confirmed the absence of local sources and the potential use of these ecosystems as sentinels of regional to global Hg contamination. While inorganic mercury (iHg) did not show seasonal variations and dissolved gaseous mercury (DGM) varied strongly within and among lakes reaching concentration values never recorded until now for pristine areas in some specific samples. Incubation experiments confirmed that drastic environmental changes occurring daily and seasonally in alpine lakes are providing conditions that can promote Hg methylation (stratified anoxic waters), MMHg demethylation and iHg photoreduction (intense UV light). The historical Hg record in sediment archives (**Chapter** Erreur ! Source du renvoi introuvable.) highlighted temporal trends in Hg accumulation rates (HgARs) with a progressive increase since the 16th Century and the industrialization, mirroring the mercury production in Almadén Hg mines (Southern Spain). Hg stable isotopes in these cores also emphasized the anthropogenic pressure characterized by higher odd MIF- $\Delta^{199}\text{Hg}$ values and provided new insights on the dry and wet deposition processes occurring in alpine lakes using even MIF- $\Delta^{200}\text{Hg}$ as a new paleoclimate proxy. About the last point, future work must be conducted on selected alpine lakes to confirm the use of Hg as a paleoclimate proxy.

Overall, environmental changes in lake ecosystems, induced by either Climate Change (temperature, and light intensity) or anthropogenic pressure (lake productivity, atmospheric CO₂) are likely to produce unexpected cascading impacts among CO₂, specific PHTEs (arsenic, copper, nickel, molybdenum, cobalt and cadmium) and Hg biogeochemical cycles in mountainous ecosystems.

Annexe 1: Major, trace and ultra-trace elements results obtained by Q- ICP-MS

REPLIM 1	Ca	Na	Mg	K	Al	Sr	Fe	Mn	Ba
	$\mu\text{g L}^{-1}$								
LOD	7	19	3	3	2	0.1	0.7	0.01	0.01
ARA-R1-F-1	8492	450	262	90	<LOD	21.8	5.0	0.67	0.42
ARA-R1-F-2	8367	182	207	64	<LOD	21.3	4.4	0.54	0.35
ARA-R1-F-3	8593	189	222	72	<LOD	21.2	4.6	0.61	0.44
BAD-R1-F-1	9754	268	258	79	<LOD	25.4	0.9	0.71	0.27
BAD-R1-F-2	9836	280	264	105	<LOD	25.1	1.6	0.74	0.28
BAD-R1-F-3	9733	273	259	79	<LOD	25.2	1.4	0.69	0.27
CAM-R1-F-1	1806	220	79	100	<LOD	3.2	1.1	0.66	0.53
CAM-R1-F-2	1679	195	75	65	<LOD	3.2	1.1	0.70	0.51
CAM-R1-F-3	1748	199	75	68	<LOD	3.2	1.1	0.78	0.52
PEY-R1-F-1	1115	150	52	47	<LOD	1.9	<LOD	1.25	0.33
PEY-R1-F-2	1111	142	52	43	5.0	1.9	4.8	1.37	0.39
PEY-R1-F-3	n.d.								
OPA-R1-F-1	3780	237	138	178	2.9	8.3	1.4	0.18	1.10
OPA-R1-F-2	3725	253	139	188	<LOD	8.3	1.3	0.18	1.06
OPA-R1-F-3	3765	237	139	169	3.0	8.1	0.9	0.39	1.03
PAR-R1-F-1	7074	1022	231	203	10.2	20.0	13.7	1.19	0.60
PAR-R1-F-2	7220	966	234	181	9.5	19.8	14.2	1.10	1.21
PAR-R1-F-3	7260	947	235	171	9.9	18.8	13.8	1.05	0.58
NER-R1-F-1	1486	205	57	62	<LOD	3.2	0.7	0.45	1.08
NER-R1-F-2	1422	191	55	53	<LOD	3.2	<LOD	0.42	1.16
NER-R1-F-3	1480	191	57	55	<LOD	3.2	<LOD	0.43	1.09
POU-R1-F-1	2712	272	53	72	<LOD	4.8	<LOD	0.65	0.47
POU-R1-F-2	2758	284	57	78	4.0	4.9	1.4	0.66	0.33
POU-R1-F-3	2675	260	54	69	4.1	4.8	2.8	0.81	0.40
AZU-R1-F-1	10410	182	241	99	<LOD	29.1	<LOD	1.13	6.42
AZU-R1-F-2	10450	166	244	90	<LOD	29.3	<LOD	1.01	5.71
AZU-R1-F-3	10470	173	250	99	2.4	30.5	<LOD	0.83	4.56
ARN-R1-F-1	3838	256	105	78	<LOD	6.7	<LOD	0.17	0.50

ARN-R1-F-2	3740	264	104	79	<LOD	6.7	<LOD	0.15	0.40
ARN-R1-F-3	3760	240	104	80	6.1	6.7	<LOD	0.14	0.31
BAC-R1-F-1	3912	184	148	76	<LOD	13.2	1.4	1.45	0.77
BAC-R1-F-2	3899	357	151	125	4.5	13.1	2.1	1.65	0.87
BAC-R1-F-3	3826	188	145	88	5.9	13.4	1.2	1.19	0.82
PEC-R1-F-1	5669	123	192	60	<LOD	18.8	<LOD	1.99	0.26
PEC-R1-F-2	5632	131	191	66	<LOD	19.0	<LOD	1.98	0.28
PEC-R1-F-3	5819	121	193	60	<LOD	18.9	<LOD	1.69	0.17
COA-R1-F-1	1984	176	76	52	<LOD	3.3	1.8	0.47	1.04
COA-R1-F-2	1953	183	75	53	<LOD	3.3	1.8	0.47	0.79
COA-R1-F-3	1999	186	77	64	5.2	3.4	2.2	0.57	0.99
PAN-R1-F-1	4917	437	164	117	3.9	14.4	3.6	1.17	0.90
PAN-R1-F-2	5587	407	172	100	<LOD	15.7	1.9	0.90	0.72
PAN-R1-F-3	4985	474	166	115	<LOD	14.6	2.4	1.00	0.81
ORD-R1-F-1	8504	395	251	168	<LOD	18.5	11.9	0.89	0.82
ORD-R1-F-2	8123	315	239	86	6.3	18.4	9.7	0.73	0.58
ORD-R1-F-3	8723	373	247	174	3.8	19.1	4.1	0.75	0.44
XUA-R1-F-1	2839	165	91	80	<LOD	4.6	<LOD	0.60	0.62
XUA-R1-F-2	2967	166	95	79	<LOD	4.5	<LOD	0.55	0.76
XUA-R1-F-3	2963	159	93	92	<LOD	4.6	<LOD	0.59	0.69
ARA-R1-UF-1	8079	389	249	78	<LOD	21.4	16.3	2.90	0.45
ARA-R1-UF-2	7964	141	240	61	<LOD	21.2	14.3	2.53	0.36
ARA-R1-UF-3	7898	160	241	69	<LOD	21.0	15.1	2.62	0.48
BAD-R1-UF-1	9758	152	278	86	9.0	25.4	6.9	1.42	0.33
BAD-R1-UF-2	9171	128	252	67	5.5	25.0	6.2	1.36	0.30
BAD-R1-UF-3	9785	141	274	74	5.4	25.1	6.4	1.35	0.30
CAM-R1-UF-1	1592	145	75	62	<LOD	3.1	4.0	0.72	0.55
CAM-R1-UF-2	1580	145	72	58	3.4	3.2	4.2	0.76	0.61
CAM-R1-UF-3	1595	144	73	61	2.4	3.2	4.6	0.83	0.54
PEY-R1-UF-1	1017	99	55	44	13.3	1.9	10.0	1.44	0.45
PEY-R1-UF-2	1315	104	51	37	35.5	2.1	11.5	1.52	0.46

PEY-R1-UF-3	n.d.	n.d.	n.d.	n.d.	n.d.	n.d.	n.d.	n.d.	n.d.
OPA-R1-UF-1	2516	110	96	116	23.4	8.0	9.6	0.47	1.27
OPA-R1-UF-2	2424	98	93	111	13.4	8.1	8.1	0.43	1.22
OPA-R1-UF-3	n.d.	n.d.	n.d.	n.d.	n.d.	n.d.	n.d.	n.d.	n.d.
PAR-R1-UF-1	7532	1035	241	177	12.4	18.8	20.6	1.99	0.77
PAR-R1-UF-2	7713	1003	249	189	11.3	17.7	54.5	2.81	1.63
PAR-R1-UF-3	7932	1020	252	168	11.5	17.3	19.9	1.25	0.57
NER-R1-UF-1	1443	155	57	51	3.3	3.2	1.9	0.49	1.07
NER-R1-UF-2	n.d.	n.d.	n.d.	n.d.	n.d.	n.d.	n.d.	n.d.	n.d.
NER-R1-UF-3	1372	152	55	49	3.8	3.2	1.6	0.48	1.17
POU-R1-UF-1	2530	222	52	57	6.8	4.7	3.2	0.76	0.48
POU-R1-UF-2	2415	210	49	51	6.7	4.6	3.3	0.68	0.30
POU-R1-UF-3	2362	199	49	54	7.6	4.7	3.8	0.77	0.43
AZU-R1-UF-1	11040	220	215	97	<LOD	29.7	4.5	1.29	6.55
AZU-R1-UF-2	10880	195	211	86	<LOD	29.5	4.4	1.29	5.79
AZU-R1-UF-3	10920	201	215	88	3.0	31.3	3.1	1.05	4.70
ARN-R1-UF-1	3352	270	109	72	8.8	6.8	1.2	0.23	0.48
ARN-R1-UF-2	3413	285	112	79	7.4	6.9	1.4	0.23	0.44
ARN-R1-UF-3	3299	269	108	73	7.4	6.8	1.0	0.21	0.31
BAC-R1-UF-1	4092	226	151	75	4.3	13.3	11.8	4.49	0.81
BAC-R1-UF-2	4118	224	152	76	6.5	13.1	15.5	5.06	0.80
BAC-R1-UF-3	4041	223	145	86	<LOD	13.4	13.6	3.68	0.85
PEC-R1-UF-1	6058	162	199	61	<LOD	18.6	2.4	3.40	0.28
PEC-R1-UF-2	5944	171	195	66	<LOD	18.8	2.6	3.48	0.30
PEC-R1-UF-3	5839	154	192	55	<LOD	18.6	2.2	2.99	0.18
COA-R1-UF-1	2057	203	78	47	13.8	3.4	4.9	0.56	1.00
COA-R1-UF-2	2050	205	80	48	12.2	3.4	5.0	0.57	0.85
COA-R1-UF-3	2033	206	78	49	14.7	3.5	4.9	0.60	0.97
PAN-R1-UF-1	5060	442	163	105	3.9	14.4	8.6	2.00	0.87
PAN-R1-UF-2	6042	440	178	102	<LOD	15.9	7.2	1.60	0.74
PAN-R1-UF-3	5074	463	161	99	<LOD	14.6	7.6	1.68	0.81

ORD-R1-UF-1	8753	325	212	77	5.6	18.5	14.9	2.19	0.82
ORD-R1-UF-2	8559	320	208	78	5.9	18.3	14.9	2.17	0.56
ORD-R1-UF-3	9435	339	215	107	<LOD	19.1	6.2	0.90	0.36
XUA-R1-UF-1	3003	192	99	85	11.1	4.6	16.4	1.77	0.70
XUA-R1-UF-2	2978	178	99	73	10.4	4.6	16.3	1.88	0.87
XUA-R1-UF-3	2977	186	96	79	9.8	4.5	16.5	2.01	0.75

REPLIM 1	As	Cu	Ti	Mo	V	Ni	Cr	Pb	Se	Sb	Co	Cd	Tl
	ng L ⁻¹												
LOD	46	15	3	6	10	20	7	4	1	10	4	9	3
ARA-R1-F-1	930	41	124	141	63	<LOD	126	<LOD	68	14	6	<LOD	<LOD
ARA-R1-F-2	916	30	106	136	57	<LOD	126	<LOD	68	12	5	<LOD	<LOD
ARA-R1-F-3	867	51	103	131	57	<LOD	117	<LOD	70	<LOD	5	<LOD	<LOD
BAD-R1-F-1	594	49	129	113	89	<LOD	183	<LOD	74	12	7	<LOD	<LOD
BAD-R1-F-2	619	23	143	105	89	<LOD	180	<LOD	75	<LOD	7	<LOD	<LOD
BAD-R1-F-3	628	38	132	112	87	<LOD	171	<LOD	73	<LOD	7	<LOD	6
CAM-R1-F-1	327	20	68	19	58	<LOD	<LOD	<LOD	14	<LOD	<LOD	<LOD	<LOD
CAM-R1-F-2	362	<LOD	69	16	45	<LOD	<LOD	<LOD	15	54	7	<LOD	4
CAM-R1-F-3	357	20	53	14	55	<LOD	<LOD	<LOD	15	24	<LOD	<LOD	<LOD
PEY-R1-F-1	154	27	37	<LOD	34	<LOD	<LOD	<LOD	13	13	6	<LOD	<LOD
PEY-R1-F-2	101	<LOD	175	<LOD	43	<LOD	<LOD	76	13	10	6	<LOD	<LOD
PEY-R1-F-3	n.d.	13	n.d.	n.d.	n.d.	n.d.							
OPA-R1-F-1	432	16	100	38	71	<LOD	20	<LOD	21	15	<LOD	<LOD	<LOD
OPA-R1-F-2	402	<LOD	221	35	68	<LOD	16	<LOD	21	13	<LOD	<LOD	<LOD
OPA-R1-F-3	415	18	80	41	63	<LOD	15	<LOD	20	15	<LOD	<LOD	<LOD
PAR-R1-F-1	1573	<LOD	217	529	377	<LOD	136	17	37	24	19	<LOD	<LOD
PAR-R1-F-2	1545	56	215	511	371	<LOD	141	<LOD	39	11	16	<LOD	<LOD
PAR-R1-F-3	1561	50	215	527	363	<LOD	138	<LOD	39	<LOD	13	<LOD	<LOD
NER-R1-F-1	165	60	50	<LOD	35	<LOD	<LOD	8	13	<LOD	<LOD	<LOD	<LOD
NER-R1-F-2	160	34	49	<LOD	40	<LOD	<LOD	<LOD	13	<LOD	<LOD	<LOD	<LOD
NER-R1-F-3	121	31	51	<LOD	31	<LOD	<LOD	9	13	<LOD	<LOD	<LOD	<LOD
POU-R1-F-1	202	55	58	<LOD	37	<LOD	<LOD	<LOD	13	55	6	<LOD	<LOD
POU-R1-F-2	153	24	101	<LOD	28	<LOD	<LOD	<LOD	13	35	<LOD	<LOD	<LOD
POU-R1-F-3	196	54	145	<LOD	38	<LOD	<LOD	31	13	20	<LOD	<LOD	<LOD
AZU-R1-F-1	4301	30	91	95	36	<LOD	36	<LOD	75	94	5	<LOD	<LOD
AZU-R1-F-2	4590	<LOD	82	95	41	<LOD	39	<LOD	77	69	<LOD	<LOD	<LOD
AZU-R1-F-3	5064	15	152	107	41	<LOD	46	<LOD	82	64	<LOD	<LOD	<LOD
ARN-R1-F-1	1367	<LOD	85	259	132	<LOD	33	<LOD	24	15	<LOD	<LOD	<LOD

ARN-R1-F-2	1296	<LOD	56	252	130	<LOD	31	<LOD	23	15	<LOD	<LOD	<LOD
ARN-R1-F-3	1298	<LOD	51	256	123	<LOD	27	<LOD	23	14	<LOD	<LOD	<LOD
BAC-R1-F-1	2666	30	67	92	64	<LOD	29	<LOD	35	18	<LOD	<LOD	<LOD
BAC-R1-F-2	2692	102	167	93	83	<LOD	41	10	<LOD	21	<LOD	<LOD	<LOD
BAC-R1-F-3	2824	30	59	95	90	<LOD	32	<LOD	<LOD	16	<LOD	<LOD	<LOD
PEC-R1-F-1	8281	<LOD	64	73	59	<LOD	55	<LOD	49	37	<LOD	<LOD	<LOD
PEC-R1-F-2	8094	<LOD	64	71	54	<LOD	49	<LOD	47	38	<LOD	<LOD	<LOD
PEC-R1-F-3	8468	<LOD	69	71	60	<LOD	51	<LOD	48	82	<LOD	<LOD	<LOD
COA-R1-F-1	852	69	51	7	93	<LOD	8	<LOD	19	13	<LOD	<LOD	<LOD
COA-R1-F-2	846	67	52	6	90	<LOD	8	<LOD	17	13	5	<LOD	<LOD
COA-R1-F-3	875	74	53	7	100	<LOD	11	<LOD	18	12	<LOD	<LOD	<LOD
PAN-R1-F-1	2820	46	145	179	110	<LOD	39	26	29	30	<LOD	<LOD	<LOD
PAN-R1-F-2	2872	29	87	184	105	<LOD	39	<LOD	31	27	<LOD	<LOD	<LOD
PAN-R1-F-3	2831	34	121	195	115	<LOD	35	<LOD	31	26	<LOD	<LOD	<LOD
ORD-R1-F-1	1650	122	193	82	142	<LOD	81	46	25	68	13	<LOD	<LOD
ORD-R1-F-2	1637	67	141	85	138	<LOD	77	19	26	59	15	<LOD	<LOD
ORD-R1-F-3	1535	75	152	98	116	<LOD	93	12	31	35	10	<LOD	<LOD
XUA-R1-F-1	366	44	62	40	81	<LOD	12	<LOD	22	22	<LOD	<LOD	<LOD
XUA-R1-F-2	300	54	38	40	83	<LOD	8	<LOD	22	16	<LOD	<LOD	<LOD
XUA-R1-F-3	305	32	52	40	71	<LOD	<LOD	<LOD	22	13	<LOD	<LOD	<LOD
ARA-R1-UF-1	1037	45	150	108	87	<LOD	136	29	62	54	18	<LOD	3
ARA-R1-UF-2	1041	29	138	107	81	<LOD	110	<LOD	63	24	14	<LOD	<LOD
ARA-R1-UF-3	974	50	145	114	83	<LOD	125	11	64	19	12	<LOD	<LOD
BAD-R1-UF-1	695	27	248	84	109	<LOD	170	17	70	<LOD	12	<LOD	<LOD
BAD-R1-UF-2	743	<LOD	212	83	107	<LOD	164	47	67	<LOD	9	<LOD	<LOD
BAD-R1-UF-3	675	23	228	84	104	<LOD	170	12	67	<LOD	11	<LOD	<LOD
CAM-R1-UF-1	456	<LOD	87	<LOD	69	<LOD	<LOD	16	14	<LOD	<LOD	<LOD	<LOD
CAM-R1-UF-2	550	<LOD	154	<LOD	66	<LOD	<LOD	18	14	<LOD	<LOD	<LOD	<LOD
CAM-R1-UF-3	646	<LOD	137	<LOD	64	<LOD	<LOD	19	17	<LOD	<LOD	<LOD	<LOD
PEY-R1-UF-1	500	<LOD	304	<LOD	73	<LOD	<LOD	37	12	<LOD	8	<LOD	<LOD
PEY-R1-UF-2	808	458	307	<LOD	100	<LOD	35	65	13	47	11	<LOD	<LOD

PEY-R1-UF-3	n.d.	12	n.d.	n.d.	n.d.	n.d.							
OPA-R1-UF-1	1361	89	313	24	135	<LOD	33	48	19	23	<LOD	<LOD	<LOD
OPA-R1-UF-2	1465	<LOD	361	27	128	<LOD	23	42	20	17	<LOD	<LOD	<LOD
OPA-R1-UF-3	n.d.	19	n.d.	n.d.	n.d.	n.d.							
PAR-R1-UF-1	1422	<LOD	337	551	319	<LOD	143	26	38	73	32	<LOD	7
PAR-R1-UF-2	1624	169	466	589	409	<LOD	185	61	36	27	26	<LOD	<LOD
PAR-R1-UF-3	1520	101	287	593	357	<LOD	154	10	36	17	21	<LOD	<LOD
NER-R1-UF-1	150	30	93	<LOD	33	<LOD	<LOD	7	13	<LOD	<LOD	<LOD	<LOD
NER-R1-UF-2	n.d.	13	n.d.	n.d.	n.d.	n.d.							
NER-R1-UF-3	276	37	65	<LOD	35	<LOD	<LOD	14	13	<LOD	<LOD	<LOD	<LOD
POU-R1-UF-1	467	33	115	<LOD	46	<LOD	<LOD	8	14	<LOD	<LOD	<LOD	<LOD
POU-R1-UF-2	323	<LOD	101	<LOD	42	<LOD	<LOD	7	14	<LOD	<LOD	<LOD	<LOD
POU-R1-UF-3	824	24	96	<LOD	50	<LOD	<LOD	14	13	<LOD	<LOD	<LOD	<LOD
AZU-R1-UF-1	4409	25	105	135	<LOD	<LOD	38	8	69	86	8	<LOD	<LOD
AZU-R1-UF-2	4638	15	116	138	<LOD	<LOD	43	5	74	76	7	<LOD	<LOD
AZU-R1-UF-3	5139	18	159	149	15	<LOD	44	<LOD	76	66	7	<LOD	<LOD
ARN-R1-UF-1	1242	28	71	303	110	<LOD	31	<LOD	26	17	<LOD	<LOD	<LOD
ARN-R1-UF-2	1412	98	132	310	134	<LOD	56	9	25	19	<LOD	73	8
ARN-R1-UF-3	1257	34	71	304	109	<LOD	31	<LOD	24	16	5	<LOD	<LOD
BAC-R1-UF-1	2890	41	107	130	51	<LOD	35	<LOD	33	21	7	<LOD	<LOD
BAC-R1-UF-2	2975	54	163	129	67	<LOD	42	13	34	18	9	<LOD	<LOD
BAC-R1-UF-3	2942	87	288	136	83	<LOD	42	16	<LOD	18	7	<LOD	<LOD
PEC-R1-UF-1	8292	33	212	108	31	<LOD	49	<LOD	45	41	5	<LOD	<LOD
PEC-R1-UF-2	8136	34	116	107	43	<LOD	57	<LOD	45	41	6	<LOD	<LOD
PEC-R1-UF-3	8129	34	89	110	32	<LOD	57	<LOD	47	41	4	<LOD	<LOD
COA-R1-UF-1	719	69	62	43	74	<LOD	11	13	19	26	7	<LOD	<LOD
COA-R1-UF-2	708	131	95	43	83	<LOD	18	15	19	19	7	<LOD	<LOD
COA-R1-UF-3	742	73	83	44	69	<LOD	13	16	19	15	6	<LOD	<LOD
PAN-R1-UF-1	2825	56	139	221	99	<LOD	41	13	30	24	7	<LOD	<LOD
PAN-R1-UF-2	2935	50	187	232	87	<LOD	50	11	31	78	11	<LOD	6
PAN-R1-UF-3	2796	44	134	232	98	<LOD	43	9	31	37	7	<LOD	<LOD

ORD-R1-UF-1	1670	88	162	124	115	<LOD	80	36	31	13	24	<LOD	<LOD
ORD-R1-UF-2	1569	105	154	118	125	<LOD	77	33	31	11	18	<LOD	<LOD
ORD-R1-UF-3	1623	48	172	133	96	<LOD	92	<LOD	30	11	12	<LOD	<LOD
XUA-R1-UF-1	241	49	484	77	73	<LOD	22	25	20	<LOD	13	<LOD	<LOD
XUA-R1-UF-2	<LOD	36	290	79	63	<LOD	16	21	20	<LOD	12	<LOD	<LOD
XUA-R1-UF-3	197	52	221	78	91	<LOD	22	26	22	63	18	<LOD	<LOD

REPLIM 2	Ca	Na	Mg	K	Al	Sr	Fe	Mn	Ba
	$\mu\text{g L}^{-1}$								
LOD	6	26	4	12	0.4	0.0	0.6	0.04	0.02
ARA-R2-F-1	18646	296	221	36	2.2	34.5	35.0	0.71	0.34
ARA-R2-F-2	18661	299	224	33	1.4	29.8	37.5	0.85	0.23
ARA-R2-F-3	18464	329	220	35	1.7	30.5	31.4	0.67	0.20
BAD-R2-F-1	18060	293	217	45	4.2	43.3	1.8	0.21	0.32
BAD-R2-F-2	17953	313	218	48	4.5	41.9	1.0	0.17	0.32
BAD-R2-F-3	18175	312	222	47	4.0	44.4	1.8	0.23	0.29
CAM-R2-F-1	2379	368	71	48	3.2	4.6	2.3	0.94	0.56
CAM-R2-F-2	2364	373	72	46	4.9	4.4	3.1	0.97	0.53
CAM-R2-F-3	n.d.								
PEY-R2-F-1	1143	215	42	27	8.2	2.1	<LOD	0.34	0.25
PEY-R2-F-2	1149	185	42	23	8.9	2.1	<LOD	0.33	0.25
PEY-R2-F-3	1167	188	43	27	14.8	2.1	<LOD	0.34	0.28
OPA-R2-F-1	4779	392	100	89	6.0	7.8	<LOD	0.27	1.00
OPA-R2-F-2	4612	376	96	85	6.3	7.8	<LOD	0.23	1.01
OPA-R2-F-3	4730	372	97	86	6.4	7.9	<LOD	0.20	0.93
PAR-R2-F-1	12846	1101	197	127	5.0	18.0	9.9	1.00	0.46
PAR-R2-F-2	12934	1039	191	109	6.0	17.4	10.1	0.93	0.42
PAR-R2-F-3	13024	1028	205	123	2.9	16.5	11.5	0.94	0.59
AZU-R2-F-1	21500	280	210	52	4.6	51.7	<LOD	0.13	5.03
AZU-R2-F-2	21236	268	205	50	4.8	51.3	<LOD	0.15	5.03
AZU-R2-F-3	21608	274	210	52	4.5	51.3	<LOD	0.15	5.05
ARN-R2-F-1	5614	437	103	49	18.5	10.0	1.0	0.19	0.33
ARN-R2-F-2	5681	447	105	49	17.4	9.9	0.8	0.19	0.32
ARN-R2-F-3	5801	458	109	51	17.5	9.8	1.1	0.17	0.31
BAC-R2-F-1	6510	279	114	46	13.9	15.3	2.3	0.75	1.27
BAC-R2-F-2	6370	272	109	40	12.6	14.8	2.2	0.78	1.24
BAC-R2-F-3	6545	273	111	43	15.7	15.0	1.9	1.03	1.19
COA-R2-F-1	2718	299	76	19	4.7	4.4	7.0	0.49	0.71

COA-R2-F-2	2673	287	77	19	23.3	4.6	14.6	0.62	0.71
COA-R2-F-3	2740	293	77	21	22.1	4.5	12.4	0.53	0.70
PAN-R2-F-1	6529	828	119	58	8.9	14.0	4.9	0.59	1.10
PAN-R2-F-2	6354	517	113	51	9.1	14.1	4.3	0.52	1.06
PAN-R2-F-3	6652	522	119	57	1.2	14.0	2.1	0.54	1.08
ARA-R2-UF-1	18440	286	215	31	2.1	34.1	57.6	3.87	0.33
ARA-R2-UF-2	18893	296	225	34	1.8	31.2	61.5	4.33	0.24
ARA-R2-UF-3	18854	292	223	33	1.6	35.7	58.6	3.86	0.20
BAD-R2-UF-1	18468	296	224	47	5.3	44.0	6.2	2.88	0.32
BAD-R2-UF-2	17968	307	221	49	8.1	42.2	5.3	2.36	0.31
BAD-R2-UF-3	18341	293	222	49	5.4	44.1	6.1	2.99	0.30
CAM-R2-UF-1	2352	356	72	47	7.9	4.5	12.3	1.97	0.60
CAM-R2-UF-2	2342	356	72	46	7.4	4.6	11.9	1.96	0.54
CAM-R2-UF-3	2346	355	72	46	8.4	4.6	12.4	1.97	0.53
PEY-R2-UF-1	1180	187	45	26	22.8	2.1	2.8	0.60	0.28
PEY-R2-UF-2	1138	178	44	25	34.6	2.1	9.1	0.85	0.31
PEY-R2-UF-3	1147	181	43	24	23.3	2.1	2.6	0.56	0.29
OPA-R2-UF-1	4735	380	100	89	10.5	8.2	5.4	0.62	1.02
OPA-R2-UF-2	4820	387	100	89	9.7	7.9	5.2	0.61	0.98
OPA-R2-UF-3	4795	368	98	86	10.9	7.9	5.3	0.61	0.96
PAR-R2-UF-1	13074	1091	197	128	8.2	18.0	20.2	1.19	0.46
PAR-R2-UF-2	12393	1009	193	112	17.8	17.4	38.8	1.95	0.47
PAR-R2-UF-3	12914	1037	206	124	6.9	16.5	17.5	1.01	0.59
AZU-R2-UF-1	20868	269	206	50	4.7	50.2	1.1	1.15	4.93
AZU-R2-UF-2	20813	267	203	50	5.3	49.9	1.2	1.19	5.03
AZU-R2-UF-3	20594	261	202	49	5.2	50.5	1.2	1.20	5.07
ARN-R2-UF-1	5680	438	107	51	18.1	9.8	3.1	0.46	0.32
ARN-R2-UF-2	5640	433	106	49	19.0	10.0	3.1	0.44	0.32
ARN-R2-UF-3	5740	444	107	49	19.4	9.9	3.0	0.46	0.29
BAC-R2-UF-1	6569	273	113	41	14.4	15.1	9.8	2.26	1.29
BAC-R2-UF-2	6278	262	112	39	21.4	15.2	35.8	6.28	1.36

BAC-R2-UF-3	6618	276	115	45	17.1	15.4	11.0	2.78	1.29
COA-R2-UF-1	2671	286	76	18	23.8	4.4	20.7	0.60	0.70
COA-R2-UF-2	2617	280	75	20	23.9	4.4	20.4	0.61	0.72
COA-R2-UF-3	2705	289	76	19	24.6	4.4	20.8	0.65	0.69
PAN-R2-UF-1	6440	785	117	58	10.3	14.2	14.0	1.84	1.13
PAN-R2-UF-2	6598	515	119	54	11.3	14.8	14.9	1.94	1.11
PAN-R2-UF-3	6717	517	122	55	11.3	14.6	14.5	1.94	1.11

REPLIM 2	As	Cu	Ti	Mo	V	Ni	Cr	Pb	Se	Sb	Co	Cd	Tl
	ng L ⁻¹												
LOD	93	66	66	9	39	62	40	45	1	4	26	9	5
ARA-R2-F-1	1609	161	<LOD	252	90	<LOD	<LOD	<LOD	45	17	<LOD	<LOD	<LOD
ARA-R2-F-2	1555	146	<LOD	250	86	<LOD	<LOD	<LOD	45	16	<LOD	<LOD	<LOD
ARA-R2-F-3	1496	154	<LOD	251	88	<LOD	<LOD	<LOD	46	17	<LOD	<LOD	<LOD
BAD-R2-F-1	799	239	83	277	139	<LOD	48	<LOD	49	11	<LOD	<LOD	<LOD
BAD-R2-F-2	876	227	142	283	140	<LOD	44	<LOD	51	12	<LOD	<LOD	<LOD
BAD-R2-F-3	817	248	104	270	140	<LOD	44	<LOD	51	10	<LOD	<LOD	<LOD
CAM-R2-F-1	683	98	<LOD	126	59	<LOD	<LOD	<LOD	17	17	<LOD	<LOD	<LOD
CAM-R2-F-2	681	82	<LOD	124	65	<LOD	<LOD	<LOD	17	17	<LOD	<LOD	<LOD
CAM-R2-F-3	n.d.	17	n.d.	n.d.	n.d.	n.d.							
PEY-R2-F-1	173	114	<LOD	15	81	<LOD	<LOD	<LOD	13	13	<LOD	<LOD	<LOD
PEY-R2-F-2	153	113	<LOD	13	78	<LOD	<LOD	<LOD	13	14	<LOD	<LOD	<LOD
PEY-R2-F-3	242	234	<LOD	14	86	<LOD	<LOD	<LOD	14	13	<LOD	<LOD	<LOD
OPA-R2-F-1	513	107	<LOD	123	87	<LOD	<LOD	<LOD	21	17	<LOD	<LOD	<LOD
OPA-R2-F-2	538	179	74	124	89	<LOD	<LOD	<LOD	17	18	<LOD	<LOD	<LOD
OPA-R2-F-3	479	90	70	122	86	<LOD	<LOD	<LOD	16	19	<LOD	<LOD	<LOD
PAR-R2-F-1	1635	588	168	727	338	<LOD	87	<LOD	n.d.	11	<LOD	<LOD	<LOD
PAR-R2-F-2	1552	99	171	703	334	<LOD	68	<LOD	n.d.	10	<LOD	<LOD	<LOD
PAR-R2-F-3	1424	91	150	674	309	<LOD	75	<LOD	n.d.	9	<LOD	<LOD	<LOD
AZU-R2-F-1	5597	175	119	231	<LOD	<LOD	<LOD	<LOD	52	78	<LOD	<LOD	<LOD
AZU-R2-F-2	5554	150	208	236	57	<LOD	<LOD	<LOD	52	78	<LOD	<LOD	<LOD
AZU-R2-F-3	5546	160	149	239	64	<LOD	<LOD	<LOD	54	80	<LOD	<LOD	<LOD
ARN-R2-F-1	1939	151	116	661	157	<LOD	<LOD	<LOD	25	23	<LOD	<LOD	<LOD
ARN-R2-F-2	1936	107	<LOD	669	156	<LOD	<LOD	<LOD	24	24	<LOD	<LOD	<LOD
ARN-R2-F-3	1967	129	67	679	154	<LOD	<LOD	<LOD	25	26	<LOD	<LOD	<LOD
BAC-R2-F-1	2578	114	130	211	94	<LOD	<LOD	<LOD	25	34	<LOD	<LOD	<LOD
BAC-R2-F-2	2471	117	95	201	91	<LOD	<LOD	<LOD	25	35	<LOD	<LOD	<LOD
BAC-R2-F-3	2558	100	79	204	94	<LOD	<LOD	<LOD	24	32	<LOD	<LOD	<LOD
COA-R2-F-1	906	251	<LOD	67	85	<LOD	<LOD	<LOD	18	18	<LOD	<LOD	<LOD

COA-R2-F-2	967	206	<LOD	70	83	<LOD	<LOD	<LOD	18	19	<LOD	<LOD	<LOD
COA-R2-F-3	967	215	<LOD	69	70	<LOD	<LOD	<LOD	18	18	<LOD	<LOD	<LOD
PAN-R2-F-1	2604	115	157	367	113	<LOD	<LOD	<LOD	21	32	<LOD	<LOD	<LOD
PAN-R2-F-2	2494	108	90	280	112	<LOD	<LOD	<LOD	21	31	<LOD	<LOD	<LOD
PAN-R2-F-3	2573	111	112	287	108	<LOD	<LOD	<LOD	21	30	<LOD	<LOD	<LOD
ARA-R2-UF-1	1633	166	<LOD	247	86	<LOD	<LOD	<LOD	59	16	<LOD	<LOD	<LOD
ARA-R2-UF-2	1654	149	<LOD	242	96	<LOD	<LOD	<LOD	58	16	<LOD	<LOD	<LOD
ARA-R2-UF-3	1605	149	75	253	96	<LOD	<LOD	301	58	17	<LOD	<LOD	<LOD
BAD-R2-UF-1	842	255	133	271	146	<LOD	47	<LOD	67	12	30	<LOD	<LOD
BAD-R2-UF-2	891	476	183	287	142	<LOD	65	<LOD	67	11	<LOD	<LOD	<LOD
BAD-R2-UF-3	884	270	116	274	138	<LOD	47	<LOD	65	12	<LOD	<LOD	<LOD
CAM-R2-UF-1	761	159	109	124	70	<LOD	<LOD	<LOD	23	16	<LOD	<LOD	<LOD
CAM-R2-UF-2	754	112	90	130	65	<LOD	<LOD	<LOD	23	16	<LOD	<LOD	<LOD
CAM-R2-UF-3	726	102	145	128	71	<LOD	<LOD	<LOD	24	17	<LOD	<LOD	<LOD
PEY-R2-UF-1	210	127	92	14	77	<LOD	<LOD	<LOD	20	15	<LOD	<LOD	<LOD
PEY-R2-UF-2	212	271	141	15	90	<LOD	<LOD	128	20	14	<LOD	<LOD	<LOD
PEY-R2-UF-3	179	129	<LOD	14	72	<LOD	<LOD	<LOD	22	16	<LOD	<LOD	<LOD
OPA-R2-UF-1	549	92	152	123	95	<LOD	<LOD	<LOD	27	17	<LOD	<LOD	<LOD
OPA-R2-UF-2	577	101	161	120	102	<LOD	<LOD	<LOD	25	18	<LOD	<LOD	<LOD
OPA-R2-UF-3	503	96	143	120	104	<LOD	<LOD	<LOD	24	17	<LOD	<LOD	<LOD
PAR-R2-UF-1	1646	115	268	736	355	<LOD	78	<LOD	n.d.	11	<LOD	<LOD	<LOD
PAR-R2-UF-2	1654	530	406	728	381	<LOD	112	51	n.d.	12	<LOD	<LOD	<LOD
PAR-R2-UF-3	1450	98	211	687	327	<LOD	71	<LOD	n.d.	11	<LOD	<LOD	<LOD
AZU-R2-UF-1	5456	175	156	232	49	<LOD	<LOD	<LOD	67	77	<LOD	<LOD	<LOD
AZU-R2-UF-2	5296	179	140	237	55	<LOD	<LOD	<LOD	67	78	<LOD	<LOD	<LOD
AZU-R2-UF-3	5318	183	156	239	55	<LOD	<LOD	<LOD	68	79	<LOD	<LOD	<LOD
ARN-R2-UF-1	1969	117	96	651	150	<LOD	<LOD	<LOD	35	23	<LOD	<LOD	<LOD
ARN-R2-UF-2	1974	137	107	662	156	<LOD	<LOD	<LOD	38	23	<LOD	<LOD	<LOD
ARN-R2-UF-3	1949	113	144	675	149	<LOD	<LOD	<LOD	40	24	<LOD	<LOD	<LOD
BAC-R2-UF-1	2524	111	584	198	96	<LOD	<LOD	<LOD	34	35	<LOD	<LOD	<LOD
BAC-R2-UF-2	2811	214	524	205	130	<LOD	<LOD	<LOD	33	35	<LOD	<LOD	<LOD

BAC-R2-UF-3	2695	110	245	206	101	<LOD	<LOD	<LOD	32	33	<LOD	<LOD	<LOD
COA-R2-UF-1	1007	255	<LOD	67	92	<LOD	<LOD	<LOD	27	16	<LOD	<LOD	<LOD
COA-R2-UF-2	924	207	69	69	75	<LOD	<LOD	<LOD	25	18	<LOD	<LOD	<LOD
COA-R2-UF-3	955	209	75	66	82	<LOD	<LOD	<LOD	26	17	<LOD	<LOD	<LOD
PAN-R2-UF-1	2799	115	207	366	127	<LOD	<LOD	<LOD	28	34	<LOD	<LOD	<LOD
PAN-R2-UF-2	2694	114	186	289	124	<LOD	<LOD	<LOD	36	31	<LOD	<LOD	<LOD
PAN-R2-UF-3	2801	121	197	290	124	<LOD	<LOD	<LOD	27	29	<LOD	<LOD	<LOD

REPLIM 3	Ca	Na	Mg	K	Al	Sr	Fe	Mn	Ba
	$\mu\text{g L}^{-1}$								
LOD	15	18	15	4	2	0.2	8.1	0.39	0.23
ARA-R3-F-T1	7939	255	196	71	<LOD	21.3	<LOD	2.60	0.52
ARA-R3-F-T3	8196	204	199	57	<LOD	21.4	<LOD	2.52	0.26
ARA-R3-F-T4	7841	208	192	60	<LOD	21.2	<LOD	2.34	0.29
ARA-R3-F-P1=T2	7616	185	184	50	<LOD	21.1	<LOD	2.52	0.25
ARA-R3-F-P2	8544	206	203	57	<LOD	22.5	<LOD	2.66	0.29
ARA-R3-F-P3	8320	193	198	53	<LOD	23.0	<LOD	2.42	0.23
ARA-R3-F-P4	8561	209	204	60	<LOD	22.8	8.3	6.69	0.33
BAD-R3-F	13210	200	327	63	<LOD	35.1	<LOD	<LOD	<LOD
CAM-R3-F	1322	194	55	47	<LOD	2.5	<LOD	<LOD	0.39
PEY-R3-F	81	36	<LOD	17	<LOD	<LOD	<LOD	1.27	0.31
OPA-R3-F	3824	226	102	141	<LOD	7.0	<LOD	<LOD	0.91
PAR-R3-F	7992	1028	257	173	3.8	20.5	<LOD	0.57	0.66
GEN-R3-F-T1	1708	176	46	23	<LOD	4.7	<LOD	0.63	0.57
GEN-R3-F-T3	3857	401	101	58	<LOD	13.0	<LOD	2.20	1.73
GEN-R3-F-T4	4017	450	111	56	<LOD	13.3	<LOD	8.58	1.80
GEN-R3-F-P1=T2	3825	446	105	53	<LOD	13.4	<LOD	1.90	1.68
GEN-R3-F-P2	3931	399	98	54	<LOD	13.4	<LOD	3.24	1.79
GEN-R3-F-P3	4184	422	113	64	<LOD	13.4	<LOD	1.92	1.72
GEN-R3-F-P4	6647	542	161	165	<LOD	20.4	<LOD	162.20	3.99
GEN-R3-F-P5	9397	681	215	294	<LOD	26.7	2727.0	724.90	10.06
ROU-R3-F	4100	433	101	57	<LOD	13.5	<LOD	1.96	1.72
BER-R3-F	1398	206	50	33	<LOD	6.4	<LOD	1.45	1.78
AZU-R3-F-T2	35820	627	630	217	22.9	100.7	<LOD	8.85	18.57
AZU-R3-F-P1=T1	10140	203	185	73	<LOD	28.6	<LOD	2.71	5.12
AZU-R3-F-P2	10380	184	187	68	<LOD	30.7	<LOD	2.86	5.81
AZU-R3-F-P3	10610	181	191	68	<LOD	31.3	<LOD	3.06	5.75
ARN-R3-F	2750	233	70	64	<LOD	5.3	<LOD	<LOD	<LOD
BAC-R3-F	3948	178	100	69	3.3	12.1	<LOD	1.36	1.11

PEC-R3-F	4563	143	121	44	<LOD	13.5	<LOD	<LOD	<LOD
COA-R3-F	1323	166	49	48	<LOD	2.4	<LOD	<LOD	0.40
PAN-R3-F	4678	335	111	73	<LOD	12.6	<LOD	0.83	0.83
ORD-R3-F	9101	305	185	100	11.8	19.4	20.1	4.45	0.51
SAB-R3-F-T1	16520	162	5504	98	<LOD	72.3	<LOD	1.39	5.33
SAB-R3-F-T3	15880	139	5299	77	<LOD	72.8	<LOD	0.67	5.35
SAB-R3-F-P1=T2	17080	159	5657	91	<LOD	75.6	<LOD	1.90	5.65
SAB-R3-F-P2	16580	154	5450	104	<LOD	72.6	<LOD	0.56	5.43
SAB-R3-F-P3	19470	172	6582	114	<LOD	89.5	<LOD	0.82	8.05
SAB-R3-F-P4	19810	185	6419	127	63.0	93.1	<LOD	2.17	9.10
SAB-R3-F-P5	20550	174	6615	136	<LOD	100.8	<LOD	20.37	11.00
SAB-R3-F-P6	21410	190	6890	162	<LOD	102.0	208.2	189.50	12.69
ARA-R3-UF-T1	8279	233	203	58	3.9	22.5	<LOD	3.08	0.57
ARA-R3-UF-T3	10210	239	244	68	2.8	27.9	12.7	3.74	0.39
ARA-R3-UF-T4	8138	201	208	57	44.1	22.4	<LOD	2.75	0.39
ARA-R3-UF-P1=T2	7779	180	194	50	16.2	21.8	9.8	2.98	0.29
ARA-R3-UF-P2	8458	194	204	55	4.9	23.2	9.7	3.06	0.32
ARA-R3-UF-P3	8423	187	200	53	<LOD	22.6	8.8	2.82	0.24
ARA-R3-UF-P4	8183	182	197	54	6.3	22.9	47.2	7.00	0.37
BAD-R3-UF	13520	209	347	76	15.9	36.8	8.7	0.55	<LOD
CAM-R3-UF	1250	171	57	42	7.5	2.5	<LOD	0.49	0.43
PEY-R3-UF	122	22	51	34	72.4	0.3	51.2	2.72	1.05
OPA-R3-UF	3874	218	113	147	29.2	7.1	15.0	<LOD	1.13
PAR-R3-UF	7910	989	255	176	16.0	20.8	<LOD	0.61	0.69
GEN-R3-UF-T1	4078	398	106	53	6.4	13.6	<LOD	2.77	1.79
GEN-R3-UF-T3	4074	399	105	56	4.8	13.3	<LOD	2.79	1.81
GEN-R3-UF-T4	3956	432	108	58	5.3	14.0	14.9	9.54	2.03
GEN-R3-UF-P1=T2	4237	472	121	58	7.1	14.7	<LOD	2.83	1.87
GEN-R3-UF-P2	3954	381	99	52	4.3	13.6	<LOD	4.84	1.89
GEN-R3-UF-P3	4470	433	117	66	5.3	14.6	<LOD	5.70	1.94
GEN-R3-UF-P4	6693	532	168	168	3.7	20.8	38.0	192.70	4.35

GEN-R3-UF-P5	10110	747	239	361	4.6	28.1	3357.0	784.90	10.65
ROU-R3-UF	4303	446	108	62	10.4	14.2	9.8	4.01	1.87
BER-R3-UF	1649	226	66	39	19.4	7.8	11.9	2.01	2.32
AZU-R3-UF-T2	9630	172	174	64	5.8	28.5	<LOD	2.69	5.23
AZU-R3-UF-P1=T1	9989	180	182	68	8.3	29.4	<LOD	3.03	5.39
AZU-R3-UF-P2	10870	186	202	71	62.5	32.9	9.0	3.43	6.21
AZU-R3-UF-P3	12720	208	226	77	7.3	36.8	8.1	4.17	7.01
ARN-R3-UF	2737	227	72	60	9.6	5.5	<LOD	<LOD	<LOD
BAC-R3-UF	4288	197	118	74	10.9	12.5	11.5	3.05	1.23
PEC-R3-UF	4379	131	122	44	14.3	12.8	<LOD	0.54	<LOD
COA-R3-UF	1429	177	54	51	7.3	2.7	<LOD	<LOD	0.48
PAN-R3-UF	5023	351	119	79	6.3	12.9	<LOD	1.83	0.86
ORD-R3-UF	9475	332	192	119	5.0	19.7	<LOD	1.09	0.50
SAB-R3-UF-T1	16900	151	5551	87	<LOD	73.5	<LOD	2.47	5.47
SAB-R3-UF-T3	15880	143	5298	79	4.5	71.6	<LOD	1.64	5.31
SAB-R3-UF-P1=T2	15330	136	5128	76	5.5	73.8	<LOD	2.89	5.65
SAB-R3-UF-P2	16400	135	5345	86	<LOD	73.8	<LOD	1.29	5.66
SAB-R3-UF-P3	18570	154	6212	108	<LOD	92.5	<LOD	2.35	8.60
SAB-R3-UF-P4	19570	165	6388	118	4.1	95.8	18.6	4.24	9.66
SAB-R3-UF-P5	20740	171	6695	140	<LOD	99.2	61.7	24.90	11.03
SAB-R3-UF-P6	20510	170	6530	150	<LOD	102.2	448.5	189.00	13.17

REPLIM 3	As	Cu	Ti	Mo	V	Ni	Cr	Pb	Se	Sb	Co	Cd	Tl
	ng L ⁻¹												
LOD	131	83	13	22	41	82	33	117	1	6	111	90	19
ARA-R3-F-T1	788	<LOD	181	112	55	<LOD	49	<LOD	47	12	<LOD	<LOD	<LOD
ARA-R3-F-T3	840	<LOD	90	120	58	<LOD	49	<LOD	47	15	<LOD	<LOD	<LOD
ARA-R3-F-T4	805	<LOD	102	115	57	<LOD	42	<LOD	47	12	<LOD	<LOD	<LOD
ARA-R3-F-P1=T2	784	<LOD	84	114	61	<LOD	52	<LOD	47	13	<LOD	<LOD	<LOD
ARA-R3-F-P2	836	<LOD	79	116	60	<LOD	48	<LOD	46	12	<LOD	<LOD	<LOD
ARA-R3-F-P3	820	<LOD	78	117	60	<LOD	44	<LOD	44	12	<LOD	<LOD	<LOD
ARA-R3-F-P4	822	<LOD	95	118	64	<LOD	50	<LOD	47	13	<LOD	<LOD	<LOD
BAD-R3-F	497	<LOD	165	102	90	<LOD	163	<LOD	68	9	<LOD	<LOD	<LOD
CAM-R3-F	262	<LOD	<LOD	22	<LOD	<LOD	<LOD	<LOD	13	11	<LOD	<LOD	<LOD
PEY-R3-F	<LOD	7	<LOD	<LOD	<LOD	<LOD							
OPA-R3-F	228	<LOD	<LOD	36	52	<LOD	<LOD	<LOD	19	13	<LOD	<LOD	<LOD
PAR-R3-F	1230	<LOD	290	500	341	<LOD	105	<LOD	29	12	<LOD	<LOD	<LOD
GEN-R3-F-T1	144	227	<LOD	75	<LOD	<LOD	<LOD	<LOD	12	23	<LOD	<LOD	<LOD
GEN-R3-F-T3	193	<LOD	31	69	44	<LOD	<LOD	<LOD	13	58	<LOD	<LOD	<LOD
GEN-R3-F-T4	235	<LOD	72	51	46	<LOD	<LOD	<LOD	13	59	<LOD	<LOD	<LOD
GEN-R3-F-P1=T2	197	<LOD	63	68	<LOD	<LOD	<LOD	<LOD	14	58	<LOD	<LOD	<LOD
GEN-R3-F-P2	217	<LOD	18	29	<LOD	<LOD	<LOD	<LOD	14	62	<LOD	<LOD	<LOD
GEN-R3-F-P3	260	<LOD	30	28	<LOD	<LOD	<LOD	<LOD	14	57	<LOD	<LOD	<LOD
GEN-R3-F-P4	319	<LOD	62	23	<LOD	<LOD	<LOD	<LOD	14	54	<LOD	<LOD	<LOD
GEN-R3-F-P5	3026	<LOD	265	41	44	<LOD	<LOD	<LOD	23	43	<LOD	<LOD	<LOD
ROU-R3-F	160	<LOD	25	<LOD	<LOD	<LOD	<LOD	<LOD	13	58	<LOD	<LOD	<LOD
BER-R3-F	<LOD	14	10	<LOD	<LOD	<LOD							
AZU-R3-F-T2	12520	<LOD	639	1155	113	<LOD	144	<LOD	49	201	<LOD	<LOD	<LOD
AZU-R3-F-P1=T1	4075	<LOD	44	99	<LOD	<LOD	<LOD	<LOD	51	64	<LOD	<LOD	<LOD
AZU-R3-F-P2	3932	<LOD	39	115	<LOD	<LOD	273	<LOD	54	68	<LOD	<LOD	<LOD
AZU-R3-F-P3	4041	<LOD	53	103	<LOD	<LOD	<LOD	<LOD	57	65	<LOD	<LOD	<LOD
ARN-R3-F	973	<LOD	16	206	109	<LOD	<LOD	<LOD	18	14	<LOD	<LOD	<LOD
BAC-R3-F	2479	<LOD	<LOD	101	65	<LOD	<LOD	<LOD	20	22	<LOD	<LOD	<LOD

PEC-R3-F	7640	<LOD	14	65	47	<LOD	<LOD	3203	27	36	<LOD	<LOD	<LOD
COA-R3-F	522	<LOD	<LOD	<LOD	79	<LOD	<LOD	<LOD	11	11	<LOD	<LOD	<LOD
PAN-R3-F	2511	<LOD	33	158	100	<LOD	<LOD	<LOD	22	24	<LOD	<LOD	<LOD
ORD-R3-F	1620	<LOD	247	92	165	<LOD	36	<LOD	25	17	<LOD	<LOD	<LOD
SAB-R3-F-T1	228	<LOD	87	26	<LOD	<LOD	<LOD	<LOD	16	31	<LOD	<LOD	<LOD
SAB-R3-F-T3	288	<LOD	77	28	<LOD	<LOD	<LOD	<LOD	18	34	<LOD	<LOD	<LOD
SAB-R3-F-P1=T2	362	<LOD	106	26	<LOD	340	<LOD	<LOD	16	35	<LOD	<LOD	<LOD
SAB-R3-F-P2	345	<LOD	73	34	<LOD	<LOD	<LOD	<LOD	17	30	<LOD	<LOD	<LOD
SAB-R3-F-P3	414	<LOD	149	26	<LOD	<LOD	<LOD	<LOD	20	30	<LOD	<LOD	<LOD
SAB-R3-F-P4	493	<LOD	194	30	65	<LOD	<LOD	<LOD	20	29	<LOD	<LOD	<LOD
SAB-R3-F-P5	429	<LOD	182	25	<LOD	<LOD	<LOD	<LOD	20	25	<LOD	<LOD	<LOD
SAB-R3-F-P6	485	<LOD	265	29	<LOD	<LOD	<LOD	<LOD	17	28	<LOD	<LOD	<LOD
ARA-R3-UF-T1	925	<LOD	145	116	77	<LOD	54	<LOD	62	12	<LOD	<LOD	<LOD
ARA-R3-UF-T3	1062	<LOD	186	151	76	<LOD	86	<LOD	59	17	<LOD	<LOD	<LOD
ARA-R3-UF-T4	980	140	173	114	90	<LOD	69	<LOD	60	12	<LOD	<LOD	<LOD
ARA-R3-UF-P1=T2	867	<LOD	155	116	81	<LOD	65	<LOD	59	11	<LOD	<LOD	<LOD
ARA-R3-UF-P2	927	<LOD	173	114	81	<LOD	68	<LOD	62	12	<LOD	<LOD	<LOD
ARA-R3-UF-P3	859	<LOD	132	111	65	<LOD	55	<LOD	62	13	<LOD	<LOD	<LOD
ARA-R3-UF-P4	962	<LOD	146	112	72	<LOD	62	<LOD	61	16	<LOD	<LOD	<LOD
BAD-R3-UF	490	<LOD	664	106	113	<LOD	181	<LOD	89	10	<LOD	<LOD	<LOD
CAM-R3-UF	255	<LOD	319	<LOD	48	<LOD	<LOD	<LOD	18	10	<LOD	<LOD	<LOD
PEY-R3-UF	<LOD	<LOD	2084	<LOD	125	<LOD	47	<LOD	13	<LOD	<LOD	<LOD	<LOD
OPA-R3-UF	276	<LOD	580	33	80	<LOD	<LOD	<LOD	24	14	<LOD	<LOD	<LOD
PAR-R3-UF	1283	<LOD	280	521	345	<LOD	96	<LOD	41	13	<LOD	<LOD	<LOD
GEN-R3-UF-T1	247	<LOD	331	46	45	<LOD	<LOD	<LOD	16	59	<LOD	<LOD	<LOD
GEN-R3-UF-T3	245	<LOD	259	35	44	<LOD	<LOD	<LOD	17	54	<LOD	<LOD	<LOD
GEN-R3-UF-T4	237	<LOD	311	32	50	<LOD	<LOD	<LOD	17	62	<LOD	<LOD	<LOD
GEN-R3-UF-P1=T2	186	<LOD	295	46	94	<LOD	35	<LOD	19	63	<LOD	<LOD	<LOD
GEN-R3-UF-P2	196	<LOD	378	<LOD	<LOD	<LOD	<LOD	<LOD	17	60	<LOD	<LOD	<LOD
GEN-R3-UF-P3	187	<LOD	367	<LOD	<LOD	<LOD	<LOD	<LOD	17	59	<LOD	<LOD	<LOD
GEN-R3-UF-P4	296	<LOD	317	<LOD	<LOD	97	<LOD	<LOD	17	55	<LOD	<LOD	<LOD

GEN-R3-UF-P5	3434	305	524	38	67	<LOD	<LOD	<LOD	14	53	<LOD	<LOD	<LOD
ROU-R3-UF	181	<LOD	247	<LOD	60	<LOD	<LOD	<LOD	19	61	<LOD	<LOD	<LOD
BER-R3-UF	<LOD	<LOD	610	<LOD	53	<LOD	<LOD	<LOD	29	12	<LOD	<LOD	<LOD
AZU-R3-UF-T2	4329	<LOD	183	98	44	<LOD	<LOD	<LOD	51	60	<LOD	<LOD	<LOD
AZU-R3-UF-P1=T1	4277	<LOD	162	100	46	<LOD	<LOD	<LOD	53	66	<LOD	<LOD	<LOD
AZU-R3-UF-P2	4294	<LOD	203	105	73	<LOD	43	<LOD	57	67	<LOD	<LOD	<LOD
AZU-R3-UF-P3	4954	<LOD	176	121	<LOD	<LOD	<LOD	<LOD	58	79	<LOD	<LOD	<LOD
ARN-R3-UF	985	<LOD	75	207	108	<LOD	<LOD	<LOD	21	16	<LOD	<LOD	<LOD
BAC-R3-UF	2913	<LOD	202	76	78	<LOD	<LOD	<LOD	27	23	<LOD	<LOD	<LOD
PEC-R3-UF	7418	<LOD	394	61	65	<LOD	<LOD	<LOD	29	35	<LOD	<LOD	<LOD
COA-R3-UF	544	<LOD	142	<LOD	71	<LOD	<LOD	<LOD	14	12	<LOD	<LOD	<LOD
PAN-R3-UF	2722	<LOD	165	155	126	<LOD	<LOD	<LOD	27	24	<LOD	<LOD	<LOD
ORD-R3-UF	1679	<LOD	114	95	150	<LOD	<LOD	<LOD	25	16	<LOD	<LOD	<LOD
SAB-R3-UF-T1	330	<LOD	86	26	<LOD	<LOD	<LOD	<LOD	24	32	<LOD	<LOD	<LOD
SAB-R3-UF-T3	305	<LOD	154	26	<LOD	<LOD	<LOD	<LOD	18	32	<LOD	<LOD	<LOD
SAB-R3-UF-P1=T2	318	<LOD	162	26	<LOD	<LOD	<LOD	<LOD	19	32	<LOD	<LOD	<LOD
SAB-R3-UF-P2	376	<LOD	100	29	<LOD	<LOD	<LOD	<LOD	21	32	<LOD	<LOD	<LOD
SAB-R3-UF-P3	385	<LOD	138	26	<LOD	<LOD	<LOD	<LOD	21	31	<LOD	<LOD	<LOD
SAB-R3-UF-P4	563	<LOD	191	25	<LOD	<LOD	<LOD	<LOD	22	29	<LOD	<LOD	<LOD
SAB-R3-UF-P5	511	<LOD	170	31	<LOD	<LOD	<LOD	<LOD	20	25	<LOD	<LOD	<LOD
SAB-R3-UF-P6	571	<LOD	281	27	<LOD	<LOD	<LOD	<LOD	19	28	<LOD	<LOD	<LOD

REPLIM 4	Ca	Na	Mg	K	Al	Sr	Fe	Mn	Ba
	$\mu\text{g L}^{-1}$								
LOD	15	1	2	1	1	0.2	0.7	0.35	0.11
ARA-R4-F-P1	11230	273	232	49	<LOD	21.3	7.3	<LOD	0.27
ARA-R4-F-P2	10650	257	220	43	1.9	21.4	7.4	<LOD	<LOD
ARA-R4-F-P3	10500	254	220	45	<LOD	22.4	6.8	1.83	0.11
BAD-R4-F	10740	251	231	60	4.6	23.7	4.0	<LOD	0.16
CAM-R4-F	2117	335	72	70	<LOD	3.4	1.5	0.82	0.31
PEY-R4-F	915	178	40	30	<LOD	1.3	<LOD	<LOD	0.11
OPA-R4-F	4074	324	97	120	<LOD	6.6	1.6	<LOD	0.68
PAR-R4-F	8163	1017	216	207	<LOD	15.9	10.7	0.97	0.31
GEN-R4-F-T1	2056	274	69	27	54.7	7.0	3.4	0.57	0.84
GEN-R4-F-T3	4956	516	113	34	<LOD	13.1	1.2	1.65	1.53
GEN-R4-F-P1=T2	520	1427	23	8710	<LOD	<LOD	<LOD	<LOD	<LOD
GEN-R4-F-P2	4830	516	110	31	<LOD	13.2	2.0	1.29	1.53
GEN-R4-F-P3	4718	505	108	31	<LOD	14.0	7.7	1.73	1.63
GEN-R4-F-P4	7246	578	158	129	<LOD	16.9	4.4	136.60	2.77
GEN-R4-F-P5	10200	711	208	303	<LOD	22.4	1261.0	763.30	8.25
ROU-R4-F	4727	508	109	64	<LOD	11.1	4.0	0.67	1.19
BER-R4-F	2930	359	75	34	<LOD	11.1	1.2	0.83	2.12
AZU-R4-F-P1=T1	10950	227	189	62	2.8	24.5	<LOD	0.37	3.38
AZU-R4-F-P2	10820	213	185	54	<LOD	24.3	<LOD	<LOD	3.28
AZU-R4-F-P3	10700	215	180	54	<LOD	24.1	<LOD	<LOD	3.29
ARN-R4-F	3746	312	85	54	<LOD	5.9	<LOD	0.62	0.18
BAC-R4-F	4452	205	100	67	<LOD	9.4	2.7	0.73	0.76
PEC-R4-F	6288	189	138	37	6.5	13.5	9.2	<LOD	<LOD
COA-R4-F	5334	575	221	157	33.6	7.4	12.9	1.24	1.44
PAN-R4-F	4762	619	143	122	1.9	10.0	7.2	2.31	0.84
ORD-R4-F	7868	397	179	150	4.9	10.8	6.2	0.95	0.39
SAB-R4-F-T1	13810	152	5185	63	<LOD	51.6	2.4	<LOD	3.22
SAB-R4-F-T3	13200	139	5036	61	<LOD	49.5	3.3	<LOD	3.13

SAB-R4-F-P1=T2	14020	151	5319	67	<LOD	49.8	3.9	<LOD	3.11
SAB-R4-F-P2	12890	139	4920	63	<LOD	48.9	3.1	<LOD	3.05
SAB-R4-F-P3	13210	142	5048	63	<LOD	49.0	2.7	<LOD	3.07
SAB-R4-F-P4	17110	154	5501	82	<LOD	55.7	2.4	<LOD	4.80
SAB-R4-F-P5	17190	167	5246	84	1.7	63.0	1.6	9.64	6.10
SAB-R4-F-P6	18270	161	5667	97	<LOD	63.8	1.0	16.56	6.42
ARA-R4-UF-P1	10710	253	222	42	<LOD	21.6	19.7	2.42	0.30
ARA-R4-UF-P2	10720	251	224	41	<LOD	21.8	19.2	2.26	<LOD
ARA-R4-UF-P3	11230	269	235	49	<LOD	22.5	26.7	5.14	0.11
BAD-R4-UF	10990	248	232	57	<LOD	24.7	3.0	1.36	0.14
CAM-R4-UF	2115	312	72	67	2.7	3.5	8.2	1.60	0.34
PEY-R4-UF	917	171	53	45	60.1	1.3	44.1	3.31	0.28
OPA-R4-UF	3964	303	98	113	14.9	6.3	15.5	1.13	0.79
PAR-R4-UF	7927	986	214	201	8.7	15.6	15.6	1.22	0.30
GEN-R4-UF-T1	5051	523	118	33	<LOD	13.4	14.8	7.67	1.55
GEN-R4-UF-T3	5152	528	118	36	5.4	14.0	22.1	7.91	1.72
GEN-R4-UF-P1=T2	4888	512	114	33	<LOD	13.5	17.0	10.63	1.67
GEN-R4-UF-P2	5409	574	125	39	<LOD	12.7	15.8	7.21	1.49
GEN-R4-UF-P3	4877	510	113	31	<LOD	13.6	14.7	7.76	1.60
GEN-R4-UF-P4	6479	506	139	106	<LOD	16.5	23.2	144.30	2.85
GEN-R4-UF-P5	10430	709	214	313	<LOD	21.2	1465.0	766.60	8.12
ROU-R4-UF	5025	541	117	72	4.6	11.8	14.0	2.98	1.26
BER-R4-UF	3012	343	76	31	1.7	11.3	2.4	1.43	2.19
AZU-R4-UF-P1=T1	10890	210	192	57	7.0	23.6	10.7	1.85	3.27
AZU-R4-UF-P2	10830	206	195	54	6.7	24.7	12.3	1.71	3.36
AZU-R4-UF-P3	10790	200	186	53	5.7	23.9	11.8	1.66	3.36
ARN-R4-UF	3998	312	90	54	7.9	5.9	2.7	1.04	0.19
BAC-R4-UF	4650	211	106	70	8.2	9.6	10.3	3.23	0.75
PEC-R4-UF	5884	164	129	33	<LOD	12.4	1.4	1.06	<LOD
COA-R4-UF	1537	170	56	43	14.8	2.1	8.3	0.44	0.40
PAN-R4-UF	4707	613	143	129	14.2	10.2	32.0	4.03	0.83

ORD-R4-UF	7360	343	163	119	11.6	10.7	8.0	1.30	0.35
SAB-R4-UF-T1	14050	155	5388	66	<LOD	50.3	8.0	1.29	3.13
SAB-R4-UF-T3	13210	138	5054	62	<LOD	49.0	8.0	0.86	3.10
SAB-R4-UF-P1=T2	13340	136	5028	60	<LOD	47.0	7.5	0.84	2.97
SAB-R4-UF-P2	14140	144	5299	66	<LOD	57.9	9.1	1.01	3.67
SAB-R4-UF-P3	15310	161	5775	75	<LOD	55.8	8.2	0.95	3.49
SAB-R4-UF-P4	19370	171	6282	94	<LOD	73.0	8.0	1.42	6.42
SAB-R4-UF-P5	19760	171	5980	100	<LOD	66.5	4.7	15.60	6.56
SAB-R4-UF-P6	19590	168	6124	107	<LOD	71.1	42.3	49.07	7.30

REPLIM 4	As	Cu	Ti	Mo	V	Ni	Cr	Pb	Se	Sb	Co	Cd	Tl
	ng L ⁻¹												
LOD	68	41	30	8	27	77	37	15	1	17	51	30	11
ARA-R4-F-P1	1196	<LOD	153	151	99	<LOD	85	<LOD	40	<LOD	<LOD	<LOD	<LOD
ARA-R4-F-P2	1123	<LOD	209	151	98	<LOD	79	<LOD	39	<LOD	<LOD	<LOD	<LOD
ARA-R4-F-P3	1065	<LOD	137	161	88	<LOD	84	<LOD	40	<LOD	<LOD	<LOD	<LOD
BAD-R4-F	622	<LOD	263	169	124	<LOD	110	32	43	<LOD	<LOD	<LOD	<LOD
CAM-R4-F	600	<LOD	64	92	62	<LOD	<LOD	<LOD	17	<LOD	<LOD	<LOD	<LOD
PEY-R4-F	84	<LOD	46	16	73	<LOD	<LOD	<LOD	11	<LOD	<LOD	<LOD	<LOD
OPA-R4-F	288	<LOD	90	86	87	<LOD	<LOD	<LOD	13	<LOD	<LOD	<LOD	<LOD
PAR-R4-F	1297	<LOD	210	462	301	<LOD	123	<LOD	31	<LOD	<LOD	<LOD	<LOD
GEN-R4-F-T1	319	942	150	61	106	<LOD	53	177	11	25	74	68	<LOD
GEN-R4-F-T3	285	114	69	55	46	<LOD	<LOD	<LOD	12	50	<LOD	<LOD	<LOD
GEN-R4-F-P1=T2	n.d.	4186	914	<LOD	34	<LOD	<LOD	<LOD	12	<LOD	777	n.d.	<LOD
GEN-R4-F-P2	208	<LOD	70	46	39	<LOD	<LOD	<LOD	11	51	<LOD	<LOD	<LOD
GEN-R4-F-P3	234	<LOD	59	34	38	<LOD	<LOD	<LOD	11	54	<LOD	<LOD	<LOD
GEN-R4-F-P4	269	<LOD	72	34	<LOD	<LOD	<LOD	<LOD	13	43	<LOD	<LOD	<LOD
GEN-R4-F-P5	1198	<LOD	171	27	<LOD	<LOD	<LOD	<LOD	14	29	77	<LOD	<LOD
ROU-R4-F	138	<LOD	56	30	57	<LOD	<LOD	<LOD	14	53	<LOD	<LOD	<LOD
BER-R4-F	<LOD	<LOD	45	16	44	<LOD	<LOD	<LOD	12	20	<LOD	<LOD	<LOD
AZU-R4-F-P1=T1	3685	<LOD	95	119	50	<LOD	40	19	48	49	<LOD	<LOD	<LOD
AZU-R4-F-P2	3651	<LOD	90	113	39	<LOD	<LOD	<LOD	47	47	<LOD	<LOD	<LOD
AZU-R4-F-P3	3640	<LOD	81	113	47	<LOD	39	<LOD	48	48	<LOD	<LOD	<LOD
ARN-R4-F	1156	<LOD	63	295	122	<LOD	<LOD	<LOD	23	<LOD	<LOD	<LOD	<LOD
BAC-R4-F	2028	<LOD	93	96	73	<LOD	<LOD	21	22	22	<LOD	<LOD	<LOD
PEC-R4-F	6746	82	220	85	59	<LOD	70	<LOD	32	40	<LOD	<LOD	<LOD
COA-R4-F	1529	549	274	93	208	<LOD	110	85	20	42	<LOD	<LOD	<LOD
PAN-R4-F	1825	<LOD	127	150	89	<LOD	46	<LOD	23	22	<LOD	<LOD	<LOD
ORD-R4-F	986	96	178	76	101	<LOD	73	46	20	<LOD	<LOD	<LOD	<LOD
SAB-R4-F-T1	75	<LOD	73	28	<LOD	<LOD	<LOD	<LOD	15	25	<LOD	<LOD	<LOD
SAB-R4-F-T3	<LOD	<LOD	76	28	<LOD	<LOD	<LOD	<LOD	15	24	<LOD	<LOD	<LOD

SAB-R4-F-P1=T2	93	<LOD	83	27	<LOD	<LOD	<LOD	<LOD	15	25	<LOD	<LOD	<LOD
SAB-R4-F-P2	<LOD	<LOD	72	26	<LOD	<LOD	<LOD	<LOD	16	24	<LOD	<LOD	<LOD
SAB-R4-F-P3	94	<LOD	75	26	<LOD	<LOD	<LOD	<LOD	15	23	<LOD	<LOD	<LOD
SAB-R4-F-P4	200	<LOD	117	24	<LOD	<LOD	<LOD	<LOD	14	20	<LOD	<LOD	<LOD
SAB-R4-F-P5	125	<LOD	239	25	<LOD	<LOD	<LOD	<LOD	15	20	<LOD	<LOD	<LOD
SAB-R4-F-P6	215	<LOD	159	25	<LOD	<LOD	<LOD	<LOD	17	19	<LOD	<LOD	<LOD
ARA-R4-UF-P1	1169	<LOD	157	151	110	<LOD	81	<LOD	n.d.	<LOD	<LOD	<LOD	<LOD
ARA-R4-UF-P2	1149	<LOD	141	152	102	<LOD	79	<LOD	54	<LOD	<LOD	<LOD	<LOD
ARA-R4-UF-P3	1243	<LOD	138	155	93	<LOD	81	<LOD	49	<LOD	<LOD	<LOD	<LOD
BAD-R4-UF	659	<LOD	141	168	121	<LOD	104	<LOD	52	<LOD	<LOD	<LOD	<LOD
CAM-R4-UF	599	<LOD	113	89	71	<LOD	<LOD	<LOD	20	<LOD	<LOD	<LOD	<LOD
PEY-R4-UF	115	<LOD	1238	12	124	<LOD	39	356	20	<LOD	<LOD	<LOD	<LOD
OPA-R4-UF	329	<LOD	271	79	103	<LOD	<LOD	79	23	<LOD	<LOD	<LOD	<LOD
PAR-R4-UF	1229	<LOD	261	459	349	<LOD	125	<LOD	36	<LOD	<LOD	<LOD	<LOD
GEN-R4-UF-T1	277	85	76	61	50	<LOD	<LOD	<LOD	17	50	<LOD	<LOD	<LOD
GEN-R4-UF-T3	252	64	355	38	49	<LOD	<LOD	<LOD	16	54	<LOD	<LOD	<LOD
GEN-R4-UF-P1=T2	225	100	93	41	44	<LOD	<LOD	<LOD	16	51	<LOD	<LOD	<LOD
GEN-R4-UF-P2	165	<LOD	211	30	33	<LOD	<LOD	<LOD	18	47	<LOD	<LOD	<LOD
GEN-R4-UF-P3	125	<LOD	83	27	35	<LOD	<LOD	<LOD	16	51	<LOD	<LOD	<LOD
GEN-R4-UF-P4	181	<LOD	84	25	28	<LOD	<LOD	<LOD	17	42	<LOD	<LOD	<LOD
GEN-R4-UF-P5	1337	<LOD	193	26	<LOD	1068	<LOD	<LOD	22	31	84	<LOD	<LOD
ROU-R4-UF	174	72	96	24	68	377	<LOD	<LOD	19	54	<LOD	<LOD	<LOD
BER-R4-UF	<LOD	<LOD	70	13	48	<LOD	<LOD	<LOD	18	20	<LOD	<LOD	<LOD
AZU-R4-UF-P1=T1	3703	<LOD	197	110	57	<LOD	44	37	57	45	<LOD	<LOD	<LOD
AZU-R4-UF-P2	3694	<LOD	249	114	54	<LOD	44	30	56	48	<LOD	<LOD	<LOD
AZU-R4-UF-P3	3729	<LOD	198	111	47	<LOD	38	28	57	46	<LOD	<LOD	<LOD
ARN-R4-UF	1194	<LOD	98	299	120	<LOD	39	<LOD	29	<LOD	<LOD	<LOD	<LOD
BAC-R4-UF	2251	266	290	101	86	<LOD	56	46	30	23	<LOD	<LOD	<LOD
PEC-R4-UF	6393	<LOD	93	76	56	<LOD	52	<LOD	39	35	<LOD	<LOD	<LOD
COA-R4-UF	490	160	182	24	74	<LOD	<LOD	29	26	<LOD	<LOD	<LOD	<LOD
PAN-R4-UF	2243	56	354	146	114	<LOD	92	37	31	28	<LOD	<LOD	<LOD

ORD-R4-UF	866	<LOD	174	72	108	<LOD	76	28	26	<LOD	<LOD	<LOD	<LOD
SAB-R4-UF-T1	<LOD	<LOD	206	25	<LOD	<LOD	<LOD	<LOD	20	24	<LOD	<LOD	<LOD
SAB-R4-UF-T3	<LOD	<LOD	112	33	<LOD	<LOD	<LOD	<LOD	19	24	<LOD	<LOD	<LOD
SAB-R4-UF-P1=T2	123	<LOD	95	24	30	<LOD	<LOD	<LOD	21	22	<LOD	<LOD	<LOD
SAB-R4-UF-P2	141	<LOD	83	30	36	<LOD	<LOD	<LOD	21	27	<LOD	<LOD	<LOD
SAB-R4-UF-P3	193	<LOD	268	30	29	<LOD	<LOD	<LOD	23	27	<LOD	<LOD	<LOD
SAB-R4-UF-P4	254	<LOD	179	32	30	<LOD	<LOD	<LOD	19	27	<LOD	<LOD	<LOD
SAB-R4-UF-P5	202	<LOD	149	26	<LOD	<LOD	<LOD	<LOD	20	20	<LOD	<LOD	<LOD
SAB-R4-UF-P6	235	<LOD	172	26	27	<LOD	<LOD	<LOD	21	18	<LOD	<LOD	<LOD

Annexe 2: Major, trace and ultra-trace elements results obtained by HR- ICP-MS

REPLIM 1	Ca	Na	Mg	K	Al	Sr	Fe	Mn	Ba
	$\mu\text{g L}^{-1}$								
LOD	7	1	0.3	9	0.3	0.002	0.07	0.004	0.002
ARA-R1-UF-1	n.d.								
ARA-R1-UF-2	13604	253	232.9	85	19.8	12.101	15.90	2.629	0.429
ARA-R1-UF-3	13056	222	226.6	63	11.7	11.756	16.10	2.672	0.476
BAD-R1-UF-1	15390	198	295.9	66	27.1	16.119	13.75	1.454	0.366
BAD-R1-UF-2	14871	178	274.9	52	20.9	14.933	12.88	1.455	0.328
BAD-R1-UF-3	14791	177	277.7	52	19.2	14.377	12.69	1.420	0.327
CAM-R1-UF-1	1934	198	68.1	48	13.6	1.503	6.92	0.725	0.524
CAM-R1-UF-2	1933	204	67.7	47	14.2	1.484	7.09	0.764	0.572
CAM-R1-UF-3	2043	204	68.4	50	16.6	1.522	8.17	0.834	0.525
PEY-R1-UF-1	1830	200	72.0	57	52.9	1.122	23.25	1.675	0.554
PEY-R1-UF-2	2352	205	66.1	38	62.8	1.214	23.09	1.654	0.530
PEY-R1-UF-3	n.d.								
OPA-R1-UF-1	5733	265	134.8	149	49.9	3.901	17.86	0.625	1.273
OPA-R1-UF-2	5500	253	132.2	148	39.4	3.895	17.39	0.617	1.254
OPA-R1-UF-3	5241	231	128.3	137	36.1	3.852	18.49	0.582	1.148
PAR-R1-UF-1	11211	1087	253.6	172	20.9	10.070	19.68	1.883	0.761
PAR-R1-UF-2	n.d.								
PAR-R1-UF-3	11522	1076	267.2	165	22.7	10.116	18.04	1.158	0.557
NER-R1-UF-1	2160	223	51.6	48	22.6	1.704	3.87	0.535	1.068
NER-R1-UF-2	2064	218	52.3	45	20.5	1.638	3.99	0.544	1.091
NER-R1-UF-3	n.d.								
POU-R1-UF-1	3252	291	51.6	56	20.0	2.248	7.36	0.839	0.480
POU-R1-UF-2	3258	260	48.2	45	22.3	2.205	6.92	0.741	0.306
POU-R1-UF-3	3328	273	51.9	56	23.4	2.219	7.26	0.824	0.419
AZU-R1-UF-1	16384	222	228.0	73	15.2	17.717	6.61	1.258	6.155
AZU-R1-UF-2	16683	236	234.6	107	16.4	18.372	6.98	1.320	5.537
AZU-R1-UF-3	16598	202	228.7	64	10.7	19.388	4.72	1.042	4.360
ARN-R1-UF-1	4520	261	87.1	58	26.9	2.969	2.90	0.261	0.449

ARN-R1-UF-2	4212	251	85.5	54	17.3	2.885	3.00	0.226	0.369
ARN-R1-UF-3	3953	235	82.6	49	12.3	2.807	2.34	0.202	0.266
BAC-R1-UF-1	6003	211	127.1	50	15.0	6.117	14.26	4.627	0.768
BAC-R1-UF-2	6049	213	129.5	53	16.3	6.141	20.00	5.059	0.785
BAC-R1-UF-3	6084	217	127.7	61	24.8	6.171	16.74	3.653	0.825
PEC-R1-UF-1	8909	165	168.1	44	12.7	8.932	5.48	3.356	0.309
PEC-R1-UF-2	8890	176	168.7	47	12.6	8.817	5.23	3.235	0.303
PEC-R1-UF-3	8838	160	167.8	40	10.8	8.813	4.98	2.908	0.190
COA-R1-UF-1	2579	215	73.7	40	23.1	1.737	6.88	0.611	1.007
COA-R1-UF-2	n.d.	n.d.	n.d.	n.d.	n.d.	n.d.	n.d.	n.d.	n.d.
COA-R1-UF-3	2983	247	78.8	57	33.0	1.868	7.74	0.733	0.998
PAN-R1-UF-1	n.d.	n.d.	n.d.	n.d.	n.d.	n.d.	n.d.	n.d.	n.d.
PAN-R1-UF-2	8883	405	152.5	74	16.4	7.539	9.16	1.615	0.721
PAN-R1-UF-3	7853	446	145.6	78	14.3	7.019	9.45	1.687	0.792
ORD-R1-UF-1	12775	298	199.8	54	16.0	8.834	14.10	2.125	0.795
ORD-R1-UF-2	13042	324	201.4	60	25.4	8.857	15.10	2.155	0.577
ORD-R1-UF-3	n.d.	n.d.	n.d.	n.d.	n.d.	n.d.	n.d.	n.d.	n.d.
XUA-R1-UF-1	3812	216	98.2	76	37.1	2.290	23.56	1.877	0.750
XUA-R1-UF-2	3608	190	95.5	59	28.6	2.227	23.20	2.007	0.884
XUA-R1-UF-3	3555	189	97.5	60	28.2	2.229	23.58	2.031	0.805

REPLIM 1	As	U	Cu	Ti	Mo	V	Ni	Cr	Pb	Sb	Co	Cd	Tl
	ng L ⁻¹												
LOD	0.5	0.1	18	2	2	0.1	11	3	2	2	0.1	0.5	0.2
ARA-R1-UF-1	n.d.												
ARA-R1-UF-2	946.6	197.0	276	127	159	97.7	121	376	66	18	16.4	4.4	0.5
ARA-R1-UF-3	936.1	193.4	195	173	152	93.5	88	183	46	20	16.6	3.4	0.4
BAD-R1-UF-1	573.0	247.9	139	249	134	125.6	80	205	40	11	15.6	2.0	0.6
BAD-R1-UF-2	560.5	242.0	117	214	129	122.6	52	197	65	9	15.4	1.6	0.5
BAD-R1-UF-3	563.0	242.5	105	215	129	122.6	46	195	31	10	15.4	1.5	0.5
CAM-R1-UF-1	293.5	683.5	78	127	42	57.9	30	27	35	14	7.0	1.7	0.5
CAM-R1-UF-2	294.5	626.2	103	116	41	58.3	58	26	34	13	7.2	1.6	0.5
CAM-R1-UF-3	299.6	679.5	102	142	42	59.4	45	29	39	13	7.1	1.7	0.5
PEY-R1-UF-1	89.6	147.6	214	478	15	76.8	104	66	78	16	21.3	3.1	1.0
PEY-R1-UF-2	88.4	144.6	n.d.	488	18	77.8	53	58	90	11	19.6	3.0	1.0
PEY-R1-UF-3	n.d.												
OPA-R1-UF-1	352.9	1260.7	n.d.	427	75	96.9	120	87	87	18	15.9	3.0	1.0
OPA-R1-UF-2	352.6	1250.3	136	392	73	93.5	70	76	73	18	15.1	2.4	0.9
OPA-R1-UF-3	354.6	1339.2	104	417	71	99.1	36	59	72	16	16.1	1.8	0.9
PAR-R1-UF-1	1430.0	2302.5	431	229	533	379.1	94	166	38	24	25.1	4.3	1.3
PAR-R1-UF-2	n.d.												
PAR-R1-UF-3	1502.6	2501.3	195	262	564	406.6	n.d.	167	29	14	17.7	4.2	1.3
NER-R1-UF-1	71.8	725.6	158	89	12	43.2	87	23	46	15	6.3	2.6	0.7
NER-R1-UF-2	70.8	691.0	139	112	13	42.6	75	26	36	12	6.0	2.7	0.6
NER-R1-UF-3	n.d.												
POU-R1-UF-1	122.7	840.6	172	116	14	46.7	115	37	39	16	8.7	2.7	0.6
POU-R1-UF-2	121.6	903.4	131	145	13	47.2	54	31	32	241	7.4	1.9	0.5
POU-R1-UF-3	121.8	839.5	211	125	15	48.1	113	41	42	18	8.3	2.2	0.5
AZU-R1-UF-1	4512.0	113.0	136	80	135	42.4	46	61	29	83	8.3	3.3	0.4
AZU-R1-UF-2	4848.7	107.3	n.d.	83	142	46.2	n.d.	87	73	85	8.6	4.8	0.4
AZU-R1-UF-3	5463.4	107.6	84	49	151	44.1	29	69	19	72	7.1	2.3	0.3
ARN-R1-UF-1	1142.4	534.1	134	67	258	129.6	52	60	19	18	5.3	2.2	0.5

ARN-R1-UF-2	1146.3	519.4	133	54	259	128.3	72	61	18	17	5.1	2.1	0.4
ARN-R1-UF-3	1128.6	513.2	123	50	256	124.7	30	49	15	18	4.6	1.8	0.4
BAC-R1-UF-1	3032.2	167.4	100	140	138	97.9	30	65	21	24	11.7	1.9	0.6
BAC-R1-UF-2	3184.5	180.1	103	255	139	112.7	31	69	31	25	14.1	2.1	0.6
BAC-R1-UF-3	3146.8	165.7	162	356	141	117.9	34	73	35	25	12.8	2.5	0.8
PEC-R1-UF-1	8909.0	76.8	94	97	116	63.8	30	75	17	47	8.1	1.1	0.3
PEC-R1-UF-2	8819.4	73.6	104	90	114	60.9	33	76	20	48	8.5	1.3	0.3
PEC-R1-UF-3	9002.0	69.4	105	81	116	63.7	28	76	13	48	7.0	1.1	0.3
COA-R1-UF-1	792.4	452.8	167	81	56	100.9	76	40	39	18	10.3	5.6	1.1
COA-R1-UF-2	n.d.	n.d.	n.d.	n.d.	n.d.	n.d.	n.d.	n.d.	n.d.	n.d.	n.d.	n.d.	n.d.
COA-R1-UF-3	807.8	464.0	237	115	58	106.5	104	55	56	20	12.2	6.7	1.2
PAN-R1-UF-1	n.d.	n.d.	n.d.	n.d.	n.d.	n.d.	n.d.	n.d.	n.d.	n.d.	n.d.	n.d.	n.d.
PAN-R1-UF-2	3073.2	598.0	132	102	228	132.2	33	69	27	30	8.6	2.4	0.9
PAN-R1-UF-3	3039.5	622.3	131	103	242	135.7	31	69	31	29	9.2	2.6	0.7
ORD-R1-UF-1	1645.7	495.9	182	93	125	164.7	76	102	52	17	18.1	2.2	0.6
ORD-R1-UF-2	1650.7	372.1	340	132	124	167.8	117	107	67	19	18.8	2.7	0.7
ORD-R1-UF-3	n.d.	n.d.	n.d.	n.d.	n.d.	n.d.	n.d.	n.d.	n.d.	n.d.	n.d.	n.d.	n.d.
XUA-R1-UF-1	280.0	367.5	191	292	93	123.7	87	69	57	17	19.4	3.5	1.0
XUA-R1-UF-2	269.0	337.3	128	308	91	111.9	39	55	43	15	19.7	2.9	0.9
XUA-R1-UF-3	270.9	355.9	129	305	91	112.1	62	56	44	16	20.6	2.8	1.2

REPLIM 2	Ca	Na	Mg	K	Al	Sr	Fe	Mn	Ba
	$\mu\text{g L}^{-1}$								
LOD	7	1	0.3	9	0.3	0.002	0.07	0.004	0.002
ARA-R2-UF-1	16104	261	267.0	43	6.9	17.311	49.66	4.029	0.338
ARA-R2-UF-2	16211	260	267.3	44	7.4	17.277	49.83	4.357	0.250
ARA-R2-UF-3	15282	254	247.8	42	11.8	14.607	47.12	3.836	0.203
BAD-R2-UF-1	16453	279	276.0	79	13.6	20.143	8.66	2.893	0.351
BAD-R2-UF-2	15870	278	270.6	71	11.0	19.774	7.06	2.539	0.301
BAD-R2-UF-3	16319	266	276.1	73	9.9	20.446	8.12	2.927	0.306
CAM-R2-UF-1	2826	314	90.3	67	11.2	2.493	14.85	2.019	0.595
CAM-R2-UF-2	2775	310	90.9	65	11.2	2.471	14.59	2.015	0.535
CAM-R2-UF-3	n.d.								
PEY-R2-UF-1	1221	156	48.7	27	20.7	0.978	6.80	0.544	0.258
PEY-R2-UF-2	n.d.								
PEY-R2-UF-3	1392	175	54.7	29	23.9	1.105	7.36	0.630	0.304
OPA-R2-UF-1	5474	322	124.9	127	15.7	4.399	10.38	0.704	0.994
OPA-R2-UF-2	5495	321	122.7	129	15.8	4.377	10.56	0.689	0.966
OPA-R2-UF-3	5499	311	118.7	123	15.9	4.343	10.20	0.691	0.936
PAR-R2-UF-1	11658	1159	242.1	210	14.4	11.310	22.06	1.286	0.457
PAR-R2-UF-2	11865	1089	240.9	214	25.0	11.256	46.60	2.051	0.489
PAR-R2-UF-3	11391	1004	233.5	182	11.4	10.395	16.55	0.992	0.566
AZU-R2-UF-1	18222	232	228.2	69	10.0	22.542	2.85	1.210	4.779
AZU-R2-UF-2	18295	233	230.7	70	10.8	22.432	3.15	1.258	4.688
AZU-R2-UF-3	18100	234	229.5	70	11.5	22.344	3.23	1.246	4.660
ARN-R2-UF-1	6730	378	125.3	70	19.8	5.331	5.43	0.512	0.332
ARN-R2-UF-2	6796	372	121.9	71	21.3	5.342	5.51	0.489	0.333
ARN-R2-UF-3	5609	310	107.3	56	16.7	4.453	4.42	0.418	0.245
BAC-R2-UF-1	n.d.								
BAC-R2-UF-2	n.d.								
BAC-R2-UF-3	n.d.								
COA-R2-UF-1	3242	245	94.4	19	22.6	2.277	21.86	0.723	0.696

COA-R2-UF-2	3284	245	91.3	23	22.3	2.325	21.35	0.705	0.710
COA-R2-UF-3	3180	241	90.4	19	23.1	2.237	21.13	0.710	0.671
PAN-R2-UF-1	8123	763	142.8	84	13.4	8.297	13.63	1.832	1.100
PAN-R2-UF-2	8014	429	138.9	73	13.5	8.123	14.21	1.968	1.071
PAN-R2-UF-3	7994	433	140.3	74	13.8	7.973	14.73	2.005	1.052

REPLIM 2	As	U	Cu	Ti	Mo	V	Ni	Cr	Pb	Sb	Co	Cd	Tl
	ng L ⁻¹												
LOD	0.5	0.1	18	2	2	0.1	11	3	2	2	0.1	0.5	0.2
ARA-R2-UF-1	1620.8	421.7	206	20	218	109.5	110	121	21	20	22.7	2.9	0.7
ARA-R2-UF-2	1621.4	381.3	218	24	218	111.0	93	120	22	19	23.6	2.3	0.5
ARA-R2-UF-3	1526.9	352.6	274	36	204	105.3	100	123	n.d.	20	22.0	2.3	0.5
BAD-R2-UF-1	853.0	346.8	392	44	244	151.5	159	150	43	17	206.9	3.4	0.9
BAD-R2-UF-2	887.2	350.6	288	32	253	152.2	100	144	25	15	16.5	2.8	0.8
BAD-R2-UF-3	858.2	342.9	323	32	244	152.9	112	142	29	16	18.0	2.9	0.8
CAM-R2-UF-1	728.6	1648.1	167	66	115	61.0	48	29	39	19	10.2	2.4	1.2
CAM-R2-UF-2	723.6	1652.9	161	63	113	58.7	44	23	37	19	10.5	2.2	1.1
CAM-R2-UF-3	n.d.												
PEY-R2-UF-1	115.1	111.6	173	104	15	74.0	44	22	60	15	5.2	2.9	1.1
PEY-R2-UF-2	n.d.												
PEY-R2-UF-3	134.9	129.0	199	108	16	86.3	45	25	64	17	7.7	3.6	1.2
OPA-R2-UF-1	486.2	1823.2	157	126	109	99.8	41	48	51	19	11.8	1.8	1.0
OPA-R2-UF-2	490.4	1795.2	154	135	108	100.3	38	47	50	18	11.5	1.8	0.9
OPA-R2-UF-3	501.0	1769.7	166	125	107	98.8	55	49	52	19	11.8	2.0	0.9
PAR-R2-UF-1	1677.7	2347.2	276	251	649	400.3	73	166	35	14	20.4	4.1	1.4
PAR-R2-UF-2	1724.6	2490.4	230	531	631	442.1	50	200	74	15	28.0	5.4	1.5
PAR-R2-UF-3	1429.8	2230.3	166	120	573	349.3	33	154	19	13	13.3	4.2	1.5
AZU-R2-UF-1	6446.6	160.8	220	25	200	51.0	92	63	15	73	8.8	3.3	0.5
AZU-R2-UF-2	6476.4	136.5	274	26	200	50.5	108	64	18	72	9.0	3.3	0.6
AZU-R2-UF-3	6462.1	133.0	288	32	195	51.5	87	65	19	71	8.8	2.9	0.5
ARN-R2-UF-1	2179.3	1162.4	240	60	569	185.8	39	70	15	25	7.4	4.2	1.0
ARN-R2-UF-2	2201.4	1162.7	242	63	580	181.6	44	64	17	25	6.7	4.0	0.9
ARN-R2-UF-3	1879.6	968.6	170	57	483	154.9	32	54	12	20	5.8	2.9	0.9
BAC-R2-UF-1	n.d.												
BAC-R2-UF-2	n.d.												
BAC-R2-UF-3	n.d.												
COA-R2-UF-1	1103.2	574.9	277	79	63	88.2	60	45	54	20	9.8	3.6	1.0

COA-R2-UF-2	1118.1	578.1	237	70	64	88.2	61	40	55	20	13.0	3.7	1.0
COA-R2-UF-3	1070.0	565.3	244	141	61	86.5	55	38	55	19	10.1	3.5	1.0
PAN-R2-UF-1	3279.3	661.2	186	89	325	138.9	39	61	22	35	7.8	3.3	1.0
PAN-R2-UF-2	3097.3	586.2	165	79	252	131.0	44	62	21	33	8.1	2.5	1.0
PAN-R2-UF-3	3001.6	570.8	173	85	243	133.6	50	60	22	33	8.8	2.3	0.9

REPLIM 3	Ca	Na	Mg	K	Al	Sr	Fe	Mn	Ba
	$\mu\text{g L}^{-1}$								
LOD	7	1	0.3	9	0.3	0.002	0.07	0.002	0.004
ARA-R3-UF-T1	12051	244	226.4	56	9.5	11.497	13.73	0.666	3.228
ARA-R3-UF-T3	11577	199	215.8	52	9.0	11.011	14.85	0.368	3.056
ARA-R3-UF-T4	11700	206	215.8	52	13.1	11.040	13.03	0.396	2.963
ARA-R3-UF-P1=T2	11373	205	225.4	53	9.8	10.812	15.41	0.352	3.298
ARA-R3-UF-P2	11951	196	215.2	49	10.4	11.254	27.85	0.385	3.079
ARA-R3-UF-P3	11847	189	208.9	47	9.4	11.072	13.54	0.323	2.812
ARA-R3-UF-P4	11804	190	213.1	50	9.3	11.029	42.58	0.409	7.005
BAD-R3-UF	18913	193	346.8	69	25.4	18.739	16.84	0.284	0.712
CAM-R3-UF	1660	177	62.0	40	14.8	1.349	7.73	0.518	0.634
PEY-R3-UF	180	35	63.0	37	94.6	0.219	64.44	1.165	2.927
OPA-R3-UF	4692	218	118.3	140	37.1	3.453	20.48	1.169	0.561
PAR-R3-UF	11238	1077	269.7	180	20.6	9.949	8.86	0.748	0.747
GEN-R3-UF-T1	6362	444	129.6	62	17.8	8.057	11.82	2.240	3.278
GEN-R3-UF-T3	6103	426	123.7	60	15.9	7.741	11.75	2.245	3.269
GEN-R3-UF-T4	6364	503	137.3	70	17.6	7.974	22.90	2.478	10.882
GEN-R3-UF-P1=T2	6191	501	137.6	63	20.8	7.859	11.38	2.164	3.048
GEN-R3-UF-P2	6070	439	124.8	60	16.5	7.654	14.82	2.234	5.579
GEN-R3-UF-P3	6530	463	136.5	70	17.8	8.010	15.73	2.234	6.068
GEN-R3-UF-P4	10422	586	192.4	202	14.2	11.549	43.20	4.959	212.672
GEN-R3-UF-P5	15781	829	282.1	436	12.2	15.854	4285.14	11.621	985.436
ROU-R3-UF	6414	462	125.2	63	19.1	7.509	16.78	2.037	4.252
BER-R3-UF	2379	259	81.1	45	36.4	4.390	23.65	2.683	2.140
AZU-R3-UF-T2	13341	178	185.7	58	11.6	12.616	10.25	4.275	2.610
AZU-R3-UF-P1=T1	13828	181	186.4	60	13.9	13.130	11.00	4.480	2.968
AZU-R3-UF-P2	14841	183	197.3	61	14.1	14.139	12.16	5.052	3.179
AZU-R3-UF-P3	14818	174	191.4	57	12.0	14.075	10.49	4.980	3.317
ARN-R3-UF	3563	237	82.0	57	14.5	2.611	3.79	0.258	0.269
BAC-R3-UF	5888	202	131.5	70	17.6	5.882	16.85	1.153	3.046

PEC-R3-UF	6041	136	130.0	40	23.9	6.096	13.85	0.262	0.692
COA-R3-UF	1696	163	51.5	39	13.1	1.190	4.04	0.437	0.301
PAN-R3-UF	6718	332	124.8	69	13.0	6.072	10.77	0.835	1.776
ORD-R3-UF	13339	320	202.8	101	18.3	9.186	23.23	0.523	4.487
SAB-R3-UF-T1	22175	152	5666.3	75	10.0	38.556	7.84	4.250	2.396
SAB-R3-UF-T3	21777	149	5587.4	68	10.9	38.108	8.09	4.251	1.667
SAB-R3-UF-P1=T2	22229	149	5587.1	66	12.2	38.731	9.84	4.314	2.704
SAB-R3-UF-P2	22646	146	5798.3	74	8.9	38.631	6.71	4.277	1.319
SAB-R3-UF-P3	25712	163	6661.4	94	4.6	46.562	11.32	6.258	2.284
SAB-R3-UF-P4	26816	169	6670.4	101	6.6	48.784	18.80	7.052	4.040
SAB-R3-UF-P5	28736	171	6875.7	118	3.9	52.020	49.81	8.352	22.307
SAB-R3-UF-P6	28745	170	6719.7	126	5.2	51.590	298.70	9.514	156.810

REPLIM 3	As	U	Cu	Ti	Mo	V	Ni	Cr	Pb	Sb	Co	Cd	Tl
	ng L ⁻¹												
LOD	0.5	0.1	18	2	2	0.1	11	3	2	2	0.1	0.5	0.2
ARA-R3-UF-T1	864.9	179.4	161	99	148	77.1	120	125	42	16	17.8	3.0	0.3
ARA-R3-UF-T3	873.0	177.3	141	87	143	75.6	102	121	39	15	16.7	2.5	0.3
ARA-R3-UF-T4	865.0	191.4	204	89	144	76.8	109	141	48	15	15.6	2.5	0.3
ARA-R3-UF-P1=T2	884.7	180.2	145	90	143	78.6	103	126	20	14	17.8	2.3	0.3
ARA-R3-UF-P2	815.2	162.0	152	85	142	74.8	104	123	49	15	18.1	2.9	0.3
ARA-R3-UF-P3	817.1	155.7	151	79	136	72.0	658	117	31	14	16.1	2.3	0.3
ARA-R3-UF-P4	880.7	155.4	153	81	136	71.4	83	116	21	20	25.3	2.0	0.3
BAD-R3-UF	444.5	218.1	170	524	116	115.7	93	241	58	11	14.8	1.2	0.5
CAM-R3-UF	221.9	517.5	106	184	32	47.9	57	27	43	12	7.1	1.7	0.5
PEY-R3-UF	31.0	4.9	251	1523	6	151.9	221	127	218	5	61.4	3.2	1.2
OPA-R3-UF	274.0	1021.9	129	641	48	92.7	161	64	67	15	17.0	1.5	0.8
PAR-R3-UF	1312.7	2245.5	176	141	532	391.8	60	162	29	14	15.2	3.2	1.2
GEN-R3-UF-T1	254.3	28.6	202	382	29	66.2	164	58	58	81	11.0	1.9	0.6
GEN-R3-UF-T3	248.3	25.2	196	317	30	61.9	150	54	40	78	9.9	1.7	0.5
GEN-R3-UF-T4	265.4	14.3	434	329	33	65.4	797	69	174	85	13.4	2.6	0.6
GEN-R3-UF-P1=T2	251.9	14.3	256	356	30	67.7	260	59	93	78	11.6	3.7	0.6
GEN-R3-UF-P2	253.6	25.2	203	314	29	60.6	131	56	41	77	11.3	1.5	0.5
GEN-R3-UF-P3	249.5	13.1	227	422	29	59.9	223	57	69	75	13.6	2.4	0.5
GEN-R3-UF-P4	357.9	19.5	206	296	77	34.5	458	40	38	73	32.0	1.8	0.5
GEN-R3-UF-P5	4021.6	21.1	4043	291	239	101.0	418	90	156	66	107.7	5.6	0.5
ROU-R3-UF	251.3	13.3	196	277	31	78.8	92	59	39	74	11.9	2.0	0.7
BER-R3-UF	92.1	6.6	236	628	14	84.1	132	65	104	14	22.6	4.2	0.7
AZU-R3-UF-T2	4222.9	69.0	132	101	105	42.1	91	59	35	63	11.5	2.8	0.2
AZU-R3-UF-P1=T1	4211.8	73.1	158	131	109	43.8	98	61	44	66	12.5	3.0	0.3
AZU-R3-UF-P2	4258.5	78.0	144	145	115	45.3	97	62	39	71	12.8	2.9	0.2
AZU-R3-UF-P3	4261.7	75.2	120	116	113	40.3	71	58	33	69	12.2	3.0	0.2
ARN-R3-UF	949.3	401.7	163	97	221	117.0	74	50	29	18	5.7	2.1	0.5
BAC-R3-UF	2927.9	102.1	180	214	95	86.7	66	65	49	24	11.5	2.2	0.5

PEC-R3-UF	7744.5	38.7	167	312	75	72.3	75	84	99	38	11.3	1.1	0.4
COA-R3-UF	439.2	256.2	211	100	33	69.7	98	29	37	12	8.0	4.5	0.6
PAN-R3-UF	2684.2	462.8	177	115	170	118.6	66	63	43	25	9.7	2.2	0.5
ORD-R3-UF	1656.0	330.8	278	206	108	185.5	75	115	105	18	23.0	2.3	0.7
SAB-R3-UF-T1	129.5	146.1	231	31	38	26.7	114	47	21	33	12.5	1.2	0.3
SAB-R3-UF-T3	124.3	97.9	263	92	38	28.0	86	44	18	33	12.1	0.9	0.3
SAB-R3-UF-P1=T2	127.9	101.9	285	39	39	35.4	85	47	42	33	12.9	0.9	0.3
SAB-R3-UF-P2	119.2	106.8	239	34	41	19.6	70	43	21	33	9.6	1.7	0.3
SAB-R3-UF-P3	128.7	121.8	144	25	37	10.4	84	36	7	31	10.8	0.6	0.2
SAB-R3-UF-P4	130.8	119.7	192	34	37	9.4	99	32	19	30	13.2	1.0	0.2
SAB-R3-UF-P5	158.6	126.1	122	21	44	7.9	89	25	7	27	28.9	0.7	0.2
SAB-R3-UF-P6	235.8	109.0	157	31	73	6.9	163	17	42	28	129.8	1.0	0.2

REPLIM 4	Ca	Na	Mg	K	Al	Sr	Fe	Mn	Ba
	$\mu\text{g L}^{-1}$								
LOD	7	1	0.3	9	0.3	0.002	0.07	0.004	0.002
ARA-R4-UF-P1	14319	231	229.8	45	7.9	13.069	22.34	2.741	0.435
ARA-R4-UF-P2	14305	231	234.3	42	6.4	13.137	21.98	2.607	0.194
ARA-R4-UF-P3	14413	240	242.3	50	6.2	13.149	29.21	5.633	0.205
BAD-R4-UF	13559	217	227.4	54	9.3	13.631	4.48	1.572	0.215
CAM-R4-UF	2543	277	82.5	66	10.9	2.146	9.77	1.715	0.448
PEY-R4-UF	1209	163	73.4	55	95.9	0.952	67.58	4.072	0.518
OPA-R4-UF	5104	289	120.6	123	29.4	3.919	20.54	1.421	0.958
PAR-R4-UF	10276	1019	222.9	197	16.4	9.500	15.71	1.294	0.408
GEN-R4-UF-T1	5715	429	118.8	28	7.1	7.792	15.26	7.772	1.699
GEN-R4-UF-T3	5687	428	120.1	29	13.9	7.810	24.91	7.883	1.770
GEN-R4-UF-P1=T2	5715	432	118.7	29	6.6	7.838	17.58	10.402	1.786
GEN-R4-UF-P2	5610	429	117.4	28	9.6	7.675	17.60	7.501	1.718
GEN-R4-UF-P3	5555	426	117.6	27	6.2	7.631	15.49	8.035	1.695
GEN-R4-UF-P4	8880	475	154.4	112	5.5	9.692	24.54	141.459	3.084
GEN-R4-UF-P5	12544	592	206.2	281	5.6	12.168	2138.38	905.614	8.622
ROU-R4-UF	5984	454	121.5	63	12.0	7.138	16.21	3.331	1.459
BER-R4-UF	3576	301	84.5	28	9.2	6.846	2.91	1.410	2.472
AZU-R4-UF-P1=T1	16150	212	220.9	69	17.9	18.369	16.65	2.448	4.525
AZU-R4-UF-P2	16542	207	219.6	67	18.7	18.864	18.39	2.220	4.625
AZU-R4-UF-P3	16269	202	217.1	66	17.5	18.416	17.93	2.203	4.594
ARN-R4-UF	5365	302	115.1	63	16.7	4.161	4.38	1.412	0.337
BAC-R4-UF	6654	210	126.0	82	15.5	6.581	14.03	4.033	1.062
PEC-R4-UF	8207	154	142.8	38	8.3	8.009	2.63	1.310	0.147
COA-R4-UF	2071	167	70.2	50	24.7	1.464	12.56	0.660	0.581
PAN-R4-UF	6605	570	165.8	142	25.0	6.720	39.03	4.702	1.125
ORD-R4-UF	10003	311	174.5	123	20.0	6.978	9.79	1.563	0.504
SAB-R4-UF-T1	20732	160	6126.9	76	11.0	42.687	10.70	1.797	4.298
SAB-R4-UF-T3	20939	152	6129.5	78	8.7	43.444	10.95	1.261	4.411

SAB-R4-UF-P1=T2	20099	145	6092.0	73	6.3	41.950	10.37	1.236	4.234
SAB-R4-UF-P2	20182	149	6179.1	76	6.2	42.106	10.72	1.268	4.301
SAB-R4-UF-P3	20004	150	6189.7	75	7.3	41.843	10.56	1.271	4.252
SAB-R4-UF-P4	26131	164	6868.8	96	5.0	50.255	9.63	1.645	6.942
SAB-R4-UF-P5	27608	173	7010.5	111	5.4	54.805	6.38	17.839	8.547
SAB-R4-UF-P6	28378	171	7225.6	120	4.4	55.964	48.77	53.548	9.143

REPLIM 4	As	U	Cu	Ti	Mo	V	Ni	Cr	Pb	Sb	Co	Cd	Tl
	ng L ⁻¹												
LOD	0.5	0.1	18	2	2	0.1	11	3	2	2	0.1	0.5	0.2
ARA-R4-UF-P1	1407.8	321.7	178	81	205	126.2	95	111	36	19	21.2	2.5	0.3
ARA-R4-UF-P2	1433.8	328.8	164	54	208	123.2	93	105	24	19	20.5	2.3	0.3
ARA-R4-UF-P3	1433.1	333.6	144	36	209	110.7	86	101	22	18	25.1	2.4	0.3
BAD-R4-UF	723.8	277.8	188	46	206	133.5	88	128	23	12	11.2	1.9	0.3
CAM-R4-UF	695.7	1446.1	133	76	110	62.7	46	23	37	17	8.7	3.6	0.9
PEY-R4-UF	188.5	303.2	192	1882	18	153.0	116	70	503	14	39.3	3.8	2.5
OPA-R4-UF	462.0	1627.8	151	654	98	111.7	63	60	128	16	22.8	2.0	0.9
PAR-R4-UF	1459.8	2247.3	150	192	581	386.3	87	141	34	13	15.0	3.5	1.1
GEN-R4-UF-T1	289.0	9.7	192	43	35	30.5	36	27	38	58	9.3	1.4	0.3
GEN-R4-UF-T3	299.1	9.7	242	485	27	42.4	50	49	34	59	14.1	1.4	0.4
GEN-R4-UF-P1=T2	291.6	8.8	137	45	28	30.8	25	29	35	58	9.8	1.1	0.3
GEN-R4-UF-P2	290.2	9.8	158	223	26	34.6	46	30	19	58	9.0	1.0	0.3
GEN-R4-UF-P3	288.4	9.7	117	65	26	30.1	100	26	9	58	8.3	1.0	0.3
GEN-R4-UF-P4	320.0	10.3	136	37	55	20.3	25	21	9	51	31.8	1.4	0.4
GEN-R4-UF-P5	1538.8	7.3	158	47	214	20.9	1477	22	16	33	89.0	2.3	0.4
ROU-R4-UF	287.1	11.2	231	79	31	73.3	603	49	40	66	10.2	3.1	0.7
BER-R4-UF	205.5	11.6	153	39	13	45.8	28	28	17	23	4.7	2.0	0.4
AZU-R4-UF-P1=T1	5068.4	118.3	190	251	171	64.3	87	76	76	66	25.6	3.4	0.4
AZU-R4-UF-P2	5201.3	111.2	183	395	173	67.7	83	75	81	69	25.8	3.4	0.4
AZU-R4-UF-P3	5072.4	107.7	165	271	169	64.5	79	74	79	67	25.7	3.5	0.4
ARN-R4-UF	1702.9	837.4	142	75	443	163.2	23	57	22	22	7.6	2.9	0.6
BAC-R4-UF	3176.7	155.7	207	175	152	104.7	65	80	54	32	9.9	2.5	0.6
PEC-R4-UF	8589.0	51.0	123	45	109	56.8	37	77	19	47	6.0	1.0	0.2
COA-R4-UF	693.5	444.3	433	208	37	87.0	58	59	76	15	15.6	12.2	1.1
PAN-R4-UF	2941.1	966.5	274	674	212	143.5	106	129	87	39	27.7	3.5	1.1
ORD-R4-UF	1112.1	231.0	207	150	104	125.3	59	106	70	17	20.0	2.7	0.8
SAB-R4-UF-T1	171.8	111.6	197	125	42	25.6	61	35	17	35	13.3	0.9	0.3
SAB-R4-UF-T3	158.6	110.1	208	36	55	23.4	64	38	36	36	12.7	0.8	0.3

SAB-R4-UF-P1=T2	155.3	111.2	171	22	42	22.5	64	29	13	35	13.2	0.8	0.3
SAB-R4-UF-P2	157.1	112.8	179	16	42	24.0	57	47	12	35	13.2	0.7	0.3
SAB-R4-UF-P3	153.2	110.8	179	20	42	23.5	57	30	15	35	12.9	0.8	0.3
SAB-R4-UF-P4	136.6	125.5	153	79	42	10.0	59	33	11	31	13.3	0.8	0.2
SAB-R4-UF-P5	135.9	129.5	147	12	46	8.8	53	36	6	29	24.6	0.9	0.2
SAB-R4-UF-P6	177.4	125.7	102	12	53	6.7	56	23	8	24	54.7	0.8	<LOD

Annexe 3: Organometals results (Hg and Sn)

REPLIM 1	iHg(II)	MMHg	non-gaseous Hg	% MMHg	DGM	total Hg	% DGM	FD 1 m s ⁻¹	FD 3 m s ⁻¹	MBT	DBT	TBT
	ng L ⁻¹	ng L ⁻¹	ng L ⁻¹	%	ng L ⁻¹	ng L ⁻¹	%	ng m ⁻² day ⁻¹	ng m ⁻² day ⁻¹	ng L ⁻¹	ng L ⁻¹	ng L ⁻¹
LOD	0.03	0.003			0.0004					0.1	0.1	0.01
ARA-R1-F-1	0.15	<LOD	0.15	<LOD	n.d.	n.d.	n.d.	n.d.	n.d.	n.d.	4.0	0.02
ARA-R1-F-2	1.98	0.010	1.99	1	n.d.	n.d.	n.d.	n.d.	n.d.	2.0	n.d.	<LOD
ARA-R1-F-3	0.85	0.012	0.86	1	n.d.	n.d.	n.d.	n.d.	n.d.	n.d.	4.0	0.01
BAD-R1-F-1	0.14	<LOD	0.15	<LOD	n.d.	n.d.	n.d.	n.d.	n.d.	0.2	0.2	<LOD
BAD-R1-F-2	0.20	0.004	0.21	2	n.d.	n.d.	n.d.	n.d.	n.d.	0.4	0.3	<LOD
BAD-R1-F-3	0.14	<LOD	0.15	<LOD	n.d.	n.d.	n.d.	n.d.	n.d.	0.3	0.2	<LOD
CAM-R1-F-1	0.29	<LOD	0.29	<LOD	n.d.	n.d.	n.d.	n.d.	n.d.	1.0	1.4	0.01
CAM-R1-F-2	0.24	0.005	0.25	2	n.d.	n.d.	n.d.	n.d.	n.d.	0.7	1.3	<LOD
CAM-R1-F-3	0.25	<LOD	0.26	<LOD	n.d.	n.d.	n.d.	n.d.	n.d.	0.8	1.7	<LOD
PEY-R1-F-1	0.21	0.004	0.21	2	n.d.	n.d.	n.d.	n.d.	n.d.	0.3	0.1	<LOD
PEY-R1-F-2	0.18	0.012	0.19	6	n.d.	n.d.	n.d.	n.d.	n.d.	0.4	0.2	<LOD
PEY-R1-F-3	0.18	<LOD	0.18	<LOD	n.d.	n.d.	n.d.	n.d.	n.d.	n.d.	0.3	<LOD
OPA-R1-F-1	0.12	<LOD	0.12	<LOD	n.d.	n.d.	n.d.	n.d.	n.d.	0.3	0.9	0.01
OPA-R1-F-2	0.10	0.007	0.10	6	n.d.	n.d.	n.d.	n.d.	n.d.	0.5	1.1	<LOD
OPA-R1-F-3	0.12	<LOD	0.12	<LOD	n.d.	n.d.	n.d.	n.d.	n.d.	0.4	0.5	<LOD
PAR-R1-F-1	0.53	0.023	0.56	4	n.d.	n.d.	n.d.	n.d.	n.d.	n.d.	0.1	0.01
PAR-R1-F-2	0.67	0.038	0.71	5	n.d.	n.d.	n.d.	n.d.	n.d.	0.8	0.2	<LOD
PAR-R1-F-3	0.61	0.037	0.65	6	n.d.	n.d.	n.d.	n.d.	n.d.	1.2	0.2	<LOD
NER-R1-F-1	0.36	<LOD	0.36	<LOD	n.d.	n.d.	n.d.	n.d.	n.d.	0.5	1.6	<LOD
NER-R1-F-2	0.46	0.008	0.47	2	n.d.	n.d.	n.d.	n.d.	n.d.	0.6	1.5	<LOD
NER-R1-F-3	0.40	<LOD	0.40	<LOD	n.d.	n.d.	n.d.	n.d.	n.d.	0.7	1.4	0.02
POU-R1-F-1	0.22	<LOD	0.22	<LOD	n.d.	n.d.	n.d.	n.d.	n.d.	0.6	1.3	<LOD
POU-R1-F-2	0.28	0.005	0.29	2	n.d.	n.d.	n.d.	n.d.	n.d.	0.6	1.2	<LOD
POU-R1-F-3	0.27	<LOD	0.28	<LOD	n.d.	n.d.	n.d.	n.d.	n.d.	n.d.	n.d.	0.01
AZU-R1-F-1	0.07	<LOD	0.07	<LOD	n.d.	n.d.	n.d.	n.d.	n.d.	0.4	1.8	<LOD
AZU-R1-F-2	0.12	<LOD	0.12	<LOD	n.d.	n.d.	n.d.	n.d.	n.d.	0.6	2.2	<LOD
AZU-R1-F-3	0.09	<LOD	0.09	<LOD	n.d.	n.d.	n.d.	n.d.	n.d.	0.8	1.6	0.03
ARN-R1-F-1	0.16	<LOD	0.16	<LOD	n.d.	n.d.	n.d.	n.d.	n.d.	0.6	0.9	0.01
ARN-R1-F-2	0.20	<LOD	0.20	<LOD	n.d.	n.d.	n.d.	n.d.	n.d.	1.0	n.d.	<LOD
ARN-R1-F-3	0.19	<LOD	0.19	<LOD	n.d.	n.d.	n.d.	n.d.	n.d.	0.7	1.3	<LOD

BAC-R1-F-1	n.d.	n.d.	n.d.	n.d.	n.d.	n.d.	n.d.	n.d.	n.d.	n.d.	n.d.	n.d.
BAC-R1-F-2	n.d.	n.d.	n.d.	n.d.	n.d.	n.d.	n.d.	n.d.	n.d.	n.d.	n.d.	n.d.
BAC-R1-F-3	n.d.	n.d.	n.d.	n.d.	n.d.	n.d.	n.d.	n.d.	n.d.	n.d.	n.d.	n.d.
PEC-R1-F-1	0.25	<LOD	0.25	<LOD	n.d.	n.d.	n.d.	n.d.	n.d.	n.d.	1.7	<LOD
PEC-R1-F-2	0.24	<LOD	0.24	<LOD	n.d.	n.d.	n.d.	n.d.	n.d.	0.5	1.3	<LOD
PEC-R1-F-3	0.23	<LOD	0.23	<LOD	n.d.	n.d.	n.d.	n.d.	n.d.	0.4	n.d.	<LOD
COA-R1-F-1	0.38	<LOD	0.38	<LOD	n.d.	n.d.	n.d.	n.d.	n.d.	0.6	1.1	0.01
COA-R1-F-2	n.d.	n.d.	n.d.	n.d.	n.d.	n.d.	n.d.	n.d.	n.d.	n.d.	n.d.	n.d.
COA-R1-F-3	0.48	<LOD	0.48	<LOD	n.d.	n.d.	n.d.	n.d.	n.d.	0.9	1.2	<LOD
PAN-R1-F-1	0.20	<LOD	0.20	<LOD	n.d.	n.d.	n.d.	n.d.	n.d.	0.6	1.4	<LOD
PAN-R1-F-2	0.26	0.006	0.26	2	n.d.	n.d.	n.d.	n.d.	n.d.	0.7	1.3	0.02
PAN-R1-F-3	0.26	<LOD	0.26	<LOD	n.d.	n.d.	n.d.	n.d.	n.d.	1.0	1.7	0.02
ORD-R1-F-1	0.49	0.010	0.50	2	n.d.	n.d.	n.d.	n.d.	n.d.	1.7	2.8	0.01
ORD-R1-F-2	0.54	0.017	0.56	3	n.d.	n.d.	n.d.	n.d.	n.d.	1.5	2.3	<LOD
ORD-R1-F-3	n.d.	n.d.	n.d.	n.d.	n.d.	n.d.	n.d.	n.d.	n.d.	n.d.	n.d.	<LOD
XUA-R1-F-1	0.26	0.009	0.26	3	n.d.	n.d.	n.d.	n.d.	n.d.	0.5	1.7	<LOD
XUA-R1-F-2	0.34	0.008	0.35	2	n.d.	n.d.	n.d.	n.d.	n.d.	n.d.	2.0	0.02
XUA-R1-F-3	0.28	<LOD	0.28	<LOD	n.d.	n.d.	n.d.	n.d.	n.d.	0.8	1.7	0.02
ARA-R1-UF-1	0.26	0.012	0.27	4	0.33	0.60	55	178	270	n.d.	n.d.	0.02
ARA-R1-UF-2	n.d.	n.d.	n.d.	n.d.	n.d.	n.d.	n.d.	n.d.	n.d.	1.9	2.4	0.01
ARA-R1-UF-3	0.25	0.012	0.26	5	n.d.	0.03						
BAD-R1-UF-1	0.29	0.009	0.30	3	0.02	0.33	7	7	11	0.3	0.2	<LOD
BAD-R1-UF-2	0.27	0.008	0.28	3	n.d.	n.d.	n.d.	n.d.	n.d.	0.3	0.1	0.01
BAD-R1-UF-3	0.23	0.009	0.24	4	n.d.	0.02						
CAM-R1-UF-1	0.36	0.020	0.38	5	0.12	0.49	24	61	93	0.9	1.7	0.02
CAM-R1-UF-2	0.36	0.016	0.38	4	n.d.	n.d.	n.d.	n.d.	n.d.	0.6	1.2	0.02
CAM-R1-UF-3	0.41	0.018	0.43	4	n.d.	n.d.	n.d.	n.d.	n.d.	1.2	1.0	0.02
PEY-R1-UF-1	0.31	0.012	0.32	4	0.12	0.44	27	60	92	0.4	0.1	0.01
PEY-R1-UF-2	0.40	0.018	0.42	4	n.d.	n.d.	n.d.	n.d.	n.d.	0.4	0.2	<LOD
PEY-R1-UF-3	0.21	0.013	0.23	6	n.d.	0.02						
OPA-R1-UF-1	0.12	0.004	0.13	3	0.07	0.20	35	34	52	0.5	1.0	<LOD
OPA-R1-UF-2	0.11	0.008	0.12	6	n.d.	n.d.	n.d.	n.d.	n.d.	0.9	1.3	<LOD
OPA-R1-UF-3	0.13	0.007	0.14	5	n.d.	n.d.	n.d.	n.d.	n.d.	0.9	0.3	<LOD
PAR-R1-UF-1	0.56	0.065	0.62	10	n.d.	n.d.	n.d.	n.d.	n.d.	0.4	0.1	0.02

PAR-R1-UF-2	0.75	0.078	0.83	9	n.d.	n.d.	n.d.	n.d.	n.d.	0.4	0.1	<LOD
PAR-R1-UF-3	0.71	0.073	0.78	9	n.d.	n.d.	n.d.	n.d.	n.d.	0.4	0.1	0.02
NER-R1-UF-1	0.48	0.010	0.49	2	0.13	0.62	21	68	103	0.7	1.1	0.02
NER-R1-UF-2	0.48	0.011	0.49	2	n.d.	n.d.	n.d.	n.d.	n.d.	0.6	1.4	0.02
NER-R1-UF-3	0.44	0.008	0.45	2	n.d.	n.d.	n.d.	n.d.	n.d.	n.d.	1.1	0.02
POU-R1-UF-1	0.37	0.012	0.38	3	0.11	0.49	22	57	86	0.6	1.0	0.01
POU-R1-UF-2	0.47	0.009	0.48	2	n.d.	n.d.	n.d.	n.d.	n.d.	0.9	1.3	0.03
POU-R1-UF-3	0.50	0.009	0.50	2	n.d.	n.d.	n.d.	n.d.	n.d.	1.1	n.d.	<LOD
AZU-R1-UF-1	0.23	0.004	0.23	2	0.06	0.29	21	29	44	0.4	1.8	0.02
AZU-R1-UF-2	0.13	<LOD	0.13	<LOD	n.d.	n.d.	n.d.	n.d.	n.d.	1.6	2.4	0.02
AZU-R1-UF-3	0.38	<LOD	0.38	<LOD	n.d.	n.d.	n.d.	n.d.	n.d.	0.9	1.9	0.03
ARN-R1-UF-1	0.26	<LOD	0.26	<LOD	0.06	0.31	18	26	39	0.7	1.2	<LOD
ARN-R1-UF-2	0.30	<LOD	0.30	<LOD	n.d.	n.d.	n.d.	n.d.	n.d.	1.2	2.6	0.02
ARN-R1-UF-3	0.37	0.005	0.37	1	n.d.	n.d.	n.d.	n.d.	n.d.	0.8	1.9	0.03
BAC-R1-UF-1	0.43	0.008	0.44	2	n.d.	n.d.	n.d.	n.d.	n.d.	0.4	0.2	0.02
BAC-R1-UF-2	0.37	0.008	0.38	2	n.d.	n.d.	n.d.	n.d.	n.d.	0.5	0.2	<LOD
BAC-R1-UF-3	0.29	0.007	0.30	2	n.d.	n.d.	n.d.	n.d.	n.d.	0.7	0.3	<LOD
PEC-R1-UF-1	0.30	0.009	0.31	3	0.04	0.34	11	17	26	1.2	1.6	<LOD
PEC-R1-UF-2	0.28	0.007	0.28	2	n.d.	n.d.	n.d.	n.d.	n.d.	1.3	1.7	0.03
PEC-R1-UF-3	0.23	0.006	0.24	2	n.d.	n.d.	n.d.	n.d.	n.d.	1.6	n.d.	0.02
COA-R1-UF-1	0.53	0.011	0.54	2	0.20	0.75	27	109	165	0.9	1.2	<LOD
COA-R1-UF-2	0.61	<LOD	0.61	<LOD	n.d.	n.d.	n.d.	n.d.	n.d.	1.2	1.6	0.02
COA-R1-UF-3	0.67	0.010	0.68	1	n.d.	n.d.	n.d.	n.d.	n.d.	1.5	1.6	0.02
PAN-R1-UF-1	0.31	0.014	0.32	4	0.10	0.43	24	54	82	1.2	1.8	<LOD
PAN-R1-UF-2	0.32	0.010	0.33	3	n.d.	n.d.	n.d.	n.d.	n.d.	0.8	1.3	0.02
PAN-R1-UF-3	0.40	0.013	0.41	3	n.d.	n.d.	n.d.	n.d.	n.d.	1.7	2.0	0.03
ORD-R1-UF-1	0.63	0.049	0.68	7	0.18	0.87	21	98	148	2.2	3.1	0.02
ORD-R1-UF-2	0.82	0.046	0.87	5	n.d.	n.d.	n.d.	n.d.	n.d.	2.8	2.6	0.02
ORD-R1-UF-3	n.d	n.d	n.d	n.d	n.d.	0.02						
XUA-R1-UF-1	0.36	0.022	0.39	6	0.13	0.52	26	70	106	1.4	1.8	0.02
XUA-R1-UF-2	0.58	0.025	0.61	4	n.d.	n.d.	n.d.	n.d.	n.d.	1.5	2.1	0.03
XUA-R1-UF-3	0.53	0.026	0.56	5	n.d.	n.d.	n.d.	n.d.	n.d.	n.d.	2.1	0.03

REPLIM 2	iHg(II)	MMHg	non-gaseous Hg	% MMHg	DGM	total Hg	% DGM	FD 1 m s ⁻¹	FD 3 m s ⁻¹	MBT	DBT	TBT
	ng L ⁻¹	ng L ⁻¹	ng L ⁻¹	%	ng L ⁻¹	ng L ⁻¹	%	ng m ⁻² day ⁻¹	ng m ⁻² day ⁻¹	ng L ⁻¹	ng L ⁻¹	ng L ⁻¹
LOD	0.03	0.003			0.0001					0.1	0.1	0.01
ARA-R2-F-1	0.14	0.005	0.14	3	n.d.	n.d.	n.d.	n.d.	n.d.	n.d.	n.d.	0.03
ARA-R2-F-2	0.10	0.007	0.11	6	n.d.	n.d.	n.d.	n.d.	n.d.	1.3	2.3	0.01
ARA-R2-F-3	0.11	0.005	0.12	4	n.d.	n.d.	n.d.	n.d.	n.d.	0.8	1.4	<LOD
BAD-R2-F-1	0.15	0.005	0.15	3	n.d.	n.d.	n.d.	n.d.	n.d.	0.6	1.0	0.02
BAD-R2-F-2	n.d.	n.d.	n.d.	n.d.	n.d.	n.d.	n.d.	n.d.	n.d.	n.d.	n.d.	n.d.
BAD-R2-F-3	0.53	0.003	0.53	1	n.d.	n.d.	n.d.	n.d.	n.d.	1.0	1.0	<LOD
CAM-R2-F-1	0.51	0.005	0.52	1	n.d.	n.d.	n.d.	n.d.	n.d.	1.1	0.8	0.02
CAM-R2-F-2	0.54	0.008	0.55	2	n.d.	n.d.	n.d.	n.d.	n.d.	0.6	1.1	<LOD
CAM-R2-F-3	0.45	0.004	0.45	1	n.d.	n.d.	n.d.	n.d.	n.d.	1.3	0.9	<LOD
PEY-R2-F-1	0.14	<LOD	0.14	<LOD	n.d.	n.d.	n.d.	n.d.	n.d.	0.4	0.1	<LOD
PEY-R2-F-2	0.14	<LOD	0.14	<LOD	n.d.	n.d.	n.d.	n.d.	n.d.	0.2	<LOD	<LOD
PEY-R2-F-3	0.23	<LOD	0.23	<LOD	n.d.	n.d.	n.d.	n.d.	n.d.	0.3	0.2	<LOD
OPA-R2-F-1	0.25	0.003	0.25	1	n.d.	n.d.	n.d.	n.d.	n.d.	0.7	0.9	0.02
OPA-R2-F-2	0.18	0.005	0.19	3	n.d.	n.d.	n.d.	n.d.	n.d.	0.5	0.8	<LOD
OPA-R2-F-3	0.24	0.003	0.24	1	n.d.	n.d.	n.d.	n.d.	n.d.	0.5	0.6	<LOD
PAR-R2-F-1	n.d.	n.d.	n.d.	n.d.	n.d.	n.d.	n.d.	n.d.	n.d.	n.d.	n.d.	n.d.
PAR-R2-F-2	n.d.	n.d.	n.d.	n.d.	n.d.	n.d.	n.d.	n.d.	n.d.	n.d.	n.d.	n.d.
PAR-R2-F-3	n.d.	n.d.	n.d.	n.d.	n.d.	n.d.	n.d.	n.d.	n.d.	n.d.	n.d.	n.d.
AZU-R2-F-1	0.29	<LOD	0.29	<LOD	n.d.	n.d.	n.d.	n.d.	n.d.	0.5	0.8	0.03
AZU-R2-F-2	0.27	<LOD	0.27	<LOD	n.d.	n.d.	n.d.	n.d.	n.d.	0.5	1.0	<LOD
AZU-R2-F-3	0.26	<LOD	0.26	<LOD	n.d.	n.d.	n.d.	n.d.	n.d.	0.5	1.0	0.02
ARN-R2-F-1	0.13	<LOD	0.13	<LOD	n.d.	n.d.	n.d.	n.d.	n.d.	0.5	0.8	0.02
ARN-R2-F-2	0.21	<LOD	0.21	<LOD	n.d.	n.d.	n.d.	n.d.	n.d.	0.3	0.8	<LOD
ARN-R2-F-3	0.34	<LOD	0.34	<LOD	n.d.	n.d.	n.d.	n.d.	n.d.	0.5	0.6	0.02
BAC-R2-F-1	0.23	0.010	0.24	4	n.d.	n.d.	n.d.	n.d.	n.d.	0.4	0.1	0.02
BAC-R2-F-2	0.17	0.008	0.17	5	n.d.	n.d.	n.d.	n.d.	n.d.	0.3	0.1	<LOD
BAC-R2-F-3	0.22	0.008	0.23	4	n.d.	n.d.	n.d.	n.d.	n.d.	0.4	0.2	0.02
COA-R2-F-1	0.49	0.006	0.50	1	n.d.	n.d.	n.d.	n.d.	n.d.	0.7	0.7	0.02
COA-R2-F-2	0.58	0.005	0.59	1	n.d.	n.d.	n.d.	n.d.	n.d.	0.5	0.7	<LOD
COA-R2-F-3	0.51	0.006	0.52	1	n.d.	n.d.	n.d.	n.d.	n.d.	0.9	0.8	0.02

PAN-R2-F-1	0.47	0.008	0.47	2	n.d.	n.d.	n.d.	n.d.	n.d.	0.8	0.8	<LOD
PAN-R2-F-2	0.71	0.013	0.72	2	n.d.	n.d.	n.d.	n.d.	n.d.	0.8	1.3	<LOD
PAN-R2-F-3	0.75	0.008	0.75	1	n.d.	n.d.	n.d.	n.d.	n.d.	0.8	1.0	0.03
ARA-R2-UF-1	0.15	0.006	0.15	4	0.04	0.20	23	20	30	n.d.	n.d.	0.03
ARA-R2-UF-2	0.18	0.007	0.18	4	n.d.	n.d.	n.d.	n.d.	n.d.	0.9	2.5	<LOD
ARA-R2-UF-3	0.13	0.005	0.14	4	n.d.	n.d.	n.d.	n.d.	n.d.	1.2	1.4	0.02
BAD-R2-UF-1	0.37	0.007	0.38	2	0.26	0.64	41	141	214	0.8	1.1	0.02
BAD-R2-UF-2	n.d.	0.006	n.d.	0.9	1.5	0.01						
BAD-R2-UF-3	0.55	0.004	0.55	1	n.d.	n.d.	n.d.	n.d.	n.d.	1.8	1.4	0.11
CAM-R2-UF-1	0.53	0.008	0.54	1	0.42	0.96	44	233	352	1.1	0.9	0.02
CAM-R2-UF-2	0.56	0.011	0.57	2	n.d.	n.d.	n.d.	n.d.	n.d.	0.8	1.1	<LOD
CAM-R2-UF-3	0.45	0.009	0.45	2	n.d.	n.d.	n.d.	n.d.	n.d.	0.7	0.6	0.02
PEY-R2-UF-1	0.31	0.008	0.32	3	0.12	0.44	28	65	98	0.5	0.1	0.02
PEY-R2-UF-2	0.27	0.005	0.28	2	n.d.	n.d.	n.d.	n.d.	n.d.	0.2	<LOD	<LOD
PEY-R2-UF-3	0.29	0.005	0.29	2	n.d.	n.d.	n.d.	n.d.	n.d.	0.3	0.1	0.03
OPA-R2-UF-1	0.31	0.005	0.32	1	0.10	0.41	24	50	75	0.7	0.9	0.02
OPA-R2-UF-2	0.41	0.006	0.41	2	n.d.	n.d.	n.d.	n.d.	n.d.	0.8	0.9	<LOD
OPA-R2-UF-3	0.54	0.006	0.54	1	n.d.	n.d.	n.d.	n.d.	n.d.	0.5	0.6	0.03
PAR-R2-UF-1	n.d.	n.d.	n.d.	n.d.	n.d.	n.d.	n.d.	n.d.	n.d.	n.d.	n.d.	n.d.
PAR-R2-UF-2	n.d.	n.d.	n.d.	n.d.	n.d.	n.d.	n.d.	n.d.	n.d.	n.d.	n.d.	n.d.
PAR-R2-UF-3	n.d.	n.d.	n.d.	n.d.	n.d.	n.d.	n.d.	n.d.	n.d.	n.d.	n.d.	n.d.
AZU-R2-UF-1	0.43	0.005	0.44	1	0.21	0.64	32	111	168	0.6	0.9	0.04
AZU-R2-UF-2	0.32	0.005	0.32	1	n.d.	n.d.	n.d.	n.d.	n.d.	0.7	1.0	<LOD
AZU-R2-UF-3	0.39	0.005	0.39	1	n.d.	n.d.	n.d.	n.d.	n.d.	0.9	1.1	0.02
ARN-R2-UF-1	0.26	0.004	0.26	2	0.15	0.41	36	78	119	0.6	1.0	0.03
ARN-R2-UF-2	0.31	0.004	0.32	1	n.d.	n.d.	n.d.	n.d.	n.d.	0.6	1.1	<LOD
ARN-R2-UF-3	0.50	0.004	0.51	1	n.d.	n.d.	n.d.	n.d.	n.d.	0.7	0.9	0.03
BAC-R2-UF-1	0.29	0.011	0.30	4	0.05	0.35	15	25	38	0.4	0.2	0.01
BAC-R2-UF-2	0.45	0.018	0.47	4	n.d.	n.d.	n.d.	n.d.	n.d.	0.3	0.2	<LOD
BAC-R2-UF-3	0.31	0.012	0.32	4	n.d.	n.d.	n.d.	n.d.	n.d.	0.4	0.2	0.03
COA-R2-UF-1	0.75	0.012	0.77	2	0.37	1.13	32	200	303	1.2	0.9	0.02
COA-R2-UF-2	0.73	0.013	0.74	2	n.d.	n.d.	n.d.	n.d.	n.d.	0.6	0.8	<LOD
COA-R2-UF-3	0.69	0.009	0.70	1	n.d.	n.d.	n.d.	n.d.	n.d.	0.7	0.8	0.02
PAN-R2-UF-1	1.00	0.014	1.01	1	0.68	1.69	40	375	568	0.9	0.9	0.02

PAN-R2-UF-2	1.30	0.015	1.31	1	n.d.	n.d.	n.d.	n.d.	n.d.	0.8	1.3	<LOD
PAN-R2-UF-3	1.28	0.018	1.30	1	n.d.	n.d.	n.d.	n.d.	n.d.	0.9	1.0	0.03

REPLIM 3	iHg(II)	MMHg	non-gaseous Hg	% MMHg	DGM	total Hg	% DGM	FD 1 m s ⁻¹	FD 3 m s ⁻¹	MBT	DBT	TBT
	ng L ⁻¹	ng L ⁻¹	ng L ⁻¹	%	ng L ⁻¹	ng L ⁻¹	%	ng m ⁻² day ⁻¹	ng m ⁻² day ⁻¹	ng L ⁻¹	ng L ⁻¹	ng L ⁻¹
LOD	0.06	0.003			0.0005					0.1	0.1	0.01
ARA-R3-F-T1	0.08	0.005	0.09	6	n.d.	n.d.	n.d.	n.d.	n.d.	0.3	0.3	0.04
ARA-R3-F-T3	0.17	0.007	0.17	4	n.d.	n.d.	n.d.	n.d.	n.d.	0.4	0.5	0.02
ARA-R3-F-T4	0.15	0.004	0.15	3	n.d.	n.d.	n.d.	n.d.	n.d.	0.6	1.0	0.03
ARA-R3-F-P1=T2	0.14	0.004	0.14	3	n.d.	n.d.	n.d.	n.d.	n.d.	0.4	0.8	0.04
ARA-R3-F-P2	0.16	0.005	0.16	3	n.d.	n.d.	n.d.	n.d.	n.d.	0.3	0.2	<LOD
ARA-R3-F-P3	0.20	0.009	0.21	4	n.d.	n.d.	n.d.	n.d.	n.d.	0.3	0.3	<LOD
ARA-R3-F-P4	0.19	0.006	0.19	3	n.d.	n.d.	n.d.	n.d.	n.d.	0.3	0.3	<LOD
BAD-R3-F	0.16	0.005	0.16	3	n.d.	n.d.	n.d.	n.d.	n.d.	0.2	0.3	<LOD
CAM-R3-F	0.19	0.009	0.19	4	n.d.	n.d.	n.d.	n.d.	n.d.	0.2	0.3	<LOD
CAM-R3-F-Melt	0.53	0.010	0.54	2	n.d.	n.d.	n.d.	n.d.	n.d.	n.d.	n.d.	n.d.
CAM-R3-F-Ice	1.03	0.054	1.08	5	n.d.	n.d.	n.d.	n.d.	n.d.	n.d.	n.d.	n.d.
PEY-R3-F	0.31	0.015	0.33	5	n.d.	n.d.	n.d.	n.d.	n.d.	0.1	0.1	<LOD
OPA-R3-F	0.19	0.007	0.19	4	n.d.	n.d.	n.d.	n.d.	n.d.	0.2	0.6	<LOD
PAR-R3-F	0.39	0.026	0.42	6	n.d.	n.d.	n.d.	n.d.	n.d.	0.1	0.1	<LOD
GEN-R3-F-T1	0.16	0.007	0.17	4	n.d.	n.d.	n.d.	n.d.	n.d.	0.8	1.4	0.07
GEN-R3-F-T3	0.19	0.009	0.20	4	n.d.	n.d.	n.d.	n.d.	n.d.	0.4	1.2	0.05
GEN-R3-F-T4	0.17	0.009	0.18	5	n.d.	n.d.	n.d.	n.d.	n.d.	0.3	0.3	0.06
GEN-R3-F-P1=T2	0.21	0.006	0.22	3	n.d.	n.d.	n.d.	n.d.	n.d.	0.3	0.3	0.07
GEN-R3-F-P2	0.20	0.009	0.21	4	n.d.	n.d.	n.d.	n.d.	n.d.	0.4	1.2	0.07
GEN-R3-F-P3	0.18	0.009	0.19	5	n.d.	n.d.	n.d.	n.d.	n.d.	0.3	0.3	0.06
GEN-R3-F-P4	0.18	0.023	0.20	12	n.d.	n.d.	n.d.	n.d.	n.d.	0.4	0.5	0.06
GEN-R3-F-P5	0.66	0.318	0.98	32	n.d.	n.d.	n.d.	n.d.	n.d.	0.1	0.4	0.04
ROU-R3-F	0.18	0.014	0.20	7	n.d.	n.d.	n.d.	n.d.	n.d.	0.2	0.2	0.06
BER-R3-F	0.35	0.016	0.36	4	n.d.	n.d.	n.d.	n.d.	n.d.	0.2	0.2	0.04
AZU-R3-F-T2	0.34	0.005	0.34	2	n.d.	n.d.	n.d.	n.d.	n.d.	0.2	0.2	0.03
AZU-R3-F-P1=T1	0.31	0.003	0.31	1	n.d.	n.d.	n.d.	n.d.	n.d.	0.2	0.3	0.03
AZU-R3-F-P2	0.28	0.005	0.28	2	n.d.	n.d.	n.d.	n.d.	n.d.	0.3	0.2	<LOD
AZU-R3-F-P3	0.30	0.005	0.31	2	n.d.	n.d.	n.d.	n.d.	n.d.	0.4	0.3	0.03
ARN-R3-F	0.31	0.006	0.31	2	n.d.	n.d.	n.d.	n.d.	n.d.	0.2	0.3	0.03
BAC-R3-F	0.30	0.010	0.31	3	n.d.	n.d.	n.d.	n.d.	n.d.	n.d.	n.d.	n.d.

PEC-R3-F	0.20	0.006	0.21	3	n.d.	n.d.	n.d.	n.d.	n.d.	0.2	0.1	0.02
COA-R3-F	0.42	0.009	0.43	2	n.d.	n.d.	n.d.	n.d.	n.d.	0.3	0.2	0.03
PAN-R3-F	0.36	0.009	0.37	2	n.d.	n.d.	n.d.	n.d.	n.d.	0.2	0.2	0.03
ORD-R3-F	0.54	0.027	0.57	5	n.d.	n.d.	n.d.	n.d.	n.d.	0.3	0.1	0.02
SAB-R3-F-T1	0.58	0.010	0.59	2	n.d.	n.d.	n.d.	n.d.	n.d.	1.3	4.0	0.04
SAB-R3-F-T3	0.67	0.010	0.68	1	n.d.	n.d.	n.d.	n.d.	n.d.	0.6	1.2	0.04
SAB-R3-F-P1=T2	0.53	0.008	0.54	2	n.d.	n.d.	n.d.	n.d.	n.d.	0.4	0.4	0.04
SAB-R3-F-P2	0.47	0.009	0.48	2	n.d.	n.d.	n.d.	n.d.	n.d.	0.6	1.6	0.04
SAB-R3-F-P3	0.35	0.012	0.36	3	n.d.	n.d.	n.d.	n.d.	n.d.	0.4	0.9	0.04
SAB-R3-F-P4	0.33	0.011	0.34	3	n.d.	n.d.	n.d.	n.d.	n.d.	0.3	0.2	0.04
SAB-R3-F-P5	0.29	0.012	0.30	4	n.d.	n.d.	n.d.	n.d.	n.d.	0.7	0.7	0.03
SAB-R3-F-P6	0.32	0.025	0.34	7	n.d.	n.d.	n.d.	n.d.	n.d.	0.3	0.3	0.03
ARA-R3-UF-T1	0.11	0.007	0.12	6	0.05	0.17	30	24	37	0.8	0.5	0.11
ARA-R3-UF-T3	0.17	0.007	0.18	4	0.20	0.37	53	106	160	0.5	0.6	0.02
ARA-R3-UF-T4	0.20	0.010	0.21	5	0.12	0.32	36	60	91	0.8	1.0	0.05
ARA-R3-UF-P1=T2	0.21	0.007	0.21	3	0.18	0.39	46	96	146	0.7	0.8	0.05
ARA-R3-UF-P2	0.17	0.005	0.17	3	0.14	0.32	45	n.d.	n.d.	0.2	0.5	0.14
ARA-R3-UF-P3	0.22	0.010	0.23	4	0.22	0.45	50	n.d.	n.d.	0.6	1.1	<LOD
ARA-R3-UF-P4	0.26	0.009	0.26	3	0.17	0.44	40	n.d.	n.d.	0.7	1.3	0.15
BAD-R3-UF	0.18	0.006	0.19	3	0.12	0.31	39	62	95	0.3	0.4	0.21
CAM-R3-UF	0.26	0.012	0.27	4	0.19	0.45	41	100	152	0.2	0.6	<LOD
CAM-R3-UF-Melt	1.01	0.035	1.05	3	n.d.	n.d.	n.d.	n.d.	n.d.	n.d.	n.d.	n.d.
CAM-R3-UF-Ice	18.80	0.612	19.41	3	n.d.	n.d.	n.d.	n.d.	n.d.	n.d.	n.d.	n.d.
PEY-R3-UF	0.67	0.023	0.69	3	0.39	1.08	36	217	328	0.1	0.1	<LOD
OPA-R3-UF	0.24	0.007	0.25	3	0.04	0.29	15	19	29	0.3	0.9	<LOD
PAR-R3-UF	0.41	0.026	0.43	6	n.d.	n.d.	n.d.	n.d.	n.d.	0.4	0.4	0.23
GEN-R3-UF-T1	0.84	0.008	0.85	1	0.09	0.94	10	46	69	1.5	2.4	0.10
GEN-R3-UF-T3	0.68	0.013	0.69	2	0.26	0.95	27	143	216	0.9	1.7	0.07
GEN-R3-UF-T4	0.39	0.014	0.40	3	0.26	0.66	39	140	213	0.6	0.4	0.07
GEN-R3-UF-P1=T2	0.38	0.008	0.39	2	10.79	11.18	97	6090	9226	0.6	0.4	0.07
GEN-R3-UF-P2	0.31	0.010	0.32	3	3.04	3.36	90	n.d.	n.d.	0.9	1.2	0.07
GEN-R3-UF-P3	0.34	0.013	0.36	4	0.31	0.66	46	n.d.	n.d.	0.5	0.3	0.08
GEN-R3-UF-P4	0.19	0.057	0.25	23	0.23	0.48	47	n.d.	n.d.	1.0	0.8	0.06
GEN-R3-UF-P5	0.75	0.426	1.17	36	0.14	1.31	10	n.d.	n.d.	0.1	0.4	0.05

ROU-R3-UF	0.30	0.014	0.32	5	0.13	0.44	29	n.d.	n.d.	0.3	0.2	0.07
BER-R3-UF	0.70	0.018	0.71	2	0.27	0.98	27	n.d.	n.d.	0.3	0.2	0.05
AZU-R3-UF-T2	0.38	0.006	0.39	2	0.09	0.49	19	48	73	0.2	0.3	0.04
AZU-R3-UF-P1=T1	0.31	0.006	0.31	2	0.17	0.48	35	89	135	0.4	0.4	0.03
AZU-R3-UF-P2	0.39	0.006	0.39	1	0.10	0.50	21	n.d.	n.d.	0.6	0.3	0.03
AZU-R3-UF-P3	0.40	0.006	0.40	1	0.09	0.49	18	n.d.	n.d.	0.4	0.3	0.03
ARN-R3-UF	0.38	0.007	0.38	2	0.08	0.46	17	39	59	0.4	0.3	0.04
BAC-R3-UF	0.44	0.012	0.45	3	0.11	0.56	20	57	87	0.3	0.2	0.04
PEC-R3-UF	0.25	0.007	0.26	3	0.05	0.31	16	23	34	0.2	0.1	0.03
COA-R3-UF	0.60	0.011	0.61	2	0.20	0.81	25	108	164	0.4	0.3	0.03
PAN-R3-UF	0.53	0.011	0.54	2	n.d.	n.d.	n.d.	n.d.	n.d.	0.3	0.3	0.03
ORD-R3-UF	0.55	0.030	0.58	5	n.d.	n.d.	n.d.	n.d.	n.d.	0.4	0.1	0.03
SAB-R3-UF-T1	0.70	0.012	0.72	2	1.27	1.98	64	693	1050	2.9	4.0	0.05
SAB-R3-UF-T3	0.73	0.018	0.75	2	1.18	1.94	61	645	977	1.4	1.5	0.04
SAB-R3-UF-P1=T2	0.64	0.019	0.66	3	4.65	5.31	88	2553	3867	0.7	0.7	0.04
SAB-R3-UF-P2	1.29	0.013	1.31	1	2.36	3.66	64	n.d.	n.d.	3.4	2.2	0.04
SAB-R3-UF-P3	0.42	0.017	0.44	4	0.31	0.74	41	n.d.	n.d.	0.7	1.0	0.04
SAB-R3-UF-P4	0.55	0.017	0.57	3	0.22	0.79	28	n.d.	n.d.	0.8	0.3	0.05
SAB-R3-UF-P5	0.39	0.026	0.42	6	1.43	1.85	77	n.d.	n.d.	1.1	1.0	0.03
SAB-R3-UF-P6	0.56	0.060	0.62	10	0.56	1.17	48	n.d.	n.d.	0.3	0.4	0.04

REPLIM 4	iHg(II)	MMHg	non-gaseous Hg	% MMHg	DGM	total Hg	% DGM	FD 1 m s ⁻¹	FD 3 m s ⁻¹	MBT	DBT	TBT
	ng L ⁻¹	ng L ⁻¹	ng L ⁻¹	%	ng L ⁻¹	ng L ⁻¹	%	ng m ⁻² day ⁻¹	ng m ⁻² day ⁻¹	ng L ⁻¹	ng L ⁻¹	ng L ⁻¹
LOD	0.01	0.004			0.0002					0.1	0.1	0.01
ARA-R4-F-P1	0.27	0.010	0.28	3	n.d.	n.d.	n.d.	n.d.	n.d.	0.9	1.1	n.d.
ARA-R4-F-P2	0.12	0.008	0.13	6	n.d.	n.d.	n.d.	n.d.	n.d.	0.4	0.2	n.d.
ARA-R4-F-P3	0.17	0.013	0.18	7	n.d.	n.d.	n.d.	n.d.	n.d.	0.4	0.2	n.d.
BAD-R4-F	0.23	0.010	0.24	4	n.d.	n.d.	n.d.	n.d.	n.d.	0.2	<LOD	n.d.
CAM-R4-F	0.19	0.008	0.19	4	n.d.	n.d.	n.d.	n.d.	n.d.	0.3	0.2	n.d.
PEY-R4-F	0.20	0.009	0.21	4	n.d.	n.d.	n.d.	n.d.	n.d.	0.2	<LOD	n.d.
OPA-R4-F	0.20	0.008	0.21	4	n.d.	n.d.	n.d.	n.d.	n.d.	0.3	<LOD	n.d.
PAR-R4-F	0.29	0.058	0.35	17	n.d.	n.d.	n.d.	n.d.	n.d.	0.2	<LOD	n.d.
GEN-R4-F-T1	0.12	0.024	0.15	16	n.d.	n.d.	n.d.	n.d.	n.d.	1.0	0.4	n.d.
GEN-R4-F-T3	0.14	0.026	0.17	15	n.d.	n.d.	n.d.	n.d.	n.d.	0.9	0.9	n.d.
GEN-R4-F-P1=T2	0.13	0.026	0.15	17	n.d.	n.d.	n.d.	n.d.	n.d.	0.3	0.2	n.d.
GEN-R4-F-P2	0.14	0.017	0.16	11	n.d.	n.d.	n.d.	n.d.	n.d.	0.7	1.0	n.d.
GEN-R4-F-P3	0.14	0.020	0.16	13	n.d.	n.d.	n.d.	n.d.	n.d.	0.7	0.8	n.d.
GEN-R4-F-P4	0.08	0.011	0.10	12	n.d.	n.d.	n.d.	n.d.	n.d.	1.5	1.6	n.d.
GEN-R4-F-P5	0.36	0.341	0.70	49	n.d.	n.d.	n.d.	n.d.	n.d.	3.1	0.1	n.d.
ROU-R4-F	0.21	0.017	0.23	7	n.d.	n.d.	n.d.	n.d.	n.d.	0.2	<LOD	n.d.
BER-R4-F	0.17	0.005	0.17	3	n.d.	n.d.	n.d.	n.d.	n.d.	0.8	<LOD	n.d.
AZU-R4-F-P1=T1	0.27	0.009	0.28	3	n.d.	n.d.	n.d.	n.d.	n.d.	0.4	0.8	n.d.
AZU-R4-F-P2	0.71	0.010	0.72	1	n.d.	n.d.	n.d.	n.d.	n.d.	0.3	0.5	n.d.
AZU-R4-F-P3	2.46	0.021	2.48	1	n.d.	n.d.	n.d.	n.d.	n.d.	0.2	0.5	n.d.
ARN-R4-F	0.37	0.008	0.37	2	n.d.	n.d.	n.d.	n.d.	n.d.	0.8	0.6	n.d.
BAC-R4-F	0.33	0.014	0.35	4	n.d.	n.d.	n.d.	n.d.	n.d.	0.4	0.1	n.d.
PEC-R4-F	0.24	0.005	0.25	2	n.d.	n.d.	n.d.	n.d.	n.d.	0.2	<LOD	n.d.
COA-R4-F	2.68	0.022	2.70	1	n.d.	n.d.	n.d.	n.d.	n.d.	0.7	0.5	n.d.
PAN-R4-F	0.68	0.035	0.72	5	n.d.	n.d.	n.d.	n.d.	n.d.	4.2	1.0	n.d.
ORD-R4-F	1.10	0.023	1.12	2	n.d.	n.d.	n.d.	n.d.	n.d.	0.3	<LOD	n.d.
SAB-R4-F-T1	0.39	0.025	0.42	6	n.d.	n.d.	n.d.	n.d.	n.d.	3.6	1.3	n.d.
SAB-R4-F-T3	0.44	0.022	0.46	5	n.d.	n.d.	n.d.	n.d.	n.d.	1.1	0.5	n.d.
SAB-R4-F-P1=T2	0.39	0.018	0.40	5	n.d.	n.d.	n.d.	n.d.	n.d.	1.2	0.4	n.d.
SAB-R4-F-P2	0.68	0.015	0.69	2	n.d.	n.d.	n.d.	n.d.	n.d.	1.0	0.8	n.d.

SAB-R4-F-P3	0.51	0.024	0.53	5	n.d.	n.d.	n.d.	n.d.	n.d.	1.3	0.4	n.d.
SAB-R4-F-P4	0.44	0.012	0.45	3	n.d.	n.d.	n.d.	n.d.	n.d.	1.5	0.8	n.d.
SAB-R4-F-P5	0.43	0.015	0.44	3	n.d.	n.d.	n.d.	n.d.	n.d.	1.2	0.3	n.d.
SAB-R4-F-P6	0.17	0.015	0.18	8	n.d.	n.d.	n.d.	n.d.	n.d.	0.8	0.3	n.d.
ARA-R4-UF-P1	0.47	0.017	0.49	3	0.08	0.57	13	38	58	1.4	1.3	n.d.
ARA-R4-UF-P2	0.25	0.011	0.26	4	0.07	0.34	21	n.d.	n.d.	0.4	0.3	n.d.
ARA-R4-UF-P3	0.22	0.014	0.24	6	0.05	0.29	19	n.d.	n.d.	0.4	0.3	n.d.
BAD-R4-UF	0.28	0.010	0.29	4	0.04	0.33	13	19	29	0.2	<LOD	n.d.
CAM-R4-UF	0.45	0.011	0.46	2	0.09	0.55	16	44	67	0.6	0.4	n.d.
PEY-R4-UF	0.40	0.010	0.41	2	0.09	0.50	19	48	72	0.3	<LOD	n.d.
OPA-R4-UF	0.31	0.009	0.32	3	0.06	0.38	15	27	41	0.3	<LOD	n.d.
PAR-R4-UF	0.36	0.092	0.45	21	n.d.	n.d.	n.d.	n.d.	n.d.	0.3	<LOD	n.d.
GEN-R4-UF-T1	0.24	0.024	0.26	9	0.03	0.29	10	12	18	1.3	0.4	n.d.
GEN-R4-UF-T3	0.16	0.027	0.19	15	0.04	0.23	19	19	29	1.6	1.0	n.d.
GEN-R4-UF-P1=T2	0.31	0.029	0.34	9	0.06	0.40	16	30	46	0.4	0.2	n.d.
GEN-R4-UF-P2	0.15	0.055	0.20	28	0.06	0.26	22	n.d.	n.d.	1.3	1.1	n.d.
GEN-R4-UF-P3	0.23	0.041	0.27	15	0.05	0.33	17	n.d.	n.d.	1.1	0.9	n.d.
GEN-R4-UF-P4	0.09	0.027	0.11	24	0.04	0.15	24	n.d.	n.d.	3.9	1.7	n.d.
GEN-R4-UF-P5	0.39	0.388	0.78	50	0.03	0.80	3	n.d.	n.d.	3.4	0.2	n.d.
ROU-R4-UF	0.38	0.034	0.41	8	0.03	0.44	8	14	22	0.3	<LOD	n.d.
BER-R4-UF	0.21	0.007	0.21	3	0.05	0.26	18	21	32	0.8	<LOD	n.d.
AZU-R4-UF-P1=T1	0.39	0.009	0.40	2	0.09	0.49	18	45	68	0.8	0.8	n.d.
AZU-R4-UF-P2	1.11	0.010	1.12	1	0.85	1.97	43	n.d.	n.d.	0.4	0.7	n.d.
AZU-R4-UF-P3	2.81	0.021	2.83	1	1.33	4.17	32	n.d.	n.d.	0.3	0.5	n.d.
ARN-R4-UF	0.52	0.011	0.53	2	0.20	0.74	28	110	167	0.9	0.7	n.d.
BAC-R4-UF	0.38	0.026	0.41	6	0.11	0.52	21	56	85	0.7	0.1	n.d.
PEC-R4-UF	0.34	0.009	0.35	3	n.d.	n.d.	n.d.	n.d.	n.d.	0.5	0.1	n.d.
COA-R4-UF	2.88	0.025	2.91	1	0.20	3.10	6	107	162	0.7	0.6	n.d.
PAN-R4-UF	0.96	0.062	1.02	6	n.d.	n.d.	n.d.	n.d.	n.d.	6.9	1.9	n.d.
ORD-R4-UF	1.16	0.025	1.18	2	0.18	1.37	13	97	147	0.9	<LOD	n.d.
SAB-R4-UF-T1	0.58	0.027	0.61	4	0.52	1.13	46	288	436	4.6	1.6	n.d.
SAB-R4-UF-T3	0.53	0.029	0.56	5	n.d.	n.d.	n.d.	n.d.	n.d.	1.8	0.6	n.d.
SAB-R4-UF-P1=T2	0.58	0.029	0.61	5	0.29	0.90	32	156	237	1.3	0.5	n.d.
SAB-R4-UF-P2	0.90	0.032	0.93	3	0.38	1.31	29	n.d.	n.d.	1.7	0.8	n.d.

SAB-R4-UF-P3	0.54	0.026	0.57	5	0.43	1.00	43	n.d.	n.d.	2.1	0.5	n.d.
SAB-R4-UF-P4	0.53	0.024	0.55	4	0.52	1.08	49	n.d.	n.d.	n.d.	0.8	n.d.
SAB-R4-UF-P5	0.61	0.017	0.63	3	1.15	1.78	65	n.d.	n.d.	2.1	0.3	n.d.
SAB-R4-UF-P6	0.79	0.026	0.81	3	0.41	1.23	34	n.d.	n.d.	0.8	0.4	n.d.

REPLIM 5	iHg(II)	MMHg	non-gaseous Hg	% MMHg	DGM	total Hg	% DGM	FD 1 m s ⁻¹	FD 3 m s ⁻¹	MBT	DBT	TBT
	ng L ⁻¹	ng L ⁻¹	ng L ⁻¹	%	ng L ⁻¹	ng L ⁻¹	%	ng m ⁻² day ⁻¹	ng m ⁻² day ⁻¹	ng L ⁻¹	ng L ⁻¹	ng L ⁻¹
LOD	0.03	0.004			0.0002					0.1	0.1	0.01
GEN-R5-F-T1	0.17	0.012	0.18	7	n.d.	n.d.	n.d.	n.d.	n.d.	1.4	1.3	0.03
GEN-R5-F-T3	0.16	0.014	0.17	8	n.d.	n.d.	n.d.	n.d.	n.d.	0.7	0.8	0.02
GEN-R5-F-T4	0.19	0.006	0.20	3	n.d.	n.d.	n.d.	n.d.	n.d.	0.6	0.7	0.03
GEN-R5-F-P1=T2	0.18	0.015	0.20	8	n.d.	n.d.	n.d.	n.d.	n.d.	0.5	1.0	0.03
GEN-R5-F-P2	0.15	0.006	0.16	4	n.d.	n.d.	n.d.	n.d.	n.d.	0.5	0.9	0.02
GEN-R5-F-P3	0.07	0.004	0.07	6	n.d.	n.d.	n.d.	n.d.	n.d.	0.5	0.6	0.03
GEN-R5-F-P4	0.08	0.019	0.10	18	n.d.	n.d.	n.d.	n.d.	n.d.	0.3	0.6	0.02
GEN-R5-F-P5	0.11	0.157	0.26	60	n.d.	n.d.	n.d.	n.d.	n.d.	0.4	0.4	0.04
ROU-R5-F	0.29	0.012	0.30	4	n.d.	n.d.	n.d.	n.d.	n.d.	0.3	0.2	0.03
BER-R5-F	0.41	0.012	0.42	3	n.d.	n.d.	n.d.	n.d.	n.d.	0.5	0.2	0.03
AZU-R5-F	n.d.	n.d.	n.d.	n.d.	n.d.	n.d.	n.d.	n.d.	n.d.	n.d.	n.d.	n.d.
ARN-R5-F	n.d.	n.d.	n.d.	n.d.	n.d.	n.d.	n.d.	n.d.	n.d.	n.d.	n.d.	n.d.
BAC-R5-F	n.d.	n.d.	n.d.	n.d.	n.d.	n.d.	n.d.	n.d.	n.d.	n.d.	n.d.	n.d.
PEC-R5-F	n.d.	n.d.	n.d.	n.d.	n.d.	n.d.	n.d.	n.d.	n.d.	n.d.	n.d.	n.d.
COA-R5-F	n.d.	n.d.	n.d.	n.d.	n.d.	n.d.	n.d.	n.d.	n.d.	n.d.	n.d.	n.d.
PAN-R5-F	n.d.	n.d.	n.d.	n.d.	n.d.	n.d.	n.d.	n.d.	n.d.	n.d.	n.d.	n.d.
ORD-R5-F	n.d.	n.d.	n.d.	n.d.	n.d.	n.d.	n.d.	n.d.	n.d.	n.d.	n.d.	n.d.
SAB-R5-F-T1	0.19	0.005	0.19	3	n.d.	n.d.	n.d.	n.d.	n.d.	0.9	0.6	0.03
SAB-R5-F-T3	0.18	0.005	0.19	3	n.d.	n.d.	n.d.	n.d.	n.d.	1.1	0.7	0.04
SAB-R5-F-P1=T2	0.21	0.014	0.22	6	n.d.	n.d.	n.d.	n.d.	n.d.	1.0	0.8	0.03
SAB-R5-F-P2	0.18	0.010	0.19	5	n.d.	n.d.	n.d.	n.d.	n.d.	0.8	0.7	0.04
SAB-R5-F-P3	0.03	0.006	0.04	15	n.d.	n.d.	n.d.	n.d.	n.d.	0.5	0.8	0.04
SAB-R5-F-P4	0.02	0.004	0.03	13	n.d.	n.d.	n.d.	n.d.	n.d.	0.4	0.5	0.05
SAB-R5-F-P5	0.03	0.005	0.03	18	n.d.	n.d.	n.d.	n.d.	n.d.	0.5	1.0	0.05
SAB-R5-F-P6	0.03	0.021	0.05	42	n.d.	n.d.	n.d.	n.d.	n.d.	0.5	0.5	0.05
GEN-R5-UF-T1	0.24	0.018	0.25	7	0.09	0.34	25	43	65	2.5	1.3	0.03
GEN-R5-UF-T3	0.30	0.011	0.31	4	0.10	0.41	25	52	79	1.1	0.8	0.03
GEN-R5-UF-T4	0.25	0.014	0.26	5	0.10	0.36	27	50	76	0.9	0.8	0.04
GEN-R5-UF-P1=T2	0.27	0.012	0.28	4	0.10	0.38	26	50	75	0.9	1.3	0.04
GEN-R5-UF-P2	0.20	0.007	0.20	3	0.08	0.29	29	n.d.	n.d.	0.7	0.9	0.03

GEN-R5-UF-P3	0.18	0.037	0.22	17	0.04	0.26	17	n.d.	n.d.	1.0	0.8	0.03
GEN-R5-UF-P4	0.14	0.059	0.20	30	0.02	0.22	8	n.d.	n.d.	1.0	0.8	0.04
GEN-R5-UF-P5	0.18	0.236	0.42	56	0.01	0.43	3	n.d.	n.d.	0.7	0.6	0.04
ROU-R5-UF	0.42	0.025	0.45	6	0.17	0.62	28	90	136	0.3	0.2	0.04
BER-R5-UF	0.55	0.021	0.57	4	0.23	0.80	29	126	191	1.1	0.3	0.06
AZU-R5-UF	0.11	0.005	0.11	5	n.d.	n.d.	n.d.	n.d.	n.d.	0.5	0.3	0.08
ARN-R5-UF	0.29	0.005	0.29	2	n.d.	n.d.	n.d.	n.d.	n.d.	0.7	0.4	0.10
BAC-R5-UF	0.44	0.011	0.45	2	n.d.	n.d.	n.d.	n.d.	n.d.	0.2	0.2	<LOD
PEC-R5-UF	0.39	0.024	0.41	6	n.d.	n.d.	n.d.	n.d.	n.d.	0.2	0.1	<LOD
COA-R5-UF	0.65	0.008	0.66	1	n.d.	n.d.	n.d.	n.d.	n.d.	0.3	0.1	<LOD
PAN-R5-UF	3.12	0.008	3.13	0	n.d.	n.d.	n.d.	n.d.	n.d.	0.5	0.3	0.08
ORD-R5-UF	1.03	0.028	1.05	3	n.d.	n.d.	n.d.	n.d.	n.d.	0.3	0.1	<LOD
SAB-R5-UF-T1	0.34	0.005	0.35	2	0.06	0.41	15	31	46	0.9	0.8	0.04
SAB-R5-UF-T3	0.35	0.018	0.36	5	0.16	0.53	31	87	132	1.4	0.8	0.05
SAB-R5-UF-P1=T2	0.32	0.022	0.34	6	1.34	1.67	80	741	1122	1.3	1.0	0.04
SAB-R5-UF-P2	0.34	0.011	0.35	3	0.12	0.47	25	n.d.	n.d.	0.9	0.8	0.06
SAB-R5-UF-P3	0.08	0.018	0.09	19	0.11	0.20	54	n.d.	n.d.	0.6	0.8	0.05
SAB-R5-UF-P4	0.13	0.020	0.15	13	0.09	0.24	39	n.d.	n.d.	0.5	0.6	0.06
SAB-R5-UF-P5	0.13	0.022	0.15	14	0.04	0.19	21	n.d.	n.d.	1.0	1.5	0.11
SAB-R5-UF-P6	0.15	0.052	0.20	25	0.06	0.26	22	n.d.	n.d.	0.7	0.8	0.08

Annexe 4: Results for other parameters (temperature, conductivity, redox potential, TOC, Silicate, DIC, TA, pH, fCO₂, major anions)

REPLIM 1	Temperature	Conductivity	Redox Potential	TOC	Silicate	DIC	TA	pH	fCO ₂	Cl ⁻	NO ₃ ⁻	SO ₄ ²⁻
	°C	μS cm ⁻¹	mV	mg L ⁻¹	mg L ⁻¹	μmol kg ⁻¹	μmol kg ⁻¹		μatm	mg L ⁻¹	mg L ⁻¹	mg L ⁻¹
LOD										0.02	0.05	0.03
ARA-R1-1	9.53	46	271	1.71	4.69	682	698	7.36	1360	0.20	0.62	2.88
ARA-R1-2	9.53	46	271	1.35	4.60	680	697	7.32	1482	0.17	0.66	2.90
ARA-R1-3	9.53	46	271	1.65	4.63	676	700	7.36	1364	0.22	n.d.	2.94
BAD-R1-1	n.d.	n.d.	n.d.	1.98	4.98	788	n.d.	n.d.	n.d.	0.25	0.78	3.56
BAD-R1-2	n.d.	n.d.	n.d.	2.18	5.42	785	817	7.46	1266	0.18	0.75	3.54
BAD-R1-3	n.d.	n.d.	n.d.	1.85	4.85	n.d.	n.d.	n.d.	n.d.	0.18	0.78	3.66
CAM-R1-1	8.71	8	160	0.64	1.62	n.d.	121	n.d.	n.d.	0.18	0.46	0.39
CAM-R1-2	8.71	8	160	0.67	1.60	125	132	6.41	1200	0.17	0.34	0.40
CAM-R1-3	8.71	8	160	0.74	1.58	123	112	6.43	1144	0.17	0.41	0.38
PEY-R1-1	5.45	17	208	0.64	1.39	90	79	6.01	1083	0.16	0.46	0.26
PEY-R1-2	5.45	17	208	0.62	1.37	94	81	6.01	1128	0.15	0.37	0.30
PEY-R1-3	5.45	17	208	n.d.	n.d.	n.d.	n.d.	n.d.	n.d.	n.d.	n.d.	n.d.
OPA-R1-1	n.d.	n.d.	n.d.	1.15	1.79	312	303	6.94	1350	0.16	0.60	0.51
OPA-R1-2	n.d.	n.d.	n.d.	1.02	1.74	308	305	6.92	1378	0.16	0.74	0.52
OPA-R1-3	n.d.	n.d.	n.d.	1.01	1.70	304	299	6.92	1357	0.16	0.62	0.51
PAR-R1-1	10.61	41	118	3.27	6.47	662	655	7.17	1975	0.52	0.61	1.80
PAR-R1-2	10.61	41	118	2.75	6.15	664	644	7.22	1802	0.48	0.42	1.71
PAR-R1-3	10.61	41	118	2.54	6.07	n.d.	649	n.d.	n.d.	0.47	0.60	1.78
NER-R1-1	11.13	7	119	0.80	1.62	110	107	6.29	1254	0.16	0.23	0.39
NER-R1-2	11.13	7	119	0.78	1.54	107	103	6.24	1280	0.16	0.38	0.37
NER-R1-3	11.13	7	119	0.77	1.57	n.d.	106	n.d.	n.d.	0.16	0.29	0.38
POU-R1-1	9.46	12	202	0.86	1.61	191	193	6.71	1257	0.25	0.37	0.41
POU-R1-2	9.46	12	202	1.20	1.68	189	208	6.78	1113	0.19	0.42	0.43
POU-R1-3	9.46	12	202	0.99	1.56	n.d.	201	n.d.	n.d.	0.25	<LOD	0.43
AZU-R1-1	8.22	58	131	2.39	2.68	797	815	7.47	1243	0.22	0.87	6.53
AZU-R1-2	8.22	58	131	1.97	2.81	n.d.	836	n.d.	n.d.	0.18	0.74	6.46
AZU-R1-3	8.22	58	131	2.06	2.82	n.d.	842	n.d.	n.d.	0.20	1.06	6.53
ARN-R1-1	8.43	18	122	0.88	2.37	226	243	6.83	1204	0.16	0.67	1.37
ARN-R1-2	8.43	18	122	1.09	2.35	225	240	6.81	1237	0.16	0.66	1.39
ARN-R1-3	8.43	18	122	1.11	2.33	225	244	6.84	1177	0.18	0.66	1.42

BAC-R1-1	n.d.	n.d.	n.d.	1.18	2.08	311	323	6.95	1351	0.24	0.84	1.70
BAC-R1-2	n.d.	n.d.	n.d.	1.33	2.11	306	321	6.92	1410	0.22	0.69	1.75
BAC-R1-3	n.d.	n.d.	n.d.	1.18	2.13	311	309	6.94	1387	0.23	0.54	1.69
PEC-R1-1	8.84	36	198	1.51	2.61	457	475	7.12	1467	0.19	0.77	2.64
PEC-R1-2	8.84	36	198	1.49	2.42	456	475	7.13	1446	0.18	0.74	2.61
PEC-R1-3	8.84	36	198	1.53	2.51	459	482	7.15	1381	0.17	0.85	2.57
COA-R1-1	7.11	23	97	0.98	1.67	134	138	6.42	1223	0.14	0.23	0.46
COA-R1-2	7.11	23	97	1.08	1.61	n.d.	142	n.d.	n.d.	0.16	0.21	0.46
COA-R1-3	7.11	23	97	1.02	1.69	n.d.	135	n.d.	n.d.	0.14	0.19	0.49
PAN-R1-1	10.29	27	195	1.73	3.26	402	405	7.02	1591	0.27	0.71	2.18
PAN-R1-2	10.29	27	195	1.48	3.36	n.d.	473	n.d.	n.d.	0.29	0.61	2.46
PAN-R1-3	10.29	27	195	1.40	3.32	n.d.	421	n.d.	n.d.	0.44	0.87	2.24
ORD-R1-1	18.29	61	157	3.16	2.94	676	695	7.31	1708	0.17	0.13	1.84
ORD-R1-2	18.29	61	157	2.69	2.99	676	699	7.38	1479	0.18	0.10	1.79
ORD-R1-3	18.29	61	157	2.38	3.42	732	743	7.34	1741	0.19	n.d.	1.96
XUA-R1-1	4.63	12	110	0.90	1.20	196	207	6.71	1176	0.23	0.91	0.64
XUA-R1-2	4.63	12	110	0.81	1.19	203	199	6.67	1287	0.16	0.84	0.61
XUA-R1-3	4.63	12	110	0.84	1.22	206	200	6.66	1315	0.20	0.96	0.57

REPLIM 2	Temperature	Conductivity	Redox Potential	TOC	Silicate	DIC	TA	pH	fCO ₂	Cl ⁻	NO ₃ ⁻	SO ₄ ²⁻
	°C	μS cm ⁻¹	mV	mg L ⁻¹	mg L ⁻¹	μmol kg ⁻¹	μmol kg ⁻¹		μatm	mg L ⁻¹	mg L ⁻¹	mg L ⁻¹
LOD										0.03	0.14	0.10
ARA-R2-1	9.85	65	80	3.15	4.55	819	949	7.93	468	0.14	0.23	3.79
ARA-R2-2	9.85	65	80	2.45	4.80	825	892	7.92	488	0.16	0.19	3.73
ARA-R2-3	9.85	65	80	2.80	4.74	821	882	7.87	534	0.14	0.22	3.71
BAD-R2-1	9.72	67	46	2.58	4.12	868	893	7.57	1088	0.18	<LOD	3.83
BAD-R2-2	9.72	67	46	2.86	3.99	842	870	7.57	1065	0.26	0.47	3.61
BAD-R2-3	9.72	67	46	3.70	3.92	865	908	7.64	944	0.17	0.36	3.71
CAM-R2-1	9.71	14	121	1.14	1.76	170	178	6.63	1263	0.20	0.22	0.62
CAM-R2-2	9.71	14	121	1.52	1.71	175	179	6.67	1219	0.20	0.20	0.62
CAM-R2-3	9.71	14	121	1.15	n.d.	170	191	n.d.	n.d.	0.19	0.21	0.65
PEY-R2-1	9.57	7	108	1.40	0.62	87	84	6.00	1184	0.15	<LOD	0.38
PEY-R2-2	9.57	7	108	n.d.	0.62	n.d.	n.d.	n.d.	n.d.	0.17	<LOD	0.33
PEY-R2-3	9.57	7	108	n.d.	0.68	n.d.	n.d.	n.d.	n.d.	0.18	<LOD	0.33
OPA-R2-1	9.89	25	141	1.28	1.83	324	334	6.95	1443	0.16	0.54	0.71
OPA-R2-2	9.89	25	141	1.31	1.91	n.d.	321	n.d.	n.d.	0.16	0.59	0.69
OPA-R2-3	9.89	25	141	1.39	1.86	320	325	6.90	1556	0.16	0.62	0.74
PAR-R2-1	7.22	49	153	3.08	6.91	738	692	7.16	2103	0.48	0.75	1.86
PAR-R2-2	7.22	49	153	3.31	6.79	721	690	7.21	1859	0.47	0.73	1.84
PAR-R2-3	7.22	49	153	2.89	7.27	723	699	7.23	1819	0.48	0.77	1.87
AZU-R2-1	8.77	72	102	2.44	2.40	876	903	7.57	1079	0.17	0.70	7.51
AZU-R2-2	8.77	72	102	2.45	2.38	888	906	7.57	1097	0.16	0.68	7.62
AZU-R2-3	8.77	72	102	2.62	2.33	882	909	7.65	917	0.16	0.65	7.54
ARN-R2-1	10.19	31	117	2.01	2.48	355	353	7.04	1354	0.19	0.67	2.68
ARN-R2-2	10.19	31	117	1.37	2.38	353	355	7.07	1267	0.20	0.64	2.68
ARN-R2-3	10.19	31	117	1.45	2.40	360	362	7.11	1209	0.18	0.66	2.79
BAC-R2-1	10.71	36	114	n.d.	1.23	427	384	n.d.	n.d.	0.17	0.36	2.36
BAC-R2-2	10.71	36	114	2.00	1.19	408	428	7.07	1485	0.18	0.39	2.29
BAC-R2-3	10.71	36	114	1.60	1.21	404	427	7.13	1299	0.19	0.36	2.40
COA-R2-1	11.08	15	81	1.80	0.57	186	190	6.65	1376	0.20	<LOD	0.61
COA-R2-2	11.08	15	81	2.02	0.57	197	220	6.72	1308	0.20	<LOD	0.55
COA-R2-3	11.08	15	81	1.87	0.49	188	193	6.63	1443	0.20	<LOD	0.56

PAN-R2-1	11.12	51	146	n.d.	3.01	435	355	n.d.	n.d.	0.47	0.42	2.86
PAN-R2-2	11.12	51	146	1.88	2.25	427	420	6.97	1876	0.27	0.43	2.42
PAN-R2-3	11.12	51	146	2.25	2.17	427	441	7.07	1558	0.26	0.43	2.44

REPLIM 3	Temperature	Conductivity	Redox Potential	TOC	Silicate	DIC	TA	pH	fCO ₂	Cl ⁻	NO ₃ ⁻	SO ₄ ²⁻
	°C	µS cm ⁻¹	mV	mg L ⁻¹	mg L ⁻¹	µmol kg ⁻¹	µmol kg ⁻¹		µatm	mg L ⁻¹	mg L ⁻¹	mg L ⁻¹
LOD										0.02	0.01	0.21
ARA-R3-T1	5.86	38	176	0.88	4.61	597	604	7.09	1929	0.27	0.85	2.64
ARA-R3-T3	5.72	35	317	0.79	5.01	590	605	6.94	2475	0.18	0.71	2.65
ARA-R3-T4	6.64	36	310	0.82	4.30	580	597	6.88	2759	0.19	0.61	2.80
ARA-R3-P1=T2	5.70	38	84	0.85	4.64	597	603	6.99	2321	0.17	0.58	2.75
ARA-R3-P2	4.91	37	101	0.80	4.90	601	614	6.96	2391	0.15	0.78	2.82
ARA-R3-P3	4.87	37	106	0.81	4.55	607	617	6.95	2454	0.15	0.74	2.75
ARA-R3-P4	4.79	138	-188	0.78	4.56	624	629	6.96	2507	0.18	0.71	2.83
BAD-R3	5.89	34	207	0.89	5.27	915	956	7.21	2321	0.19	1.13	5.43
CAM-R3	2.43	5	172	0.85	1.66	108	85	5.80	1303	0.13	0.34	0.35
PEY-R3	6.41	16	36	0.84	0.09	33	14	4.87	526	0.07	0.10	<LOD
OPA-R3	3.29	15	91	0.71	1.60	270	266	6.48	2078	0.17	0.56	0.49
PAR-R3	n.d.	n.d.	n.d.	2.18	6.38	705	676	n.d.	n.d.	0.50	0.46	1.71
GEN-R3-T1	6.89	20	269	0.85	2.35	341	342	6.70	2172	0.25	0.10	0.49
GEN-R3-T3	6.87	20	202	0.62	2.84	339	325	6.90	1576	0.26	0.21	0.49
GEN-R3-T4	7.21	20	75	1.09	2.52	340	338	6.64	2367	0.38	0.16	0.47
GEN-R3-P1=T2	6.87	20	202	0.86	2.38	346	340	6.72	2113	0.36	0.18	0.42
GEN-R3-P2	4.97	20	199	0.75	2.34	347	339	6.68	2163	0.27	0.18	0.43
GEN-R3-P3	4.37	38	211	1.03	2.56	375	363	6.74	2129	0.34	0.04	0.49
GEN-R3-P4	4.23	47	38	1.41	3.37	684	575	6.76	3712	0.60	0.03	0.68
GEN-R3-P5	4.40	67	-69	1.44	6.75	1307	862	6.77	6938	0.92	0.08	0.66
ROU-R3	n.d.	n.d.	n.d.	0.87	2.81	345	357	n.d.	n.d.	0.30	0.14	0.50
BER-R3	n.d.	n.d.	n.d.	0.77	1.29	168	114	n.d.	n.d.	0.23	0.37	0.32
AZU-R3-T2	5.03	43	39	0.65	2.35	661	n.d.	n.d.	n.d.	0.17	0.69	4.76
AZU-R3-P1=T1	4.87	46	149	0.70	2.55	675	704	7.17	1852	0.18	0.76	4.91
AZU-R3-P2	4.82	48	143	0.63	2.37	719	753	7.39	1270	0.19	1.17	5.23
AZU-R3-P3	4.67	48	140	0.72	2.29	734	759	7.21	1843	0.15	0.64	5.26
ARN-R3	7.45	13	200	0.77	1.94	184	188	6.33	1836	0.19	0.62	1.13
BAC-R3	12.45	25	129	0.94	1.98	290	302	6.55	2537	0.16	0.57	1.68
PEC-R3	4.33	21	149	0.65	1.92	314	316	6.64	2039	0.17	1.03	1.68
COA-R3	10.09	7	169	1.03	1.14	108	90	5.85	1619	0.24	0.41	0.35

PAN-R3	11.18	28	176	1.01	2.57	359	366	6.67	2595	0.27	0.71	1.88
ORD-R3	17.50	57	97	2.26	2.68	722	733	7.02	3188	0.20	0.20	1.86
SAB-R3-T1	16.65	130	37	2.37	1.63	1727	1810	7.65	2011	0.20	0.43	2.23
SAB-R3-T3	18.67	120	201	1.52	1.57	1720	1808	7.47	3049	0.17	0.29	2.32
SAB-R3-P1=T2	17.25	115	207	1.71	1.48	1723	1803	7.53	2615	0.21	0.49	2.33
SAB-R3-P2	10.70	115	61	2.07	2.02	1814	1877	7.51	2610	0.21	0.48	2.51
SAB-R3-P3	7.57	119	65	1.93	3.15	2137	2171	7.54	2747	0.27	0.45	3.21
SAB-R3-P4	6.01	120	66	1.54	3.63	2192	2209	7.56	2656	0.29	0.54	3.07
SAB-R3-P5	5.13	124	95	1.55	5.13	2320	2298	7.51	3087	0.31	0.50	3.02
SAB-R3-P6	4.80	127	-61	1.32	7.38	2483	2381	7.42	3971	0.35	0.46	2.74

REPLIM 4	Temperature	Conductivity	Redox Potential	TOC	Silicate	DIC	TA	pH	fCO ₂	Cl ⁻	NO ₃ ⁻	SO ₄ ²⁻
	°C	µS cm ⁻¹	mV	mg L ⁻¹	mg L ⁻¹	µmol kg ⁻¹	µmol kg ⁻¹		µatm	mg L ⁻¹	mg L ⁻¹	mg L ⁻¹
LOD										0.01	0.06	0.29
ARA-R4-P1	8.32	50	170	1.79	4.76	777	815	7.23	1998	0.15	0.17	3.23
ARA-R4-P2	8.38	50	130	1.40	4.73	778	851	7.44	1291	0.14	0.17	3.22
ARA-R4-P3	5.64	54	71	1.16	4.95	805	871	7.39	1446	0.16	0.22	3.33
BAD-R4	5.33	45	136	1.26	4.11	778	825	7.37	1450	0.15	0.29	2.96
CAM-R4	8.47	10	222	1.08	1.87	162	154	6.36	1618	0.18	0.21	0.40
PEY-R4	6.81	5	151	1.64	0.81	79	85	5.94	1034	0.14	<LOD	<LOD
OPA-R4	5.90	17	127	1.13	2.38	307	291	6.74	1788	0.17	0.51	0.48
PAR-R4	9.53	34	240	2.30	6.43	642	618	6.99	2639	0.68	0.57	1.66
GEN-R4-T1	12.63	24	166	1.30	1.40	368	378	6.74	2462	0.30	<LOD	<LOD
GEN-R4-T3	12.81	24	137	1.25	1.40	359	364	6.71	2497	0.37	<LOD	0.38
GEN-R4-P1=T2	12.80	24	96	1.38	1.38	358	349	6.75	2338	0.26	<LOD	0.31
GEN-R4-P2	12.68	24	88	1.41	1.34	357	355	6.65	2696	0.22	<LOD	0.30
GEN-R4-P3	12.62	24	90	1.23	1.43	364	365	6.77	2287	0.24	<LOD	0.33
GEN-R4-P4	8.52	44	196	1.77	2.39	635	585	6.96	2734	0.55	<LOD	0.47
GEN-R4-P5	6.05	56	-64	1.52	5.60	1151	858	6.90	5189	0.87	0.14	<LOD
ROU-R4	13.38	25	36	1.86	1.15	359	377	6.85	2009	0.29	<LOD	0.47
BER-R4	12.09	15	38	1.58	0.88	237	223	7.43	430	0.31	<LOD	<LOD
AZU-R4-P1=T1	5.39	50	110	0.94	2.72	803	853	7.27	1803	0.16	0.76	6.78
AZU-R4-P2	5.08	50	86	1.08	2.74	814	846	7.25	1912	0.17	0.78	6.70
AZU-R4-P3	4.98	50	79	0.95	2.76	818	847	7.27	1823	0.20	0.90	6.73
ARN-R4	7.41	20	221	n.d.	2.47	309	309	6.79	1737	0.21	0.81	2.19
BAC-R4	8.97	32	207	1.05	1.48	358	350	6.75	2194	0.22	0.82	1.89
PEC-R4	8.13	35	216	1.08	2.21	444	438	6.79	2489	0.19	0.69	2.39
COA-R4	6.18	7	163	1.87	1.16	125	106	6.02	1523	0.25	0.09	<LOD
PAN-R4	9.87	25	193	2.03	2.98	372	334	6.64	2718	0.68	0.63	2.20
ORD-R4	9.32	48	225	4.63	2.86	573	540	6.90	2740	0.39	0.14	1.50
SAB-R4-T1	10.42	100	188	3.02	1.10	1691	1839	7.71	1584	0.23	0.13	2.48
SAB-R4-T3	10.80	101	262	2.62	1.27	1692	1810	7.67	1755	0.22	<LOD	2.56
SAB-R4-P1=T2	10.70	101	245	1.96	1.24	1694	1838	7.64	1853	0.20	0.37	2.54
SAB-R4-P2	10.56	102	62	2.25	1.25	1693	1850	7.73	1521	0.22	0.15	2.54

SAB-R4-P3	10.53	102	54	2.10	1.39	1701	1849	7.55	2255	0.22	0.17	2.55
SAB-R4-P4	7.87	119	66	2.01	3.12	2133	2272	7.60	2459	0.30	0.34	3.09
SAB-R4-P5	5.97	117	78	2.16	4.32	2225	2227	7.64	2262	0.46	0.44	3.10
SAB-R4-P6	5.70	121	84	2.01	6.76	2395	2469	7.34	4565	0.30	0.20	3.03

Annexe 5: Hg isotope data (Lake Marboré and Lake Estanya)

Lake Marbore	Age	[Hg]	HgARs	$\delta^{204}\text{Hg}$	$\delta^{202}\text{Hg}$	$\delta^{201}\text{Hg}$	$\delta^{200}\text{Hg}$	$\delta^{199}\text{Hg}$	$\Delta^{204}\text{Hg}$	$\Delta^{201}\text{Hg}$	$\Delta^{200}\text{Hg}$	$\Delta^{199}\text{Hg}$
	Year	ng g ⁻¹	$\mu\text{g m}^{-2} \text{y}^{-1}$	‰	‰	‰	‰	‰	‰	‰	‰	‰
MAR11-1A-1U-1, 8-9 cm	2004	58	40	-0.96	-0.51	-0.15	-0.18	0.00	-0.19	0.24	0.08	0.13
MAR11-1A-1G-1, 10-11 cm	1992	64	49	-1.15	-0.63	-0.24	-0.22	0.13	-0.21	0.23	0.10	0.29
MAR11-1A-1G-1, 12-13 cm	1969	106	70	-1.00	-0.51	0.00	-0.14	0.24	-0.24	0.38	0.12	0.37
MAR11-1A-1G-1, 14-15 cm	1946	53	39	-1.14	-0.64	-0.25	-0.21	0.09	-0.19	0.23	0.11	0.26
MAR11-1A-1U-1, 14-15 cm	1927	53	39	-0.04	0.11	0.22	0.07	0.12	-0.20	0.13	0.01	0.09
MAR11-1A-1U-1, 16-17 cm	1906	67	54	-0.74	-0.37	-0.06	-0.04	0.19	-0.18	0.22	0.15	0.28
MAR11-1A-1U-1, 18-19 cm	1885	58	44	-0.55	-0.23	0.00	0.01	0.19	-0.20	0.17	0.13	0.25
MAR11-1A-1U-1, 20-21 cm	1865	67	48	-0.52	-0.27	-0.13	-0.01	0.04	-0.12	0.07	0.13	0.10
MAR11-1A-1U-1, 22-23 cm	1841	50	30	-0.62	-0.35	-0.17	-0.08	-0.01	-0.10	0.09	0.10	0.07
MAR11-1A-1U-1, 24-25 cm	1817	37	25	-1.24	-0.74	-0.54	-0.27	-0.15	-0.13	0.01	0.10	0.03
MAR11-1A-1U-1, 28-29 cm	1770	38	22	-0.75	-0.38	-0.34	-0.08	-0.06	-0.19	-0.05	0.11	0.03
MAR11-1A-1U-1, 32-33 cm	1722	32	23	-1.07	-0.59	-0.48	-0.21	-0.20	-0.18	-0.03	0.09	-0.05
MAR11-1A-1U-1, 36-37 cm	1674	26	15	-0.90	-0.52	-0.27	-0.13	-0.02	-0.13	0.11	0.13	0.11
MAR11-1A-1U-1, 40-41 cm	1595	26	17	-0.88	-0.39	-0.31	-0.13	-0.16	-0.30	-0.02	0.07	-0.06
MAR11-1A-1U-1, 42-43 cm	1498	25	18	-0.68	-0.35	-0.35	-0.08	-0.04	-0.15	-0.09	0.10	0.05
MAR11-1A-1U-2, 15-16 cm	1436	22	14	-1.66	-0.99	-0.84	-0.39	-0.27	-0.18	-0.10	0.11	-0.02
MAR11-1A-1U-2, 19-20 cm	1355	20	14	-1.61	-1.03	-0.87	-0.40	-0.38	-0.08	-0.10	0.11	-0.12
MAR11-1A-1U-2, 23-24 cm	1273	25	13	-2.12	-1.23	-1.19	-0.63	-0.49	-0.28	-0.27	-0.01	-0.18
MAR11-1A-1U-2, 29-30 cm	1152	27	16	-1.99	-1.33	-1.13	-0.63	-0.46	0.00	-0.13	0.04	-0.12
MAR11-1A-1U-2, 45-46 cm	829	22	14	-2.18	-1.31	-1.06	-0.54	-0.43	-0.22	-0.07	0.12	-0.09
MAR11-1A-1U-2, 57-58 cm	600	19	14	-1.71	-1.04	-0.90	-0.43	-0.35	-0.16	-0.12	0.09	-0.09
MAR11-1A-1U-2, 67-68 cm	438	23	14	-2.24	-1.46	-1.13	-0.61	-0.44	-0.05	-0.03	0.12	-0.07
MAR11-1A-1U-2, 77-78 cm	278	20	17	-2.64	-1.73	-1.36	-0.80	-0.47	-0.05	-0.05	0.07	-0.04
MAR11-1A-1U-2, 89-90 cm	85	19	14	-3.12	-1.99	-1.67	-0.96	-0.66	-0.14	-0.17	0.04	-0.16
MAR11-1A-1U-2, 93-94 cm	20	31	18	-2.94	-1.83	-1.51	-0.91	-0.58	-0.20	-0.13	0.01	-0.12
MAR11-1A-1U-2, 117-118 cm	-366	24	13	-2.17	-1.35	-1.19	-0.62	-0.41	-0.16	-0.17	0.06	-0.07

MAR11-1A-1U-2, 147-148 cm	-835	19	12	-1.89	-1.17	-1.02	-0.45	-0.34	-0.15	-0.15	0.13	-0.04
Lake Estanya	Age	[Hg]	HgARs	$\delta^{204}\text{Hg}$	$\delta^{202}\text{Hg}$	$\delta^{201}\text{Hg}$	$\delta^{200}\text{Hg}$	$\delta^{199}\text{Hg}$	$\Delta^{204}\text{Hg}$	$\Delta^{201}\text{Hg}$	$\Delta^{200}\text{Hg}$	$\Delta^{199}\text{Hg}$
	Year	ng g ⁻¹	$\mu\text{g m}^{-2} \text{y}^{-1}$	‰	‰	‰	‰	‰	‰	‰	‰	‰
LEG04-1A-1M, 1-6 cm	2001	37	29	-0.93	-0.70	-0.56	-0.30	-0.19	0.12	-0.03	0.05	-0.01
LEG04-1A-1M, 9-15 cm	1976	29	23	-0.99	-0.62	-0.42	-0.27	-0.17	-0.06	0.05	0.04	-0.01
LEG04-1A-1K-1, 6-7 cm	1952	79	37	-0.81	-0.45	-0.08	-0.12	0.20	-0.14	0.26	0.11	0.31
LEG04-1A-1K-1, 7-8 cm	1940	77	54	-0.69	-0.56	-0.25	-0.18	0.10	0.15	0.17	0.10	0.24
LEG04-1A-1K-1, 12-13 cm	1873	97	51	-0.35	-0.28	-0.11	-0.11	0.14	0.07	0.10	0.03	0.21
LEG04-1A-1K-1, 16-17 cm	1808	75	48	-1.07	-0.69	-0.37	-0.27	-0.10	1.54	0.15	0.07	0.08
LEG04-1A-1K-1, 18-19 cm	1776	86	40	-0.61	-0.45	-0.13	-0.17	0.09	0.06	0.21	0.06	0.20
LEG04-1A-1K-1, 24-25 cm	1687	31	21	-0.98	-0.69	-0.50	-0.26	-0.15	0.06	0.02	0.09	0.02
LEG04-1A-1K-1, 41-42 cm	1501	31	24	-1.38	-0.84	-0.61	-0.43	-0.26	-0.12	0.02	-0.01	-0.05
LEG04-1A-1K-2, 4-5 cm	1269	20	5	-1.20	-0.79	-0.65	-0.42	-0.20	-0.02	-0.06	-0.02	0.00
LEG04-1A-1K-2, 38-39 cm	852	16	4	-1.29	-0.87	-0.64	-0.49	-0.23	0.00	0.01	-0.05	-0.01
LEG04-1A-1K-2, 72-73 cm	-825	17	4	-1.22	-0.85	-0.52	-0.47	-0.16	0.04	0.12	-0.04	0.05
LEG04-1A-1K-2, 82-83 cm	-1467	24	6	-0.95	-0.72	-0.59	-0.34	-0.16	0.12	-0.05	0.02	0.02
LEG04-1A-1K-2, 92-93 cm	-2086	15	4	-0.91	-0.71	-0.49	-0.36	-0.02	0.15	0.05	0.00	0.16